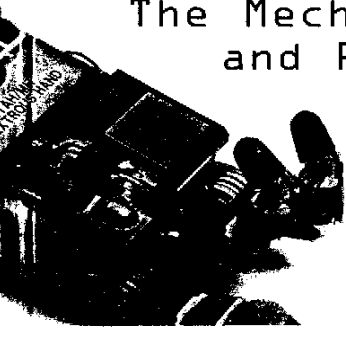


ROBOT ANALYSIS

The Mechanics of Serial
and Parallel Manipulators



LUNG-WEN TSAI

ROBOT ANALYSIS



ROBOT ANALYSIS

The Mechanics of Serial and Parallel Manipulators

LUNG-WEN TSAI

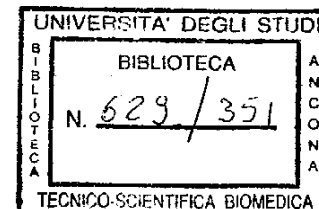
Department of Mechanical Engineering
and
Institute for Systems Research
University of Maryland



A Wiley-Interscience Publication

JOHN WILEY & SONS, INC.

New York / Chichester / Weinheim / Brisbane / Singapore / Toronto



This book is printed on acid-free paper. ☺

Copyright © 1999 by John Wiley & Sons, Inc. All rights reserved.

Published simultaneously in Canada.

No part of this publication may be reproduced, stored in a retrieval system or transmitted in any form or by any means, electronic, mechanical, photocopying, recording, scanning or otherwise, except as permitted under Section 107 or 108 of the 1976 United States Copyright Act, without either the prior written permission of the Publisher, or authorization through payment of the appropriate per-copy fee to the Copyright Clearance Center, 222 Rosewood Drive, Danvers, MA 01923, (978) 750-8400, fax (978) 750-4744. Requests to the Publisher for permission should be addressed to the Permissions Department, John Wiley & Sons, Inc., 605 Third Avenue, New York, NY 10158-0012, (212) 850-6011, fax (212) 850-6008, E-Mail: PERMREQ@WILEY.COM.

This publication is designed to provide accurate and authoritative information in regard to the subject matter covered. It is sold with the understanding that the publisher is not engaged in rendering professional services. If professional advice or other expert assistance is required, the services of a competent professional person should be sought.

Library of Congress Cataloging-in-Publication Data:

Tsai, Lung-Wen.

Robot analysis : the mechanics of serial and parallel manipulators / by Lung-Wen Tsai.

p. cm.

Includes index.

ISBN 0-471-32593-7 (cloth : alk. paper)

1. Robotics. 2. Manipulators (Mechanism) 1. Title.

TJ211.T75 1999

629.8'92—dc21

98-36463

Printed in the United States of America

10 9 8 7 6 5 4 3 2



CONTENTS

Preface

1 Introduction

- 1.1 Historical Development / 2
- 1.2 A Sense of Mechanisms / 6
- 1.3 Robotic Systems / 17
- 1.4 Classification of Robots / 19
- 1.5 Position, Orientation, and Location of a Rigid Body / 29
- 1.6 Homogeneous Transformations / 42
- 1.7 Mechanics of Robot Manipulators / 45
- 1.8 Summary / 48
- References / 48
- Exercises / 50

2 Position Analysis of Serial Manipulators

- 2.1 Introduction / 54
- 2.2 Link Parameters and Link Coordinate Systems / 56
- 2.3 Denavit-Hartenberg Homogeneous Transformation Matrices / 60
- 2.4 Loop-Closure Equations / 65

xi

1

54

v

2.5 Other Coordinate Systems / 69		4.9 Relationship between the Two Methods / 211	
2.6 Denavit–Hartenberg Method / 69		4.10 Condition Number / 211	
2.7 Method of Successive Screw Displacements / 91		4.11 Singularity Analysis / 215	
2.8 Summary / 109		4.12 Summary / 219	
References / 109		References / 220	
Exercises / 111		Exercises / 221	
3 Position Analysis of Parallel Manipulators	116	5 Jacobian Analysis of Parallel Manipulators	223
3.1 Introduction / 116		5.1 Introduction / 223	
3.2 Structure Classification of Parallel Manipulators / 118		5.2 Jacobian Matrices / 224	
3.3 Denavit–Hartenberg Method versus Geometric Method / 123		5.3 Singularity Conditions / 225	
3.4 Position Analysis of a Planar 3RRR Parallel Manipulator / 124	-	5.4 Conventional Jacobian / 226	
3.5 Position Analysis of a Spatial Orientation Mechanism / 129		5.5 Wrenches and Reciprocal Screws / 241	
3.6 Position Analysis of the University of Maryland Manipulator / 134		5.6 Screw-Based Jacobian / 247	
3.7 Position Analysis of a Spatial 3RPS Parallel Manipulator / 142		5.7 Summary / 257	
3.8 Position Analysis of a General Stewart–Gough Platform / 151		References / 257	
3.9 Position Analysis of a Nearly General Stewart–Gough Platform / 156		Exercises / 259	
3.10 Position Analysis of a 3–3 Stewart–Gough Platform / 158		6 Statics and Stiffness Analysis	260
3.11 Summary / 161		6.1 Introduction / 260	
References / 161		6.2 Statics of Serial Manipulators / 261	
Exercises / 164		6.3 Transformation of Forces and Moments / 275	
4 Jacobian Analysis of Serial Manipulators	169	6.4 Stiffness Analysis of Serial Manipulators / 279	
4.1 Introduction / 169		6.5 Statics of Parallel Manipulators / 282	
4.2 Differential Kinematics of a Rigid Body / 171		6.6 Stiffness Analysis of Parallel Manipulators / 288	
4.3 Differential Kinematics of Serial Manipulators / 177		6.7 Summary / 293	
4.4 Screw Coordinates and Screw Systems / 182		References / 293	
4.5 Manipulator Jacobian Matrix / 184		Exercises / 294	
4.6 Conventional Jacobian / 186		7 Wrist Mechanisms	298
4.7 Screw-Based Jacobian / 192		7.1 Introduction / 298	
4.8 Transformation of Screw Coordinates / 205		7.2 Bevel-Gear Wrist Mechanisms / 301	
		7.3 Structure Representation of Mechanisms / 303	
		7.4 Structure Characteristics of Epicyclic Gear Trains / 307	
		7.5 Classification of Wrist Mechanisms / 308	
		7.6 Kinematics of Epicyclic Gear Drives / 309	

7.7 Kinematics of Robotic Wrist Mechanisms / 317		10.3 Principle of Virtual Work / 437
7.8 Static Force Analysis / 321		10.4 Lagrangian Formulation / 447
7.9 Summary / 326		10.5 Summary / 453
References / 326		References / 454
Exercises / 328		Exercises / 455
8 Tendon-Driven Manipulators	333	APPENDIXES
8.1 Introduction / 333		A Continuation Method
8.2 Classification of Tendon-Driven Manipulators / 334		A.1 Bezout Number / 458
8.3 Planar Schematic Representation / 339		A.2 Traditional Homogeneous Formulation / 458
8.4 Kinematics of Tendon-Driven Manipulators / 340		A.3 M -Homogenization / 460
8.5 Static Force Analysis / 348		A.4 Solutions at Infinity / 461
8.6 Feasible Structure Matrices / 351		A.5 Continuation Method / 462
8.7 Redundant Forces Resolution / 354		A.6 Cheater's Homotopy / 469
8.8 Summary / 366		References / 470
References / 367		B Sylvester Dialytic Elimination Method
Exercises / 369		B.1 Elimination Procedure / 473
9 Dynamics of Serial Manipulators	372	B.2 Example / 474
9.1 Introduction / 372		References / 475
9.2 Mass Properties / 375		C Raghavan and Roth's Solution
9.3 Momentum / 379		C.1 Loop-Closure Equation / 477
9.4 Transformation of Inertia Matrix / 381		C.2 Elimination of θ_1 and θ_2 / 480
9.5 Kinetic Energy / 382		C.3 Elimination of θ_4 and θ_5 / 480
9.6 Newton-Euler Laws / 383		References / 482
9.7 Recursive Newton-Euler Formulation / 386		D List of Symbols
9.8 Lagrangian Formulation / 395		Index
9.9 Inertia Effects of the Rotors / 410		
9.10 End-Effector Space Dynamical Equations / 417		
9.11 Summary / 419		
References / 419		
Exercises / 421		
10 Dynamics Of Parallel Manipulators	424	
10.1 Introduction / 424		
10.2 Newton-Euler Formulation / 426		

PREFACE

This book has evolved from class notes used for a graduate-level course in robot analysis that the author has taught for over a decade at the University of Maryland, College Park, Maryland. It provides both fundamental and advanced topics on the kinematics, statics, and dynamics of robot manipulators. Both serial and parallel manipulators are covered in depth. In addition, it contains chapters on geared robotic mechanisms and tendon-driven manipulators. An overview of the state of the art in solving systems of nonlinear equations that arise in robot kinematics is given in the appendixes. An extensive reference list is provided at the end of each chapter to provide readers with plenty of resources for more advanced study.

Prerequisites for readers of this book consist of the fundamentals of kinematics, dynamics, vector space analysis, and matrix theory. These basics are usually taught at the undergraduate level. A one-semester course will cover most of the fundamentals presented in the book. The more advanced topics, such as the screw-based Jacobian and singularity analysis and the two chapters on geared robotic wrists and tendon-driven manipulators, can be taught in a second semester or be used as reference material. It is anticipated that after studying the kinematics and dynamics of robot manipulators, students will be motivated to take an advanced course in robot sensing, control, and machine intelligence.

Chapter 1 provides a brief review of the historical development and a classification of robot manipulators. The science of *robotics* and the *mechanics* of robot manipulators are defined. A brief review of some of the fundamentals that are essential for an understanding of the mechanics of robot manipulators

is given. Finally, the rotation matrix and homogeneous transformation matrix are described.

Chapter 2 lays the mathematical foundation for the position analysis of serial manipulators. The concept of loop closure equation is introduced. Both the Denavit–Hartenberg method and the method of successive screw displacements are presented. Several industrial and research robots are analyzed to illustrate the methodologies.

Chapter 3 provides the fundamental knowledge needed for the position analysis of parallel manipulators. Parallel manipulators are classified according to their kinematic structures. The method of vector-loop equation is introduced. Several parallel manipulators, including a planar 3-dof manipulator, a spatial 3-dof orientation mechanism, a parallel manipulator with only translational degrees of freedom, and the well-known Stewart–Gough platform are analyzed.

Chapter 4 extends the study of serial manipulators from the position analysis to the velocity analysis. The differential kinematic properties of a link in an open-loop chain and their propagation from link to link are studied. Both the conventional Jacobian and the screw-based Jacobian are defined. The screw-based Jacobian analysis is shown to be more efficient than the conventional method of analysis. Finally, the singularities of serial manipulators are studied.

Chapter 5 covers the Jacobian and singularity analyses of parallel manipulators. The velocity vector-loop approach is employed for derivation of the conventional Jacobian matrices, and the concept of reciprocal screws is used for derivation of the screw-based Jacobian matrices. The singularities of parallel manipulators are classified into three types. For the first type of singularity, the manipulator loses 1 or more degrees of freedom, while for the second type of singularity, the manipulator gains 1 or more degrees of freedom. The third type of singularity occurs when the first and second types of singularity occur simultaneously. The physical meanings of each type of singularity are illustrated by several parallel manipulators.

Chapter 6 addresses the statics and stiffness of serial and parallel manipulators. Both the free-body diagram method and the method of virtual work are presented. By applying the principle of virtual work, it is shown that in the absence of gravity, the actuated joint torques are related to the end-effector output forces by the transpose of the Jacobian matrix. The statics and stiffness of several manipulators are analyzed to illustrate the principles.

Chapter 7 deals with the kinematics and statics of robotic wrist mechanisms. The structural characteristics of epicyclic gear trains are analyzed. The theory of fundamental circuits and the coaxiality conditions associated with epicyclic gear drives are derived. A systematic methodology for the kinematic analysis of epicyclic gear trains and robotic wrist mechanisms is developed.

Chapter 8 covers the kinematics and statics of tendon-driven manipulators. The concept of transmission lines is introduced. It is shown that tendon displacements are related to the joint angles by a structure matrix, and the structure matrix can be derived by inspection of the structural topology of the tendon routing. Furthermore, force transmission characteristics from the tendon space to the end-effector space are analyzed. An efficient method for the resolution of redundant tendon forces is developed. The Stanford/JPL hand and the Utah/MIT hand are analyzed to demonstrate the methodology.

Chapter 9 deals with the dynamics of serial manipulators. Both the recursive Newton–Euler formulation and the Lagrangian formulation are presented. The concepts of the Lagrangian function, manipulator inertia matrix, and generalized forces are introduced. Furthermore, the inertia effects of rotors on the dynamics of a serial manipulator are discussed.

Chapter 10 concerns the dynamics of parallel manipulators. The dynamical analysis of parallel manipulators is complicated by the existence of multiple closed loops. First, a numerical solution technique based on the laws of Newton and Euler is presented. Then a more efficient method based on the principle of virtual work is developed. Finally, it is shown that explicit equations of motion for some relatively simple manipulators can be derived by applying Lagrangian equations of the first type.

In the appendixes, the state-of-the-art continuation method and the methods of elimination for solving systems of nonlinear equations are presented. Furthermore, Raghavan and Roth's solution of the kinematics of the 6R manipulator of general geometry is presented.

Some of the materials presented in this book is based on the author's research in collaboration with friends, professional colleagues, and a former advisor: Ferdinand Freudenstein, Krishna Gupta, Tien Yien Li, Alexander Morgan, Madhusudan Raghavan, Bernard Roth, and Gregory Walsh—and with former students: Sun-Lai Chang, Dar-Zen Chen, Hsin-I Hsieh, Jyh-Jone Lee, Chen-Chou Lin, Yeong-Jeong Ou, Tai-Kang Shing, Richard Stamper, and Farhad Tahmasbi. Their efforts are deeply appreciated.

The author would like to acknowledge the anonymous reviewers for their constructive comments on the manuscript, and the editor of the book, Bob Argentieri, for his enthusiasm and support in making this publication possible.

Finally, the author appreciates the patience and sacrifice of his family members, Lung-Chu Tsai, Jule Ann Tsai, and David Jeanchung Tsai, over the past few years while the book was being written.

LUNG-WEN TSAI
College Park, Maryland

CHAPTER 1

INTRODUCTION

Since the industrial revolution, there has been an ever-increasing demand to improve product quality and reduce manufacturing cost. At first, most products were manufactured by craftsmen. The product quality depended highly on the skill of the craftsmanship, and the product cost was prohibitively high. This is known as *manual production*.

At the beginning of the twentieth century (1905), Ford Motor Company introduced the concept of *mass production*. In a mass-production environment, most manufacturing processes are carried out by special-purpose machines. This method of production drastically reduces the cost of manufacturing and makes the automobile and other industrial products affordable to the general population. However, since each production machine is designed to perform a predetermined task, every time a new model is introduced, the entire production line has to be shut down and retooled. Retooling a production line during each model change can be very expensive. We call this type of automation *hard automation*.

The inflexibility and relatively high cost of hard automation have led to an entirely new approach. Recently, *robot manipulators* have been introduced by manufacturing industries for performing certain production tasks, such as material handling, spot welding, spray painting, and assembling. Because robot manipulators are controlled by computers or microprocessors, they can easily be reprogrammed for different tasks. Hence there is no need to replace these machines during a model change. We call this type of automation *flexible automation*.

There are compromises between manual production, hard automation, and flexible automation. In general, manual production tends to be slow and makes it difficult to achieve consistent product quality. Although hard automation is faster and more precise than the other two production methods, the retooling cost for each model change can be high. With flexible automation, on the other hand, much less time is required to set up a production line because robot manipulators can readily be purchased off the shelf. In addition, the manipulators can be preprogrammed off the line and are almost immune to obsolescence. Typically, when the production volume is very low, manual production is more economical. As the production volume increases, flexible automation becomes more cost-effective. As the production volume increases further, hard automation becomes the most effective production method. In this book, we study the mechanics of robot manipulators essential for the design, programming, and control of such devices in a flexible manufacturing environment.

1.1 HISTORICAL DEVELOPMENT

The word *robot* means different things to different people. Webster's *New World College Dictionary* defines a *robot* as "any anthropomorphic mechanical being built to do routine manual work for human beings." On the other hand, the definition used by the Robotics Institute of America is more specific: "A robot is a re-programmable multi-functional manipulator designed to move material, parts, tools, or specialized devices, through variable programmed motions for the performance of a variety of tasks." The latter definition includes mechanical manipulators, numerical control machines, walking machines, and the humanoids of science fiction. Although most people perceive robots anthropomorphically, today's industrial robots are only somewhat humanoid in appearance. In fact, most industrial robots are mechanical manipulators. Figure 1.1 shows a typical humanoid of science fiction; by contrast, Fig. 1.2 shows a typical industrial robot.

Although the word *robot* entered the English vocabulary as early as 1923 (Capek, 1923), the actual development of robot manipulators did not occur until after the 1940s. The emergence of industrial robots was due initially to the need to handle hazardous materials and in space exploration, and later to achieve flexible automation. During the late 1940s, the Oak Ridge and Argonne National Laboratories began their development of *master-slave manipulators* (Fig. 1.3) for handling radioactive materials. The master manipulator is guided by an operator, while the slave manipulator duplicates the motion produced by the master in a remote site. Force feedback can be incorporated

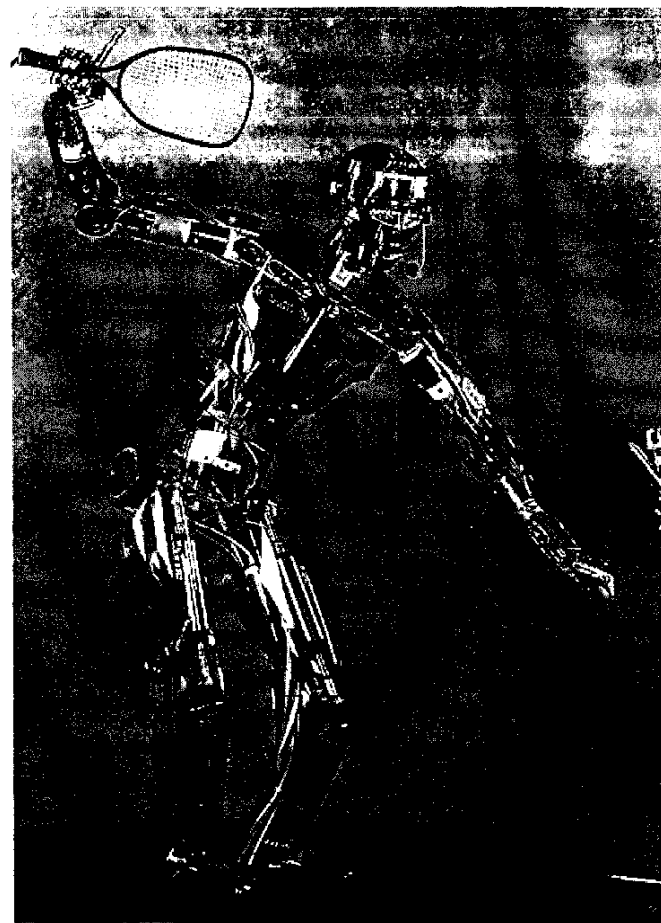


FIGURE 1.1. Humanoid. (Courtesy of SARCOS, Salt Lake City, Utah.)

to provide the operator with some feedback on the load the slave manipulator encountered.

In the late 1950s, George Devol conceived a programmable mechanical manipulator, subsequently refined by him together with Engelberger into the Unimate industrial robot (Engelberger, 1980). An important feature of an industrial robot is the incorporation of a computer- or microprocessor-based

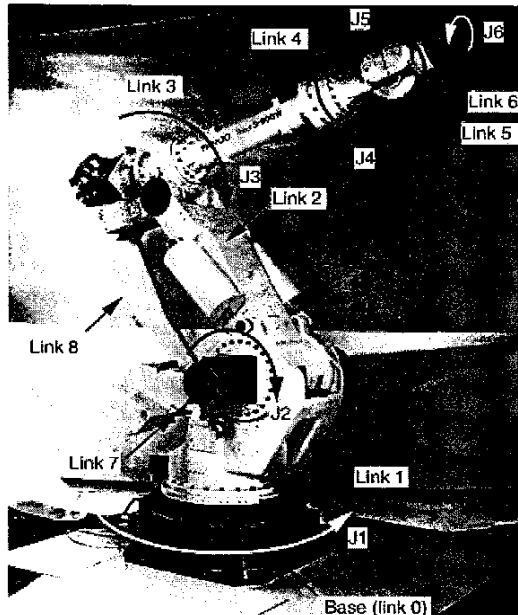


FIGURE 1.2. FANUC S-900W robot. (Courtesy of FANUC Robotics North America, Inc., Rochester Hills, Michigan.)

controller with sensory feedback to achieve programmable multifunctional capability. In the 1960s, the Stanford Artificial Intelligence Laboratory (McCarthy et al., 1968) and MIT Lincoln Laboratory (Ernst, 1962) began their development of robot manipulators with tactile sensors and computer vision. The Stanford robot was capable of doing some simple assembly tasks. In 1974, Cincinnati Milacron introduced a heavy-duty industrial robot called the Cincinnati Milacron T³ (The Tomorrow Tool) robot. Later, Unimation Incorporated introduced a new series of robots called the *PUMA robots*. Meanwhile, other companies and countries also began robotics research and development activities.

In the 1980s, there was a big boom in the robotics industry, due to the huge demand for more economical and flexible automation from the automotive industry and for space exploration. In 1982, General Motors, the largest user of robots, signed an agreement with FANUC Ltd. to form a robotic company called GMF in Rochester Hills, Michigan, to produce robots for use primarily in the automotive industry. During the same period, many other U.S.

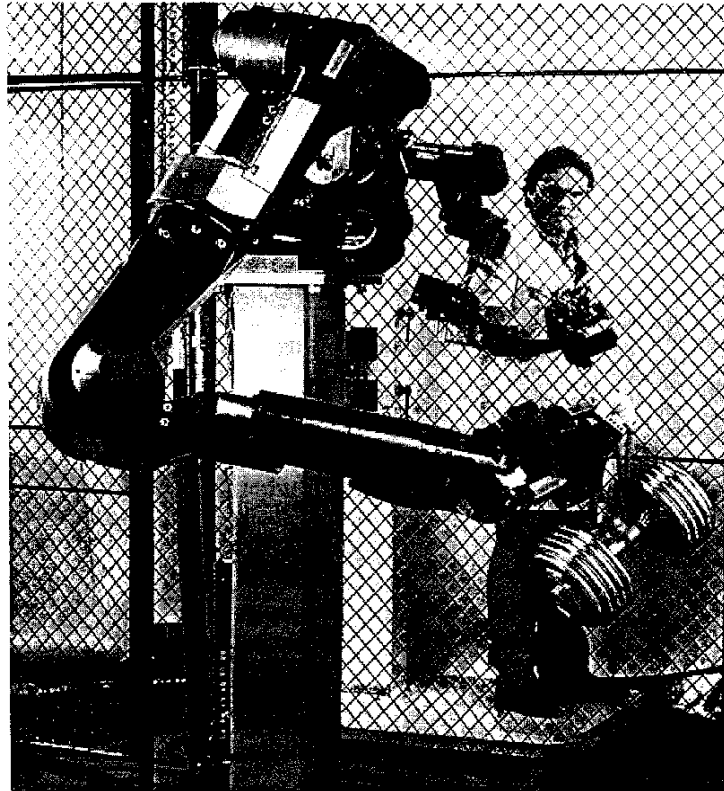


FIGURE 1.3. Master-slave robot. (Courtesy of SARCOS, Salt Lake City, Utah.)

companies, including Adept Technology, Bendix, General Electric, IBM, Intelleddex, SARCOS, Westinghouse, and Zebra Robotics, also ventured into the business, but only a few were successful. In the early 1990s, GMF was sold back to FANUC Ltd. and renamed FANUC Robotics North America, Inc. Currently, there are more European and, in particular, Japanese robotic companies than U.S. firms. The leading Japanese robotic companies include such industrial giants as FANUC, Hitachi, Kawasaki Robotics, Mitsubishi Electric, and Seiko Instruments. Some European companies, such as ASEA and KUKA International, also play an important role in both research and development and in marketing robot manipulators. Recently, Honda Laboratory invested

nearly \$80 million in the development of a 200-kg humanoid that is capable of walking up and down stairs. In 1997, NASA sent a rover called *Pathfinder* to Mars. A historical review of the early development of robot manipulators is given in Engelberger (1980).

During recent decades, robot manipulators have been used primarily for repetitive operations and in hazardous environments. Typical repetitive operation tasks include materials handling, parts loading and unloading, sealant application, and component assembling. Applications in hazardous environments include radioactive material handling, space and undersea exploration, spot welding, spray painting, and so on. Other robotic applications include construction robots, flight and vehicle simulators (Stewart, 1965), mining machines (Arai et al., 1991), pointing devices (Gosselin and Hamcl, 1994), and intelligent machining centers (Giddings & Lewis, 1995). Recently, there has been increasing interest in making robots more intelligent and user friendly, and medical surgery robots, household service robots, and so on, are becoming available. Although much effort has been spent on the development of robot manipulators, the ultimate goal of developing intelligent, user-friendly robots that can emulate human functions is still in its infancy. Major obstacles can be attributed to the fact that some of the key technologies have not yet been fully developed.

1.2 A SENSE OF MECHANISMS

A mechanism or mechanical manipulator is made up of several links connected by joints. The number of degrees of freedom (dof) of a mechanism depends on the number of links and joints and the types of joints used for construction of the mechanism. In this section we define links, joints, kinematic chains, mechanisms, and machines, then introduce the concepts of degrees of freedom and the loop mobility criterion.

1.2.1 Links and Joints

The individual bodies that make up a mechanism are called the *members* or *links*. In this book, unless stated otherwise, we treat all links as rigid bodies. The assumption of rigid bodies makes the study of mechanisms and robot manipulators a lot easier to understand. However, for high-speed or highly loaded mechanisms, the elastic effects of a material body may become significant and should be taken into consideration. For convenience, certain non-rigid bodies, such as chains, cables, or belts, which momentarily serve the same function as rigid bodies, may also be considered as links. From the kinematic point of view, two or more members connected together such that

no relative motion can occur between them will be considered as a single link. For example, an assembly of two gears connected by a common shaft is treated kinematically as one link.

Links in a mechanism or mechanical manipulator are connected in pairs. The connection between two links is called a *joint*. A joint provides some physical constraints on the relative motion between the two members. The kind of relative motion permitted by a joint is governed by the form of the contact surfaces between the members. The contact surface of a link is called a *pair element*. Two pair elements form a *kinematic pair*. Kinematic pairs can be classified into lower pairs and higher pairs, according to the type of contact. A kinematic pair is called a *lower pair* if the two elements contact each other with a substantial surface area. Typically, the forms of two mating lower-pair elements are geometrically identical, one being solid and the other hollow. A kinematic pair is called a *higher pair* if the pair elements are in contact at a point or along a line. There are six basic types of lower pairs and two of higher pairs that are frequently used in mechanisms and robot manipulators.

A *revolute joint*, *R*, permits two paired elements to rotate with respect to each other about an axis that is defined by the geometry of the joint. Hence the revolute joint imposes five constraints between the paired elements and is a 1-dof joint. The revolute joint is sometimes called a *turning pair*, a *hinge*, or a *pin joint*.

A *prismatic joint*, *P*, allows two paired elements to slide with respect to each other along an axis that is defined by the geometry of the joint. Hence the prismatic joint imposes five constraints between the paired elements and is a 1-dof joint. The prismatic joint is sometimes called a *sliding pair*.

A *cylindrical joint*, *C*, permits rotation about, and independent translation along, an axis that is defined by the geometry of the joint. Hence the cylindrical joint imposes four constraints on the paired elements and is a 2-dof joint.

A *helical joint*, *H*, allows two paired elements to rotate about, and translate along, an axis defined by the geometry of the joint. However, the translation is related to rotation by the pitch of a screw. Hence the helical joint imposes five constraints on the paired elements and is a 1-dof joint. The helical joint is sometimes called a *screw pair*.

A *spherical joint*, *S*, allows one element to rotate freely with respect to the other about the center of the sphere in all possible orientations. No translation between the paired elements is permitted. Hence the spherical joint imposes three constraints on the paired elements and is a 3-dof joint.

A *plane pair*, *E*, permits two translational degrees of freedom along the plane of contact and a rotational degree of freedom about an axis normal to

the plane of contact. Hence it imposes three constraints on the paired elements and is a 3-dof joint.

A *gear pair*, G , permits one gear to roll and slide with respect to the other at the point of contact between two meshing teeth. In addition, the motion space of a spur, helical, or bevel gear is also assumed to be constrained on a plane. Hence a gear pair imposes four constraints on the paired elements and is a 2-dof joint.

A *cam pair*, C_p , is similar to the gear pair except that a spring is usually used to keep the two paired elements in contact. Hence the cam pair is a 2-dof joint.

Revolute, prismatic, cylindrical, helical, spherical, and plane pairs are lower pairs. Gear and cam pairs are higher pairs. Another frequently used joint is the *universal joint*, shown in Fig. 1.4. The universal joint is essentially a combination of two intersecting revolute joints, hence is a 2-dof joint.

1.2.2 Kinematic Chains, Mechanisms, and Machines

A *kinematic chain* is an assemblage of links that are connected by joints. When every link in a kinematic chain is connected to every other link by at least two distinct paths, the kinematic chain forms one or more closed loops and is called a *closed-loop chain*. On the other hand, if every link is connected to every other link by one and only one path, the kinematic chain is called an *open-loop chain*. It is also possible for a kinematic chain to be made up of both closed- and open-loop chains. We call such a chain a *hybrid kinematic chain*.

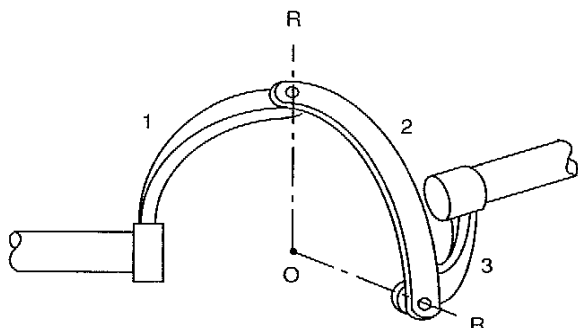


FIGURE 1.4. Universal joint.

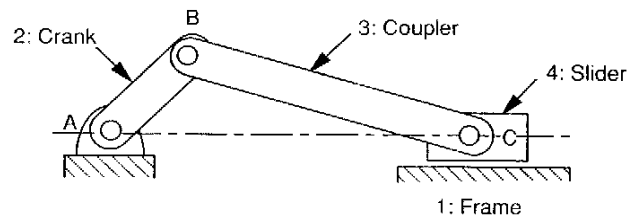


FIGURE 1.5. Slider-and-crank mechanism.

A kinematic chain is called a *mechanism* when one of its links is fixed to the ground. The fixed link is sometimes called the *base*. In a mechanism, one or more links may be assigned as the input links. As the input link(s) move with respect to the fixed link, all the other links will move according to the kinematic constraints imposed by the joints. Thus a mechanism is a device that transforms motion or torque from one or more input links to the others. Figure 1.5 shows a slider-and-crank mechanism that can transform the crank rotation into a reciprocating motion of the slider, and vice versa.

A *machine* is an assemblage of one or more mechanisms, along with other electrical and/or hydraulic components, used to transform external energy into useful work or other form of energy. For example, an electric drill is a machine. It consists of an electric motor, a speed reduction unit, a keyed chuck, and a trigger switch for the purpose of transforming electric energy into drilling work. However, the speed reduction unit itself is a mechanism and not a machine.

The terms *mechanism* and *machine* are sometimes used synonymously. According to the definitions above, however, there is a definite difference. An assemblage of parts is called a *mechanism* if it is used only for the transmission of motion, and it is called a *machine* if it is used to transform external energy into useful work. The mechanical manipulator of a robotic system is a mechanism. For the mechanism to become a machine, a microprocessor-based controller, encoders and/or force sensors, and other accessories, such as a computer vision system, must be incorporated so that an external source of energy can be converted into useful work. Although a machine may consist of one or more mechanisms, a mechanism is not necessarily a machine since it does not necessarily have to do work but serves merely as a motion transformation device.

1.2.3 Degrees of Freedom of a Mechanism

Perhaps the first concern in a study of the kinematics of mechanisms is the number of *degrees of freedom*. The degrees of freedom of a mechanism are

the number of independent parameters or inputs needed to specify the configuration of the mechanism completely. Except for some special cases, it is possible to derive a general expression for the degrees of freedom of a mechanism in terms of the number of links, number of joints, and types of joints incorporated in the mechanism. The following notations are defined to facilitate the derivation of an equation:

c_i : number of constraints imposed by joint i .

F : degrees of freedom of a mechanism.

f_i : degrees of relative motion permitted by joint i .

j : number of joints in a mechanism, assuming that all the joints are binary.

j_i : number of joints with i degrees of freedom.

L : number of independent loops in a mechanism.

n : number of links in a mechanism, including the fixed link.

λ : degrees of freedom of the space in which a mechanism is intended to function.

Since we assume that all the joints are binary, a ternary joint is counted as two binary joints, a quaternary joint is counted as three binary joints, and so on. We also assume that a single value of λ applies to the motions of all the moving links. That is, they all operate in the same working space; hence $\lambda = 6$ for spatial mechanisms, and $\lambda = 3$ for planar and spherical mechanisms.

Intuitively, the degree-of-freedom value of a mechanism is equal to the degrees of freedom associated with all the moving links minus the number of constraints imposed by the joints. Hence, if the links are all free of constraints, the degrees of freedom of an n -link mechanism, with one of its links fixed to the ground, would be equal to $\lambda(n - 1)$. However, the total number of constraints imposed by the joints is equal to $\sum_{i=1}^j c_i$. Hence the degree-of-freedom value of a mechanism is generally given by

$$F = \lambda(n - 1) - \sum_{i=1}^j c_i. \quad (1.1)$$

The number of constraints imposed by a joint and the degrees of freedom permitted by the joint are equal to the motion parameter, λ ; that is,

$$\lambda = c_i + f_i. \quad (1.2)$$

Hence the total number of constraints imposed by the joints is

$$\sum_{i=1}^j c_i = \sum_{i=1}^j (\lambda - f_i) = j\lambda - \sum_{i=1}^j f_i. \quad (1.3)$$

Substituting Eq. (1.3) into (1.1) yields

$$F = \lambda(n - j - 1) + \sum_i f_i. \quad (1.4)$$

Equation (1.4) is known as the *Grübler* (1917) or *Kutzbach* (1929) criterion. In reality, the criterion was established much earlier by Ball (1900) and probably by others. However, unlike earlier researchers, Grübler and Kutzbach developed the equation specifically for mechanisms.

Example 1.2.1 Four-Bar Linkage Figure 1.6 shows a planar four-bar linkage. There are four links connected in a loop by four revolute joints. Hence $\lambda = 3$, $n = 4$, $j = j_1 = 4$, and Eq. (1.4) yields $F = 3(4 - 4 - 1) + 4 \times 1 = 1$. The planar four-bar linkage is often employed in a manipulator as a push-rod linkage for transmitting the rotation of a base- or near-base-connected actuator to the rotation of a link at the far end of a manipulator, as shown in Fig. 1.2, links 2–3–8–7.

Example 1.2.2 Five-Bar Linkage Figure 1.7 shows a planar five-bar linkage in which all the joints are revolute. We have $\lambda = 3$, $n = 5$, and $j = j_1 = 5$. Hence Eq. (1.4) yields $F = 3(5 - 5 - 1) + 5 \times 1 = 2$. The planar five-linkage is often used as a 2-dof manipulator. Using 1 and 2 as the input links, point Q can be positioned anywhere on the plane.

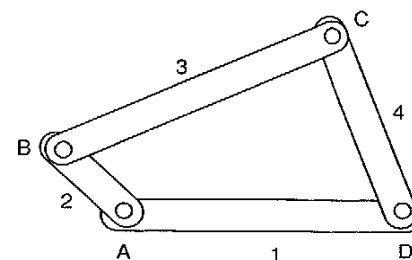


FIGURE 1.6. Four-bar linkage.

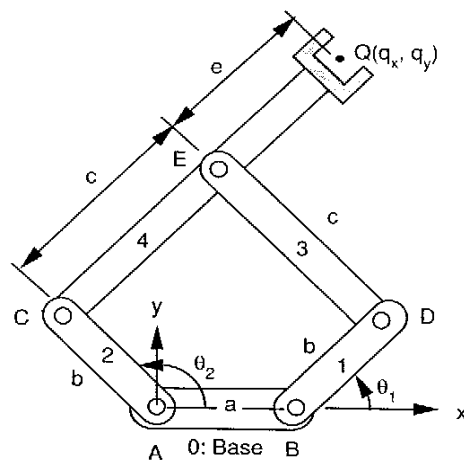


FIGURE 1.7. Five-bar, 5R manipulator.

Example 1.2.3 Pantograph Mechanism Figure 1.8 shows a planar pantograph mechanism in which the two ground-connected joints are prismatic and the remaining joints are revolute. For this mechanism we have $\lambda = 3$, $n = 7$ (including the ground link), and $j = j_i = 8$. Equation (1.4) yields $F = 3(7 - 8 - 1) + 8 \times 1 = 2$. Hence the pantograph mechanism is often employed as a 2-dof manipulator. Using 1 and 2 as the input links, point Q can be positioned anywhere on the plane.

The Grubler criterion is valid provided that the constraints imposed by the joints are independent of one another and do not introduce redundancies. For example, a revolute-spherical binary link chain with the revolute joint axis passing through the center of the spherical joint introduces a redundant degree of freedom. This type of freedom, called a *passive degree of freedom*, allows an intermediate link to rotate freely about an axis defined by the two joints. Although the intermediate link does have the ability to transmit forces or torques and therefore motion about some other axes, it has no torque transmission capability about the passive axis. In general, binary links with $S-S$, $S-E$, and $E-E$ pairs possess a passive degree of freedom (Table 1.1). A sequence of binary links with $S-S$, $S-E$, and $E-E$ pairs as their terminal joints also possesses a passive degree of freedom.

A passive degree of freedom cannot transmit torque, and therefore motion, about the passive axis. When such a joint pair exists in a mechanism, 1 degree

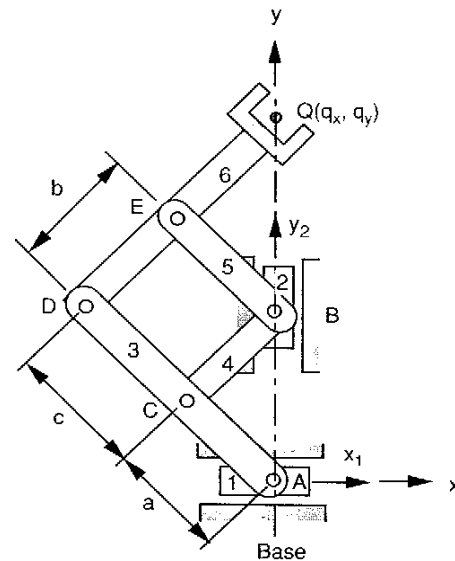


FIGURE 1.8. Pantograph mechanism.

of freedom should be subtracted from the degree-of-freedom equation. Let f_p be the number of passive degrees of freedom in a mechanism; then the remaining active degrees of freedom is given by

$$F = \lambda(n - j - 1) + \sum_i f_i - f_p. \quad (1.5)$$

Example 1.2.4 Stewart-Gough Platform Figure 1.9 shows a spatial mechanism in which a moving platform is connected to a fixed base with six extensible limbs by spherical joints. Each limb is made up of two

TABLE 1.1. Binary Links with Passive Degrees of Freedom

Type	Passive Degrees of Freedom
$S-S$	Rotation about an axis through centers of ball joints.
$S-E$	Rotation about an axis through the center of the ball and perpendicular to the plane of the plane pair.
$E-E$	Sliding along an axis parallel to the line of intersection of the planes of the plane pairs. If the two planes are parallel, 3 passive degrees of freedom exist.

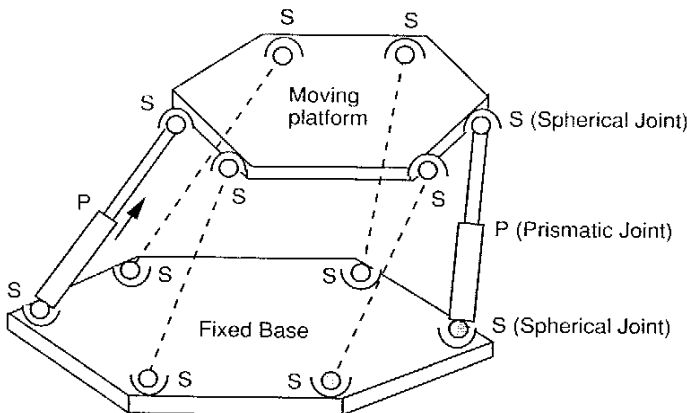


FIGURE 1.9. Stewart-Gough platform.

binary links that are connected by a prismatic joint. This construction is called an *S-P-S* limb. Because of the *S-P-S* combination, there is a passive degree of freedom associated with each limb. Hence we have $\lambda = 6$, $n = 14$, $j_1 = 6$, $j_3 = 12$, and $f_p = 6$. The degree-of-freedom value of the manipulator is given by $F = 6(14 - 18 - 1) + (12 \times 3 + 6) - 6 = 6$.

Since Eq. (1.5) is derived by using a single value of λ for all the moving links, the degree of freedom of a spatial mechanism with a planar or spherical linkage as a subsystem should be counted with care. Specifically, $\lambda = 3$ should be used for the planar or spherical subsystem, while $\lambda = 6$ is used for the spatial portion of the mechanism. For example, the manipulator shown in Fig. 1.2 consists of a planar four-bar linkage (links 2, 3, 8, and 7) and a spherical wrist mechanism (links 3, 4, 5, and 6) as two subsystems. The four-bar linkage provides 1 degree of freedom, the spherical linkage gives 3 degrees of freedom, and the open-loop chain 0-1-2 provides 2 additional degrees of freedom. Overall, it is a 6-dof spatial manipulator.

In general, if the Grubler criterion yields $F > 0$, the mechanism has F degrees of freedom. If the criterion yields $F = 0$, the mechanism becomes a structure with zero degrees of freedom. On the other hand, if the criterion yields $F < 0$, the mechanism becomes a statically indeterminate structure with redundant constraints. However, it should be noted that there are mechanisms that do not obey the Grubler criterion. Those mechanisms that require special link lengths to achieve mobility are called *overconstrained mechanisms* (Mavroidis and Roth, 1994).

For closed-loop mechanisms and mechanical manipulators, the number and locations of actuated joints should be chosen carefully such that the end effector can be controlled at will. In general, the number of actuated joints should be equal to the number of degrees of freedom of the mechanism, and the locations of actuated joints should be chosen such that they form a set of independent coordinates. If the number of actuators is less than the number of degrees of freedom, the output link cannot be controlled at will. On the other hand, if the number of actuators is greater than the number of degrees of freedom, the motion of these actuators must be coordinated in accordance with their kinematic constraints. A redundantly driven manipulator can be employed for the purpose of eliminating gear backlash and clearances associated with the geometry of the joints (Chang and Tsai, 1993; Tsai and Chang, 1994).

1.2.4 Loop Mobility Criterion

As stated earlier, a kinematic chain is an assemblage of links connected by joints. If every link is connected to at least two other links, the chain forms one or more closed loops. It is possible to establish an equation relating the number of independent loops to the number of links and joints in a kinematic chain. Here the term *number of independent loops* refers to the total number of loops, excluding the external loop.

We observe that the four-bar linkage shown in Fig. 1.6 is a kinematic chain with one independent loop. It is made up of four links and four joints. The five-bar linkage shown in Fig. 1.7 is also a kinematic chain with one independent loop, and it is made up of five links and five joints. We conclude that for a single-loop kinematic chain (planar, spherical, or spatial), the number of links is equal to the number of joints. That is, $n = j$ for all single-loop kinematic chains.

We now extend a single-loop chain into a two-loop chain. This can be accomplished by taking an open-loop chain and joining its two ends to any two members of a single-loop chain by two joints, as depicted in Fig. 1.10, where *A* and *B* are the attachment points. Note that by extending from one to two loops, the number of joints added exceeds the number of links by one. Similarly, an open-loop chain can be added to a two-loop chain to form a three-loop chain, and so on. In general, extending a kinematic chain from one to L loops, the difference between the number of joints and number of links is increased by $L - 1$. Hence we can write

$$j = n + L - 1, \quad (1.6)$$

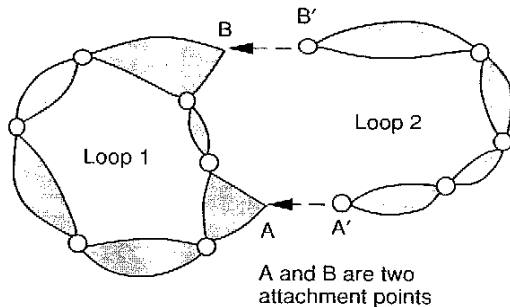


FIGURE 1.10. Formation of a multiloop chain.

or

$$L = j - n + 1. \quad (1.7)$$

Equation (1.7) is known as *Euler's equation*. It states that the number of independent loops exceeds the difference between the number of joints and the number of links by one. Combining Eq. (1.7) with (1.4) yields

$$\sum f_i = F + \lambda L. \quad (1.8)$$

Equation (1.8) is known as the *loop mobility criterion*. Equation (1.7) or (1.8) is useful for predicting the number of independent loops in a kinematic chain. Generally, the number of *loop-closure equations* that can be established for a mechanism is equal to the number of independent loops in the mechanism. This is demonstrated in Chapters 3 and 5.

Example 1.2.5 Pantograph Mechanism For the planar pantograph mechanism shown in Fig. 1.8, we have $\lambda = 3$, $n = 7$, and $j = 8$. Hence there are $L = 8 - 7 + 1 = 2$ independent loops. The first loop consists of the base link and links 1, 3, 4, and 2. The second loop consists of links 3, 4, 5, and 6.

Example 1.2.6 Stewart-Gough Platform For the Stewart-Gough platform shown in Fig. 1.9, we have $\lambda = 6$, $n = 14$, and $j = 18$. Hence there are $L = 18 - 14 + 1 = 5$ independent loops. The right-hand side of Eq. (1.8) yields $F + \lambda L = 6 + 6 \times 5 = 36$, while the left-hand side gives $\sum f_i = 3 \times 12 + 6 = 42$. The difference is due to the existence of the 6 passive degrees of freedom.

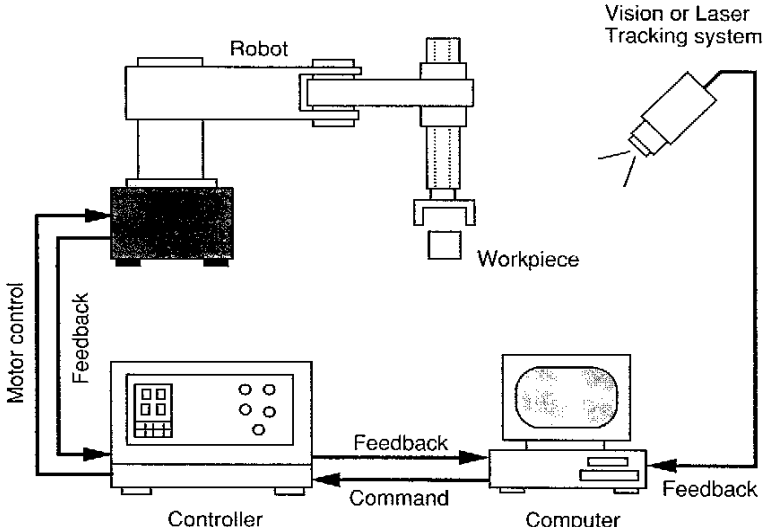


FIGURE 1.11. Typical robotic system.

1.3 ROBOTIC SYSTEMS

A robotic system typically consists of a mechanical manipulator, an end effector, a microprocessor-based controller, a computer, and perhaps, a vision system or other noncontact sensing devices (Fig. 1.11).

A *mechanical manipulator* is made up of several links connected by joints. One link is fixed to the ground, while another is designated as the *output link*. Some of the joints in the manipulator are actuated; the others are passive. Typically, the number of actuated joints is equal to the number of degrees of freedom so that the manipulator can be controlled at will. The manipulator shown in Fig. 1.2 is a 6-dof manipulator in which link 0 is fixed to the ground and link 6 is the output link. The joints between links (0 and 1), (1 and 2), (1 and 7), (3 and 4), (4 and 5), and (5 and 6) are actuated; the others are passive.

End effectors are devices attached at the output link of a mechanical manipulator to grasp, lift, and manipulate workpieces. We may think of the end effector as a mechanical interface between a mechanical manipulator and its environment. Generally, an end effector is a specialized device that is used for handling a few objects of similar shape, size, and weight in a repetitive operation where the requirement for dexterity and versatility is not essential. Such

an end effector is sometimes called a *gripper*. Most simple grippers are 1-dof devices. Figure 1.12 shows a rack-and-pinion gripper driven by a pneumatic source, and Fig. 1.13 shows a gripper equipped with force sensor.

For some applications, an end effector may be required to handle a variety of objects of different shapes, sizes, and materials. We call an end effector that requires certain dexterity and versatility a *universal gripper* or *dextrous hand*. The Stanford/JPL hand (Salisbury, 1982; Salisbury and Roth, 1983) and the Utah/MIT hand (Jacobsen et al., 1984, 1986) are dextrous hands. Figure 1.14 shows a Utah/MIT hand and the mechanical components and some sensing elements of the hand are shown in Fig. 1.15. The basics of gripping and a variety of grippers can be found in Pham and Hegbinbotham (1986).

The *controller* may range from a simple low-level PID controller to a high-level model-based intelligent controller. Encoders and/or tachometers are installed at the joints of a manipulator to measure the relative motion between two connected bodies for the purpose of feedback control. Some advanced intelligent controllers may require the manipulator to be equipped with force and/or touch sensors along with a vision system or some other sensor. In addition, the controller is often equipped with a *teach pendant* that is capable of teaching position, editing and running programs, and interfacing with the computer.

The computer may be microprocessor-based hardware, a personal computer, or a mainframe computer capable of high-speed real-time computation, reasoning, and issuing intelligent control commands.

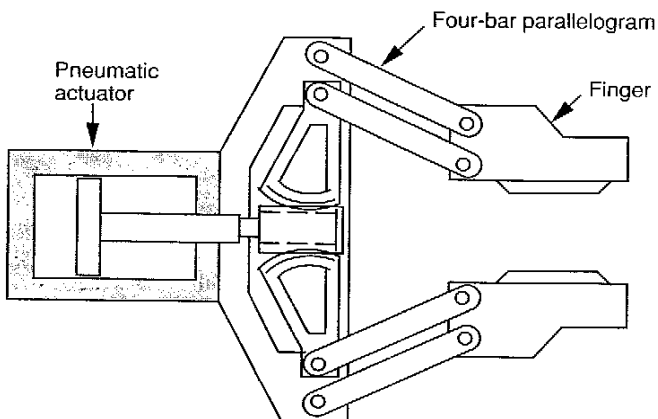


FIGURE 1.12. Dual rack-and-pinion gripper mechanism.

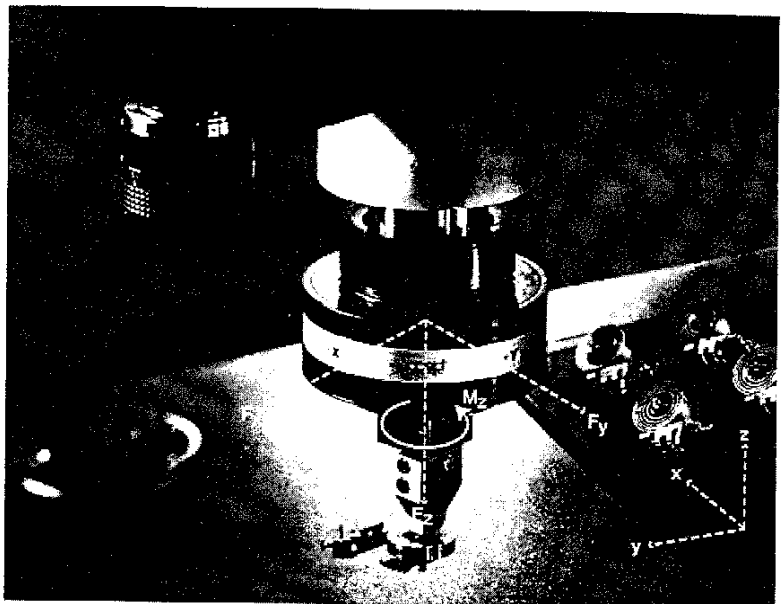


FIGURE 1.13. Adept gripper. (Courtesy of Adept Technology, Inc., San Jose, California.)

1.4 CLASSIFICATION OF ROBOTS

Robots can be classified according to various criteria, such as their degrees of freedom, kinematic structure, drive technology, workspace geometry, and motion characteristics. We discuss each of these in turn.

1.4.1 Classification by Degrees of Freedom

One obvious classification scheme is to categorize robots according to their degrees of freedom. Ideally, a manipulator should possess 6 degrees of freedom in order to manipulate an object freely in three-dimensional space. From this point of view, we call a robot a *general-purpose robot* if it possesses 6 degrees of freedom, a *redundant robot* if it possesses more than 6 degrees of freedom, and a *deficient robot* if it possesses less than 6 degrees of freedom. A redundant robot provides more freedom to move around obstacles and operate in a tightly confined workspace. On the other hand, for some special applications, such as assembling components on a plane, a robot with just

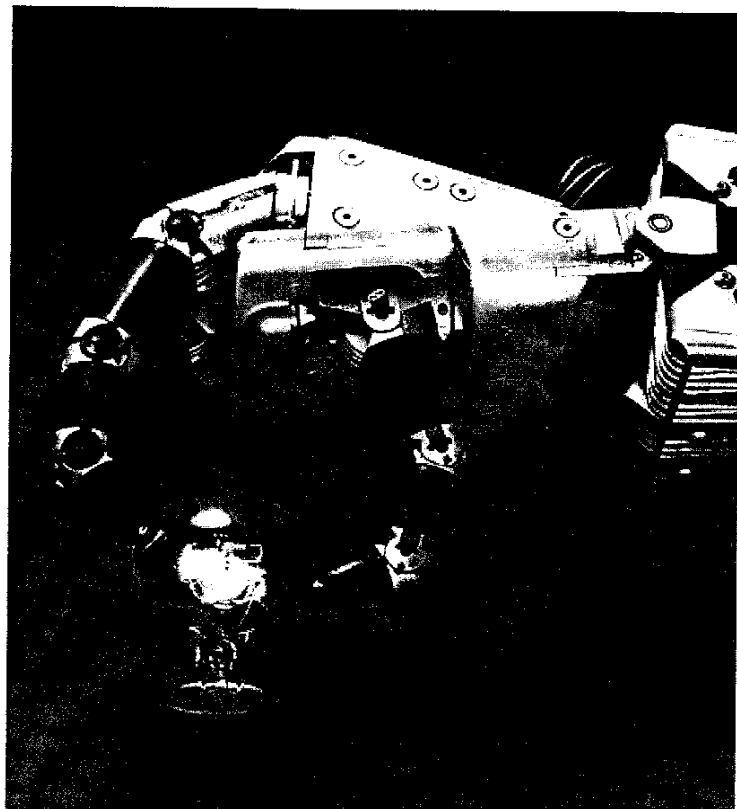


FIGURE 1.14. Utah/MIT dexterous hand. (Courtesy of SARCOS, Salt Lake City, Utah.)

4 degrees of freedom would be sufficient. The Fanuc S-900W robot shown in Fig. 1.2 is a 6-dof general-purpose manipulator and the Adept-One robot shown in Fig. 1.16 is a 4-dof manipulator.

1.4.2 Classification by Kinematic Structure

Another scheme is to classify robots according to their structural topologies. A robot is said to be a *serial robot* or *open-loop manipulator* if its kinematic structure takes the form of an open-loop chain, a *parallel manipulator* if it is

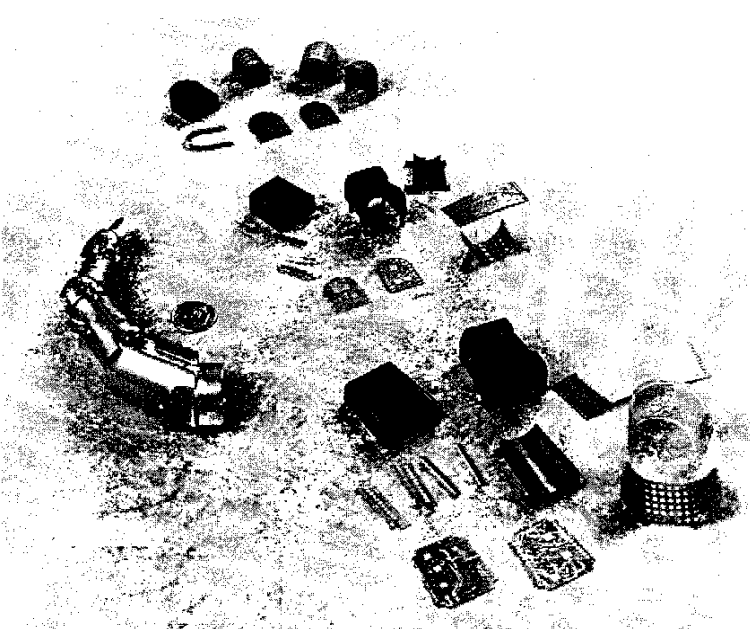


FIGURE 1.15. Components of the Utah/MIT hand. (Courtesy of SARCOS, Salt Lake City, Utah.)

made up of a closed-loop chain, and a *hybrid manipulator* if it consists of both open- and closed-loop chains. The Adept-One robot shown in Fig. 1.16 is a serial manipulator, and the manipulator shown in Fig. 1.17 is a parallel manipulator. Most engineers consider the Fanuc S-900W robot shown in Fig. 1.2 to be a serial manipulator. In reality, it is a hybrid manipulator, since it incorporates a four-bar (push-rod) linkage to drive the third joint. Many industrial robots employ this type of construction because it allows the third motor to be mounted on the waist and therefore reduces the inertia of the manipulator. In general, a parallel manipulator has the advantages of higher stiffness, higher payload capacity, and lower inertia to the manipulation problem than a comparable serial manipulator, at the price of a smaller workspace and more complex mechanism.

1.4.3 Classification by Drive Technology

Manipulators can also be classified by their drive technology. The three popular drive technologies are *electric*, *hydraulic*, and *pneumatic*. Most manip-

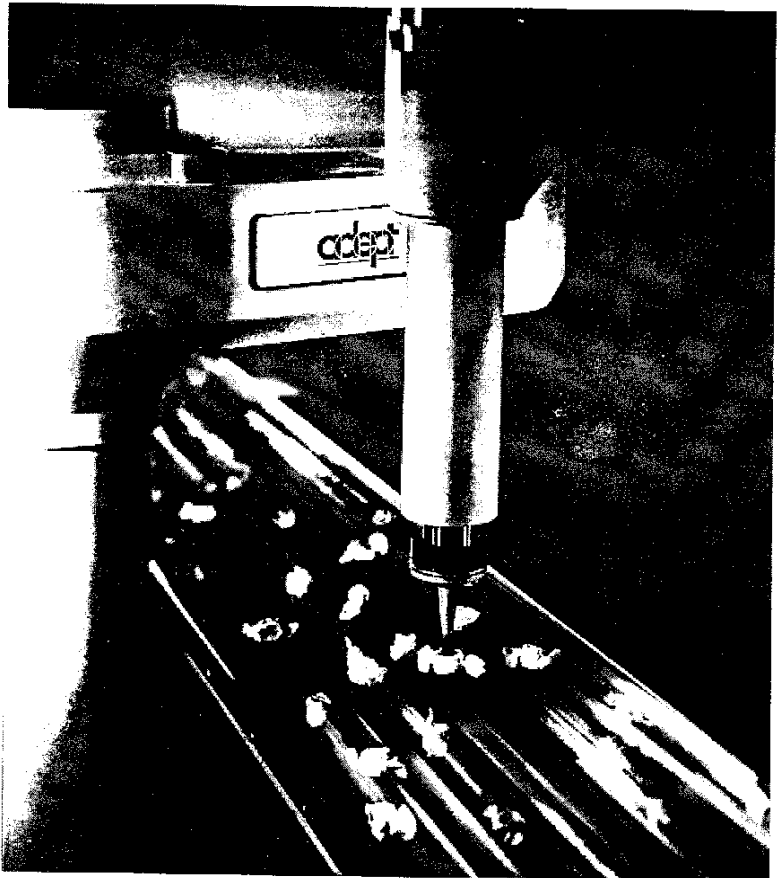


FIGURE 1.16. Adept-One robot. (Courtesy of Adept Technology, Inc., San Jose, California.)

ulators use either electric dc servomotors or stepper motors, because they are clean and relatively easy to control. However, when high-speed and/or high-load-carrying capabilities are needed, hydraulic or pneumatic drive is preferred. A major disadvantage associated with the use of a hydraulic drive is the possibility of leaking oils. Additionally, a hydraulic drive is inherently flexible, due to the bulk modulus of oil. Although a pneumatic drive is clean and fast, it is difficult to control because air is a compressible fluid.

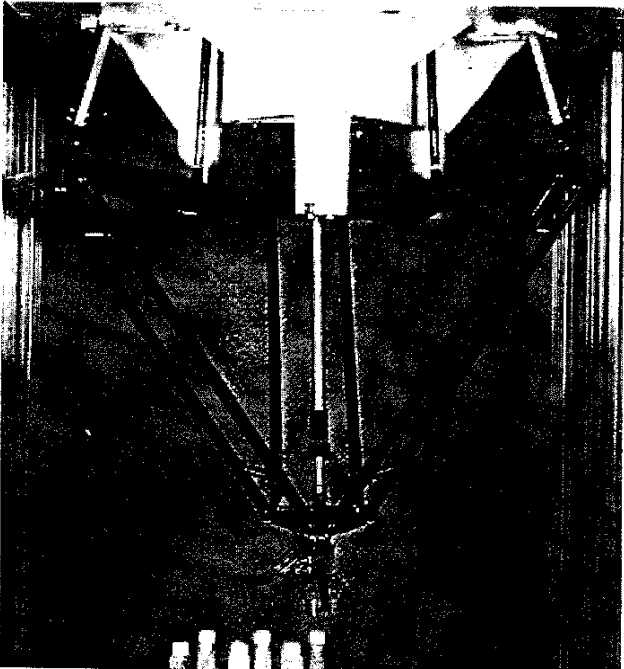


FIGURE 1.17. A 4-dof parallel robot. (Courtesy of Demaurex Robotique & Microtechnique S.A., Switzerland.)

In a serial manipulator, typically, one actuator is used to control the motion of each joint. If every moving link is driven by one actuator mounted on its preceding link through a gear reduction unit, the joint displacements are kinematically independent of one another. We call this type of manipulator a *conventional serial manipulator*. On the other hand, if each joint is driven directly by an actuator without a speed reducer, the manipulator is called a *direct-drive manipulator*.

Employing a gear reduction unit permits the use of a smaller motor, which in turn reduces the inertia of a manipulator. However, backlash in a gear reduction unit can cause position error at the end effector. Direct-drive technique eliminates the problems associated with gear backlash and can possibly increase the speed of a manipulator. However, direct-drive motors are bulky and heavy. Consequently, they are commonly used to drive the first joint of

a manipulator where the motor can be installed on the base. Alternatively, they can also be installed on the base to drive the second or third joint via a push-rod linkage or a metal belt. The first joint of the Adept-One robot shown in Fig. 1.16 is directly driven by a direct-drive motor, and the second joint is driven by a direct-drive motor via two pretensioned opposing metal belts.

Some manipulators employ gear trains, tendons, or chain-and-sprocket devices to drive their joints. When such transmission mechanisms are used to drive a manipulator across several joints, the joint displacements are no longer independent of each other. Strictly speaking, such manipulators should be considered as closed-loop manipulators, although there may be several articulation points. Figure 1.18 shows a 5-dof educational robot. The mechanical transmission system of this robot consists of gears, timing belts, and lead screws.

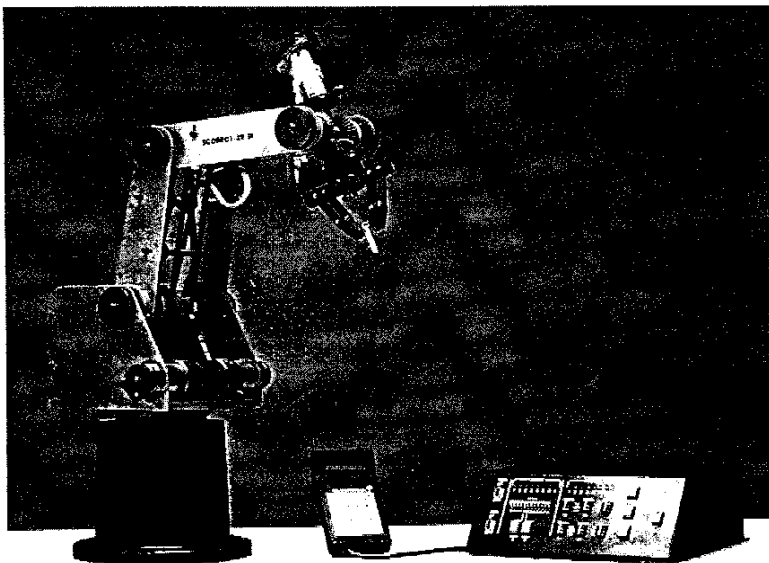


FIGURE 1.18. Scorpion-ER III robot. (Courtesy of Eshed Robotec Inc., Princeton, New Jersey.)

1.4.4 Classification by Workspace Geometry

The *workspace* of a manipulator is defined as the volume of space the end effector can reach. Two different definitions of workspace are frequently used. A *reachable workspace* is the volume of space within which every point can be reached by the end effector in at least one orientation. A *dextrous workspace* is the volume of space within which every point can be reached by the end effector in all possible orientations. Clearly, the dextrous workspace is a subset of the reachable workspace.

Although it is not a necessary condition, many serial manipulators are designed with their first three moving links longer than the remaining links. Thus the first three links are used primarily for manipulating the position and the remaining links for controlling the orientation of the end effector. For this reason, the subassembly associated with the first three links is called the *arm*, and the subassembly associated with the remaining links is called the *wrist*. Except for redundant manipulators, the arm usually possesses 3 degrees of freedom while the wrist may have 1 to 3 degrees of freedom. Furthermore, the wrist assembly is often designed with its joint axes intersecting at a common point called the *wrist center*. The arm assembly can assume various kinematic structures and therefore generates different work envelopes called *regional workspaces*. The workspace supplied by robotic manufacturers usually shows the regional workspace.

Perhaps the simplest kinematic structure of a robot arm is made up of three mutually perpendicular *prismatic joints*. This type of robot is known as a *Cartesian robot*. The wrist center position of a Cartesian robot can be conveniently described by three Cartesian coordinates associated with the three prismatic joints. Obviously, the regional workspace of a Cartesian robot is a rectangular box. Figure 1.19 shows a Cartesian robot manufactured by Seiko Instruments. When a Cartesian robot is mounted on rails above its workspace, it is called a *gantry robot*.

A robot arm is called a *cylindrical robot* if either the first or second joint of a Cartesian robot is replaced by a *revolute joint*. The wrist center position of a cylindrical robot can be described by a set of cylindrical coordinates associated with the three joint variables. The prismatic joints usually have mechanical limits on both ends. Hence the workspace of a cylindrical robot is confined by two concentric cylinders of finite length. Figure 1.20 shows a cylindrical robot.

A robot arm is called a *spherical robot* if the first two joints are made up of two intersecting revolute joints and the third is a prismatic joint. Normally, the prismatic joint is not parallel to the second joint axis. The wrist center position of a spherical robot can be described by a set of spherical coordinates

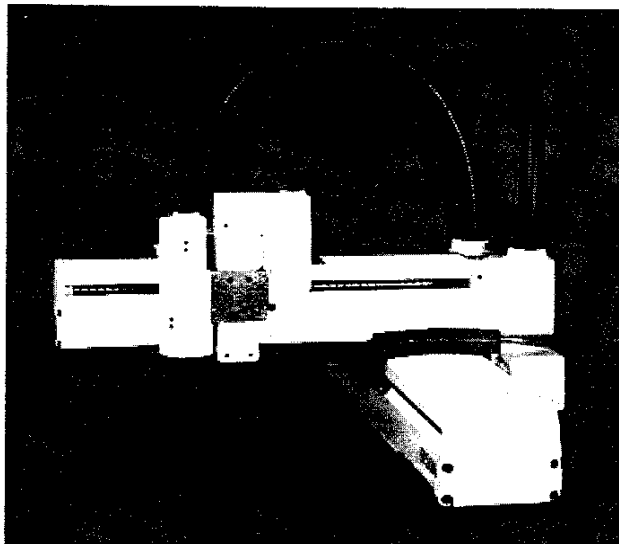


FIGURE 1.19. Cartesian robot. (Courtesy of Seiko Instruments USA, Inc., Torrance, California.)

associated with the three joint variables. Hence the workspace of a spherical robot is confined by two concentric spheres.

A robot arm is said to be an *articulated robot* if all three joints are revolute. The workspace of an articulated robot is very complex, typically a crescent-shaped cross section. Many industrial robots are of the articulated type. The PUMA robot is an articulated robot, as is the master-slave robot shown in Fig. 1.3.

The *SCARA* (selective compliance assembly robot arm) *robot* is a special type of robot. It consists of two revolute joints followed by a prismatic joint. In addition, all three joint axes are parallel to each other and usually point along the direction of gravity. Thus the first two actuators do not have to work against the gravitational forces of the links and the payload. The wrist usually has only 1 degree of freedom. Hence the entire robot has 4 degrees of freedom. This type of manipulators is useful for assembling parts on a plane. The Adept robot shown in Fig. 1.16 is a SCARA robot.

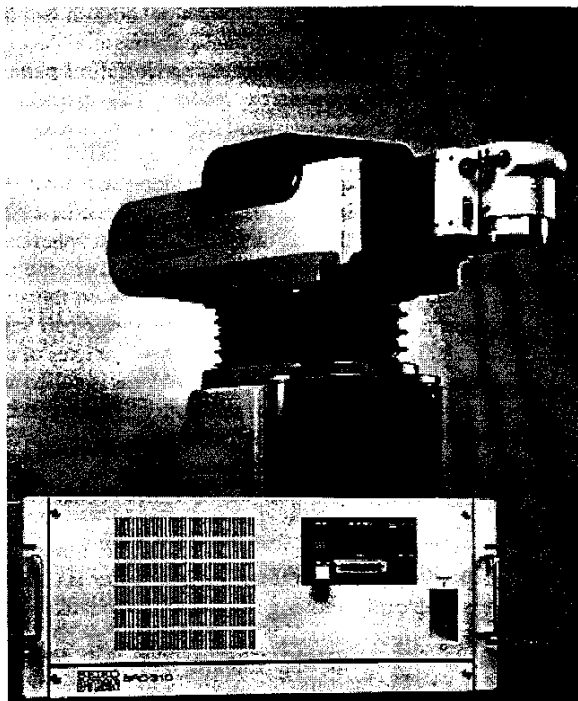


FIGURE 1.20. Cylindrical robot. (Courtesy of Seiko Instruments USA, Inc., Torrance, California.)

1.4.5 Classification by Motion Characteristics

Robot manipulators can also be classified according to their nature of motion. A rigid body is said to perform a *planar motion* if all particles in the body describe plane curves that lie in parallel planes. A mechanism is said to be a *planar mechanism* if all the moving links in the mechanism perform planar motions that are parallel to one another. For a planar mechanism, the loci of all points in all links can be drawn conveniently on a plane. Planar mechanisms that utilize only lower-pair joints are called *planar linkages*. Revolute and prismatic joints are the only permissible lower pairs for planar linkages. In a planar linkage, the axes of all revolute joints must be normal to the plane of motion, while the direction of translation of a prismatic joint must be parallel to the plane of motion. A manipulator is called a *planar manipulator* if its

mechanism is a planar mechanism, as are the manipulators shown in Figs. 1.7 and 1.8. Planar manipulators are useful for manipulating an object on a plane.

A rigid body is said to be under a *spherical motion* if all particles in the body describe curves that lie on concentric spheres. Thus when a rigid body performs a spherical motion, there exists at least one stationary point. Following the definition above, a rigid body rotating about a fixed axis can be considered as a special case of spherical motion since any point on the axis of revolution can be treated as the stationary point. A mechanism is said to be a *spherical mechanism* if all the moving links perform spherical motions about a common stationary point. In a spherical mechanism, the motions of all particles can be described by their radial projections on the surface of a unit sphere. A revolute joint is the only permissible lower-pair joint for the construction of spherical linkages. In addition, all the joint axes of a spherical linkage must intersect at a common point. A manipulator is called a *spherical manipulator* if it is made up of a spherical mechanism. Figure 1.21 shows a 3-dof spherical parallel manipulator. In this mechanism, all the revolute joints intersect at a common center point O . Links 1, 2, and 3 are considered as the input links, and link 7 is designated as the output link. A spherical manipulator can be used as a pointing device.

A rigid body is said to perform a *spatial motion* if its motion cannot be characterized as planar or spherical motion. A manipulator is called a *spatial manipulator* if at least one of the moving links in the mechanism possesses a

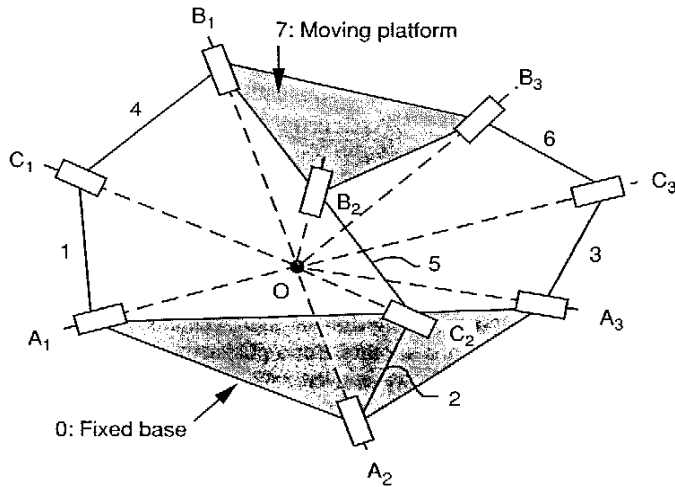


FIGURE 1.21. Spherical 3RRR manipulator.



general spatial motion. In general, we cannot associate unique motion characteristics with a spatial mechanism. The mechanism shown in Fig. 1.9 is a spatial 6-dof parallel manipulator. Planar and spherical mechanisms can be considered as special cases of spatial mechanisms. They occur as a consequence of special geometry in the particular orientations of their joint axes. Because of the special geometric conditions, the synthesis and analysis problems associated with planar and spherical mechanisms are greatly simplified. The selection of a robot manipulator depends on the application, the working environment, and other considerations.

1.5 POSITION, ORIENTATION, AND LOCATION OF A RIGID BODY

In the study of the kinematics of robot manipulators, we are constantly dealing with the *location* of several bodies in space. The bodies of interest include the links of a manipulator, the tools, the workpieces, and so on. To identify the location of a body, a reference coordinate system is established. We call this reference coordinate system the *fixed frame*, although in reality, it may not necessarily be fixed to the ground. In what follows we employ a Cartesian coordinate system to describe the location of a body, although other types of coordinate systems, such as the *cylindrical coordinate system* and *spherical coordinate system*, may also be used.

The *location* of a body with respect to a reference coordinate system is known if the *position* of all the points of the body are known. If the body of interest is rigid, six independent parameters would be sufficient to describe its location in three-dimensional space. As shown in Fig. 1.22, we take the (x, y, z) coordinate system as the fixed frame. We also attach an (u, v, w) Cartesian coordinate system to the moving body and refer to it as the *moving frame*. Clearly, the positions of all the points of the rigid body can be determined when the location of the moving frame with respect to the fixed frame is known. This relative *location* can be considered as composed of the *position* of a point, say the origin Q , and the *orientation* of the moving frame with respect to the fixed frame. Further, if we assume that the moving frame coincides with the fixed frame initially, the location of the moving frame with respect to the fixed frame and the spatial displacement of a rigid body from the initial coincident position are equivalent.

1.5.1 Description of a Position

The *position* of any point with respect to the reference frame can be described by a 3×1 *position vector*. For example, the position of a point P in the

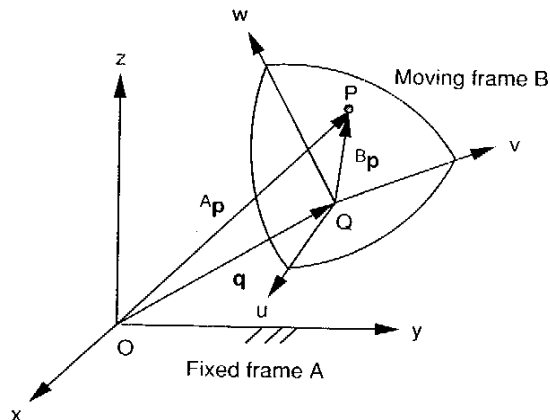


FIGURE 1.22. General spatial displacement.

reference frame *A* as shown in Fig. 1.23 is written as

$${}^A\mathbf{p} = \begin{bmatrix} p_x \\ p_y \\ p_z \end{bmatrix}, \quad (1.9)$$

where the subscripts *x*, *y*, and *z* represent the projections of the position vector onto the three coordinate axes of the reference frame. Since we are dealing

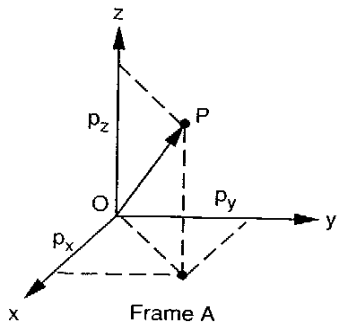


FIGURE 1.23. Position vector of a point *P* in space.

with several coordinate systems, a leading superscript is used to indicate the coordinate system to which the vector is referred.

1.5.2 Description of an Orientation

The *orientation* of a rigid body with respect to the fixed frame can be described in several different ways. In what follows we first describe the *direction cosine representation* followed by the *screw axis representation* and then the *Euler angle representation*. To describe the orientation of a rigid body, we consider the motion of a moving frame *B* with respect to a fixed frame *A* with one point fixed. This is known as a *rotation* or a *spherical motion*. Without losing generality, we assume that the origin of the moving frame is fixed to that of the fixed frame, as shown in Fig. 1.24.

(a) Direction Cosine Representation. One convenient way of describing the orientation of a rigid body is by means of the *direction cosines* of the coordinate axes of the moving frame with respect to the fixed frame. Let *i*, *j*, and *k* denote three unit vectors pointing along the coordinate axes of the fixed frame *A*, and *u*, *v*, and *w* denote three unit vectors pointing along the coordinate axes of the moving frame *B*, respectively, as shown in Fig. 1.24. The three unit vectors *u*, *v*, and *w* can be expressed in the fixed frame *A* as follows:

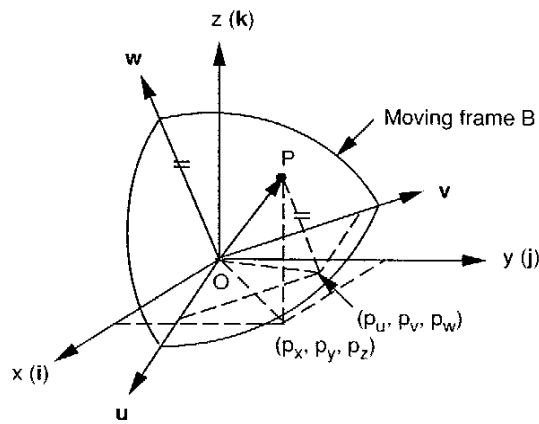


FIGURE 1.24. Spherical displacement.

$$\begin{aligned} {}^A\mathbf{u} &= u_x \mathbf{i} + u_y \mathbf{j} + u_z \mathbf{k}, \\ {}^A\mathbf{v} &= v_x \mathbf{i} + v_y \mathbf{j} + v_z \mathbf{k}, \\ {}^A\mathbf{w} &= w_x \mathbf{i} + w_y \mathbf{j} + w_z \mathbf{k}. \end{aligned} \quad (1.10)$$

The position vector of a point P of the rigid body can be expressed either in the fixed frame A as

$${}^A\mathbf{p} = p_x \mathbf{i} + p_y \mathbf{j} + p_z \mathbf{k}, \quad (1.11)$$

or in the rotated frame B as

$${}^B\mathbf{p} = p_u \mathbf{u} + p_v \mathbf{v} + p_w \mathbf{w}. \quad (1.12)$$

Since P is a point of the rigid body, ${}^B\mathbf{p}$ is constant. However, ${}^A\mathbf{p}$ depends on the orientation of B relative to A . Substituting Eq. (1.10) in (1.12), we obtain the vector \mathbf{p} expressed in the fixed frame A as

$$\begin{aligned} {}^A\mathbf{p} &= (p_u u_x + p_v v_x + p_w w_x) \mathbf{i} + (p_u u_y + p_v v_y + p_w w_y) \mathbf{j} \\ &\quad + (p_u u_z + p_v v_z + p_w w_z) \mathbf{k}. \end{aligned} \quad (1.13)$$

Equating the x , y , and z components of ${}^A\mathbf{p}$ in Eq. (1.13) to the corresponding components in (1.11) yields

$$\begin{aligned} p_x &= u_x p_u + v_x p_v + w_x p_w, \\ p_y &= u_y p_u + v_y p_v + w_y p_w, \\ p_z &= u_z p_u + v_z p_v + w_z p_w. \end{aligned} \quad (1.14)$$

Writing Eq. (1.14) in a matrix form we obtain

$${}^A\mathbf{p} = {}^A\mathbf{R}_B {}^B\mathbf{p}, \quad (1.15)$$

where

$${}^A\mathbf{R}_B = \begin{bmatrix} u_x & v_x & w_x \\ u_y & v_y & w_y \\ u_z & v_z & w_z \end{bmatrix} = \begin{bmatrix} a_{11} & a_{12} & a_{13} \\ a_{21} & a_{22} & a_{23} \\ a_{31} & a_{32} & a_{33} \end{bmatrix}, \quad (1.16)$$

where the leading superscript A and the trailing subscript B indicate the order of transformation. In what follows we omit the leading superscript and trailing subscript from time to time whenever there are only two frames of reference and the order of transformation is clear.

We call the matrix ${}^A\mathbf{R}_B$ the *rotation matrix* of the moving frame B with respect to the fixed frame A . The rotation matrix specifies the orientation of B completely with respect to A . It transforms the position vector of any point P from the moving frame B to the fixed frame A . From the definition above, we see that the columns of a rotation matrix represent three orthogonal unit vectors of the moving coordinate axes expressed in the fixed frame. Therefore, the rotation matrix is orthogonal. The orthogonality conditions can be stated as

$$\begin{aligned} \mathbf{u}^2 &= 1, \\ \mathbf{v}^2 &= 1, \\ \mathbf{w}^2 &= 1, \end{aligned} \quad (1.17)$$

and

$$\begin{aligned} \mathbf{u}^T \mathbf{v} &= 0, \\ \mathbf{v}^T \mathbf{w} &= 0, \\ \mathbf{w}^T \mathbf{u} &= 0. \end{aligned} \quad (1.18)$$

Because of the orthogonality conditions above, only three of the nine elements of ${}^A\mathbf{R}_B$ are independent. Using the orthogonality conditions above, it can be shown that

$$\begin{aligned} \mathbf{u} \times \mathbf{v} &= \mathbf{w}, \\ \mathbf{v} \times \mathbf{w} &= \mathbf{u}, \\ \mathbf{w} \times \mathbf{u} &= \mathbf{v}. \end{aligned} \quad (1.19)$$

It can also be shown that

$$\det({}^A\mathbf{R}_B) = 1. \quad (1.20)$$

Furthermore, due to the orthogonality conditions, the inverse transformation of a rotation matrix is equal to its transpose:

$${}^B\mathbf{R}_A = {}^A\mathbf{R}_B^{-1} = {}^A\mathbf{R}_B^T. \quad (1.21)$$

Since the columns of ${}^A\mathbf{R}_B$ represent three unit vectors of the coordinate axes of frame B expressed in frame A , it follows that the rows of ${}^A\mathbf{R}_B$ represent the three unit vectors defined along the coordinate axes of frame A and expressed in frame B . Therefore, the rotation matrix can be interpreted as a

set of three column vectors or a set of three row vectors:

$${}^A R_B = [{}^A \mathbf{u} \quad {}^A \mathbf{v} \quad {}^A \mathbf{w}] = \begin{bmatrix} {}^B \mathbf{i}^T \\ {}^B \mathbf{j}^T \\ {}^B \mathbf{k}^T \end{bmatrix}. \quad (1.22)$$

Euler's Theorem. Euler's theorem states that the general displacement of a rigid body with one point fixed is a *rotation* about some axis. This unique axis of rotation is called the *screw axis*. In what follows, we show how the screw axis can be derived from a given rotation matrix.

Equation (1.15) provides an orthogonal transformation of the position of a point P in a moving frame B to a fixed frame A . Since the moving frame B coincides with the fixed frame A at the initial location, we may consider ${}^B \tilde{\mathbf{p}}$ as the first position and ${}^A \tilde{\mathbf{p}}$ as the second position of P of the rigid body B . Since the origin O is a stationary point, the screw axis passes through this point. Furthermore, if \tilde{P} lies on the axis of rotation, its position vector will not be affected by the rotation; that is,

$${}^B \tilde{\mathbf{p}} = {}^A \tilde{\mathbf{p}}. \quad (1.23)$$

The second position of P is governed by the orthogonal transformation given by Eq. (1.15). Substituting Eq. (1.23) into (1.15) and rearranging yields

$$({}^A R_B - I) {}^A \tilde{\mathbf{p}} = 0, \quad (1.24)$$

where I denotes a 3×3 identity matrix.

We note that Eq. (1.24) is a special case of the following general eigenvalue problem:

$$({}^A R_B - \lambda I) {}^A \tilde{\mathbf{p}} = 0, \quad (1.25)$$

where λ is called the *eigenvalue value* or *characteristic value*. Equation (1.25) consists of three linear homogeneous equations in three unknowns, \tilde{p}_x , \tilde{p}_y , and \tilde{p}_z . The compatibility condition for the existence of nontrivial solutions is that the determinant of the coefficients must vanish; that is,

$$|{}^A R_B - \lambda I| = \begin{vmatrix} a_{11} - \lambda & a_{12} & a_{13} \\ a_{21} & a_{22} - \lambda & a_{23} \\ a_{31} & a_{32} & a_{33} - \lambda \end{vmatrix} = 0, \quad (1.26)$$

where a_{ij} represents the (i, j) element of ${}^A R_B$.

Equation (1.26) is known as the *characteristic equation* and the values of λ for which the equation is satisfied are the eigenvalues. In general, the characteristic equation will have three roots with three corresponding eigen-

vectors. Expanding Eq. (1.26), say along the first column of ${}^A R_B$ and applying Eqs. (1.19) and (1.20), we obtain

$$\lambda^3 - \text{tr}({}^A R_B) \lambda^2 + \text{tr}({}^A R_B) \lambda - 1 = 0, \quad (1.27)$$

where $\text{tr}({}^A R_B) = a_{11} + a_{22} + a_{33}$.

We note that Eq. (1.27) contains $\lambda - 1$ as a factor. Solving Eq. (1.27) yields

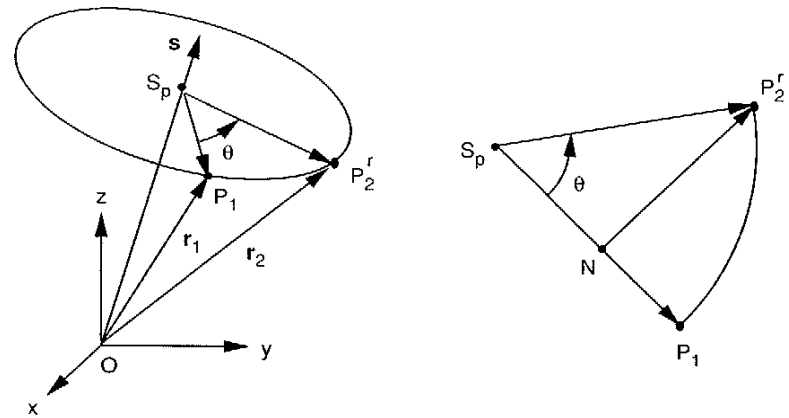
$$\lambda = 1, e^{i\theta}, e^{-i\theta},$$

where

$$\theta = \cos^{-1} \frac{a_{11} + a_{22} + a_{33} - 1}{2} \quad (1.28)$$

defines the angle of rotation about the screw axis and where $\cos^{-1} x$ is the arccosine function. The eigenvector corresponding to the eigenvalue of $\lambda = 1$ gives the direction of the screw axis. Hence the direction of the screw axis is obtained by solving Eq. (1.24) for the ratio $\tilde{p}_x/\tilde{p}_y/\tilde{p}_z$.

(b) Screw Axis Representation. In this section we seek a description of the orientation of a rigid body in terms of a rotation about a screw axis. As shown in Fig. 1.25a, let the moving frame B be rotated an angle θ about an



(a) Spherical displacement

(b) Plane normal to the axis of rotation

FIGURE 1.25. Vector diagram of a spherical displacement.

axis passing through the origin of the fixed frame A . The first position of a point P of the rigid body B is denoted by the vector $\mathbf{r}_1 = \overline{OP_1}$. The second position is denoted by $\mathbf{r}_2 = \overline{OP'_2}$, and the direction of rotation is denoted by a unit vector $\mathbf{s}(s_x, s_y, s_z)$. From the geometry of the figure, we obtain

$$\overline{S_p P_1} = \mathbf{r}_1 - (\mathbf{r}_1^T \mathbf{s})\mathbf{s}, \quad (1.29)$$

$$\overline{S_p P'_2} = \mathbf{r}_2 - (\mathbf{r}_2^T \mathbf{s})\mathbf{s}. \quad (1.30)$$

Figure 1.25b shows a plane that contains both points P_1 and P'_2 and is normal to the axis of rotation. The point of intersection between the plane and the axis of rotation is taken as S_p . Let $\overline{NP'_2} \perp \overline{S_p P_1}$. Then, using of the fact that $|S_p P_1| = |S_p P'_2|$ and $\mathbf{s} \times \overline{S_p P_1} = \mathbf{s} \times \mathbf{r}_1$, we have

$$\overline{S_p N} = \overline{S_p P_1} c\theta, \quad (1.31)$$

$$\overline{NP'_2} = \mathbf{s} \times \mathbf{r}_1 s\theta, \quad (1.32)$$

where $c\theta$ is a shorthand notation for $\cos \theta$ and $s\theta$ for $\sin \theta$. To derive a relation between \mathbf{r}_2 and \mathbf{r}_1 , we express $\overline{S_p P'_2}$ as a sum of two vectors:

$$\overline{S_p P'_2} = \overline{S_p N} + \overline{NP'_2}. \quad (1.33)$$

Substituting Eqs. (1.29) through (1.32) into (1.33), we obtain

$$\mathbf{r}_2 - (\mathbf{r}_2^T \mathbf{s})\mathbf{s} = [\mathbf{r}_1 - (\mathbf{r}_1^T \mathbf{s})\mathbf{s}]c\theta + \mathbf{s} \times \mathbf{r}_1 s\theta. \quad (1.34)$$

Substituting $\mathbf{r}_1^T \mathbf{s} = \mathbf{r}_2^T \mathbf{s}$ into Eq. (1.34) and rearranging yields

$$\mathbf{r}_2 = \mathbf{r}_1 c\theta + \mathbf{s} \times \mathbf{r}_1 s\theta + \mathbf{s}(\mathbf{r}_1^T \mathbf{s})(1 - c\theta). \quad (1.35)$$

Equation (1.35) is known as *Rodrigues's formula* for a spherical displacement of a rigid body. By considering \mathbf{r}_1 as ${}^B\mathbf{p}$ and \mathbf{r}_2 as ${}^A\mathbf{p}$, Eq. (1.35) can be written in matrix form as

$${}^A\mathbf{p} = {}^A R_B {}^B\mathbf{p}, \quad (1.36)$$

where the elements of the rotation matrix are given by:

$$a_{11} = (s_x^2 - 1)(1 - c\theta) + 1,$$

$$a_{12} = s_x s_y (1 - c\theta) - s_z s\theta,$$

$$a_{13} = s_x s_z (1 - c\theta) + s_y s\theta,$$

$$a_{21} = s_y s_x (1 - c\theta) + s_z s\theta,$$

$$\begin{aligned} a_{22} &= (s_y^2 - 1)(1 - c\theta) + 1, \\ a_{23} &= s_y s_z (1 - c\theta) - s_x s\theta, \\ a_{31} &= s_z s_x (1 - c\theta) - s_y s\theta, \\ a_{32} &= s_z s_y (1 - c\theta) + s_x s\theta, \\ a_{33} &= (s_z^2 - 1)(1 - c\theta) + 1. \end{aligned} \quad (1.37)$$

Equation (1.37) is called the *screw axis representation* of the orientation of a rigid body. This representation uses four parameters: three associated with the direction of the screw axis and one associated with the angle of rotation. However, only two of the three parameters associated with the direction of the screw axis are independent since they must satisfy the condition of a unit vector, $\mathbf{s}^T \mathbf{s} = 1$.

Given the screw axis and angle of rotation, we can compute the elements of the rotation matrix from Eq. (1.37). On the other hand, given a rotation matrix, we can compute the screw axis and the angle of rotation. The angle of rotation is obtained by summing the diagonal elements of the rotation matrix given by Eq. (1.37):

$$\theta = \cos^{-1} \frac{a_{11} + a_{22} + a_{33} - 1}{2}. \quad (1.38)$$

The direction of the screw axis is obtained by taking the differences between each pair of two opposing off-diagonal elements:

$$\begin{aligned} s_x &= \frac{a_{32} - a_{23}}{2s\theta}, \\ s_y &= \frac{a_{13} - a_{31}}{2s\theta}, \\ s_z &= \frac{a_{21} - a_{12}}{2s\theta}. \end{aligned} \quad (1.39)$$

From Eqs. (1.38) and (1.39) it appears that there are two solutions of the screw axis, one being the negative of the other. In reality, these two solutions represent the same screw, since a $-\theta$ rotation about the $-s$ axis produces the same result as a $+\theta$ rotation about the s axis.

(c) Euler Angle Representations. The direction cosine representation of an orientation contains nine parameters, and the screw axis representation requires four. Since rotation is a motion with 3 degrees of freedom, a set of three independent parameters are sufficient to describe the orientation of a rigid body in space. Several sets of three-parameter representations have been reported in the literature. Perhaps, the most commonly used sets are the Euler

angles. In an Euler angle representation, three successive rotations about the coordinate axes of either a fixed coordinate system or a moving coordinate system are used to describe the orientation of a rigid body.

For convenience, we introduce three basic rotation matrices from which an Euler angle representation can be derived in terms of their product. When a rigid body performs a rotation of θ about the z -axis, $s_x = s_y = 0$ and $s_z = 1$. Hence the rotation matrix, Eq. (1.37), reduces to

$$R(z, \theta) = \begin{bmatrix} c\theta & -s\theta & 0 \\ s\theta & c\theta & 0 \\ 0 & 0 & 1 \end{bmatrix}. \quad (1.40)$$

Similarly, when a rigid body performs a rotation of ψ about the x -axis, $s_y = s_z = 0$ and $s_x = 1$. Hence the rotation matrix, Eq. (1.37), reduces to

$$R(x, \psi) = \begin{bmatrix} 1 & 0 & 0 \\ 0 & c\psi & -s\psi \\ 0 & s\psi & c\psi \end{bmatrix}. \quad (1.41)$$

and when a rigid body performs a rotation of ϕ about the y -axis, $s_x = s_z = 0$ and $s_y = 1$. Hence the rotation matrix, Eq. (1.37), reduces to

$$R(y, \phi) = \begin{bmatrix} c\phi & 0 & s\phi \\ 0 & 1 & 0 \\ -s\phi & 0 & c\phi \end{bmatrix}. \quad (1.42)$$

Roll–Pitch–Yaw Angles. We first consider three successive rotations of the moving frame B about the coordinate axes of the fixed frame A . Starting with the moving frame B coinciding with the fixed frame A , we rotate B about the x -axis by an angle ψ , resulting in an (u', v', w') system; followed by a second rotation of θ about the y -axis, resulting in an (u'', v'', w'') system; and then a third rotation of ϕ about the z -axis, resulting in the final (u, v, w) system, as shown in Fig. 1.26.

Since all rotations take place about the coordinate axes of a fixed frame, the resulting rotation matrix is obtained by premultiplying three basic rotation matrices:

$$\begin{aligned} R(\psi, \theta, \phi) &= R(z, \phi) R(y, \theta) R(x, \psi) \\ &= \begin{bmatrix} c\phi c\theta & c\phi s\theta s\psi - s\phi c\psi & c\phi s\theta c\psi + s\phi s\psi \\ s\phi c\theta & s\phi s\theta s\psi + c\phi c\psi & s\phi s\theta c\psi - c\phi s\psi \\ -s\theta & c\theta s\psi & c\theta c\psi \end{bmatrix}. \end{aligned} \quad (1.43)$$

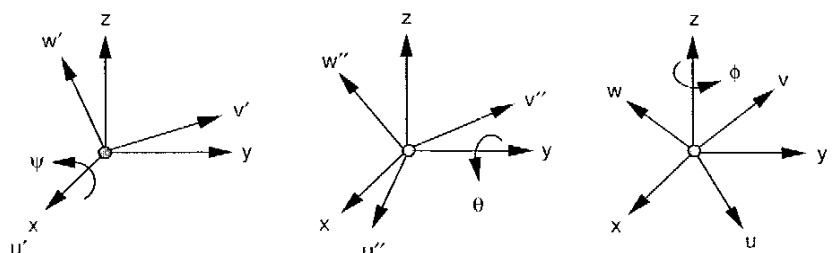


FIGURE 1.26. Successive rotations about the fixed coordinate axes.

The rotation about the x -axis is called a *roll*, the rotation about the y -axis is called a *pitch*, and the rotation about the z -axis is called a *yaw*. We call the convention of describing the orientation of a rigid body the *roll-pitch-yaw* angles representation. We note that successive rotations about the fixed coordinate axes result in a *premultiplication* of the matrices. Since finite rotations do not commute (Goldstein, 1980), the order of rotations cannot be exchanged arbitrarily.

Given the roll, pitch, and yaw angles, we can compute the overall rotation matrix from Eq. (1.43). On the other hand, given a rotation matrix, we can compute the equivalent roll–pitch–yaw angles as follows:

$$\begin{aligned} \theta &= \sin^{-1}(-a_{31}), \\ \psi &= \text{Atan2}(a_{32}/c\theta, a_{33}/c\theta), \\ \phi &= \text{Atan2}(a_{21}/c\theta, a_{11}/c\theta), \end{aligned} \quad (1.44)$$

provided that $c\theta \neq 0$, where $\sin^{-1} x$ is the arcsine function and $\text{Atan2}(y, x)$ is a two-argument arctangent function that yields one unique solution for the angle. Hence corresponding to a given rotation matrix, there are generally two possible solutions of the roll–pitch–yaw angles. However, if $\theta = \pm 90^\circ$, the solutions of Eq. (1.44) degenerate. For this special case, only the sum or the difference of ϕ and ψ can be computed.

w–u–w Euler Angles. Next, we consider three successive rotations of the rigid body about the coordinate axes of a moving frame B . Starting with the moving frame B coinciding with the fixed frame A , we rotate B about the body-attached w -axis by an angle ϕ , followed by a second rotation of θ about the rotated u' -axis, and then a third rotation of ψ about the rotated w'' -axis as shown in Fig. 1.27. We note that each rotation occurs about an axis whose location depends on the preceding rotations. The first rotation causes

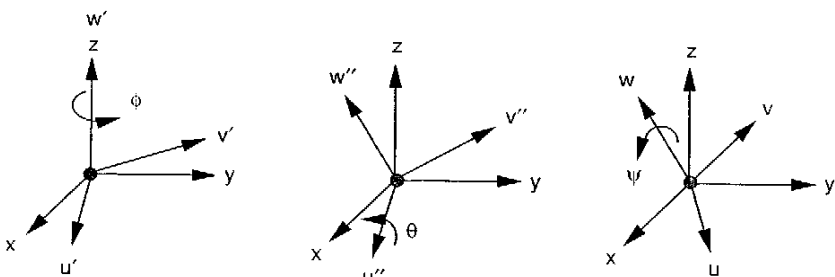


FIGURE 1.27. Successive rotations about the moving coordinate axes.

the (u, v, w) frame to move into the (u', v', w') location. The second rotation causes the (u', v', w') frame to move into the (u'', v'', w'') location. The third rotation causes the (u'', v'', w'') frame to rotate into the final (u, v, w) location. Three such successive rotations are called $w-u-w$ or $z-x-z$ Euler angles.

The resulting rotation matrix can be derived by a kinematic inversion, that is, by considering the orientation of frame A with respect to frame B . The inverse kinematics problem can be stated as a rotation of frame A about the w -axis by angle $-\phi$, followed by a second rotation of $-\theta$ about the u -axis, and followed by a third rotation of $-\psi$ about the w -axis. Under the kinematic inversion, the coordinate axes of frame B are considered as fixed. Hence the overall rotation matrix, ${}^B R_A(-\phi, -\theta, -\psi)$, can be written as

$${}^B R_A(-\phi, -\theta, -\psi) = {}^B R_A(w, -\psi) {}^B R_A(u, -\theta) {}^B R_A(w, -\phi). \quad (1.45)$$

Since ${}^A R_B = [{}^B R_A]^{-1}$ and ${}^B R_A^{-1}(w, -\phi) = {}^B R_A(w, \phi)$, we can expand Eq. (1.45) as follows:

$$\begin{aligned} {}^A R_B(\phi, \theta, \psi) &= [{}^B R_A(-\phi, -\theta, -\psi)]^{-1} \\ &= R(w, \phi) R(u, \theta) R(w, \psi) \\ &= \begin{bmatrix} c\phi c\psi - s\phi c\theta s\psi & -c\phi s\psi - s\phi c\theta c\psi & s\phi s\theta \\ s\phi c\psi + c\phi c\theta s\psi & -s\phi s\psi + c\phi c\theta c\psi & -c\phi s\theta \\ s\theta s\psi & s\theta c\psi & c\theta \end{bmatrix}. \end{aligned} \quad (1.46)$$

We note that successive rotations about the rotated coordinate axes of a moving frame result in a *postmultiplication* by the matrices. Given the $w-u-w$ Euler angles, we can compute the resulting rotation matrix from

Eq. (1.46). On the other hand, given a rotation matrix, we can compute the $w-u-w$ Euler angles as follows:

$$\begin{aligned} \theta &= \cos^{-1} a_{33}, \\ \phi &= \text{Atan2}(a_{13}/s\theta, -a_{23}/s\theta), \\ \psi &= \text{Atan2}(a_{31}/s\theta, a_{32}/s\theta), \end{aligned} \quad (1.47)$$

provided that $s\theta \neq 0$. When $\theta = 0$ or 180° , the solutions of Eq. (1.47) degenerates. For this degenerated case, only the sum or the difference of ϕ and ψ can be computed.

$w-v-w$ Euler Angles. Another type of Euler angle representation consists of a rotation of angle ϕ about the w -axis, followed by a second rotation of θ about the rotated v -axis, and followed by a third rotation of ψ about the rotated w -axis. The resulting rotation matrix is obtained by a postmultiplication of three basic rotation matrices as follows:

$$\begin{aligned} {}^A R_B(\phi, \theta, \psi) &= R(w, \phi) R(v, \theta) R(w, \psi) \\ &= \begin{bmatrix} c\phi c\theta c\psi - s\phi s\psi & -c\phi c\theta s\psi - s\phi c\psi & c\phi s\theta \\ s\phi c\theta c\psi + c\phi s\psi & -s\phi c\theta s\psi + c\phi c\psi & s\phi s\theta \\ -s\theta c\psi & s\theta s\psi & c\theta \end{bmatrix}. \end{aligned} \quad (1.48)$$

Again, given the $w-v-w$ Euler angles, we can compute the resulting rotation matrix from Eq. (1.48). On the other hand, given a rotation matrix, we can compute the $w-v-w$ Euler angles as follows:

$$\begin{aligned} \theta &= \cos^{-1} a_{33}, \\ \phi &= \text{Atan2}(a_{23}/s\theta, a_{13}/s\theta), \\ \psi &= \text{Atan2}(a_{32}/s\theta, -a_{31}/s\theta), \end{aligned} \quad (1.49)$$

provided that $s\theta \neq 0$. When $\theta = 0$ or 180° , the solutions of Eq. (1.49) degenerates. In this case, only the sum or the difference of ϕ and ψ can be computed.

1.5.3 Description of a Location

As pointed out earlier, the location of the rigid body can be described by the position of the origin Q and the orientation of the moving frame with respect to the fixed frame. Figure 1.22 shows that the position of a point P of the rigid body can be expressed in the fixed frame A as ${}^A p = \overline{OP}$. It can also be

expressed in the moving frame B as ${}^B\mathbf{p} = \overline{QP}$. To derive a relation between ${}^A\mathbf{p}$ and ${}^B\mathbf{p}$, we construct the vector \overline{OP} as a sum of two vectors:

$$\overline{OP} = \overline{OQ} + \overline{QP}, \quad (1.50)$$

where $\overline{OQ} = {}^A\mathbf{q}$ denotes the position of Q with respect to the fixed frame A .

Let the orientation of the moving frame B with respect to the fixed frame A be defined by the rotation matrix ${}^A R_B$. Then Eq. (1.50) can be written as

$${}^A\mathbf{p} = {}^A R_B {}^B\mathbf{p} + {}^A\mathbf{q}. \quad (1.51)$$

Equation (1.51) describes the position of a point in a rigid body in terms of the position of the origin Q and the orientation of the moving frame B with respect to the fixed frame A . The leading superscript of ${}^B\mathbf{p}$ cancels with the trailing subscript of ${}^A R_B$, leaving all quantities as vectors expressed in the fixed frame A .

Since we assume that initially, the moving frame coincides with the fixed frame, we may consider ${}^B\mathbf{p}$ as the first position of a point P and ${}^A\mathbf{p}$ as the second position of the same point expressed in the fixed frame A . The first term on the right-hand side of Eq. (1.51) represents the contribution due to a rotation of the rigid body about some axis, and the second term represents the contribution due a translation along the direction of ${}^A\mathbf{q}$. We observe that the general spatial displacement of a rigid body can be considered as a rotation plus a translation. This is well known as *Chasles' theorem*.

1.6 HOMOGENEOUS TRANSFORMATIONS

Equation (1.51) provides a general transformation of a position vector from the moving frame to the fixed frame. The first term on the right-hand side of the equation represents the contribution due to a rotation and the second term that due to a translation of the moving frame respect to the fixed frame. The equation is not in a compact form, because the 3×3 rotation matrix does not provide for the translation. To write Eq. (1.51) in a better-appearing form, we introduce the concepts of homogeneous coordinates and homogeneous transformation matrix.

1.6.1 Homogeneous Coordinates

Let $\mathbf{p} = [p_x, p_y, p_z]^T$ be the position vector of a point with respect to a reference frame A in three-dimensional space. We define the *homogeneous*

coordinates of \mathbf{p} as

$$\hat{\mathbf{p}} = [\rho p_x, \rho p_y, \rho p_z, \rho]^T. \quad (1.52)$$

Thus the homogeneous coordinates of a point \mathbf{p} in frame A are represented by a vector $\hat{\mathbf{p}}$ in a four-dimensional space. The fourth coordinate ρ is a nonzero scaling factor. In general, an N -dimensional position vector becomes an $(N+1)$ -dimensional vector in a homogeneous coordinate system. The concept of homogeneous coordinates is useful in developing matrix transformations that include rotation, translation, scaling, and perspective transformation (Ballard and Brown, 1982).

From the definition above, we see that a three-dimensional vector can be recovered from its four-dimensional homogeneous coordinates by dividing the first three homogeneous coordinates by the fourth coordinate; that is,

$$p_x = \frac{\hat{p}_x}{\rho}, \quad p_y = \frac{\hat{p}_y}{\rho}, \quad \text{and} \quad p_z = \frac{\hat{p}_z}{\rho}. \quad (1.53)$$

We note that the homogeneous coordinates $\hat{\mathbf{p}}$ are not unique, since any nonzero scaling factor ρ will yield the same three-dimensional vector \mathbf{p} . For example, $\hat{\mathbf{p}}_1 = [\rho_1 p_x, \rho_1 p_y, \rho_1 p_z, \rho_1]^T$ and $\hat{\mathbf{p}}_2 = [\rho_2 p_x, \rho_2 p_y, \rho_2 p_z, \rho_2]^T$ represent the same position vector $\mathbf{p} = [p_x, p_y, p_z]^T$ in a three-dimensional space. For the kinematics of mechanisms and robot manipulators, we choose a scaling factor of $\rho = 1$ for convenience. When the scaling factor is set to unity, the first three homogeneous coordinates represent the actual coordinates of a three-dimensional vector. Hence the position vector of a point is given simply as

$$\hat{\mathbf{p}} = [p_x, p_y, p_z, 1]^T. \quad (1.54)$$

In subsequent chapters, we omit the hats from the equation for brevity.

1.6.2 Homogeneous Transformation Matrix

The *homogeneous transformation matrix* is a 4×4 matrix that is defined for the purpose of mapping a homogeneous position vector from one coordinate system into another. The matrix can be partitioned into four submatrices as follows:

$${}^A T_B = \begin{bmatrix} {}^A R_B (3 \times 3) & \vdots & {}^A \mathbf{q} (3 \times 1) \\ \dots & \vdots & \dots \\ {}^A \mathbf{q} (1 \times 3) & \vdots & \rho (1 \times 1) \end{bmatrix}. \quad (1.55)$$

The upper left 3×3 submatrix ${}^A R_B$ denotes the *orientation* of a moving frame B with respect to a reference frame A , the upper right 3×1 submatrix ${}^A \mathbf{q}$ denotes the *position* of the origin of the moving frame relative to the fixed frame, the lower left 1×3 submatrix \mathbf{p} represents a *perspective transformation*, and the lower right element ρ is a *scaling factor*. For kinematics of mechanisms and robot manipulators, the scaling factor is set to unity and the 1×3 perspective transformation matrix is set to zero. See Nevatia (1982) for a more detailed description of the matrix.

Using the homogeneous coordinates, Eq. (1.51) can be written in the following compact form:

$${}^A \hat{\mathbf{p}} = {}^A T_B {}^B \hat{\mathbf{p}}, \quad (1.56)$$

where

$${}^A T_B = \begin{bmatrix} {}^A R_B & : & {}^A \mathbf{q} \\ \dots & : & \dots \\ 0 & 0 & 0 \end{bmatrix},$$

$${}^A \hat{\mathbf{p}} = [p_x, p_y, p_z, 1]^T,$$

$${}^B \hat{\mathbf{p}} = [p_u, p_v, p_w, 1]^T.$$

For example, the homogeneous transformation matrix for a simple rotation about the z -axis is given by

$${}^A T_B(z, \theta) = \begin{bmatrix} \cos \theta & -\sin \theta & 0 & 0 \\ \sin \theta & \cos \theta & 0 & 0 \\ 0 & 0 & 1 & 0 \\ 0 & 0 & 0 & 1 \end{bmatrix}. \quad (1.57)$$

The transformation matrix for a pure translation is given by

$${}^A T_B(\mathbf{q}) = \begin{bmatrix} 1 & 0 & 0 & q_x \\ 0 & 1 & 0 & q_y \\ 0 & 0 & 1 & q_z \\ 0 & 0 & 0 & 1 \end{bmatrix}. \quad (1.58)$$

In summary, Eq. (1.56) provides a transformation of homogeneous coordinates from one frame to another. Given the transformation matrix ${}^A T_B$, we can locate the moving frame B with respect to the fixed frame A ; and given the location of a moving frame B with respect to a fixed frame A , we can find the transformation matrix ${}^A T_B$.

Although the transformation matrix ${}^A T_B$ is not orthogonal (i.e., ${}^A T_B^{-1} \neq {}^A T_B^T$), its inverse transformation does exist. Multiplying both sides of

Eq. (1.51) by ${}^A T_B^{-1}$ and making use of the fact that ${}^A T_B^{-1} = {}^A R_B^T$, we obtain

$${}^B \mathbf{p} = {}^A R_B^T {}^A \mathbf{p} + {}^A R_B^T {}^A \mathbf{q}. \quad (1.59)$$

Using the homogeneous coordinates, Eq. (1.59) can be written as

$${}^B \hat{\mathbf{p}} = {}^A T_B^{-1} {}^A \hat{\mathbf{p}}. \quad (1.60)$$

Hence

$${}^A T_B^{-1} = {}^B T_A = \begin{bmatrix} {}^A R_B^T & : & -{}^A R_B^T {}^A \mathbf{q} \\ \dots & : & \dots \\ 0 & 0 & 0 \end{bmatrix}. \quad (1.61)$$

1.6.3 Composite Homogeneous Transformation

Homogeneous transformation matrices can be multiplied together to obtain a composite transformation matrix. However, special attention should be paid to the order of multiplication since finite rotations are not commutative. The problem is further complicated, since a rigid body can rotate about the coordinate axes of either a fixed reference frame or the body-attached moving frame. The following rules are helpful for the determination of a composite transformation matrix:

1. At the initial position, the moving frame B and the fixed frame A are coincident. Hence $T = I$ is an identity matrix.
2. Rotation and translation about the coordinate axes of a fixed frame results in a premultiplication of the two matrices.
3. Rotation and translation about the coordinate axes of a moving frame results in a postmultiplication of the two matrices.

1.7 MECHANICS OF ROBOT MANIPULATORS

Robotics is the science or study of the basic technologies associated with the theory and application of robotic systems. The study involves both theoretical and applied research, which can be divided into manipulator design, basic mechanics, trajectory planning and control, programming and machine intelligence, and so on. *Mechanics* is a branch of science that deals with energy and forces and their effect on the motion of a mechanical system. The study involves three interrelated subjects: kinematics, statics, and dynamics.

1.7.1 Kinematics

Kinematics deals with the aspects of motion without regard to the forces and/or torques that cause it. The science of kinematics deals with the position, velocity, acceleration, and higher-order derivatives of the position variables with respect to time or other variables. Hence kinematics is concerned only with the geometrical and time properties of a motion. The joint variables of a robot manipulator are related to the position and orientation of the end effector by the constraints imposed by the joints. These kinematic relations are the focal points of interest in a study of the kinematics of robot manipulators. The study can be approached from two different points of view: kinematic analysis and kinematic synthesis. However, the processes of kinematic analysis and kinematic synthesis are intertwined. A designer needs a skillful analysis ability to evaluate various design alternatives under consideration and to arrive at the best design. Hence a better understanding of the kinematics is the first concern in the design and control of robot manipulators.

Kinematic analysis deals with the derivation of relative motions among various links of a given manipulator. There are two types of kinematic analysis problems: direct kinematics and inverse kinematics. In the programming of a robot manipulator, typically a set of desired positions and orientations, and perhaps the time derivatives of the positions and orientations of the end effector, are specified in space. The problem is to find all possible sets of actuated joint variables and their corresponding time derivatives which will bring the end effector to the set of desired positions and orientations with the desired motion characteristics. This is known as *inverse kinematics*. On the other hand, sometimes the actuated joint variables and possibly their time derivatives are obtained from readings of sensors installed at the joints, from which we wish to find all possible sets of end effector positions and orientations and their corresponding time derivatives. This is called *direct kinematics* or *forward kinematics*. Both direct and inverse kinematics problems can be solved by various methods of analysis, such as geometric vector analysis, matrix algebra, screw algebra, and so on (Erdman and Sandor, 1991; Kimbrell, 1991; Lange, 1995; Martin, 1982).

Kinematic synthesis is the reverse process of kinematic analysis. In this case, a designer is challenged to devise a new manipulator or machine that will possess certain desired kinematic properties. Specifically, given a set of desirable positions and orientations of the end effector and possibly their time derivatives in space, the corresponding actuated joint variables and the type and geometry of a manipulator are to be determined. Some researchers have focused on the synthesis of manipulators with the workspace as an optimality criterion. The kinematic synthesis problem can be further divided into three interrelated phases: *type synthesis*, *number synthesis*, and *dimensional syn-*

thesis. See Erdman and Sandor (1991) or Hartenberg and Denavit (1964) for a description of these three phases of kinematic synthesis.

1.7.2 Statics

Statics deals with the relations of forces that produce equilibrium among the various members of a robot manipulator. A manipulator may be acted upon by forces that arise from various sources, such as forces of gravity, forces of applied loads, frictional forces, inertia forces, and so on. These forces must be considered carefully during the design stage of a robot manipulator so that its parts can be sized properly and the manipulator will function correctly. Obviously, inertia forces are excluded from the static force analysis. The forces of equilibrium depend on the *configuration* or *posture* of a robot manipulator and are not time dependent.

1.7.3 Dynamics

Dynamics deals with the forces and/or torques required to cause the motion of a system of bodies. The study includes inertia forces as one of the principal concerns. The dynamics of a robot manipulator is a very complicated subject. Typically, the end effector is to be guided through a given path with certain prescribed motion characteristics. A set of torque and/or force functions must be applied at the actuated joints in order to produce that motion. These actuating torque and/or force functions depend not only on the spatial and temporal attributes of the given path but also on the mass properties of the links, the payload, the externally applied forces, and so on.

The dynamics of robot manipulators can also be approached from two different points of view: dynamical analysis and dynamical synthesis.

Dynamical analysis deals with derivation of the equations of motion of a given manipulator. There are two types of dynamical analysis problems: direct dynamics and inverse dynamics. *Direct dynamics* can be defined as follows: Given a set of actuated joint torque and/or force functions, calculate the resulting motion of the end effector as a function of time; and *inverse dynamics* as: Given a trajectory of the end effector as a function of time, find a set actuated joint torque and/or force functions which will produce that motion. The computational efficiency of direct dynamics is not as critical since it is used primarily for computer simulations of a robot manipulator. On the other hand, an efficient inverse dynamical model becomes extremely important for real-time, model-based control of a robot manipulator. Various methods of analysis, such as the Newton–Euler equations, the Lagrangian equations of motion, and the principle of virtual work can be applied for the dynamical analysis of robot manipulators.

Dynamical synthesis is the reverse of dynamical analysis. Specifically, a new manipulator is to be designed with certain desired dynamical motion characteristics. The dynamical synthesis problem is much more complicated than the dynamical analysis problem and is not treated in this book, which concentrates on recent advances in the kinematic, static, and dynamical analysis of robot manipulators. Both serial and parallel manipulators are covered. A thorough understanding of the mechanics of robot manipulators is a prerequisite for achieving better design, path planning, and control of such electromechanical systems. Readers of this book are strongly encouraged to consult other textbooks on robot sensing, control, path planning, programming languages, and machine intelligence (e.g., Asada and Slotine, 1986; Craig, 1986; Fu et al., 1987; Paul, 1981; Rivin, 1987; Schilling, 1990).

1.8 SUMMARY

We first gave a brief description of the background and historical development of robot manipulators. Then we provided a review of the definitions of links, joints, kinematic chains, mechanisms, and machines. The concepts of degrees of freedom and the loop-mobility criterion of a mechanism were introduced. The essential components of a robotic system were described. Robot manipulators were classified according to their degrees of freedom, kinematic structure, drive technology, workspace envelope, and motion characteristics. Several industrial robots were used to demonstrate the state-of-the-art development. Furthermore, descriptions of the position, orientation, and location of a rigid body with respect to a fixed frame were presented. Several different methods of specifying the orientation of a rigid body with respect to a fixed frame were studied. Finally, the concepts of homogeneous coordinates, homogeneous transformation, and composite homogeneous transformation were introduced. These fundamental concepts will be useful for the development of the mechanics of robot manipulators in subsequent chapters.

REFERENCES

- Arai, T., Cleary, K., Homma, K., Adachi, H., and Nakamura, T., 1991, "Development of Parallel Link Manipulator for Underground Excavation Task," *Proc. 1991 International Symposium on Advanced Robot Technology*, pp. 541–548.
- Asada, H. and Slotine, J.-J. E., 1986, *Robot Analysis and Control*, Wiley, New York.
- Ball, R. S., 1900, *A Treatise on the Theory of Screws*, Cambridge University Press, Cambridge.

- Ballard, D. and Brown, C., 1982, *Computer Vision*, Prentice Hall, Upper Saddle River, NJ.
- Capek, K., 1923, *Rossum's Universal Robots (R.U.R)* (a play), Doubleday Page, New York.
- Chang, S. L. and Tsai, L. W., 1993, "On the Redundant-Drive Backlash-Free Robotic Mechanisms," *ASME J. Mech. Des.*, Vol. 115, No. 2, pp. 247–254.
- Craig, J., 1986, *Introduction to Robotics. Mechanics and Control*, Addison-Wesley, Reading, MA.
- Engelberger, J. F., 1980, *Robotics in Practice*, AMACOM, New York.
- Erdman, A. G. and Sandor, G. N., 1991, *Mechanism Design: Analysis and Synthesis*, Prentice Hall, Upper Saddle River, NJ.
- Ernst, H. A., 1962, "A Computer-Operated Mechanical Hand," Sc.D. thesis, Massachusetts Institute of Technology, Cambridge, MA.
- Fu, K. S., Gonzalez, R. C., and Lee, C. S. G., 1987, *Robotics: Control, Sensing, Vision, and Intelligence*, McGraw-Hill, New York.
- Giddings & Lewis, 1995, Giddings & Lewis Machine Tools, 142 Doty Street, Fond du Lac, WI.
- Goldstein, H., 1980, *Classical Mechanics*, Addison-Wesley, Reading, MA.
- Gosselin, C. and Hamel, J., 1994, "The Agile Eye: A High-Performance Three-Degree-of-Freedom Camera-Orienting Device," *Proc. IEEE International Conference on Robotics and Automation*, pp. 781–786.
- Grübler, M., 1917, *Getriebelehre*, Springer-Verlag, Berlin.
- Hartenberg, R. S. and Denavit, J., 1964, *Kinematic Synthesis of Linkages*, McGraw-Hill, New York.
- Jacobsen, S. C., Wood, J. E., Knutti, D. F., and Biggers, K. B., 1984, "The Utah/MIT Dextrous Hand: Work in Progress," *Int. J. Robot. Res.*, Vol. 3, No. 4, pp. 21–50.
- Jacobsen, S. C., Iversen, E. K., Knutti, D. F., Johnson, R. T., and Biggers, K. B., 1986, "The Design of the Utah/MIT Dextrous Hand," *Proc. IEEE International Conference on Robotics and Automation*, pp. 1520–1532.
- Kimbrell, J. T., 1991, *Kinematics Analysis and Synthesis*, McGraw-Hill, New York.
- Kutzbach, K., 1929, "Mechanische Leitungsverzweigung, Maschinenbau," *Der Betrieb* 8, No. 21, pp. 710–716.
- Lange, J., 1995, *Kinematics: A Graphical Approach*, Prentice Hall, Upper Saddle River, NJ.
- Martin, G. H., 1982, *Kinematics and Dynamics of Machines*, McGraw-Hill, New York.
- Mavroidis, C., and Roth, B., 1994, "Analysis and Synthesis of Overconstrained Mechanisms," *Proc. ASME 1994 Mechanisms Conference*, Minneapolis, MN.
- McCarthy, J., et al., 1968, "A Computer with Hands, Eyes, and Ears," *1968 Fall Joint Computer Conference, AFIPS Proc.*, pp. 329–338.
- Nevatia, R., 1982, *Machine Perception*, Prentice Hall, Upper Saddle River, NJ.

- Paul, R. P., 1981, *Robot Manipulators: Mathematics, Programming, and Control*, MIT Press, Cambridge, MA.
- Pham, D. T. and Heginbotham, W. B., 1986, *Robot Grippers*, Springer-Verlag, New York.
- Rivin, E. I., 1987, *Mechanical Design of Robots*, McGraw-Hill, New York.
- Salisbury, J. K., 1982, "Kinematic and Force Analysis of Articulated Mechanical Hands," Ph.D. dissertation, Mechanical Engineering Department, Stanford University, Stanford, CA.
- Salisbury, J. K. and Roth, B., 1983, "Kinematic and Force Analysis of Articulated Mechanical Hands," *ASME J. Mech. Trans. Autom. Des.*, Vol. 105, No. 1, pp. 35–41.
- Schilling, R. J., 1990, *Fundamentals of Robotics: Analysis and Control*, Prentice Hall, Upper Saddle River, NJ.
- Stewart, D. 1965, "A Platform with Six Degrees of Freedom," *Proc. Inst. Mech. Eng. London*, Vol. 180, pp. 371–386.
- Tsai, L. W. and Chang, S. L., 1994, "Backlash Control via Redundant Drives: An Experimental Verification," *ASME J. Mech. Des.*, Vol. 116, No. 3, pp. 963–967.

EXERCISES

1. Find the number of degrees of freedom associated with the planar manipulator shown in Fig. 1.28, where a moving platform is shown connected to a fixed base by three limbs. Each limb consists of two binary links and three parallel revolute joints. Is this a serial or a parallel manipulator?

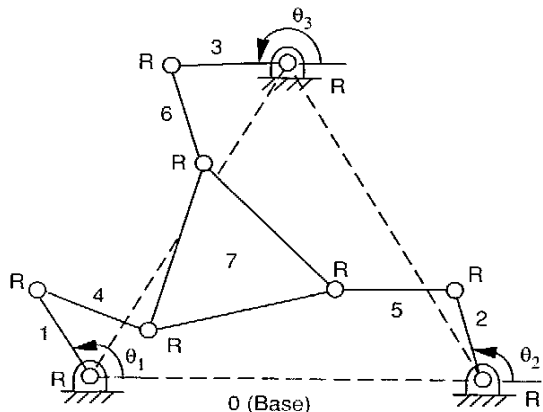


FIGURE 1.28. Planar 3RRR manipulator.

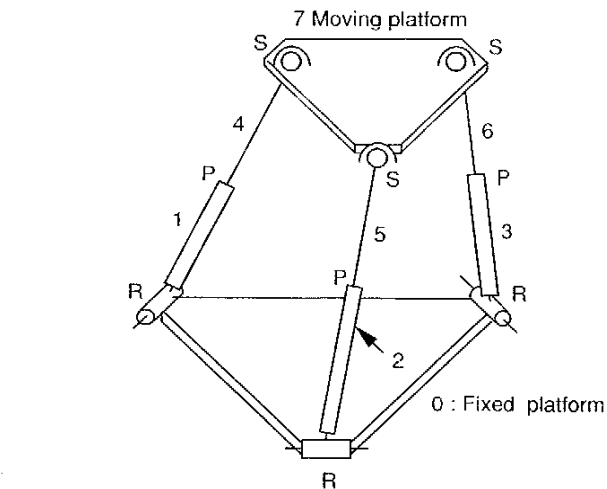


FIGURE 1.29. Spatial 3RPS manipulator.

- Figure 1.29 shows a spatial mechanism in which a moving platform is connected to a fixed base by three extensible limbs with a spherical joint at the upper end and a revolute joint at the lower end. Furthermore, each limb is made up of two binary links connected by a prismatic joint. Find the number of degrees of freedom of the mechanism.
- Figure 1.30 shows a moving platform that is connected to a fixed base by three limbs with a universal joint on each end. Each limb is made up of two binary links connected by a prismatic joint. Find the degrees of freedom associated with this spatial manipulator.
- A rigid body is first rotated about the fixed x -axis by 45° and then about the fixed y -axis by 30° . Find the resulting rotation matrix.
- A rigid body is first rotated about the body-attached w -axis by 30° and then about the rotated v -axis by 45° . Find the resulting rotation matrix.
- What is the resulting rotation matrix for a rotation of 60° about the fixed x -axis, followed by a rotation of 45° about the y -axis, followed by another rotation of 30° about the z -axis?

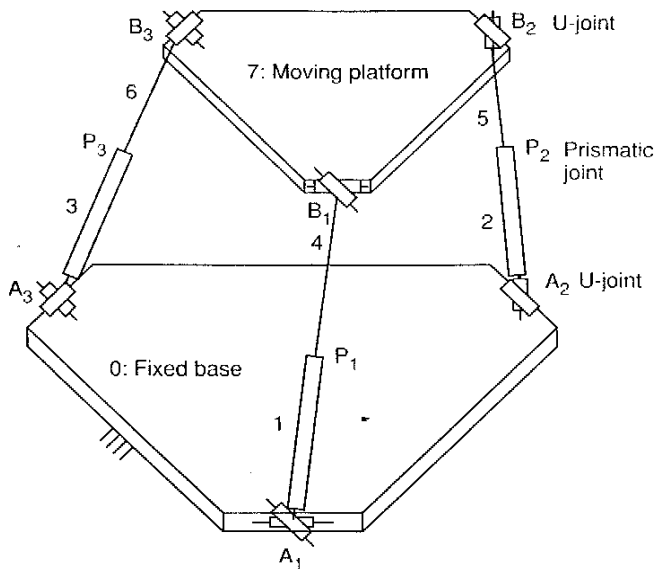


FIGURE 1.30. Spatial 3UPU manipulator.

7. Find the axis of rotation associated with the rotation matrix

$${}^A R_B = \begin{bmatrix} a_{11} & a_{12} & a_{13} \\ a_{21} & a_{22} & a_{23} \\ a_{31} & a_{32} & a_{33} \end{bmatrix},$$

8. Find the equivalent screw axis and the angle of rotation associated with the rotation matrix

$${}^A R_B = \begin{bmatrix} 0.866 & -0.500 & 0.000 \\ 0.500 & 0.866 & 0.000 \\ 0.000 & 0.000 & 1.000 \end{bmatrix}.$$

9. Find the equivalent $x-y-z$ roll-pitch-yaw angles associated with the rotation matrix

$${}^A R_B = \begin{bmatrix} 1.000 & 0.000 & 0.000 \\ 0.000 & 0.866 & -0.500 \\ 0.000 & 0.500 & 0.866 \end{bmatrix}.$$

10. Find the equivalent $w-u-w$ Euler angles associated with the rotation matrix

$${}^A R_B = \begin{bmatrix} 0.866 & -0.500 & 0.000 \\ 0.433 & 0.750 & -0.500 \\ 0.250 & 0.433 & 0.866 \end{bmatrix}.$$

11. A rigid body is rotated about the fixed z -axis by 30° followed by a translation of 2 units in the x direction and 4 units in the y -direction. Find the transformation matrix ${}^A T_B$ and its inverse transformation, ${}^B T_A$.

CHAPTER 2

POSITION ANALYSIS OF SERIAL MANIPULATORS

2.1 INTRODUCTION

A serial manipulator consists of several links connected in series by various types of joints, typically revolute and prismatic joints. One end of the manipulator is attached to the ground and the other end is free to move in space. For this reason a serial manipulator is sometimes called an *open-loop manipulator*. We call the fixed link the *base*, and the free end where a gripper or a mechanical hand is attached, the *end effector*.

For a robot to perform a specific task, the location of the end effector relative to the base should be established first. This is called the *position analysis problem*. There are two types of position analysis problems: *direct position* or *direct kinematics* and *inverse position* or *inverse kinematics problems*. For direct kinematics, the joint variables are given and the problem is to find the location of the end effector. For inverse kinematics, the location of the end effector is given and the problem is to find the joint variables necessary to bring the end effector to the desired location. For a serial manipulator, direct kinematics is fairly straightforward, whereas inverse kinematics becomes very difficult. On the other hand, for a parallel manipulator, inverse kinematics is very straightforward, whereas direct kinematics becomes very difficult. We note that for a deficient manipulator the end effector cannot be positioned freely in space, and for a redundant manipulator there may be several infinities of inverse kinematic solutions corresponding to a given end-effector location, depending on the degrees of redundancy.

In solving the inverse kinematics problem, we are often interested in obtaining a *closed-form solution*, that is, in reducing the problem to an algebraic equation relating the end-effector location to a single joint variable. In this way, all possible solutions and manipulator postures can be accounted for. To achieve this goal, various methods of formulation have been proposed. Perhaps the most commonly used methods are the *vector algebra method* (Chase, 1963; Lee and Liang, 1988a,b), the *geometric method* (Duffy and Rooney, 1975; Duffy, 1980), the 4×4 *matrix method* (Denavit and Hartenberg, 1955), the 3×3 *dual matrix method* (Yang, 1969; Pennock and Yang, 1985), the *iterative method* (Uicker et al., 1964; Albala and Angeles, 1979), the *screw algebra method* (Yuan and Freudenstein, 1971; Kohli and Soni, 1975), and the *quaternion algebra method* (Yang and Freudenstein, 1964).

The number of possible inverse kinematics solutions depends on the type and location of a robot manipulator. In general, closed-form solutions can be found for manipulators with simple geometry, such as manipulators with three consecutive joint axes intersecting at a common point or three consecutive joint axes parallel to one another. For a manipulator of general geometry, the inverse kinematics problem becomes a very difficult task. Following is a brief review of the historical development of the inverse kinematics problem.

- Pieper and Roth (1969) applied the 4×4 matrix method to solve the inverse kinematics of serial manipulators. They found that a sufficient condition for a serial manipulator to yield a closed-form inverse kinematics solution is to have any three consecutive joint axes intersecting at a common point or any three consecutive joint axes parallel to each other. They also pointed out that the analysis of a serial manipulator is related to the displacement analysis of a single-loop spatial mechanism. Therefore, the results using all methods of solution developed for single-loop spatial mechanisms can be applied to the analysis of serial manipulators. Closed-form solutions were obtained for several robot manipulators of special geometry (Pieper, 1968).
- Roth, Rastegar, and Scheinman (1972) concluded by deductive reasoning that there are at most 32 inverse kinematics solutions for the general $6R$ manipulator.
- Freudenstein (1973) referred to the inverse kinematics problem of the most general $6R$ manipulator as the “Mount Everest” of kinematic problems.
- Duffy and Crane (1980) derived a closed-form solution for the general $7R$ single-loop spatial mechanism. The solution was obtained in the form of a 16×16 determinant in which every element is a second-degree polynomial in one joint variable. The determinant, when expended,

should yield a 32nd-degree polynomial equation and hence confirms the upper limit predicted by Roth et al. (1973).

- Albal (1982) used the indicial notation to formulate the general 7R spatial mechanism problem and obtained the solution in a 12×12 determinant form in which every element is a quadratic polynomial in the tangent of one-half of a joint angle.
- Tsai and Morgan (1985) used the homotopy continuation method to solve the inverse kinematics of the general 6R manipulator and found only 16 solutions. Since the continuation method is capable of finding all possible solutions of a set of polynomial equations, they conjectured that the most general 6R manipulator has at most 16 real solutions.
- Primrose (1986) proved that the 32nd-degree polynomial derived by Duffy and Crane contains 16 extraneous solutions.
- Lee and Liang (1988a,b) derived a 16th-degree polynomial for the input-output displacement equation of the general 7R spatial mechanism.
- Raghavan and Roth (1989, 1990) used the dyadic elimination method to derive a 16th-degree polynomial for the general 6R inverse kinematics problem. See Appendix C for the derivation.

In this chapter we focus on the position problem of serial manipulators. Two commonly used methods, Denavit and Hartenberg's method and the method of successive screw displacements, are introduced. Both methods are systematic in nature and more suitable for the kinematic analysis of serial manipulators. The kinematics of several frequently used robotic structures will be analyzed to demonstrate the methodologies. The inverse kinematics of the 6R manipulator of general geometry, which is the most difficult problem in kinematics, is presented in Appendix C. Although the geometric method is often employed by some researchers and engineers, it is judged to be more suitable for serial manipulators with relatively simple geometry and for the analysis of parallel manipulators. We describe this method only briefly in this chapter.

2.2 LINK PARAMETERS AND LINK COORDINATE SYSTEMS

In general, an n -dof serial manipulator consists of a base link and n moving links connected in series by n joints without forming a closed loop. The relative motion associated with each joint can be controlled by an actuator such that the end effector can be positioned anywhere within its workspace. For example, the Scrbot robot shown in Fig. 2.1 is a 5-dof serial manipu-

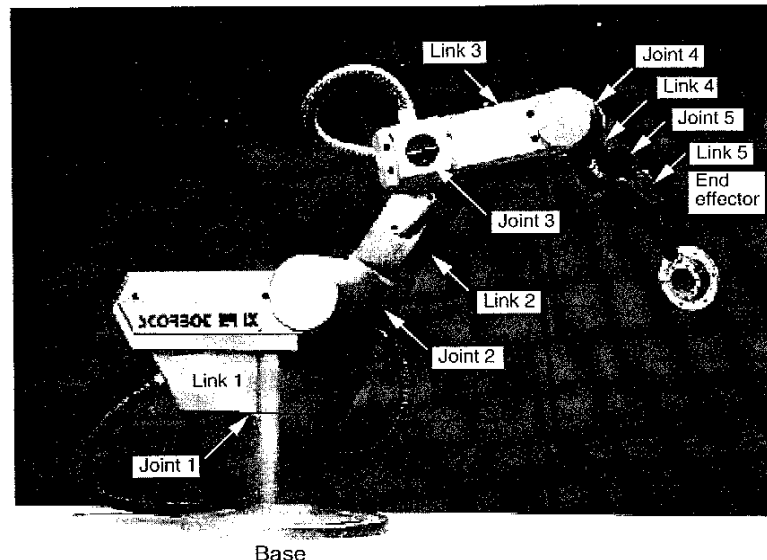


FIGURE 2.1. Scrbot robot. (Courtesy of Eshed Robotic Inc., Princeton, New Jersey.)

lator in which the first joint axis points up vertically, the second joint axis is perpendicular to the first with a small offset, the third and fourth joint axes are both parallel to the second, and the fifth joint axis intersects the fourth perpendicularly.

To describe the geometry of the links, starting from the base link, we number the links sequentially from 0 to n and the joints from 1 to n . Thus, except for the base link and the end-effector link, every link has two joints. Link 1 is connected to the base link by joint 1, link 2 is connected to link 1 by joint 2, and so on. Link i has joint i at its proximal end and joint $i + 1$ at the distal end, as shown in Fig. 2.2.

Following Denavit and Hartenberg's convention (1955), a Cartesian coordinate system is attached to each link of a manipulator. Except for the base and end-effector link, coordinate system i is attached to link i according to the following rules:

- The z_i -axis is aligned with the $(i + 1)$ th joint axis. The positive direction of rotation or translation can be chosen arbitrarily.

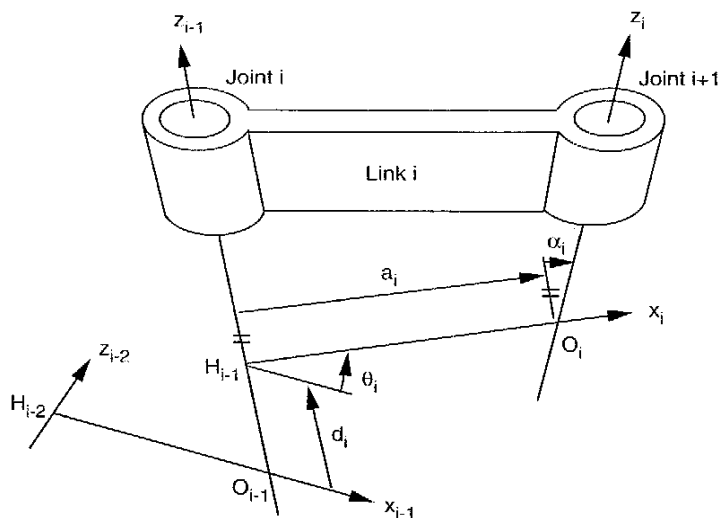


FIGURE 2.2. Definition of link parameters.

- The x_i -axis is defined along the common normal between the i th and $(i+1)$ th joint axes and points from the i th to the $(i+1)$ th joint axis. If the two joint axes are parallel, the x_i -axis can be chosen anywhere perpendicular to the two joint axes. In case of two intersecting joint axes, the x_i -axis can be defined either in the direction of the vector cross product $\mathbf{z}_{i-1} \times \mathbf{z}_i$ or in the opposite direction, and the origin is at the point of intersection.
- The y_i -axis is determined by the right-hand rule.

The zeroth coordinate system is attached to the base at any convenient location as long as the z_0 -axis is aligned with the first joint axis. Furthermore, we attach a coordinate system to the end-effector link, called the *end effector* or *hand coordinate system*, to describe the location of the end effector. The hand coordinate system can be located anywhere in the end-effector as long as the x_n -axis is normal to the last joint axis. For convenience, the z_n -axis is often defined along the direction of approach of a gripper.

Let H_{i-1} be the point of intersection of the x_i and z_{i-1} axes, and let O_i , the origin of the i th coordinate system, be the point of intersection of the x_i and z_i axes as shown in Fig. 2.2. Then, regardless of how the links are constructed physically, the following parameters are uniquely determined by the geometry of the axes:

a_i : offset distance between two adjacent joint axes, where $a_i = |H_{i-1}O_i|$.

d_i : translational distance between two incident normals of a joint axis.

$d_i = |O_{i-1}H_{i-1}|$ is positive if the vector $\overrightarrow{O_{i-1}H_{i-1}}$ points in the positive z_{i-1} -direction; otherwise, it is negative.

α_i : twist angle between two adjacent joint axes. It is the angle required to rotate the z_{i-1} -axis into alignment with the z_i -axis about the positive x_i -axis according to the right-hand rule.

θ_i : joint angle between two incident normals of a joint axis. It is the angle required to rotate the x_{i-1} -axis into alignment with the x_i -axis about the positive z_{i-1} -axis according to the right-hand rule.

For a revolute joint, a_i , α_i , and d_i are constant, and θ_i is a variable that measures the relative location of link i with respect to link $i - 1$. For a prismatic joint, a_i , α_i , and d_i are constant, and d_i is a variable that measures the relative location of link i with respect to link $i - 1$. In what follows, we refer to θ_i for a revolute joint and d_i for a prismatic joint as *joint variables* and to the constant parameters as *link parameters*. We note that a joint variable provides only the relative location between two adjacent links, it should not be confused with the term *displacement*. A displacement implies the amount of angle or distance needed to move a link from one location to another. Using the definitions above, the displacement required to move a link from one location to another is equal to the difference between two successive values of a joint variable.

For a prismatic joint, the direction of the joint axis defines the direction of relative translation between two links. Unlike a revolute joint, only the direction of the joint axis is important. Although the location of a prismatic joint has no effect on relative displacement, the physical location of the joint will be used to establish the foregoing link parameters. Note that several different coordinate systems can be defined for a manipulator, due to various possible choices of the positive z and x axes. A general procedure for establishing Denavit–Hartenberg coordinate systems can be summarized as follows:

- Starting from the base link, number the links and joints sequentially. The base is numbered as link 0 and the last link is the end effector. Except for the base and end effector link, every link contains two joints. Joint i connects link i to link $i - 1$.
- Draw the common normals between every two adjacent joint axes. Except for the first and last joint axes, every joint axis should have two incident common normals, one with the $(i - 1)$ th and the other with the $(i + 1)$ th joint axis.

3. Establish the base coordinate system such that the z_0 -axis is aligned with the first joint axis, the x_0 -axis is perpendicular to the z_0 -axis, and the y_0 -axis is determined by the right-hand rule.
4. Establish the n th hand coordinate system such that the x_n -axis is perpendicular to the last joint axis. The z_n -axis is usually chosen in the direction of approach of the end effector.
5. Attach a Cartesian coordinate system to the distal end of all the other links as follows:
 - The z_i -axis is aligned with the $(i + 1)$ th joint axis.
 - The x_i -axis is defined along the common normal between the i th and $(i + 1)$ th joint axes, pointing from the i th to the $(i + 1)$ th joint axis. If the joint axes are parallel, the x_i -axis can be chosen anywhere perpendicular to the two joint axes. In the case of two intersecting joint axes, the x_i -axis can be defined either in the direction of the vector cross product $\mathbf{z}_{i-1} \times \mathbf{z}_i$ or in the opposite direction, and the origin is located at the point of intersection.
 - The y_i -axis is defined according to the right-hand rule.
6. Determine the link parameters and joint variables, a_i , α_i , θ_i , and d_i .

There are $n + 1$ coordinate systems for an n -dof manipulator. However, if additional reference coordinate systems are defined, they can be related to one of the coordinate systems above by a transformation matrix. We note that John Craig used a different convention; he attached the i th coordinate system to the proximal end of link i , which results in a different homogeneous transformation matrix.

2.3 DENAVIT-HARTENBERG HOMOGENEOUS TRANSFORMATION MATRICES

Having established a coordinate system to each link of a manipulator, a 4×4 transformation matrix relating two successive coordinate systems can be established. Observation of Fig. 2.2 reveals that the i th coordinate system can be thought of as being displaced from the $(i - 1)$ th coordinate system by the following successive rotations and translations.

1. The $(i - 1)$ th coordinate system is translated along the z_{i-1} -axis a distance d_i . This brings the origin O_{i-1} into coincidence with H_{i-1} . The corresponding transformation matrix is

$$T(z, d) = \begin{bmatrix} 1 & 0 & 0 & 0 \\ 0 & 1 & 0 & 0 \\ 0 & 0 & 1 & d_i \\ 0 & 0 & 0 & 1 \end{bmatrix}.$$

2. The displaced $(i - 1)$ th coordinate system is rotated about the z_{i-1} -axis an angle θ_i , which brings the x_{i-1} -axis into alignment with the x_i -axis. The corresponding transformation matrix is

$$T(z, \theta) = \begin{bmatrix} c\theta_i & -s\theta_i & 0 & 0 \\ s\theta_i & c\theta_i & 0 & 0 \\ 0 & 0 & 1 & 0 \\ 0 & 0 & 0 & 1 \end{bmatrix}.$$

3. The displaced $(i - 1)$ th coordinate system is translated along the x_i -axis a distance a_i . This brings the origin O_{i-1} into coincidence with O_i . The corresponding transformation matrix is

$$T(x, a) = \begin{bmatrix} 1 & 0 & 0 & a_i \\ 0 & 1 & 0 & 0 \\ 0 & 0 & 1 & 0 \\ 0 & 0 & 0 & 1 \end{bmatrix}.$$

4. The displaced $(i - 1)$ th coordinate system is rotated about the x_i -axis an angle α_i , which brings the two coordinate systems into complete coincidence. The corresponding transformation matrix is

$$T(x, \alpha) = \begin{bmatrix} 1 & 0 & 0 & 0 \\ 0 & c\alpha_i & -s\alpha_i & 0 \\ 0 & s\alpha_i & c\alpha_i & 0 \\ 0 & 0 & 0 & 1 \end{bmatrix}.$$

We may think of the transformations above as four basic transformations about the moving coordinate axes. Therefore, the resulting transformation matrix, ${}^{i-1}A_i$, is given by

$${}^{i-1}A_i = T(z, d)T(z, \theta)T(x, a)T(x, \alpha). \quad (2.1)$$

Expanding Eq. (2.1), we obtain

$${}^{i-1}A_i = \begin{bmatrix} c\theta_i & -c\alpha_i s\theta_i & s\alpha_i s\theta_i & a_i c\theta_i \\ s\theta_i & c\alpha_i c\theta_i & -s\alpha_i c\theta_i & a_i s\theta_i \\ 0 & s\alpha_i & c\alpha_i & d_i \\ 0 & 0 & 0 & 1 \end{bmatrix}. \quad (2.2)$$

Equation (2.2) is called the *Denavit–Hartenberg (D-H) transformation matrix*. The trailing subscript i and the leading superscript $i - 1$ denote that the transformation takes place from the i th coordinate system to the $(i - 1)$ th coordinate system.

Let the homogeneous coordinates of the position vector of a point relative to the i th coordinate system be denoted by ${}^i\mathbf{p} = [p_x, p_y, p_z, 1]^T$. Also let the homogeneous coordinates of a unit vector expressed in the i th coordinate system be denoted by ${}^i\mathbf{u} = [u_x, u_y, u_z, 0]^T$. Then the transformation of a position vector and a unit vector from the i th to the $(i - 1)$ th coordinate system can be written as

$${}^{i-1}\mathbf{p} = {}^{i-1}\mathbf{A}_i {}^i\mathbf{p}, \quad (2.3)$$

$${}^{i-1}\mathbf{u} = {}^{i-1}\mathbf{A}_i {}^i\mathbf{u}. \quad (2.4)$$

Note that the leading superscript is used to indicate the coordinate system with respect to which a vector is expressed. Although the transformation matrix A is not orthogonal, the inverse transformation exists and is given by

$${}^i\mathbf{A}_{i-1} = ({}^{i-1}\mathbf{A}_i)^{-1} = \begin{bmatrix} c\theta_i & s\theta_i & 0 & -a_i \\ -c\alpha_i s\theta_i & c\alpha_i c\theta_i & s\alpha_i & -d_i s\alpha_i \\ s\alpha_i s\theta_i & -s\alpha_i c\theta_i & c\alpha_i & -d_i c\alpha_i \\ 0 & 0 & 0 & 1 \end{bmatrix}. \quad (2.5)$$

Example 2.3.1 Planar 3-DOF Manipulator Figure 2.3 shows a 3-dof planar manipulator constructed with three revolute joints located at points O_0 , A , and P , respectively. A coordinate system is attached to each link. The (x_0, y_0, z_0) coordinate system is attached to the base with its origin located at the first joint pivot and the x -axis pointing to the right. Since the joint axes are all parallel to each other, all the twist angles α_i and translational distances d_i are zero.

For the coordinate systems chosen, the link parameters are given in Table 2.1. The D-H transformation matrices are obtained by substituting the D-H link parameters into Eq. (2.2):

$${}^0\mathbf{A}_1 = \begin{bmatrix} c\theta_1 & -s\theta_1 & 0 & a_1 c\theta_1 \\ s\theta_1 & c\theta_1 & 0 & a_1 s\theta_1 \\ 0 & 0 & 1 & 0 \\ 0 & 0 & 0 & 1 \end{bmatrix}, \quad (2.6)$$

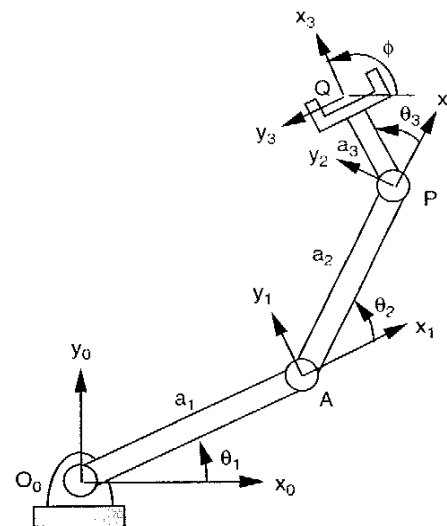


FIGURE 2.3. Planar 3-dof manipulator.

$${}^1\mathbf{A}_2 = \begin{bmatrix} c\theta_2 & -s\theta_2 & 0 & a_2 c\theta_2 \\ s\theta_2 & c\theta_2 & 0 & a_2 s\theta_2 \\ 0 & 0 & 1 & 0 \\ 0 & 0 & 0 & 1 \end{bmatrix}, \quad (2.7)$$

$${}^2\mathbf{A}_3 = \begin{bmatrix} c\theta_3 & -s\theta_3 & 0 & a_3 c\theta_3 \\ s\theta_3 & c\theta_3 & 0 & a_3 s\theta_3 \\ 0 & 0 & 1 & 0 \\ 0 & 0 & 0 & 1 \end{bmatrix}. \quad (2.8)$$

Example 2.3.2 SCARA Arm The SCARA arm is an important type of 4-dof manipulator. It has been produced by several companies, including Adept

TABLE 2.1. D-H Parameters of a 3-DOF Manipulator

Joint i	α_i	a_i	d_i	θ_i
1	0	a_1	0	θ_1
2	0	a_2	0	θ_2
3	0	a_3	0	θ_3

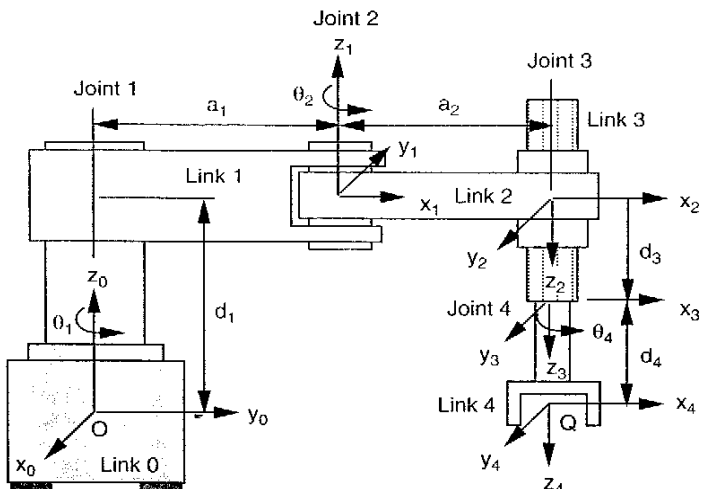


FIGURE 2.4. Schematic diagram of a SCARA arm.

Technology, IBM, Seiko, and others. A SCARA arm is constructed with four joint axes parallel to each other. The first two and the fourth are revolute joints, and the third is a prismatic joint. Figure 2.4 shows a schematic diagram of a SCARA arm. For the coordinate systems established in the figure, the corresponding link parameters are listed in Table 2.2.

Substituting the D-H link parameters into Eq. (2.2), we obtain the D-H transformation matrices:

$${}^0A_1 = \begin{bmatrix} c\theta_1 & -s\theta_1 & 0 & a_1 c\theta_1 \\ s\theta_1 & c\theta_1 & 0 & a_1 s\theta_1 \\ 0 & 0 & 1 & d_1 \\ 0 & 0 & 0 & 1 \end{bmatrix}, \quad (2.9)$$

TABLE 2.2. D-H Parameters of the SCARA Arm

Joint <i>i</i>	α_i	a_i	d_i	θ_i
1	0	a_1	d_1	θ_1
2	π	a_2	0	θ_2
3	0	0	d_3	0
4	0	0	d_4	θ_4

$${}^1A_2 = \begin{bmatrix} c\theta_2 & s\theta_2 & 0 & a_2 c\theta_2 \\ s\theta_2 & -c\theta_2 & 0 & a_2 s\theta_2 \\ 0 & 0 & -1 & 0 \\ 0 & 0 & 0 & 1 \end{bmatrix}, \quad (2.10)$$

$${}^2A_3 = \begin{bmatrix} 1 & 0 & 0 & 0 \\ 0 & 1 & 0 & 0 \\ 0 & 0 & 1 & d_3 \\ 0 & 0 & 0 & 1 \end{bmatrix}, \quad (2.11)$$

$${}^3A_4 = \begin{bmatrix} c\theta_4 & -s\theta_4 & 0 & 0 \\ s\theta_4 & c\theta_4 & 0 & 0 \\ 0 & 0 & 1 & d_4 \\ 0 & 0 & 0 & 1 \end{bmatrix}. \quad (2.12)$$

In this robot, the joint variables are θ_1 , θ_2 , d_3 , and θ_4 . The first two joint variables control the x and y coordinates, the third joint variable controls the z coordinate, and the fourth joint variable controls the orientation of the end effector. Since the robot has only 4 degrees of freedom, the orientation of the end effector cannot be specified arbitrarily. As a matter of fact, the z_4 -axis must be always pointing in the negative z_0 direction. Although the SCARA robot has only 4 degrees of freedom, it is very useful for assembling components on a plane such as a PC board.

2.4 LOOP-CLOSURE EQUATIONS

In a study of the kinematics of robot manipulators, we are interested in deriving an algebraic equation relating the location of the end effector to the joint variables. The location of the end effector can be specified by the following 4×4 homogeneous transformation matrix:

$${}^0A_n = \begin{bmatrix} \mathbf{u} & \mathbf{v} & \mathbf{w} & \mathbf{q} \\ 0 & 0 & 0 & 1 \end{bmatrix}, \quad (2.13)$$

where the upper right 3×1 submatrix describes the position of a reference point Q and the upper left 3×3 submatrix describes the orientation of the end effector. The orientation of the end effector can be specified in terms of three Euler angles, or the direction cosines of the three end-effector coordinate axes, u , v , and w . If the $w-u-w$ Euler angles are used, for example, the elements of the upper left 3×3 submatrix are given by

$$u_x = c\phi c\psi - s\phi c\theta\psi,$$

$$u_y = s\phi c\psi + c\phi c\theta\psi,$$

$$\begin{aligned}
 u_x &= s\theta s\psi, \\
 v_x &= c\phi s\psi - s\phi c\theta c\psi, \\
 v_y &= -s\phi s\psi + c\phi c\theta c\psi, \\
 v_z &= s\theta c\psi, \\
 w_x &= s\phi s\theta, \\
 w_y &= -c\phi s\theta, \\
 w_z &= c\theta.
 \end{aligned} \tag{2.14}$$

If the direction cosines are used, \mathbf{u} , \mathbf{v} , and \mathbf{w} represent three unit vectors directed along the three coordinate axes of the hand coordinate system and expressed in the base coordinate system.

From the geometry of the links, the transformation matrix 0A_n above can be thought of as the resultant of a series of coordinate transformations beginning from the base coordinate system to the end-effector coordinate system. That is,

$${}^0A_1 {}^1A_2 {}^2A_3 \cdots {}^{n-1}A_n = {}^0A_n. \tag{2.15}$$

Equation (2.15) is called the *loop-closure equation* of a serial manipulator. It contains 16 scalar equations, four of which are trivial. Equating the upper right 3×1 submatrix results in three independent equations, representing the position of the end effector. Equating the elements of the upper left 3×3 submatrix results in nine equations, representing the orientation of the end effector. However, only three of the nine orientation equations are independent because of the orthogonal conditions.

The loop-closure equation, Eq. (2.15), can be used to solve both direct and inverse kinematics problems. For direct kinematics, the joint variables are given and the problem is to find where the end effector is with respect to the base coordinate system. This can be accomplished by multiplying the D-H matrices on the left-hand side of the equation. For the inverse kinematics, the end-effector location (i.e., 0A_n) is given and the problem is to find the joint variables needed to bring the end effector to the desired location. The problem becomes very nonlinear. In what follows, we concentrate on the inverse kinematics problem.

Example 2.4.1 Scrbot Robot Figure 2.5 shows a schematic diagram of the Scrbot robot. In this diagram, the second, third, and fourth joint axes are parallel to one another and point into the paper at points A, B, and P, respectively. The first joint axis points up vertically, and the fifth joint axis intersects the fourth perpendicularly. We wish to find the overall transformation matrix for the robot.

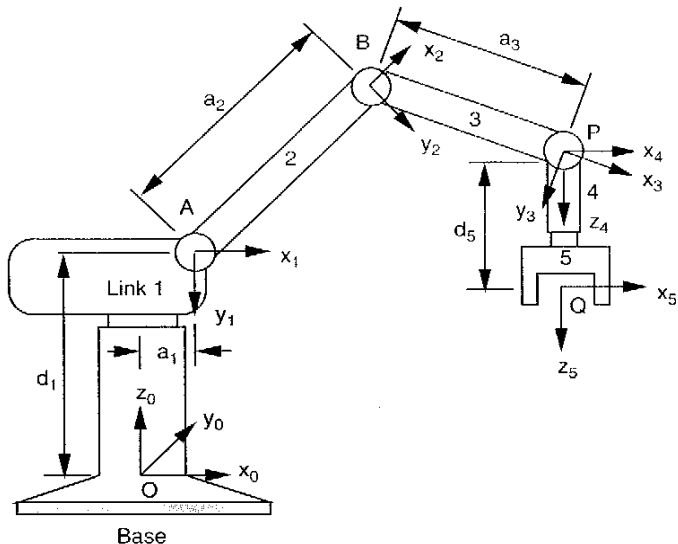


FIGURE 2.5. Schematic diagram of the Scrbot robot.

Using the coordinate systems established in Fig. 2.5, the corresponding link parameters are listed in Table 2.3. Substituting the D-H link parameters into Eq. (2.2), we obtain the D-H transformation matrices:

$${}^0A_1 = \begin{bmatrix} c\theta_1 & 0 & -s\theta_1 & a_1 c\theta_1 \\ s\theta_1 & 0 & c\theta_1 & a_1 s\theta_1 \\ 0 & -1 & 0 & d_1 \\ 0 & 0 & 0 & 1 \end{bmatrix}, \tag{2.16}$$

TABLE 2.3. D-H Parameters of a 5-DOF Manipulator

Joint i	α_i	a_i	d_i	θ_i
1	$-\pi/2$	a_1	d_1	θ_1
2	0	a_2	0	θ_2
3	0	a_3	0	θ_3
4	$-\pi/2$	0	0	θ_4
5	0	0	d_5	θ_5

$${}^1A_2 = \begin{bmatrix} c\theta_2 & -s\theta_2 & 0 & a_2 c\theta_2 \\ s\theta_2 & c\theta_2 & 0 & a_2 s\theta_2 \\ 0 & 0 & 1 & 0 \\ 0 & 0 & 0 & 1 \end{bmatrix}, \quad (2.17)$$

$${}^2A_3 = \begin{bmatrix} c\theta_3 & -s\theta_3 & 0 & a_3 c\theta_3 \\ s\theta_3 & c\theta_3 & 0 & a_3 s\theta_3 \\ 0 & 0 & 1 & 0 \\ 0 & 0 & 0 & 1 \end{bmatrix}, \quad (2.18)$$

$${}^3A_4 = \begin{bmatrix} c\theta_4 & 0 & -s\theta_4 & 0 \\ s\theta_4 & 0 & c\theta_4 & 0 \\ 0 & -1 & 0 & 0 \\ 0 & 0 & 0 & 1 \end{bmatrix}, \quad (2.19)$$

$${}^4A_5 = \begin{bmatrix} c\theta_5 & -s\theta_5 & 0 & 0 \\ s\theta_5 & c\theta_5 & 0 & 0 \\ 0 & 0 & 1 & d_5 \\ 0 & 0 & 0 & 1 \end{bmatrix}. \quad (2.20)$$

Multiplying Eqs. (2.17), (2.18), and (2.19) yields

$${}^1A_4 = \begin{bmatrix} c\theta_{234} & 0 & -s\theta_{234} & a_3 c\theta_{23} + a_2 c\theta_2 \\ s\theta_{234} & 0 & c\theta_{234} & a_3 s\theta_{23} + a_2 s\theta_2 \\ 0 & -1 & 0 & 0 \\ 0 & 0 & 0 & 1 \end{bmatrix}, \quad (2.21)$$

where $c\theta_{ij} = \cos(\theta_i + \theta_j)$, $s\theta_{ij} = \sin(\theta_i + \theta_j)$, $c\theta_{ijk} = \cos(\theta_i + \theta_j + \theta_k)$, and $s\theta_{ijk} = \sin(\theta_i + \theta_j + \theta_k)$.

Note that Eq. (2.21) provides a transformation from the fourth coordinate system to the first coordinate system. We may treat θ_2 , θ_{23} , and θ_{234} as new variables. In this way, the orientation submatrix contains only one variable, θ_{234} , while the position submatrix contains two variables, θ_2 and θ_{23} . This important fact can be used for deriving a closed-form solution for any manipulator with three consecutive parallel joint axes.

Multiplying Eqs. (2.16), (2.21), and (2.20) yields the elements of the overall transformation matrix 0A_5 :

$$u_x = c\theta_1 c\theta_{234} c\theta_5 + s\theta_1 s\theta_5,$$

$$u_y = s\theta_1 c\theta_{234} c\theta_5 - c\theta_1 s\theta_5,$$

$$u_z = -s\theta_{234} c\theta_5,$$

$$v_x = -c\theta_1 c\theta_{234} s\theta_5 + s\theta_1 c\theta_5,$$

$$v_y = -s\theta_1 c\theta_{234} s\theta_5 - c\theta_1 c\theta_5,$$

$$v_z = s\theta_{234} s\theta_5,$$

$$w_x = -c\theta_1 s\theta_{234},$$

$$w_y = -s\theta_1 s\theta_{234},$$

$$w_z = -c\theta_{234},$$

$$q_x = c\theta_1(a_1 + a_2 c\theta_2 + a_3 c\theta_{23} - d_5 s\theta_{234}),$$

$$q_y = s\theta_1(a_1 + a_2 c\theta_2 + a_3 c\theta_{23} - d_5 s\theta_{234}),$$

$$q_z = d_1 - a_2 s\theta_2 - a_3 s\theta_{23} - d_5 c\theta_{234}. \quad (2.22)$$

Since this is a 5-dof manipulator, only five of the six parameters of the end effector can be specified. Very often, the desired position of a point and the direction of a line in the end effector (e.g., the position of point Q and the direction of x_5 -axis) are specified. Five-dof manipulators are useful for spray painting, spot welding, and sealant applications for which only the position and direction of a line are essential.

2.5 OTHER COORDINATE SYSTEMS

In the preceding section, the z_0 -axis of the base coordinate system was chosen to be in line with the first joint axis, and the z_n -axis of the hand coordinate system was chosen to be in the direction of approach. If an additional coordinate system is defined in the base with a transformation matrix ${}^{\text{ref}}A_0$, and another coordinate system is defined in the tool frame with a transformation matrix ${}^nA_{\text{tool}}$, the overall loop-closure equation can be modified as

$${}^{\text{ref}}A_{\text{tool}} = {}^{\text{ref}}A_0 {}^0A_n {}^nA_{\text{tool}}, \quad (2.23)$$

where ${}^{\text{ref}}A_0$ and ${}^nA_{\text{tool}}$ are constant transformation matrices.

2.6 DENAVIT-HARTENBERG METHOD

Although the loop-closure equation, Eq. (2.15), can be applied to solve the inverse kinematics problem, in practice it is rarely solved in its present form. In general, if there are three intersecting joint axes, we may work with the position of the point of intersection first, thereby avoiding the joint variables associated with the three intersecting axes. If there are three parallel joint axes, we may combine the three joint variables as illustrated in the Scorbot

robot example. We may also pre- or postmultiply the loop-closure equation by the inverse of the matrix iA_i to obtain alternative loop-closure equations, such as

$$({}^0A_1)^{-1}{}^0A_n = {}^1A_2 {}^2A_3 \dots {}^{n-1}A_n, \quad (2.24)$$

$$({}^1A_2)^{-1}({}^0A_1)^{-1}{}^0A_n = {}^2A_3 {}^3A_4 \dots {}^{n-1}A_n, \quad (2.25)$$

$$({}^2A_3)^{-1}({}^1A_2)^{-1}({}^0A_1)^{-1}{}^0A_n = {}^3A_4 {}^4A_5 \dots {}^{n-1}A_n. \quad (2.26)$$

One reason for rearranging the loop-closure equation is to redistribute the unknown variables on both sides of the equation as evenly as possible. Another reason is to take advantage of some special conditions, such as three consecutive intersecting joint axes or three consecutive parallel joint axes. In many cases, the equation becomes decoupled and a closed-form solution can be derived.

2.6.1 Position Analysis of a Planar 3-DOF Manipulator

For the planar 3-dof manipulator shown in Fig. 2.3, the overall transformation matrix is given by

$${}^0A_3 = {}^0A_1 {}^1A_2 {}^2A_3. \quad (2.27)$$

Substituting Eqs. (2.6) through (2.8) into (2.27), we obtain

$${}^0A_3 = \begin{bmatrix} c\theta_{123} & -s\theta_{123} & 0 & a_1c\theta_1 + a_2c\theta_{12} + a_3c\theta_{123} \\ s\theta_{123} & c\theta_{123} & 0 & a_1s\theta_1 + a_2s\theta_{12} + a_3s\theta_{123} \\ 0 & 0 & 1 & 0 \\ 0 & 0 & 0 & 1 \end{bmatrix}. \quad (2.28)$$

(a) Direct Kinematics. The position vector of the origin Q expressed in the end-effector coordinate system is given by ${}^3q = [0, 0, 0, 1]^T$. Let the position vector of Q with respect to the base coordinate system be ${}^0q = [q_x, q_y, q_z, 1]^T$. Then we can relate 3q to 0q by the following transformation:

$$\begin{bmatrix} q_x \\ q_y \\ q_z \\ 1 \end{bmatrix} = {}^0A_3 \begin{bmatrix} 0 \\ 0 \\ 0 \\ 1 \end{bmatrix} = \begin{bmatrix} a_1c\theta_1 + a_2c\theta_{12} + a_3c\theta_{123} \\ a_1s\theta_1 + a_2s\theta_{12} + a_3s\theta_{123} \\ 0 \\ 1 \end{bmatrix}. \quad (2.29)$$

Hence, given θ_1, θ_2 , and θ_3 , the position of point Q can be computed by Eq. (2.29). Similarly, the position vector of any other point in the end effector,

${}^3g = [g_x, g_y, 0, 1]^T$, is given by

$$\begin{bmatrix} g_x \\ g_y \\ g_z \\ 1 \end{bmatrix} = {}^0A_3 \begin{bmatrix} g_x \\ g_y \\ 0 \\ 1 \end{bmatrix} = \begin{bmatrix} g_x c\theta_{123} - g_y s\theta_{123} + a_1 c\theta_1 + a_2 c\theta_{12} + a_3 c\theta_{123} \\ g_x s\theta_{123} + g_y c\theta_{123} + a_1 s\theta_1 + a_2 s\theta_{12} + a_3 s\theta_{123} \\ 0 \\ 1 \end{bmatrix}. \quad (2.30)$$

From Eq. (2.28), we conclude that the orientation angle of the end effector is equal to $\theta_1 + \theta_2 + \theta_3$.

(b) Inverse Kinematics. For the inverse kinematics problem, the location of the end effector is given and the problem is to find the joint angles $\theta_i, i = 1, 2, 3$, necessary to bring the end effector to the desired location. For a planar 3-dof manipulator, the end effector can be specified in terms of the position of point Q and an orientation angle ϕ of the end effector. Hence the overall transformation matrix from the end-effector coordinate system to the base coordinate system, 0A_3 , is given by

$${}^0A_3 = \begin{bmatrix} c\phi & -s\phi & 0 & q_x \\ s\phi & c\phi & 0 & q_y \\ 0 & 0 & 1 & 0 \\ 0 & 0 & 0 & 1 \end{bmatrix}. \quad (2.31)$$

Inverse kinematics solutions can be obtained by equating the elements of Eq. (2.28) to that of (2.31). To find the orientation of the end effector, we equate the (1,1) and (2,1) elements of Eq. (2.28) to that of (2.31):

$$c\theta_{123} = c\phi, \quad (2.32)$$

$$s\theta_{123} = s\phi. \quad (2.33)$$

Hence

$$\theta_{123} = \theta_1 + \theta_2 + \theta_3 = \phi. \quad (2.34)$$

Next, we equate the (1,4) and (2,4) elements of Eq. (2.28) to that of (2.31):

$$p_x = a_1 c\theta_1 + a_2 c\theta_{12}, \quad (2.35)$$

$$p_y = a_1 s\theta_1 + a_2 s\theta_{12}, \quad (2.36)$$

where $p_x = q_x - a_3 c\phi$ and $p_y = q_y - a_3 s\phi$ denote the position vector of the point P located at the third joint axis shown in Fig. 2.3. Note that by using

this substitution, θ_3 disappears from Eqs. (2.35) and (2.36). From Fig. 2.3 we observe that the distance from point O to P is independent of θ_1 . Hence we can eliminate θ_1 by summing the squares of Eqs. (2.35) and (2.36); that is,

$$p_x^2 + p_y^2 = a_1^2 + a_2^2 + 2a_1a_2c\theta_2. \quad (2.37)$$

Solving Eq. (2.37) for θ_2 , we obtain

$$\theta_2 = \cos^{-1} \kappa, \quad (2.38)$$

where

$$\kappa = \frac{p_x^2 + p_y^2 - a_1^2 - a_2^2}{2a_1a_2}.$$

Equation (2.38) yields (1) two real roots if $|\kappa| < 1$, (2) one double root if $|\kappa| = 1$, and (3) no real roots if $|\kappa| > 1$. In general, if $\theta_2 = \theta_2^*$ is a solution, $\theta_2 = -\theta_2^*$ is also a solution, where $\pi \geq \theta_2^* \geq 0$. We call $\theta_2 = \theta_2^*$ the elbow-down solution and $\theta_2 = -\theta_2^*$ the elbow-up solution. If $|\kappa| = 1$, the arm is in a fully stretched or folded configuration. If $|\kappa| > 1$, the position is not reachable.

Corresponding to each θ_2 , we can solve θ_1 by expanding Eqs. (2.35) and (2.36) as follows:

$$(a_1 + a_2c\theta_2)c\theta_1 - (a_2s\theta_2)s\theta_1 = p_x, \quad (2.39)$$

$$(a_2s\theta_2)c\theta_1 + (a_1 + a_2c\theta_2)s\theta_1 = p_y. \quad (2.40)$$

Solving Eqs. (2.39) and (2.40) for $c\theta_1$ and $s\theta_1$, yields

$$c\theta_1 = \frac{p_x(a_1 + a_2c\theta_2) + p_ya_2s\theta_2}{\Delta},$$

$$s\theta_1 = \frac{-p_xa_2s\theta_2 + p_y(a_1 + a_2c\theta_2)}{\Delta}.$$

where $\Delta = a_1^2 + a_2^2 + 2a_1a_2c\theta_2$. Hence, corresponding to each θ_2 , we obtain a unique solution for θ_1 :

$$\theta_1 = \text{Atan2}(s\theta_1, c\theta_1). \quad (2.41)$$

In a computer program we may use the function $\text{Atan2}(x, y)$ to obtain a unique solution for θ_1 . However, the solution may be real or complex. A complex solution corresponds to an end-effector location that is not reachable by the manipulator. Once θ_1 and θ_2 are known, Eq. (2.34) yields a unique solution for θ_3 . Hence, corresponding to a given end-effector location, there are

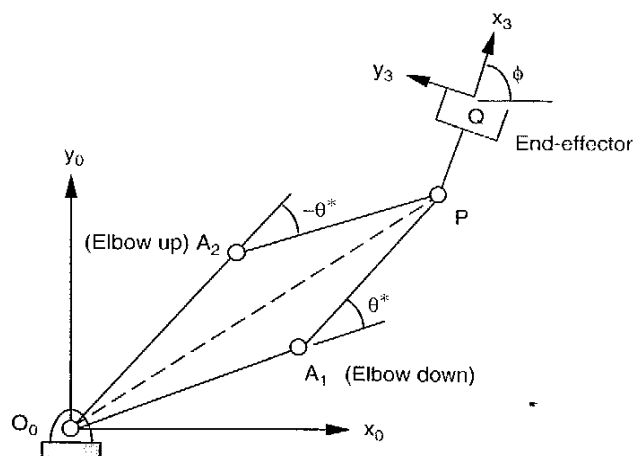


FIGURE 2.6. Two possible inverse kinematics solutions.

generally two real inverse kinematics solutions, one being the reflection of the other about a line connecting points O and P , as illustrated in Fig. 2.6.

Vector-Loop Method. Although the D-H method of analysis is a very powerful tool, the inverse kinematics problem can often be solved by other methods, such as the vector-loop method. For example, the vector-loop method becomes more efficient for analysis of the 3-dof planar manipulator shown in Fig. 2.3. For convenience, the manipulator has been resketched as shown in Fig. 2.7.

Using vector algebra, the position vector of the wrist center P can be related to the origin Q of the end effector by the equations

$$p_x = q_x - a_3c\phi, \quad (2.42)$$

$$p_y = q_y - a_3s\phi. \quad (2.43)$$

From Fig. 2.7, we observe that the orientation angle ϕ is related to the joint angles by

$$\phi = \theta_1 + \theta_2 + \theta_3. \quad (2.44)$$

We now form a fictitious vector loop equation as follows:

$$\overline{OA} + \overline{AP} = \overline{OP}. \quad (2.45)$$

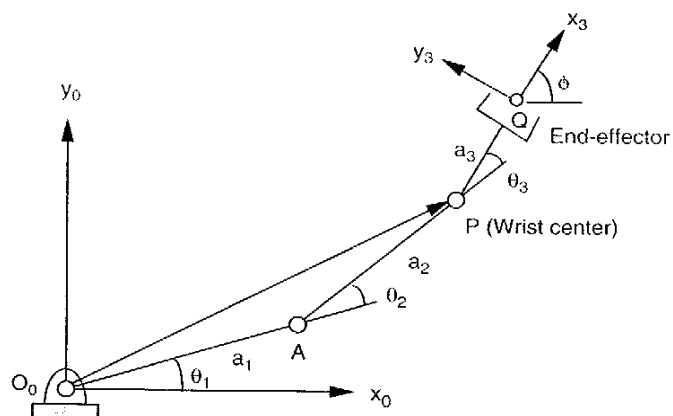


FIGURE 2.7. Vector loop of the planar 3-dof manipulator.

Taking the x and y components of Eq. (2.45) yields

$$p_x = a_1 c\theta_1 + a_2 c\theta_{12}, \quad (2.46)$$

$$p_y = a_1 s\theta_1 + a_2 s\theta_{12}. \quad (2.47)$$

Note that using the vector-loop method, we have derived Eqs. (2.35) and (2.36) with very little effort.

2.6.2 Position Analysis of the Scorbot Robot

For the Scorbot robot shown in Fig. 2.5, the overall transformation matrix is given by Eq. (2.22). We wish to solve the direct and inverse kinematics problems.

(a) Direct Kinematics. For the direct kinematics problem, we simply substitute the given joint angles into Eq. (2.22) to obtain the end-effector position, (q_x, q_y, q_z) , and the orientation in terms of the three unit vectors (u_x, u_y, u_z) , (v_x, v_y, v_z) , and (w_x, w_y, w_z) .

(b) Inverse Kinematics. For the inverse kinematics problem, only 5 of the 12 parameters associated with the end-effector position vector and rotation matrix can be specified at will. This is because the manipulator has only 5 degrees of freedom. It is obvious that the position vector \mathbf{q} and the approach

vector \mathbf{w} cannot be specified simultaneously, due to the fact that \mathbf{q} and \mathbf{w} together depend only on 4 degrees of freedom of the manipulator. For this exercise we assume that \mathbf{q} and \mathbf{u} are specified and that the other two unit vectors, \mathbf{v} and \mathbf{w} , are to be determined after the joint angles are found.

Although Eq. (2.22) can be used to solve the inverse kinematics, in what follows we take a more straightforward approach by multiplying both sides of the loop-closure equation by ${}^0A_1^{-1}$; that is,

$${}^0A_1^{-1} {}^0A_5 = {}^1A_2 {}^2A_3 {}^3A_4 {}^4A_5. \quad (2.48)$$

Equating the first column of Eq. (2.48), we obtain

$$u_x c\theta_1 + u_y s\theta_1 = c\theta_{234} c\theta_5, \quad (2.49)$$

$$-u_z = s\theta_{234} c\theta_5, \quad (2.50)$$

$$-u_x s\theta_1 + u_y c\theta_1 = -s\theta_5. \quad (2.51)$$

Similarly, equating the fourth column of Eq. (2.48), we obtain

$$q_x c\theta_1 + q_y s\theta_1 - a_1 = a_2 c\theta_2 + a_3 c\theta_{23} - d_5 s\theta_{234}, \quad (2.52)$$

$$-q_z + d_1 = a_2 s\theta_2 + a_3 s\theta_{23} + d_5 c\theta_{234}, \quad (2.53)$$

$$-q_x s\theta_1 + q_y c\theta_1 = 0. \quad (2.54)$$

The first joint angle, θ_1 , is obtained immediately from Eq. (2.54):

$$\theta_1 = \tan^{-1} \frac{q_y}{q_x}. \quad (2.55)$$

There are two solutions; that is, if $\theta_1 = \theta_1^*$ is a solution, $\theta_1 = \pi + \theta_1^*$ is also a solution. Once θ_1 is found, two solutions for θ_5 are obtained from Eq. (2.51):

$$\theta_5 = \sin^{-1} (u_x s\theta_1 - u_y c\theta_1). \quad (2.56)$$

That is, if $\theta_5 = \theta_5^*$ is a solution, $\theta_5 = \pi - \theta_5^*$ is also a solution.

Corresponding to each solution set of (θ_1, θ_5) , Eqs. (2.49) and (2.50) produce a unique solution of θ_{234} :

$$\theta_{234} = \text{Atan2} [-u_z / c\theta_5, (u_x c\theta_1 + u_y s\theta_1) / c\theta_5]. \quad (2.57)$$

Next, we solve Eqs. (2.52) and (2.53) for θ_2 and θ_3 . Equations (2.52) and (2.53) can be written

$$a_2 c \theta_2 + a_3 c \theta_{23} = k_1, \quad (2.58)$$

$$a_2 s \theta_2 + a_3 s \theta_{23} = k_2. \quad (2.59)$$

where $k_1 = q_x c \theta_1 + q_y s \theta_1 - a_1 + d_5 s \theta_{234}$ and $k_2 = -q_z + d_1 - d_5 c \theta_{234}$.

Summing the squares of Eqs. (2.58) and (2.59) yields

$$a_2^2 + a_3^2 + 2a_2 a_3 c \theta_3 = k_1^2 + k_2^2. \quad (2.60)$$

Hence

$$\theta_3 = \cos^{-1} \frac{k_1^2 + k_2^2 - a_2^2 - a_3^2}{2a_2 a_3}. \quad (2.61)$$

and there are two solutions of θ_3 ; that is, if $\theta_3 = \theta_3^*$ is a solution, $\theta_3 = -\theta_3^*$ is also a solution.

Once θ_3 is known, we can solve θ_2 by expanding Eqs. (2.58) and (2.59) as follows:

$$(a_2 + a_3 c \theta_3) c \theta_2 - (a_3 s \theta_3) s \theta_2 = k_1, \quad (2.62)$$

$$(a_3 s \theta_3) c \theta_2 + (a_2 + a_3 c \theta_3) s \theta_2 = k_2. \quad (2.63)$$

Solving Eqs. (2.62) and (2.63) for $c \theta_2$ and $s \theta_2$ yields

$$c \theta_2 = \frac{k_1(a_2 + a_3 c \theta_3) + k_2 a_3 s \theta_3}{a_2^2 + a_3^2 + 2a_2 a_3 c \theta_3},$$

$$s \theta_2 = \frac{-k_1 a_3 s \theta_3 + k_2(a_2 + a_3 c \theta_3)}{a_2^2 + a_3^2 + 2a_2 a_3 c \theta_3}.$$

Hence, corresponding to each solution set of $(\theta_1, \theta_3, \theta_5, \theta_{234})$, we obtain a unique solution of θ_2 :

$$\theta_2 = \text{Atan2}(s \theta_2, c \theta_2). \quad (2.64)$$

Finally, θ_4 is obtained by

$$\theta_4 = \theta_{234} - \theta_2 - \theta_3. \quad (2.65)$$

We conclude that corresponding to each given end-effector location, there are at most eight inverse kinematics solutions.

2.6.3 Position Analysis of the Fanuc S-900W Robot

Figure 2.8 shows a 6-dof manipulator manufactured by Fanuc. In this manipulator, the first joint axis points up vertically along the z_0 -axis, the second joint axis is perpendicular to the first joint axis with a small offset distance $a_1 = OA$, the third joint axis is parallel to the second with an offset distance $a_2 = AB$, and the fourth joint axis is perpendicular to the third joint axis with a small offset distance $a_3 = BC$. In addition, the last three joint axes intersect one another perpendicularly in sequence at a common point P , which is d_4 distance away from point C . This robot belongs to a special class of manipulators where the last three joint axes intersect at the wrist center. The kinematics problem for this type of manipulators can be partitioned into two subchains: one associated with the first three moving links and the other with the last three moving links. That is, in solving the inverse kinematics problem, the position of the wrist center can be solved independently of the orientation part, therefore reducing the complexity of the problem.

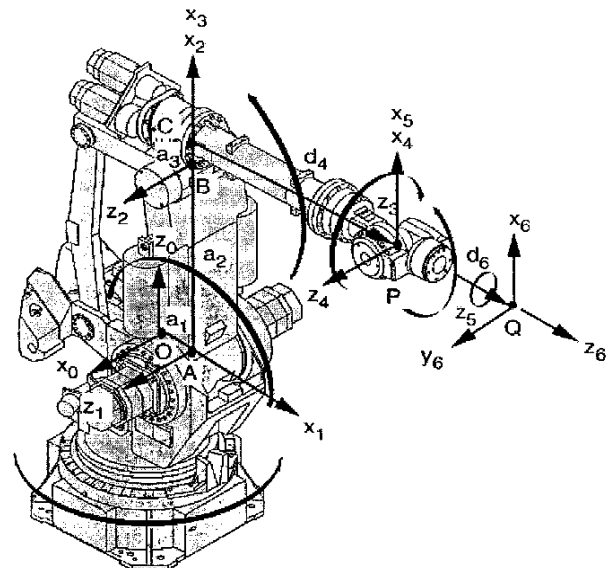


FIGURE 2.8. Fanuc S-900W robot. (Courtesy of Fanuc Robotics North America, Inc., Rochester Hills, Michigan.)

TABLE 2.4. D-H Parameters of the Fanuc S-900W Manipulator

Joint <i>i</i>	α_i	a_i	d_i	θ_i
1	$\pi/2$	a_1	0	θ_1
2	0	a_2	0	θ_2
3	$\pi/2$	a_3	0	θ_3
4	$-\pi/2$	0	d_4	θ_4
5	$\pi/2$	0	0	θ_5
6	0	0	d_6	θ_6

We note that this manipulator employs a four-bar linkage to drive the third joint. The four-bar linkage simply transmits the motion of the third motor mounted on the waist to the third joint. Otherwise, it has no effect on the kinematics of the manipulator. In the following analysis we neglect the effect of the four-bar linkage and treat the manipulator as a serial manipulator.

Using the coordinate systems established in Fig. 2.8, the corresponding link parameters are listed in Table 2.4. Substituting the D-H link parameters into Eq. (2.2), we obtain the D-H transformation matrices:

$${}^0A_1 = \begin{bmatrix} c\theta_1 & 0 & s\theta_1 & a_1 c\theta_1 \\ s\theta_1 & 0 & -c\theta_1 & a_1 s\theta_1 \\ 0 & 1 & 0 & 0 \\ 0 & 0 & 0 & 1 \end{bmatrix}, \quad (2.66)$$

$${}^1A_2 = \begin{bmatrix} c\theta_2 & -s\theta_2 & 0 & a_2 c\theta_2 \\ s\theta_2 & c\theta_2 & 0 & a_2 s\theta_2 \\ 0 & 0 & 1 & 0 \\ 0 & 0 & 0 & 1 \end{bmatrix}, \quad (2.67)$$

$${}^2A_3 = \begin{bmatrix} c\theta_3 & 0 & s\theta_3 & a_3 c\theta_3 \\ s\theta_3 & 0 & -c\theta_3 & a_3 s\theta_3 \\ 0 & 1 & 0 & 0 \\ 0 & 0 & 0 & 1 \end{bmatrix}, \quad (2.68)$$

$${}^3A_4 = \begin{bmatrix} c\theta_4 & 0 & -s\theta_4 & 0 \\ s\theta_4 & 0 & c\theta_4 & 0 \\ 0 & -1 & 0 & d_4 \\ 0 & 0 & 0 & 1 \end{bmatrix}, \quad (2.69)$$

$${}^4A_5 = \begin{bmatrix} c\theta_5 & 0 & s\theta_5 & 0 \\ s\theta_5 & 0 & -c\theta_5 & 0 \\ 0 & 1 & 0 & 0 \\ 0 & 0 & 0 & 1 \end{bmatrix}, \quad (2.70)$$

$${}^5A_6 = \begin{bmatrix} c\theta_6 & -s\theta_6 & 0 & 0 \\ s\theta_6 & c\theta_6 & 0 & 0 \\ 0 & 0 & 1 & d_6 \\ 0 & 0 & 0 & 1 \end{bmatrix}. \quad (2.71)$$

The end-effector location is given by

$${}^0A_6 = \begin{bmatrix} u_x & v_x & w_x & q_x \\ u_y & v_y & w_y & q_y \\ u_z & v_z & w_z & q_z \\ 0 & 0 & 0 & 1 \end{bmatrix}. \quad (2.72)$$

The loop-closure equation is obtained in two steps. First, we multiply Eqs. (2.66), (2.67), and (2.68):

$$\begin{aligned} {}^0A_3 &= {}^0A_1 {}^1A_2 {}^2A_3 \\ &= \begin{bmatrix} c\theta_1 c\theta_{23} & s\theta_1 & c\theta_1 s\theta_{23} & c\theta_1(a_1 + a_2 c\theta_2 + a_3 c\theta_{23}) \\ s\theta_1 c\theta_{23} & -c\theta_1 & s\theta_1 s\theta_{23} & s\theta_1(a_1 + a_2 c\theta_2 + a_3 c\theta_{23}) \\ s\theta_{23} & 0 & -c\theta_{23} & a_2 s\theta_2 + a_3 s\theta_{23} \\ 0 & 0 & 0 & 1 \end{bmatrix}. \end{aligned} \quad (2.73)$$

Next, we multiply Eqs. (2.69), (2.70), and (2.71):

$$\begin{aligned} {}^3A_6 &= {}^3A_4 {}^4A_5 {}^5A_6 \\ &= \begin{bmatrix} c\theta_4 c\theta_5 c\theta_6 - s\theta_4 s\theta_6 & -c\theta_4 c\theta_5 s\theta_6 - s\theta_4 c\theta_6 & c\theta_4 s\theta_5 & d_6 c\theta_4 s\theta_5 \\ s\theta_4 c\theta_5 c\theta_6 + c\theta_4 s\theta_6 & -s\theta_4 c\theta_5 s\theta_6 + c\theta_4 c\theta_6 & s\theta_4 s\theta_5 & d_6 s\theta_4 s\theta_5 \\ -s\theta_5 c\theta_6 & s\theta_5 s\theta_6 & c\theta_5 & d_4 + d_6 c\theta_5 \\ 0 & 0 & 0 & 1 \end{bmatrix}. \end{aligned} \quad (2.74)$$

Hence the resulting transformation matrix is given by

$${}^0A_6 = {}^0A_3 {}^3A_6, \quad (2.75)$$

where 0A_6 describes the end effector location.

Substituting Eqs. (2.73) and (2.74) into (2.75) yields the elements of 0A_6 as follows:

$$\begin{aligned} u_x &= c\theta_1 [c\theta_{23}(c\theta_4 c\theta_5 c\theta_6 - s\theta_4 s\theta_6) - s\theta_{23} s\theta_5 c\theta_6] + s\theta_1 (s\theta_4 c\theta_5 c\theta_6 + c\theta_4 s\theta_6), \\ u_y &= s\theta_1 [c\theta_{23}(c\theta_4 c\theta_5 c\theta_6 - s\theta_4 s\theta_6) - s\theta_{23} s\theta_5 c\theta_6] - c\theta_1 (s\theta_4 c\theta_5 c\theta_6 + c\theta_4 s\theta_6), \\ u_z &= s\theta_{23}(c\theta_4 c\theta_5 c\theta_6 - s\theta_4 s\theta_6) + c\theta_{23} s\theta_5 c\theta_6, \end{aligned}$$

$$\begin{aligned}
 v_x &= c\theta_1[-c\theta_{23}(c\theta_4c\theta_5s\theta_6 + s\theta_4c\theta_6) + s\theta_{23}s\theta_5s\theta_6] \\
 &\quad + s\theta_1(-s\theta_4c\theta_5s\theta_6 + c\theta_4c\theta_6), \\
 v_y &= s\theta_1[-c\theta_{23}(c\theta_4c\theta_5s\theta_6 + s\theta_4c\theta_6) + s\theta_{23}s\theta_5s\theta_6] \\
 &\quad - c\theta_1(-s\theta_4c\theta_5s\theta_6 + c\theta_4c\theta_6), \\
 v_z &= -s\theta_{23}(c\theta_4c\theta_5s\theta_6 + s\theta_4c\theta_6) - c\theta_{23}s\theta_5s\theta_6, \\
 w_x &= c\theta_1(c\theta_{23}c\theta_4s\theta_5 + s\theta_{23}c\theta_5) + s\theta_1s\theta_4s\theta_5, \\
 w_y &= s\theta_1(c\theta_{23}c\theta_4s\theta_5 + s\theta_{23}c\theta_5) - c\theta_1s\theta_4s\theta_5, \\
 w_z &= s\theta_{23}c\theta_4s\theta_5 - c\theta_{23}c\theta_5, \\
 q_x &= c\theta_1[a_1 + a_2c\theta_2 + a_3c\theta_{23} + d_4s\theta_{23} + d_6(c\theta_{23}c\theta_4s\theta_5 + s\theta_{23}c\theta_5)] \\
 &\quad + d_6s\theta_1s\theta_4s\theta_5, \\
 q_y &= s\theta_1[a_1 + a_2c\theta_2 + a_3c\theta_{23} + d_4s\theta_{23} + d_6(c\theta_{23}c\theta_4s\theta_5 + s\theta_{23}c\theta_5)] \\
 &\quad - d_6c\theta_1s\theta_4s\theta_5, \\
 q_z &= a_2s\theta_2 + a_3s\theta_{23} - d_4c\theta_{23} + d_6(s\theta_{23}c\theta_4s\theta_5 - c\theta_{23}c\theta_5).
 \end{aligned}$$

Although the equations above can be used to solve the inverse kinematics, they are highly nonlinear and difficult to solve. In what follows we present a more efficient method of solution by separating the wrist-center-position problem from the orientation problem.

(a) Wrist Center Position. Note that the last three joint axes intersect at the wrist center point P as shown in Fig. 2.8. Hence rotations of the last three joints do not affect the position of P . Figure 2.9 shows the end-effector coordinate system (x_6, y_6, z_6) , the wrist center P , and the vector relation between them.

The wrist center position with respect to and expressed in the end-effector coordinate system is

$${}^6\mathbf{p} = \overline{QP} = [0, 0, -d_6, 1]^T. \quad (2.76)$$

The wrist center position with respect to and expressed in the base coordinate system is

$${}^0\mathbf{p} = \overline{OP} = \begin{bmatrix} p_x \\ p_y \\ p_z \\ 1 \end{bmatrix} = \begin{bmatrix} q_x - d_6w_x \\ q_y - d_6w_y \\ q_z - d_6w_z \\ 1 \end{bmatrix}. \quad (2.77)$$

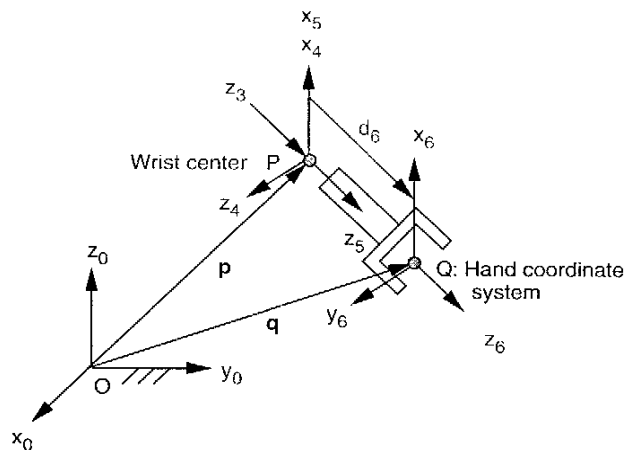


FIGURE 2.9. Hand coordinate system and wrist center position.

Hence, given the end-effector location, we can find the position of the wrist center point P with respect to the base coordinate system. Furthermore, we observe from Fig. 2.8 that the position of the wrist center P with respect to the link 3 coordinate system is given by

$${}^3\mathbf{p} = \overline{CP} = [0, 0, d_4, 1]^T. \quad (2.78)$$

Transforming ${}^3\mathbf{p}$ into the base coordinate system, we obtain

$${}^0\mathbf{p} = {}^0A_3 {}^3\mathbf{p}. \quad (2.79)$$

Equation (2.79) consists of three scalar equations in three unknowns. Hence the position and orientation of the inverse kinematics problem are decoupled.

Theoretically, we can solve Eq. (2.79) for the three joint angles. In what follows we take a simpler approach. Multiplying both sides Eq. (2.79) by the inverse of 0A_1 , we obtain

$$({}^0A_1)^{-1} {}^0\mathbf{p} = {}^1A_3 {}^3\mathbf{p}. \quad (2.80)$$

Substituting Eqs. (2.66) through (2.68) into (2.80) yields

$$p_x c\theta_1 + p_y s\theta_1 - a_1 = a_2 c\theta_2 + a_3 c\theta_{23} + d_4 s\theta_{23}, \quad (2.81)$$

$$p_z = a_2 s\theta_2 + a_3 s\theta_{23} - d_4 c\theta_{23}. \quad (2.82)$$

$$p_x s\theta_1 - p_y c\theta_1 = 0, \quad (2.83)$$

where p_x , p_y , and p_z are given by Eq. (2.77).

A solution for θ_1 is found immediately by solving Eq. (2.83).

$$\theta_1 = \tan^{-1} \frac{p_y}{p_x}, \quad (2.84)$$

Hence there are two solutions of θ_1 . Specifically, if $\theta_1 = \theta_1^*$ is a solution, $\theta_1 = \theta_1^* + \pi$ is also a solution, where $\pi \geq \theta_1^* \geq 0$. We call $\theta_1 = \theta_1^*$ the front-reach solution and $\theta_1 = \theta_1^* + \pi$ the back-reach solution. Because of the four-bar linkage and other mechanical constraints, the back-reach solution is physically impossible.

An observation of the kinematic structure reveals that the distance between point A and the wrist center P is independent of θ_1 and θ_2 , which implies that these two variables can be eliminated simultaneously. Summing the squares of Eqs. (2.81), (2.82), and (2.83), gives

$$\kappa_1 s\theta_3 + \kappa_2 c\theta_3 = \kappa_3, \quad (2.85)$$

where $\kappa_1 = 2a_2 d_4$, $\kappa_2 = 2a_2 a_3$, and $\kappa_3 = p_x^2 + p_y^2 + p_z^2 - 2p_x a_1 c\theta_1 - 2p_y a_1 s\theta_1 + a_1^2 - a_2^2 - a_3^2 - d_4^2$.

We can convert Eq. (2.85) into a polynomial by making use of the following trigonometric identities:

$$c\theta_3 = \frac{1 - t_3^2}{1 + t_3^2} \quad \text{and} \quad s\theta_3 = \frac{2t_3}{1 + t_3^2}, \quad \text{where} \quad t_3 = \tan \frac{\theta_3}{2}.$$

Substituting the trigonometric identities above into Eq. (2.85) yields

$$(\kappa_3 + \kappa_2)t_3^2 - 2\kappa_1 t_3 + (\kappa_3 - \kappa_2) = 0. \quad (2.86)$$

Hence

$$\frac{\theta_3}{2} = \tan^{-1} \frac{\kappa_1 \pm \sqrt{\kappa_1^2 + \kappa_2^2 - \kappa_3^2}}{\kappa_3 + \kappa_2}. \quad (2.87)$$

Equation (2.86) yields (1) two real roots if $\kappa_1^2 + \kappa_2^2 - \kappa_3^2 > 0$, (2) one double root if $\kappa_1^2 + \kappa_2^2 - \kappa_3^2 = 0$, and (3) no real roots if $\kappa_1^2 + \kappa_2^2 - \kappa_3^2 < 0$. When Eq. (2.86) yields a double root, the arm is either in a fully stretched or a folded-back configuration. On the other hand, if Eq. (2.86) yields no real roots, the position is not reachable. Figure 2.10 shows two different arm configurations, corresponding to the two solutions of θ_3 .

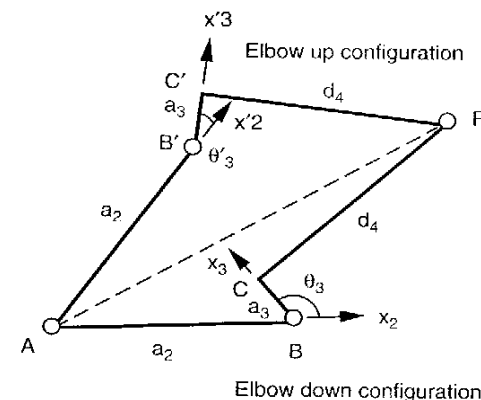


FIGURE 2.10. Two different arm configurations.

Once θ_1 and θ_3 are known, θ_2 can be obtained by back substitution. Expanding Eqs. (2.81) and (2.82), we obtain

$$\mu_1 c\theta_2 + v_1 s\theta_2 = \gamma_1, \quad (2.88)$$

$$\mu_2 c\theta_2 + v_2 s\theta_2 = \gamma_2, \quad (2.89)$$

where

$$\mu_1 = a_2 + a_3 c\theta_3 + d_4 s\theta_3,$$

$$v_1 = -a_3 s\theta_3 + d_4 c\theta_3,$$

$$\gamma_1 = p_x c\theta_1 + p_y s\theta_1 - a_1,$$

$$\mu_2 = a_3 s\theta_3 - d_4 c\theta_3,$$

$$v_2 = a_2 + a_3 c\theta_3 + d_4 s\theta_3,$$

$$\gamma_2 = p_z.$$

Therefore, we can solve Eqs. (2.88) and (2.89) for $c\theta_2$ and $s\theta_2$. Once $s\theta_2$ and $c\theta_2$ are found, a unique value of θ_2 is obtained by taking

$$\theta_2 = \text{Atan2}(s\theta_2, c\theta_2). \quad (2.90)$$

We conclude that given the wrist center position, mathematically there are at most four possible arm configurations, but due to the mechanical limits, only two are physically possible.

(b) End-Effector Orientation. Once θ_1 , θ_2 , and θ_3 are solved, 0A_3 is completely known. The remaining joint angles can be found by multiplying both sides of Eq. (2.75) by $({}^0A_3)^{-1}$:

$${}^3A_6 = ({}^0A_3)^{-1} {}^0A_6. \quad (2.91)$$

We note that the elements on the right-hand side of Eq. (2.91) are known, and only the rotation part of Eq. (2.91) is needed for computation of the last three joint angles. The rotation matrices 0R_3 and 3R_6 are given by the upper 3×3 submatrices of Eqs. (2.73) and (2.74), respectively.

Equating the 3×3 element of Eq. (2.91) yields

$$\theta_5 = \cos^{-1} r_{33}, \quad (2.92)$$

where $r_{33} = w_x c\theta_1 s\theta_{23} + w_y s\theta_1 s\theta_{23} - w_z c\theta_{23}$. Hence, corresponding to each solution set of θ_1 , θ_2 , and θ_3 , Eq. (2.92) yields (1) two real roots if $|r_{33}| < 1$, and (2) $\theta_5 = 0$ or π if $|r_{33}| = 1$. When $\theta_5 = 0$ or π , the sixth joint axis, z_5 , is in line with the fourth joint axis, z_3 , and the wrist is said to be in a *singular configuration*. The condition $|r_{33}| > 1$ cannot physically arise.

Assuming that $s\theta_5 \neq 0$, we can solve θ_4 and θ_6 as follows. Equating the 1×3 element of Eq. (2.91) yields

$$c\theta_4 = \frac{w_x c\theta_1 c\theta_{23} + w_y s\theta_1 c\theta_{23} + w_z s\theta_{23}}{s\theta_5}. \quad (2.93)$$

Equating the 2×3 element of Eq. (2.91) yields

$$s\theta_4 = \frac{w_x s\theta_1 - w_y c\theta_1}{s\theta_5}. \quad (2.94)$$

Hence, corresponding to each solution set of θ_1 , θ_2 , θ_3 , and θ_5 , Eqs. (2.93) and (2.94) yield a unique solution of θ_4 :

$$\theta_4 = \text{Atan2}(s\theta_4, c\theta_4). \quad (2.95)$$

Similarly, equating the 3×1 element of Eq. (2.91) yields

$$c\theta_6 = -\frac{u_x c\theta_1 s\theta_{23} + u_y s\theta_1 s\theta_{23} - u_z c\theta_{23}}{s\theta_5}. \quad (2.96)$$

Equating the 3×2 element of Eq. (2.91) yields

$$s\theta_6 = \frac{v_x c\theta_1 s\theta_{23} + v_y s\theta_1 s\theta_{23} - v_z c\theta_{23}}{s\theta_5}. \quad (2.97)$$

Hence, corresponding to each solution set of θ_1 , θ_2 , θ_3 , θ_4 , and θ_5 , Eqs. (2.96) and (2.97) yield a unique solution of θ_6 :

$$\theta_6 = \text{Atan2}(s\theta_6, c\theta_6). \quad (2.98)$$

We conclude that corresponding to each solution set of the first three joint angles, there are two possible wrist configurations. Since there are four possible upper arm configurations, a total of eight manipulator postures are possible. However, due to mechanical limits, fewer than eight manipulator postures are physically realizable. When $s\theta_5 = 0$, Eqs. (2.93) through (2.98) degenerate. For such a singular condition, only the sum or difference of θ_4 and θ_6 can be computed.

2.6.4 Tsai and Morgan's Solution

In this section we outline a solution method developed by Tsai and Morgan (1985), who reduced the problem to a system of four equations and then employed a numerical method, known as the *homotopy method*, to find all solutions to the inverse kinematics of a general 6R manipulator. They also derived closed-form solutions for manipulators in which three consecutive joint axes either intersect at a common point or are parallel to one another.

Figure 2.11 shows a general 6R manipulator where point Q denotes the origin and \mathbf{u} , \mathbf{v} , and \mathbf{w} denote three orthogonal unit vectors of the end effector coordinate system. Using the Denavit–Hartenberg method, a loop-closure equation can be written as

$${}^0A_1 {}^1A_2 {}^2A_3 {}^3A_4 {}^4A_5 {}^5A_6 = {}^0A_6. \quad (2.99)$$

For convenience, we introduce a position vector \mathbf{p} of the origin and a unit vector \mathbf{e} of the z_5 -axis of the fifth coordinate system as shown in Fig. 2.11. These two vectors can be expressed in the fifth coordinate system as ${}^5\mathbf{p} = [0, 0, 0, 1]^T$ and ${}^5\mathbf{e} = [0, 0, 1, 0]^T$, or in the fixed coordinate system as $\mathbf{p} = {}^0\mathbf{p} = [p_x, p_y, p_z, 1]^T$ and $\mathbf{e} = {}^0\mathbf{e} = [e_x, e_y, e_z, 0]^T$. Since both the point P and the vector \mathbf{e} are attached to the end effector, \mathbf{p} and \mathbf{e} can be computed from the given end-effector location as follows:

$$\begin{bmatrix} p_x \\ p_y \\ p_z \\ 1 \end{bmatrix} = {}^0A_6 {}^6A_5 \begin{bmatrix} 0 \\ 0 \\ 0 \\ 1 \end{bmatrix} = \begin{bmatrix} -u_x a_6 - (v_x s\alpha_6 + w_x c\alpha_6) d_6 + q_x \\ -u_y a_6 - (v_y s\alpha_6 + w_y c\alpha_6) d_6 + q_y \\ -u_z a_6 - (v_z s\alpha_6 + w_z c\alpha_6) d_6 + q_z \\ 1 \end{bmatrix}, \quad (2.100)$$

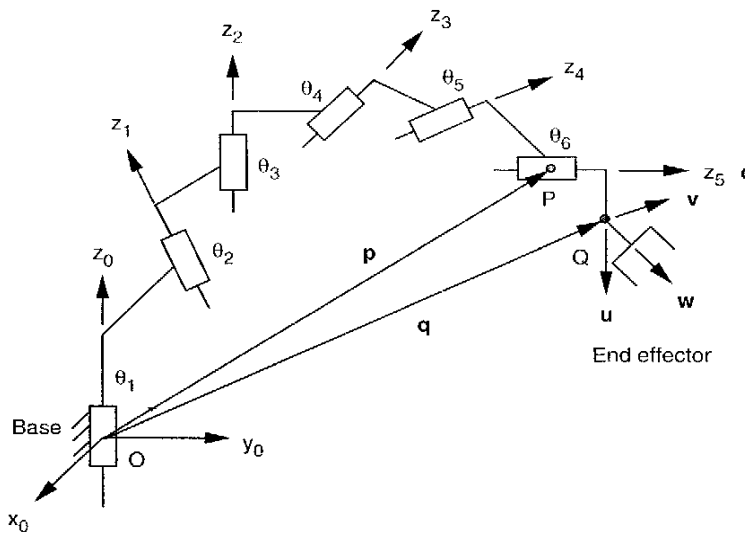


FIGURE 2.11. General 6R manipulator.

$$\begin{bmatrix} e_x \\ e_y \\ e_z \\ 0 \end{bmatrix} = {}^0A_6 {}^6A_5 \begin{bmatrix} 0 \\ 0 \\ 1 \\ 0 \end{bmatrix} = \begin{bmatrix} v_x s\alpha_6 + w_x c\alpha_6 \\ v_y s\alpha_6 + w_y c\alpha_6 \\ v_z s\alpha_6 + w_z c\alpha_6 \\ 0 \end{bmatrix}. \quad (2.101)$$

Equations (2.100) and (2.101) imply that once the end-effector location is given, the point P and the direction of z_5 -axis can be found.

The transformation between 5p and 0p and between 5e and 0e can be written as

$${}^0p = {}^0A_1 {}^1A_2 {}^2A_3 {}^3A_4 {}^4A_5 {}^5p, \quad (2.102)$$

$${}^0e = {}^0A_1 {}^1A_2 {}^2A_3 {}^3A_4 {}^4A_5 {}^5e. \quad (2.103)$$

To simplify the analysis, we multiply both sides of Eqs. (2.102) and (2.103) by $({}^0A_1 {}^1A_2)^{-1}$. The resulting equations can be written

$${}^3p = {}^2p', \quad (2.104)$$

$${}^3e = {}^2e'. \quad (2.105)$$

where

$${}^2p = {}^2A_3 {}^3A_4 {}^4A_5 {}^5p,$$

$${}^2p' = ({}^1A_2)^{-1}({}^0A_1)^{-1}{}^0p,$$

$${}^2e = {}^2A_3 {}^3A_4 {}^4A_5 {}^5e,$$

$${}^2e' = ({}^1A_2)^{-1}({}^0A_1)^{-1}{}^0e$$

are the position vectors of P and the direction of the z_5 -axis with reference to the (x_2, y_2, z_2) coordinate system.

Equations (2.104) and (2.105) constitute a set of six scalar equations free of the variable θ_6 . However, only two of the three scalar equations in Eq. (2.105) are independent, because the components of e must satisfy the condition of a unit vector. Hence there are only five independent equations in five unknowns, $\theta_1, \dots, \theta_5$. The x and y components in Eqs. (2.104) and (2.105) are third-degree polynomials, while the z -component is a second-degree polynomial in the sines and cosines of five joint angles. We note that by using this approach, θ_6 does not appear in the system of equations and therefore reduces the complexity of the problem. In the following we eliminate θ_3 from the system of equations above.

Elimination of θ_3 . First, we notice that both z -components of Eqs. (2.104) and (2.105) are already free of the variable θ_3 . Expanding the z -components of Eqs. (2.104) and (2.105), yields

$$\begin{aligned} h_x s\alpha_2 s\theta_2 - h_y s\alpha_2 c\theta_2 - g_x s\alpha_3 s\theta_4 + g_y s\alpha_3 c\theta_4 \\ = -h_z c\alpha_2 + d_2 c\alpha_2 + g_z c\alpha_3 + d_3, \end{aligned} \quad (2.106)$$

$$\begin{aligned} n_x s\alpha_2 s\theta_2 - n_y s\alpha_2 c\theta_2 - m_x s\alpha_3 s\theta_4 + m_y s\alpha_3 c\theta_4 \\ = -n_z c\alpha_2 + m_z c\alpha_3, \end{aligned} \quad (2.107)$$

where

$$g_x = a_5 c\theta_5 + a_4,$$

$$g_y = -a_5 c\alpha_4 s\theta_5 + d_5 s\alpha_4,$$

$$g_z = a_5 s\alpha_4 s\theta_5 + d_5 c\alpha_4 + d_4,$$

$$h_x = p_x c\theta_1 + p_y s\theta_1 - a_1,$$

$$h_y = -p_x c\alpha_1 s\theta_1 + p_y c\alpha_1 c\theta_1 + (p_z - d_1) s\alpha_1,$$

$$h_z = p_x s\alpha_1 s\theta_1 - p_y s\alpha_1 c\theta_1 + (p_z - d_1) c\alpha_1,$$

$$m_x = c\alpha_5 s\theta_5,$$

$$\begin{aligned}m_y &= c\alpha_4 s\alpha_5 c\theta_5 + s\alpha_4 c\alpha_5, \\m_z &= -s\alpha_4 s\alpha_5 c\theta_5 + c\alpha_4 c\alpha_5, \\n_x &= e_x c\theta_1 + e_y s\theta_1, \\n_y &= -e_x c\alpha_1 s\theta_1 + e_y c\alpha_1 c\theta_1 + e_z s\alpha_1, \\n_z &= e_x s\alpha_1 s\theta_1 - e_y s\alpha_1 c\theta_1 + e_z c\alpha_1.\end{aligned}$$

A third equation that is free of θ_3 is obtained by performing the dot product ${}^2\mathbf{p} \cdot {}^2\mathbf{e} = {}^2\mathbf{p}' \cdot {}^2\mathbf{e}'$. Substituting Eqs. (2.104) and (2.105) into the dot product and simplifying, we obtain

$$\begin{aligned}a_2 n_y s\theta_2 + a_2 n_x c\theta_2 + (a_3 m_y + d_3 m_x s\alpha_3) s\theta_4 + (a_3 m_x - d_3 m_y s\alpha_3) c\theta_4 \\= -a_1 n_x - d_2 n_z - a_4 m_x - m_z (d_3 c\alpha_3 + d_4) + k_1,\end{aligned}\quad (2.108)$$

where $k_1 = -d_5 c\alpha_5 + p_x e_x + p_y e_y + (p_z - d_1) e_z$.

A fourth equation that is free of θ_3 is obtained by equating the sum of the squares of the x , y , and z components on both sides of Eq. (2.104). Expanding $({}^2\mathbf{p})^2 = ({}^2\mathbf{p}')^2$ yields

$$\begin{aligned}a_2 h_y s\theta_2 + a_2 h_x c\theta_2 + (a_3 g_y + d_3 g_x s\alpha_3) s\theta_4 + (a_3 g_x - d_3 g_y s\alpha_3) c\theta_4 \\= -a_1 h_x - d_2 h_z - a_4 g_x - g_z (d_3 c\alpha_3 + d_4) + k_2,\end{aligned}\quad (2.109)$$

where

$$k_2 = 0.5 [p_x^2 + p_y^2 + (p_z - d_1)^2 - a_1^2 + a_2^2 + d_2^2 - a_3^2 - d_3^2 + a_4^2 + d_4^2 - a_5^2 - d_5^2].$$

Equations (2.106) through (2.109) represent a system of four second-degree polynomials in the sines and cosines of four joint angles. We may consider $\sin \theta_i$ and $\cos \theta_i$ as two independent variables and add the following trigonometric identities as supplementary equations of constraint:

$$s^2\theta_i + c^2\theta_i = 1, \quad \text{for } i = 1, 2, 4, 5. \quad (2.110)$$

In this way, we obtain a system of eight second-degree polynomials in eight variables. Tsai and Morgan employed a continuation method to solve the system of equations above and showed that the most general 6-dof, 6R robot has at most 16 significant solutions. See Appendix A for more details.

The system of equations will decouple when any three consecutive joint axes either intersect at a common point or are parallel to one another. For these special geometries, closed-form solutions can be derived. In what follows we illustrate the decoupling by solving the inverse kinematics of two special cases that are most commonly implemented in industrial robots. Other special cases can be derived by applying the kinematic inversions.

(a) Last Three Joint Axes Intersecting at a Common Point. When the last three joint axes intersect at a common point, $a_4 = a_5 = d_5 = 0$ identically. Substituting these values into Eqs. (2.106) and (2.109) yields

$$h_x s\theta_2 - h_y c\theta_2 = \mu_1 / s\alpha_2, \quad (2.111)$$

$$h_y s\theta_2 + h_x c\theta_2 = \mu_2 / a_2, \quad (2.112)$$

provided that $s\alpha_2 \neq 0$ and $a_2 \neq 0$, where

$$\mu_1 = -h_z c\alpha_2 + d_2 c\alpha_2 + d_3 + d_4 c\alpha_3,$$

$$\mu_2 = -a_1 h_x - d_2 h_z - d_3 d_4 c\alpha_3$$

$$+ 0.5 [p_x^2 + p_y^2 + (p_z - d_1)^2 - a_1^2 + a_2^2 + d_2^2 - a_3^2 - d_3^2 - d_4^2].$$

Equations (2.111) and (2.112) contain only two unknown variables and hence are completely decoupled from Eqs. (2.107) and (2.108). To eliminate θ_2 , we sum the squares of Eqs. (2.111) and (2.112).

$$h_x^2 + h_y^2 = (\mu_1 / s\alpha_2)^2 + (\mu_2 / a_2)^2. \quad (2.113)$$

Equation (2.113) contains only one variable, θ_1 . We may convert it into a fourth-degree polynomial in t_1 by replacing $s\theta_1$ with $2t_1/(1+t_1^2)$ and $c\theta_1$ with $(1-t_1^2)/(1+t_1^2)$, where $t_1 = \tan(\theta_1/2)$. Hence, for each given end-effector position, there are at most four real solutions of θ_1 . Once θ_1 is found, a unique solution of θ_2 can be obtained by solving Eqs. (2.111) and (2.112) simultaneously for $s\theta_2$ and $c\theta_2$, and then applying the two-argument arctangent function. Following that, a unique solution of θ_3 can be found by solving the two scalar equations associated with the x and y components of Eq. (2.104).

Corresponding to each solution set of $(\theta_1, \theta_2, \theta_3)$, two sets of $(\theta_4, \theta_5, \theta_6)$ can be found by following the procedure outlined in the earlier example. Hence we conclude that there are at most eight possible solutions sets (manipulator postures).

(b) Joint Axes 2, 3, and 4 Parallel to One Another. When the second, third, and fourth joint axes are parallel to one another, $\alpha_2 = \alpha_3 = 0$ identically. Further, since the common normals between the second and third joint axes and between the third and fourth joint axes are indeterminate, we can always define these two common normals such that $d_2 = d_3 = 0$. With these values, Eqs. (2.106) and (2.107) reduce to

$$s\alpha_4 s\theta_5 = \frac{h_z - d_5 c\alpha_4 - d_4}{a_5}, \quad (2.114)$$

$$s\alpha_4 c\theta_5 = \frac{-n_z + c\alpha_4 c\alpha_5}{s\alpha_5}, \quad (2.115)$$

provided that $a_5 \neq 0$ and $s\alpha_5 \neq 0$.

Again, Eqs. (2.114) and (2.115) contain only two unknown variables and hence are completely decoupled from Eqs. (2.108) and (2.109). We can eliminate θ_5 by summing the squares of Eq. (2.114) and (2.115):

$$s^2\alpha_4 = \left(\frac{h_z - d_5 c\alpha_4 - d_4}{a_5} \right)^2 + \left(\frac{-n_z + c\alpha_4 c\alpha_5}{s\alpha_5} \right)^2. \quad (2.116)$$

Equation (2.116) contains only one variable, θ_1 . We may convert it into a fourth-degree polynomial in t_1 by replacing $s\theta_1$ with $2t_1/(1+t_1^2)$ and $c\theta_1$ with $(1-t_1^2)/(1+t_1^2)$, where $t_1 = \tan(\theta_1/2)$. Hence for each given end-effector position and orientation, there are at most four real solutions of θ_1 . Once θ_1 is known, a unique solution of θ_5 can be obtained by solving Eqs. (2.114) and (2.115) simultaneously for $s\theta_5$ and $c\theta_5$ and then applying the two-argument arctangent function.

When $\alpha_2 = \alpha_3 = 0$, the two scalar equations corresponding to the x and y components of Eq. (2.105) reduce to

$$m_x c\theta_{34} + m_z s\theta_{34} = n_x c\theta_2 + n_y s\theta_2, \quad (2.117)$$

$$m_x s\theta_{34} - m_y c\theta_{34} = -n_x s\theta_2 + n_y c\theta_2. \quad (2.118)$$

Equations (2.117) and (2.118) contain two unknown variables, θ_{34} and θ_2 . We may reduce these two equations to a single equation in one variable by the following procedure. Subtracting Eq. (2.118) $\times s\theta_2$ from (2.117) $\times c\theta_2$ yields

$$m_x c\theta_{234} + m_y s\theta_{234} = n_x. \quad (2.119)$$

Adding Eq. (2.118) $\times c\theta_2$ to (2.117) $\times s\theta_2$ yields

$$m_x s\theta_{234} - m_y c\theta_{234} = n_y. \quad (2.120)$$

Hence, corresponding to each solution set of θ_1 and θ_5 , a unique solution of θ_{234} can be obtained by solving Eqs. (2.119) and (2.120) for $s\theta_{234}$ and $c\theta_{234}$, and then applying the two-argument arctangent function.

Similarly, the two scalar equations corresponding to the x and y components of Eq. (2.104) reduce to

$$g_x c\theta_{34} + g_z s\theta_{34} + a_3 c\theta_3 = h_x c\theta_2 + h_y s\theta_2 - a_2, \quad (2.121)$$

$$g_x s\theta_{34} - g_y c\theta_{34} + a_3 s\theta_3 = -h_x s\theta_2 + h_y c\theta_2. \quad (2.122)$$

Subtracting Eq. (2.122) $\times s\theta_2$ from (2.121) $\times c\theta_2$ yields

$$g_x c\theta_{234} + g_y s\theta_{234} + a_3 c\theta_{23} = h_x - a_2 c\theta_2. \quad (2.123)$$

Adding Eq. (2.122) $\times c\theta_2$ to (2.121) $\times s\theta_2$ yields

$$g_x s\theta_{234} - g_y c\theta_{234} + a_3 s\theta_{23} = h_y - a_2 s\theta_2. \quad (2.124)$$

Summing the squares of [Eq. (2.123) - h_x] and [Eq. (2.124) - h_y] yields

$$2a_3(k_3 c\theta_{23} + k_4 s\theta_{23}) + k_5 = 0, \quad (2.125)$$

where

$$k_3 = g_x c\theta_{234} + g_y s\theta_{234} - h_x,$$

$$k_4 = g_x s\theta_{234} - g_y c\theta_{234} - h_y,$$

$$k_5 = -a_2^2 + a_3^2 + k_3^2 + k_4^2.$$

Hence, corresponding to each solution set of $(\theta_1, \theta_5, \theta_{234})$, Eq. (2.125) yields two solutions of θ_{23} . Once θ_{23} is found, Eqs. (2.123) and (2.124) yield a unique solution of θ_2 . We conclude that there are at most eight possible solution sets.

2.7 METHOD OF SUCCESSIVE SCREW DISPLACEMENTS

In this section we study a method of analysis based on the concept of *successive screw displacements*. First, the transformation matrix associated with a screw displacement is derived. Then the concept of the *resultant screw* of two successive screw displacements is described. Then the concept is applied to the position analysis of serial manipulators.

2.7.1 Transformation Based on Screw Displacement

Chasles' theorem states that the general spatial displacement of a rigid body is a translation plus a rotation. A stronger form of the theorem states that regardless of how a rigid body is displaced from one location to another, the displacement can be regarded as a rotation about and a translation along some axis. Such a combination of translation and rotation is called a *screw displacement* (Bottema and Roth, 1979). In what follows we derive a homogeneous transformation based on the concept of screw displacement.

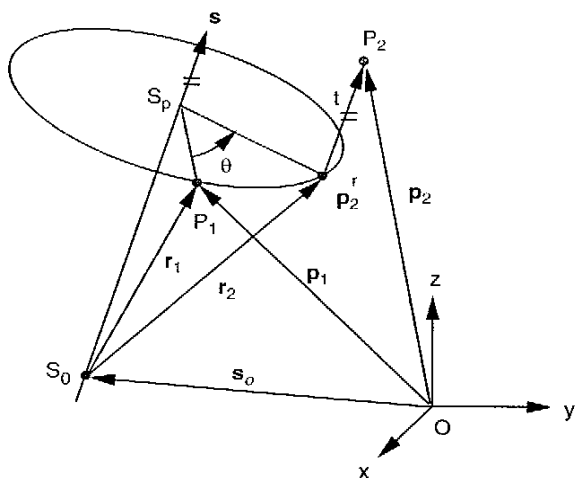


FIGURE 2.12. Vector diagram of a spatial displacement.

Figure 2.12 shows a point P that is displaced from a first position P_1 to a second position P_2 by a rotation of θ about a screw axis followed by a translation of t along the same axis. The rotation brings P from P_1 to P'_2 , and the translation brings P from P'_2 to P_2 . In the figure, $s = [s_x, s_y, s_z]^T$ denotes a unit vector along the direction of the screw axis, and $s_o = [s_{ox}, s_{oy}, s_{oz}]^T$ denotes the position vector of a point lying on the screw axis. The rotation angle θ and the translational distance t are called the *screw parameters*. The screw axis together with the screw parameters completely define the general displacement of a rigid body. Note that for a general displacement of a rigid body, the screw axis does not necessarily pass through the origin of the fixed frame.

The displacement equation due to a rotation about an axis passing through the origin was derived in Chapter 1. Hence we only need to take care of the fact that the screw axis does not pass through the origin and add the contribution due to a translation along the screw axis. Referring to Fig. 2.12, we observe that

$$\mathbf{r}_1 = \mathbf{p}_1 - \mathbf{s}_o, \quad (2.126)$$

$$\mathbf{r}_2 = \mathbf{p}_2 - \mathbf{s}_o - ts. \quad (2.127)$$

Substituting Eqs. (2.126) and (2.127) into (1.35), we obtain

$$\mathbf{p}_2 = \mathbf{s}_o + ts + (\mathbf{p}_1 - \mathbf{s}_o)c\theta + \mathbf{s} \times (\mathbf{p}_1 - \mathbf{s}_o)s\theta + [(\mathbf{p}_1 - \mathbf{s}_o)^T \mathbf{s}]s(1 - c\theta). \quad (2.128)$$

Equation (2.128) is known as *Rodrigues's formula* for the general spatial displacement of a rigid body. Expanding Eq. (2.128) and replacing \mathbf{p}_1 by ${}^B\mathbf{p}$ and \mathbf{p}_2 by ${}^A\mathbf{p}$, we obtain

$${}^A\mathbf{p} = {}^A\mathbf{R}_B {}^B\mathbf{p} + {}^A\mathbf{q}, \quad (2.129)$$

where the elements of the rotation matrix, a_{ij} , are given by Eq. (1.37), and the position of the origin, ${}^A\mathbf{q}$, of the moving frame is given by

$$\begin{aligned} q_x &= ts_x - s_{ox}(a_{11} - 1) - s_{oy}a_{12} - s_{oz}a_{13}, \\ q_y &= ts_y - s_{ox}a_{21} - s_{oy}(a_{22} - 1) - s_{oz}a_{23}, \\ q_z &= ts_z - s_{ox}a_{31} - s_{oy}a_{32} - s_{oz}(a_{33} - 1). \end{aligned} \quad (2.130)$$

Equation (2.129) can be written as a homogeneous transformation:

$${}^A\hat{\mathbf{p}} = A {}^B\hat{\mathbf{p}} \quad (2.131)$$

where A is a 4×4 transformation matrix the elements of which are given by

$$\begin{aligned} a_{11} &= (s_x^2 - 1)(1 - c\theta) + 1, \\ a_{12} &= s_x s_y (1 - c\theta) - s_z s\theta, \\ a_{13} &= s_x s_z (1 - c\theta) + s_y s\theta, \\ a_{21} &= s_y s_x (1 - c\theta) + s_z s\theta, \\ a_{22} &= (s_y^2 - 1)(1 - c\theta) + 1, \\ a_{23} &= s_y s_z (1 - c\theta) - s_x s\theta, \\ a_{31} &= s_z s_x (1 - c\theta) - s_y s\theta, \\ a_{32} &= s_z s_y (1 - c\theta) + s_x s\theta, \\ a_{33} &= (s_z^2 - 1)(1 - c\theta) + 1, \\ a_{14} &= ts_x - s_{ox}(a_{11} - 1) - s_{oy}a_{12} - s_{oz}a_{13}, \\ a_{24} &= ts_y - s_{ox}a_{21} - s_{oy}(a_{22} - 1) - s_{oz}a_{23}, \\ a_{34} &= ts_z - s_{ox}a_{31} - s_{oy}a_{32} - s_{oz}(a_{33} - 1), \end{aligned}$$

$$\begin{aligned} a_{41} &= 0, \\ a_{42} &= 0, \\ a_{43} &= 0, \\ a_{44} &= 1. \end{aligned} \quad (2.132)$$

The upper left 3×3 submatrix of A represents the rotation of the rigid body. The upper right 3×1 submatrix represents the translation of the origin Q (i.e., $a_{14} = q_x$, $a_{24} = q_y$, and $a_{34} = q_z$). This representation of a spatial displacement requires eight parameters: three associated with the direction of the screw axis, three associated with the location of the screw axis, one associated with the rotation angle, and one associated with the translational distance. However, only two of the three parameters associated with the direction of the screw axis are independent since they must satisfy the condition of a unit vector:

$$\mathbf{s}^T \mathbf{s} = 1. \quad (2.133)$$

Similarly, only two of the three parameters associated with the location of the screw axis are independent, since S_o can be any point on the screw axis. For convenience, we may choose \mathbf{s}_o to be normal to the screw axis:

$$\mathbf{s}_o^T \mathbf{s} = 0. \quad (2.134)$$

Given the screw axis and screw parameters, we can compute the elements of the transformation matrix by Eq. (2.132). On the other hand, given the spatial displacement of a rigid body in terms of a rotation matrix, ${}^A R_B$, and a translation vector, ${}^A \mathbf{q}$, we can compute the screw axis and the screw parameters as follows. The angle of rotation is given by

$$\theta = \cos^{-1} \frac{a_{11} + a_{22} + a_{33} - 1}{2}. \quad (2.135)$$

There are two solutions of θ , one being the negative of the other. Once the rotation angle is known, the direction of the screw axis is computed by

$$\begin{aligned} s_x &= \frac{a_{32} - a_{23}}{2s\theta}, \\ s_y &= \frac{a_{13} - a_{31}}{2s\theta}, \\ s_z &= \frac{a_{21} - a_{12}}{2s\theta}. \end{aligned} \quad (2.136)$$

The translational distance is calculated by

$$t = \mathbf{q}^T \mathbf{s}, \quad (2.137)$$

and the screw axis location is obtained by solving any two of the three equations in Eq. (2.130) along with Eq. (2.134). Since these equations are linear, there exists one solution corresponding to each solution set of \mathbf{s} , θ , and t .

From the derivation above, it appears that there are two solutions of the screw axis, one being the negative of the other. In reality, these two solutions represent the same screw, since a $-\theta$ rotation about and a $-t$ translation along the $-(\mathbf{s}, \mathbf{s}_o)$ screw axis produces the same result as a $+\theta$ rotation about and a $+t$ translation along the $(\mathbf{s}, \mathbf{s}_o)$ screw axis.

2.7.2 Successive Screw Displacements

We now apply the concept of screw displacements to kinematic analysis of open-loop chains. Figure 2.13 shows a rigid body σ which is guided to a fixed base by a dyad that is made up of two kinematic pairs, denoted by $\$_1$ and $\$_2$, respectively. The first kinematic pair connects the first moving link to the fixed base, and the second kinematic pair connects the second moving

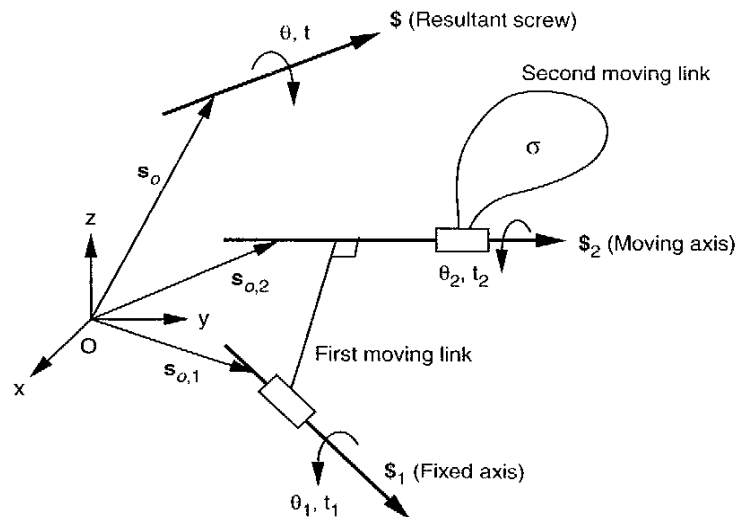


FIGURE 2.13. Two-link chain and its associated screw displacements.

link (σ) to the first. We call the axis of the first kinematic pair the *fixed joint axis* and the axis of the second kinematic pair the *moving joint axis*.

As the rigid body is rotated about and/or translated along these two joint axes, we may think of its displacement as the resultant of a screw displacement of (θ_1, t_1) about the fixed joint axis followed by another displacement of (θ_2, t_2) about the displaced moving joint axis. We may also think of the displacement as the resultant of a screw displacement of (θ_2, t_2) about the moving joint axis in its initial location followed by another displacement of (θ_1, t_1) about the fixed joint axis. As a matter of fact, these two screw displacements can occur in any order or simultaneously as long as the total amounts of rotations and/or translations about these two joint axes are correct. That is, the order in which the joint variables change their values can be arbitrary. The changes can be one at a time in any order or simultaneous.

A difficult scheme is to consider the resultant screw, $\$,$ as a screw displacement of $\$_1$ about the fixed joint axis followed by another screw displacement of $\$_2$ about the displaced moving joint axis. This is because a rotation of θ_1 about the fixed joint axis will displace the moving joint axis, $\$_2,$ to a new location, and this must be accounted for the subsequent displacement.

The best scheme is to rotate the rigid body σ about the moving joint axis followed by another rotation about the fixed joint axis. In this way, the initial location of the moving joint axis can be used for derivation of the transformation matrices, and the resulting transformation matrix can be obtained by a premultiplication of the two successive screw displacements; that is,

$$A_r = A_1 A_2, \quad (2.138)$$

where A_1 and A_2 denote the screw displacements about the initial locations of the fixed and moving joint axes, respectively.

The commutative property with regard to the change in joint variables in an open-loop chain should not be confused with the fact that finite rotations about body-fixed (or space fixed) axes do not commute. This property was first discovered and applied to the kinematic synthesis of spatial linkages by Tsai and Roth (Tsai, 1972; Tsai and Roth, 1972, 1973). Gupta (1984, 1986, 1997) subsequently provided a more rigorous proof of the property and applied it for the kinematic analysis of serial manipulators.

The proposition above can be extended to an n -link serial manipulator as shown in Fig. 2.14. Toward this goal, we first define a *reference position* for the manipulator. Although the reference position can be chosen arbitrarily, it is usually chosen at a location where the coordinates of all the joint axes can easily be identified. The reference position is sometimes called the *zero position*, and the desired position is called the *target position*. In this way, we may consider the manipulator as being displaced from the reference position

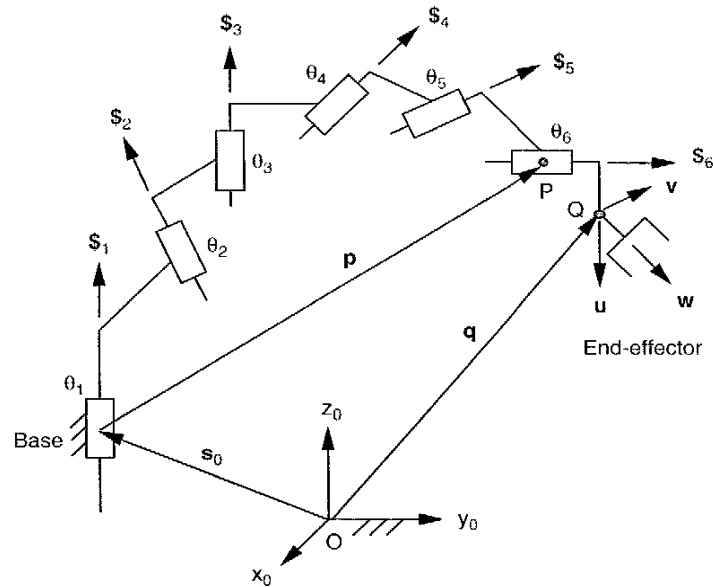


FIGURE 2.14. Screw axes of a serial manipulator.

to the target position by a series of finite screw displacements about all the joint axes.

(a) Reference Position. The reference position of a manipulator is specified in terms of the end effector location,

$$\mathbf{u}_0, \mathbf{v}_0, \mathbf{w}_0, \text{ and } \mathbf{q}_0,$$

and the direction and orientation of the joint axes:

$$\mathbf{s}_i \text{ and } \mathbf{s}_{oi}, \text{ for } i = 1, 2, \dots, n.$$

(b) Target Position. The target position of a manipulator is specified in terms of the desired end-effector location:

$$\mathbf{u}, \mathbf{v}, \mathbf{w}, \text{ and } \mathbf{q}.$$

(c) Loop-Closure Equation. The end-effector displacement from a reference position to a target position can be considered as the resultant of n

successive screw displacements: that is, a rotation about the n th joint axis, followed by another about the $(n - 1)$ th joint axis, and so on. Since all screw displacements take place about the joint axes at the reference position, the resulting screw displacement is obtained by premultiplying these screw displacements:

$$A_h = A_1 A_2 \cdots A_{n-1} A_n. \quad (2.139)$$

Using the method of successive screw displacements, only one fixed coordinate system and one end effector coordinate system are needed. The screw parameters used in Eq. (2.132) should not be confused with the Denavit–Hartenberg parameters. The joint variables of a screw displacement represent the actual angles of rotation and/or distances of translation needed to bring the end effector from a reference position to a target position. Specifically, for a revolute joint, θ_i is a variable and $t_i = 0$ identically, while for a prismatic joint, t_i is a variable and $\theta_i = 0$ identically.

The D-II parameters do not represent the angle of rotation or the distance of translation about a joint axis. To obtain the actual displacements, it is necessary to subtract the joint variables associated with a reference position from that of a target position. One of the advantages of using successive screw displacements is that the reference position can be chosen arbitrarily. For example, it can be chosen at the *home position* of a robot, where all the information regarding the location of the end effector and the locations of the joint axes are known.

For direct kinematics, we compute Eq. (2.139) directly by using the given joint variables. For inverse kinematics, the left-hand side of Eq. (2.139) is given and the problem is to find the joint displacements needed to bring the hand to a desired location.

2.7.3 Position Analysis of an Elbow Manipulator

Figure 2.15 shows the schematic diagram of an elbow manipulator. In this manipulator, the second joint axis intersects the first perpendicularly, the third and fourth joint axes are parallel to the second, the fifth joint axis is perpendicular to the fourth with a small offset distance a_4 , and the sixth joint axis is perpendicular to the fifth. We wish to solve the inverse kinematics problem of this manipulator using the method of successive screw displacements.

(a) Reference Position. First we identify a reference configuration with respect to which the displacement of the manipulator will be measured. Figure 2.16 shows such a reference configuration, where the first joint axis, S_1 ,

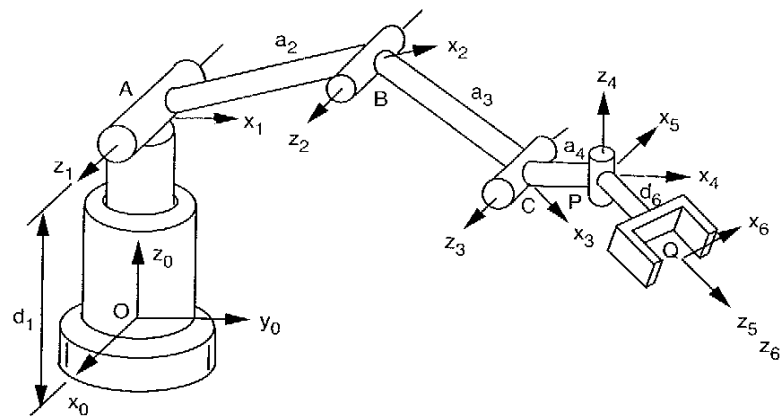


FIGURE 2.15. A 6-dof elbow manipulator.

points up vertically in the positive z -direction; the second, third, and fourth joint axes, S_2 , S_3 , and S_4 , are all pointing out of the paper; the fifth joint axis, S_5 , points in the positive z -direction; and the sixth joint axis, S_6 , points in the positive x -direction. The hand coordinate system is located at point Q such that the w_0 -axis points in the positive x -direction and the u_0 -axis points in the

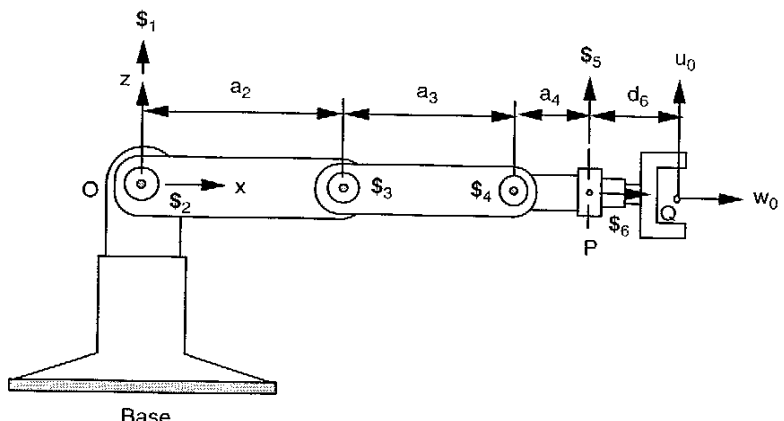


FIGURE 2.16. Reference position of the elbow manipulator.

TABLE 2.5. Screw Axis Locations of the Elbow Manipulator

Joint i	s_i	s_{oi}
1	(0, 0, 1)	(0, 0, 0)
2	(0, -1, 0)	(0, 0, 0)
3	(0, -1, 0)	(a_2 , 0, 0)
4	(0, -1, 0)	($a_2 + a_3$, 0, 0)
5	(0, 0, 1)	($a_2 + a_3 + a_4$, 0, 0)
6	(1, 0, 0)	(0, 0, 0)

positive z -direction. At this reference position, the locations of the screw axes with respect to the fixed reference frame are listed in Table 2.5. The reference position of the end effector is

$$\begin{aligned} \mathbf{u}_0 &= [0, 0, 1]^T, \quad \mathbf{v}_0 = [0, -1, 0]^T, \quad \mathbf{w}_0 = [1, 0, 0]^T, \quad \text{and} \\ \mathbf{p}_0 &= [a_2 + a_3 + a_4, 0, 0]^T. \end{aligned}$$

(b) Target Position. Let the target position of the end effector be

$$\begin{aligned} \mathbf{u} &= [u_x, u_y, u_z]^T, \quad \mathbf{v} = [v_x, v_y, v_z]^T, \quad \mathbf{w} = [w_x, w_y, w_z]^T, \quad \text{and} \\ \mathbf{p} &= [p_x, p_y, p_z]^T. \end{aligned}$$

(c) Transformation Matrices. Substituting the coordinates of the joint axes into Eq. (2.132), we obtain the screw transformation matrices:

$$A_1 = \begin{bmatrix} c\theta_1 & -s\theta_1 & 0 & 0 \\ s\theta_1 & c\theta_1 & 0 & 0 \\ 0 & 0 & 1 & 0 \\ 0 & 0 & 0 & 1 \end{bmatrix}, \quad A_1^{-1} = \begin{bmatrix} c\theta_1 & s\theta_1 & 0 & 0 \\ -s\theta_1 & c\theta_1 & 0 & 0 \\ 0 & 0 & 1 & 0 \\ 0 & 0 & 0 & 1 \end{bmatrix},$$

$$A_2 = \begin{bmatrix} c\theta_2 & 0 & -s\theta_2 & 0 \\ 0 & 1 & 0 & 0 \\ s\theta_2 & 0 & c\theta_2 & 0 \\ 0 & 0 & 0 & 1 \end{bmatrix},$$

$$A_3 = \begin{bmatrix} c\theta_3 & 0 & -s\theta_3 & a_2(1 - c\theta_3) \\ 0 & 1 & 0 & 0 \\ s\theta_3 & 0 & c\theta_3 & -a_2s\theta_3 \\ 0 & 0 & 0 & 1 \end{bmatrix},$$

$$\begin{aligned} A_4 &= \begin{bmatrix} c\theta_4 & 0 & -s\theta_4 & (a_2 + a_3)(1 - c\theta_4) \\ 0 & 1 & 0 & 0 \\ s\theta_4 & 0 & c\theta_4 & (a_2 + a_3)s\theta_4 \\ 0 & 0 & 0 & 1 \end{bmatrix}, \\ A_5 &= \begin{bmatrix} c\theta_5 & -s\theta_5 & 0 & (a_2 + a_3 + a_4)(1 - c\theta_5) \\ s\theta_5 & c\theta_5 & 0 & -(a_2 + a_3 + a_4)s\theta_5 \\ 0 & 0 & 1 & 0 \\ 0 & 0 & 0 & 1 \end{bmatrix}, \\ A_6 &= \begin{bmatrix} 1 & 0 & 0 & 0 \\ 0 & c\theta_6 & -s\theta_6 & 0 \\ 0 & s\theta_6 & c\theta_6 & 0 \\ 0 & 0 & 0 & 1 \end{bmatrix}. \end{aligned}$$

The matrix products $A_2A_3A_4$ and $A_1A_2A_3A_4$ are computed as

$$A_2A_3A_4 = \begin{bmatrix} c\theta_{234} & 0 & -s\theta_{234} & a_2c\theta_2 + a_3c\theta_{23} - (a_2 + a_3)c\theta_{234} \\ 0 & 1 & 0 & 0 \\ s\theta_{234} & 0 & c\theta_{234} & a_2s\theta_2 + a_3s\theta_{23} - (a_2 + a_3)s\theta_{234} \\ 0 & 0 & 0 & 1 \end{bmatrix}, \quad (2.140)$$

$$A_1A_2A_3A_4 = \begin{bmatrix} c\theta_1c\theta_{234} & -s\theta_1 & -c\theta_1s\theta_{234} & c\theta_1[a_2c\theta_2 + a_3c\theta_{23} - (a_2 + a_3)c\theta_{234}] \\ s\theta_1c\theta_{234} & c\theta_1 & -s\theta_1s\theta_{234} & s\theta_1[a_2c\theta_2 + a_3c\theta_{23} - (a_2 + a_3)c\theta_{234}] \\ s\theta_{234} & 0 & c\theta_{234} & [a_2s\theta_2 + a_3s\theta_{23} - (a_2 + a_3)s\theta_{234}] \\ 0 & 0 & 0 & 1 \end{bmatrix}. \quad (2.141)$$

(d) Inverse Kinematics. The transformation of the wrist center point P is given by

$$\mathbf{p} = A_1A_2A_3A_4\mathbf{p}_0. \quad (2.142)$$

Multiplying both sides of the equation above by A_1^{-1} , we obtain

$$A_1^{-1} \begin{bmatrix} p_x \\ p_y \\ p_z \\ 1 \end{bmatrix} = A_2A_3A_4 \begin{bmatrix} a_2 + a_3 + a_4 \\ 0 \\ 0 \\ 1 \end{bmatrix}. \quad (2.143)$$

Substituting A_1^{-1} and Eq. (2.140) into (2.143) yields

$$p_x c\theta_1 + p_y s\theta_1 = a_2 c\theta_2 + a_3 c\theta_{23} + a_4 c\theta_{234}, \quad (2.144)$$

$$-p_x s\theta_1 + p_y c\theta_1 = 0. \quad (2.145)$$

$$p_z = a_2 s\theta_2 + a_3 s\theta_{23} + a_4 s\theta_{234}. \quad (2.146)$$

From Eq. (2.145), two solutions of θ_1 are found immediately:

$$\theta_1 = \tan^{-1} \frac{p_y}{p_x}. \quad (2.147)$$

For this manipulator, the position and orientation are not decoupled. Therefore, we need to work on both simultaneously. Applying the transformation matrix to the approach vector \mathbf{w} gives

$$R_1^T \mathbf{w} = R_2 R_3 R_4 R_5 \mathbf{w}_0, \quad (2.148)$$

where R_i denotes the upper left 3×3 submatrix of A_i . Expanding Eq. (2.148), we obtain

$$w_x c\theta_1 + w_y s\theta_1 = c\theta_{234} c\theta_5, \quad (2.149)$$

$$-w_x s\theta_1 + w_y c\theta_1 = s\theta_5, \quad (2.150)$$

$$w_z = s\theta_{234} c\theta_5. \quad (2.151)$$

Corresponding to each solution of θ_1 , Eq. (2.150) yields two solutions of θ_5 :

$$\theta_5 = \sin^{-1}(-w_x s\theta_1 + w_y c\theta_1). \quad (2.152)$$

That is, if $\theta_5 = \theta_5^*$ is a solution, $\theta_5 = \pi - \theta_5^*$ is also a solution. Once θ_1 and θ_5 are known, Eqs. (2.149) and (2.151) can be solved for $s\theta_{234}$ and $c\theta_{234}$. This leads to a unique solution for θ_{234} :

$$\theta_{234} = \text{Atan2}\left[w_z/c\theta_5, (w_x c\theta_1 + w_y s\theta_1)/c\theta_5\right]. \quad (2.153)$$

Next, we solve Eqs. (2.144) and (2.146) for θ_2 and θ_3 . For convenience, we rewrite Eqs. (2.144) and (2.146) as follows:

$$a_2 c\theta_2 + a_3 c\theta_{23} = k_1, \quad (2.154)$$

$$a_2 s\theta_2 + a_3 s\theta_{23} = k_2, \quad (2.155)$$

where $k_1 = p_x c\theta_1 + p_y s\theta_1 - a_4 c\theta_{234}$ and $k_2 = p_z - a_4 s\theta_{234}$. Summing the squares of Eqs. (2.154) and (2.155), we obtain

$$a_2^2 + a_3^2 + 2a_2 a_3 c\theta_3 = k_1^2 + k_2^2. \quad (2.156)$$

Hence

$$\theta_3 = \cos^{-1} \frac{k_1^2 + k_2^2 - a_2^2 - a_3^2}{2a_2 a_3}. \quad (2.157)$$

Therefore, corresponding to each solution set of θ_1 , θ_5 , and θ_{234} , there are at most two real solutions of θ_3 . Namely, if θ_3^* is a solution, $\theta_3 = -\theta_3^*$ is also a solution. Once θ_3 is known, θ_2 can be obtained by solving Eqs. (2.154) and (2.155) simultaneously for $s\theta_2$ and $c\theta_2$. This produces one solution of θ_2 . Finally, the solutions of θ_4 are obtained from the relation $\theta_4 = \theta_{234} - \theta_2 - \theta_3$.

To solve for θ_6 , we apply the transformation to the unit vector \mathbf{u} :

$$(R_1 R_2 R_3 R_4)^T \mathbf{u} = R_5 R_6 \mathbf{u}_0. \quad (2.158)$$

Expanding Eq. (2.158), we obtain

$$u_x c\theta_1 c\theta_{234} + u_y s\theta_1 c\theta_{234} + u_z s\theta_{234} = s\theta_5 s\theta_6, \quad (2.159)$$

$$-u_x s\theta_1 + u_y c\theta_1 = -c\theta_5 s\theta_6, \quad (2.160)$$

$$-u_x c\theta_1 s\theta_{234} - u_y s\theta_1 s\theta_{234} + u_z c\theta_{234} = c\theta_6. \quad (2.161)$$

We can solve Eqs. (2.159) and (2.160) for $s\theta_6$:

$$s\theta_6 = s\theta_5(u_x c\theta_1 c\theta_{234} + u_y s\theta_1 c\theta_{234} + u_z s\theta_{234}) - c\theta_5(-u_x s\theta_1 + u_y c\theta_1). \quad (2.162)$$

Equations (2.161) and (2.162) together determine a unique solution for θ_6 :

$$\theta_6 = \text{Atan2}(s\theta_6, c\theta_6). \quad (2.163)$$

We conclude that there are at most eight real inverse kinematic solutions.

2.7.4 Position Analysis of the Stanford Arm

Figure 2.17 shows a 6-dof manipulator developed at Stanford University (Scheinman, 1969). In this manipulator, the third joint is a prismatic joint (or sliding pair) while all the others are revolute. The first joint axis, $\$_1$, points up vertically in the positive z -direction. The second joint axis, $\$_2$, intersects the first perpendicularly at point A and points in the positive x -direction. The third joint axis intersects the second perpendicularly at point B and points

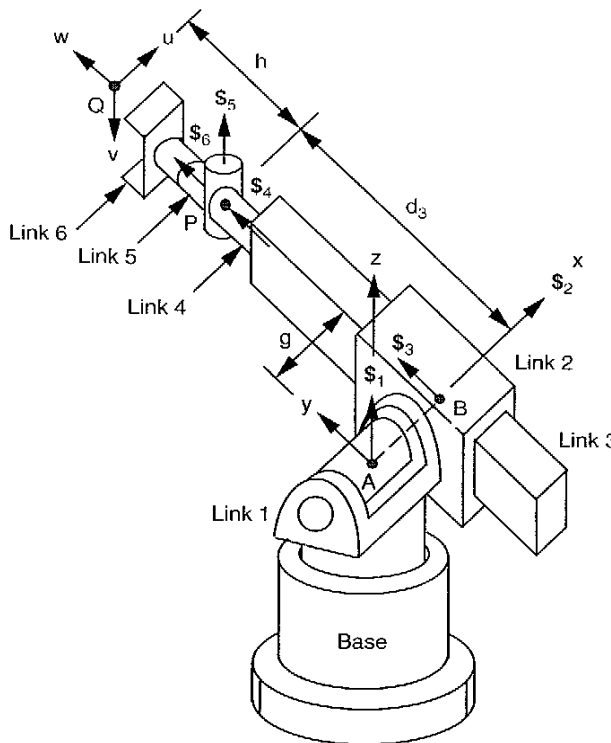


FIGURE 2.17. Screw axes associated with the Stanford manipulator.

in the positive y -direction. The fourth joint axis is in line with the third. Furthermore, the last three joint axes intersect one another perpendicularly at the wrist center point P as shown in Fig. 2.17.

(a) Reference Position. The reference position is chosen at the location where the wrist center point P is retracted back into coincident with B . At this reference position, the locations of the joint axes with respect to the fixed coordinate system are listed in Table 2.6, where g denotes the offset distance between the first and third joint axes.

The reference position of the end effector is given by

$$\mathbf{u}_0 = [1, 0, 0]^T, \quad \mathbf{v}_0 = [0, 0, -1]^T, \quad \mathbf{w}_0 = [0, 1, 0]^T, \quad \text{and} \\ \mathbf{q}_0 = [g, h, 0]^T.$$

TABLE 2.6. Screw Axis Locations of the Stanford Arm

Joint i	$s_i(s_x, s_y, s_z)$	$s_{oi}(s_{ox}, s_{oy}, s_{oz})$
1	(0, 0, 1)	(0, 0, 0)
2	(1, 0, 0)	(0, 0, 0)
3	(0, 1, 0)	(g , 0, 0)
4	(0, 1, 0)	(g , 0, 0)
5	(0, 0, 1)	(g , 0, 0)
6	(0, 1, 0)	(g , 0, 0)

Furthermore, the reference position of the wrist center P is given by

$$\mathbf{p}_0 = [g, 0, 0]^T.$$

(b) Target Position. Let the target position of the end effector be

$$\mathbf{u} = [u_x, u_y, u_z]^T, \quad \mathbf{v} = [v_x, v_y, v_z]^T, \quad \mathbf{w} = [w_x, w_y, w_z]^T, \quad \text{and} \\ \mathbf{q} = [q_x, q_y, q_z]^T.$$

Then the target position of the wrist center is given by

$$\mathbf{p} = \mathbf{q} + h\mathbf{w}, \quad (2.164)$$

where h is the distance between points P and Q .

In what follows, we first relate the position of the wrist center P to the first three joint variables. Then we solve the last three joint variables in terms of the end-effector orientation.

(c) Wrist Center Position. We observe that the position of the wrist center P depends only on the first three joint variables, θ_1 , θ_2 , and d_3 . Substituting the coordinates of the first three joint axes into Eq. (2.132), we obtain

$$A_1 A_2 A_3 = \begin{bmatrix} c\theta_1 & -s\theta_1 & 0 & 0 \\ s\theta_1 & c\theta_1 & 0 & 0 \\ 0 & 0 & 1 & 0 \\ 0 & 0 & 0 & 1 \end{bmatrix} \begin{bmatrix} 1 & 0 & 0 & 0 \\ 0 & c\theta_2 & -s\theta_2 & 0 \\ 0 & s\theta_2 & c\theta_2 & 0 \\ 0 & 0 & 0 & 1 \end{bmatrix} \begin{bmatrix} 1 & 0 & 0 & 0 \\ 0 & 1 & 0 & d_3 \\ 0 & 0 & 1 & 0 \\ 0 & 0 & 0 & 1 \end{bmatrix} \\ = \begin{bmatrix} c\theta_1 & -s\theta_1 c\theta_2 & s\theta_1 s\theta_2 & -d_3 s\theta_1 c\theta_2 \\ s\theta_1 & c\theta_1 c\theta_2 & -c\theta_1 s\theta_2 & d_3 c\theta_1 c\theta_2 \\ 0 & s\theta_2 & c\theta_2 & d_3 s\theta_2 \\ 0 & 0 & 0 & 1 \end{bmatrix}. \quad (2.165)$$

The target position of the wrist center is related to its initial reference position by

$$\mathbf{p} = A_1 A_2 A_3 \mathbf{p}_0. \quad (2.166)$$

Substituting Eq. (2.165) into (2.166) yields

$$p_x = g \cos \theta_1 - d_3 s \theta_1 \cos \theta_2, \quad (2.167)$$

$$p_y = g \sin \theta_1 + d_3 \cos \theta_1 \cos \theta_2, \quad (2.168)$$

$$p_z = d_3 \sin \theta_2. \quad (2.169)$$

We note that the distance between point A and the wrist center P as shown in Fig. 2.17 does not depend on the joint variables θ_1 and θ_2 . We can eliminate both θ_1 and θ_2 by the following operation. Summing the squares of Eqs. (2.167), (2.168), and (2.169) yields

$$p_x^2 + p_y^2 + p_z^2 = g^2 + d_3^2. \quad (2.170)$$

Hence

$$d_3 = \pm \sqrt{p_x^2 + p_y^2 + p_z^2 - g^2}. \quad (2.171)$$

Equation (2.171) yields (1) two real roots if $p_x^2 + p_y^2 + p_z^2 - g^2 > 0$, (2) one double root if $p_x^2 + p_y^2 + p_z^2 - g^2 = 0$, and (3) no real roots if $p_x^2 + p_y^2 + p_z^2 - g^2 < 0$. Although there may be two real values of d_3 , the negative d_3 cannot be realized physically because of the mechanical structure limitation of the robot. When Eq. (2.171) yields a double root, $d_3 = 0$, the wrist center is retracted to point B and the manipulator is said to be in a singular configuration. When Eq. (2.171) yields no real roots, the target point is not reachable. Furthermore, let d_{\max} be the maximum extension of the prismatic joint. Then a target point is not reachable if $d_3 > d_{\max}$, even though Eq. (2.171) may yield two real roots.

Once d_3 is known, we can solve Eq. (2.169) for θ_2 as

$$\theta_2 = \sin^{-1} \frac{p_z}{d_3}. \quad (2.172)$$

Hence, corresponding to each d_3 , Eq. (2.172) yields at most two real solutions of θ_2 . In general, if $\theta_2 = \theta_2^*$ is a solution, $\theta_2 = \pi - \theta_2^*$ is also a solution. We note that $p_x^2 + p_y^2 - g^2 = 0$ represents a cylinder of radius g with the z -axis as its longitudinal axis. It can be shown that Eq. (2.172) yields (1) two real roots if the target point falls outside the cylinder ($p_x^2 + p_y^2 - g^2 > 0$), (2) one

double root if the target point falls on the cylinder ($p_x^2 + p_y^2 - g^2 = 0$), and (3) no real roots if the target point falls inside the cylinder ($p_x^2 + p_y^2 - g^2 < 0$). When the target point falls outside the cylinder, Eq. (2.171) also yields two real roots.

Once d_3 and θ_2 are known, we can solve Eqs. (2.167) and (2.168) simultaneously for $s\theta_1$ and $c\theta_1$:

$$c\theta_1 = \frac{gp_x + d_3 p_y \cos \theta_2}{g^2 + d_3^2 c^2 \theta_2}, \quad (2.173)$$

$$s\theta_1 = \frac{gp_y - d_3 p_x \cos \theta_2}{g^2 + d_3^2 c^2 \theta_2}. \quad (2.174)$$

Therefore, corresponding to each solution set of θ_2 and d_3 , Eqs. (2.173) and (2.174) yield one solution of θ_1 :

$$\theta_1 = \text{Atan2}(s\theta_1, c\theta_1). \quad (2.175)$$

We conclude that corresponding to each given end-effector location, there are at most four upper arm configurations.

(d) End-Effector Orientation. We now proceed to find the last three joint angles. The end-effector orientation depends only on the rotational part of the transformation matrices A_i . Substituting the coordinates of the last three joint axes into Eq. (2.132), we obtain

$$\begin{aligned} R_4 R_5 R_6 &= \begin{bmatrix} c\theta_4 & 0 & s\theta_4 \\ 0 & 1 & 0 \\ -s\theta_4 & 0 & c\theta_4 \end{bmatrix} \begin{bmatrix} c\theta_5 & -s\theta_5 & 0 \\ s\theta_5 & c\theta_5 & 0 \\ 0 & 0 & 1 \end{bmatrix} \begin{bmatrix} c\theta_6 & 0 & s\theta_6 \\ 0 & 1 & 0 \\ -s\theta_6 & 0 & c\theta_6 \end{bmatrix} \\ &= \begin{bmatrix} c\theta_4 c\theta_5 c\theta_6 - s\theta_4 s\theta_6 & -c\theta_4 s\theta_5 & c\theta_4 c\theta_5 s\theta_6 + s\theta_4 c\theta_6 \\ s\theta_5 c\theta_6 & c\theta_5 & s\theta_5 s\theta_6 \\ -s\theta_4 c\theta_5 c\theta_6 - c\theta_4 s\theta_6 & s\theta_4 s\theta_5 & -s\theta_4 c\theta_5 s\theta_6 + c\theta_4 c\theta_6 \end{bmatrix}, \end{aligned} \quad (2.176)$$

where R_i denotes the upper left 3×3 submatrix of A_i .

The transformation of the approach vector \mathbf{w} is

$$\mathbf{w} = R_1 R_2 R_3 R_4 R_5 R_6 \mathbf{w}_0. \quad (2.177)$$

Multiplying both sides of Eq. (2.177) by $(R_1 R_2 R_3)^{-1}$, we obtain

$$R_3^T R_2^T R_1^T \mathbf{w} = R_4 R_5 R_6 \mathbf{w}_0. \quad (2.178)$$

The quantities on the left-hand side of Eq. (2.178) are known. For convenience, we define ${}^3\mathbf{w} \equiv R_3^T R_2^T R_1^T \mathbf{w}$. Expanding Eq. (2.178), we obtain

$$-c\theta_4 s\theta_5 = {}^3w_x, \quad (2.179)$$

$$c\theta_5 = {}^3w_y, \quad (2.180)$$

$$s\theta_4 s\theta_5 = {}^3w_z, \quad (2.181)$$

where

$${}^3w_x = w_x c\theta_1 + w_y s\theta_1,$$

$${}^3w_y = (-w_x s\theta_1 + w_y c\theta_1)c\theta_2 + w_z s\theta_2,$$

$${}^3w_z = (w_x s\theta_1 - w_y c\theta_1)s\theta_2 + w_z c\theta_2.$$

Note that the approach vector \mathbf{w} does not depend on the sixth joint angle, θ_6 . Solving Eq. (2.180) for θ_5 yields

$$\theta_5 = \cos^{-1}({}^3w_y). \quad (2.182)$$

Equation (2.182) yields two real roots of θ_5 if $|{}^3w_y| < 1$. When $|{}^3w_y| = 1$, Eq. (2.182) yields $\theta_5 = 0$ or π . For this case the sixth joint axis is in line with the fourth, and the wrist is said to be at a singular configuration. The condition $|{}^3w_y| > 1$ cannot occur physically. Assuming that $s\theta_5 \neq 0$, we solve θ_4 from Eqs. (2.179) and (2.181):

$$\theta_4 = \text{Atan2}({}^3w_z/s\theta_5, -{}^3w_x/s\theta_5). \quad (2.183)$$

Finally, we solve θ_6 by applying the transformation to the unit vector \mathbf{u} .

$$\mathbf{u} = R_1 R_2 R_3 R_4 R_5 R_6 \mathbf{u}_0. \quad (2.184)$$

Multiplying both sides of Eq. (2.184) by $(R_1 R_2 R_3)^{-1}$, we obtain

$$R_3^T R_2^T R_1^T \mathbf{u} = R_4 R_5 R_6 \mathbf{u}_0. \quad (2.185)$$

For convenience, we define ${}^3\mathbf{u} \equiv R_3^T R_2^T R_1^T \mathbf{u}$. Expanding Eq. (2.185) yields

$${}^3u_x = c\theta_4 c\theta_5 c\theta_6 - s\theta_4 s\theta_6, \quad (2.186)$$

$${}^3u_y = s\theta_5 c\theta_6, \quad (2.187)$$

$${}^3u_z = -s\theta_4 c\theta_5 c\theta_6 - c\theta_4 s\theta_6, \quad (2.188)$$

where

$${}^3u_x = u_x c\theta_1 + u_y s\theta_1,$$

$${}^3u_y = (-u_x s\theta_1 + u_y c\theta_1)c\theta_2 + u_z s\theta_2,$$

$${}^3u_z = (u_x s\theta_1 - u_y c\theta_1)s\theta_2 + u_z c\theta_2.$$

Multiplying Eq. (2.186) by $s\theta_4$ and (2.188) by $c\theta_4$ and summing produces

$$s\theta_4 {}^3u_x + c\theta_4 {}^3u_z = -s\theta_6. \quad (2.189)$$

From Eqs. (2.187) and (2.189), we obtain a unique solution for θ_6 :

$$\theta_6 = \text{Atan2}(-s\theta_4 {}^3u_x - c\theta_4 {}^3u_z, {}^3u_y/s\theta_5). \quad (2.190)$$

We conclude that corresponding to a given end-effector location, there are up to eight inverse kinematics solutions, but only four are physically realizable.

2.8 SUMMARY

In this chapter, two methods for solving the inverse kinematics of serial manipulators have been presented. First, the Denavit–Hartenberg parameters were defined. Then the D-H transformation matrices were developed for derivation of the kinematic equations. The D-H method was demonstrated by a planar 3-dof manipulator, the Scorbot robot, and the Fanuc S-900W robot. In addition, Tsai and Morgan's solution for the cases of three intersecting joint axes and three parallel joint axes was presented. Second, the concept of successive screw displacements and its application to the inverse kinematics of serial manipulators were described. It is shown that the inverse kinematics can be solved in a straightforward manner by applying the method of successive screw displacements. The inverse kinematics of an elbow manipulator and the Stanford manipulator were solved to illustrate the concept.

REFERENCES

- Albala, H., 1982, "Displacement Analysis of the General N -Bar, Single-Loop, Spatial Linkages," *ASME J. Mech. Des.*, Vol. 104, No. 2, pp. 504–525.
- Albala, H. and Angeles, J., 1979, "Numerical Solution to the Input–Output Displacement Equation of the General 7R Spatial Mechanism," *Proc. 5th World Congress on Theory of Machines and Mechanisms*, pp. 1008–1011.
- Bottema, O. and Roth, B., 1979, *Theoretical Kinematics*, North Holland, New York.

- Chase, M. A., 1963, "Vector Analysis of Linkages," *ASME J. Eng. Ind.*, Vol. 85, pp. 289–297.
- Denavit, J. and Hartenberg, R. S., 1955, "A Kinematic Notation for Lower Pair Mechanisms Based on Matrices," *ASME J. Appl. Mech.*, Vol. 77, pp. 215–221.
- Duffy, J., 1980, *Analysis of Mechanisms and Robot Manipulators*, Wiley, New York.
- Duffy, J. and Crane, C., 1980, "A Displacement Analysis of the General Spatial 7R Mechanism," *Mech. Mach. Theory*, Vol. 15, pp. 153–169.
- Duffy, J. and Rooney, J., 1975, "A Foundation for a Unified Theory of Analysis of Spatial Mechanisms," *ASME J. Eng. Ind.*, Vol. 97, No. 4, pp. 1159–1164.
- Freudentstein, F., 1973, "Kinematics: Past, Present, and Future," *Mech. Mach. Theory*, Vol. 8, No. 2, pp. 151–161.
- Gupta, K. C., 1984, "A Note on Position Analysis of Manipulators," *Mech. Mach. Theory*, Vol. 19, pp. 5–8.
- Gupta, K. C., 1986, "Kinematic Analysis of Manipulators Using Zero Reference Position Description," *Int. J. Robot. Res.*, Vol. 5, No. 2, pp. 5–13.
- Gupta, K. C., 1997, *Mechanics and Control of Robots*, Springer-Verlag, New York.
- Kohli, D. and Soni, A. H., 1975, "Kinematic Analysis of Spatial Mechanisms via Successive Screw Displacements," *ASME J. Eng. Ind.*, Vol. 97, No. 2, pp. 739–747.
- Lee, H. Y. and Liang, C. G., 1988a, "A New Vector Theory for the Analysis of Spatial Mechanisms," *Mech. Mach. Theory*, Vol. 23, No. 3, pp. 209–217.
- Lee, H. Y. and Liang, C. G., 1988b, "Displacement Analysis of the General Spatial 7-Link 7R Mechanism," *Mech. Mach. Theory*, Vol. 23, No. 3, pp. 219–226.
- Pennock, G. R. and Yang, A. T., 1985, "Application of Dual-Number Matrices to the Inverse Kinematics Problem of Robot Manipulators," *ASME J. Mech. Transm. Autom. Des.*, Vol. 107, No. 2, pp. 201–208.
- Pieper, D., 1968, "The Kinematics of Manipulators Under Computer Control," Ph.D. dissertation, Department of Mechanical Engineering, Stanford University, Stanford, CA.
- Pieper, D. L. and Roth, B., 1969, "The Kinematics of Manipulators Under Computer Control," *Proc. 2nd International Congress for the Theory of Machines and Mechanisms*, Zakopane, Poland, Vol. 2, pp. 159–168.
- Primrose, E. J. F., 1986, "On the Input–Output Equation of the General 7R-Mechanism," *Mech. Mach. Theory*, Vol. 21, No. 6, pp. 509–510.
- Raghavan, M. and Roth, B., 1989, "Kinematic Analysis of the 6R Manipulator of General Geometry," *Proc. 5th International Symposium on Robotics Research*, edited by H. Miura and S. Arimoto, MIT Press, Cambridge, MA; preprint 1989, final 1990.
- Raghavan, M. and Roth, B., 1990, "A General Solution for the Inverse Kinematics of All Series Chains," *Proc. 8th CISM-IFToMM Symposium on Robots and Manipulators* (ROMANSY-90), Cracow, Poland.

- Roth, B., Rastegar, J., and Scheinman, V., 1973, "On the Design of Computer Controlled Manipulators: On the Theory and Practice of Robots and Manipulators," *Proc. First CISM-IFToMM Symposium*, Vol. 1, pp. 93–113.
- Scheinman, V., 1969, "Design of Computer Controlled Manipulators," Report AIM 92, Stanford Artificial Intelligence Laboratory, Stanford, CA.
- Tsai, L. W., 1972, "Design of Open-Loop Chains for Rigid Body Guidance," Ph.D. dissertation, Department of Mechanical Engineering, Stanford University, Stanford, CA.
- Tsai, L. W. and Morgan, A., 1985, "Solving the Kinematics of the Most General Six- and Five-Degree-of-Freedom Manipulators by Continuation Methods," *ASME J. Mech. Transm. Autom. Des.*, Vol. 107, June, pp. 189–200.
- Tsai, L. W. and Roth, B., 1972, "Design of Dyads with Helical, Cylindrical, Spherical, Revolute, and Prismatic Joints," *Mech. Mach. Theory*, Vol. 7, pp. 85–102.
- Tsai, L. W. and Roth, B., 1973, "Incompletely Specified Displacement: Geometry and Spatial Linkage Synthesis," *ASME J. Eng. Ind.*, Vol. 95, Ser. B, No. 2, pp. 603–611.
- Uicker, J. J., Denavit, J., and Hartenberg, R. S., 1964, "An Iterative Method for Displacement Analysis of Spatial Mechanisms," *ASME J. Appl. Mech.*, Vol. 86, Ser. E, No. 2, pp. 309–314.
- Yang, A. T., 1969, "Displacement Analysis of Spatial Five-Link Mechanisms Using (3×3) Matrices with Dual-Number Elements," *ASME J. Eng. Ind.*, Vol. 9, No. 1, pp. 152–157.
- Yang, A. T. and Freudentstein, F., 1964, "Application of Dual Number Quaternion Algebra to the Analysis of Spatial Mechanisms," *ASME J. Appl. Mech.*, Vol. 86, pp. 300–308.
- Yuan, M. S. C. and Freudentstein, F., 1971, "Kinematic Analysis of Spatial Mechanisms by Means of Screw Coordinates," *ASME J. Eng. Ind.*, Vol. 93, No. 1, pp. 61–73.

EXERCISES

- Figure 2.18 shows an alternative method of coordinate frame assignment for the SCARA arm. Establish the D-H transformation matrices. Compare these transformation matrices with those given in Eqs. (2.9) through (2.12). Are there other methods of assigning the coordinate frames?
- Figure 2.19 shows a spatial 3-dof, 3R manipulator where the second joint axis is perpendicular to the first while the third joint axis is parallel to the second. Establish the D-H and overall transformation matrices ${}^{i-1}A_i$ for $i = 1, 2, \dots, 4$ and 0A_4 .
- For the elbow manipulator shown in Fig. 2.15, establish the D-H and overall transformation matrices ${}^{i-1}A_i$ for $i = 1, 2, \dots, 6$ and 0A_6 .

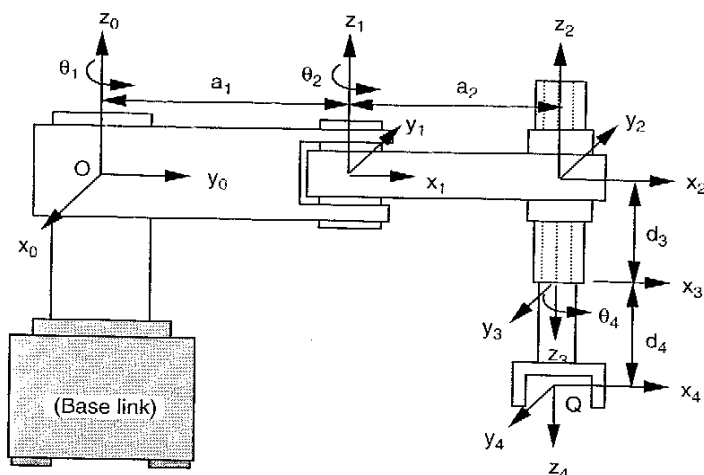


FIGURE 2.18. Alternative method of frame assignment for the SCARA arm.

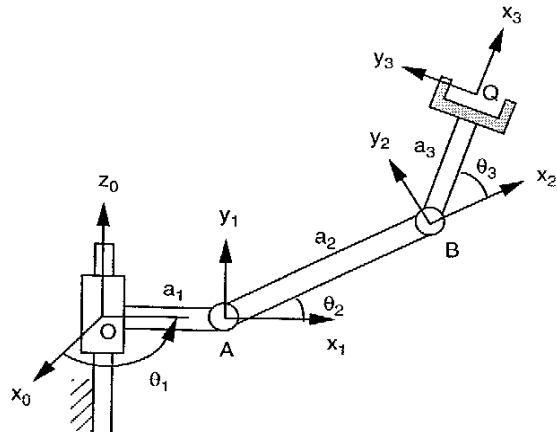


FIGURE 2.19. Spatial 3-dof, 3R manipulator.

4. Find the joint angles needed to bring the end effector of the manipulator shown in Fig. 2.19 to a given position \mathbf{q} by the D-H method. Corresponding to a given position of \mathbf{q} , how many number of possible arm configurations exist?
5. Solve the inverse kinematics of the 4-dof SCARA arm shown in Fig. 2.4 using the D-H method. Discuss how the orientation of the end effector can be specified.
6. For the elbow-type manipulator shown in Fig. 2.15, solve the joint angles in terms of a given end-effector location, \mathbf{q} and $\mathbf{u}, \mathbf{v}, \mathbf{w}$. How many possible solutions exist?
7. Figure 2.20 shows a schematic diagram of the Stanford arm. Find the joint angles needed to bring the end effector to a given position and orienta-

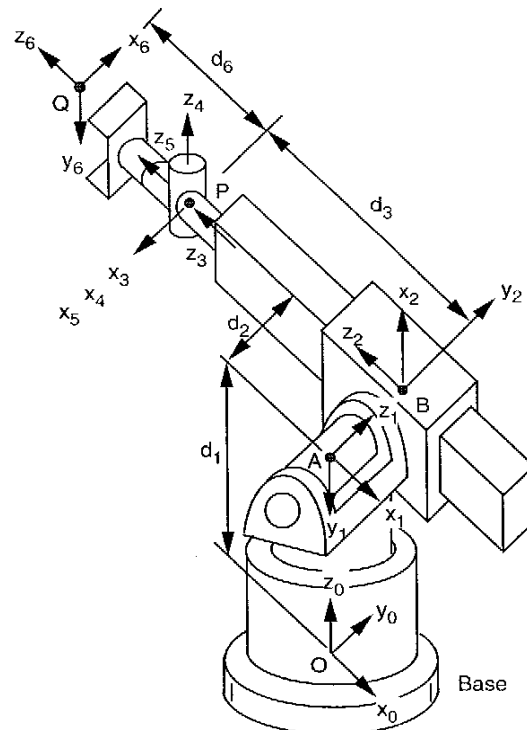


FIGURE 2.20. D-H coordinate systems associated with the Stanford manipulator.

- tation, \mathbf{q} and $\mathbf{u}, \mathbf{v}, \mathbf{w}$. Under what conditions will the manipulator possess no real solutions?
8. Solve the inverse kinematics of the 3-dof manipulator shown in Fig. 2.19 using the vector-loop approach.
 9. Solve the inverse kinematics of the 4-dof SCARA arm shown in Fig. 2.4 using the vector-loop approach.
 10. For the 3-dof manipulator shown in Fig. 2.19, find the joint angles needed to bring the end effector to a given position \mathbf{q} using the method of successive screw displacements.
 11. Figure 2.21 shows a reference position of the Scorbot robot. At this reference position, the first joint axis points up vertically along the positive z -direction; the second, third, and fourth joint axes point out of the paper, the fifth joint axis points to the right and intersects the fourth at P . The wrist center is located at Q . Solve the inverse kinematics problem using the method of successive screw displacements.

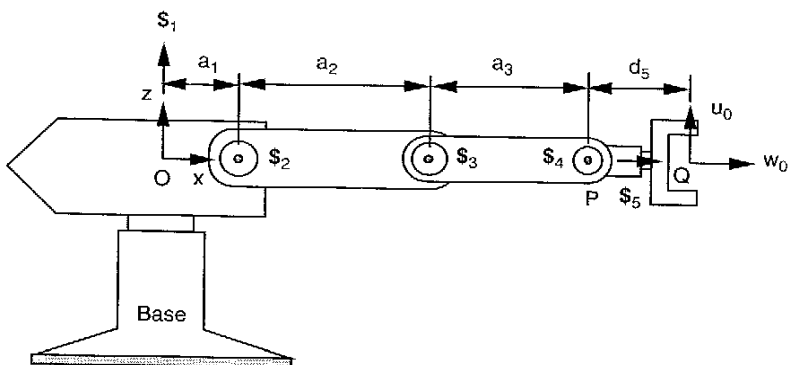


FIGURE 2.21. Reference position of the Scorbot robot.

12. Figure 2.22 shows a reference position of the Fanuc S-900W robot. Solve the inverse kinematics using the method of successive screw displacements.

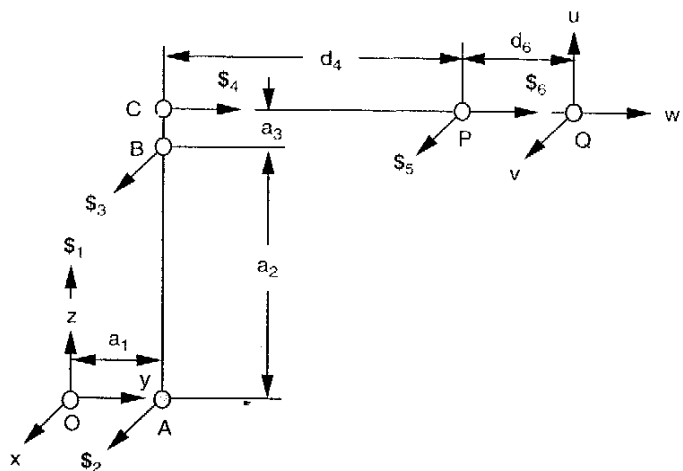


FIGURE 2.22. Reference position of the Fanuc S-900W robot.

CHAPTER 3

POSITION ANALYSIS OF PARALLEL MANIPULATORS

3.1 INTRODUCTION

In this chapter, the position analysis of a class of spatial multi-dof mechanisms known as *parallel manipulators* is studied. Parallel manipulators are classified as planar, spherical, or spatial manipulators in accordance with their motion characteristics. Then the direct and inverse kinematics of several parallel manipulators are analyzed.

As shown in Fig. 3.1, a parallel manipulator typically consists of a moving platform that is connected to a fixed base by several *limbs* or *legs*. Typically, the number of limbs is equal to the number of degrees of freedom such that every limb is controlled by one actuator and all the actuators can be mounted at or near the fixed base. For this reason, parallel manipulators are sometimes called *platform manipulators*. Because the external load can be shared by the actuators, parallel manipulators tend to have a large load-carrying capacity.

Parallel manipulators can be found in many applications, such as airplane simulators (Stewart, 1965), adjustable articulated trusses (Reinholtz and Gokhale, 1987), mining machines (Arai et al., 1991), pointing devices (Gosselin and Hamel, 1994), and walking machines (Waldron et al., 1984). Recently, it has also been developed as a high-speed, high-precision, multi-dof machining center, shown in Fig. 3.1 (Giddings & Lewis, 1995).

The design of parallel manipulators can be dated back to 1962, when Gough and Whitehall (1962) devised a six-linear jack system for use as a universal tire-testing machine. Stewart (1965) designed a platform manipulator for use as an aircraft simulator in 1965. Hunt (1983) made a systematic

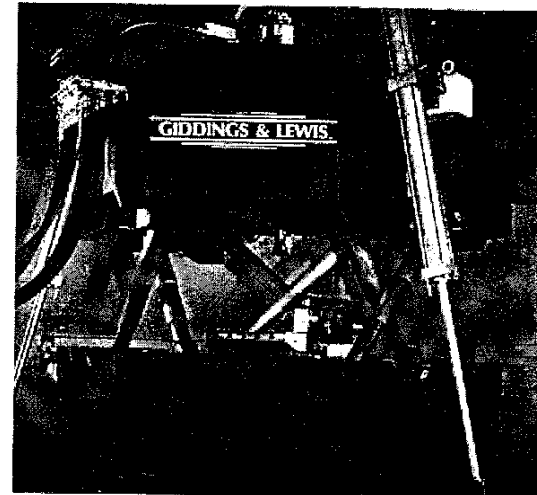


FIGURE 3.1. VARIAX® machining center. (Courtesy of Giddings & Lewis Machine Tools, Fond du Lac, Wisconsin.)

study of the kinematic structure of parallel manipulators. Since then, parallel manipulators have been studied extensively by numerous researchers (Clearly and Arai, 1991; Fichter, 1986; Griffis and Duffy, 1989; Innocenti and Parenti-Castelli, 1990; Mohamed and Duffy, 1985; Nanua et al., 1990; Zhang and Song, 1994).

Most of the 6-dof parallel manipulators studied to date consist of six extensible limbs. These parallel manipulators possess the advantages of high stiffness, low inertia, and large payload capacity. However, they suffer the problems of relatively small useful workspace and design difficulties. Furthermore, their direct kinematics is a very difficult problem. Perhaps, the only six-limbed, 6-dof parallel manipulators for which closed-form direct kinematic solutions have been reported in the literature are special forms of the Stewart-Gough platform (Chen and Song, 1994; Griffis and Duffy, 1989; Hussain and Waldron, 1994; Lin et al., 1994; Nanua et al., 1990). In these special forms, pairs of concentric spherical joints may present manufacturing problems. As to the general Stewart-Gough platform, researchers have to resort to numerical techniques for the solutions. Raghavan (1993) applied the continuation method, while Innocenti and Parenti-Castelli (1993a) developed an exhaustive monodimensional search algorithm to solve the direct kinematics of the general Stewart-Gough platform.

Other variations of the Stewart-Gough platform have also been proposed in an attempt to overcome the aforementioned shortcomings. See Clavel (1988), Hudgens and Tesar (1988), Kohli et al. (1988), Lee and Shah (1987), Pierrot et al. (1990, 1991), Sternheim (1987), Tahmasebi and Tsai (1994, 1995), Tsai (1996), Tsai and Tahmasebi (1993), and Tsai et al. (1996) for examples.

3.2 STRUCTURE CLASSIFICATION OF PARALLEL MANIPULATORS

A parallel manipulator is said to be *symmetrical* if it satisfies the following conditions:

1. The number of limbs is equal to the number of degrees of freedom of the moving platform.
2. The type and number of joints in all the limbs are arranged in an identical pattern.
3. The number and location of actuated joints in all the limbs are the same.

When the conditions above are not satisfied, the manipulator is called *asymmetrical*. In this chapter we are concerned primarily with symmetrical manipulators. We observe that in a symmetrical manipulator the number of limbs, m , is equal to the number of degrees of freedom, F , which is also equal to the total number of loops, $L + 1$ (including the external loop); that is,

$$m = F = L + 1. \quad (3.1)$$

Let the *connectivity*, C_k , of a limb be the degrees of freedom associated with all the joints in the limb. It follows that

$$\sum_{k=1}^m C_k = \sum_{i=1}^j f_i, \quad (3.2)$$

where j is the number of joints in a mechanism. Substituting Eq. (1.8) into (3.2) and eliminating L by making use of (3.1), we obtain

$$\sum_{k=1}^m C_k = (\lambda + 1)F - \lambda. \quad (3.3)$$

Furthermore, the connectivity of each limb should not be greater than the motion parameter and less than the degrees of freedom of the moving plat-

form; that is,

$$\lambda \geq C_k \geq F. \quad (3.4)$$

Equations (3.3) and (3.4) are useful for enumeration and classification of parallel manipulators. Parallel mechanisms can generally be classified as planar, spherical, or spatial mechanisms. In what follows, we discuss the enumeration of each of these three types of manipulators.

3.2.1 Planar Parallel Manipulators

For planar 3-dof, three-limbed parallel manipulators, we have $\lambda = 3$ and $m = F = 3$. Substituting $\lambda = 3$ and $F = 3$ into Eq. (3.3), we obtain

$$C_1 + C_2 + C_3 = 4F - 3 = 9. \quad (3.5)$$

At the same time, Eq. (3.4) reduces to

$$3 \geq C_k \geq 3. \quad (3.6)$$

Hence the connectivity of each limb should be equal to 3; that is, each limb should have 3 degrees of freedom in its joints. Assuming that each limb consists of two links and three joints, each joint must be a 1-dof joint. Using revolute and prismatic joints as the kinematic pairs, we obtain seven possible limb arrangements: *RRR*, *RRP*, *RPR*, *PRR*, *RPP*, *PRP*, and *PPR*. Further, if we limit ourselves to manipulators with three identical limb structures, only seven 3-dof planar parallel manipulators are feasible.

Figure 3.2 shows a planar 3-dof parallel manipulator using the *3RRR* limb structure (Gosselin and Angeles, 1988); Figure 3.3 shows a planar 3-dof parallel manipulator using the *3PRP* limb structure, where the three revolute joint axes are perpendicular to the plane of motion while the prismatic joint axes lie on the plane of motion (Mohammadi et al., 1993).

3.2.2 Spherical Parallel Manipulators

The motion parameter for spherical mechanisms is also equal to 3. Hence the connectivity requirement for spherical parallel manipulators is identical to that of planar parallel manipulators. For spherical linkage manipulators, the only permissible joint type is the revolute joint, and all the joint axes must intersect at a common point, called the *spherical center*. Hence the only possible limb structure is the *RRR* configuration. The manipulator shown in Fig. 1.21 is a 3-dof, *3RRR* spherical parallel manipulator.

We note that one spherical joint can be installed at the center of a spherical parallel manipulator. However, such a spherical joint can only be used

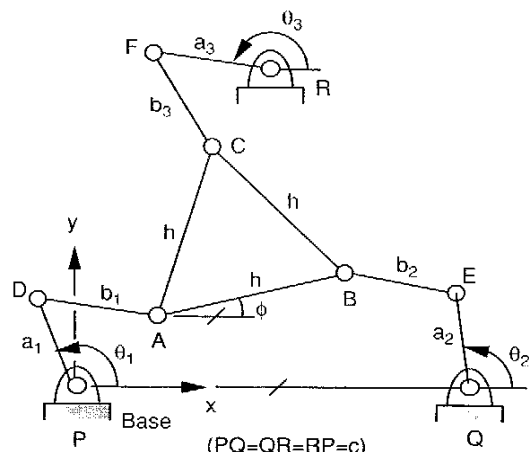


FIGURE 3.2. Planar 3-dof, 3RRR parallel manipulator.

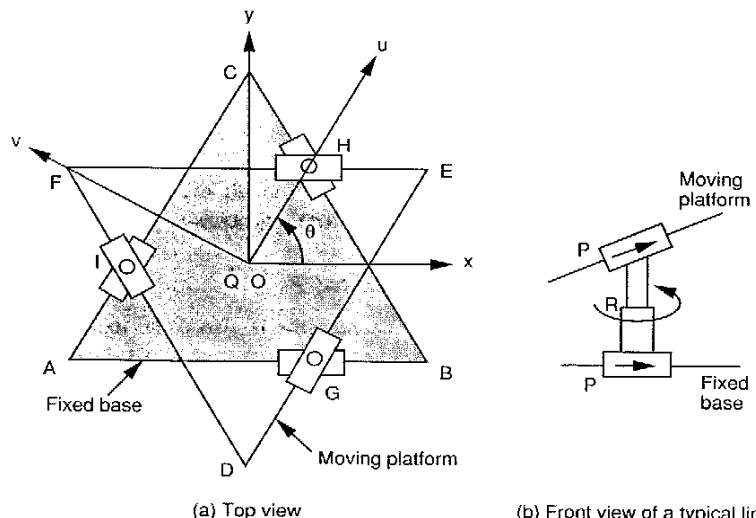


FIGURE 3.3. Planar 3-dof, 3PRP parallel manipulator.

as a passive joint, since it cannot be actuated by existing actuators. Hence, if a spherical joint is used, three additional limbs would be needed for parallel actuation of the moving platform. In this case, the number of limbs, including the limb with a spherical joint of zero length, is no longer equal to the number of degrees of freedom. Readers can refer to several articles related to the design and analysis of spherical parallel manipulators (Gosselin and Angeles, 1989; Gosselin and Hamel, 1994; Innocenti and Parenti-Castelli, 1993b; Wohlhart, 1994).

3.2.3 Spatial Parallel Manipulators

Substituting $\lambda = 6$ into Eqs. (3.3) and (3.4) for spatial mechanisms, we obtain

$$\sum_k^m C_k = 7F - 6 \quad (3.7)$$

and

$$6 \geq C_k \geq F. \quad (3.8)$$

Solving Eqs. (3.7) and (3.8) simultaneously for positive integers of C_k , $k = 1, 2, 3, \dots$, we can classify spatial parallel manipulators according to their degrees of freedom and connectivity listing as given in Table 3.1 (Hunt, 1983).

The number of links incorporated in each limb can be any as long as the sum of all joint freedoms is equal to the required connectivity. The maximum number of links occurs when all the joints are 1-dof joints. In practice, it is desirable to employ just two major links connecting the moving platform to

TABLE 3.1. Classification of Spatial Parallel Manipulators

Degrees of Freedom F	Number of Loops L	Sum of All Joint Freedoms $\sum_i f_i$	Connectivity Listing $C_k, k = 1, 2, 3, \dots$
2	1	8	4,4 5,3 6,2
3	2	15	5,5,5 6,5,4 6,6,3
4	3	22	6,6,5,5 6,6,6,4
5	4	29	6,6,6,6,5
6	5	36	6,6,6,6,6,6

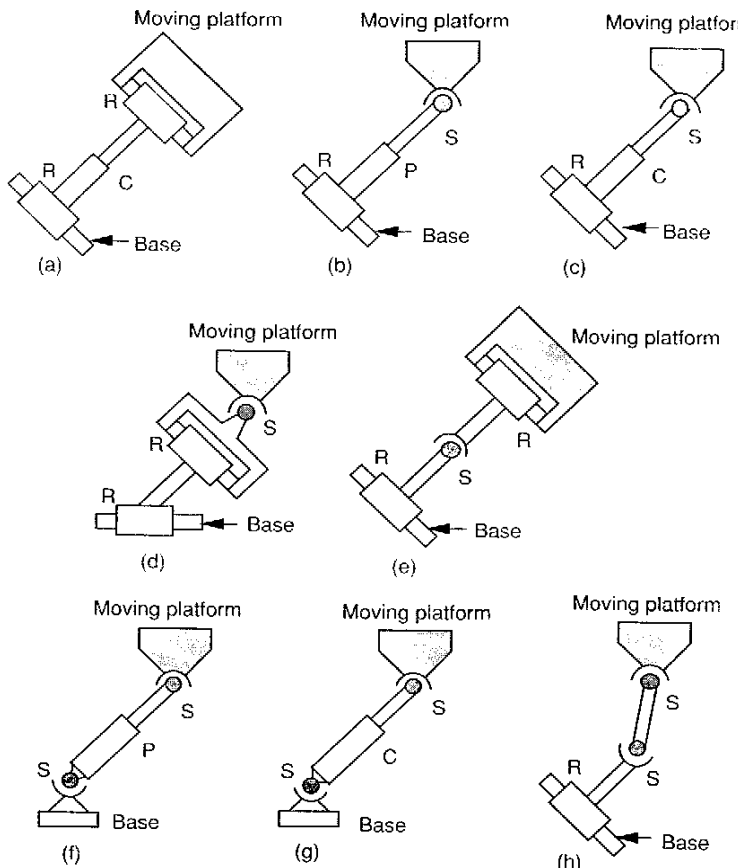


FIGURE 3.4. Eight possible limb configurations.

the base by three joints. Figure 3.4 illustrates a few such limb configurations. Figure 3.4a is a 4-dof limb, Fig. 3.4b-e are 5-dof limbs, and Fig. 3.4f-h are 6-dof limbs. Note that each of the limbs shown in Fig. 3.4c, f, and h contains 1 passive degree of freedom, while the one shown in Fig. 3.4g contains 2 passive degrees of freedom.

If limbs of identical kinematic structure are desired, the (4,4), (5,5,5), and (6,6,6,6,6) connectivity listings are the only feasible limb arrangements for

the 2-, 3-, and 6-dof parallel manipulators. For example, the 6-dof machining center developed by Giddings & Lewis (1995) shown in Fig. 3.1 has a connectivity listing of (6,6,6,6,6,6). Six 6UPS limbs connect a moving platform to the fixed base. The prismatic joint in the middle of each limb is driven by a dc motor using a linear ball screw as the force transmission mechanism. Extending and retracting of the limbs alter the location of the moving platform on which a spindle is mounted, making six-axis machining feasible.

3.3 DENAVIT-HARTENBERG METHOD VERSUS GEOMETRIC METHOD

In this section we present the Denavit-Hartenberg matrix method of analysis. To facilitate the analysis, a Cartesian coordinate system is defined on each link in accordance with the Denavit-Hartenberg convention as shown in Fig. 3.5. Unlike open-loop manipulators, all the coordinate systems in a closed-loop mechanism are defined completely by the geometry of the linkage. In particular, the end-effector (n th) coordinate system coincides with the base (zeroth) coordinate system.

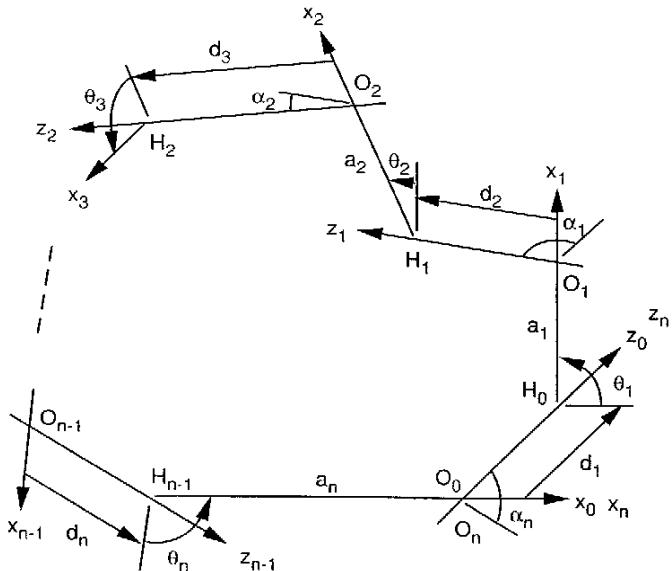


FIGURE 3.5. Closed-loop mechanism and its D-H parameters.

A change of coordinates between the i th coordinate system and the $(i+1)$ th coordinate system is given in Eq. (2.2). When the change of coordinates is taken in succession, the corresponding matrices are multiplied. When all the changes of coordinates are taken, starting from the (x_0, y_0, z_0) system, going around the chain, and returning to the (x_0, y_0, z_0) system, the resulting matrix of transformation is given by ${}^0A_1 {}^1A_2 \dots {}^{n-2}A_{n-1} {}^{n-1}A_n$. But this transformation is an identity transformation because of the return to the original system. Hence we can write

$${}^0A_1 {}^1A_2 \dots {}^{n-2}A_{n-1} {}^{n-1}A_n = I, \quad (3.9)$$

where I is a 4×4 identity matrix.

For a multiple-loop mechanism, we formulate the loop-closure equation above once for each independent loop of the mechanism to obtain a set of constraint equations. We note that a universal joint can be modeled by two intersecting revolute joints, and a spherical joint can be modeled by three intersecting revolute joints.

Although the Denavit–Hartenberg method is very general, the method is complicated by the existence of multiple closed loops. For parallel manipulators, it is often more convenient to employ the geometric method. Generally, a *vector-loop equation* is written for each limb, and the passive joint variables are eliminated among these equations. In the following sections, we analyze the kinematics of several parallel manipulators to illustrate the methodology.

3.4 POSITION ANALYSIS OF A PLANAR 3RRR PARALLEL MANIPULATOR

For the planar 3-dof parallel manipulator shown in Fig. 3.2, the three fixed pivots P , Q , and R define the geometry of a fixed base, and the three moving pivots A , B , and C define the geometry of a moving platform. Three limbs connect the moving platform at points A , B , and C to the fixed base at points P , Q , and R by revolute joints. Each limb consists of two links connected by a revolute joint. Together, the mechanism consists of eight links and nine revolute joints. The degrees of freedom of the mechanism are computed from Eq. (1.4):

$$F = \lambda(n - j - 1) + \sum_i f_i = 3(8 - 9 - 1) + 9 = 3.$$

Hence the mechanism has 3 degrees of freedom. We consider the moving platform as the output link and links PD , QE , and RF as the input links. Thus all actuators can be installed on the fixed base.

3.4.1 Geometry of the Manipulator

Referring to Fig. 3.2, the origin of the fixed coordinate frame is located at point P . The x -axis points along the direction of \overline{PQ} and the y -axis is perpendicular to \overline{PQ} . We assume that both the moving platform ABC and the fixed platform PQR are equilateral triangles (i.e., $AB = BC = AC = h$ and $PQ = QR = RP = c$). Figure 3.6 shows the link lengths and joint angles of a typical limb i .

The location of the moving platform can be specified in terms of the position of point A , and an orientation angle, ϕ . Then the coordinates of points B and C can be written in terms of A and ϕ as follows:

$$\begin{aligned} x_B &= x_A + hc\phi, \\ y_B &= y_A + hs\phi, \end{aligned} \quad (3.10)$$

and

$$\begin{aligned} x_C &= x_A + hc \left(\phi + \frac{\pi}{3} \right), \\ y_C &= y_A + hs \left(\phi + \frac{\pi}{3} \right). \end{aligned} \quad (3.11)$$

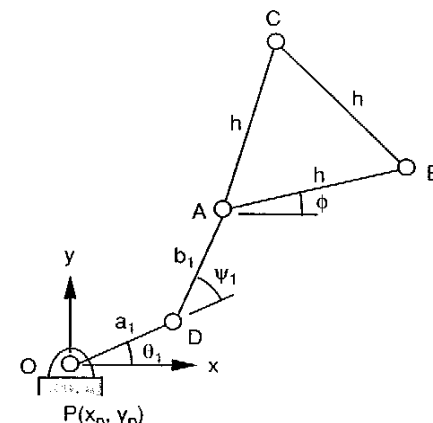


FIGURE 3.6. Joint angles associated with a typical limb of the 3RRR planar parallel manipulator.

From the geometry of Fig. 3.6, a vector-loop equation can be written as

$$\overline{OA} = \overline{OP} + \overline{PD} + \overline{DA}. \quad (3.12)$$

Expressing the vector-loop equation above in the fixed coordinate frame gives

$$\begin{aligned} x_A &= x_P + a_1 c\theta_1 + b_1 c(\theta_1 + \psi_1), \\ y_A &= y_P + a_1 s\theta_1 + b_1 s(\theta_1 + \psi_1). \end{aligned} \quad (3.13)$$

Since P is located at the origin, $x_P = y_P = 0$, identically. Since ψ_1 is a passive joint angle, it should be eliminated from the equations above. Toward this goal, we write Eq. (3.13) in the following form:

$$\begin{aligned} x_A - a_1 c\theta_1 &= b_1 c(\theta_1 + \psi_1), \\ y_A - a_1 s\theta_1 &= b_1 s(\theta_1 + \psi_1). \end{aligned} \quad (3.14)$$

Summing the squares of the two equations in (3.14) yields

$$x_A^2 + y_A^2 - 2x_A a_1 c\theta_1 - 2y_A a_1 s\theta_1 + a_1^2 - b_1^2 = 0. \quad (3.15)$$

Similarly, two additional equations can be derived for limbs 2 and 3:

$$\begin{aligned} x_A^2 + y_A^2 - 2x_{AQ} - 2y_{AQ} + x_Q^2 + y_Q^2 + h^2 + a_2^2 - b_2^2 + 2x_A h c\phi \\ + 2y_A h s\phi - 2x_A a_2 c\theta_2 - 2y_A a_2 s\theta_2 - 2a_2 h c\phi c\theta_2 - 2x_Q h c\phi - 2y_Q h s\phi \\ + 2x_Q a_2 c\theta_2 + 2y_Q a_2 s\theta_2 - 2a_2 h s\phi s\theta_2 = 0, \end{aligned} \quad (3.16)$$

$$\begin{aligned} x_A^2 + y_A^2 - 2x_{AR} - 2y_{AR} + x_R^2 + y_R^2 + h^2 + a_3^2 - b_3^2 \\ + 2x_A h c\left(\phi + \frac{\pi}{3}\right) + 2y_A h s\left(\phi + \frac{\pi}{3}\right) - 2x_A a_3 c\theta_3 \\ - 2y_A a_3 s\theta_3 - 2a_3 h c\left(\phi + \frac{\pi}{3}\right) c\theta_3 \\ - 2x_R h c\left(\phi + \frac{\pi}{3}\right) - 2y_R h s\left(\phi + \frac{\pi}{3}\right) + 2x_R a_3 c\theta_3 \\ + 2y_R a_3 s\theta_3 - 2a_3 h s\left(\phi + \frac{\pi}{3}\right) s\theta_3 = 0. \end{aligned} \quad (3.17)$$

3.4.2 Inverse Kinematics

For the inverse kinematics, x_A , y_A , and ϕ are given, and the joint angles θ_1 , θ_2 , and θ_3 are to be found. This can be accomplished on a limb-by-limb basis. For

limb 1 we arrange Eq. (3.15) in the following form:

$$e_1 s\theta_1 + e_2 c\theta_1 + e_3 = 0, \quad (3.18)$$

where

$$\begin{aligned} e_1 &= -2y_A a_1, \\ e_2 &= -2x_A a_1, \\ e_3 &= x_A^2 + y_A^2 + a_1^2 - b_1^2. \end{aligned}$$

Substituting the trigonometric identities

$$s\theta_i = \frac{2t_i}{1+t_i^2} \quad \text{and} \quad c\theta_i = \frac{1-t_i^2}{1+t_i^2}, \quad \text{where} \quad t_i = \tan \frac{\theta_i}{2}$$

into Eq. (3.18), we obtain

$$(e_3 - e_2)t_1^2 + 2e_1 t_1 + (e_3 + e_2) = 0. \quad (3.19)$$

Solving Eq. (3.19) for t_1 yields

$$\theta_1 = 2 \tan^{-1} \frac{-e_1 \pm \sqrt{e_1^2 + e_2^2 - e_3^2}}{e_3 - e_2}. \quad (3.20)$$

Hence, corresponding to each given moving platform location, there are generally two solutions of θ_1 and therefore two configurations of limb 1. When Eq. (3.18) yields a double root, the two links PD and DA are in a fully stretched-out or folded-back configuration called the *singular configuration*. When Eq. (3.18) yields no real root, the specified moving platform location is not reachable. Once θ_1 is solved, ψ_1 can be found from Eq. (3.13) by back substitution.

Following the same procedure, the other two limb configurations can be solved. We conclude that, in general, there are a total of eight possible manipulator postures corresponding to a given end-effector location.

3.4.3 Direct Kinematics

For the direct kinematics, θ_1 , θ_2 , and θ_3 are given, and the position (x_A, y_A) and the orientation angle ϕ of the moving platform are to be found. This can be accomplished by eliminating x_A and y_A from Eqs. (3.15), (3.16), and (3.17) as follows. First, we write Eqs. (3.15), (3.16), and (3.17) in the follow-

ing forms:

$$x_A^2 + y_A^2 + e_{11}x_A + e_{12}y_A + e_{13} = 0, \quad (3.21)$$

$$x_A^2 + y_A^2 + e_{21}x_A + e_{22}y_A + e_{23} = 0, \quad (3.22)$$

$$x_A^2 + y_A^2 + e_{31}x_A + e_{32}y_A + e_{33} = 0. \quad (3.23)$$

where

$$e_{11} = -2a_1c\theta_1,$$

$$e_{12} = -2a_1s\theta_1,$$

$$e_{13} = a_1^2 - b_1^2,$$

$$e_{21} = -2x_Q + 2hc\phi - 2a_2c\theta_2,$$

$$e_{22} = -2y_Q + 2hs\phi - 2a_2s\theta_2,$$

$$e_{23} = x_Q^2 + y_Q^2 + h^2 + a_2^2 - b_2^2 - 2a_2hc\phi c\theta_2 - 2a_2hs\phi s\theta_2 \\ - 2x_Qhc\phi - 2y_Qhs\phi + 2x_Qa_2c\theta_2 + 2y_Qa_2s\theta_2,$$

$$e_{31} = -2x_R + 2hc\left(\phi + \frac{\pi}{3}\right) - 2a_3c\theta_3,$$

$$e_{32} = -2y_R + 2hs\left(\phi + \frac{\pi}{3}\right) - 2a_3s\theta_3,$$

$$e_{33} = x_R^2 + y_R^2 + h^2 + a_3^2 - b_3^2 - 2a_3hc\left(\phi + \frac{\pi}{3}\right)c\theta_3 - 2a_3hs\left(\phi + \frac{\pi}{3}\right)s\theta_3 \\ - 2x_Rhc\left(\phi + \frac{\pi}{3}\right) - 2y_Rhs\left(\phi + \frac{\pi}{3}\right) + 2x_Ra_3c\theta_3 + 2y_Ra_3s\theta_3.$$

Note that e_{11} , e_{12} , and e_{13} are constants, while e_{21} , e_{22} , e_{23} , e_{31} , e_{32} , and e_{33} are linear functions of $s\phi$ and $c\phi$.

Equations (3.21), (3.22), and (3.23) constitute three nonlinear equations in three unknowns, x_A , y_A , and ϕ . This system of equations can be simplified by performing the following operations. Subtracting Eq. (3.22) from (3.21) yields

$$e'_{11}x_A + e'_{12}y_A + e'_{13} = 0. \quad (3.24)$$

Subtracting Eq. (3.23) from (3.21) yields

$$e'_{21}x_A + e'_{22}y_A + e'_{23} = 0. \quad (3.25)$$

Here $e'_{11} = e_{11} - e_{21}$, $e'_{12} = e_{12} - e_{22}$, $e'_{13} = e_{13} - e_{23}$, $e'_{21} = e_{11} - e_{31}$, $e'_{22} = e_{12} - e_{32}$, and $e'_{23} = e_{13} - e_{33}$ are linear functions of $\sin\phi$ and $\cos\phi$.

Equations (3.21) together with (3.24) and (3.25) form a new system of equations. We may solve Eqs. (3.24) and (3.25) for x_A and y_A and then sub-

stitute the resulting expressions into Eq. (3.21). This results in a fourth-degree polynomial in $s\phi$ and $c\phi$:

$$\delta_1^2 + \delta_2^2 + e_{11}\delta\delta_1 + e_{12}\delta\delta_2 + e_{13}\delta^2 = 0, \quad (3.26)$$

where

$$\delta = e'_{11}e'_{22} - e'_{12}e'_{21},$$

$$\delta_1 = e'_{12}e'_{23} - e'_{13}e'_{22},$$

$$\delta_2 = e'_{13}e'_{21} - e'_{11}e'_{23}.$$

Equation (3.26) can be converted into an eighth-degree polynomial by using the half-tangent angle expressions. Hence, corresponding to each given set of input joint angles, there are at most eight possible manipulator configurations. A numerical method of solution can be found in Gosselin and Sefrioui (1991).

3.5 POSITION ANALYSIS OF A SPATIAL ORIENTATION MECHANISM

In this section the kinematics of a 3-dof orientation platform is studied. First, we describe the kinematic structure of the manipulator. Then the inverse and direct kinematics are solved in closed form.

Figure 3.7 shows a spatial parallel manipulator that is made up of a moving platform, a fixed base, and three extensible limbs. Both the moving platform $OB_1B_2B_3$ and the fixed base $OA_1A_2A_3$ take the form of a tetrahedron. The moving platform is connected directly to the fixed base by a spherical joint at point O . In addition, three extensible limbs connect the moving platform at points B_i to the fixed base at points A_i by spherical joints. Each limb consists of an upper member and a lower member connected by a prismatic joint. Ball screws or hydraulic jacks can be used to vary the lengths of the prismatic joints and therefore to control the motion of the moving platform. Overall, there are eight links connected together by seven spherical and three prismatic joints. We note that this mechanism is not a spherical mechanism, because the three limbs and the moving platform do not have a common stationary point. In fact, the upper members of the three limbs do not possess spherical motions at all.

Substituting $\lambda = 6$, $n = 8$, $j = 10$, and the appropriate f_i for each joint into Eq. (1.4) yields

$$F = \lambda(n - j - 1) + \sum_i f_i = 6(8 - 10 - 1) + (7 \times 3 + 3) = 6.$$



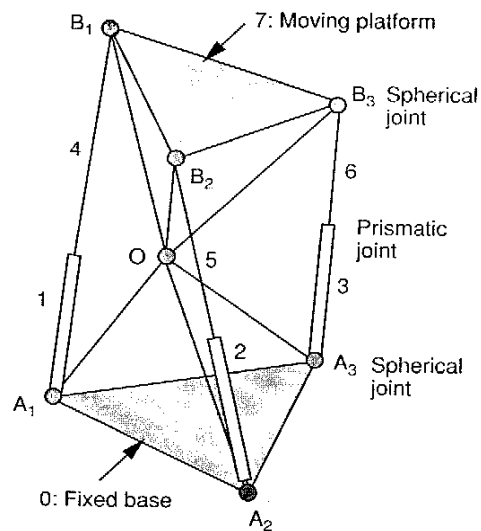


FIGURE 3.7. A 3-dof orientation platform.

However, there is a passive degree of freedom associated with each of the three limbs. Hence the moving platform possesses only 3 degrees of freedom. Although the motion of the whole mechanism is not spherical, the moving platform does possess a spherical motion because of the existence of a fixed point O . This mechanism can be used as an orienting device in which the moving platform is treated as the output link, and the three prismatic joints are employed as the input means.

3.5.1 Geometry of the Manipulator

For the purpose of analysis, two Cartesian coordinate systems $A(x, y, z)$ and $B(u, v, w)$ are attached to the fixed base and moving platform, respectively, as shown in Fig. 3.8. Without losing generality, we assume that the origin of frame A is located at the fixed point O , the z -axis points along the direction of OA_1 , the x -axis lies on the plane of OA_1A_2 , and the y -axis is defined according to the right-hand rule. Similarly, we assume that the origin of frame B is located at the fixed point O , the w -axis points along the direction of OB_1 , the u -axis lies on the plane of OB_1B_2 , and the v -axis is defined according to the right-hand rule.

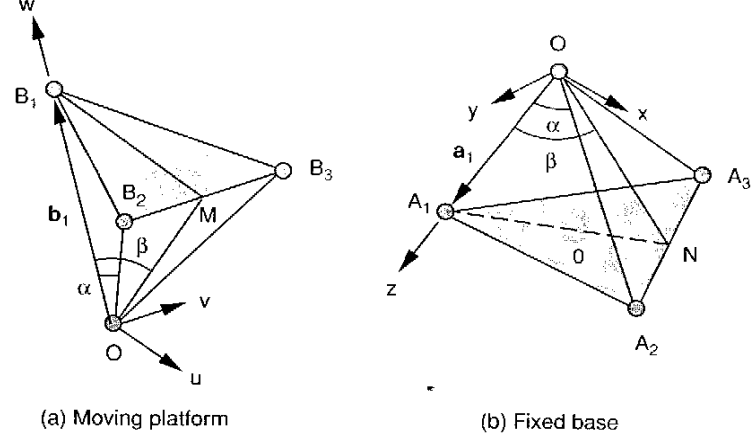


FIGURE 3.8. Coordinate systems of the orientation mechanism.

The transformation from the moving frame B to the fixed frame A can be described by a 3×3 rotation matrix ${}^A R_B$ defined by the following three Euler angles. Assume that the initial location of the moving frame B coincides with the fixed frame A and that the final location is obtained by a rotation of ϕ about the w -axis, followed by a second rotation of θ about the displaced u -axis, followed by a third rotation of ψ about the displaced w -axis. Then the resulting rotation matrix is given by:

$${}^A R_B = \begin{bmatrix} c\phi c\psi - s\phi c\theta s\psi & -c\phi s\psi - s\phi c\theta c\psi & s\phi s\theta \\ s\phi c\psi + c\phi c\theta s\psi & -s\phi s\psi + c\phi c\theta c\psi & -c\phi s\theta \\ s\theta s\psi & s\theta c\psi & c\theta \end{bmatrix}. \quad (3.27)$$

Let the position vector of point B_i with respect to the moving frame B be given by

$${}^B \mathbf{b}_i = [b_{iu}, b_{iv}, b_{iw}]^T. \quad (3.28)$$

Then the position vector of point B_i expressed in the fixed frame A is

$$\begin{aligned} {}^B \mathbf{b}_i &= [b_{ix}, b_{iy}, b_{iz}]^T = {}^A R_B \cdot {}^B \mathbf{b}_i \\ &= \begin{bmatrix} b_{iu}(c\phi c\psi - s\phi c\theta s\psi) - b_{iv}(c\phi s\psi + s\phi c\theta c\psi) + b_{iw}s\phi s\theta \\ b_{iu}(s\phi c\psi + c\phi c\theta s\psi) - b_{iv}(s\phi s\psi - c\phi c\theta c\psi) - b_{iw}c\phi s\theta \\ b_{iu}s\theta s\psi + b_{iv}s\theta c\psi + b_{iw}c\theta \end{bmatrix}. \end{aligned} \quad (3.29)$$

Also let the position vector of point A_i with respect to the fixed frame A be given by

$$\mathbf{a}_i = [a_{ix}, a_{iy}, a_{iz}]^T. \quad (3.30)$$

Then a loop-closure equation can be written for limb i as

$$\mathbf{d}_i = \mathbf{b}_i - \mathbf{a}_i, \quad (3.31)$$

where $\mathbf{d}_i = \overline{A_i B_i}$.

Dot-multiplying Eq. (3.31) with itself produces an equation of constraint imposed by limb i as follows:

$$d_i^2 = \mathbf{a}_i^2 + \mathbf{b}_i^2 - 2\mathbf{a}_i^T \mathbf{b}_i, \quad (3.32)$$

where d_i denotes the length of the i th limb. Substituting Eqs. (3.29) and (3.30) into (3.32) yields

$$e_{i1}c\phi + e_{i2}s\phi + e_{i3} = 0 \quad \text{for } i = 1, 2, 3, \quad (3.33)$$

where

$$e_{i1} = \lambda_{i1}c\psi + \lambda_{i2}s\psi + \lambda_{i3}, \quad (3.34)$$

$$e_{i2} = \mu_{i1}c\psi + \mu_{i2}s\psi + \mu_{i3}, \quad (3.35)$$

$$e_{i3} = \nu_{i1}c\psi + \nu_{i2}s\psi + \nu_{i3}, \quad (3.36)$$

$$\lambda_{i1} = a_{iy}b_{iv}c\theta + a_{ix}b_{iu},$$

$$\lambda_{i2} = a_{iy}b_{iu}c\theta - a_{ix}b_{iv},$$

$$\lambda_{i3} = -a_{iy}b_{iw}s\theta,$$

$$\mu_{i1} = -a_{ix}b_{iv}c\theta + a_{iy}b_{iu},$$

$$\mu_{i2} = -a_{ix}b_{iu}c\theta - a_{iy}b_{iv},$$

$$\mu_{i3} = a_{ix}b_{iw}s\theta,$$

$$\nu_{i1} = a_{iz}b_{iv}s\theta,$$

$$\nu_{i2} = a_{iz}b_{iu}s\theta,$$

$$\nu_{i3} = a_{iz}b_{iw}c\theta - \frac{1}{2}(\mathbf{a}_i^2 + \mathbf{b}_i^2 - d_i^2).$$

Equation (3.32) or (3.33) written three times, once for each $i = 1, 2$, and 3, yields three equations of constraint for the moving platform.

3.5.2 Inverse Kinematics

For inverse kinematics, the orientation of the moving platform is known, and the problem is to find the limb lengths d_1 , d_2 , and d_3 . The orientation of the moving platform is described by the three Euler's angles, ϕ , θ , and ψ . Once the orientation of the moving platform is known, the position of points B_i for $i = 1, 2$, and 3 can be computed from Eq. (3.29). Hence the corresponding limb lengths d_i , $i = 1, 2, 3$, can be computed from Eq. (3.32):

$$d_i^2 = \pm \sqrt{\mathbf{a}_i^2 + \mathbf{b}_i^2 - 2\mathbf{a}_i^T \mathbf{b}_i} \quad \text{for } i = 1, 2, 3. \quad (3.37)$$

There are generally two solutions of d_i . However, only the positive limb length is physically realizable.

3.5.3 Direct Kinematics

For direct kinematics, the limb lengths d_1 , d_2 , and d_3 are given, and the problem is to find the orientation of the moving platform. Equation (3.33) written three times yields a system of three trigonometric equations that can be solved for the three variables ϕ , θ , and ψ . For the coordinate systems chosen, we have $a_{1x} = a_{1y} = a_{2y} = 0$, $b_{1u} = b_{1v} = b_{2v} = 0$, $a_{1z} = \ell_1 = OA_1$, and $b_{1w} = \ell_2 = OB_1$. Equation (3.33) written for $i = 1$ yields

$$\theta = \cos^{-1} \frac{\ell_1^2 + \ell_2^2 - d_1^2}{2\ell_1\ell_2}. \quad (3.38)$$

Hence Eq. (3.38) yields two solutions of θ . However, these two solutions represent only one manipulator orientation. Hence they will be counted as one solution. This is a common problem associated with the Euler angle representation of the orientation of a rigid body.

Once θ is found, we can write Eq. (3.33) twice for $i = 2$ and 3 and solve them for $c\phi$ and $s\phi$ as follows:

$$c\phi = \frac{e_{22}e_{33} - e_{23}e_{32}}{e_{21}e_{32} - e_{22}e_{31}}, \quad (3.39)$$

$$s\phi = \frac{e_{23}e_{31} - e_{21}e_{33}}{e_{21}e_{32} - e_{22}e_{31}}, \quad (3.40)$$

provided that $e_{21}e_{32} - e_{22}e_{31} \neq 0$. Then we eliminate ϕ by substituting Eqs. (3.39) and (3.40) into the trigonometric identity $c^2\phi + s^2\phi = 1$. This results in the following equation:

$$(e_{22}e_{33} - e_{23}e_{32})^2 + (e_{23}e_{31} - e_{21}e_{33})^2 - (e_{21}e_{32} - e_{22}e_{31})^2 = 0. \quad (3.41)$$

Substituting Eqs. (3.34)–(3.36) into Eq. (3.41) and making use of the trigonometric identities

$$\cos \psi = \frac{1-t^2}{1+t^2} \quad \text{and} \quad \sin \psi = \frac{2t}{1+t^2}, \quad \text{where} \quad t = \tan \frac{\psi}{2},$$

we obtain an eighth-degree polynomial in t :

$$\kappa_0 t^8 + \kappa_1 t^7 + \cdots + \kappa_7 t + \kappa_8 = 0, \quad (3.42)$$

where $\kappa_i, i = 0, 1, \dots, 8$, are functions of the geometric parameters \mathbf{a}_i and \mathbf{b}_i , limb lengths d_i , and the angle θ . It follows that corresponding to each solution of θ , there are at most eight solutions of ψ . Once θ and ψ are known, Eqs. (3.39) and (3.40) yield a single value of ϕ . We conclude that the direct kinematics of the orientation platform has at most eight feasible postures.

3.6 POSITION ANALYSIS OF THE UNIVERSITY OF MARYLAND MANIPULATOR

In this section the kinematics of a 3-dof parallel manipulator developed at the University of Maryland (Tsai and Stamper, 1996) is studied. This manipulator, shown in Fig. 3.9, employs only revolute joints to constrain the moving platform output to translational motion. A schematic diagram of the manipulator is sketched in Fig. 3.10, where the fixed base is labeled as link 0 and the moving platform is labeled as link 16. Three identical limbs connect the moving platform to the fixed base. Each limb consists of an upper arm and a lower arm. The lower arms are labeled as links 1, 2, and 3. Each upper arm is made up of a planar four-bar parallelogram: links 4, 7, 10, and 13 for the first limb; 5, 8, 11, and 14 for the second limb; and 6, 9, 12, and 15 for the third limb. For each limb, the upper and lower arms and the two platforms are connected by three parallel revolute joints at points A , B , and C . The ground-connected joint axes lie on a plane. Similarly, the moving platform connected joint axes also lie on a plane. Furthermore, the two joint axes at B and C intersect the axes of the four-bar parallelogram perpendicularly. A more general configuration includes a small offset in each of links 4, 5, 6, 13, 14, and 15 (Tsai and Stamper, 1996). Revolute joints are used for the parallelogram as opposed to ball joints employed in the DELTA robot (Pierrot et al., 1990). Overall, there are 17 links and 21 revolute joints. The general degrees-of-freedom equation predicts that

$$F = \lambda(n - j - 1) + \sum_i f_i = 6(17 - 21 - 1) + 21 = -9.$$

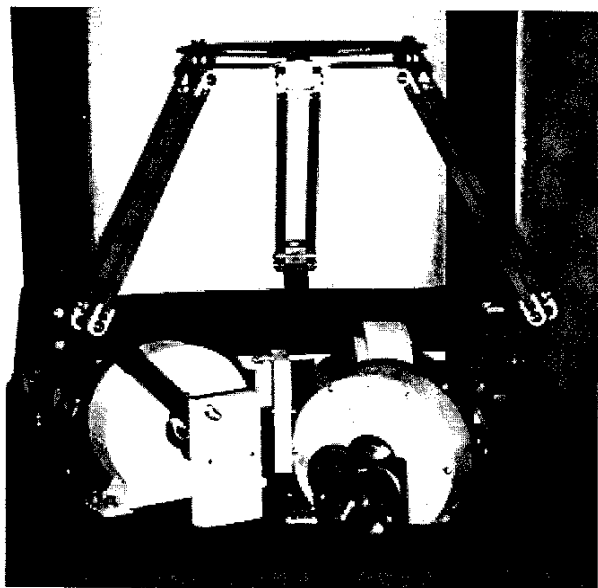


FIGURE 3.9. University of Maryland manipulator.

However, due to the special arrangement of the links and joints, many of the constraints imposed by the joints are redundant, and the resulting mechanism does have 3 translational degrees of freedom. Due to the four-bar parallelogram and the three parallel revolute joints at points A , B , and C , any single limb constrains the moving platform from rotating about the z and x_i axes. Hence any two limbs constrain the moving platform from rotating about any axis. This leaves the mechanism with 3 translational degrees of freedom and forces the moving platform to remain in the same orientation at all times. This unique characteristic is useful in many applications, such as an x - y - z positioning device. A hybrid manipulator can also be constructed by mounting a wrist mechanism onto the moving platform.

3.6.1 Geometry of the Manipulator

As shown in Fig. 3.10, a reference coordinate system (x, y, z) is attached to the center O of the fixed platform, with its x and y axes lie on the fixed plane and the z -axis points up vertically. Another coordinate system (x_i, y_i, z_i) is attached to the fixed base at point A_i , such that the x_i -axis is in line with the

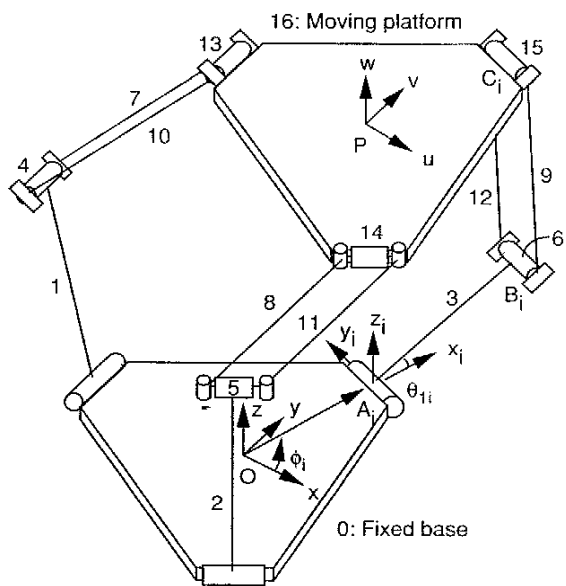


FIGURE 3.10. Platform manipulator with only translational degrees of freedom.

extended line of \overline{OA}_i , the y_i -axis is directed along the revolute joint axis at A_i , and the z_i -axis is parallel to the z -axis. The angle ϕ_i is measured from the x -axis to the x_i -axis and is a constant parameter of the manipulator design. Figure 3.11 defines the joint angles associated with the i th limb, wherein \mathbf{p} is the position vector of the centroid of the moving platform, θ_{1i} is measured from the x_i axis to \overline{AB}_i , θ_{2i} is defined from the extended line of \overline{AB}_i to the line defined by the intersection of the plane of the parallelogram and the x_i-z_i plane, and θ_{3i} is measured from the y_i direction to \overline{B}_iC_i . Overall, there are nine joint angles, θ_{1i} , θ_{2i} , and θ_{3i} for $i = 1, 2$, and 3 , associated with the manipulator.

For this manipulator, θ_{11} , θ_{12} , and θ_{13} are considered as the actuated joints. Other combinations of actuated joints are also possible, but actuating θ_{11} , θ_{12} , and θ_{13} offers the advantage of attaching all actuators to the fixed base. A loop-closure equation can be written for each limb:

$$\overline{A}_i\overline{B}_i + \overline{B}_i\overline{C}_i = \overline{OP} + \overline{PC}_i - \overline{OA}_i. \quad (3.43)$$

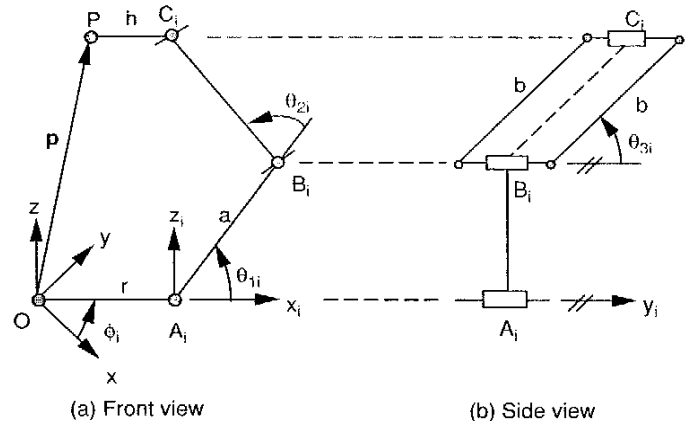


FIGURE 3.11. Description of the joint angles.

Expressing Eq. (3.43) in the (x_i, y_i, z_i) coordinate frame, we obtain

$$\begin{bmatrix} ac\theta_{1i} + bs\theta_{3i}c(\theta_{1i} + \theta_{2i}) \\ bc\theta_{3i} \\ as\theta_{1i} + bs\theta_{3i}s(\theta_{1i} + \theta_{2i}) \end{bmatrix} = \begin{bmatrix} c_{xi} \\ c_{yi} \\ c_{zi} \end{bmatrix}, \quad (3.44)$$

where

$$\begin{bmatrix} c_{xi} \\ c_{yi} \\ c_{zi} \end{bmatrix} = \begin{bmatrix} c\phi_i & s\phi_i & 0 \\ -s\phi_i & c\phi_i & 0 \\ 0 & 0 & 1 \end{bmatrix} \begin{bmatrix} p_x \\ p_y \\ p_z \end{bmatrix} + \begin{bmatrix} h - r \\ 0 \\ 0 \end{bmatrix} \quad (3.45)$$

denotes the position of point C_i relative to the (x_i, y_i, z_i) coordinate frame, a and b are the lengths of links A_iB_i and B_iC_i , respectively, and $\mathbf{p} = [p_x, p_y, p_z]^T$ is the position vector of point P relative to the (x, y, z) coordinate system.

3.6.2 Inverse Kinematics

For inverse kinematics, the position vector \mathbf{p} of the moving platform is given and the problem is to find the joint angles θ_{1i} , θ_{12} , and θ_{13} required to bring the moving platform to the desired position. An intuitive approach for the solution is to consider the problem geometrically. We notice that once the position of P is given, the position of C_i is also known. Now consider the surface

generated by the full range of motion of $C_i B_i$ about point C_i . It is a sphere centered at point C_i . The full range of motion of $A_i B_i$ is a circle centered about A_i in the plane of motion of $A_i B_i$. The solution of the inverse kinematics problem is found at the intersection of this circle and the sphere as shown in Fig. 3.12. Four cases are possible:

1. *Generic solution.* The circle penetrates the sphere, resulting in two solutions.
2. *Singular solution.* The circle is tangent to the sphere, resulting in one solution.
3. *Singular solution.* The circle lies on the sphere, producing an infinite number of solutions. This is unlikely since it requires the moving and stationary platforms to occupy the same plane simultaneously.
4. *No real solution.* The circle and the sphere may not intersect at all.

With the geometry of the problem in mind, algebraic solutions are developed by solving Eq. (3.44). Two solutions of θ_{3i} are found by solving the second element of Eq. (3.44):

$$\theta_{3i} = \cos^{-1} \frac{c_{yi}}{b}. \quad (3.46)$$

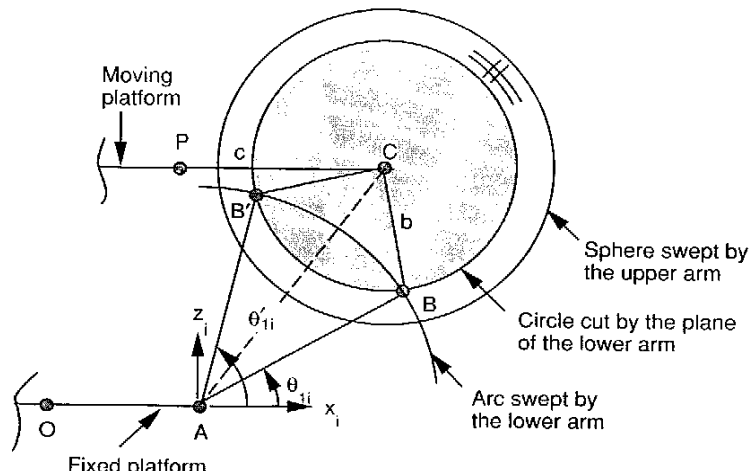


FIGURE 3.12. Two inverse kinematic solutions of a limb.

However, it will be shown later that either of the two solutions for θ_{3i} results in the same physical pose for limb i .

With θ_{3i} determined, an equation with θ_{2i} as the only unknown is generated by summing the squares of c_{xi} , c_{yi} , and c_{zi} in Eq. (3.44):

$$2abs\theta_{3i}c\theta_{2i} + a^2 + b^2 = c_{xi}^2 + c_{yi}^2 + c_{zi}^2. \quad (3.47)$$

Hence

$$\theta_{2i} = \cos^{-1} \kappa. \quad (3.48)$$

where $\kappa = (c_{xi}^2 + c_{yi}^2 + c_{zi}^2 - a^2 - b^2) / (2abs\theta_{3i})$. Therefore, corresponding to each solution of θ_{3i} , Eq. (3.48) yields two solutions of θ_{2i} . This results in four solution sets for θ_{2i} and θ_{3i} .

Furthermore, corresponding to each solution set of θ_{2i} and θ_{3i} , Eq. (3.44) yields a unique solution for θ_{1i} . However, the four solution sets contain only two distinct values of θ_{1i} . Moreover, for each solution of θ_{1i} , the two associated values of θ_{2i} differ by π , while the sum of the two associated values of θ_{3i} is 0. By virtue of these relationships and the geometry of the limb, each limb assumes the same physical pose for each θ_{1i} . Hence for each limb the four solution sets are realized in only two distinct poses.

The inverse kinematics solution is tested for special cases by examining Eq. (3.48). If $|c_{yi}| < b$ and $|\kappa| < 1$, the two solutions correspond to the configuration where the circle swept by $A_i B_i$ intersects the sphere swept by $C_i B_i$ in two locations. If $|c_{yi}| = b$ and $c_{xi}^2 + c_{zi}^2 = a^2$, the circle and sphere are tangent and the manipulator is in a singular location. If $|c_{yi}| > b$, the circle and sphere do not intersect and there are no real solutions.

3.6.3 Direct Kinematics

For the direct kinematics, the input joint angles θ_{11} , θ_{12} , and θ_{13} are given and the problem is to find the position of the moving platform. First, we consider the surface composed of all possible positions of P for limb i with a given θ_{1i} . The surface is a sphere centered at a point, which is located at a distance h from B_i in the direction of $C_i P$. Next, we consider all three limbs. Point P must fall simultaneously on the three spheres created by a sweep of P for each limb. The intersections of these three spheres represent the solutions to the direct kinematics problem. In the generic case, there are two solutions, since the intersection of two spheres forms a circle, which is generally intersected by the third sphere in two locations. Four cases are possible:

1. *Generic solution.* The two solutions are realized at the intersection of three spheres.
2. *Singular solution.* One sphere is tangent to the circle of intersection of the other two spheres. Hence there is only one solution possible.
3. *Singular solution.* The centers of any two spheres coincide, resulting in an infinite number of solutions. This is an unlikely configuration for most practical embodiments of the manipulator, except for the situation when $\theta_{11} = \theta_{12} = \theta_{13} = \pi/2$ and $r = h$.
4. *No solution.* The three spheres do not intersect.

Algebraically, the solution is found by writing the equations that describe the three spheres and then solving those equations for the points of intersection. Substituting c_{xi} , c_{yi} , and c_{zi} from Eq. (3.45) into (3.44) and rearranging, we obtain

$$\begin{bmatrix} bs\theta_{3i}c(\theta_{1i} + \theta_{2i}) \\ bc\theta_{3i} \\ bs\theta_{3i}s(\theta_{1i} + \theta_{2i}) \end{bmatrix} = \begin{bmatrix} c\phi_i & s\phi_i & 0 \\ -s\phi_i & c\phi_i & 0 \\ 0 & 0 & 1 \end{bmatrix} \begin{bmatrix} p_x \\ p_y \\ p_z \end{bmatrix} + \begin{bmatrix} -ac\theta_{1i} - r + h \\ 0 \\ -as\theta_{1i} \end{bmatrix}. \quad (3.49)$$

An equation for the sphere swept by point P for limb i is obtained by summing the squares of the three components of Eq. (3.49):

$$\begin{aligned} b^2 &= p_x^2 + p_y^2 + p_z^2 - 2(p_x c\phi_i + p_y s\phi_i)(ac\theta_{1i} + r - h) \\ &\quad - 2p_z as\theta_{1i} + (ac\theta_{1i} + r - h)^2 + a^2 s^2 \theta_{1i} \end{aligned} \quad (3.50)$$

for $i = 1, 2$, and 3 .

The plane that contains the circle of intersection created by the spheres of limb 1 and limb j is found by subtracting Eq. (3.50) for $i = 1$ from Eq. (3.50) for $i = j$:

$$e_{1j}p_x + e_{2j}p_y + e_{3j}p_z + e_{4j} = 0 \quad \text{for } j = 2, 3, \quad (3.51)$$

where

$$\begin{aligned} e_{1j} &= 2c\phi_j(ac\theta_{1j} + r - h) - 2c\phi_1(ac\theta_{11} + r - h), \\ e_{2j} &= 2s\phi_j(ac\theta_{1j} + r - h) - 2s\phi_1(ac\theta_{11} + r - h), \\ e_{3j} &= 2as\theta_{1j} - 2as\theta_{11}, \\ e_{4j} &= (ac\theta_{11} + r - h)^2 + a^2 s^2 \theta_{11} - (ac\theta_{1j} + r - h)^2 - a^2 s^2 \theta_{1j}. \end{aligned}$$

Equation (3.51) written twice for $j = 2$ and 3 results in a system of two linearly independent equations as long as the centers of the spheres are not collinear. This system of equations defines a line that contains point P if there are real solutions. The intersections of this line with one of the spheres described by Eq. (3.50) solve the the direct kinematics problem. In this case, solving Eq. (3.51) for p_y and p_z in terms of p_x and then substituting the resulting expressions into Eq. (3.50) for $i = 1$ yields

$$k_0 p_y^2 + k_1 p_x + k_2 = 0. \quad (3.52)$$

The coefficients of the quadratic are

$$k_0 = 1 + \frac{l_1^2}{l_2^2} + \frac{l_4^2}{l_2^2},$$

$$k_1 = \frac{2l_0 l_1}{l_2^2} + \frac{2l_1 l_4}{l_2^2} - 2l_5 c\phi_1 - \frac{2l_5 l_1}{l_2} s\phi_1 - \frac{2al_4}{l_2} s\theta_{11},$$

$$k_2 = l_5^2 - b^2 + \frac{l_0^2}{l_2^2} + \frac{l_3^2}{l_2^2} + a^2 s^2 \theta_{11} - \frac{2l_0 l_5}{l_2} s\phi_1 - \frac{2al_3}{l_2} s\theta_{11},$$

where

$$l_0 = e_{32}e_{43} - e_{33}e_{42},$$

$$l_1 = e_{13}e_{32} - e_{12}e_{33},$$

$$l_2 = e_{22}e_{33} - e_{23}e_{32},$$

$$l_3 = e_{23}e_{42} - e_{22}e_{43},$$

$$l_4 = e_{12}e_{23} - e_{13}e_{22},$$

$$l_5 = ac\theta_{11} + r - h,$$

and where e_{12} , e_{13} , e_{22} , e_{23} , e_{32} , e_{33} , e_{42} , and e_{43} are as defined in Eq. (3.51).

The following four cases are possible:

1. If $k_1^2 - 4k_0 k_2 > 0$, two solutions are realized where the circle created by the intersection of two spheres is intersected by the third sphere in two places. The two manipulator postures form a mirror image of each other about a plane defined by the centers of the three spheres.
2. If $k_1^2 - 4k_0 k_2 = 0$, the circle created by the intersection of two spheres is tangent to the third sphere, resulting in one real solution.

3. If $k_1^2 - 4k_0k_2 < 0$, the three spheres do not intersect and there are no real solutions.
4. If the system of equations produced by Eq. (3.51) for $j = 2$ and 3 are linearly dependent, the centers of the spheres are collinear, resulting in either an infinite number of solutions if the centers of the spheres are coincident or no solutions if they are not coincident.

Once p_x is found, the values for p_y and p_z are found by back substitution into Eq. (3.51).

In summary, a parallel manipulator with 3 translational degrees of freedom is described. The general design of the manipulator is discussed. Closed-formed solutions are developed for both the direct and inverse kinematics. These solutions demonstrate that, in general, there are two possible poses for the forward kinematics and two possible poses for each limb for the inverse kinematics. A geometric approach to both the forward and inverse kinematics problems is also considered that provides some insights into the nature of the inverse and forward kinematics of this manipulator.

3.7 POSITION ANALYSIS OF A SPATIAL 3RPS PARALLEL MANIPULATOR

Figure 3.13 shows a spatial 3-dof, 3RPS parallel manipulator (Lee and Shah, 1987). Three identical limbs connect the moving platform at points B_i by spherical joints to the fixed base at points A_i by revolute joints. Each limb consists of an upper and a lower member connected by a prismatic joint. These three prismatic joints are used as the inputs to the manipulator. Overall, there are eight links, three revolute joints, three prismatic joints, and three spherical joints. Hence the degrees of freedom of the mechanism is

$$F = \lambda(n - j - 1) + \sum_i f_i = 6(8 - 9 - 1) + (3 + 3 + 9) = 3. \quad (3.53)$$

3.7.1 Geometry of the Manipulator

For the purpose of analysis, two Cartesian coordinate systems $A(x, y, z)$ and $B(u, v, w)$ are attached to the fixed base and moving platform, respectively, as shown in Fig. 3.13. The following assumptions are made. Points A_1 , A_2 , and A_3 lie on the x - y plane and B_1 , B_2 , and B_3 lie on the u - v plane. As shown in Fig. 3.14, the origin O of the fixed coordinate system is located at the centroid of $\Delta A_1A_2A_3$ and the x -axis points in the direction of \overrightarrow{OA}_1 . Similarly, the origin P of the moving coordinate system is located at the

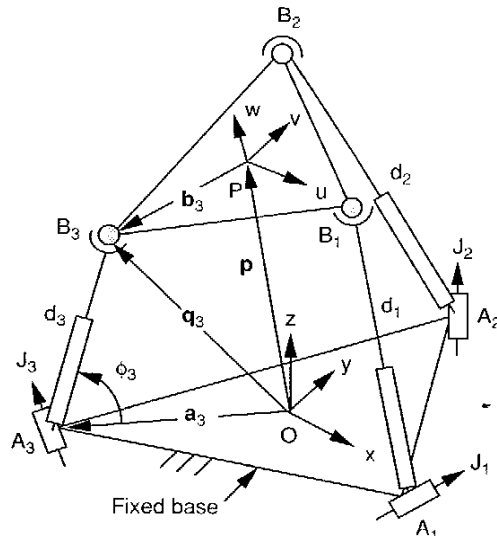


FIGURE 3.13. Spatial 3-dof, 3RPS parallel manipulator.

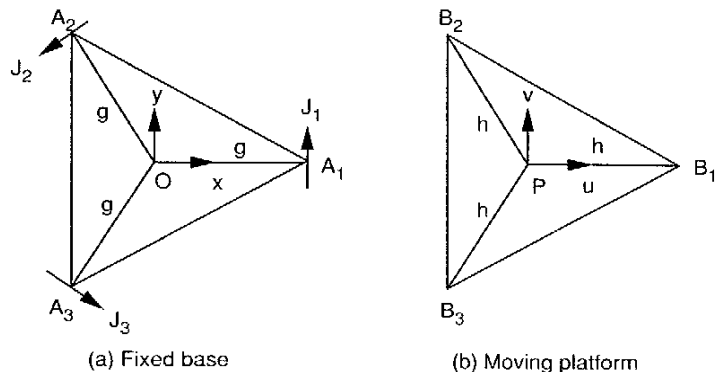


FIGURE 3.14. Top views of the 3RPS parallel manipulator.

centroid of $\triangle B_1B_2B_3$ and the u -axis points in the direction of $\overline{PB_1}$. Both $\triangle A_1A_2A_3$ and $\triangle B_1B_2B_3$ are equilateral triangles with $|OA_1| = |OA_2| = |OA_3| = g$ and $|PB_1| = |PB_2| = |PB_3| = h$. Furthermore, the axis of each revolute joint, J_i , lies on the x - y plane and is perpendicular to the vector $\overline{OA_i}$.

The transformation from the moving platform to the fixed base can be described by a position vector $\mathbf{p} = \overline{OP}$, and a 3×3 rotation matrix ${}^A R_B$. Let \mathbf{u} , \mathbf{v} , and \mathbf{w} be three unit vectors defined along the u , v , and w axes of the moving coordinate system B , respectively; then the rotation matrix can be expressed in terms of the direction cosines of \mathbf{u} , \mathbf{v} , and \mathbf{w} as

$${}^A R_B = \begin{bmatrix} u_x & v_x & w_x \\ u_y & v_y & w_y \\ u_z & v_z & w_z \end{bmatrix}. \quad (3.54)$$

We note that the elements of ${}^A R_B$ must satisfy the following orthogonal conditions:

$$u_x^2 + u_y^2 + u_z^2 = 1, \quad (3.55)$$

$$v_x^2 + v_y^2 + v_z^2 = 1, \quad (3.56)$$

$$w_x^2 + w_y^2 + w_z^2 = 1, \quad (3.57)$$

$$u_x v_x + u_y v_y + u_z v_z = 0, \quad (3.58)$$

$$u_x w_x + u_y w_y + u_z w_z = 0, \quad (3.59)$$

$$v_x w_x + v_y w_y + v_z w_z = 0. \quad (3.60)$$

Let \mathbf{a}_i and ${}^B \mathbf{b}_i$ be the position vectors of points A_i and B_i in the coordinate systems A and B , respectively. Then the coordinates of A_i and B_i are given by

$$\mathbf{a}_1 = [g, 0, 0]^T, \quad (3.61)$$

$$\mathbf{a}_2 = \left[-\frac{1}{2}g, \frac{\sqrt{3}}{2}g, 0 \right]^T, \quad (3.62)$$

$$\mathbf{a}_3 = \left[-\frac{1}{2}g, -\frac{\sqrt{3}}{2}g, 0 \right]^T, \quad (3.63)$$

$${}^B \mathbf{b}_1 = [h, 0, 0]^T, \quad (3.64)$$

$${}^B \mathbf{b}_2 = \left[-\frac{1}{2}h, \frac{\sqrt{3}}{2}h, 0 \right]^T, \quad (3.65)$$

$${}^B \mathbf{b}_3 = \left[-\frac{1}{2}h, -\frac{\sqrt{3}}{2}h, 0 \right]^T. \quad (3.66)$$

The position vector \mathbf{q}_i of B_i with respect to the fixed coordinate system is obtained by the following transformation:

$$\mathbf{q}_i = \mathbf{p} + {}^A R_B {}^B \mathbf{b}_i. \quad (3.67)$$

Substituting Eqs. (3.54) and (3.64) through (3.66) into (3.67) yields

$$\mathbf{q}_1 = \begin{bmatrix} p_x + hu_x \\ p_y + hu_y \\ p_z + hu_z \end{bmatrix}, \quad (3.68)$$

$$\mathbf{q}_2 = \begin{bmatrix} p_x - \frac{1}{2}hu_x + \frac{\sqrt{3}}{2}hv_x \\ p_y - \frac{1}{2}hu_y + \frac{\sqrt{3}}{2}hv_y \\ p_z - \frac{1}{2}hu_z + \frac{\sqrt{3}}{2}hv_z \end{bmatrix}, \quad (3.69)$$

$$\mathbf{q}_3 = \begin{bmatrix} p_x - \frac{1}{2}hu_x - \frac{\sqrt{3}}{2}hv_x \\ p_y - \frac{1}{2}hu_y - \frac{\sqrt{3}}{2}hv_y \\ p_z - \frac{1}{2}hu_z - \frac{\sqrt{3}}{2}hv_z \end{bmatrix}. \quad (3.70)$$

3.7.2 Constraints Imposed by the Revolute Joints

Since the each limb is connected to the fixed base by a revolute joint located at A_i , its motion is constrained in one of the following three planes:

$$q_{1y} = 0 \quad \text{for } i = 1, \quad (3.71)$$

$$q_{2y} = -\sqrt{3}q_{2x} \quad \text{for } i = 2, \quad (3.72)$$

$$q_{3y} = +\sqrt{3}q_{3x} \quad \text{for } i = 3. \quad (3.73)$$

Substituting the y -component of \mathbf{q}_i from Eqs. (3.68) through (3.70) into the three equations above, we obtain

$$p_y + hu_y = 0, \quad (3.74)$$

$$p_x - \frac{1}{2}hu_y + \frac{\sqrt{3}}{2}hv_y = -\sqrt{3} \left(p_x - \frac{1}{2}hu_x + \frac{\sqrt{3}}{2}hv_x \right), \quad (3.75)$$

$$p_y - \frac{1}{2}hu_y - \frac{\sqrt{3}}{2}hv_y = \sqrt{3} \left(p_x - \frac{1}{2}hu_x - \frac{\sqrt{3}}{2}hv_x \right). \quad (3.76)$$

Equations (3.75) and (3.76) can be simplified further. Subtracting the sum of Eqs. (3.75) and (3.76) from $2 \times (3.74)$, we obtain

$$v_x = u_y. \quad (3.77)$$

Subtracting Eq. (3.76) from (3.75), we obtain

$$p_x = \frac{1}{2}h(u_x - v_y). \quad (3.78)$$

Hence Eqs. (3.74), (3.77), and (3.78) impose three constraints on the motion of the moving platform.

3.7.3 Length of Limb i

The length of a limb, d_i , shown in Fig. 3.13, is given by

$$d_i^2 = [\mathbf{q}_i - \mathbf{a}_i]^T [\mathbf{q}_i - \mathbf{a}_i] \quad \text{for } i = 1, 2, 3. \quad (3.79)$$

Substituting Eqs. (3.61) through (3.63) and (3.68) through (3.70) into (3.79) yields

$$\begin{aligned} d_1^2 &= p_x^2 + p_y^2 + p_z^2 + 2h(p_x u_x + p_y u_y + p_z u_z) \\ &\quad - 2gp_x - 2ghu_x + g^2 + h^2, \end{aligned} \quad (3.80)$$

$$\begin{aligned} d_2^2 &= p_x^2 + p_y^2 + p_z^2 - h(p_x u_x + p_y u_y + p_z u_z) \\ &\quad + \sqrt{3}h(p_x v_x + p_y v_y + p_z v_z) + g(p_x - \sqrt{3}p_y) \\ &\quad - \frac{1}{2}gh(u_x - \sqrt{3}u_y) + \frac{1}{2}gh(\sqrt{3}v_x - 3v_y) + g^2 + h^2, \end{aligned} \quad (3.81)$$

$$\begin{aligned} d_3^2 &= p_x^2 + p_y^2 + p_z^2 - h(p_x u_x + p_y u_y + p_z u_z) \\ &\quad - \sqrt{3}h(p_x v_x + p_y v_y + p_z v_z) + g(p_x + \sqrt{3}p_y) \\ &\quad - \frac{1}{2}gh(u_x + \sqrt{3}u_y) - \frac{1}{2}gh(\sqrt{3}v_x + 3v_y) + g^2 + h^2. \end{aligned} \quad (3.82)$$

Equations (3.80), (3.81), and (3.82) relate the limb lengths to the moving platform location.

3.7.4 Inverse Kinematics

The inverse kinematic problem is: *Given the location of the moving platform, find the limb lengths d_1 , d_2 , and d_3 .* Since the manipulator has only 3 degrees of freedom, the position and orientation must be specified in accordance with the constraints imposed by the revolute joints. Equation (3.77) imposes a constraint on the orientation of the moving platform, while Eqs. (3.74) and (3.78) relate the x and y components of \mathbf{p} to the orientation of the moving platform. Hence only three of the 12 parameters in ${}^A R_B$ and \mathbf{p} can be specified arbitrarily. In any case, the z -component of \mathbf{p} must be specified, since it does not appear in the constraint equations, while the other two parameters can be chosen from either the position vector \mathbf{p} or the three unit vectors \mathbf{u} , \mathbf{v} , and \mathbf{w} . Once three parameters are chosen, the remaining parameters are determined from Eqs. (3.74), (3.77), and (3.78) and the orthogonal conditions. It can be shown that if the three components of \mathbf{p} are chosen as the independent parameters, there are eight corresponding platform orientations (Song and Zhang, 1995). If the roll and pitch angles of the Euler roll-pitch-yaw angles and p_z are chosen as the independent parameters, there are two corresponding platform locations. Once the position vector and the rotation matrix of the moving platform are known, the limb lengths can be computed directly from Eqs. (3.80), (3.81), and (3.82).

3.7.5 Direct Kinematics

The direct kinematic problem is: *Given the limb lengths d_1 , d_2 , and d_3 , find the location of the moving platform.* Equations (3.55), (3.56), (3.58), (3.74), (3.77), (3.78), and (3.80) through (3.82) form a system of nine polynomial equations in nine unknowns: p_x , p_y , p_z , u_x , u_y , u_z , v_x , v_y , and v_z . Equations (3.55), (3.56), (3.58), (3.80), (3.81), and (3.82) are second-degree polynomials, while Eqs. (3.74), (3.77), and (3.78) are linear equations. Two linear equations can be obtained by manipulating Eqs. (3.80), (3.81), and (3.82) algebraically. This results in a new system with four second-degree polynomials and five linear equations. Since the traditional Bezout number is $2^4 = 16$, the system of equations has at most 16 solutions.

In what follows we introduce the tilt angles of the limbs, ϕ_i , as intermediate variables and show how to use these angles to reduce the problem to a 16th-degree polynomial. Let ϕ_i be measured from line A_iO to A_iB_i as shown in Fig. 3.13. Then the position vector of point B_i with respect to the fixed coordinate system can be written as

$$\mathbf{q}_1 = \begin{bmatrix} g - d_1 c\phi_1 \\ 0 \\ d_1 s\phi_1 \end{bmatrix}, \quad (3.83)$$

$$\mathbf{q}_2 = \begin{bmatrix} -\frac{1}{2}(g - d_2 c\phi_2) \\ \frac{\sqrt{3}}{2}(g - d_2 c\phi_2) \\ d_2 s\phi_2 \end{bmatrix}, \quad (3.84)$$

$$\mathbf{q}_3 = \begin{bmatrix} -\frac{1}{2}(g - d_3 c\phi_3) \\ -\frac{\sqrt{3}}{2}(g - d_3 c\phi_3) \\ d_3 s\phi_3 \end{bmatrix}. \quad (3.85)$$

We note that once the limb lengths are given, the resulting mechanism is equivalent to a 3RS spatial mechanism with zero degrees of freedom. Hence the position and orientation of the mechanism can be obtained by equating $|B_i B_{i+1}| = \sqrt{3}h$; that is,

$$[\mathbf{q}_i - \mathbf{q}_{i+1}]^T [\mathbf{q}_i - \mathbf{q}_{i+1}] - 3h^2 = 0 \quad \text{for } i = 1, 2, 3 \pmod{3}. \quad (3.86)$$

Note that the subscripts in Eq. (3.86) are cyclic of modulo 3. Thus if $i = 3$, then $i + 1$ is equal to 1. Substituting Eqs. (3.83) through (3.85) into (3.86) yields

$$e_{1i} c\phi_i c\phi_{i+1} + e_{2i} s\phi_i s\phi_{i+1} + e_{3i} c\phi_i + e_{4i} c\phi_{i+1} + e_{5i} = 0, \quad (3.87)$$

for $i = 1, 2, 3$ (modulo 3), where

$$e_{1i} = d_i d_{i+1},$$

$$e_{2i} = -2d_i d_{i+1},$$

$$e_{3i} = -3g d_i,$$

$$e_{4i} = -3g d_{i+1},$$

$$e_{5i} = 3g^2 + d_i^2 + d_{i+1}^2 - 3h^2.$$

We now convert Eqs. (3.87) to a system of polynomial equations in order to eliminate two unknown variables. Substituting the trigonometric identities

$$s\phi_i = \frac{2t_i}{1+t_i^2} \quad \text{and} \quad c\phi_i = \frac{1-t_i^2}{1+t_i^2}, \quad \text{where } t_i = \tan \frac{\phi_i}{2}$$

into Eq. (3.87) yields three fourth-degree polynomials in t_1 , t_2 , and t_3 :

$$\tilde{e}_{1i} t_i^2 t_{i+1}^2 + \tilde{e}_{2i} t_i^2 + \tilde{e}_{3i} t_{i+1}^2 + \tilde{e}_{4i} t_i t_{i+1} + \tilde{e}_{5i} = 0 \quad \text{for } i = 1, 2, 3 \pmod{3} \quad (3.88)$$

where

$$\begin{aligned} \tilde{e}_{1i} &= e_{1i} - e_{3i} - e_{4i} + e_{5i}, \\ \tilde{e}_{2i} &= -e_{1i} - e_{3i} + e_{4i} + e_{5i}, \\ \tilde{e}_{3i} &= -e_{1i} + e_{3i} - e_{4i} + e_{5i}, \\ \tilde{e}_{4i} &= 4e_{2i}, \\ \tilde{e}_{5i} &= e_{1i} + e_{3i} + e_{4i} + e_{5i}. \end{aligned}$$

Although, the traditional 1-homogeneous Bezout number is $4^3 = 64$, the 3-homogeneous Bezout number is 16. To prove this, we arrange the variables into three groups:

group 1: $[t_1]$, group 2: $[t_2]$, and group 3: $[t_3]$.

The degrees of the three equations in the variables of each group are listed in Table 3.2. Following the procedure outlined in Appendix A, we compute the product

$$\prod_{i=1}^3 \left(\sum_{j=1}^3 d_{ij} \beta_j \right) = (2\beta_1 + 2\beta_2)(2\beta_2 + 2\beta_3)(2\beta_1 + 2\beta_3),$$

where d_{ij} is taken from the (i, j) element of Table 3.2. Since each group contains only one variable, the 3-homogeneous Bezout number, determined by the coefficient of the term $\beta_1 \beta_2 \beta_3$, is 16. Hence the system of equations has at most 16 solutions.

TABLE 3.2. Degrees of the Equations

Equation	Group 1	Group 2	Group 3
1, Eq. (3.88) for $i = 1$	2	2	0
2, Eq. (3.88) for $i = 2$	0	2	2
3, Eq. (3.88) for $i = 3$	2	0	2

In what follows, we apply the Sylvester dialytic elimination method to reduce the system of equations to a 16th-degree polynomial. See Appendix B for a brief description of the method.

(a) Elimination of t_3 . To eliminate t_3 , we write Eq. (3.88) for $i = 2$ and 3 as two second-degree polynomials in t_3 :

$$At_3^2 + Bt_3 + C = 0, \quad (3.89)$$

$$Dt_3^2 + Et_3 + F = 0, \quad (3.90)$$

where A , B , and C are second-degree polynomials in t_2 whose coefficients can be derived from Eq. (3.88) for $i = 2$, whereas D , E , and F are second-degree polynomials in t_1 whose coefficients can be derived from Eq. (3.88) for $i = 3$.

Multiplying Eq. (3.89) by D and Eq. (3.90) by A , and subtracting, we obtain

$$(AE - BD)t_3 + (AF - CD) = 0. \quad (3.91)$$

Multiplying Eq. (3.89) by F and Eq. (3.90) by C and subtracting, we obtain

$$(CD - AF)t_3 + (CE - BF) = 0. \quad (3.92)$$

Equations (3.91) and (3.92) constitute a system of two equations linear in t_3 and 1. The following eliminant is obtained by equating the determinant of the coefficient matrix to zero.

$$(AF - CD)^2 + (AE - BD)(CE - BF) = 0. \quad (3.93)$$

(b) Elimination of t_2 . For the purpose of eliminating t_2 , we write Eq. (3.93) in the form

$$Lt_2^4 + Mt_2^3 + Nt_2^2 + Pt_2 + Q = 0, \quad (3.94)$$

where L , M , N , P , and Q are fourth-degree polynomials in t_1 . We also write Eq. (3.88) for $i = 1$ in the form

$$Gt_2^2 + Ht_2 + I = 0, \quad (3.95)$$

where G , H , and I are second-degree polynomials in t_1 .

We now eliminate the unknown t_2 from Eqs. (3.94) and (3.95) as follows. Multiplying Eq. (3.94) by G , Eq. (3.95) by Lt_2^2 , and subtracting, we obtain

$$(HL - GM)t_2^3 + (IL - GN)t_2^2 - GPt_2 - GQ = 0. \quad (3.96)$$

Multiplying Eq. (3.94) by $Gt_2 + H$, Eq. (3.95) by $Lt_2^3 + Mt_2^2$, and subtracting, we obtain

$$(GN - LI)t_2^3 + (GP + HN - MI)t_2^2 + (GQ + HP)t_2 + HQ = 0. \quad (3.97)$$

Multiplying Eq. (3.95) by t_2 , we obtain

$$Gt_2^3 + Lt_2^2 + It_2 = 0. \quad (3.98)$$

We may consider Eqs. (3.95) through (3.98) as four linear homogeneous equations in the four variables t_2^3 , t_2^2 , t_2 , and 1. Vanishing of their eliminant yields

$$\begin{vmatrix} HL - GM & IL - GN & -GP & -GQ \\ GN - LI & GP + HN - MI & GQ + HP & HQ \\ G & H & I & 0 \\ 0 & G & H & I \end{vmatrix} = 0. \quad (3.99)$$

Expanding Eq. (3.99) results in an eighth-degree polynomial in the square of t_1 . It follows that there are at most eight pairs of solutions for t_1 , one being the negative of the other.

(c) Location of the Moving Platform. Once ϕ_1 is found, ϕ_2 and ϕ_3 can be solved by back substitution using Eqs. (3.95) and (3.89). Next, the position vectors \mathbf{q}_1 , \mathbf{q}_2 , and \mathbf{q}_3 are found by substituting the values of ϕ_i into Eqs. (3.83), (3.84), and (3.85), respectively. Since the ball joints are located at the vertices of the equilateral triangle, the position vector of the moving platform, \mathbf{p} , is obtained as

$$\mathbf{p} = \frac{1}{3}(\mathbf{q}_1 + \mathbf{q}_2 + \mathbf{q}_3). \quad (3.100)$$

Finally, the orientation of the moving platform is found by solving Eqs. (3.74), (3.77), and (3.78) along with the orthogonal conditions.

In summary, there are at most 16 solutions for the direct kinematics problem. These 16 solutions form eight pairs of manipulator postures, one being the mirror image of another about the fixed plane $A_1A_2A_3$.

3.8 POSITION ANALYSIS OF A GENERAL STEWART-GOUGH PLATFORM

Figure 3.15 shows a spatial 6-dof, 6SPS parallel manipulator known as a Stewart-Gough platform. Six identical limbs connect the moving platform to the fixed base by spherical joints at points B_i and A_i , $i = 1, 2, \dots, 6$,

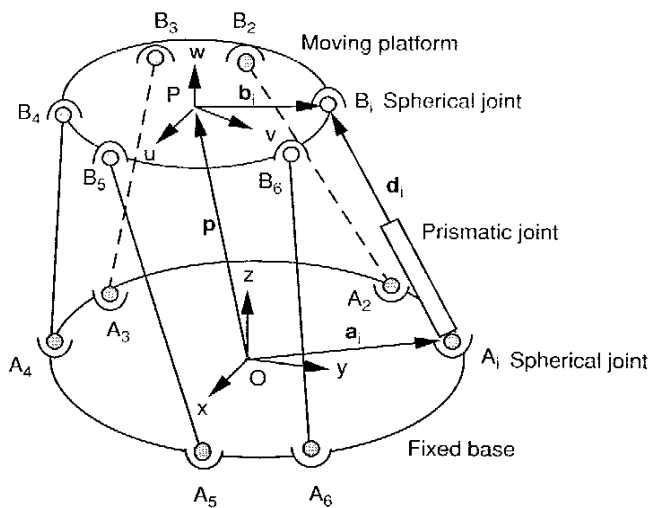


FIGURE 3.15. Spatial 6-dof, 6SPS parallel manipulator.

respectively. Each limb consists of an upper member and a lower member connected by a prismatic joint. Ball screws or hydraulic jacks can be used to vary the lengths of the prismatic joints and therefore to control the location of the moving platform.

Note that in Fig. 3.15, the attachment points A_i for $i = 1$ to 6 are sketched in a plane on the fixed base. Similarly, B_i for $i = 1$ to 6 are sketched in a plane on the moving platform. For a general Stewart platform, however, these attachment points do not necessarily lie on one plane. There are 14 links connected by 6 prismatic joints and 12 spherical joints. Hence the number of degrees of freedom of the mechanism is

$$F = \lambda(n - j - 1) + \sum_i f_i = 6(14 - 18 - 1) + (6 + 3 \times 12) = 12. \quad (3.101)$$

However, there are 6 passive degrees of freedom associated with the six SPS limbs. Therefore, the moving platform possesses 6 degrees of freedom. Note that an SPS limb can be replaced by an SPU limb without compromising the overall degrees of freedom of the mechanism.

Since the limbs are connected to the moving platform and the fixed base by spherical joints, no bending moments or twisting torques will transmit to

the limbs. The force acting on each limb is directed along the longitudinal axis of the limb. Consequently, these limbs can be made of hollow cylindrical rods to produce a light-weight, high-stiffness, high-speed manipulator.

3.8.1 Geometry of the Manipulator

For the purpose of analysis, two Cartesian coordinate systems, frames $A(x, y, z)$ and $B(u, v, w)$ as shown in Fig. 3.15, are attached to the fixed base and moving platform, respectively. The transformation from the moving platform to the fixed base can be described by the position vector \mathbf{p} of the centroid P and the rotation matrix R_B^A of the moving platform. Let \mathbf{u} , \mathbf{v} , and \mathbf{w} be three unit vectors defined along the u , v , and w axes of the moving coordinate system; then the rotation matrix can be written as

$$R_B^A = \begin{bmatrix} u_x & v_x & w_x \\ u_y & v_y & w_y \\ u_z & v_z & w_z \end{bmatrix}. \quad (3.102)$$

Note that the elements of R_B^A must satisfy the following orthogonal conditions:

$$u_x^2 + v_x^2 + w_x^2 = 1, \quad (3.103)$$

$$u_y^2 + v_y^2 + w_y^2 = 1, \quad (3.104)$$

$$w_x^2 + w_y^2 + w_z^2 = 1, \quad (3.105)$$

$$u_x v_x + u_y v_y + u_z v_z = 0, \quad (3.106)$$

$$u_x w_x + u_y w_y + u_z w_z = 0, \quad (3.107)$$

$$v_x w_x + v_y w_y + v_z w_z = 0. \quad (3.108)$$

As shown in Fig. 3.15, let $\mathbf{a}_i = [a_{ix}, a_{iy}, a_{iz}]^T$ and $\mathbf{b}_i = [b_{iu}, b_{iv}, b_{iw}]^T$ be the position vectors of points A_i and B_i in the coordinate frames A and B , respectively. We can write a vector-loop equation for the i th limb of the manipulator as follows:

$$\overline{A_i B_i} = \mathbf{p} + R_B^A \mathbf{b}_i - \mathbf{a}_i. \quad (3.109)$$

The length of the i th limb is obtained by taking the dot product of the vector $\overline{A_i B_i}$ with itself:

$$d_i^2 = [\mathbf{p} + R_B^A \mathbf{b}_i - \mathbf{a}_i]^T [\mathbf{p} + R_B^A \mathbf{b}_i - \mathbf{a}_i], \quad \text{for } i = 1, 2, \dots, 6, \quad (3.110)$$

where d_i denotes the length of the i th limb. Expanding Eq. (3.110) yields

$$d_i^2 = \mathbf{p}^T \mathbf{p} + [{}^B\mathbf{b}_i]^T [{}^B\mathbf{b}_i] + \mathbf{a}_i^T \mathbf{a}_i + 2\mathbf{p}^T [{}^A R_B {}^B \mathbf{b}_i] - 2\mathbf{p}^T \mathbf{a}_i - 2[{}^A R_B {}^B \mathbf{b}_i]^T \mathbf{a}_i. \quad (3.111)$$

Equation (3.111) written six times, once for each $i = 1, 2, \dots, 6$, yields six equations describing the location of the moving platform with respect to the fixed base. Note that ${}^B\mathbf{b}_i$ and \mathbf{a}_i are constant vectors defined by the geometry of the manipulator.

3.8.2 Inverse Kinematics

For the inverse kinematics problem, the position vector \mathbf{p} and rotation matrix ${}^A R_B$ of frame B with respect to A are given and the limb lengths d_i , $i = 1, 2, \dots, 6$, are to be found. The solution is very straightforward. Taking the square root of Eq. (3.111) we obtain

$$d_i = \pm \sqrt{\mathbf{p}^T \mathbf{p} + {}^B\mathbf{b}_i^T {}^B\mathbf{b}_i + \mathbf{a}_i^T \mathbf{a}_i + 2\mathbf{p}^T {}^A R_B {}^B \mathbf{b}_i - 2\mathbf{p}^T \mathbf{a}_i - 2[{}^A R_B {}^B \mathbf{b}_i]^T \mathbf{a}_i} \quad (3.112)$$

for $i = 1, 2, \dots, 6$. Hence, corresponding to each given location of the moving platform, there are generally two possible solutions for each limb. However, the negative limb length is physically not feasible. When the solution of d_i becomes a complex number, the location of the moving platform is not reachable.

3.8.3 Direct Kinematics

For the direct kinematics problem, the limb lengths d_i , for $i = 1, 2, \dots, 6$, are given, and the position vector \mathbf{p} and rotation matrix ${}^A R_B$ of the moving platform are to be found. The position vector contains three scalar unknowns, while the rotation matrix contains nine scalar unknowns. However, the nine scalar unknowns in ${}^A R_B$ are related by the six orthogonal conditions given by Eqs. (3.103) through (3.108). Without losing generality, we may assume that

1. The origin O of the fixed frame is located at the center of the fixed spherical joint A_1 .
2. The origin P of the moving frame is located at the center of the moving spherical joint B_1 .

Based on the assumptions above, we have $a_{1x} = a_{1y} = a_{1z} = 0$ and $b_{1u} = b_{1v} = b_{1w} = 0$. Hence Eq. (3.111) for $i = 1$ reduces to

$$d_1^2 = p_x^2 + p_y^2 + p_z^2. \quad (3.113)$$

Expanding (3.111) for $i = 2, 3, \dots, 6$, and then subtracting Eq. (3.113) from each of the resulting equations yields

$$\begin{aligned} & b_{iu}(p_x u_x + p_y u_y + p_z u_z) + b_{iv}(p_x v_x + p_y v_y + p_z v_z) \\ & + b_{iw}(p_x w_x + p_y w_y + p_z w_z) - a_{ix} p_x - a_{iy} p_y - a_{iz} p_z \\ & - b_{iu}(a_{ix} u_x + a_{iy} u_y + a_{iz} u_z) - b_{iv}(a_{ix} v_x + a_{iy} v_y + a_{iz} v_z) \\ & - b_{iw}(a_{ix} w_x + a_{iy} w_y + a_{iz} w_z) + k_i = 0 \quad \text{for } i = 2, 3, \dots, 6, \end{aligned} \quad (3.114)$$

$$\text{where } k_i = (a_{ix}^2 + a_{iy}^2 + a_{iz}^2 + b_{iu}^2 + b_{iv}^2 + b_{iw}^2 + d_1^2 - d_i^2)/2.$$

Equations (3.113) and (3.114) for $i = 2$ to 6, together with the six orthogonal conditions, yields 12 equations in 12 unknowns. These 12 equations can be solved for the direct kinematics problem of the general Stewart-Gough platform. The equations are highly nonlinear and extremely difficult to solve. Since each equation is of second degree, the traditional 1-homogeneous Bezout number is $2^{12} = 4096$, which contains many extraneous solutions.

For the 2-homogeneous formulation, we arrange the variables into two groups:

$$\text{group 1: } [p_x, p_y, p_z] \quad \text{and} \quad \text{group 2: } [u_x, u_y, u_z, v_x, v_y, v_z, w_x, w_y, w_z].$$

The degrees of the 12 equations in the variables of each group are listed in Table 3.3. Following the procedure outlined in Appendix A, we form the

TABLE 3.3. Degrees of the 12 Equations

Equation	Group 1	Group 2
1, Eq. (3.113)	2	0
2, Eq. (3.114) for $i = 2$	1	1
3, Eq. (3.114) for $i = 3$	1	1
4, Eq. (3.114) for $i = 4$	1	1
5, Eq. (3.114) for $i = 5$	1	1
6, Eq. (3.114) for $i = 6$	1	1
7, Eq. (3.103)	0	2
8, Eq. (3.104)	0	2
9, Eq. (3.105)	0	2
10, Eq. (3.106)	0	2
11, Eq. (3.107)	0	2
12, Eq. (3.108)	0	2

product

$$\prod_{i=1}^{12} \left(\sum_{j=1}^2 d_{ij} \beta_j \right) = (2\beta_1)(\beta_1 + \beta_2)^5 (2\beta_2)^6,$$

where d_{ij} is taken from the (i, j) element of Table 3.3.

Since the first group contains three variables and the second group contains nine variables, the 2-homogeneous Bezout number is given by the coefficient of the $\beta_1^3 \beta_2^9$ term in the polynomial above and is found to be 1280. Hence the system of equations has at most 1280 solutions. Although the 2-homogeneous Bezout number is much lower than the 1-homogeneous Bezout number, it still contains numerous extraneous solutions. Raghavan (1993) applied the continuation method and found that the general Stewart–Gough platform has 40 direct kinematics solutions.

3.9 POSITION ANALYSIS OF A NEARLY GENERAL STEWART–GOUGH PLATFORM

In this section we study the direct kinematics of a nearly general Stewart–Gough platform by introducing the following additional assumptions (Zhang and Song, 1994):

1. The six spherical joints on the moving platform lie on the u – v plane.
2. The six spherical joints on the fixed platform lie on the x – y plane.

Based on the assumptions above, we have $a_{iz} = b_{iw} = 0$ for $i = 1, 2, \dots, 6$. Hence Eq. (3.114) can be further reduced to

$$\begin{aligned} b_{iu}\xi_1 + b_{iv}\xi_2 - a_{ix}p_x - a_{iy}p_y - a_{ix}b_{iu}u_x - a_{iy}b_{iu}u_y \\ - a_{ix}b_{iv}v_x - a_{iy}b_{iv}v_y + k_i = 0 \quad \text{for } i = 2, 3, \dots, 6. \end{aligned} \quad (3.115)$$

where $k_i = (a_{ix}^2 + a_{iy}^2 + b_{iu}^2 + b_{iv}^2 - d_i^2 + d_1^2)/2$ and where the variables ξ_1 and ξ_2 are defined as follows:

$$\xi_1 = p_x u_x + p_y u_y + p_z u_z, \quad (3.116)$$

$$\xi_2 = p_x v_x + p_y v_y + p_z v_z. \quad (3.117)$$

We note that the unit vector w disappears from Eq. (3.115). Hence only three of the six orthogonal conditions are needed for the analysis. By considering ξ_1 and ξ_2 as two intermediate variables, we have a system of 11

equations in 11 unknowns. The system of equations consists of Eqs. (3.103), (3.104), (3.106), (3.113), (3.115) for $i = 2$ to 6, (3.116), and (3.117). The unknowns are $p_x, p_y, p_z, u_x, u_y, u_z, v_x, v_y, v_z, \xi_1$, and ξ_2 . Equations (3.115) for $i = 2$ to 6 are linear, while the remaining equations are second-degree polynomials.

In what follows, we derive six polynomial equations in three unknowns: u_x, u_y , and v_y . First, we rewrite Eqs. (3.103), (3.104), and (3.113) as a group, and (3.106), (3.116), and (3.117) as another group, as follows:

$$u_z^2 = 1 - u_x^2 - u_y^2, \quad (3.118)$$

$$v_z^2 = 1 - v_x^2 - v_y^2, \quad (3.119)$$

$$p_z^2 = d_1^2 - p_x^2 - p_y^2, \quad (3.120)$$

and

$$u_z v_z = -u_x v_x - u_y v_y, \quad (3.121)$$

$$p_z u_z = \xi_1 - p_x u_x - p_y u_y, \quad (3.122)$$

$$p_z v_z = \xi_2 - p_x v_x - p_y v_y. \quad (3.123)$$

Next, we substitute Eqs. (3.118) through (3.123) into the following six identities:

$$(u_z^2)(v_z^2) - (u_z v_z)^2 = 0, \quad (3.124)$$

$$(p_z^2)(u_z^2) - (p_z u_z)^2 = 0, \quad (3.125)$$

$$(p_z^2)(v_z^2) - (p_z v_z)^2 = 0, \quad (3.126)$$

$$(u_z v_z)(p_z^2) - (p_z u_z)(p_z v_z) = 0, \quad (3.127)$$

$$(p_z u_z)(v_z^2) - (u_z v_z)(p_z v_z) = 0, \quad (3.128)$$

$$(p_z v_z)(u_z^2) - (u_z v_z)(p_z u_z) = 0. \quad (3.129)$$

This results in six equations free of the variables u_z, v_z , and p_z .

Equations (3.115), $i = 2, 3, \dots, 6$, represent five linear equations in eight unknowns. Hence we can solve five unknowns in terms of the remaining three. For example, we can express ξ_1, ξ_2, p_x, p_y , and v_x in terms of u_x, u_y , and v_y as follows:

$$\xi_1 = e_{11}u_x + e_{12}u_y + e_{13}v_y + e_{14}, \quad (3.130)$$

$$\xi_2 = e_{21}u_x + e_{22}u_y + e_{23}v_y + e_{24}, \quad (3.131)$$

$$p_x = e_{31}u_x + e_{32}u_y + e_{33}v_y + e_{34}, \quad (3.132)$$

$$p_y = e_{41}u_x + e_{42}u_y + e_{43}v_y + e_{44}, \quad (3.133)$$

$$v_x = e_{51}u_x + e_{52}u_y + e_{53}v_y + e_{54}, \quad (3.134)$$

where $e_{i,j}$'s are constants that can be found by solving Eqs. (3.115) for $i = 2, 3, \dots, 6$.

Upon substitution of Eqs. (3.130) through (3.134) into Eqs. (3.124) through (3.129), we obtain six fourth-degree polynomials in three unknowns: u_x , u_y , and v_y . Any three of the six polynomials can be used to solve for the three unknowns. Since the traditional Bezout number is $4^3 = 64$, the system of equations has at most 64 solutions. Zhang and Song (1994) applied the Sylvester dialytic method to further reduce the six polynomial equations to a 20th-degree polynomial in one unknown and showed that after back substitution, there are at most 40 direct kinematics solutions. Closed-form solutions of this manipulator have also been derived by Wen and Liang (1994).

3.10 POSITION ANALYSIS OF A 3-3 STEWART-GOUGH PLATFORM

A major problem associated with the general Stewart-Gough platform manipulator is that its direct kinematics cannot be solved in a closed form, although it has been shown that there exist up to 40 direct kinematic solutions. To avoid the problems associated with the general Stewart-Gough platform, special configurations of the Stewart-Gough platform have been proposed. These special designs usually contain concentric spherical joints either at the moving platform or at the fixed base. Figure 3.16 shows a 3-3 Stewart-Gough platform whose six limbs meet in a pairwise fashion at three points each in the moving platform and the base. This type of special construction makes closed-form direct kinematics solutions feasible.

Figure 3.17 shows the top view of the 3-3 Stewart-Gough platform, where the moving platform is symbolically represented by three pairs of concentric spherical joints located at points B_1 , B_2 , and B_3 , and the fixed base is represented by another three pairs of concentric spherical joints located at points A_1 , A_2 , and A_3 . For the purpose of analysis, we attach a Cartesian coordinate system to the fixed base with its origin located at point A_1 , the x -axis pointing along line A_1A_2 , the z -axis perpendicular to the plane defined by the triangle $\Delta A_1A_2A_3$, and the y -axis defined by the right-hand screw rule as shown in Fig. 3.17.

For the direct kinematics problem, the limb lengths are given and the platform location is to be found. Because of the special configuration, once the limb lengths are given, three triangles $\Delta A_1A_2B_1$, $\Delta A_2A_3B_2$, and $\Delta A_3A_1B_3$

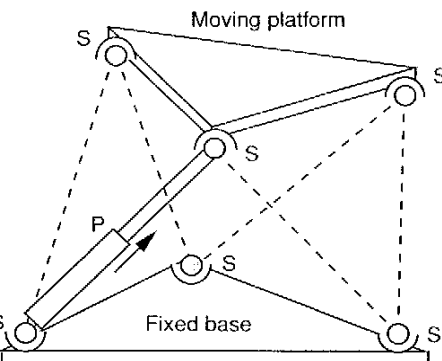


FIGURE 3.16. Spatial 6-dof, 3-3 Stewart-Gough platform.

can be uniquely determined. Hence the locus of B_i is constrained on a circle that is centered at and perpendicular to line A_iA_{i+1} . This constraint is equivalent to a simple RS (revolute-spherical) joint pair. Hence the overall mechanism is kinematically equivalent to a spatial 3 RS mechanism with zero degrees of freedom, as shown in Fig. 3.18.

To perform the analysis, we first identify the center C_i and equivalent radius r_i of the circle on which point B_i lies. Then we express the coordinates of point B_i in terms of an angle ϕ_i which the triangle $\Delta A_iA_{i+1}B_i$ makes with

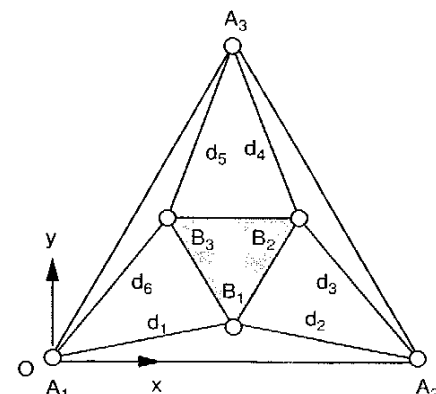


FIGURE 3.17. Top view of the 3-3 Stewart-Gough platform.

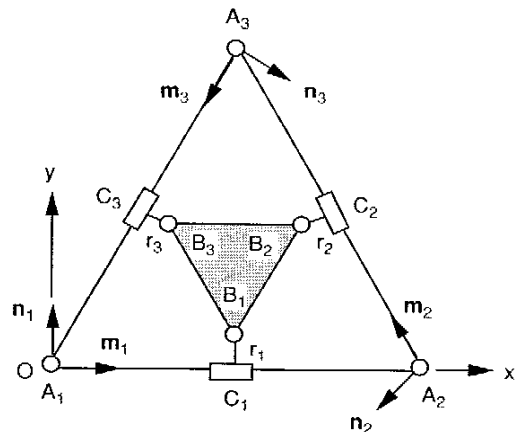


FIGURE 3.18. Equivalent 3RS spatial mechanism.

the base plane:

$$\mathbf{b}_i = \mathbf{c}_i + r_i(\mathbf{n}_i c\phi_i + \mathbf{k} s\phi_i) \quad \text{for } i = 1, 2, 3 \quad (3.135)$$

where \mathbf{b}_i and \mathbf{c}_i denote the position vectors of B_i and C_i , respectively; \mathbf{n}_i denotes a unit vector that lies on the base plane and is perpendicular to line $A_i A_{i+1}$ as shown in Fig. 3.18; and \mathbf{k} is a unit vector pointing in the positive z-axis.

Finally, we formulate the equations associated with the loop closure of the mechanism. Since the distance between points B_i and B_{i+1} is constant, we have

$$[\mathbf{b}_i - \mathbf{b}_{i+1}]^T [\mathbf{b}_i - \mathbf{b}_{i+1}] = h_i^2 \quad \text{for } i = 1, 2, 3 \pmod{3}, \quad (3.136)$$

where $h_i = |B_i B_{i+1}|$. Substituting Eq. (3.135) into (3.136) yields

$$e_{1i} c\phi_i c\phi_{i+1} + e_{2i} s\phi_i s\phi_{i+1} + e_{3i} c\phi_i + e_{4i} c\phi_{i+1} + e_{5i} = 0 \quad (3.137)$$

for $i = 1, 2, 3$ (modulo 3), where

$$e_{1i} = r_i r_{i+1} \mathbf{n}_i^T \mathbf{n}_{i+1},$$

$$e_{2i} = r_i r_{i+1},$$

$$e_{3i} = r_i \mathbf{n}_i^T [\mathbf{c}_{i+1} - \mathbf{c}_i],$$

$$e_{4i} = -r_{i+1} \mathbf{n}_{i+1}^T [\mathbf{c}_{i+1} - \mathbf{c}_i],$$

$$e_{5i} = \frac{h_i^2 + r_i^2 - r_{i+1}^2 - (\mathbf{c}_{i+1} - \mathbf{c}_i)^2}{2}.$$

Equation (3.137) takes the same form as Eq. (3.87). Following the same procedure, Eq. (3.137) can be reduced to an eighth-degree polynomial in the square of one unknown. Therefore, there are at most 16 solutions for the direct kinematics problem. Again, these 16 solutions form eight pairs of manipulator postures, one being the mirror image of another about a plane defined by A_1 , A_2 , and A_3 .

3.11 SUMMARY

Parallel manipulators have been introduced and classified into planar, spherical, and spatial manipulators in accordance with their motion characteristics and their connectivity listings. The Denavit–Hartenberg method for the kinematic analysis of closed-loop mechanisms was reviewed. However, it was judged that the geometric method is more appropriate for the kinematic analysis of most parallel manipulators. The direct and inverse kinematics of several well-known parallel manipulators were analyzed.

The direct kinematics of a 3-dof planar manipulator and a 3-dof orientation platform were both reduced to an eighth-degree polynomial. A spatial parallel manipulators with only translational degrees of freedom was shown to possess two solutions for both the direct and inverse kinematics problems. The direct kinematics of a spatial 3-dof manipulator with coupled position and orientation characteristics was shown to have at most eight pairs of possible poses. Furthermore, the kinematics of a general Stewart–Gough platform and a nearly general Stewart–Gough platform were studied. Finally, a 3–3 Stewart–Gough platform was shown to possess at most eight pairs of possible manipulator postures for its direct kinematics problem. In general, the solutions to the direct kinematics of a parallel manipulator form several pairs of postures, one being the mirror image of the other about some plane of symmetry.

REFERENCES

- Arai, T., Cleary, K., Homma, K., Adachi, H., and Nakamura, T., 1991, "Development of Parallel Link Manipulator for Underground Excavation Task," *Proc. 1991 International Symposium on Advanced Robot Technology*, pp. 541–548.

- Chen, N. X. and Song, S. M., 1994, "Direct Position Analysis of the 4-6 Stewart Platforms," *ASME J. Mech. Des.*, Vol. 116, pp. 61-66.
- Clavel, R., 1988, "A Fast Robot with Parallel Geometry," *Proc. 18th International Symposium on Industrial Robots*, Sydney, Australia, pp. 91-100.
- Clearly, K. and Arai, T., 1991, "A Prototype Parallel Manipulator: Kinematics, Construction, Software, Workspace Results, and Singularity Analysis," *Proc. IEEE International Conference on Robotics and Automation*, Vol. 1, pp. 561-571.
- Fichter, E. F., 1986, "A Stewart Platform Based Manipulator: General Theory and Practical Construction," *Int. J. Robot. Res.*, Vol. 5, pp. 157-182.
- Giddings & Lewis, 1995, Giddings and Lewis Machine Tools, Fond du Lac, WI.
- Gosselin, C. and Angeles, J., 1988, "The Optimum Kinematic Design of a Planar Three-Degree-of-Freedom Parallel Manipulator," *ASME J. Mech. Transm. Autom. Des.*, Vol. 110, pp. 35-41.
- Gosselin, C. and Angeles, J., 1989, "The Optimum Kinematic Design of a Spherical Three-Degree-of-Freedom Parallel Manipulator," *ASME J. Mech. Transm. Autom. Des.*, Vol. 111, pp. 202-207.
- Gosselin, C. and Hamel, J., 1994, "The Agile Eye: A High-Performance Three-Degree-of-Freedom Camera-Orienting Device," *Proc. IEEE International Conference on Robotics and Automation*, pp. 781-786.
- Gosselin, C. and Sefrioui, J., 1991, "Polynomial Solutions for the Direct Kinematic Problem of Planar Three-Degree-of-Freedom Parallel Manipulator," *Proc. International Conference on Advanced Robotics*, Pisa, Italy, pp. 1124-1129.
- Gough, V. E. and Whitehall, S. G., 1962, "Universal Tyre Test Machine," *Proc. 9th International Technical Congress, F.I.S.I.T.A.*, p. 177 (Institution of Mechanical Engineers).
- Griffis, M. and Duffy, J., 1989, "Forward Displacement Analysis of a Class of Stewart Platforms," *J. Robot. Syst.*, Vol. 6, pp. 703-720.
- Hudgens, J. C. and Tesar, D., 1988, "A Fully-Parallel Six Degree-of-Freedom Micromanipulator: Kinematic Analysis and Dynamic Model," *Trends and Developments in Mechanisms, Machines, and Robotics*, *Proc. 20th ASME Biennial Mechanisms Conference*, DE-Vol. 15.3, pp. 29-37.
- Hunt, K. H., 1983, "Structural Kinematics of In-Parallel-Actuated Robot Arms," *ASME J. Mech. Transm. Autom. Des.*, Vol. 105, pp. 705-712.
- Husain, M. and Waldron, K. J., 1994, "Direct Position Kinematics of the 3-1-1-1 Stewart Platform," *ASME J. Mech. Des.*, Vol. 116, pp. 1102-1107.
- Innocenti, C. and Parenti-Castelli, V., 1990, "Direct Position Analysis of the Stewart Platform Mechanism," *Mech. Mach. Theory*, Vol. 25, pp. 611-612.
- Innocenti, C. and Parenti-Castelli, V., 1993a, "Forward Kinematics of the General 6-6 Fully Parallel Mechanism: An Exhaustive Numerical Approach via a Monodimensional Search Algorithm," *ASME J. Mech. Des.*, Vol. 115, pp. 932-937.
- Innocenti, C. and Parenti-Castelli, V., 1993b, "Echelon Form Solution of Direct Kinematics for the General Fully Parallel Spherical Wrist," *Mech. Mach. Theory*, Vol. 28, No. 4, pp. 553-561.
- Kohli, D., Lee, S. H., Tsai, K. Y., and Sandor, G. N., 1988, "Manipulator Configurations Based on Rotary-Linear (R-L) Actuators and Their Direct and Inverse Kinematics," *ASME J. Mech. Transm. Autom. Des.*, Vol. 110, pp. 397-404.
- Lee, K. and Shah, D. K., 1987, "Kinematic Analysis of a Three Degrees of Freedom In-Parallel Actuated Manipulator," *Proc. IEEE International Conference on Robotics and Automation*, Vol. 1, pp. 345-350.
- Lin, W., Crane, C. D., and Duffy, J., 1994, "Closed Form Forward Displacement Analysis of the 4-5 In-Parallel Platforms," *ASME J. Mech. Des.*, Vol. 116, pp. 47-53.
- Mohamed, M. G. and Duffy, J., 1985, "A Direct Determination of the Instantaneous Kinematics of Fully Parallel Robotic Manipulators," *ASME J. Mech. Transm. Autom. Des.*, Vol. 107, pp. 226-229.
- Mohammadi, H. R., Daniali, P. J., Zsombor-Murray, P. J., and Angeles, J., 1993, "The Kinematics of 3-DOF Planar and Spherical Double-Triangular Parallel Manipulators," in *Computational Kinematics*, edited by J. Angeles, G. Hommel, and P. Kovacs, Kluwer Academic Publishers, Dordrecht, The Netherlands, pp. 153-164.
- Nanua, P., Waldron, K. J., and Murthy, V., 1990, "Direct Kinematic Solution of a Stewart Platform," *IEEE Trans. Robot. Autom.*, Vol. 6, pp. 438-444.
- Pierrot, F., Reynaud, C., and Fournier, A., 1990, "DELTa: A Simple and Efficient Parallel Robot," *Robotica*, Vol. 8, pp. 105-109.
- Pierrot, F., Fournier, A., and Dauchez, P., 1991, "Toward a Fully Parallel 6-DOF Robot for High-Speed Applications," *Proc. 1991 IEEE International Conference on Robotics and Automation*, pp. 1288-1293.
- Raghavan, M., 1993, "The Stewart Platform of General Geometry Has 40 Configurations," *ASME J. Mech. Des.*, Vol. 115, pp. 277-282.
- Reinholtz, C. and Gokhale, D., 1987, "Design and Analysis of Variable Geometry Truss Robot," *Proc. 9th Applied Mechanisms Conference*, Oklahoma State University, Stillwater, OK.
- Sternheim, F., 1987, "Computation of the Direct and Inverse Kinematic Model of the Delta 4 Parallel Robot," *Robotersysteme*, Vol. 3, pp. 199-203.
- Stewart, D., 1965, "A Platform with Six Degrees of Freedom," *Proc. Inst. Mech. Eng. London*, Vol. 180, pp. 371-386.
- Song, S. M. and Zhang, M. D., 1995, "A Study of Reaction Force Compensation Based on Three-Degree-of-Freedom Parallel Platform," *J. Robot. Syst.*, Vol. 12, No. 12, pp. 783-794.
- Tahmasebi, F. and Tsai, L. W., 1994, "Closed-Form Direct Kinematics Solution of a New Parallel Mini-manipulator," *ASME J. Mech. Des.*, Vol. 116, No. 4, pp. 1141-1147.
- Tahmasebi, F. and Tsai, L. W., 1995, "On the Stiffness of a Novel Six-DOF Parallel Mini-manipulator," *J. Robot. Syst.*, Vol. 12, No. 12, pp. 845-856.
- Tsai, L. W., 1996, "Kinematics of a Three-DOF Platform with Three Extensible Limbs," in *Recent Advances in Robot Kinematics*, edited by J. Lenarcic and

- V. Parenti-Castelli, Kluwer Academic Publishers, Boston, pp. 401–410, *Proc. 5th International Symposium on Advances in Robot Kinematics*.
- Tsai, L. W. and Stamper, R., 1996, "A Parallel Manipulator with Only Translational Degrees of Freedom," 96-DETC-MECH-1152, ASME 1996 Design Engineering Technical Conferences, Irvine, CA.
- Tsai, L. W. and Tahmasebi, F., 1993, "Synthesis and Analysis of a New Class of Six-DOF Parallel Mini-manipulators," *J. Robot. Sys.*, Vol. 10, No. 5, pp. 561–580.
- Tsai, L. W., Walsh, G. C., and Stamper, R., 1996, "Kinematics of a Novel Three-DOF Translational Platform," *Proc. IEEE 1996 International Conference on Robotics and Automation*, Minneapolis, MN, pp. 3446–3451.
- Waldron, K. J., Vohnout, V. J., Pery, A., and McGhee, R.B., 1984, "Configuration Design of the Adaptive Suspension Vehicle," *Int. J. Robot. Res.*, Vol. 3, pp. 37–48.
- Wen, F. and Liang, C., 1994, "Displacement Analysis of the 6 6 Stewart Platform Mechanism," *Mech. Mach. Theory*, Vol. 29, No. 4, pp. 547–557.
- Wohlhart, K., 1994, "Displacement Analysis of the General Spherical Stewart Platform," *Mech. Mach. Theory*, Vol. 29, No. 4, pp. 581–589.
- Zhang, C. and Song, S. M., 1994, "Forward Position Analysis of Nearly General Stewart Platforms," *ASME J. Mech. Des.*, Vol. 116, pp. 54–60.

EXERCISES

- Sketch as many feasible spatial 3-dof parallel manipulators with a connectivity listing of (5,5,5) as possible. Using the limb configurations shown in Fig. 3.4, identify those mechanisms with identical limb structure.
- Using the limb configurations shown in Fig. 3.4, sketch as many feasible spatial 4-dof parallel manipulators with a connectivity listing of (6,6,5,5) as possible. Identify those mechanisms with linear input actuators.
- Referring to the planar five-bar linkage shown in Fig. 1.7, find the end-effector position \mathbf{q} as a function of the two input joint angles, θ_1 and θ_2 .
- Figure 3.19 shows the schematic diagram of a planar 2-dof five-bar manipulator that is constructed with one prismatic and four revolute joints. Find the end-effector position \mathbf{q} as a function of the two input joint variables, d_1 and θ_2 .
- Referring to the planar 2-dof pantograph mechanism shown in Fig. 1.8, let 1 and 2 be the input links and 6 be the output link. Also let $BC \parallel DE$, $BE \parallel CD$, and points A , B , and Q lie on a straight line. Find the end-effector position \mathbf{q} as a function of the linear displacements, x_1 and y_2 , of the two input links.

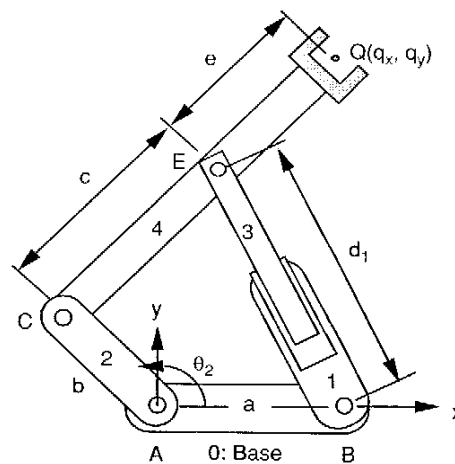


FIGURE 3.19. Five-bar, 4R1P manipulator.

- Consider the planar 3-dof, 3PRP manipulator shown in Fig. 3.3. Let the three ground-connected prismatic joints be the actuated joints. Assuming that $AB = BC = CA = DE = EF = FD = a$, find the moving platform location in terms of the input displacements.
- For the spherical 3RRR manipulator shown in Fig. 1.21, let the three ground-connected joints be the input variables. Solve the moving platform orientation as a function of input joint angles. Discuss the number of possible configurations corresponding to a given set of input joint angles.
- Figure 3.20 shows the schematic diagram of a spatial 3UPU platform manipulator. Three identical limbs connect the moving platform to the fixed base by universal joints at points B_i and A_i , $i = 1, 2$, and 3 , respectively. Each limb consists of an upper member and a lower member that are connected by a prismatic joint. The three base-connected axes of the universal joints are coplanar. Similarly, the three moving-platform connected axes of the universal joints are also coplanar. The second axes of the universal joints that are directly attached to the upper and lower members of each limb are parallel to each other and are both perpendicular to the axis of the prismatic joint. It can be shown that this manipulator possesses three translational degrees of freedom. Considering the three prismatic joints as the input joints, solve the direct kinematics problem.

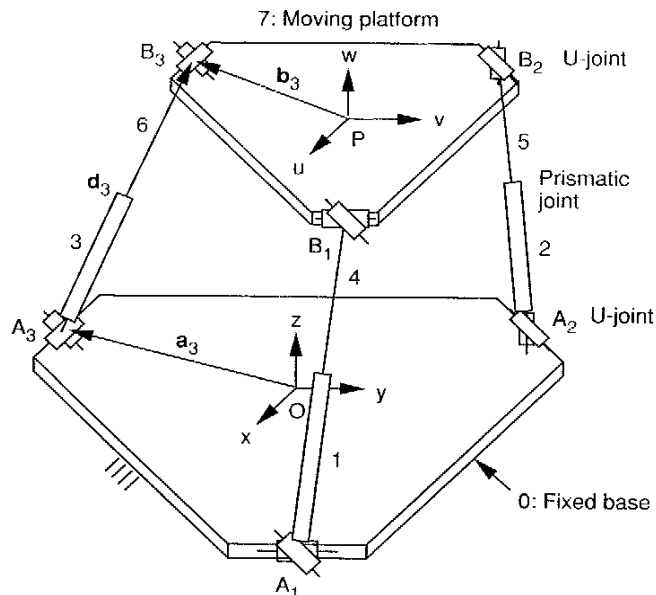


FIGURE 3.20. A 3-dof, 3U PU parallel manipulator.

Also discuss the number of possible configurations corresponding to a given set of input joint variables.

9. Figure 3.21 shows a schematic diagram of the DELTA robot without the gripper (Pierrot et al., 1990, 1991). This robot is made up of a fixed base, a moving platform, and three major limbs. Each major limb connects the moving platform to the fixed platform by an upper arm and a lower arm. The upper arm is made up of a spatial parallelogram (connected by ball joints at the ends of each rod). The moving platform possesses three translational degrees of freedom. Links 1, 2, and 3 are the input links. Three rotary actuators can be mounted on the fixed base to drive the manipulator. Derive the moving platform position \mathbf{p} in terms of the input joint angles.
10. The original flight simulator designed by Stewart (1965) consists of three major limbs, as shown in Fig. 3.22. Each limb consists of two hydraulic jacks. The first jack has its piston connected to the moving platform by a spherical joint, and the cylinder connected to the base by two revolute

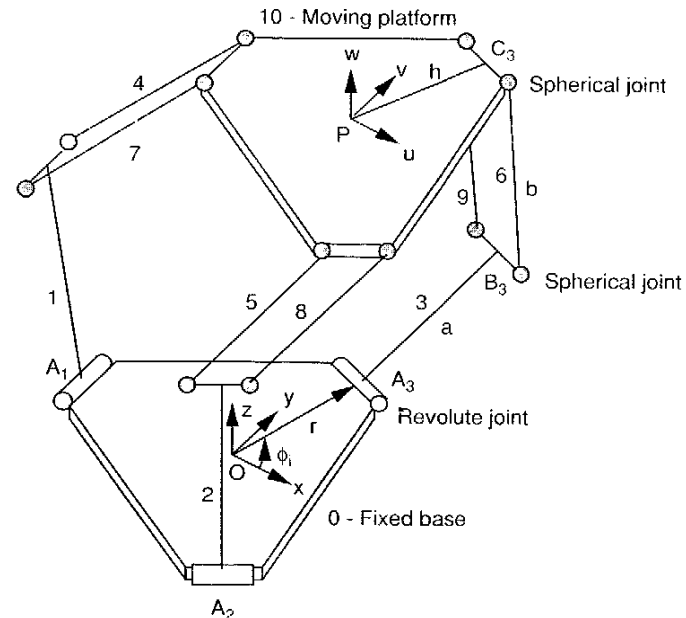


FIGURE 3.21. DELTA platform.

joints. The second jack has its piston connected to the cylinder of the first jack, and the cylinder connected to the base by two revolute joints. The two base-connected revolute joints share one common axis, while the remaining revolute joint axes are parallel to one another and are perpendicular to the base-connected revolute joints. The hydraulic jacks serve as the inputs of the manipulator. Derive the location of the moving platform in terms of the linear displacements of the hydraulic jacks.

11. Figure 3.23 shows a 6-dof parallel manipulator developed by Tsai and Tahmasebi (1993). This manipulator consists of three inextensible limbs. One end of each limb is connected to the moving platform by a revolute joint, while the other end is connected to a 2-dof planar motor by a spherical joint. The three moving-platform-connected revolute joints are coplanar. Derive the moving platform location in terms of the linear displacements of the planar motors.

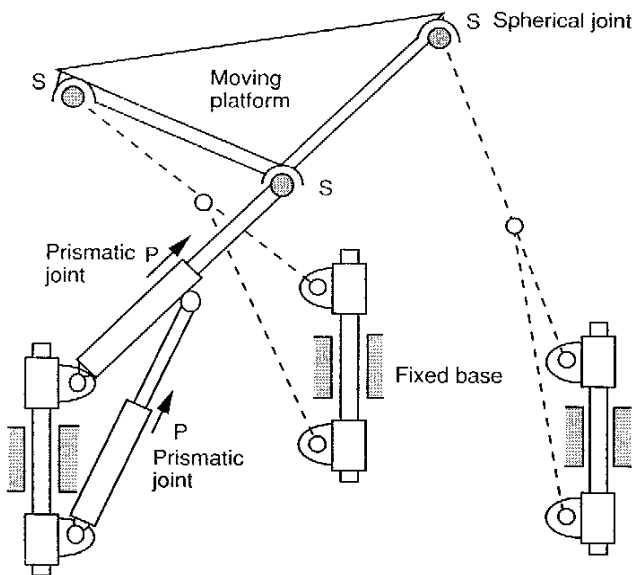


FIGURE 3.22. A 6-dof Stewart platform.

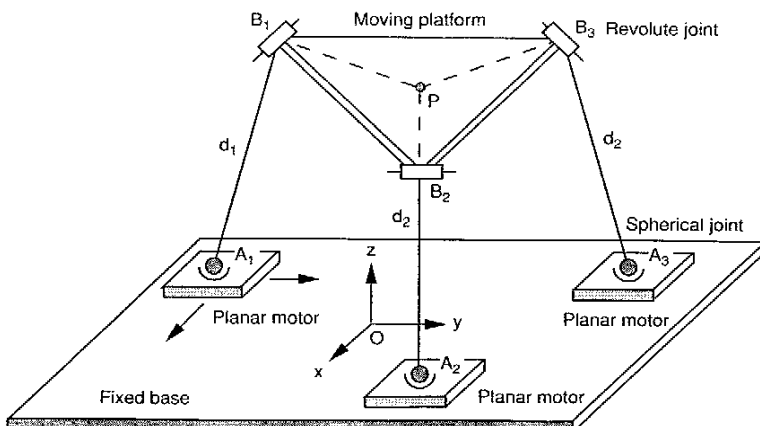


FIGURE 3.23. Spatial 6-dof, 3PPSR platform.

CHAPTER 4

JACOBIAN ANALYSIS OF SERIAL MANIPULATORS

4.1 INTRODUCTION

In previous chapters we have studied the kinematic relations between the end-effector location and the joint variables of serial and parallel manipulators. Both the direct and inverse kinematics have been analyzed. This knowledge enables us to bring the end effector to some desired locations in space. In this chapter we extend our study from a position analysis problem to a velocity analysis problem of serial manipulators.

For some applications, such as spray painting (Fig. 4.1), it is necessary to move the end effector of a manipulator along some desired paths with a prescribed speed. To achieve this goal, the motion of the individual joints of a manipulator must be carefully coordinated. There are two types of velocity coordination problems, called direct velocity and inverse velocity problems. For the *direct velocity problem*, the input joint rates are given and the objective is to find the velocity state of the end effector. For the *inverse velocity problem*, the velocity state of the end effector is given and the input joint rates required to produce the desired velocity are to be found. In this chapter, the fundamental knowledge needed to achieve such a coordinated motion is developed.

We call the vector space spanned by the joint variables the *joint space*, and the vector space spanned by the end-effector location, the *end-effector space*. For robot manipulators, the *Jacobian matrix*, or simply *Jacobian*, is defined as the matrix that transforms the joint rates in the actuator space to the velocity state in the end-effector space.



FIGURE 4.1. Spray painting robot. (Courtesy of Fanuc Robotics North America, Inc., Rochester Hills, Michigan.)

The Jacobian matrix is a critical component for generating trajectories of prescribed geometry in the end-effector space. Most coordination algorithms employed by industrial robots avoid numerical inversion of the Jacobian matrix by deriving analytical inverse solutions on an ad hoc basis. Therefore, it is important that efficient algorithms be developed. Since the velocity state of the end effector can be defined in various ways, a variety of Jacobian matrices and consequently, different methods of formulation have appeared in the literature (Craig, 1986; Featherstone, 1983; Hollerbach and Saher, 1983; Hunt, 1986, 1987a,b; Orin and Schrader, 1984; Waldron et al., 1985; Whitney, 1972). In what follows, two different definitions of the Jacobian matrix are described. The first is a *conventional Jacobian* and the second is a *screw-based Jacobian*.

The Jacobian matrix is also useful in other applications. For some configurations of a manipulator, the Jacobian matrix may lose its full rank. Such conditions are called *singular conditions*. At a singular condition, a serial manipulator may lose one or more degrees of freedom while a parallel manipulator may gain one or more degrees of freedom. In this chapter, the singular conditions of serial manipulators are also studied.

4.2 DIFFERENTIAL KINEMATICS OF A RIGID BODY

We first study the differential kinematics of a rigid body. Then these kinematic properties are applied for a derivation of the differential kinematics of the links in a manipulator and for a development of the Jacobian matrix. Since we will be dealing with many frames of reference, the following notations are made to identify the frame with respect to which a vector is defined. A vector \mathbf{p} can be a function of time in one reference frame but constant in another reference frame. Thus, in general, we need two frames of references to describe the nature of a vector: one with respect to which the change of a vector is measured and another in which the vector is expressed. In this book we use an inner leading superscript to denote the frame with respect to which a vector is being measured, and an outer leading superscript to indicate the frame in which the vector is expressed.

For example, ${}^B\mathbf{p}$ denotes the position vector of a point P with respect to frame B , and ${}^A({}^B\mathbf{p})$ denotes ${}^B\mathbf{p}$ expressed in frame A . Similarly, the velocity of P is defined by taking the derivative of ${}^B\mathbf{p}$ with respect to time:

$${}^B\mathbf{v}_P = \frac{d^B\mathbf{p}}{dt}. \quad (4.1)$$

However, once the differentiation is taken, the vector can be expressed in any other frame. Thus

$${}^A({}^B\mathbf{v}_P) = {}^A\left(\frac{d^B\mathbf{p}}{dt}\right) \quad (4.2)$$

indicates that the differentiation is taken with respect to frame B and the resulting vector is expressed in frame A .

When the two leading superscripts are the same or when the frame with respect to which a vector quantity is being measured is clearly understood, the inner superscript will be omitted. For clarity, we often use the rotation matrix ${}^A\mathbf{R}_B$ to transform a vector from one reference frame to another:

$${}^A({}^B\mathbf{p}) \equiv {}^A\mathbf{R}_B {}^B\mathbf{p}. \quad (4.3)$$

Furthermore, when no specific reference frame is mentioned, either the base frame is implied or any reference frame can be used. Note that all vectors in one equation must be expressed in the same reference frame.

4.2.1 Angular Velocity of a Rigid Body

While the linear velocity describes the rate of change of the position of a point in space, the angular velocity vector describes the rate of change of the

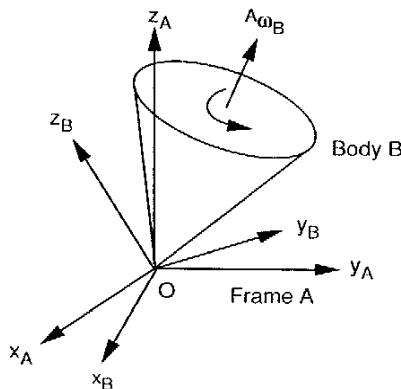


FIGURE 4.2. Instantaneous rotation of frame B with respect to A .

orientation of a rigid body. Figure 4.2 shows that frame B is rotating with respect to frame A with a fixed point O . The orientation of frame B with respect to A can be described by a rotation matrix, ${}^A R_B$. Since the rotation matrix ${}^A R_B$ is orthogonal, the inverse transformation of ${}^A R_B$ is identical to the transpose. Hence

$${}^A R_B {}^A R_B^T = I, \quad (4.4)$$

where I is a 3×3 identity matrix.

Taking the derivative of Eq. (4.4) with respect to time, we obtain

$${}^A \dot{R}_B {}^A R_B^T + {}^A R_B {}^A \dot{R}_B^T = 0. \quad (4.5)$$

Substituting ${}^A R_B^T = {}^A R_B^{-1}$ and ${}^A R_B = ({}^A R_B^{-1})^T$ into Eq. (4.5), we obtain

$$({}^A \dot{R}_B {}^A R_B^{-1}) + ({}^A \dot{R}_B {}^A R_B^{-1})^T = 0. \quad (4.6)$$

Hence ${}^A \dot{R}_B {}^A R_B^{-1}$ is a 3×3 skew-symmetric matrix. Without losing generality, we may define the skew-symmetric matrix as

$$\Omega \equiv {}^A \dot{R}_B {}^A R_B^{-1} = \begin{bmatrix} 0 & -\omega_z & \omega_y \\ \omega_z & 0 & -\omega_x \\ -\omega_y & \omega_x & 0 \end{bmatrix}. \quad (4.7)$$

Here ω_x , ω_y , and ω_z are to be identified as three independent parameters specifying the angular velocity of a rigid body. In what follows it will be shown

that these three quantities form the components of a vector called the angular velocity vector of B in A .

The position vector of a point P that is embedded in frame B and measured with respect to frame A is given by

$${}^A \mathbf{p} = {}^A R_B {}^B \mathbf{p}. \quad (4.8)$$

Note that ${}^B \mathbf{p}$ is a constant vector in frame B since P is embedded in B . The velocity of P with respect to frame A is obtained by taking the derivative of Eq. (4.8) with respect to time:

$${}^A \mathbf{v}_P = \frac{d}{dt} ({}^A R_B {}^B \mathbf{p}) = {}^A \dot{R}_B {}^B \mathbf{p}. \quad (4.9)$$

Solving ${}^B \mathbf{p}$ from Eq. (4.8) and substituting the resulting expression into Eq. (4.9) yields

$${}^A \mathbf{v}_P = {}^A \dot{R}_B {}^A R_B^{-1} {}^A \mathbf{p}. \quad (4.10)$$

Substituting Eq. (4.7) into (4.10) produces

$${}^A \mathbf{v}_P = \Omega {}^A \mathbf{p}. \quad (4.11)$$

We may ask ourselves the following question: Is there any point in B that has zero velocity at that instant? Assuming that \tilde{P} is such a point,

$${}^A \mathbf{v}_{\tilde{P}} = \Omega {}^A \tilde{\mathbf{p}} = \mathbf{0}. \quad (4.12)$$

Equation (4.12) consists of three homogeneous linear equations in three unknowns, \tilde{p}_x , \tilde{p}_y , and \tilde{p}_z . The compatibility condition for the existence of non-trivial solutions is that the determinant of the coefficient matrix must vanish (i.e., $|\Omega| = 0$). Since Ω is a 3×3 skew-symmetric matrix, this condition is satisfied automatically:

$$\begin{vmatrix} 0 & -\omega_z & \omega_y \\ \omega_z & 0 & -\omega_x \\ -\omega_y & \omega_x & 0 \end{vmatrix} = \omega_x \omega_y \omega_z - \omega_x \omega_y \omega_z = 0.$$

Hence only two of the three equations in Eq. (4.12) are independent. Solving Eq. (4.12) for the ratio $\tilde{p}_x : \tilde{p}_y : \tilde{p}_z$, we obtain

$$\tilde{p}_x : \tilde{p}_y : \tilde{p}_z = \omega_x : \omega_y : \omega_z. \quad (4.13)$$

We conclude that there exist infinitely many stationary points, and these points lie on a line that passes through the origin and is parallel to the vector

${}^A\omega_B = [\omega_x, \omega_y, \omega_z]^T$. We call the vector ${}^A\omega_B$ the *angular velocity vector* and the line the *instantaneous screw axis*. Using the vector notation, Eq. (4.11) can be written as

$${}^A\mathbf{v}_p = {}^A\omega_B \times {}^A\mathbf{p}. \quad (4.14)$$

4.2.2 Linear Velocity of a Point

Figure 4.3 shows a rigid body B that is making an instantaneous rotation as well as translation with respect to a reference frame A . The position vector of a point P , which is not necessarily fixed in frame B , relative to frame A can be written as

$${}^A\mathbf{p} = {}^A\mathbf{q} + {}^A\mathbf{R}_B {}^B\mathbf{p}, \quad (4.15)$$

where ${}^A\mathbf{q} = \overline{OQ}$ denotes the position vector of the origin Q of frame B with respect to frame A .

To derive the velocity of P , we first consider the rate of change of the second term in Eq. (4.15). This is essentially the case when frame B is rotating with respect to frame A with the origin Q fixed in A . Differentiating the second term of Eq. (4.15) with respect to time yields

$$\frac{d}{dt}({}^A\mathbf{R}_B {}^B\mathbf{p}) = {}^A\mathbf{R}_B {}^B\mathbf{v}_p + {}^A\dot{\mathbf{R}}_B {}^B\mathbf{p}, \quad (4.16)$$

where ${}^B\mathbf{v}_p = \frac{d}{dt} {}^B\mathbf{p}$ denotes the velocity of P with respect frame B .

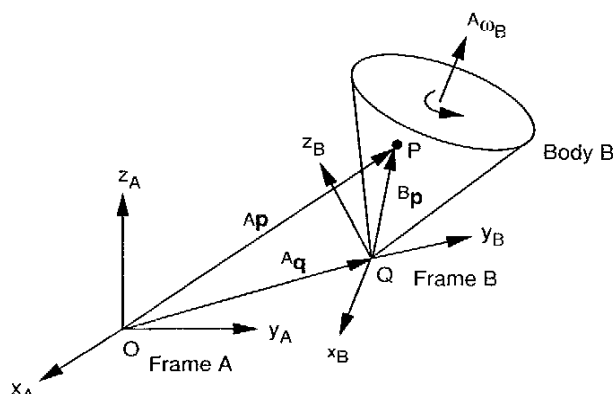


FIGURE 4.3. Instantaneous motion of a rigid body B with respect to frame A .

Postmultiplying both sides of Eq. (4.7) by ${}^A\mathbf{R}_B$, we obtain

$${}^A\dot{\mathbf{R}}_B = \Omega {}^A\mathbf{R}_B. \quad (4.17)$$

Substituting Eq. (4.17) into (4.16) yields

$$\frac{d}{dt}({}^A\mathbf{R}_B {}^B\mathbf{p}) = {}^A\mathbf{R}_B {}^B\mathbf{v}_p + \Omega {}^A\mathbf{R}_B {}^B\mathbf{p}. \quad (4.18)$$

Equation (4.18) can be written in vector form as

$$\frac{d}{dt}({}^A\mathbf{R}_B {}^B\mathbf{p}) = {}^A\mathbf{R}_B {}^B\mathbf{v}_p + {}^A\omega_B \times ({}^A\mathbf{R}_B {}^B\mathbf{p}). \quad (4.19)$$

When the origin Q of frame B is moving with respect to frame A , we simply add a component representing the linear velocity of Q in A to Eq. (4.19). Hence a general equation of motion can be written as

$${}^A\mathbf{v}_p = {}^A\mathbf{v}_q + {}^A\mathbf{R}_B {}^B\mathbf{v}_p + {}^A\omega_B \times ({}^A\mathbf{R}_B {}^B\mathbf{p}), \quad (4.20)$$

where ${}^A\mathbf{v}_q = {}^A\dot{\mathbf{q}}$ denotes the velocity of Q relative to frame A . The first term in Eq. (4.20) is contributed by the linear velocity of Q with respect to frame A , the second term is contributed by the relative motion of P with respect to frame B , and the third term is contributed by the rotation of frame B with respect to A .

Special Case. If point P is embedded in the moving frame B , ${}^B\mathbf{v}_p = 0$ identically. Equation (4.20) reduces to

$${}^A\mathbf{v}_p = {}^A\mathbf{v}_q + {}^A\omega_B \times ({}^A\mathbf{R}_B {}^B\mathbf{p}). \quad (4.21)$$

Although Eq. (4.21) is derived for the case in which Q is the origin of a moving frame, it is equally applicable to any two points fixed on the moving frame. In general, if P and Q are two points embedded in a rigid body B , their velocities are related by the equation

$${}^A\mathbf{v}_p = {}^A\mathbf{v}_q + {}^A\omega_B \times ({}^A\mathbf{p} - {}^A\mathbf{q}). \quad (4.22)$$

4.2.3 Instantaneous Screw Axis

In this section we show that a general instantaneous motion of a rigid body can be described by a differential rotation about a unique axis and a differential translation along the same axis. This concept will be applied to the Jacobian analysis of serial manipulators.

For a general spatial motion of a rigid body B , are there any stationary points in B ? If ${}^B\bar{\mathbf{p}}$ is a stationary point, ${}^A\mathbf{v}_{\bar{p}} = 0$ identically, and Eq. (4.21)

reduces to

$${}^A\omega_B \times ({}^A R_B {}^B \tilde{\mathbf{p}}) = -{}^A \mathbf{v}_q. \quad (4.23)$$

Since the angular velocity ${}^A\omega_B$ is derived from a 3×3 skew-symmetric matrix Ω , the coefficients matrix of Eq. (4.23) is singular. It follows that, in general, there are no solutions to Eq. (4.21). However, we may seek for those points whose linear velocity vectors point along the direction of the angular velocity. That is,

$${}^A \mathbf{v}_{\tilde{p}} = \lambda {}^A \omega_B, \quad (4.24)$$

where λ is called a *pitch*.

Substituting Eq. (4.24) into (4.21) yields

$${}^A \mathbf{v}_q + {}^A \omega_B \times ({}^A R_B {}^B \tilde{\mathbf{p}}) = \lambda {}^A \omega_B. \quad (4.25)$$

Dot-multiplying both sides of Eq. (4.25) by ${}^A \omega_B$, we obtain

$$\lambda = \frac{{}^A \omega_B \cdot {}^A \mathbf{v}_q}{{}^A \omega_B^2}. \quad (4.26)$$

Equation (4.25) can be written in the form

$${}^A \omega_B \times ({}^A R_B {}^B \tilde{\mathbf{p}}) = -{}^A \mathbf{v}'_q, \quad (4.27)$$

where ${}^A \mathbf{v}'_q = {}^A \mathbf{v}_q - \lambda {}^A \omega_B$ is orthogonal to ${}^A \omega_B$; that is,

$${}^A \omega_B \cdot {}^A \mathbf{v}'_q = {}^A \omega_B \cdot ({}^A \mathbf{v}_q - \lambda {}^A \omega_B) = 0. \quad (4.28)$$

We now make use of the following result derived from vector algebra. Let vectors \mathbf{a} , \mathbf{b} , and \mathbf{c} in Fig. 4.4 satisfy the following two conditions:

$$\mathbf{a} \times \mathbf{c} = \mathbf{b},$$

$$\mathbf{a} \cdot \mathbf{b} = 0.$$

Then \mathbf{c} has infinite number of solutions lying on a line:

$$\mathbf{c} = -\frac{\mathbf{a} \times \mathbf{b}}{\mathbf{a}^2} + \mu \mathbf{a},$$

where μ is an arbitrary scalar constant.

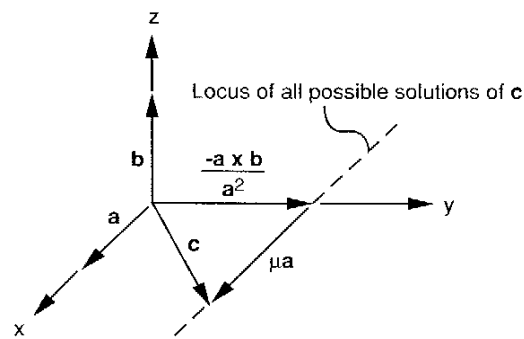


FIGURE 4.4. Vector relation.

From the vector algebra above, we conclude that all solutions to Eqs. (4.27) and (4.28) are given by

$${}^A R_B {}^B \tilde{\mathbf{p}} = \frac{{}^A \omega_B \times {}^A \mathbf{v}'_q}{{}^A \omega_B^2} + \mu {}^A \omega_B. \quad (4.29)$$

Applying Eq. (4.15), Eq. (4.29) can be written as

$${}^A \tilde{\mathbf{p}} = {}^A \mathbf{q} + \frac{{}^A \omega_B \times {}^A \mathbf{v}'_q}{{}^A \omega_B^2} + \mu {}^A \omega_B. \quad (4.30)$$

Equation (4.29) or (4.30) states that the locus of all points whose instantaneous linear velocities point along the direction of the angular velocity vector is a line. This line that is parallel to the angular velocity vector is called the *instantaneous screw axis*. We conclude that the general spatial motion of a rigid body consists of a differential rotation about, and a differential translation along, some axis.

4.3 DIFFERENTIAL KINEMATICS OF SERIAL MANIPULATORS

In this section we study the differential kinematics of a serial manipulator using the Denavit–Hartenberg transformation matrix. First, we study the differential motion of a link. Then we apply it to the differential motion of a serial manipulator.

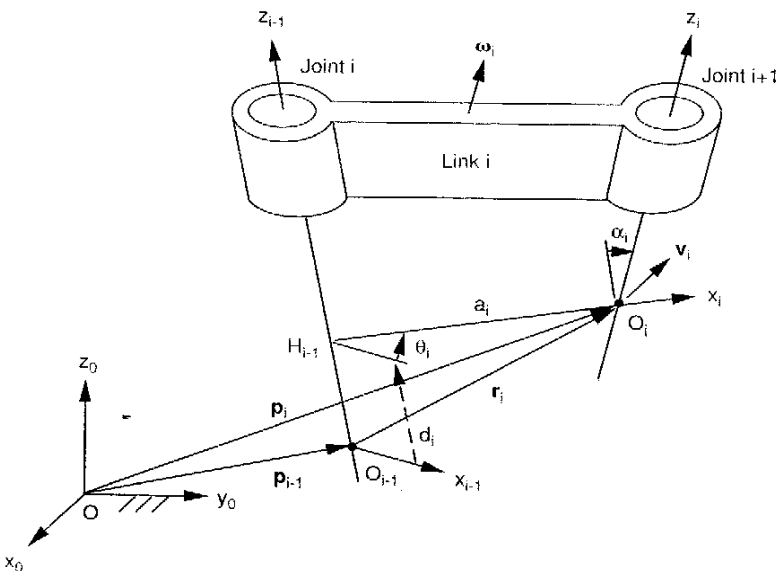


FIGURE 4.5. Geometry of link i and its motion state.

4.3.1 Link Differential Transformation Matrix

Figure 4.5 shows a typical link, i , of a manipulator. According to the D-H convention, a Cartesian coordinate system (x_i, y_i, z_i) is attached to the distal end of link i , and the fixed coordinate system is denoted by frame (x_0, y_0, z_0) . The location of link i can be described by a position vector \mathbf{p}_i of O_i , and a rotation matrix 0R_i of link i with respect to the fixed reference frame 0. The velocity state of link i can be described by the linear velocity \mathbf{v}_i of the origin O_i , and the angular velocity ω_i of link i relative to the fixed reference frame.

The D-H transformation matrix is given by Eq. (2.2) and the inverse transformation is given by Eq. (2.5). Taking the derivative of Eq. (2.2) with respect to time, we obtain

$${}^{i-1}\dot{A}_i = \begin{bmatrix} -\dot{\theta}_i s\theta_i & -\dot{\theta}_i c\alpha_i c\theta_i & \dot{\theta}_i s\alpha_i c\theta_i & -\dot{\theta}_i a_i s\theta_i \\ \dot{\theta}_i c\theta_i & -\dot{\theta}_i c\alpha_i s\theta_i & \dot{\theta}_i s\alpha_i s\theta_i & \dot{\theta}_i a_i c\theta_i \\ 0 & 0 & 0 & d_i \\ 0 & 0 & 0 & 1 \end{bmatrix}. \quad (4.31)$$

In Eq. (4.31), both θ_i and d_i are treated as variables. For a revolute joint, $\dot{d}_i = 0$, and for a prismatic joint, $\dot{\theta}_i = 0$. Postmultiplying both sides of Eq. (4.31) by $({}^{i-1}A_i)^{-1}$, we obtain

$$({}^{i-1}\dot{A}_i)({}^{i-1}A_i)^{-1} = \begin{bmatrix} \dot{\theta}_i {}^{i-1}Z_{i-1} & \dot{d}_i {}^{i-1}\mathbf{z}_{i-1} \\ \dots & \dots \\ 0 & 0 \end{bmatrix}, \quad (4.32)$$

where

$${}^{i-1}\mathbf{z}_{i-1} = \begin{bmatrix} 0 \\ 0 \\ 1 \end{bmatrix}, \quad (4.33)$$

$${}^{i-1}Z_{i-1} = \begin{bmatrix} 0 & -1 & 0 \\ 1 & 0 & 0 \\ 0 & 0 & 0 \end{bmatrix}. \quad (4.34)$$

Equation (4.33) represents a unit vector pointing along the z_{i-1} -axis. Similarly, Eq. (4.34) represents a 3×3 skew-symmetric matrix whose nonzero elements denote a unit angular velocity of link i with respect to link $i-1$. Both ${}^{i-1}\mathbf{z}_{i-1}$ and ${}^{i-1}Z_{i-1}$ are expressed in the $(i-1)$ th link frame. We conclude that the upper left 3×3 submatrix of $({}^{i-1}\dot{A}_i)({}^{i-1}A_i)^{-1}$ represents the angular velocity of link i relative to link $i-1$, and the fourth column represents the linear velocity of a point, which is embedded in link i and instantaneously coincident with O_{i-1} , relative to link $i-1$.

4.3.2 Overall Differential Transformation Matrix

We now apply the results derived earlier to the kinematic analysis of serial manipulators. Figure 4.6 shows a schematic of a typical serial manipulator, where \mathbf{p}_n denotes the position vector of the origin of the end-effector frame, and \mathbf{p}_{i-1} denotes the position vector of the origin of the $(i-1)$ th frame relative to the fixed frame. Further, ${}^{i-1}\mathbf{p}_n^*$ denotes the vector pointing from O_{i-1} to O_n and expressed in the fixed frame. The loop-closure equation for such an n -dof serial manipulator can be written as

$${}^0A_n = {}^0A_1 {}^1A_2 {}^2A_3 \cdots {}^{n-1}A_n. \quad (4.35)$$

Taking the derivative of Eq. (4.35) with respect to time, we obtain

$$\begin{aligned} {}^0\dot{A}_n = & ({}^0\dot{A}_1 {}^1A_2 \cdots {}^{n-1}A_n) + ({}^0A_1 {}^1\dot{A}_2 \cdots {}^{n-1}A_n) \\ & + \cdots + ({}^0A_1 {}^1A_2 \cdots {}^{n-1}\dot{A}_n). \end{aligned} \quad (4.36)$$

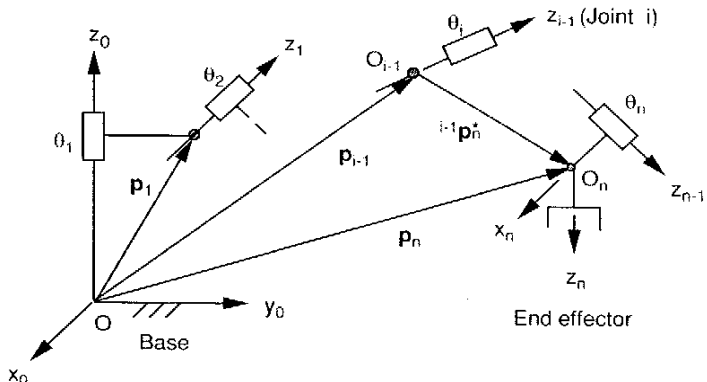


FIGURE 4.6. Link parameters of a serial manipulator.

Equation (4.36) contains 12 nontrivial scalar equations that can be reduced to a system of six independent equations as follows. Postmultiplying Eq. (4.36) by ${}^0A_n^{-1}$, we obtain

$$\begin{aligned} {}^0\dot{A}_n {}^0A_n^{-1} &= {}^0\dot{A}_1 {}^0A_1^{-1} + {}^0A_1({}^1\dot{A}_2 {}^1A_2^{-1}) {}^0A_1^{-1} \\ &\quad + ({}^0A_1 {}^1A_2)({}^2\dot{A}_3 {}^2A_3^{-1}) {}^0A_1 {}^1A_2 {}^0A_1^{-1} + \dots \end{aligned} \quad (4.37)$$

The matrix ${}^0\dot{A}_n$ can be decomposed into two submatrices:

$${}^0\dot{A}_n = \begin{bmatrix} \dot{R}_n & \mathbf{v}_o \\ 0 & 0 \end{bmatrix}, \quad (4.38)$$

where \dot{R}_n denotes the rate of change of the end-effector rotation matrix and $\mathbf{v}_o = \dot{\mathbf{p}}_n$ denotes the linear velocity of the origin of the hand coordinate system.

Similar to Eq. (4.32), we can express the matrix products in Eq. (4.37) as

$${}^0\dot{A}_n {}^0A_n^{-1} = \begin{bmatrix} \Omega_n & \mathbf{v}_o \\ 0 & 0 \end{bmatrix}, \quad (4.39)$$

$${}^{i-1}\dot{A}_i {}^{i-1}A_i^{-1} = \begin{bmatrix} \dot{\theta}_i {}^{i-1}Z_{i-1} & \dot{d}_i {}^{i-1}\mathbf{z}_{i-1} \\ 0 & 0 \end{bmatrix}. \quad (4.40)$$

Note that $\Omega_n = \dot{R}_n R_n^T$ is a 3×3 skew-symmetric matrix whose elements represent the angular velocity of the end effector, and \mathbf{v}_o represents the linear

velocity of a point in the end effector that is instantaneously coincident with the origin of the fixed reference frame. For convenience, we define

$${}^0A_1 {}^1A_2 \dots {}^{i-2}A_{i-1} = \begin{bmatrix} R_{i-1} & \mathbf{p}_{i-1} \\ 0 & 1 \end{bmatrix}, \quad (4.41)$$

where R_{i-1} and \mathbf{p}_{i-1} denote the rotation matrix and the position vector of the $(i-1)$ th frame with respect to the fixed reference frame. Substituting Eqs. (4.39) through (4.41) into (4.37) yields

$$\begin{aligned} &\begin{bmatrix} \Omega_n & \mathbf{v}_o \\ 0 & 0 \end{bmatrix} \\ &= \sum_{i=1}^n \begin{bmatrix} \dot{\theta}_i (R_{i-1} {}^{i-1}Z_{i-1} R_{i-1}^T) & -\dot{\theta}_i (R_{i-1} {}^{i-1}Z_{i-1} R_{i-1}^T) \mathbf{p}_{i-1} + \dot{d}_i R_{i-1} {}^{i-1}\mathbf{z}_{i-1} \\ \dots & \dots \\ 0 & 0 \end{bmatrix} \\ &= \sum_{i=1}^n \begin{bmatrix} \dot{\theta}_i Z_{i-1} & -\dot{\theta}_i Z_{i-1} \mathbf{p}_{i-1} + \dot{d}_i \mathbf{z}_{i-1} \\ \dots & \dots \\ 0 & 0 \end{bmatrix}, \end{aligned} \quad (4.42)$$

where

$$Z_{i-1} = R_{i-1} {}^{i-1}Z_{i-1} R_{i-1}^T, \quad (4.43)$$

$$\mathbf{z}_{i-1} = R_{i-1} {}^{i-1}\mathbf{z}_{i-1}. \quad (4.44)$$

Equation (4.42) contains only six independent equations. The (3,2), (1,3), and (2,1) elements form the angular velocity vector ω_n of the end effector, and the last column represents the linear velocity of a point in the end effector that is instantaneously coincident with the origin of the fixed frame. Writing Eq. (4.42) in vector form, we obtain

$$\omega_n = \sum_{i=1}^n \dot{\theta}_i \mathbf{z}_{i-1}, \quad (4.45)$$

$$\mathbf{v}_o = \sum_{i=1}^n (-\dot{\theta}_i \mathbf{z}_{i-1} \times \mathbf{p}_{i-1} + \dot{d}_i \mathbf{z}_{i-1}). \quad (4.46)$$

Equations (4.45) and (4.46) imply that the angular velocities of the links are additive. We may think of the end effector as rotating instantaneously about and translating along all the joint axes, and the effect of the instantaneous motion about each joint axis can be added linearly. We note that the

velocity, \mathbf{v}_n , of a point located at the origin of the hand coordinate system is related to \mathbf{v}_o by the following transformation:

$$\mathbf{v}_n = \mathbf{v}_o + \boldsymbol{\omega}_n \times \mathbf{p}_n. \quad (4.47)$$

4.4 SCREW COORDINATES AND SCREW SYSTEMS

We have shown that both finite and infinitesimal displacements of a rigid body can conveniently be expressed as a rotation about a unique axis and a translation along the same axis. This combined motion is called a *screw displacement* or *twist*, and the unique axis is called a *screw axis* of the displacement. The ratio of translation to rotation is called the *pitch*, λ . Specifically, $\lambda = d/\theta$ for finite displacements and $\lambda = \dot{d}/\dot{\theta}$ for infinitesimal displacements.

A screw can conveniently be represented by a coordinate system called the *screw coordinates*. We define the coordinates of a unit screw, $\hat{\$}$, by a pair of vectors (Ball, 1900; Beyer, 1958; Dimentberg, 1965; Roth, 1984):

$$\hat{\$} = \begin{bmatrix} \mathbf{s} \\ \mathbf{s}_o \times \mathbf{s} + \lambda \mathbf{s} \end{bmatrix} = \begin{bmatrix} S_1 \\ S_2 \\ S_3 \\ S_4 \\ S_5 \\ S_6 \end{bmatrix}, \quad (4.48)$$

where \mathbf{s} is a unit vector pointing along the direction of the screw axis and \mathbf{s}_o is the position vector of any point on the screw axis.

The vector $\mathbf{s}_o \times \mathbf{s}$ defines the moment of the screw axis about the origin of a reference frame. Since the screw axis and its moment are directed at right angles to one another, $\mathbf{s} \cdot (\mathbf{s}_o \times \mathbf{s}) = 0$ identically. Hence only five of the six coordinates are independent.

For a revolute joint, $\lambda = 0$, the unit screw reduces to

$$\hat{\$} = \begin{bmatrix} \mathbf{s} \\ \mathbf{s}_o \times \mathbf{s} \end{bmatrix}. \quad (4.49)$$

For a prismatic joint, $\lambda = \infty$, the unit screw is defined as

$$\hat{\$} = \begin{bmatrix} \mathbf{0} \\ \mathbf{s} \end{bmatrix}. \quad (4.50)$$

The screw axis and the pitch together determine the screw. However, the displacement is not determined completely until after the *amplitude* or *inten-*

sity of the screw axis is specified. Let \dot{q} be the intensity of a twist. Then the twist can be written as

$$\$ = \dot{q} \hat{\$}. \quad (4.51)$$

where $\dot{q} = \dot{\theta}$ for a revolute joint and $\dot{q} = \dot{d}$ for a prismatic joint.

Hence six screw coordinates completely specify the first-order instantaneous kinematics of a rigid body. The first three coordinates of $\$$ represent the angular velocity, and the last three coordinates represent the linear velocity of a point that is embedded in the moving body and instantaneously coincident with the origin of the fixed reference frame.

We may consider the motion of a rigid body as being twisted instantaneously about several screw axes. These screws form a screw system in three-dimensional space (Hunt, 1978). The screw system that permits a rigid body to move instantaneously with 1 degree of freedom consists of a single screw. This is called a *first-order screw system* or simply a *1-system*.

The infinitesimal motion of a rigid body with 2 degrees of freedom can generally be considered as the resulting motion of two instantaneous screws of arbitrary pitches. In fact, we can visualize the body as being connected to a fixed base by two joints with one intermediate link. These two joint axes can be arbitrarily located in space. Given the intensities of the two screws, the instantaneous velocity vectors of all points in the body are completely known, and this velocity state can be represented by a resulting twist of prescribed pitch and intensity. It can be shown that for any instantaneous motion, the ratio of the two intensities determine the location and pitch of the resulting twist, while the actual intensities determine the intensity of the resulting twist. As the intensities of these two screws change, a single infinitude of resulting twists will be generated. The axes of these screws form a line series in space known as the *screw cylindroid*. We call this system of infinite many screws a *2-system*. Similarly, the infinitesimal motion of a rigid body with n degrees of freedom, $n \leq 6$, can generally be described by an *n-system*.

For a serial manipulator, we may consider the motion of the end effector as being twisted instantaneously about the joint axes of an open-loop chain. These instantaneous twists may be added linearly to give the resulting motion of the end effector. Thus the first-order instantaneous kinematics can be written as

$$\$_n = \sum_{i=1}^n \dot{q}_i \hat{\$}_i, \quad (4.52)$$

where $\hat{\$}_i$ is a unit screw defined by the joints of the manipulator.

We note that a line in three-dimensional space can be represented by a coordinate system called the *Plücker* or *line* coordinates. If the Plücker coordinates of a line are $[L, M, N, P, Q, R]^T$, the Plücker coordinates are related to the screw coordinates by

$$\begin{bmatrix} L \\ M \\ N \\ P \\ Q \\ R \end{bmatrix} = \begin{bmatrix} S_1 \\ S_2 \\ S_3 \\ S_4 - \lambda S_1 \\ S_5 - \lambda S_2 \\ S_6 - \lambda S_3 \end{bmatrix}. \quad (4.53)$$

4.5 MANIPULATOR JACOBIAN MATRIX

Let $x_i = f_i(q_1, q_2, q_3, \dots, q_n)$ for $i = 1, 2, 3, \dots, m$ be a set of m equations, each a function of n independent variables. Then the time derivatives of x_i can be written as a function of \dot{q}_i as follows:

$$\dot{x}_i = \frac{\partial f_i}{\partial q_1} \dot{q}_1 + \frac{\partial f_i}{\partial q_2} \dot{q}_2 + \frac{\partial f_i}{\partial q_3} \dot{q}_3 + \dots + \frac{\partial f_i}{\partial q_n} \dot{q}_n, \quad i = 1, 2, 3, \dots, m. \quad (4.54)$$

Writing Eq. (4.54) in matrix form, we obtain

$$\begin{bmatrix} \dot{x}_1 \\ \dot{x}_2 \\ \vdots \\ \dot{x}_m \end{bmatrix} = \begin{bmatrix} \frac{\partial f_1}{\partial q_1} & \frac{\partial f_1}{\partial q_2} & \dots & \frac{\partial f_1}{\partial q_n} \\ \frac{\partial f_2}{\partial q_1} & \frac{\partial f_2}{\partial q_2} & \dots & \frac{\partial f_2}{\partial q_n} \\ \vdots & \vdots & \dots & \vdots \\ \frac{\partial f_m}{\partial q_1} & \frac{\partial f_m}{\partial q_2} & \dots & \frac{\partial f_m}{\partial q_n} \end{bmatrix} \begin{bmatrix} \dot{q}_1 \\ \dot{q}_2 \\ \vdots \\ \dot{q}_n \end{bmatrix}, \quad (4.55)$$

or simply

$$\dot{\mathbf{x}} = J \dot{\mathbf{q}}, \quad (4.56)$$

where $\mathbf{x} = [x_1, x_2, \dots, x_m]^T$ denotes an m -dimensional vector, $\mathbf{q} = [q_1, q_2, \dots, q_n]^T$ denotes an n -dimensional vector, and J denotes the $m \times n$ matrix of the partial derivatives in Eq. (4.55).

We call J the *Jacobian matrix*, or simply *Jacobian*. The Jacobian matrix is a linear transformation matrix that maps an n -dimensional velocity vector $\dot{\mathbf{q}}$ into an m -dimensional velocity vector $\dot{\mathbf{x}}$. We may think of the elements of J as the influence coefficients of the vector function \mathbf{x} . The (i, j) element of J

describes how a differential change in q_j affects the differential change in x_i . In general, the vector \mathbf{x} is a nonlinear function of \mathbf{q} . Hence the Jacobian matrix is also a function of \mathbf{q} . Thus, the Jacobian matrix is configuration dependent.

For robot manipulators, the Jacobian matrix is defined as the coefficient matrix of any set of equations that relates the velocity state of the end effector to the actuated joint rates. The joint rates are defined as

$$\dot{q}_i = \begin{cases} \dot{\theta}_i & \text{for a revolute joint.} \\ \dot{d}_i & \text{for a prismatic joint.} \end{cases} \quad (4.57)$$

The velocity state of the end effector, $\dot{\mathbf{x}}$, can be expressed in several different ways. Perhaps the most commonly used definitions are the *conventional Jacobian* and *screw-based Jacobian*.

1. *Conventional Jacobian.* In a conventional Jacobian, the end-effector velocity state is expressed in terms of the linear velocity of the origin of the end-effector coordinate frame, \mathbf{v}_n , and the angular velocity of the end effector, $\boldsymbol{\omega}_n$.

$$\dot{\mathbf{x}} = \begin{bmatrix} \mathbf{v}_n \\ \boldsymbol{\omega}_n \end{bmatrix}. \quad (4.58)$$

2. *Screw-based Jacobian.* The screw-based Jacobian is defined in terms of the angular velocity of the end effector, $\boldsymbol{\omega}_n$, and the linear velocity of a reference point, \mathbf{v}_o , in the end effector that is instantaneously coincident with the origin of a reference frame in which the screws are expressed:

$$\dot{\mathbf{x}} = \begin{bmatrix} \boldsymbol{\omega}_n \\ \mathbf{v}_o \end{bmatrix}. \quad (4.59)$$

We note that the end-effector velocity, $\dot{\mathbf{x}}$, for the screw-based Jacobian is defined with its angular and linear velocity vectors arranged in reverse order from the conventional Jacobian.

In general, the Jacobian matrix is an $m \times n$ matrix, where m denotes the degrees of freedom of the end-effector space and n denotes the number of actuated joint variables. For a 6-dof spatial manipulator, $m = n = 6$, the Jacobian matrix is a 6×6 square matrix. For a manipulator with less than 6 degrees of freedom, the end-effector velocity state may contain just the linear velocity vector, or the angular velocity vector, or a combination of some linear and angular velocity components. For example, the working space of a planar manipulator is confined to a two-dimensional space. A three-component vector $\dot{\mathbf{x}} = [v_x, v_y, \omega_z]^T$ is sufficient to describe the velocity state of the end effector. Hence the Jacobian reduces to a 3×3 matrix. Similarly, for a point-

positioning device $\dot{\mathbf{x}} = [v_x, v_y, v_z]^T$, and for a body-orienting mechanism $\dot{\mathbf{x}} = [\omega_x, \omega_y, \omega_z]^T$. On the other hand, for a manipulator with redundant degrees of freedom, we may have $n > 6$. In this book, we concentrate on nonredundant robot manipulators.

4.6 CONVENTIONAL JACOBIAN

As mentioned earlier, any point in the end effector can be chosen as the reference point to describe the velocity state of the end effector. A logical choice is the origin, O_n , of the end-effector frame (Whitney, 1972). Using this definition, the end-effector velocity state can be expressed in terms of the joint rates as follows:

$$\mathbf{v}_n = \sum_{i=1}^n [\dot{\theta}_i (\mathbf{z}_{i-1} \times {}^{i-1}\mathbf{p}_n^*) + \mathbf{z}_{i-1} \dot{d}_i] \quad (4.60)$$

$$\boldsymbol{\omega}_n = \sum_{i=1}^n \dot{\theta}_i \mathbf{z}_{i-1} \quad (4.61)$$

where $\dot{\theta}_i$ and \dot{d}_i are the rate of rotation about and translation along the i th joint axis, \mathbf{z}_{i-1} is a unit vector along the i th joint axis, and ${}^{i-1}\mathbf{p}_n^*$ is a vector defined from the origin of the $(i-1)$ th link frame, O_{i-1} , to the origin of the end effector frame, as shown in Fig. 4.6. Note that all vectors in Eqs. (4.60) and (4.61) are expressed in the fixed coordinate frame, (x_0, y_0, z_0) .

Writing Eqs. (4.60) and (4.61) in matrix form, we obtain

$$\dot{\mathbf{x}} = \begin{bmatrix} \mathbf{v}_n \\ \boldsymbol{\omega}_n \end{bmatrix} = J \dot{\mathbf{q}} \quad (4.62)$$

where

$$J = [J_1, J_2, \dots, J_n],$$

$$J_i = \begin{bmatrix} \mathbf{z}_{i-1} \times {}^{i-1}\mathbf{p}_n^* \\ \mathbf{z}_{i-1} \end{bmatrix} \quad \text{for a revolute joint,}$$

$$J_i = \begin{bmatrix} \mathbf{z}_{i-1} \\ \mathbf{0} \end{bmatrix} \quad \text{for a prismatic joint.}$$

The left-hand side of Eq. (4.62) is a 6×1 vector composed of the elements of \mathbf{v}_n and $\boldsymbol{\omega}_n$, while the right-hand side is a product of the Jacobian matrix and the vector of joint rates. The vector of joint rates consists of all the actuated joint rates, \dot{q}_i for $i = 1, 2, \dots, n$. The i th column of the Jacobian matrix,

J_i , represents the effect of the i th joint rate on the velocity state of the end effector.

Equation (4.62) implies that to compute the Jacobian matrix, the direction and location of each joint axis should be determined first. This can be accomplished by the following matrix operations:

$$\mathbf{z}_{i-1} = {}^0R_{i-1} \begin{bmatrix} 0 \\ 0 \\ 1 \end{bmatrix}, \quad (4.63)$$

$${}^{i-1}\mathbf{p}_n^* = {}^0R_{i-1} {}^{i-1}\mathbf{r}_i + {}^i\mathbf{p}_n^*, \quad (4.64)$$

where

$${}^{i-1}\mathbf{r}_i = \begin{bmatrix} a_i c \theta_i \\ a_i s \theta_i \\ d_i \end{bmatrix}$$

denotes the vector $\overline{O_{i-1}O_i}$ expressed in the $(i-1)$ th link frame, while ${}^{i-1}\mathbf{p}_n^*$ denotes the vector $\overline{O_{i-1}O_n}$ expressed in the fixed frame. Once the Jacobian is known, the end-effector velocity can be computed directly from Eq. (4.62) for any given joint rates. On the other hand, given a desired end-effector velocity, the inverse transformation of Eq. (4.62) can be solved for the joint rates.

4.6.1 Jacobian of a Planar 2-DOF Manipulator

In this example we derive the Jacobian of a planar 2-dof manipulator shown in Fig. 4.7. The manipulator is made up of two revolute joints, with both axes pointing out of the paper. A coordinate system is attached to each link according to the D-H convention for the purpose of analysis. The (x_0, y_0) coordinate system is attached to the base with its origin located at the fixed pivot O . The x_0 -axis points to the right.

We first compute the vectors \mathbf{z}_{i-1} and ${}^{i-1}\mathbf{p}_2^*$ by applying Eqs. (4.63) and (4.64):

$$\mathbf{z}_0 = \mathbf{z}_1 = \begin{bmatrix} 0 \\ 0 \\ 1 \end{bmatrix},$$

$${}^1\mathbf{p}_2^* = \begin{bmatrix} a_2 c \theta_{12} \\ a_2 s \theta_{12} \\ 0 \end{bmatrix},$$

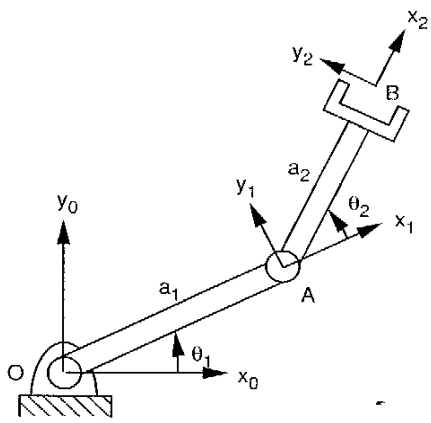


FIGURE 4.7. Planar 2-dof, 2R manipulator.

$${}^0\mathbf{p}_2^* = \begin{bmatrix} a_1 c\theta_1 + a_2 c\theta_{12} \\ a_1 s\theta_1 + a_2 s\theta_{12} \\ 0 \end{bmatrix},$$

where $\theta_{12} = \theta_1 + \theta_2$. We note that the expressions above can be obtained directly from the geometry of the links without using the Denavit–Hartenberg transformation matrices. Substituting the expressions above into Eq. (4.62), we obtain

$$\begin{bmatrix} v_x \\ v_y \end{bmatrix} = \begin{bmatrix} -a_1 s\theta_1 - a_2 s\theta_{12} & -a_2 s\theta_{12} \\ a_1 c\theta_1 + a_2 c\theta_{12} & a_2 c\theta_{12} \end{bmatrix} \begin{bmatrix} \dot{\theta}_1 \\ \dot{\theta}_2 \end{bmatrix}. \quad (4.65)$$

Hence the Jacobian matrix is given by

$$J = \begin{bmatrix} -a_1 s\theta_1 - a_2 s\theta_{12} & -a_2 s\theta_{12} \\ a_1 c\theta_1 + a_2 c\theta_{12} & a_2 c\theta_{12} \end{bmatrix}. \quad (4.66)$$

4.6.2 Jacobian of a Planar 3-DOF Manipulator

As a second example, we study the conventional Jacobian of the planar 3-dof manipulator shown in Fig. 2.3. We first compute the vectors \mathbf{z}_{i-1} and ${}^{i-1}\mathbf{p}_3^*$ from Eqs. (4.63) and (4.64), for $i = 1, 2$, and 3 as follows:

$$\mathbf{z}_0 = \mathbf{z}_1 = \mathbf{z}_2 = \begin{bmatrix} 0 \\ 0 \\ 1 \end{bmatrix},$$

$${}^2\mathbf{p}_3^* = \begin{bmatrix} a_3 c\theta_{123} \\ a_3 s\theta_{123} \\ 0 \end{bmatrix},$$

$${}^1\mathbf{p}_3^* = \begin{bmatrix} a_2 c\theta_{12} + a_3 c\theta_{123} \\ a_2 s\theta_{12} + a_3 s\theta_{123} \\ 0 \end{bmatrix},$$

$${}^0\mathbf{p}_3^* = \begin{bmatrix} a_1 c\theta_1 + a_2 c\theta_{12} + a_3 c\theta_{123} \\ a_1 s\theta_1 + a_2 s\theta_{12} + a_3 s\theta_{123} \\ 0 \end{bmatrix},$$

where $\theta_{12} = \theta_1 + \theta_2$ and $\theta_{123} = \theta_1 + \theta_2 + \theta_3$. Substituting the expressions above into Eq. (4.62), we obtain

$$\begin{bmatrix} v_x \\ v_y \\ v_z \end{bmatrix} = J \begin{bmatrix} \dot{\theta}_1 \\ \dot{\theta}_2 \\ \dot{\theta}_3 \end{bmatrix},$$

where

$$J = \begin{bmatrix} -(a_1 s\theta_1 + a_2 s\theta_{12} + a_3 s\theta_{123}) & -(a_2 s\theta_{12} + a_3 s\theta_{123}) & -a_3 s\theta_{123} \\ (a_1 c\theta_1 + a_2 c\theta_{12} + a_3 c\theta_{123}) & (a_2 c\theta_{12} + a_3 c\theta_{123}) & a_3 c\theta_{123} \\ 1 & 1 & 1 \end{bmatrix}. \quad (4.67)$$

We note that if the reference point is chosen at origin of the (x_2, y_2) frame, the Jacobian matrix reduces to

$$J = \begin{bmatrix} -(a_1 s\theta_1 + a_2 s\theta_{12}) & -(a_2 s\theta_{12}) & 0 \\ (a_1 c\theta_1 + a_2 c\theta_{12}) & (a_2 c\theta_{12}) & 0 \\ 1 & 1 & 1 \end{bmatrix}. \quad (4.68)$$

4.6.3 Jacobian of the Stanford Manipulator

Figure 4.8 shows a schematic diagram of the Stanford arm described in Chapter 2. To simplify the analysis, the origin of the fixed coordinate frame is located at the point of intersection of the first two joint axes, and the origin of the (x_6, y_6, z_6) frame is located at the point of intersection of the last three joint axes.

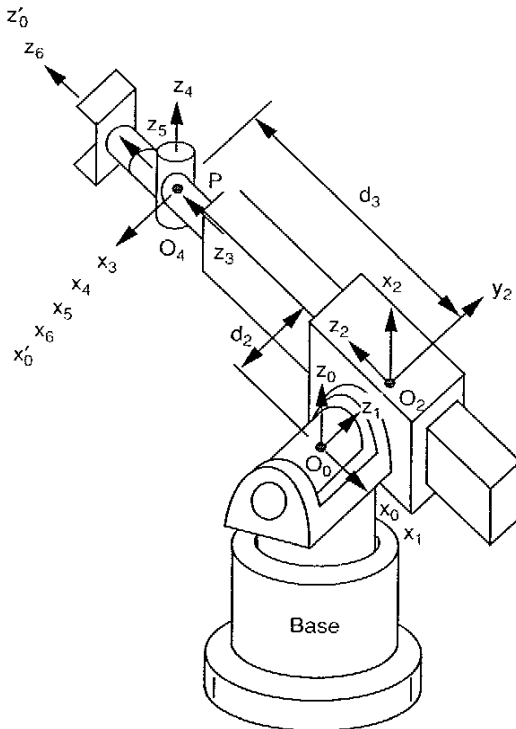


FIGURE 4.8. Stanford manipulator.

The D-H link parameters are listed in Table 4.1, from which the D-H transformation matrices are derived as follows:

$$\begin{aligned} {}^0A_1 &= \begin{bmatrix} c\theta_1 & 0 & -s\theta_1 & 0 \\ s\theta_1 & 0 & c\theta_1 & 0 \\ 0 & -1 & 0 & 0 \\ 0 & 0 & 0 & 1 \end{bmatrix}, & {}^1A_2 &= \begin{bmatrix} c\theta_2 & 0 & s\theta_2 & 0 \\ s\theta_2 & 0 & -c\theta_2 & 0 \\ 0 & 1 & 0 & d_2 \\ 0 & 0 & 0 & 1 \end{bmatrix}, \\ {}^2A_3 &= \begin{bmatrix} 0 & 1 & 0 & 0 \\ -1 & 0 & 0 & 0 \\ 0 & 0 & 1 & d_3 \\ 0 & 0 & 0 & 1 \end{bmatrix}, & {}^3A_4 &= \begin{bmatrix} c\theta_4 & 0 & -s\theta_4 & 0 \\ s\theta_4 & 0 & c\theta_4 & 0 \\ 0 & -1 & 0 & 0 \\ 0 & 0 & 0 & 1 \end{bmatrix}, \end{aligned}$$

TABLE 4.1. D-H Link Parameters of the Stanford Arm

Joint i	α_i	a_i	d_i	θ_i
1	-90°	0	0	θ_1 (variable)
2	90°	0	d_2 (constant)	θ_2 (variable)
3	0°	0	d_3 (variable)	-90° (constant)
4	-90°	0	0	θ_4 (variable)
5	90°	0	0	θ_5 (variable)
6	0°	0	0	θ_6 (variable)

$${}^4A_5 = \begin{bmatrix} c\theta_5 & 0 & s\theta_5 & 0 \\ s\theta_5 & 0 & -c\theta_5 & 0 \\ 0 & 1 & 0 & 0 \\ 0 & 0 & 0 & 1 \end{bmatrix}, \quad {}^5A_6 = \begin{bmatrix} c\theta_6 & -s\theta_6 & 0 & 0 \\ s\theta_6 & c\theta_6 & 0 & 0 \\ 0 & 0 & 1 & 0 \\ 0 & 0 & 0 & 1 \end{bmatrix}.$$

The directions of the joint axes, \mathbf{z}_{i-1} , are derived by applying Eq. (4.63):

$$\mathbf{z}_0 = \begin{bmatrix} 0 \\ 0 \\ 1 \end{bmatrix}, \quad (4.69)$$

$$\mathbf{z}_1 = {}^0R_1 \begin{bmatrix} 0 \\ 0 \\ 1 \end{bmatrix} = \begin{bmatrix} -s\theta_1 \\ c\theta_1 \\ 0 \end{bmatrix}, \quad (4.70)$$

$$\mathbf{z}_2 = \mathbf{z}_3 = {}^0R_2 \begin{bmatrix} 0 \\ 0 \\ 1 \end{bmatrix} = \begin{bmatrix} c\theta_1 s\theta_2 \\ s\theta_1 s\theta_2 \\ c\theta_2 \end{bmatrix}, \quad (4.71)$$

$$\mathbf{z}_4 = {}^0R_4 \begin{bmatrix} 0 \\ 0 \\ 1 \end{bmatrix} = \begin{bmatrix} -s\theta_1 s\theta_4 + c\theta_1 c\theta_2 c\theta_4 \\ c\theta_1 s\theta_4 + s\theta_1 c\theta_2 c\theta_4 \\ -s\theta_2 c\theta_4 \end{bmatrix}, \quad (4.72)$$

$$\mathbf{z}_5 = {}^0R_5 \begin{bmatrix} 0 \\ 0 \\ 1 \end{bmatrix} = \begin{bmatrix} s\theta_1 c\theta_4 s\theta_5 + c\theta_1 c\theta_2 s\theta_4 s\theta_5 + c\theta_1 s\theta_2 c\theta_5 \\ -c\theta_1 c\theta_4 s\theta_5 + s\theta_1 c\theta_2 s\theta_4 s\theta_5 + s\theta_1 s\theta_2 c\theta_5 \\ -s\theta_2 s\theta_4 s\theta_5 + c\theta_2 c\theta_5 \end{bmatrix}. \quad (4.73)$$

The position vectors, ${}^{i-1}\mathbf{p}_6^*$, are derived by applying Eq. (4.64):

$${}^3\mathbf{p}_6^* = {}^4\mathbf{p}_6^* = {}^5\mathbf{p}_6^* = \begin{bmatrix} 0 \\ 0 \\ 0 \end{bmatrix}, \quad (4.74)$$

$${}^2\mathbf{p}_6^* = \begin{bmatrix} d_3 c\theta_1 s\theta_2 \\ d_3 s\theta_1 s\theta_2 \\ d_3 c\theta_2 \end{bmatrix}, \quad (4.75)$$

$${}^1\mathbf{p}_6^* = \begin{bmatrix} d_3 c\theta_1 s\theta_2 - d_2 s\theta_1 \\ d_3 s\theta_1 s\theta_2 + d_2 c\theta_1 \\ d_3 c\theta_2 \end{bmatrix}, \quad (4.76)$$

$${}^0\mathbf{p}_6^* = \begin{bmatrix} d_3 c\theta_1 s\theta_2 - d_2 s\theta_1 \\ d_3 s\theta_1 s\theta_2 + d_2 c\theta_1 \\ d_3 c\theta_2 \end{bmatrix}. \quad (4.77)$$

The Jacobian matrix is derived by applying Eq. (4.62) column by column:

$$\begin{bmatrix} v_{6x} \\ v_{6y} \\ v_{6z} \\ \omega_x \\ \omega_y \\ \omega_z \end{bmatrix} = J \begin{bmatrix} \dot{\theta}_1 \\ \dot{\theta}_2 \\ \dot{\theta}_3 \\ \dot{\theta}_4 \\ \dot{\theta}_5 \\ \dot{\theta}_6 \end{bmatrix},$$

where the Jacobian matrix is given by

$$J = \begin{bmatrix} -d_3 s\theta_1 s\theta_2 - d_2 c\theta_1 & d_3 c\theta_1 c\theta_2 & c\theta_1 s\theta_2 & 0 & 0 & 0 \\ d_3 c\theta_1 s\theta_2 - d_2 s\theta_1 & d_3 s\theta_1 c\theta_2 & s\theta_1 s\theta_2 & 0 & 0 & 0 \\ 0 & -d_3 s\theta_2 & c\theta_2 & 0 & 0 & 0 \\ 0 & -s\theta_1 & 0 & c\theta_1 s\theta_2 & j_{45} & j_{46} \\ 0 & c\theta_1 & 0 & s\theta_1 s\theta_2 & j_{55} & j_{56} \\ 1 & 0 & 0 & c\theta_2 & j_{65} & j_{66} \end{bmatrix}, \quad (4.78)$$

where j_{45} , j_{55} , and j_{65} represent the x , y , and z components of the unit vector \mathbf{z}_4 , and j_{46} , j_{56} , and j_{66} are the x , y , and z components of \mathbf{z}_5 .

As a consequence of the concurrence of axes 4, 5 and 6, all the elements in the upper right 3×3 submatrix are equal to zero.

4.7 SCREW-BASED JACOBIAN

In the preceding section, the origin of the hand coordinate system was chosen as the reference point. It turns out that it is more convenient to use the origin of the fixed frame as the reference point. In this way, the screw coordinates can be used for formulating the Jacobian matrix (Hunt, 1986, 1987a; Sugimoto, 1984; Waldron, 1982). Let \mathbf{v}_o be the velocity of a point in the end-effector of

a serial manipulator that is instantaneously coincident with the origin of the fixed reference frame. Then we can apply Eq. (4.52) to get the end-effector velocity vector as

$$\dot{\mathbf{x}} = \begin{bmatrix} \omega_n \\ \mathbf{v}_o \end{bmatrix} = \sum_{i=1}^n \dot{\theta}_i \hat{s}_i, \quad (4.79)$$

where the unit twist is defined by Eq. (4.49) or (4.50).

We observe from Eq. (4.79) that the Jacobian matrix is simply an assemblage of the unit screws associated with the joint axes of a manipulator. Namely, the coordinates of the unit joint screws are the columns of the Jacobian matrix:

$$J = [\hat{s}_1, \hat{s}_2, \dots, \hat{s}_n]. \quad (4.80)$$

Therefore, to compute the Jacobian matrix, the directions and the locations of the joint axes relative to a reference frame should be determined first. This can often be accomplished by an inspection of the geometry of the manipulator. On the other hand, if the link coordinate systems, (x_0, y_0, z_0) to (x_6, y_6, z_6) , are established in accordance with the Denavit–Hartenberg convention, \mathbf{s}_i and \mathbf{s}_{oi} can be taken from the third and fourth columns of ${}^0A_{i-1}$.

Note that the coordinates of the joint screws can be described in any reference frame. It turns out that the Jacobian matrix can be greatly simplified if a reference frame is defined at a location where it is instantaneously coincident with one of the intermediate link frames, typically link 3 or 4 (Hunt, 1987b; Waldron et al., 1985). Specifically, if the link geometry contains concurrent joint axes, it is advantageous to locate the origin of the instantaneous reference frame at the point of concurrence. Similarly, if the link geometry contains parallel joint axes, it is preferable to align the coordinate axes of the instantaneous reference frame with these parallel axes and their common perpendiculars.

Let an instantaneous reference frame, (x'_0, y'_0, z'_0) , be coincident with the (x_j, y_j, z_j) link frame as shown in Fig. 4.9. Then the directions and locations of the joint axes relative to the (x'_0, y'_0, z'_0) reference frame are given by the third and fourth column of jA_i , respectively. That is,

$$\begin{bmatrix} \mathbf{s}_{i+1} \\ 0 \end{bmatrix} = {}^jA_i \begin{bmatrix} 0 \\ 0 \\ 1 \\ 0 \end{bmatrix}, \quad (4.81)$$

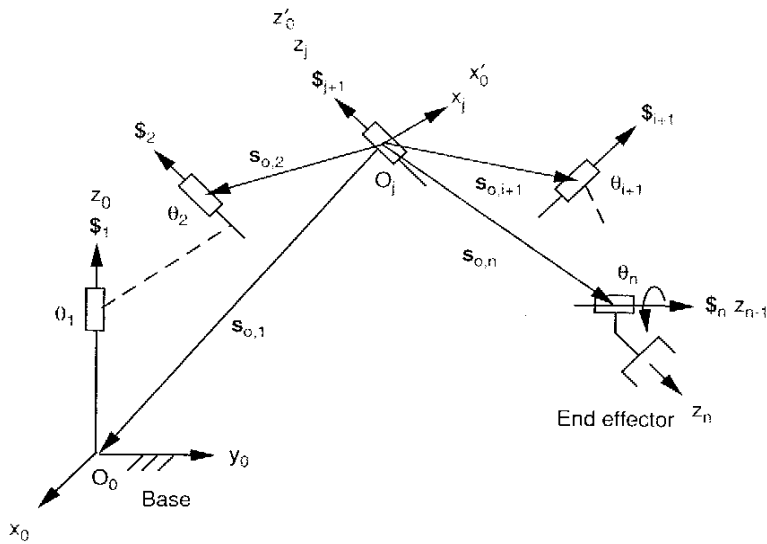


FIGURE 4.9. Screw coordinates with respect to an instantaneous reference frame.

$$\begin{bmatrix} \mathbf{s}_{o,i+1} \\ 1 \end{bmatrix} = {}^i A_i \begin{bmatrix} 0 \\ 0 \\ 0 \\ 1 \end{bmatrix}. \quad (4.82)$$

The screw coordinates above can be computed efficiently by using the following recursive formulas:

1. *Initial conditions.* We begin with $\mathbf{s}_{j+1} = [0, 0, 1]^T$ and $\mathbf{s}_{o,j+1} = [0, 0, 0]^T$.

2. *Forward computation.* For $i = j + 1, j + 2, \dots, n - 1$, we compute

$$\begin{aligned} \mathbf{s}_{i+1} &= ({}^j R_i)({}^i \mathbf{z}_i), \\ \mathbf{s}_{o,i+1} &= \mathbf{s}_{o,i} + ({}^j R_i)({}^i \mathbf{r}_i), \\ {}^j R_{i+1} &= ({}^j R_i)({}^i R_{i+1}). \end{aligned} \quad (4.83)$$

3. *Backward computation.* For $i = j - 1, j - 2, \dots, 0$, we compute

$$\begin{aligned} \mathbf{s}_{i+1} &= ({}^j R_i)({}^i \mathbf{z}_i), \\ \mathbf{s}_{o,i+1} &= \mathbf{s}_{o,i+2} - ({}^j R_{i+1})({}^{i+1} \mathbf{r}_{i+1}), \\ {}^j R_{i-1} &= ({}^j R_i)({}^i R_{i-1}), \end{aligned} \quad (4.84)$$

where ${}^{i-1} R_i$ is the rotation matrix of link i with respect to link $i - 1$, ${}^i R_{i-1} = ({}^{i-1} R_i)^T$,

$${}^i \mathbf{z}_i = \begin{bmatrix} 0 \\ 0 \\ 1 \end{bmatrix}$$

is a unit vector pointing along the z_i -axis and expressed in the i th link frame, and

$${}^i \mathbf{r}_i = \begin{bmatrix} a_i \\ d_i s \alpha_i \\ d_i c \alpha_i \end{bmatrix}$$

is the position vector defined from O_{i-1} to O_i and expressed in the i th link frame.

Assembling the unit screws derived from the recursive formulas above, we obtain

$$\begin{bmatrix} {}^j \omega_n \\ {}^j \mathbf{v}_o \end{bmatrix} = {}^j J \dot{\mathbf{q}}. \quad (4.85)$$

The leading superscript, j , indicates that the velocity state of the end effector is expressed in a reference frame that is instantaneously coincident with the j th link frame. Given the joint rates, Eq. (4.85) can be used to compute for the velocity state of the end effector. On the other hand, given a desired velocity state of the end effector, one can solve the inverse transformation of Eq. (4.85) for the joint rate. This can best be illustrated by the following examples.

4.7.1 Screw-based Jacobian of the Stanford Manipulator

To illustrate the methodology, we derive the screw-based Jacobian of the Stanford manipulator. Let the instantaneous reference frame, (x'_0, y'_0, z'_0) , be coincident with the (x_3, y_3, z_3) link frame as shown in Fig. 4.8. The initial conditions for $j = 3$ are $\mathbf{s}_4 = [0, 0, 1]^T$ and $\mathbf{s}_{o,4} = [0, 0, 0]^T$. Applying Eq. (4.83), we obtain the directions and locations of the fifth and sixth joint axes as follows. For $i = 4$, we obtain

$$\mathbf{s}_5 = {}^3R_4 {}^4\mathbf{z}_4 = \begin{bmatrix} -s\theta_4 \\ c\theta_4 \\ 0 \end{bmatrix}, \quad (4.86)$$

$$\mathbf{s}_{o,5} = \mathbf{s}_{o,4} + {}^3R_4 {}^4r_4 = \begin{bmatrix} 0 \\ 0 \\ 0 \end{bmatrix}, \quad (4.87)$$

$${}^3R_5 = {}^3R_4 {}^4R_5 = \begin{bmatrix} c\theta_4c\theta_5 & -s\theta_4 & c\theta_4s\theta_5 \\ s\theta_4c\theta_5 & c\theta_4 & s\theta_4s\theta_5 \\ -s\theta_5 & 0 & c\theta_5 \end{bmatrix}. \quad (4.88)$$

For $i = 5$, we obtain

$$\mathbf{s}_6 = {}^3R_5 {}^5\mathbf{z}_5 = \begin{bmatrix} c\theta_4s\theta_5 \\ s\theta_4s\theta_5 \\ c\theta_5 \end{bmatrix}, \quad (4.89)$$

$$\mathbf{s}_{o,6} = \mathbf{s}_{o,5} + {}^3R_5 {}^5r_5 = \begin{bmatrix} 0 \\ 0 \\ 0 \end{bmatrix}. \quad (4.90)$$

Applying Eq. (4.84), we obtain the directions and locations of the third, second, and first joint axes in turn as follows. For $i = 2$, we obtain

$$\mathbf{s}_3 = {}^3R_2 {}^2\mathbf{z}_2 = \begin{bmatrix} 0 \\ 0 \\ 1 \end{bmatrix}, \quad (4.91)$$

$$\mathbf{s}_{o,3} = \mathbf{s}_{o,4} - {}^3R_3 {}^3r_3 = \begin{bmatrix} 0 \\ 0 \\ -d_3 \end{bmatrix}, \quad (4.92)$$

$${}^3R_1 = {}^3R_2 {}^2R_1 = \begin{bmatrix} 0 & 0 & -1 \\ c\theta_2 & s\theta_2 & 0 \\ s\theta_2 & -c\theta_2 & 0 \end{bmatrix}. \quad (4.93)$$

For $i = 1$, we obtain

$$\mathbf{s}_2 = {}^3R_1 {}^1\mathbf{z}_1 = \begin{bmatrix} -1 \\ 0 \\ 0 \end{bmatrix}, \quad (4.94)$$

$$\mathbf{s}_{o,2} = \mathbf{s}_{o,3} - {}^3R_2 {}^2r_2 = \begin{bmatrix} d_2 \\ 0 \\ -d_3 \end{bmatrix}, \quad (4.95)$$

$${}^3R_0 = {}^3R_1 {}^1R_0 = \begin{bmatrix} s\theta_1 & -c\theta_1 & 0 \\ c\theta_1c\theta_2 & s\theta_1c\theta_2 & -s\theta_2 \\ c\theta_1s\theta_2 & s\theta_1s\theta_2 & c\theta_2 \end{bmatrix}. \quad (4.96)$$

For $i = 0$, we obtain

$$\mathbf{s}_1 = {}^3R_0 {}^0\mathbf{z}_0 = \begin{bmatrix} 0 \\ -s\theta_2 \\ c\theta_2 \end{bmatrix}, \quad (4.97)$$

$$\mathbf{s}_{o,1} = \mathbf{s}_{o,2} - {}^3R_1 {}^1r_1 = \begin{bmatrix} d_2 \\ 0 \\ -d_3 \end{bmatrix}. \quad (4.98)$$

We now apply Eqs. (4.49) and (4.50), column by column, to compute the Jacobian matrix. The result is

$${}^3J = \begin{bmatrix} 0 & -1 & 0 & 0 & -s\theta_4 & c\theta_4s\theta_5 \\ -s\theta_2 & 0 & 0 & 0 & c\theta_4 & s\theta_4s\theta_5 \\ c\theta_2 & 0 & 0 & 1 & 0 & c\theta_5 \\ -d_3s\theta_2 & 0 & 0 & 0 & 0 & 0 \\ d_2c\theta_2 & d_3 & 0 & 0 & 0 & 0 \\ -d_2s\theta_2 & 0 & 1 & 0 & 0 & 0 \end{bmatrix}. \quad (4.99)$$

We observe that the Jacobian matrix is greatly simplified by expressing it in the instantaneous frame of reference. Substituting Eq. (4.99) into Eq. (4.85), we obtain

$$\begin{aligned} {}^3\omega_x &= -\dot{\theta}_2 - \dot{\theta}_3s\theta_4 + \dot{\theta}_6c\theta_4s\theta_5, \\ {}^3\omega_y &= -\dot{\theta}_1s\theta_2 + \dot{\theta}_5c\theta_4 + \dot{\theta}_6s\theta_4s\theta_5, \\ {}^3\omega_z &= \dot{\theta}_1c\theta_2 + \dot{\theta}_4 + \dot{\theta}_6c\theta_5, \\ {}^3v_{ox} &= -\dot{\theta}_1d_3s\theta_2, \\ {}^3v_{oy} &= -\dot{\theta}_1d_2c\theta_2 + \dot{\theta}_2d_3, \\ {}^3v_{oz} &= -\dot{\theta}_1d_2s\theta_2 + \dot{d}_3. \end{aligned} \quad (4.100)$$

The inverse transformation of Eq. (4.100) can be easily derived as

$$\dot{\theta}_1 = -\frac{{}^3v_{ox}}{d_3s\theta_2},$$

$$\dot{\theta}_2 = \frac{{}^3v_{oy} + \dot{\theta}_1d_2c\theta_2}{d_3},$$

$$\begin{aligned}\dot{\theta}_3 &= {}^3\omega_n + \dot{\theta}_1 d_2 s\theta_2, \\ \dot{\theta}_5 &= -{}^3\omega_v s\theta_4 + {}^3\omega_v c\theta_4 + \dot{\theta}_1 s\theta_2 c\theta_4 - \dot{\theta}_2 s\theta_4, \\ \dot{\theta}_6 &= \frac{{}^3\omega_v c\theta_4 + {}^3\omega_v s\theta_4 + \dot{\theta}_1 s\theta_2 s\theta_4 + \dot{\theta}_2 c\theta_4}{s\theta_3}, \\ \dot{\theta}_4 &= {}^3\omega_v - \dot{\theta}_1 c\theta_2 - \dot{\theta}_6 c\theta_5.\end{aligned}\quad (4.101)$$

Hence given the joint rates $\dot{\mathbf{q}} = [\dot{\theta}_1, \dot{\theta}_2, \dot{\theta}_3, \dot{\theta}_4, \dot{\theta}_5, \dot{\theta}_6]$, the end-effector velocity state, ${}^3\omega_n$ and ${}^3\mathbf{v}_o$, can be computed directly from Eq. (4.100). On the other hand, given the velocity state of the end effector, the joint rates required to produce that velocity can be computed from Eq. (4.101) without going through numerical inversion of the Jacobian matrix.

4.7.2 Screw-based Jacobian of an Elbow Manipulator

Figure 4.10 shows a schematic diagram of the elbow manipulator studied in Chapter 2. We wish to derive the screw-based Jacobian of this manipulator. Using the coordinate systems established in the figure, the D-H link parameters are listed in Table 4.2, from which the D-H transformation matrices can be developed as follows:

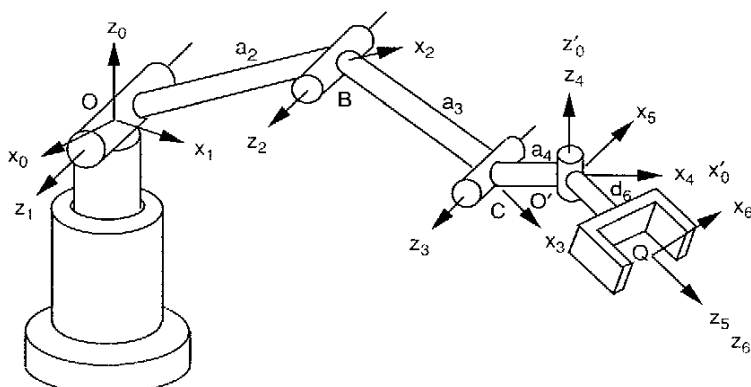


FIGURE 4.10. Elbow manipulator.

TABLE 4.2. Link Parameters of the Elbow Manipulator

Joint i	α_i	a_i	d_i	θ_i
1	$\pi/2$	0	0	variable
2	0	a_2	0	variable
3	0	a_3	0	variable
4	$\pi/2$	a_4	0	variable
5	$\pi/2$	0	0	variable
6	0	0	d_6	variable

$$\begin{aligned}{}^0A_1 &= \begin{bmatrix} c\theta_1 & 0 & s\theta_1 & 0 \\ s\theta_1 & 0 & -c\theta_1 & 0 \\ 0 & 1 & 0 & 0 \\ 0 & 0 & 0 & 1 \end{bmatrix}, \quad {}^1A_2 = \begin{bmatrix} c\theta_2 & -s\theta_2 & 0 & a_2 c\theta_2 \\ s\theta_2 & c\theta_2 & 0 & a_2 s\theta_2 \\ 0 & 0 & 1 & 0 \\ 0 & 0 & 0 & 1 \end{bmatrix}, \\ {}^2A_3 &= \begin{bmatrix} c\theta_3 & -s\theta_3 & 0 & a_3 c\theta_3 \\ s\theta_3 & c\theta_3 & 0 & a_3 s\theta_3 \\ 0 & 0 & 1 & 0 \\ 0 & 0 & 0 & 1 \end{bmatrix}, \quad {}^3A_4 = \begin{bmatrix} c\theta_4 & 0 & -s\theta_4 & a_4 c\theta_4 \\ s\theta_4 & 0 & c\theta_4 & a_4 s\theta_4 \\ 0 & 1 & 0 & 0 \\ 0 & 0 & 0 & 1 \end{bmatrix}, \\ {}^4A_5 &= \begin{bmatrix} c\theta_5 & 0 & s\theta_5 & 0 \\ s\theta_5 & 0 & -c\theta_5 & 0 \\ 0 & 1 & 0 & 0 \\ 0 & 0 & 0 & 1 \end{bmatrix}, \quad {}^5A_6 = \begin{bmatrix} c\theta_6 & s\theta_6 & 0 & 0 \\ s\theta_6 & c\theta_6 & 0 & 0 \\ 0 & 0 & 1 & d_6 \\ 0 & 0 & 0 & 1 \end{bmatrix}.\end{aligned}$$

Let an instantaneous reference frame (x'_0, y'_0, z'_0) be aligned with the (x_4, y_4, z_4) link frame as shown in Fig. 4.10. Then the initial conditions for $j = 4$ are $\mathbf{s}_5 = [0, 0, 1]^T$ and $\mathbf{s}_{o,5} = [0, 0, 0]^T$. Applying Eq. (4.83), we obtain the direction and location of the sixth joint axis as follows. For $i = 5$, we obtain

$$\mathbf{s}_6 = {}^4R_5 {}^5\mathbf{z}_5 = \begin{bmatrix} s\theta_5 \\ -c\theta_5 \\ 0 \end{bmatrix}, \quad (4.102)$$

$$\mathbf{s}_{o,6} = \mathbf{s}_{o,5} + {}^4R_5 {}^5\mathbf{r}_5 = \begin{bmatrix} 0 \\ 0 \\ 0 \end{bmatrix}. \quad (4.103)$$

Applying Eq. (4.84), we obtain the directions and locations of the third, second, and first joint axes in sequence as follows. For $i = 3$, we obtain

$$\mathbf{s}_4 = {}^4R_3 {}^3\mathbf{z}_3 = \begin{bmatrix} 0 \\ -1 \\ 0 \end{bmatrix}, \quad (4.104)$$

$$\mathbf{s}_{o,4} = \mathbf{s}_{o,5} - {}^4R_4 {}^4r_4 = \begin{bmatrix} -a_4 \\ 0 \\ 0 \end{bmatrix}, \quad (4.105)$$

$${}^4R_2 = {}^4R_3 {}^3R_2 = \begin{bmatrix} c\theta_{34} & s\theta_{34} & 0 \\ 0 & 0 & -1 \\ -s\theta_{34} & c\theta_{34} & 0 \end{bmatrix}. \quad (4.106)$$

For $i = 2$, we obtain

$$\mathbf{s}_3 = {}^4R_2 {}^2\mathbf{z}_2 = \begin{bmatrix} 0 \\ -1 \\ 0 \end{bmatrix}, \quad (4.107)$$

$$\mathbf{s}_{o,3} = \mathbf{s}_{o,4} - {}^4R_3 {}^3r_3 = \begin{bmatrix} -a_3c\theta_4 - a_4 \\ 0 \\ a_3s\theta_4 \end{bmatrix}, \quad (4.108)$$

$${}^4R_1 = {}^4R_2 {}^2R_1 = \begin{bmatrix} c\theta_{234} & s\theta_{234} & 0 \\ 0 & 0 & -1 \\ -s\theta_{234} & c\theta_{234} & 0 \end{bmatrix}. \quad (4.109)$$

For $i = 1$, we obtain

$$\mathbf{s}_2 = {}^4R_1 {}^1\mathbf{z}_1 = \begin{bmatrix} 0 \\ -1 \\ 0 \end{bmatrix}, \quad (4.110)$$

$$\mathbf{s}_{o,2} = \mathbf{s}_{o,3} - {}^4R_2 {}^2r_2 = \begin{bmatrix} -a_2c\theta_{34} - a_3c\theta_4 - a_4 \\ 0 \\ a_2s\theta_{34} + a_3s\theta_4 \end{bmatrix}, \quad (4.111)$$

$${}^4R_0 = {}^4R_1 {}^1R_0 = \begin{bmatrix} c\theta_1c\theta_{234} & s\theta_1c\theta_{234} & s\theta_{234} \\ -s\theta_1 & c\theta_1 & 0 \\ -c\theta_1s\theta_{234} & -s\theta_1s\theta_{234} & c\theta_{234} \end{bmatrix}. \quad (4.112)$$

For $i = 0$, we obtain

$$\mathbf{s}_1 = {}^4R_0 {}^0\mathbf{z}_0 = \begin{bmatrix} s\theta_{234} \\ 0 \\ c\theta_{234} \end{bmatrix}, \quad (4.113)$$

$$\mathbf{s}_{o,1} = \mathbf{s}_{o,2} - {}^4R_1 {}^1r_1 = \begin{bmatrix} -a_2c\theta_{34} - a_3c\theta_4 - a_4 \\ 0 \\ a_2s\theta_{34} + a_3s\theta_4 \end{bmatrix}. \quad (4.114)$$

We now apply Eq. (4.49) to compute the Jacobian matrix column by column:

$${}^4J = \begin{bmatrix} s\theta_{234} & 0 & 0 & 0 & 0 & s\theta_5 \\ 0 & -1 & -1 & -1 & 0 & -c\theta_5 \\ c\theta_{234} & 0 & 0 & 0 & 1 & 0 \\ 0 & a_2s\theta_{34} + a_3s\theta_4 & a_3s\theta_4 & 0 & 0 & 0 \\ x_{51} & 0 & 0 & 0 & 0 & 0 \\ 0 & a_2c\theta_{34} + a_3c\theta_4 + a_4 & a_3c\theta_4 + a_4 & a_4 & 0 & 0 \end{bmatrix}, \quad (4.115)$$

where $x_{51} = a_2c\theta_2 + a_3c\theta_{23} + a_4c\theta_{234}$. Equation (4.115) relates the joint rates to the velocity state of the end effector. The leading superscript, 4, indicates that the joint screws, \mathbf{s}_i , $i = 1, 2, \dots, n$, are expressed in a reference frame that is instantaneously coincident with the fourth link frame. Substituting Eq. (4.115) into (4.85), we obtain

$$\begin{aligned} {}^4\omega_x &= \dot{\theta}_1s\theta_{234} + \dot{\theta}_6s\theta_5, \\ {}^4\omega_y &= -\dot{\theta}_{234} - \dot{\theta}_6c\theta_5, \\ {}^4\omega_z &= \dot{\theta}_1c\theta_{234} + \dot{\theta}_5, \\ {}^4v_{ox} &= \dot{\theta}_2a_2s\theta_{34} + \dot{\theta}_{23}a_3s\theta_4, \\ {}^4v_{oy} &= \dot{\theta}_1(a_2c\theta_2 + a_3c\theta_{23} + a_4c\theta_{234}), \\ {}^4v_{oz} &= \dot{\theta}_2a_2c\theta_{34} + \dot{\theta}_{23}a_3c\theta_4 + \dot{\theta}_{234}a_4. \end{aligned} \quad (4.116)$$

Hence, given the joint rates, the end-effector velocity state can be computed directly from Eq. (4.116). On the other hand, given the velocity state of the end effector, the joint rates can be found in sequence by the following inverse transformation:

$$\begin{aligned} \dot{\theta}_1 &= \frac{{}^4v_{oy}}{a_2c\theta_2 + a_3c\theta_{23} + a_4c\theta_{234}}, \\ \dot{\theta}_5 &= {}^4\omega_z - \dot{\theta}_1c\theta_{234}, \\ \dot{\theta}_6 &= \frac{{}^4\omega_x - \dot{\theta}_1s\theta_{234}}{s\theta_5}, \\ \dot{\theta}_{234} &= -{}^4\omega_y - \dot{\theta}_6c\theta_5, \end{aligned}$$

$$\begin{aligned}\dot{\theta}_{23} &= \frac{s\theta_{34}(\dot{v}_{o_2} - a_4\dot{\theta}_{234}) - c\theta_{34}(\dot{v}_{o_3} - a_4\dot{\theta}_{234})}{a_3 s\theta_3}, \\ \dot{\theta}_2 &= \frac{c\theta_4(\dot{v}_{o_3} - s\theta_4(\dot{v}_{o_2} - a_4\dot{\theta}_{234}))}{a_2 s\theta_3}, \\ \dot{\theta}_3 &= \dot{\theta}_{23} - \dot{\theta}_2, \\ \dot{\theta}_4 &= \dot{\theta}_{234} - \dot{\theta}_{23}. \end{aligned} \quad (4.117)$$

4.7.3 Screw-based Jacobian of a Nearly General 6R Manipulator

In previous examples it was possible to derive analytical inversions of the Jacobian matrices due to the special geometric arrangement of the links. The complexity of the Jacobian increases rapidly as the geometry of a manipulator becomes more general. However, substantial simplification can still be achieved by choosing a proper reference frame. In this example, to illustrate the point, we derive the screw-based Jacobian of a nearly general 6-dof, 6R manipulator as shown in Fig. 4.11.

For this manipulator, the first and second joint axes intersect perpendicularly; the second and third joint axes are parallel to each other; and the third and fourth joint axes intersect perpendicularly, as do the fourth and fifth joint axes. The sixth joint axis is perpendicular to the fifth with an offset distance a_5 . The D-H link parameters are summarized in Table 4.3.

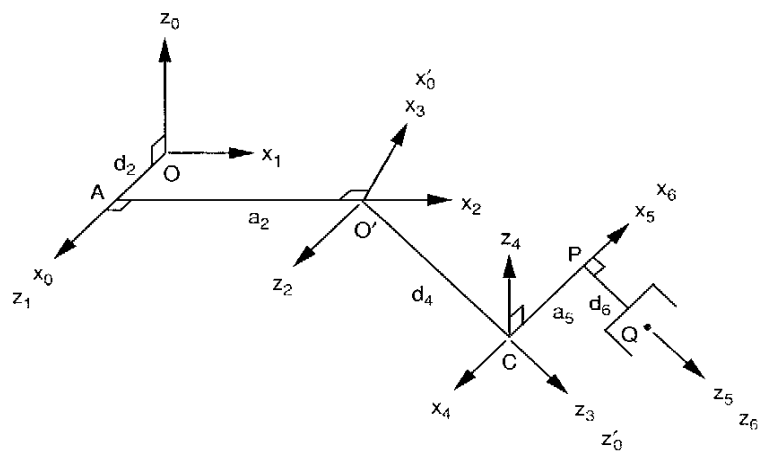


FIGURE 4.11. Nearly general manipulator.

TABLE 4.3. Link Parameters of a Nearly General Manipulator

Joint i	α_i	a_i	d_i	θ_i
1	$\pi/2$	0	0	variable
2	0	a_2	d_2	variable
3	$\pi/2$	0	0	variable
4	$\pi/2$	0	d_4	variable
5	$\pi/2$	a_5	0	variable
6	0	0	d_6	variable

Hence the D-H transformation matrices can be written as

$${}^0A_1 = \begin{bmatrix} c\theta_1 & 0 & s\theta_1 & 0 \\ s\theta_1 & 0 & -c\theta_1 & 0 \\ 0 & 1 & 0 & 0 \\ 0 & 0 & 0 & 1 \end{bmatrix}, \quad {}^1A_2 = \begin{bmatrix} c\theta_2 & -s\theta_2 & 0 & a_2 c\theta_2 \\ s\theta_2 & c\theta_2 & 0 & a_2 s\theta_2 \\ 0 & 0 & 1 & d_2 \\ 0 & 0 & 0 & 1 \end{bmatrix},$$

$${}^2A_3 = \begin{bmatrix} c\theta_3 & 0 & s\theta_3 & 0 \\ s\theta_3 & 0 & -c\theta_3 & 0 \\ 0 & 1 & 0 & 0 \\ 0 & 0 & 0 & 1 \end{bmatrix}, \quad {}^3A_4 = \begin{bmatrix} c\theta_4 & 0 & s\theta_4 & 0 \\ s\theta_4 & 0 & -c\theta_4 & 0 \\ 0 & 1 & 0 & d_4 \\ 0 & 0 & 0 & 1 \end{bmatrix}.$$

$${}^4A_5 = \begin{bmatrix} c\theta_5 & 0 & s\theta_5 & a_5 c\theta_2 \\ s\theta_5 & 0 & -c\theta_5 & a_5 s\theta_2 \\ 0 & 1 & 0 & 0 \\ 0 & 0 & 0 & 1 \end{bmatrix}, \quad {}^5A_6 = \begin{bmatrix} c\theta_6 & -s\theta_6 & 0 & 0 \\ s\theta_6 & c\theta_6 & 0 & 0 \\ 0 & 0 & 1 & d_6 \\ 0 & 0 & 0 & 1 \end{bmatrix}.$$

Let the instantaneous reference frame (x'_0, y'_0, z'_0) be aligned with the (x_3, y_3, z_3) link frame. Then the initial conditions for $j = 3$ are $s_4 = [0, 0, 1]^T$ and $s_{o,4} = [0, 0, 0]^T$. Applying Eq. (4.83), we obtain the directions and locations of the fifth and sixth joint axes as follows. For $i = 4$, we obtain

$$s_5 = {}^3R_4 {}^4z_4 = \begin{bmatrix} s\theta_4 \\ -c\theta_4 \\ 0 \end{bmatrix}, \quad (4.118)$$

$$s_{o,5} = s_{o,4} + {}^3R_4 {}^4r_4 = \begin{bmatrix} 0 \\ 0 \\ d_4 \end{bmatrix}, \quad (4.119)$$

$${}^3R_5 = {}^3R_4 {}^4R_5 = \begin{bmatrix} c\theta_4 c\theta_5 & s\theta_4 & c\theta_4 s\theta_5 \\ s\theta_4 c\theta_5 & -c\theta_4 & s\theta_4 s\theta_5 \\ s\theta_5 & 0 & -c\theta_5 \end{bmatrix}. \quad (4.120)$$

For $i = 5$, we obtain

$$\mathbf{s}_6 = {}^3R_5 {}^5\mathbf{z}_5 = \begin{bmatrix} c\theta_4 s\theta_5 \\ s\theta_4 s\theta_5 \\ -c\theta_5 \end{bmatrix}, \quad (4.121)$$

$$\mathbf{s}_{o,6} = \mathbf{s}_{o,5} + {}^3R_5 {}^5r_5 = \begin{bmatrix} a_5 c\theta_4 c\theta_5 \\ a_5 s\theta_4 c\theta_5 \\ d_4 + a_5 s\theta_5 \end{bmatrix}. \quad (4.122)$$

Applying Eq. (4.84), we obtain the directions and locations of the third, second, and first joint axes as follows. For $i = 2$, we obtain

$$\mathbf{s}_3 = {}^3R_2 {}^2\mathbf{z}_2 = \begin{bmatrix} 0 \\ 1 \\ 0 \end{bmatrix}, \quad (4.123)$$

$$\mathbf{s}_{o,3} = \mathbf{s}_{o,4} - {}^3R_3 {}^3r_3 = \begin{bmatrix} 0 \\ 0 \\ 0 \end{bmatrix}, \quad (4.124)$$

$${}^3R_1 = {}^3R_2 {}^2R_1 = \begin{bmatrix} c\theta_{23} & s\theta_{23} & 0 \\ 0 & 0 & 1 \\ s\theta_{23} & -c\theta_{23} & 0 \end{bmatrix}. \quad (4.125)$$

For $i = 1$, we obtain

$$\mathbf{s}_2 = {}^3R_1 {}^1\mathbf{z}_1 = \begin{bmatrix} 0 \\ 1 \\ 0 \end{bmatrix}, \quad (4.126)$$

$$\mathbf{s}_{o,2} = \mathbf{s}_{o,3} - {}^3R_2 {}^2r_2 = \begin{bmatrix} -a_2 c\theta_3 \\ -d_2 \\ -a_2 s\theta_3 \end{bmatrix}, \quad (4.127)$$

$${}^3R_0 = {}^3R_1 {}^1R_0 = \begin{bmatrix} c\theta_1 c\theta_{23} & s\theta_1 c\theta_{23} & s\theta_{23} \\ s\theta_1 & -c\theta_1 & 0 \\ c\theta_1 s\theta_{23} & s\theta_1 s\theta_{23} & -c\theta_{23} \end{bmatrix}. \quad (4.128)$$

For $i = 0$, we obtain

$$\mathbf{s}_1 = {}^3R_0 {}^0\mathbf{z}_0 = \begin{bmatrix} s\theta_{23} \\ 0 \\ -c\theta_{23} \end{bmatrix}, \quad (4.129)$$

$$\mathbf{s}_{o,1} = \mathbf{s}_{o,2} - {}^3R_1 {}^1r_1 = \begin{bmatrix} -a_2 c\theta_3 \\ -d_2 \\ -a_2 s\theta_3 \end{bmatrix}. \quad (4.130)$$

We now apply Eqs. (4.49) and (4.50) to compute the Jacobian matrix column by column. As a result, we obtain

$${}^3J = \begin{bmatrix} s\theta_{23} & 0 & 0 & 0 & s\theta_4 & c\theta_4 s\theta_5 \\ 0 & 1 & 1 & 0 & -c\theta_4 & s\theta_4 s\theta_5 \\ -c\theta_{23} & 0 & 0 & 1 & 0 & c\theta_5 \\ d_2 c\theta_{23} & a_2 s\theta_3 & 0 & 0 & d_4 c\theta_4 & -s\theta_4(a_5 + d_4 s\theta_5) \\ -a_2 c\theta_2 & 0 & 0 & 0 & d_4 s\theta_4 & c\theta_4(a_5 + d_4 s\theta_5) \\ d_2 s\theta_{23} & -a_2 c\theta_3 & 0 & 0 & 0 & 0 \end{bmatrix}. \quad (4.131)$$

We observe that the Jacobian is still simple enough to make an analytical inversion feasible.

4.8 TRANSFORMATION OF SCREW COORDINATES

In the preceding section we have shown that the Jacobian matrix can be greatly simplified by using a reference frame that is instantaneously coincident with an intermediate link frame of the manipulator. In practice, however, the velocity state of the end effector is often specified in a fixed reference frame (x_0, y_0, z_0) . Therefore, it is necessary to transform the velocity state from the fixed reference frame to the instantaneous reference frame such that the corresponding joint rates can be computed. In what follows, a 6×6 matrix of transformation, \bar{T} , is derived to serve this purpose (Yuan et al., 1971).

As shown in Fig. 4.12, let (x_i, y_i, z_i) and (x_j, y_j, z_j) be two reference frames of interest. The position of O_j relative to the (x_i, y_i, z_i) frame is given by ${}^i\mathbf{p} = [p_x, p_y, p_z]^T$, and the orientation of the (x_j, y_j, z_j) frame relative to the (x_i, y_i, z_i) frame is described by a rotation matrix iR_j . A screw $\$$ relative to the (x_i, y_i, z_i) frame is denoted by ${}^i\$$, and the same screw relative to the (x_j, y_j, z_j) frame is denoted by ${}^j\$$.

Following the definition of a screw, we have

$${}^i\$ = \begin{bmatrix} {}^i\mathbf{s} \\ {}^i\mathbf{s}_o \times {}^i\mathbf{s} + \lambda {}^i\mathbf{s} \end{bmatrix} \quad (4.132)$$

$${}^j\$ = \begin{bmatrix} {}^j\mathbf{s} \\ {}^j\mathbf{s}_o \times {}^j\mathbf{s} + \lambda {}^j\mathbf{s} \end{bmatrix}. \quad (4.133)$$

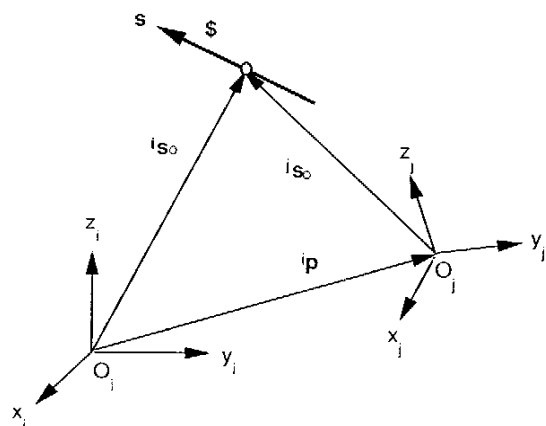


FIGURE 4.12. Coordinate transformation of a screw.

However, the line and moment vectors of the two screws are related by the following transformations:

$${}^i s = {}^i R_j {}^j s, \quad (4.134)$$

$${}^i s_o = {}^i p + {}^i R_j {}^j s_o. \quad (4.135)$$

Hence

$${}^i s_o \times {}^i s = ({}^i p + {}^i R_j {}^j s_o) \times {}^i s = {}^i p \times ({}^i R_j {}^j s) + {}^i R_j ({}^j s_o \times {}^j s). \quad (4.136)$$

Substituting Eqs. (4.134) through (4.136) into (4.132), we obtain

$${}^i \$ = \left[{}^i R_j ({}^j s_o \times {}^j s) + {}^i p \times ({}^i R_j {}^j s) + \lambda {}^i R_j {}^j s \right]. \quad (4.137)$$

Equation (4.137) can be written in the following matrix form:

$${}^i \$ = {}^i \tilde{T}_j {}^j \$, \quad (4.138)$$

where

$${}^i \tilde{T}_j = \begin{bmatrix} {}^i R_j & \vdots & \mathbf{0} \\ \dots & \vdots & \dots \\ {}^i W_j / {}^i R_j & \vdots & {}^i R_j \end{bmatrix} \quad (4.139)$$

is a 6×6 matrix, and

$${}^i W_j = \begin{bmatrix} 0 & -p_z & p_y \\ p_z & 0 & -p_x \\ -p_y & p_x & 0 \end{bmatrix} \quad (4.140)$$

is a 3×3 skew-symmetric matrix representing the vector of $\overrightarrow{O_i O_j}$ expressed in the i th frame.

Since ${}^i W_j$ is skew symmetric and ${}^i R_j$ is orthogonal, the inverse transformation matrix can be written as

$${}^i \tilde{T}_i = \begin{bmatrix} {}^i R_j^T & \vdots & \mathbf{0} \\ \dots & \vdots & \dots \\ {}^i R_j^T / {}^i W_j^T & \vdots & {}^i R_j^T \end{bmatrix}. \quad (4.141)$$

Hence given a screw in the j th frame, we can express it in the i th frame by applying Eq. (4.139), and vice versa using Eq. (4.141).

Geometrically, the six columns of ${}^i \tilde{T}_j$ in Eq. (4.139) represent three normalized screws of zero pitch along and three normalized screws of infinite pitch parallel to the coordinate axes of the (x_j, y_j, z_j) frame and expressed in the (x_i, y_i, z_i) frame, respectively. These six normalized screws, expressed in the (x_j, y_j, z_j) frame, are

$$\begin{aligned} \hat{\$}_1 &= [1, 0, 0, 0, 0, 0]^T, \\ \hat{\$}_2 &= [0, 1, 0, 0, 0, 0]^T, \\ \hat{\$}_3 &= [0, 0, 1, 0, 0, 0]^T, \\ \hat{\$}_4 &= [0, 0, 0, 1, 0, 0]^T, \\ \hat{\$}_5 &= [0, 0, 0, 0, 1, 0]^T, \\ \hat{\$}_6 &= [0, 0, 0, 0, 0, 1]^T. \end{aligned} \quad (4.142)$$

The geometric interpretation above can sometimes be very helpful in deriving the transformation matrix. In addition, it can also be used as a check on the validity of any analytical derivation of \tilde{T} .

Example 4.8.1 Stanford Manipulator Let us consider the Stanford manipulator shown in Fig. 4.8 as an example to illustrate the foregoing principle. Using the D-H link parameters listed in the preceding section, we obtain the matrix product ${}^0 A_3$ as

$${}^0A_3 = \begin{bmatrix} s\theta_1 & c\theta_1c\theta_2 & c\theta_1s\theta_2 & d_3c\theta_1s\theta_2 - d_2s\theta_1 \\ -c\theta_1 & s\theta_1c\theta_2 & s\theta_1s\theta_2 & d_3s\theta_1s\theta_2 + d_2c\theta_1 \\ 0 & -s\theta_2 & c\theta_2 & d_3c\theta_2 \\ 0 & 0 & 0 & 1 \end{bmatrix}. \quad (4.143)$$

Hence the rotation matrix 0R_3 is given by

$${}^0R_3 = \begin{bmatrix} s\theta_1 & c\theta_1c\theta_2 & c\theta_1s\theta_2 \\ -c\theta_1 & s\theta_1c\theta_2 & s\theta_1s\theta_2 \\ 0 & -s\theta_2 & c\theta_2 \end{bmatrix}. \quad (4.144)$$

The position vector of O_3 with respect to the fixed reference frame (x_0, y_0, z_0) is given by

$${}^0p_3 = {}^0A_3 \begin{bmatrix} 0 \\ 0 \\ 0 \\ 1 \end{bmatrix} = \begin{bmatrix} d_3c\theta_1s\theta_2 - d_2s\theta_1 \\ d_3s\theta_1s\theta_2 + d_2c\theta_1 \\ d_3c\theta_2 \\ 1 \end{bmatrix}. \quad (4.145)$$

Substituting Eqs. (4.144) and (4.145) into (4.139), we obtain

$$\begin{aligned} {}^0\tilde{T}_3 = & \\ & \begin{bmatrix} s\theta_1 & c\theta_1c\theta_2 & c\theta_1s\theta_2 & 0 & 0 & 0 \\ -c\theta_1 & s\theta_1c\theta_2 & s\theta_1s\theta_2 & 0 & 0 & 0 \\ 0 & -s\theta_2 & c\theta_2 & 0 & 0 & 0 \\ d_3c\theta_1c\theta_2 & -d_3s\theta_1 - d_2c\theta_1s\theta_2 & d_2c\theta_1c\theta_2 & s\theta_1 & c\theta_1c\theta_2 & c\theta_1s\theta_2 \\ d_3s\theta_1c\theta_2 & d_3c\theta_1 - d_2s\theta_1s\theta_2 & d_2s\theta_1c\theta_2 & -c\theta_1 & s\theta_1c\theta_2 & s\theta_1s\theta_2 \\ -d_3s\theta_2 & -d_2c\theta_2 & -d_2s\theta_2 & 0 & -s\theta_2 & c\theta_2 \end{bmatrix}. \end{aligned} \quad (4.146)$$

The inverse transformation is given by

$$\begin{aligned} {}^3\tilde{T}_0 = & \\ & \begin{bmatrix} s\theta_1 & -c\theta_1 & 0 & 0 & 0 & 0 \\ c\theta_1c\theta_2 & s\theta_1c\theta_2 & -s\theta_2 & 0 & 0 & 0 \\ c\theta_1s\theta_2 & s\theta_1s\theta_2 & c\theta_2 & 0 & 0 & 0 \\ d_3c\theta_1c\theta_2 & d_3s\theta_1c\theta_2 & -d_3s\theta_2 & s\theta_1 & -c\theta_1 & 0 \\ -d_3s\theta_1 - d_2c\theta_1s\theta_2 & d_3c\theta_1 - d_2s\theta_1s\theta_2 & -d_2c\theta_2 & c\theta_1c\theta_2 & s\theta_1c\theta_2 & -s\theta_2 \\ d_2c\theta_1c\theta_2 & d_2s\theta_1c\theta_2 & -d_2s\theta_2 & c\theta_1s\theta_2 & s\theta_1s\theta_2 & c\theta_2 \end{bmatrix}. \end{aligned} \quad (4.147)$$

In a path planning problem, the velocity state of the end effector is often specified by the angular velocity vector, $(\omega_x, \omega_y, \omega_z)$, and the velocity of a point in the end effector, (v_{ox}, v_{oy}, v_{oz}) , which is instantaneously coincident with the fixed origin O_0 . These six components are precisely the coordinates of a screw about which the end effector is twisting instantaneously. Consequently, these six components are related to the components of the velocity state specified in the third moving frame by the following transformation.

$$\begin{bmatrix} {}^3\omega_x \\ {}^3\omega_y \\ {}^3\omega_z \\ {}^3v_{ox} \\ {}^3v_{oy} \\ {}^3v_{oz} \end{bmatrix} = {}^3\tilde{T}_0 \begin{bmatrix} \omega_x \\ \omega_y \\ \omega_z \\ v_{ox} \\ v_{oy} \\ v_{oz} \end{bmatrix}. \quad (4.148)$$

Once the velocity state is transformed into the instantaneous reference frame, the inverse velocity problem, namely the problem of finding the joint rates needed to achieve a given velocity state, can be solved by

$$\begin{bmatrix} \dot{\theta}_1 \\ \dot{\theta}_2 \\ \dot{\theta}_3 \\ \dot{\theta}_4 \\ \dot{\theta}_5 \\ \dot{\theta}_6 \end{bmatrix} = {}^3J^{-1} \begin{bmatrix} {}^3\omega_x \\ {}^3\omega_y \\ {}^3\omega_z \\ {}^3v_{ox} \\ {}^3v_{oy} \\ {}^3v_{oz} \end{bmatrix}. \quad (4.149)$$

Example 4.8.2 Elbow Manipulator Consider the elbow manipulator shown in Fig. 4.10 as a second example. Using the D-H link parameters listed in the preceding section, we obtain the matrix product 0A_4 as

$${}^0A_4 = \begin{bmatrix} c\theta_1c\theta_{234} & -s\theta_1 & -c\theta_1s\theta_{234} & c\theta_1(a_4c\theta_{234} + a_3c\theta_{23} + a_2c\theta_2) \\ s\theta_1c\theta_{234} & c\theta_1 & -s\theta_1s\theta_{234} & s\theta_1(a_4c\theta_{234} + a_3c\theta_{23} + a_2c\theta_2) \\ s\theta_{234} & 0 & c\theta_{234} & a_4s\theta_{234} + a_3s\theta_{23} + a_2s\theta_2 \\ 0 & 0 & 0 & 1 \end{bmatrix}. \quad (4.150)$$

Hence the rotation matrix 0R_4 is given by

$${}^0R_4 = \begin{bmatrix} c\theta_1c\theta_{234} & -s\theta_1 & -c\theta_1s\theta_{234} \\ s\theta_1c\theta_{234} & c\theta_1 & -s\theta_1s\theta_{234} \\ s\theta_{234} & 0 & c\theta_{234} \end{bmatrix}. \quad (4.151)$$

The position vector of O_4 with respect to the fixed reference frame (x_0, y_0, z_0) is given by

$${}^0\mathbf{p}_4 = {}^0A_4 \begin{bmatrix} 0 \\ 0 \\ 0 \\ 1 \end{bmatrix} = \begin{bmatrix} c\theta_1(a_4c\theta_{234} + a_3c\theta_{23} + a_2c\theta_2) \\ s\theta_1(a_4c\theta_{234} + a_3c\theta_{23} + a_2c\theta_2) \\ a_4s\theta_{234} + a_3s\theta_{23} + a_2s\theta_2 \\ 1 \end{bmatrix}. \quad (4.152)$$

Substituting Eqs. (4.151) and (4.152) into (4.139), we obtain

$${}^0\tilde{T}_4 = \begin{bmatrix} c\theta_1c\theta_{234} & -s\theta_1 & -c\theta_1s\theta_{234} & 0 & 0 & 0 \\ s\theta_1c\theta_{234} & c\theta_1 & -s\theta_1s\theta_{234} & 0 & 0 & 0 \\ s\theta_{234} & 0 & c\theta_{234} & 0 & 0 & 0 \\ x_1s\theta_1 & -x_2c\theta_1 & x_4s\theta_1 & c\theta_1c\theta_{234} & -s\theta_1 & -c\theta_1s\theta_{234} \\ -x_1c\theta_1 & -x_2s\theta_1 & -x_4c\theta_1 & s\theta_1c\theta_{234} & c\theta_1 & -s\theta_1s\theta_{234} \\ 0 & x_3 & 0 & s\theta_{234} & 0 & c\theta_{234} \end{bmatrix}, \quad (4.153)$$

where $x_1 = a_3s\theta_4 + a_2s\theta_{34}$, $x_2 = a_4s\theta_{234} + a_3s\theta_{23} + a_2s\theta_2$, $x_3 = a_4c\theta_{234} + a_3c\theta_{23} + a_2c\theta_2$, and $x_4 = a_4 + a_3c\theta_4 + a_2c\theta_{34}$. The inverse transformation is given by

$${}^4\tilde{T}_0 = \begin{bmatrix} c\theta_1c\theta_{234} & s\theta_1c\theta_{234} & s\theta_{234} & 0 & 0 & 0 \\ -s\theta_1 & c\theta_1 & 0 & 0 & 0 & 0 \\ -c\theta_1s\theta_{234} & -s\theta_1s\theta_{234} & c\theta_{234} & 0 & 0 & 0 \\ x_1s\theta_1 & -x_1c\theta_1 & 0 & c\theta_1c\theta_{234} & s\theta_1c\theta_{234} & s\theta_{234} \\ -x_2c\theta_1 & -x_2s\theta_1 & x_3 & -s\theta_1 & c\theta_1 & 0 \\ x_4s\theta_1 & -x_4c\theta_1 & 0 & -c\theta_1s\theta_{234} & -s\theta_1s\theta_{234} & c\theta_{234} \end{bmatrix}. \quad (4.154)$$

Hence the velocity state of the end effector with respect to the fixed reference frame is related to that with respect to the fourth moving frame by the following matrix transformation:

$$\begin{bmatrix} {}^4\omega_x \\ {}^4\omega_y \\ {}^4\omega_z \\ {}^4v_{ox} \\ {}^4v_{oy} \\ {}^4v_{oz} \end{bmatrix} = {}^4\tilde{T}_0 \begin{bmatrix} \omega_x \\ \omega_y \\ \omega_z \\ v_{ox} \\ v_{oy} \\ v_{oz} \end{bmatrix}. \quad (4.155)$$

Similar to the Stanford manipulator, the inverse velocity problem can be solved as

$$\begin{bmatrix} \dot{\theta}_1 \\ \dot{\theta}_2 \\ \dot{\theta}_3 \\ \dot{\theta}_4 \\ \dot{\theta}_5 \\ \dot{\theta}_6 \end{bmatrix} = {}^4J^{-1} \begin{bmatrix} {}^4\omega_x \\ {}^4\omega_y \\ {}^4\omega_z \\ {}^4v_{ox} \\ {}^4v_{oy} \\ {}^4v_{oz} \end{bmatrix}. \quad (4.156)$$

4.9 RELATIONSHIP BETWEEN THE TWO METHODS

The velocity vectors, ω_n and \mathbf{v}_n , used by the conventional method are expressed in the fixed reference frame, while ${}^j\omega_n$ and ${}^j\mathbf{v}_o$ employed by the method of screw coordinates are expressed in the instantaneous reference frame. These two velocity states are related by the following transformation:

$$\omega_n = {}^0R_j {}^j\omega_n \quad (4.157)$$

$$\mathbf{v}_n = {}^0R_j({}^j\mathbf{v}_o + {}^j\omega_n \times {}^j\mathbf{p}_n) \quad (4.158)$$

where

$$\begin{bmatrix} {}^j\mathbf{p}_n \\ 1 \end{bmatrix} = {}^jA_n \begin{bmatrix} 0 \\ 0 \\ 0 \\ 1 \end{bmatrix}$$

denotes the position vector of the origin of the end-effector frame with respect to the j th link frame.

4.10 CONDITION NUMBER

The Jacobian matrix J transforms the joint rate in n -dimensional space into the end-effector velocity in m -dimensional space. In a conventional Jacobian, the first three elements of $\dot{\mathbf{x}}$ have the dimension of length per unit time, whereas the last three elements of $\dot{\mathbf{x}}$ have the dimension of radians per unit time. Further, depending on the type of joints used in a manipulator, the elements of $\dot{\mathbf{q}}$ may not necessarily have the same dimension. As a result, the elements of the Jacobian matrix do not necessarily have uniform dimensions. For example, if all the joints are revolute, the first three rows of the Jaco-

bian matrix J have the dimension of length, whereas the last three rows are dimensionless. Therefore, one should be careful in manipulating the matrix.

For those manipulators with only one type of joint and for one type of task, namely, either point positioning or body orienting but not both, the Jacobian matrix can be characterized by a measure called the *condition number*, c . The condition number of a matrix A is defined as

$$c = \|A\| \|A^{-1}\|, \quad (4.159)$$

where the *norm* of A is defined as

$$\|A\| = \max_{x \neq 0} \frac{\|Ax\|}{\|x\|}.$$

In other words, the norm of A bounds the amplifying power of the matrix:

$$\|Ax\| \leq \|A\| \|x\| \quad \text{for all vectors } x, \quad (4.160)$$

where the equality holds for at least one nonzero x (Strang, 1988). In case A is a positive-definite matrix, the condition number of A becomes the ratio of the largest eigenvalue to the smallest eigenvalue of A .

The condition number of the Jacobian matrix depends on the link lengths and the manipulator configuration. As the end effector moves from location to location, the condition number will assume different values. The minimum condition number of any matrix is 1. Those points in the workspace of a manipulator where the condition number of the Jacobian matrix is equal to 1 are called *isotropic points* (Salisbury, 1982). Depending on link dimensions, a manipulator may or may not possess isotropic points within its workspace.

Another method of comparing the transformation characteristics is to compare the joint rates required to produce a unity end-effector velocity in all possible directions. To achieve this goal, we confine the end-effector velocity vector on an m -dimensional unit sphere,

$$\dot{x}^T \dot{x} = 1 \quad (4.161)$$

and compare the corresponding joint rates in the n -dimensional joint space. Substituting Eq. (4.56) into (4.161) yields

$$\dot{q}^T J^T J \dot{q} = 1. \quad (4.162)$$

Equation (4.162) represents an ellipsoid in the n -dimensional joint space. Because the product $J^T J$ is symmetric positive semidefinite, its eigenvectors are orthogonal. The principal axes of the ellipsoid coincide with the eigenvectors of $J^T J$, and the lengths of its principal axes are equal to the reciprocals of the square roots of the eigenvalues of $J^T J$.

Since the Jacobian matrix is configuration dependent, the ellipsoid is also configuration dependent. As the end effector moves from one location to another, the shape and orientation of the ellipsoid will also change accordingly. The closer the velocity ellipsoid to a sphere, the better the transformation characteristics are. The transformation is said to be *isotropic* when the principal axes are all of equal length. At an isotropic point, a unit sphere in the m -dimensional end-effector space maps onto a sphere in the n -dimensional joint space. On the other hand, at a singular point, one or more of the principal axes becomes infinitely long and the ellipsoid degenerates into a cylinder. Under such a condition, the end effector will not be able to move in some directions.

Example 4.10.1 Planar 2-DOF Manipulator Consider the planar 2-dof manipulator shown in Fig. 4.7 as an example. Let $a_1 = \sqrt{2}$ m and $a_2 = 1$ m. Then the Jacobian matrix, Eq. (4.66), can be written as

$$J = \begin{bmatrix} -\sqrt{2}s\theta_1 - s\theta_{12} & -s\theta_{12} \\ \sqrt{2}c\theta_1 + c\theta_{12} & c\theta_{12} \end{bmatrix} \quad \text{m.} \quad (4.163)$$

The matrix product $J^T J$ is given by

$$J^T J = \begin{bmatrix} 2\sqrt{2}c\theta_2 + 3 & \sqrt{2}c\theta_2 + 1 \\ \sqrt{2}c\theta_2 + 1 & 1 \end{bmatrix} \quad \text{m}^2. \quad (4.164)$$

Note that the matrix product $J^T J$ is symmetric and independent of θ_1 . The eigenvalues of $J^T J$ are $\lambda_1 = (2 - \sqrt{2})(-c\theta_2 + 1)$ and $\lambda_2 = (2 + \sqrt{2})(c\theta_2 + 1)$, respectively. In particular, $\lambda_1 = \lambda_2 = 1$ for the configuration of $\theta_2 = 3\pi/4$ or $\theta_2 = 5\pi/4$. We conclude that the manipulator possesses a unity condition number when it assumes either one of these two configurations. Since the condition number is independent of θ_1 , all points swept by the manipulator with $\theta_2 = 3\pi/4$ or $\theta_2 = 5\pi/4$ form the locus of isotropic points as shown in Fig. 4.13.

For the purpose of discussion, let us further assume that $\theta_2 = \pi/2$. Then the matrix product $J^T J$ becomes

$$J^T J = \begin{bmatrix} 3 & 1 \\ 1 & 1 \end{bmatrix}. \quad (4.165)$$

The eigenvalues of $J^T J$ are $\lambda_1 = 2 - \sqrt{2} = 0.5858$ and $\lambda_2 = 2 + \sqrt{2} = 3.4142$. The corresponding eigenvectors, normalized to unit length, are $(-0.3827, 0.9238)$ and $(0.9238, 0.3827)$, respectively. These two eigen-

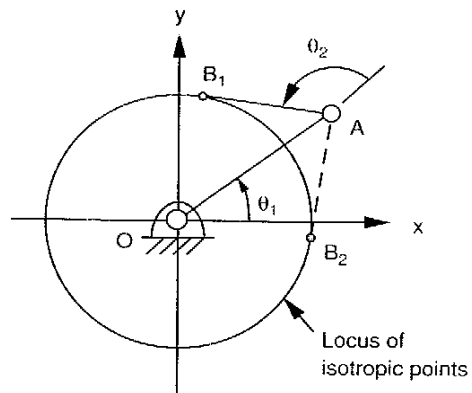


FIGURE 4.13. Locus of isotropic points.

vectors are at 22.5° angles with the $\dot{\theta}_2$ and $\dot{\theta}_1$ axes, respectively, and they are lined up with the principal axes of the ellipse.

Substituting Eq. (4.165) into (4.162) yields

$$3\dot{\theta}_1^2 + 2\dot{\theta}_1\dot{\theta}_2 + \dot{\theta}_2^2 = \frac{(0.3827\dot{\theta}_1 - 0.9238\dot{\theta}_2)^2}{1.3065^2} + \frac{(0.9238\dot{\theta}_1 + 0.3827\dot{\theta}_2)^2}{0.5412^2} = 1. \quad (4.166)$$

Equation (4.166) represents an ellipse as shown in Fig. 4.14b. The joint rates required to produce a unity end-effector velocity are $(\dot{\theta}_1, \dot{\theta}_2) = (-0.500, 1.207)$ rad/s along the major axis, and $(\dot{\theta}_1, \dot{\theta}_2) = (0.500, 0.207)$ rad/s along the minor axis.

Without loss of generality, we assume that $\theta_1 = 0$. Then the Jacobian matrix becomes

$$J = \begin{bmatrix} -1 & -1 \\ \sqrt{2} & 0 \end{bmatrix}. \quad (4.167)$$

Hence the corresponding end-effector velocities are $(v_x, v_y) = (-0.707, -0.707)$ m/s along the major axis and $(v_x, v_y) = (-0.707, 0.707)$ m/s along the minor axis, respectively, as shown in Fig. 4.14a. We notice that to produce the same end-effector speed along the principal axes, one requires the largest joint rates while the other requires the smallest joint rates.

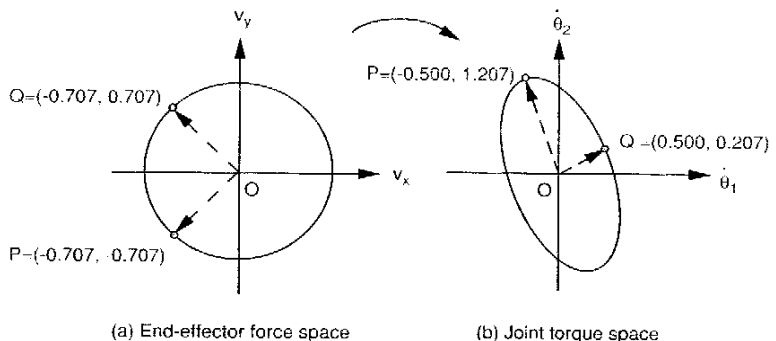


FIGURE 4.14. Velocity ellipsoid.

4.11 SINGULARITY ANALYSIS

The Jacobian matrix, J , transforms the joint rates of a manipulator into the end-effector velocity state. Thus, given the joint rates, we can compute the end-effector velocities directly. In a trajectory planning problem, however, the end-effector velocities are usually given along a desired path in the end-effector space, and these velocities must be converted into the joint rates in the joint space. This requires a computation of the inverse transformation of Eq. (4.56):

$$\dot{q} = J^{-1}\dot{x}. \quad (4.168)$$

The inverse transformation matrix, J^{-1} , can be derived by formulating the matrix of cofactors of J , transporting it, and dividing throughout by the determinant of J . Equation (4.168) provides a means of calculating the joint rates required to produce certain desired end-effector velocities. It is obvious that the required joint rates depend on the condition of the Jacobian matrix. At certain manipulator configurations, the Jacobian matrix may lose its full rank (i.e., there is a reduction of the number of linearly independent rows or columns). Hence as the manipulator approaches these configurations, the Jacobian matrix becomes ill conditioned and may not be invertible. Under such a condition, numerical solution of Eq. (4.168) results in infinite joint rates.

A manipulator is said to be at a *singular configuration* when the Jacobian matrix loses its full rank. Physically, this implies that the instantaneous screws spanning the n -dimensional space of the Jacobian matrix become linearly dependent. Therefore, at a singular configuration, a serial manipulator

may lose one or more degrees of freedom, and it won't be able to move in some directions in the end-effector space.

Singular configurations can be found by setting the determinant of the Jacobian matrix to zero. In general, this will result in a single algebraic equation. For serial manipulators, the singular condition is a function of the intermediate joint variables, not of the first and last joint variables. This is because the presence of a singularity depends solely on the relative locations of the joint axes. Rotation of the entire manipulator about the first axis does not change the relative locations of the joint axes. Similarly, rotation of the end effector about the last joint axis does not affect the location of any joint axis. Therefore, the first and last joint variables do not appear in the determinant of the Jacobian matrix. Several studies of singularity analysis can be found in the literature (Hunt, 1986, 1987a; Paul and Stevenson, 1983; Waldron and Hunt, 1988; Wang and Waldron, 1987).

There are two types of singularities for a serial manipulator: *boundary singularity* and *interior singularity*. A boundary singularity occurs when the end effector is on the surface of the workspace boundary, and it usually happens when the manipulator is either in a fully stretched-out or a folded-back configuration. Boundary singularity can also occur when one of its actuators reaches its mechanical limit. An interior singularity occurs inside the workspace boundary. Several conditions may lead to an interior singularity. For example, when two or more joint axes line up on a straight line, the effects of a rotation about one joint axis can be canceled by counterrotation about another joint axis. Thus the end effector remains stationary even though the intermediate links of the manipulator may move in space. Another example of interior singularity occurs when four revolute joint axes are parallel to one another or intersect at a common point. For a manipulator of general geometry, the problem of identifying interior singularities becomes a much more complex problem. Basically, an interior singularity occurs whenever the screws of two or more joint axes become linearly dependent. Boundary singularities are not particularly serious, since they can always be avoided by arranging the tasks of manipulation far away from the workspace boundary. Interior singularity is more troublesome because it is more difficult to predict during the path planning process. The following examples illustrate the physical meaning of boundary and interior singularities.

4.11.1 Singular Configurations of a Planar 3-DOF Manipulator

Consider the planar 3-dof manipulator shown in Fig. 2.3 as an example. To identify the singular configurations, we equate the determinant of the conven-

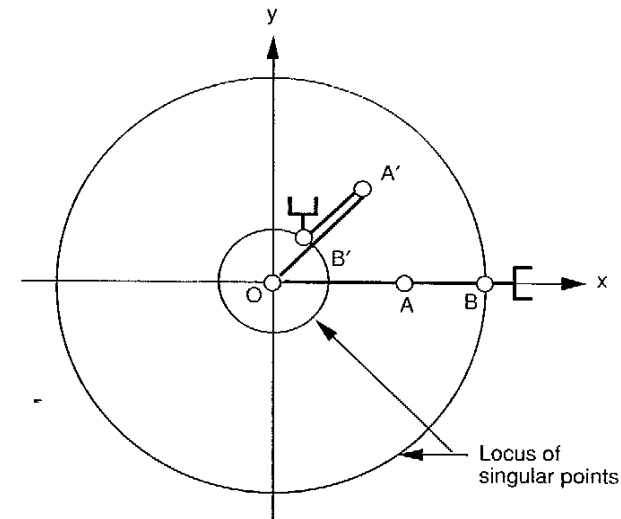


FIGURE 4.15. Locus of singular points.

tional Jacobian matrix, Eq. (4.67), to zero:

$$\det(J) = \begin{vmatrix} -(a_1 s\theta_1 + a_2 s\theta_{12} + a_3 s\theta_{123}) & -(a_2 s\theta_{12} + a_3 s\theta_{123}) & -a_3 s\theta_{123} \\ (a_1 c\theta_1 + a_2 c\theta_{12} + a_3 c\theta_{123}) & (a_2 c\theta_{12} + a_3 c\theta_{123}) & a_3 c\theta_{123} \\ 1 & 1 & 1 \end{vmatrix} = a_1 a_2 s\theta_2 = 0. \quad (4.169)$$

We note that the joint angles θ_1 and θ_3 do not appear in Eq. (4.169) as predicted. Clearly, the manipulator assumes a singular configuration when $\theta_2 = 0$ or $\theta_2 = \pi$. The condition $\theta_2 = 0$ corresponds to a stretched-out configuration, and the condition $\theta_2 = \pi$ corresponds to a folded-back configuration, as depicted in Fig. 4.15. In either case, the manipulator loses 1 degree of freedom. The end effector can only move along the tangential direction of the arm; motion along the radial direction is not possible. This is a typical example of workspace boundary singularity.

4.11.2 Singular Configurations of the Stanford Manipulator

In this example we examine the singular configurations of the Stanford manipulator shown in Fig. 4.8. Equating the determinant of the screw-based Jacobian in Eq. (4.99) to zero, we obtain

$$\det({}^3J) = \begin{vmatrix} 0 & -1 & 0 & 0 & -s\theta_4 & c\theta_4 s\theta_5 \\ -s\theta_2 & 0 & 0 & 0 & c\theta_4 & s\theta_4 s\theta_5 \\ c\theta_2 & 0 & 0 & 1 & 0 & c\theta_5 \\ -d_3 s\theta_2 & 0 & 0 & 0 & 0 & 0 \\ -d_2 c\theta_2 & d_3 & 0 & 0 & 0 & 0 \\ -d_2 s\theta_2 & 0 & 1 & 0 & 0 & 0 \end{vmatrix} = -d_3^2 s\theta_2 s\theta_5 = 0. \quad (4.170)$$

The workspace boundary of the wrist center, P , is determined by the upper and lower limits of the sliding distance along the prismatic joint, namely the extreme values of d_3 . Assuming that $d_3 \neq 0$, it can be concluded that the manipulator will lose (1) 1 degree of freedom if either $s\theta_2$ or $s\theta_5$ is equal to zero; (2) 2 degrees of freedom if both $s\theta_2$ and $s\theta_5$ are equal to zero simultaneously, and (3) 3 degrees of freedom, if condition 2 occurs at the workspace boundary.

The condition $s\theta_2 = 0$ is satisfied when $\theta_2 = 0$ or π . Under this condition, the arm points either vertically up or down, and the position of the wrist center is confined on a cylindrical surface of radius d_2 . Hence it is a workspace boundary singularity.

The condition $s\theta_5 = 0$ is satisfied when $\theta_5 = 0$ or π . In this case the sixth joint axis is in line with the fourth. Therefore, any rotation about the fourth joint axis can be canceled by a counterrotation about the sixth joint axis. That is, the wrist can perform a *self-motion* with no effect on the orientation of the end effector. This is an interior singularity.

Mathematically, another singularity occurs at $d_3 = 0$. When $d_3 = 0$, any rotation about the second joint axis (z_1) has no effects on the linear velocity of the wrist center. However, in practice, the minimum value of d_3 is determined by the physical construction of the robot arm.

4.11.3 Singular Configurations of the Elbow Manipulator

In this example we examine the singular configurations of the elbow manipulator shown in Fig. 4.10. Equating the determinant of the screw-based Jacobian given by Eq. (4.115) to zero, we obtain

$$\det({}^4J) = \begin{vmatrix} s\theta_{234} & 0 & 0 & 0 & 0 & s\theta_5 \\ 0 & -1 & -1 & -1 & 0 & -c\theta_5 \\ c\theta_{234} & 0 & 0 & 0 & 1 & 0 \\ 0 & a_2 s\theta_{34} + a_3 s\theta_4 & a_3 s\theta_4 & 0 & 0 & 0 \\ x_{51} & 0 & 0 & 0 & 0 & 0 \\ 0 & a_2 c\theta_{34} + a_3 c\theta_4 + a_4 & a_3 c\theta_4 + a_4 & a_4 & 0 & 0 \end{vmatrix} = -a_2 a_3 x_{51} s\theta_3 s\theta_5 = 0. \quad (4.171)$$

where $x_{51} = a_2 c\theta_2 + a_3 c\theta_{23} + a_4 c\theta_{234}$.

Assuming that $a_2 \neq 0$ and $a_3 \neq 0$, it can be concluded that singularities occur when at least one of the three factors $s\theta_3$, $s\theta_5$, and x_{51} is equal to zero. Specifically, the manipulator will lose (1) 1 degree of freedom if either $s\theta_3$, $s\theta_5$, or x_{51} is equal to zero; (2) 2 degrees of freedom if any two of $s\theta_3$, $s\theta_5$, and x_{51} are equal to zero simultaneously, and (3) 3 degrees of freedom if $s\theta_3$, $s\theta_5$, and x_{51} are all equal to zero. The manipulator cannot lose more than 3 degrees of freedom.

The condition $s\theta_3 = 0$ is satisfied when $\theta_3 = 0$ or π . Under this condition, the second and third links are either in a stretched-out or folded-back configuration. This can be considered as a workspace boundary singularity from a regional structure point of view.

The condition $s\theta_5 = 0$ is satisfied when $\theta_5 = 0$ or π . Under such a condition, the sixth joint axis becomes parallel to the second, third, and fourth joint axes, and the manipulator loses 1 degree of freedom. This type of singularity can occur within the workspace boundary and therefore is an interior singularity.

The condition $x_{51} = a_2 c\theta_2 + a_3 c\theta_{23} + a_4 c\theta_{234} = 0$ is satisfied when the wrist center, O_5 , is brought back to the origin of the first link frame, (x_1, y_1, z_1) . Thus any rotation about the second joint axis has no effect on the position of the wrist center. Since the first and second joint axes intersect each other, any rotation about the first joint axis has no effect on the position of the wrist center either.

4.12 SUMMARY

In this chapter, the differential kinematics of serial manipulators was studied. First, the differential kinematics of a rigid body was reviewed. The differential matrices of transformation and the concept of instantaneous screw motion were introduced for the kinematic analysis of serial manipulators. Then the manipulator Jacobian matrix was defined. Both the conventional method and the method of instantaneous screw motions were described. A recursive method for derivation of the screw-based Jacobian matrix was presented. It was shown that the Jacobian of a manipulator can be greatly simplified by expressing the screws in a properly chosen reference frame. To facilitate the inverse velocity analysis associated with the trajectory planning problem, a 6×6 transformation matrix was introduced. Finally, the singularity of a robot manipulator was defined. It was shown that the singularity of a serial manipulator is independent of the first and last joint variables. Several serial manipulators were studied to illustrate the principle.

REFERENCES

- Ball, R. S., 1900, *A Treatise on the Theory of Screws*, Cambridge University Press, Cambridge.
- Beyer, R., 1958, "Space Mechanisms," *Trans. 5th Conference on Mechanisms*, Purdue University, West Lafayette, IN, pp. 141–163.
- Craig, J., 1986, *Introduction to Robotics, Mechanics and Control*, Addison-Wesley, Reading, MA.
- Dimentberg, F. F., 1965, *Screw Calculus and Its Applications to Mechanics* (Russian), Nauka, Moscow, p. 200.
- Featherstone, R., 1983, "Position and Velocity Transformation Between Robot End-Effector Coordinates and Joint Angles," *Int. J. Robot. Res.*, Vol. 2, No. 2, pp. 35–45.
- Hollerbach, J. and Saher, G., 1983, "Wrist-Partitioned Inverse Kinematic Accelerations and Manipulator Dynamics," *Int. J. Robot. Res.*, Vol. 2, No. 4, pp. 61–76.
- Hunt, K. H., 1978, *Kinematic Geometry of Mechanisms*, Clarendon Press, Oxford.
- Hunt, K. H., 1986, "Special Configurations of Robot Arms via Screw Theory, Part 1: The Jacobian and Its Matrix of Cofactors," *Robotica*, Vol. 4, pp. 171–179.
- Hunt, K. H., 1987a, "Special Configurations of Robot Arms via Screw Theory, Part 2: Available End-Effector Displacements," *Robotica*, Vol. 5, pp. 17–22.
- Hunt, K. H., 1987b, "Robot Kinematics—A Compact Analytic Inverse Solution for Velocities," *ASME J. Mech. Transm. Autom. Des.*, Vol. 109, No. 1, pp. 42–49.
- Orin, D. E. and Schrader, W. W., 1984, "Efficient Computation of the Jacobian for Robot Manipulators," *Int. J. Robot. Res.*, Vol. 3, No. 4, pp. 66–75.
- Paul, R. P. and Stevenson, C. N., 1983, "Kinematics of Robot Wrists," *Int. J. Robot. Res.*, Vol. 2, No. 1, pp. 31–38.
- Roth, B., 1984, "Screws, Motors, and Wrenches That Cannot Be Bought in a Hardware Store," *1st International Symposium of Robotics Research*, pp. 679–693.
- Salisbury, J. K., 1982, "Kinematic and Force Analysis of Articulated Mechanical Hands," Ph.D. dissertation, Mechanical Engineering Department, Stanford University, Stanford, CA.
- Strang, G., 1988, *Linear Algebra and Its Applications*, Harcourt Brace Jovanovich, San Diego, CA.
- Sugimoto, K., 1984, "Determination of Joint Velocities of Robots by Using Screws," *ASME J. Mech. Transm. Autom. Des.*, Vol. 106, pp. 222–227.
- Waldron, K. J., 1982, "Geometrically Based Manipulator Rate Control Algorithms," *Mech. Mach. Theory*, Vol. 17, No. 6, pp. 379–385.
- Waldron, K. J. and Hunt, K. H., 1988, "Series-Parallel Dualities in Actively Coordinated Mechanisms," *Proc. 4th International Symposium on Robotic Research*, MIT Press, Cambridge, MA, pp. 175–181.

- Waldron, K. J., Wang, S. L., and Bolin, S. J., 1985, "A Study of the Jacobian Matrix of Serial Manipulators," *ASME J. Mech. Transm. Autom. Des.*, Vol. 107, No. 2, pp. 230–238.
- Wang, S. L. and Waldron, K. J., 1987, "A Study of Singular Configurations of Serial Manipulators," *ASME J. Mech. Transm. Autom. Des.*, Vol. 109, No. 1, pp. 14–20.
- Whitney, D. E., 1972, "The Mathematics of Coordinated Control of Prosthetic Arms and Manipulators," *ASME J. Dyn. Sys. Meas. Control*, Vol. 122, pp. 303–309.
- Yuan, M. S. C., Freudenstein, F., and Woo, I. S., 1971, "Kinematic Analysis of Spatial Mechanisms by Means of Screw Coordinates, Part 1: Screw Coordinates," *ASME J. Eng. Ind.*, Vol. 93, Ser. B, No. 1, pp. 61–66.

EXERCISES

- Let ${}^A v_p$ and ${}^A v_q$ be the velocities of two points in a rigid body B that is moving with respect to a fixed frame A . Derive the angular velocity of B in terms of ${}^A v_p$ and ${}^A v_q$.
- Consider the spatial 3-dof, 3R manipulator shown in Fig. 2.19. Calculate the velocity of the point Q in the end effector as a function of joint rates. Express it in the fixed frame.
- Figure 4.16 shows a planar 3-dof, 3R manipulator. We wish to move the end effector, Q , along the x -axis at 1.0 m/s and, at the same time, keep the direction of approach, the x_3 -axis, in the $-y_0$ -direction. Calculate the joint rates required to accomplish this task. Under what conditions will the joint rates approach infinity?

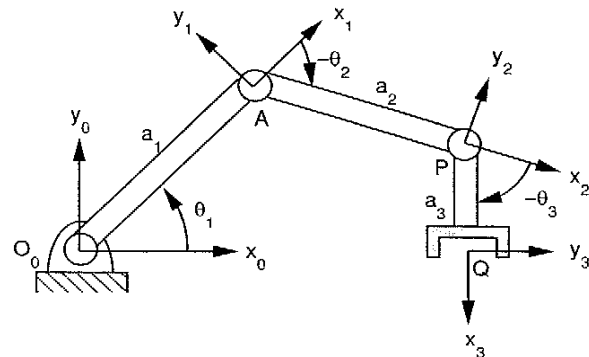


FIGURE 4.16. Planar 3-dof manipulator.

4. For the SCARA robot shown in Fig. 2.4, derive the velocity of point Q and the angular velocity of the end effector in terms of the joint rates. What is the appropriate form of a Jacobian matrix? Express it in the fixed frame.
5. For the 5-dof Scrbot robot shown in Fig. 2.5, derive the velocity of point Q and the angular velocity of the end effector in terms of the joint rates. Formulate the conventional Jacobian matrix. Is this Jacobian a square matrix?
6. Derive the conventional Jacobian matrix for the elbow manipulator shown in Fig. 4.10.
7. Calculate the screw-based Jacobian matrix of the SCARA robot shown in Fig. 2.4. Express it in the (x_3, y_3, z_3) coordinate frame.
8. Derive the screw-based Jacobian matrix for the 6-dof Fanuc S-900W robot shown in Fig. 2.8. Express it in the (x_3, y_3, z_3) coordinate frame.
9. For the spatial 3-dof robot shown in Fig. 2.19, identify a set of joint angles for which the manipulator is at a workspace boundary singularity, and another set of joint angles for which the manipulator is at a workspace interior singularity.
10. Show that a spatial manipulator with three revolute joints and nonzero link lengths always contains a locus of workspace interior singular points.
11. What are the necessary conditions for a spatial manipulator with three revolute joints and nonzero link lengths to possess isotropic points?
12. Find the singular loci associated with the SCARA robot shown in Fig. 2.4.
13. Derive the singular points associated with the 5-dof Scrbot robot shown in Fig. 2.5. Explain whether they are workspace boundary or interior singularities.

CHAPTER 5

JACOBIAN ANALYSIS OF PARALLEL MANIPULATORS

5.1 INTRODUCTION

This chapter is devoted to the Jacobian analysis of parallel manipulators. The Jacobian analysis of parallel manipulators is a much more difficult problem than that of serial manipulators because there are many links that form a number of closed loops. Study of the instantaneous motion of kinematic chains was pioneered by Waldron (1966), Davies and Primrose (1971), and later Baker (1980). Since then, various methods of analysis have been proposed. Davies (1981) developed a constraint law for a mechanical network that is analogous to Kirchhoff's circulation law. Mohamed et al. (1983) developed a procedure for determination of the instantaneous twists associated with the joints of a limb using velocity vector-loop equations. Mohamed and Duffy (1985) introduced the screw theory, and Sugimoto (1987) applied motor algebra for the Jacobian analysis of parallel manipulators.

An important limitation of a parallel manipulator is that singular configurations may exist within its workspace where the manipulator gains 1 or more degrees of freedom and therefore loses its stiffness completely. This property has attracted the attention of several researchers. Gosselin and Angeles (1990) studied the singularities of closed-loop mechanisms and suggested a separation of the Jacobian matrix into two matrices: one associated with the direct kinematics and the other with the inverse kinematics. Depending on which matrix is singular, a closed-loop mechanism may be at a direct kinematic singular configuration, an inverse kinematic singular configuration, or both. This classification has been refined by Zlatanov et al. (1994).

In this chapter, two methods of analysis are presented. The first method employs velocity vector-loop equations, and the second method applies the theory of reciprocal screws.

5.2 JACOBIAN MATRICES

A parallel manipulator such as the VARIAX® machining center shown in Fig. 5.1 typically consists of a moving platform and a fixed base connected by several limbs. The moving platform serves as the end effector. Because of the closed-loop construction, not all the joints can be controlled independently. Thus some of the joints are driven by actuators, whereas others are passive.

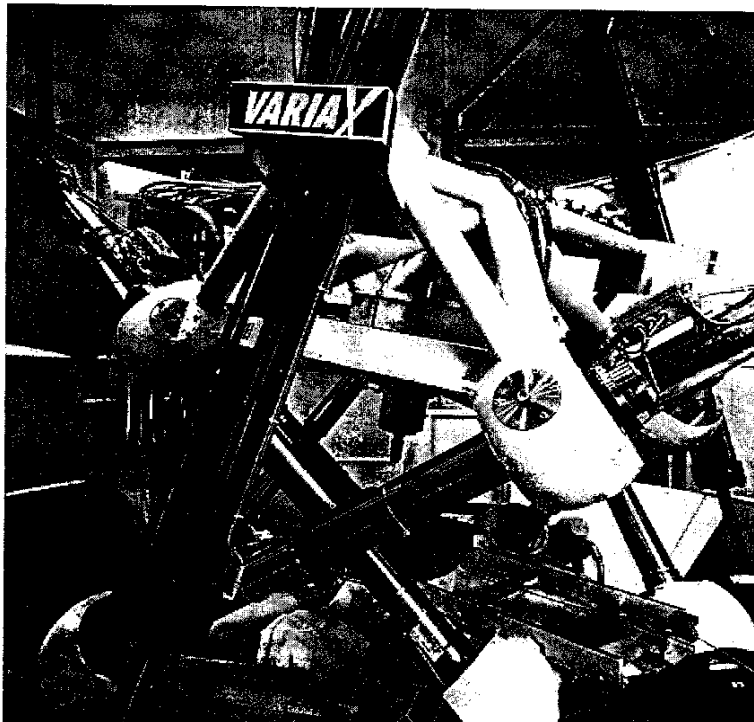


FIGURE 5.1. VARIAX® machining center. (Courtesy of Giddings & Lewis Machine Tools, Fond du Lac, Wisconsin.)

In general, the number of actuated joints should be equal to the number of degrees of freedom of the manipulator.

Let the actuated joint variables be denoted by a vector \mathbf{q} and the location of the moving platform be described by a vector \mathbf{x} . Then the kinematic constraints imposed by the limbs can be written in the general form

$$\mathbf{f}(\mathbf{x}, \mathbf{q}) = \mathbf{0}, \quad (5.1)$$

where \mathbf{f} is an n -dimensional implicit function of \mathbf{q} and \mathbf{x} and $\mathbf{0}$ is an n -dimensional zero vector.

Differentiating Eq. (5.1) with respect to time, we obtain a relationship between the input joint rates and the end-effector output velocity as follows:

$$J_x \dot{\mathbf{x}} = J_q \dot{\mathbf{q}}, \quad (5.2)$$

where

$$J_x = \frac{\partial \mathbf{f}}{\partial \mathbf{x}} \quad \text{and} \quad J_q = -\frac{\partial \mathbf{f}}{\partial \mathbf{q}}.$$

The derivation above leads to two separate Jacobian matrices. Hence the overall Jacobian matrix, J , can be written as

$$\dot{\mathbf{q}} = J \dot{\mathbf{x}}, \quad (5.3)$$

where $J = J_q^{-1} J_x$. We note that the Jacobian matrix defined in Eq. (5.3) for a parallel manipulator corresponds to the inverse Jacobian of a serial manipulator.

5.3 SINGULARITY CONDITIONS

Due to the existence of two Jacobian matrices, a parallel manipulator is said to be at a *singular configuration* when either J_x or J_q or both are singular. Three different types of singularities can be identified.

5.3.1 Inverse Kinematic Singularities

An inverse kinematic singularity occurs when the determinant of J_q goes to zero, namely,

$$\det(J_q) = 0. \quad (5.4)$$

When J_q is singular and the null space of J_q is not empty, there exist some nonzero $\dot{\mathbf{q}}$ vectors that result in zero $\dot{\mathbf{x}}$ vectors. Infinitesimal motion of the

moving platform along certain directions cannot be accomplished. Hence the manipulator loses one or more degrees of freedom. On the other hand, at an inverse kinematic singular configuration, a parallel manipulator can resist forces or moments in some directions with zero actuator forces or torques. Inverse kinematic singularities usually occur at the workspace boundary, where different branches of the inverse kinematic solutions converge. It is similar to that of a serial manipulator.

5.3.2 Direct Kinematic Singularities

A direct kinematic singularity occurs when the determinant of J_x is equal to zero, namely,

$$\det(J_x) = 0. \quad (5.5)$$

Assuming that in the presence of such a singular condition the null space of J_x is not empty, there exist some nonzero $\dot{\mathbf{x}}$ vectors that result in zero $\dot{\mathbf{q}}$ vectors. That is, the moving platform can possess infinitesimal motion in some directions while all the actuators are completely locked. Hence the moving platform gains 1 or more degrees of freedom. This is in contradiction with a serial manipulator, which loses 1 or more degrees of freedom (Waldron and Hunt, 1988). In other words, at a direct kinematic singular configuration, the manipulator cannot resist forces or moments in some directions. Direct kinematic singularities usually occur where different branches of direct kinematic solutions meet.

5.3.3 Combined Singularities

A combined singularity occurs when the determinants of J_x and J_q are both zero. Generally, this type of singularity can occur only for manipulators with special kinematic architecture. At a combined singular configuration, Eq. (5.1) will degenerate. The moving platform can undergo some infinitesimal motions while all the actuators are locked. On the other hand, it can also remain stationary while the actuators undergo some infinitesimal motions.

5.4 CONVENTIONAL JACOBIAN

In this section we introduce the conventional method of analysis. Although the methods of screw coordinates and motor algebra are very powerful, their applications to parallel manipulators are often hindered by the presence of many unactuated joints. In this regard, the conventional *velocity vector-loop method* appears to be more straightforward.

Generally, the velocity vector of a point is formulated from two different directions of a loop closure. Each loop closure consists of a fixed base, a moving platform, and all the links of a limb. The unactuated joint rates in each limb are then eliminated by performing a dot product of the velocity vector-loop equation with an appropriate vector that is normal to all vectors of the unactuated joint rates. Finally, the resulting equations are assembled into a Jacobian matrix.

For consistency, we define the end-effector velocity state of the conventional Jacobian as a six-dimensional vector with the linear velocity of a point, followed by the angular velocity of the moving platform; that is,

$$\dot{\mathbf{x}} = \begin{bmatrix} \mathbf{v}_p \\ \boldsymbol{\omega}_p \end{bmatrix}. \quad (5.6)$$

The method can best be illustrated by examples, which we provide next.

5.4.1 Jacobian of a Planar 3RRR Parallel Manipulator

We first investigate the Jacobian and singular conditions of the planar 3RRR manipulator described in Chapter 3. For convenience, a schematic diagram of the manipulator is shown here in Fig. 5.2. The moving platform is defined by the moving pivots A , B , and C , and the fixed platform is defined by the fixed pivots P , Q , and R . Point G is a point in the moving platform, \mathbf{a}_i and \mathbf{b}_i

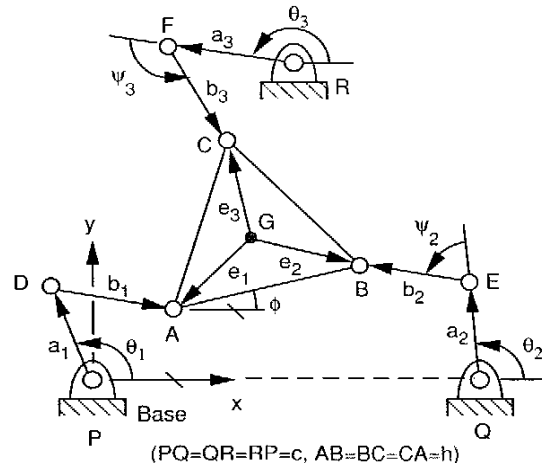


FIGURE 5.2. Schematic of a planar 3RRR manipulator.

denote the vectors of the first and second moving links of the i th limb, while θ_i and ψ_i denote the orientation angles of \mathbf{a}_i and \mathbf{b}_i with respect to the x -axis. For this manipulator, the input vector is $\mathbf{q} = [\theta_1, \theta_2, \theta_3]^T$ and the output vector is $\mathbf{x} = [x_g, y_g, \phi]^T$.

A loop-closure equation can be written for each limb. For example, for the first limb we have

$$\overline{PG} + \overline{GA} = \overline{PD} + \overline{DA}. \quad (5.7)$$

Since this is a planar mechanism, the angular velocity vectors of all links point in the positive z -direction. A velocity vector-loop equation is obtained by taking the derivative of Eq. (5.7) with respect to time:

$$\mathbf{v}_g + \dot{\phi}(\mathbf{k} \times \mathbf{e}_i) = \dot{\theta}_i(\mathbf{k} \times \mathbf{a}_i) + (\dot{\theta}_i + \dot{\psi}_i)(\mathbf{k} \times \mathbf{b}_i), \quad i = 1, 2, 3, \quad (5.8)$$

where \mathbf{v}_g is the velocity of point G and \mathbf{k} is a unit vector pointing in the positive z -axis direction. Since $\dot{\psi}_i$ is a passive variable, it should be eliminated from Eq. (5.8). To achieve this goal, we dot-multiply both sides of Eq. (5.8) by \mathbf{b}_i . This leads to

$$\mathbf{b}_i \cdot \mathbf{v}_g + \dot{\phi} \mathbf{k} \cdot (\mathbf{e} \times \mathbf{b}_i) = \dot{\theta}_i \mathbf{k} \cdot (\mathbf{a}_i \times \mathbf{b}_i). \quad (5.9)$$

Writing Eq. (5.9) three times, once for each $i = 1, 2$, and 3, yields three scalar equations, which can be arranged in matrix form:

$$J_x \dot{\mathbf{x}} = J_q \dot{\mathbf{q}}, \quad (5.10)$$

where

$$J_x = \begin{bmatrix} b_{1x} & b_{1y} & e_{1x}b_{1y} - e_{1y}b_{1x} \\ b_{2x} & b_{2y} & e_{2x}b_{2y} - e_{2y}b_{2x} \\ b_{3x} & b_{3y} & e_{3x}b_{3y} - e_{3y}b_{3x} \end{bmatrix},$$

$$J_q = \begin{bmatrix} a_{1x}b_{1y} - a_{1y}b_{1x} & 0 & 0 \\ 0 & a_{2x}b_{2y} - a_{2y}b_{2x} & 0 \\ 0 & 0 & a_{3x}b_{3y} - a_{3y}b_{3x} \end{bmatrix},$$

and where $\dot{\mathbf{x}} = [v_{gx}, v_{gy}, \dot{\phi}]^T$ and $\dot{\mathbf{q}} = [\dot{\theta}_1, \dot{\theta}_2, \dot{\theta}_3]^T$. In what follows, we discuss the physical significance of each of the three types of singularities.

(a) Inverse Kinematic Singularities. Inverse kinematic singularities occur when one of the diagonal elements of J_q vanishes, namely,

$$a_{ix}b_{iy} - a_{iy}b_{ix} = 0 \quad \text{for } i = 1, \text{ or } 2, \text{ or } 3. \quad (5.11)$$

The left-hand side of Eq. (5.11) represents the magnitude of $\mathbf{a}_i \times \mathbf{b}_i$. Consequently, an inverse kinematic singularity arises whenever any limb is in a fully stretched-out or folded-back configuration. The manipulator loses 1, 2, or 3 degrees of freedom, depending on whether one, two, or three limbs are in fully stretched-out or folded-back configurations. At an inverse kinematic singularity, infinitesimal rotation of the input link, which is in a stretched-out or folded-back configuration, results in no output motion of the moving platform.

(b) Direct Kinematic Singularities. Direct kinematic singularities occur when the determinant of J_x goes to zero. Although it is difficult to identify all possible direct kinematic singularities, the following two singularities are found by inspection of the matrix J_x . We note that the last column of J_x represents the magnitudes of the vector cross products, $\mathbf{e}_i \times \mathbf{b}_i$ for $i = 1, 2$, and 3. These three elements will vanish when the vector \mathbf{b}_i is in line with \mathbf{e}_i for all the limbs. Since G is an arbitrary point in the moving platform, a direct kinematic singularity arises whenever the three vectors \mathbf{b}_i , for $i = 1, 2$, and 3, intersect at a common point. Figure 5.3 illustrates such a singular configuration. At this configuration, the moving platform can make an infinitesimal rotation about point G while the actuators are locked. Hence the moving platform gains 1 degree of freedom and it cannot withstand any external moment about G .

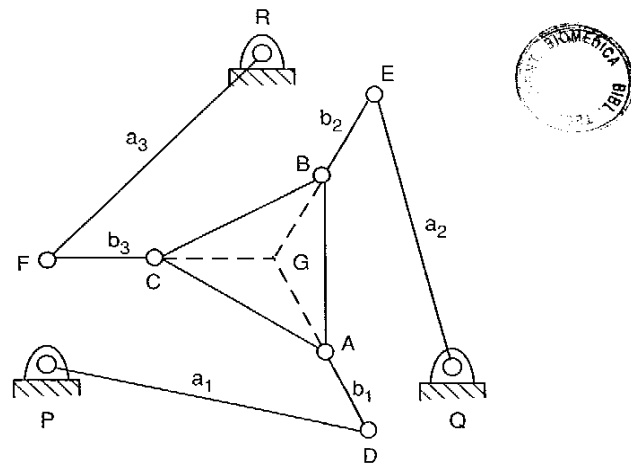


FIGURE 5.3. Direct kinematic singularity of the planar parallel manipulator.

We also note that the first and second columns of J_x represent the x and y components of the vector \mathbf{b}_i , for $i = 1, 2$, and 3. These two columns become linearly dependent when the three vectors, \mathbf{b}_i for $i = 1, 2$, and 3, point in the same direction. Hence another direct kinematic singularity occurs whenever the three vectors \mathbf{b}_i , for $i = 1, 2$, and 3, are parallel to one another. Figure 5.4 illustrates such a singular configuration. At this configuration, the moving platform can make an infinitesimal translation along a direction that is perpendicular to the vector \mathbf{b}_i while all the actuators are locked. Any force applied to the moving platform in that direction cannot be resisted by the actuators.

(c) Combined Singularities. A combined singularity occurs when the determinants of J_x and J_q are both equal to zero. As mentioned earlier, this type of singularity is not only configuration dependent but also architecture dependent. Each of the following two architectures possesses a combined singularity (Gosselin and Angeles, 1990).

Architecture 1

$$PQ = QR = RP, \quad AB = BA = CA, \quad a_i = PQ/\sqrt{3}, \\ \text{and } b_i = e_i \quad \text{for } i = 1, 2, \text{ and } 3.$$

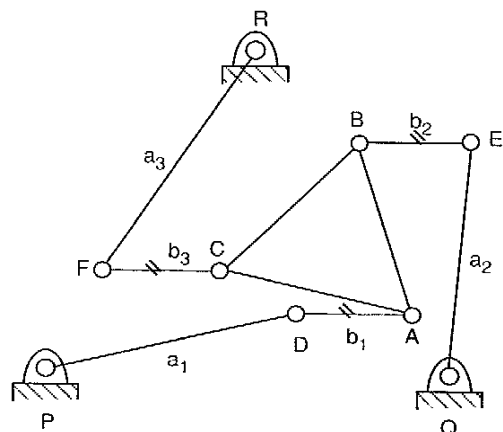


FIGURE 5.4. Another direct kinematic singularity of the planar parallel manipulator.

This type of manipulator can be positioned in a configuration in which pivots D , E , and F meet at the centroid of the base triangle. Because of the special link length ratios, the centroid of the moving platform also coincides with the centroid of the base triangle. Therefore, the moving platform can rotate about the centroid while the actuators are locked. On the other hand, the moving platform can be held stationary at $\phi = 0$ while the input links make some infinitesimal rotations about their corresponding pivots. This is due to the fact that the elements of J_q and the last column of J_x are all equal to zero.

Architecture 2

$$PQ = QR = RP = AB = BC = CA \\ \text{and } a_i = b_i \quad \text{for } i = 1, 2, \text{ and } 3.$$

A manipulator of this type can be positioned in a configuration in which the three moving pivots A , B , and C are coincident with the three fixed pivots P , Q , and R , respectively. Hence the three input links can make arbitrary rotations while the moving platform is locked. Furthermore, with the actuators locked at $\theta_1 = -150^\circ$, $\theta_2 = -30^\circ$, and $\theta_3 = 90^\circ$, the moving platform can perform an infinitesimal rotation about its centroid.

5.4.2 Jacobian of a Spatial Orientation Mechanism

In this example we study the Jacobian and singular conditions of the spatial orientation mechanism shown in Fig. 3.7. Since the manipulator possesses only 3 rotational degrees of freedom, the input vector can be written as $\dot{\mathbf{q}} = [d_1, d_2, d_3]^T$, and the output vector can be described by the angular velocity of the moving platform, $\dot{\mathbf{x}} = \boldsymbol{\omega}_B = [\omega_x, \omega_y, \omega_z]^T$.

Referring to Fig. 3.7, a loop-closure equation for the i th limb can be written as

$$\overline{OB_i} = \overline{OA_i} + \overline{A_iB_i}. \quad (5.12)$$

Taking the derivative of Eq. (5.12) with respect to time yields a velocity vector-loop equation as follows:

$$\boldsymbol{\omega}_B \times \mathbf{b}_i = d_i \boldsymbol{\omega}_i \times \mathbf{s}_i + \dot{d}_i \mathbf{s}_i \quad \text{for } i = 1, 2, 3, \quad (5.13)$$

where \mathbf{b}_i denotes the vector of $\overline{OB_i}$, \mathbf{s}_i is a unit vector pointing along $\overline{A_iB_i}$, and $\boldsymbol{\omega}_i$ denotes the angular velocity of limb i with respect to the fixed frame.

To eliminate ω_i , we dot-multiply both sides of Eq. (5.13) by s_i . This produces

$$(\mathbf{b}_i \times \mathbf{s}_i) \cdot \boldsymbol{\omega}_B = \dot{d}_i \quad \text{for } i = 1, 2, 3. \quad (5.14)$$

Equation (5.14) written three times, once for each $i = 1, 2$, and 3, yields three scalar equations, which can be arranged in matrix form:

$$J_x \boldsymbol{\omega}_B = J_q \dot{\mathbf{q}}, \quad (5.15)$$

where

$$J_x = \begin{bmatrix} (\mathbf{b}_1 \times \mathbf{s}_1)^T \\ (\mathbf{b}_2 \times \mathbf{s}_2)^T \\ (\mathbf{b}_3 \times \mathbf{s}_3)^T \end{bmatrix},$$

$$J_q = I \quad (3 \times 3 \text{ identity matrix}).$$

Note that each row of J_x represents a vector that is normal to a plane defined by the triangle $\triangle A_i O B_i$. For convenience, we define this vector as \mathbf{n}_i ; that is,

$$\mathbf{n}_i = \mathbf{b}_i \times \mathbf{s}_i. \quad (5.16)$$

In what follows, we discuss the physical meaning of the three types of singularities.

(a) Inverse Kinematic Singularities. Since J_q is an identity matrix, there exists no inverse kinematic singularity within the workspace of the manipulator. However, inverse kinematic singularities can occur at the workspace boundary where one or more limbs are in fully stretched or retracted positions.

(b) Direct Kinematic Singularities. Consider the kinematic constraints imposed by limb i . From Eq. (5.14), we observe that the elongation rate of the i th limb, d_i , contributes to a rotation of the moving platform about an axis that passes through the origin O and points in the direction of the vector \mathbf{n}_i . Thus when the i th actuator is locked, the moving platform is prohibited from rotating about this axis. However, it can still rotate freely about the two axes defined by $\overline{OA_i}$ and $\overline{OB_i}$. To completely immobilize the moving platform by three linear actuators, the three vectors \mathbf{n}_i for $i = 1, 2$, and 3 must be well defined and span the three-dimensional rotation space of the end effector. Hence the determinant of J_x goes to zero and the manipulator gains an extra degree of freedom, when these three vectors become linearly dependent or when one of the three vectors vanishes identically. Three different direct kinematic singularities can be identified.

Case 1. One of the three vectors, say \mathbf{n}_i , vanishes. For this condition to hold, points A_i , O , and B_i must lie on a straight line. Under such a condition, the manipulator gains 1 degree of freedom. That is, with all actuators locked, the moving platform can make an infinitesimal rotation about a line of intersection of the two planes defined by triangles $\triangle A_j O B_j$ and $\triangle A_k O B_k$, where $i \neq j \neq k$. Figure 5.5 shows such a singular configuration, in which points A_1 , O , and B_1 lie on a straight line.

Case 2. Two of the three vectors, say \mathbf{n}_i and \mathbf{n}_j , are linearly dependent. When the two planes defined by triangles $\triangle A_i O B_i$ and $\triangle A_j O B_j$ are coincident, the manipulator gains 1 degree of freedom. Specifically, with all actuators locked, the moving platform can make an infinitesimal rotation about a line of intersection of the plane defined by the triangle $\triangle A_i O B_i$ and the plane defined by the triangle $\triangle A_k O B_k$, where $k \neq j$. Figure 5.6 shows such a singular configuration, where the two faces $\triangle A_1 O B_1$ and $\triangle A_2 O B_2$ lie on a plane.

Case 3. The three vectors \mathbf{n}_1 , \mathbf{n}_2 , and \mathbf{n}_3 are linearly dependent. This condition happens when the three planes defined by triangles $\triangle A_1 O B_1$, $\triangle A_2 O B_2$, and $\triangle A_3 O B_3$ intersect in a common line. In other words, when the three

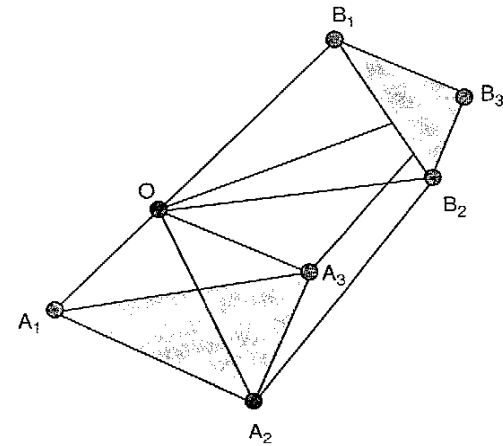


FIGURE 5.5. Direct kinematic singularity of the orientation mechanism.

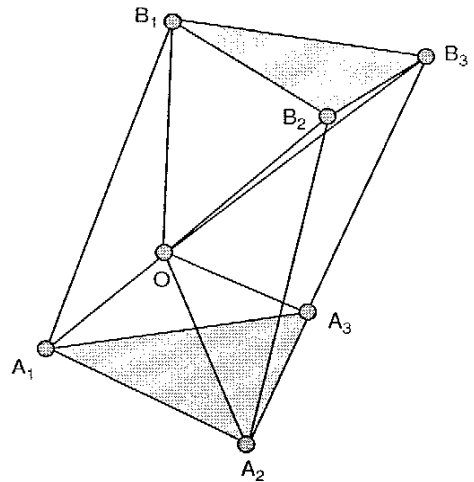


FIGURE 5.6. Another direct kinematic singularity of the orientation mechanism.

normal vectors \mathbf{n}_1 , \mathbf{n}_2 , and \mathbf{n}_3 lie on a plane, one of the three vectors can be expressed as a linear summation of the other two. Hence, with all actuators locked, the moving platform can make an infinitesimal rotation about the line of intersection of the three planes. For example, if the moving tetrahedron $OB_1B_2B_3$ is geometrically similar to the fixed tetrahedron $OA_1A_2A_3$, a singular condition occurs when the moving tetrahedron $OB_1B_2B_3$ is directly on top of the fixed tetrahedron $OA_1A_2A_3$.

(c) Combined Singularities. Combined singularities cannot occur within the workspace of the manipulator. However, it can occur at the workspace boundary if the following three conditions are satisfied simultaneously: (1) the tetrahedron $OA_1A_2A_3$ is similar to $OB_1B_2B_3$; (2) the three planes of triangle $\Delta A_i O B_i$, for $i = 1, 2, 3$, intersect at a common line; and (3) one of the three limbs is at its extreme reach.

5.4.3 Jacobian of the University of Maryland's Manipulator

In this example we develop the Jacobian matrix and examine some singular configurations of the University of Maryland manipulator shown in Fig. 3.10. Recall that this manipulator possesses only 3 translational degrees of freedom. Referring to Fig. 3.11, a loop-closure equation for the i th limb can be

written as

$$\overline{OP} + \overline{PC_i} = \overline{OA_i} + \overline{A_iB_i} + \overline{B_iC_i}. \quad (5.17)$$

Differentiating Eq. (5.17) with respects to time yields

$$\mathbf{v}_p = \boldsymbol{\omega}_{1i} \times \mathbf{a}_i + \boldsymbol{\omega}_{2i} \times \mathbf{b}_i, \quad (5.18)$$

where \mathbf{v}_p is the linear velocity of the moving platform, $\mathbf{a}_i = \overline{A_iB_i}$, $\mathbf{b}_i = \overline{B_iC_i}$, and $\boldsymbol{\omega}_{ji}$ is the angular velocity of the j th link of the i th limb. Here link A_iB_i is treated as the first link and B_iC_i as the second link.

For this manipulator, the input vector is $\dot{\mathbf{q}} = [\dot{\theta}_{11}, \dot{\theta}_{12}, \dot{\theta}_{13}]^T$, and the output vector is $\mathbf{v}_p = [v_{p,x}, v_{p,y}, v_{p,z}]^T$. All other joint rates are passive variables. To eliminate the passive joint rate, we dot-multiply both sides of Eq. (5.18) by \mathbf{b}_i . This produces

$$\mathbf{b}_i \cdot \mathbf{v}_p = \boldsymbol{\omega}_{1i} \cdot (\mathbf{a}_i \times \mathbf{b}_i). \quad (5.19)$$

Expressing the vectors in Eq. (5.19) in the (x_i, y_i, z_i) coordinate frame, we have

$$\begin{aligned} {}^i\mathbf{a}_i &= a \begin{bmatrix} c\theta_{1i} \\ 0 \\ s\theta_{1i} \end{bmatrix}, & {}^i\mathbf{b}_i &= b \begin{bmatrix} s\theta_{3i}c(\theta_{1i} + \theta_{2i}) \\ c\theta_{3i} \\ s\theta_{3i}s(\theta_{1i} + \theta_{2i}) \end{bmatrix}, & {}^i\boldsymbol{\omega}_{1i} &= \begin{bmatrix} 0 \\ -\dot{\theta}_{1i} \\ 0 \end{bmatrix}, \\ {}^i\mathbf{v}_p &= \begin{bmatrix} v_{p,x}c\phi_i + v_{p,y}s\phi_i \\ -v_{p,x}s\phi_i + v_{p,y}c\phi_i \\ v_{p,z} \end{bmatrix}. \end{aligned}$$

Substituting the expressions above into Eq. (5.19), after simplification we obtain

$$j_{ix}v_{p,x} + j_{iy}v_{p,y} + j_{iz}v_{p,z} = as\theta_{2i}s\theta_{3i}\dot{\theta}_{1i}, \quad (5.20)$$

where

$$j_{ix} = c(\theta_{1i} + \theta_{2i})s\theta_{3i}c\phi_i - c\theta_{3i}s\phi_i,$$

$$j_{iy} = c(\theta_{1i} + \theta_{2i})s\theta_{3i}s\phi_i + c\theta_{3i}c\phi_i,$$

$$j_{iz} = s(\theta_{1i} + \theta_{2i})s\theta_{3i}.$$

Note that $\mathbf{j}_i = [j_{ix}, j_{iy}, j_{iz}]^T$ represents a unit vector that is directed from B_i to C_i and expressed in the fixed (x, y, z) coordinate frame.

Writing Eq. (5.20) three times, once for each $i = 1, 2$, and 3, yields three scalar equations, which can be assembled in matrix form as

$$J_x \mathbf{v}_p = J_q \dot{\mathbf{q}}, \quad (5.21)$$

where

$$J_x = \begin{bmatrix} j_{1x} & j_{1y} & j_{1z} \\ j_{2x} & j_{2y} & j_{2z} \\ j_{3x} & j_{3y} & j_{3z} \end{bmatrix},$$

$$J_q = a \begin{bmatrix} s\theta_{21}s\theta_{31} & 0 & 0 \\ 0 & s\theta_{22}s\theta_{32} & 0 \\ 0 & 0 & s\theta_{23}s\theta_{33} \end{bmatrix}.$$

(a) Inverse Kinematic Singularities. From Eq. (5.21), we observe that an inverse kinematic singularity occurs when one of the following conditions is satisfied:

$$\theta_{2i} = 0 \text{ or } \pi, \quad (5.22)$$

or

$$\theta_{3i} = 0 \text{ or } \pi, \quad (5.23)$$

for $i = 1$ or 2 or 3 . Physically, the condition $\theta_{2i} = 0$ or π occurs when the upper arm linkage and the input link of a limb are in the same plane. The condition $\theta_{3i} = 0$ or π occurs when all the links of the four-bar parallelogram that comprise the upper arm of a limb are collinear.

(b) Direct Kinematic Singularities. Direct kinematic singularities occur when the condition $\det(J_x) = 0$ is satisfied. Although it is difficult to solve for all possible singularities, several manipulator postures that satisfy this condition are identified below. We note that each row of J_x represents a unit vector, \mathbf{j}_i , which points along the direction of a coupling link B_iC_i of the four-bar parallelogram. Hence J_x becomes singular when these three unit vectors become linearly dependent; that is,

$$\mu_1 \mathbf{j}_1 + \mu_2 \mathbf{j}_2 + \mu_3 \mathbf{j}_3 = \mathbf{0} \quad (5.24)$$

for some real values of μ_1 , μ_2 , and μ_3 , where not all μ 's are zero.

One condition that satisfies Eq. (5.24) is found when all three unit vectors \mathbf{j}_i for $i = 1$ to 3 lie on a plane. For example, when the three four-bar parallelograms lie on a plane that is parallel to the x - y plane, the z -component of Eq. (5.24) is equal to zero identically. Hence some nonzero values of μ_1 , μ_2 , and μ_3 can always be found from the first two equations. In terms of manip-

ulator variables, this condition can be written as

$$s(\theta_{11} + \theta_{21})s\theta_{31} = s(\theta_{12} + \theta_{22})s\theta_{32} = s(\theta_{13} + \theta_{23})s\theta_{33} = 0. \quad (5.25)$$

Equation (5.25) indicates that the manipulator is in a direct kinematic singularity whenever all limbs are in a posture such that

$$\theta_{1i} + \theta_{2i} = 0 \text{ or } \pi,$$

or

$$\theta_{3i} = 0 \text{ or } \pi,$$

for all $i = 1$ and 2 and 3. The condition $\theta_{3i} = 0$ or π is a combined singularity.

The geometrical interpretation of this condition is that the manipulator displays a direct kinematic singularity when the four-bar linkages of all three limbs are in the same plane as the moving platform. At such a configuration, the manipulator actuators cannot resist any force applied to the moving platform in the z -direction. One example of this type of singular configuration is shown in Fig. 5.7. Note that this example configuration is possible only if $a + r \geq b + h$.

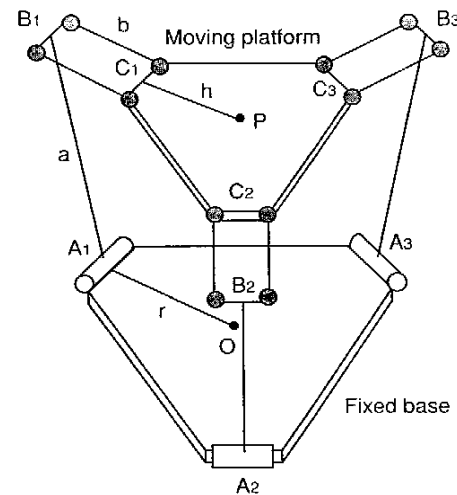


FIGURE 5.7. Direct kinematic singular configuration in which all the upper arm linkages are in the plane of the moving platform.

A second set of postures that satisfies Eq. (5.24) is found when any two of the upper arm linkages are parallel; that is,

$$\mathbf{j}_i = \pm \mathbf{j}_k \quad \text{for } i \neq k. \quad (5.26)$$

Figure 5.8 shows such a singular configuration. At this singular configuration, the manipulator cannot resist any force applied in the plane of the moving platform. Note that in this example we have sketched all three upper arm linkages to be parallel to one another. However, it is only necessary that two of the upper arm linkages be parallel to each other to yield a singular configuration.

(c) Combined Singularities. One combined singularity occurs when the following two conditions are satisfied simultaneously: (1) the geometry of the moving platform is identical to that of the fixed platform, and (2) all three input links are perpendicular to the fixed base (i.e., $\mathbf{A}_i \mathbf{B}_i \perp \mathbf{O} \mathbf{A}_i$ for $i = 1, 2$, and 3). At this configuration the moving platform gains 2 degrees of freedom. Specifically, with the input links completely locked, point P can be positioned anywhere on a spherical surface centered at a distance a above the centroid of

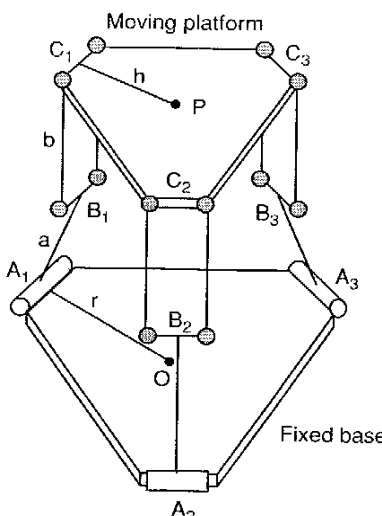


FIGURE 5.8. Another direct kinematic singular configuration, in which two upper arm linkages are parallel to each other.

the fixed base. On the other hand, with the moving platform held stationary, the input links can make some infinitesimal rotations.

5.4.4 Jacobian of a Stewart-Gough Platform

In this example we investigate the Jacobian and singular conditions of the Stewart-Gough platform shown in Fig. 3.15. For this manipulator, the input vector is given by $\dot{\mathbf{q}} = [\dot{d}_1, \dot{d}_2, \dots, \dot{d}_6]^T$, and the output vector can be described by the velocity of the centroid P and the angular velocity of the moving platform:

$$\dot{\mathbf{x}} = \begin{bmatrix} \mathbf{v}_p \\ \boldsymbol{\omega}_B \end{bmatrix}. \quad (5.27)$$

The Jacobian matrix can be derived by formulating a velocity loop-closure equation for each limb. Referring to Fig. 3.15, a loop-closure equation for the i th limb can be written as

$$\overline{OP} + \overline{PB_i} = \overline{OA_i} + \overline{A_i B_i}. \quad (5.28)$$

Differentiating Eq. (5.28) with respect to time yields

$$\mathbf{v}_p + \boldsymbol{\omega}_B \times \mathbf{b}_i = d_i \boldsymbol{\omega}_i \times \mathbf{s}_i + \dot{d}_i \mathbf{s}_i, \quad (5.29)$$

where \mathbf{b}_i and \mathbf{s}_i denote the vector $\overline{PB_i}$ and a unit vector along $\overline{A_i B_i}$, respectively, and $\boldsymbol{\omega}_i$ denotes the angular velocity of the i th limb with respect to the fixed frame A . To eliminate $\boldsymbol{\omega}_i$, we dot-multiply both sides of Eq. (5.29) by \mathbf{s}_i :

$$\mathbf{s}_i \cdot \mathbf{v}_p + (\mathbf{b}_i \times \mathbf{s}_i) \cdot \boldsymbol{\omega}_B = \dot{d}_i. \quad (5.30)$$

Equation (5.30) written six times, once for each $i = 1$ to 6, yields six scalar equations, which can be assembled in matrix form:

$$J_x \dot{\mathbf{x}} = J_q \dot{\mathbf{q}}, \quad (5.31)$$

where

$$J_x = \begin{bmatrix} \mathbf{s}_1^T & (\mathbf{b}_1 \times \mathbf{s}_1)^T \\ \mathbf{s}_2^T & (\mathbf{b}_2 \times \mathbf{s}_2)^T \\ \vdots & \vdots \\ \mathbf{s}_6^T & (\mathbf{b}_6 \times \mathbf{s}_6)^T \end{bmatrix},$$

$$J_q = I \quad (6 \times 6 \text{ identity matrix})$$

Let

$$\mathbf{n}_i = \mathbf{b}_i \times \mathbf{s}_i. \quad (5.32)$$

Then \mathbf{n}_i represents a vector that is normal to the plane containing points A_i , B_i , and P . In what follows, we discuss the physical meaning of the three types of singularities.

(a) Inverse Kinematic Singularities. Inverse kinematic singularities cannot occur within the workspace of the manipulator since J_q is an identity matrix. However, inverse kinematic singularities can occur at the workspace boundary where one or more limbs are in fully stretched or retracted positions.

(b) Direct Kinematic Singularities. This type of singularity is very difficult to solve (Merlet, 1989; St.-Onge and Gosselin, 1996). Although it is impossible to find all singularities, some of them can be identified by an examination of the matrix J_x . For example, when the moving platform falls on top of the fixed base, $\mathbf{n}_i = 0$, identically, for $i = 1$ to 6. The manipulator gains 3 degrees of freedom. That is, the moving platform can make an infinitesimal rotation about any axis on the x - y plane. It can also make an infinitesimal translation along the z -axis.

Another direct kinematic singularity occurs when the geometry of the manipulator satisfies the following conditions:

1. The geometry of the moving platform is identical to that of the fixed platform.
2. The manipulator assumes a configuration in which the limb lengths are equal to one another.
3. All the limbs are parallel to each other.

When the foregoing conditions are met, the moving platform gains 2 translational degrees of freedom. Namely, it can be positioned anywhere on a spherical surface of a radius equal to the length of a limb and centered at the geometric center of the fixed platform. The orientation of the moving platform remains unchanged throughout this motion. There are infinitely many such configurations, whenever the condition $d_1 = d_2 = \dots = d_6$ is met. Finally, we note that a combined singularity cannot occur within the workspace of the manipulator since J_q is an identity matrix.

5.5 WRENCHES AND RECIPROCAL SCREWS

The concept of twist is a convenient way of describing either finite or infinitesimal displacements of a rigid body in three-dimensional space. For statics, a similar concept can be defined. It is well known that any system of forces and couples acting on a rigid body can be reduced to a resultant force and a couple about any point of interest. In general, the resultant force vector and the couple are not collinear. However, it can be shown that there exists a unique axis with respect to which the system of forces and couples can be reduced to a resulting force, \mathbf{f} , acting along the axis and a couple, \mathbf{c} , about the same axis. This force and couple combination is called a *wrench* (Roth, 1984; Yuan et al., 1971). The unique axis is called the *wrench axis* or *screw axis* of the system of forces and couples. Similar to a twist, the *pitch* of a wrench is defined as the ratio of the couple to the force (i.e., $\lambda_r = c/f$).

A unit wrench, $\hat{\$}_r$, is defined with respect to a reference frame by a pair of vectors:

$$\hat{\$}_r = \begin{bmatrix} \mathbf{s}_r \\ \mathbf{s}_{ro} \times \mathbf{s}_r + \lambda_r \mathbf{s}_r \end{bmatrix} = \begin{bmatrix} S_{r1} \\ S_{r2} \\ S_{r3} \\ S_{r4} \\ S_{r5} \\ S_{r6} \end{bmatrix}, \quad (5.33)$$

where \mathbf{s}_r is a unit vector pointing along the direction of the screw axis, \mathbf{s}_{ro} is the position vector of any point on the screw axis, and the vector $\mathbf{s}_{ro} \times \mathbf{s}_r$ defines the moment of the screw axis about the origin of the reference frame chosen. For a pure force, $\lambda_r = 0$, the unit wrench reduces to

$$\hat{\$}_r = \begin{bmatrix} \mathbf{s}_r \\ \mathbf{s}_{ro} \times \mathbf{s}_r \end{bmatrix}. \quad (5.34)$$

For a pure couple, $\lambda_r = \infty$, the unit wrench is defined as

$$\hat{\$}_r = \begin{bmatrix} \mathbf{0} \\ \mathbf{s}_r \end{bmatrix}. \quad (5.35)$$

Following the definition above, a wrench of intensity ρ can be written in terms of the unit wrench as

$$\$_r = \rho \hat{\$}_r. \quad (5.36)$$

We observe that the first three components of a wrench represent the resulting force, \mathbf{f} , and the last three components represent the resulting moment due to the combined effects of the force \mathbf{f} and the couple \mathbf{c} about the origin of the reference frame.

The concept of reciprocal screws was first studied by Ball (1900), followed by Waldron (1969), Hunt (1970, 1978), Roth (1984), and others. If a wrench acts on a rigid body in such a way that it produces no work while the body is undergoing an infinitesimal twist, the two screws are said to be *reciprocal screws*. Figure 5.9 shows a rigid body that is exerted by a wrench $\$_r = \rho \$_r$ while it is undergoing an infinitesimal twist $\$ = \dot{q} \$$. Recall that the first three components of a twist represent the angular velocity and the last three components represent the linear velocity of a point that is instantaneously coincident with the origin of the reference frame. Hence the virtual work performed between the wrench and the twist is given by

$$\delta W = \rho \dot{q} [\$ \cdot (\mathbf{s}_{ro} \times \mathbf{s}_r + \lambda_r \mathbf{s}_r) + \mathbf{s}_r \cdot (\mathbf{s}_o \times \mathbf{s} + \lambda \mathbf{s})] \\ = \rho \dot{q} [(\lambda + \lambda_r)(\mathbf{s} \cdot \mathbf{s}_r) + \mathbf{s}_r \cdot (\mathbf{s}_o \times \mathbf{s}) + \mathbf{s} \cdot (\mathbf{s}_{ro} \times \mathbf{s}_r)]. \quad (5.37)$$

From the geometry of the lines associated with the two screws, it can be shown that

$$\mathbf{s} \cdot \mathbf{s}_r = c\alpha, \quad (5.38)$$

$$\mathbf{s}_r \cdot (\mathbf{s}_o \times \mathbf{s}) + \mathbf{s} \cdot (\mathbf{s}_{ro} \times \mathbf{s}_r) = -\mathbf{a} \cdot (\mathbf{s} \times \mathbf{s}_r) = -as\alpha, \quad (5.39)$$

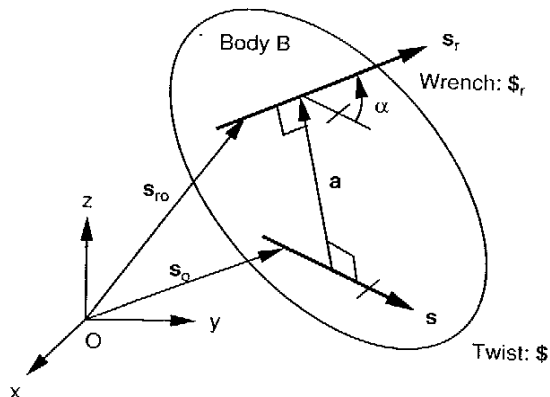


FIGURE 5.9. Twist and wrench in three-dimensional space.

where \mathbf{a} is a vector along the common perpendicular leading from the screw axis of $\$$ to $\$_r$ and α is the twist angle between the axes of $\$$ and $\$_r$, measured from $\$$ to $\$_r$ about the common perpendicular, \mathbf{a} , according to the right-hand rule. Substituting Eqs. (5.38) and (5.39) into (5.37), we obtain

$$\delta W = \rho \dot{q} [(\lambda + \lambda_r)c\alpha - as\alpha]. \quad (5.40)$$

By definition, the virtual work produced by the two reciprocal screws is equal to zero. Since ρ and \dot{q} are generally not equal to zero, the reciprocal condition can be stated as

$$\eta = (\lambda + \lambda_r)c\alpha - as\alpha = 0. \quad (5.41)$$

The quantity η in Eq. (5.41) is called the *virtual coefficient* between the twist and wrench. We note that the virtual coefficient is independent of the intensities of the twist and wrench. If $\eta = 0$, then regardless of the intensities of the twist and wrench, the wrench will not produce any work while the rigid body undergoes an infinitesimal twist. Since the virtual coefficient is symmetrical in λ and λ_r , the two screws $\$$ and $\$_r$ can be interchanged without affecting their reciprocal properties.

For convenience, we define the *transpose of a screw* as

$$\$^T = [S_4 \ S_5 \ S_6 \ S_1 \ S_2 \ S_3],$$

such that the *generalized inner product* or the *orthogonal product* of two screws $\$_r$ and $\$$ is given by

$$\$_r \$ = S_1 S_{r4} + S_2 S_{r5} + S_3 S_{r6} + S_4 S_{r1} + S_5 S_{r2} + S_6 S_{r3}.$$

Then the reciprocal condition can be stated as

$$\delta W = \$_r^T \$ = 0. \quad (5.42)$$

Equation (5.41) or (5.42) imposes one geometric constraint on the two reciprocal screws. Since a unit screw requires five independent parameters to specify its location and pitch, there is a quadruple infinitude (∞^4) of screws reciprocal to a given screw. Thus all screws that are reciprocal to a single screw form a 5-system in three-dimensional space. Theoretically, any five screws selected from the 5-system can be used as "wrenches" to constrain the rigid body to a single-degree-of-freedom motion. Similarly, there is a triple infinitude (∞^3) of screws reciprocal to the single infinitude of screws associated with a 2-system, and these reciprocal screws form a 4-system. Any four screws selected from the 4-system can be used as "wrenches" to constrain

the rigid body to a 2-dof motion. The 3-system and its reciprocal system both contain a double infinitude (∞^2) of screws. A more detailed description of screw systems can be found in Hunt (1970).

In general, the condition for reciprocity is satisfied if the point of application of a wrench remains stationary while the rigid body is undergoing an instantaneous twist about some axis. For a wrench of zero pitch (i.e., a pure force) the condition is satisfied if either the contact point does not move at all or moves in a direction orthogonal to the applied force.

In what follows, we study the reciprocal screw systems associated with some frequently used kinematic pairs and chains that can be used as guidelines for the development of Jacobian matrices of parallel manipulators.

5.5.1 Reciprocal Screws of Some Kinematic Pairs

The screws and reciprocal screws associated with some frequently used joints are listed below.

Revolute Joint. The unit screw associated with a revolute joint is a screw of zero pitch pointing along the joint axis. The reciprocal screws form a 5-system. In particular, those zero-pitch reciprocal screws lie on all planes containing the axis of the revolute joint.

Prismatic Joint. The unit screw associated with a prismatic joint is a screw of infinite pitch pointing along the direction of sliding. The reciprocal screws form a 5-system, and those zero-pitch reciprocal screws lie on all planes perpendicular to the axis of the prismatic joint.

Spherical Joint. The unit screws associated with a spherical joint form a 3-system of zero pitch passing through the center of the joint. The reciprocal screws also form a 3-system of zero pitch passing through the center of the sphere.

Universal Joint. The unit screws associated with a universal joint form a 2-system of zero pitch. It is a planar pencil radiating from the center of the universal joint and lying on a plane that contains the two axes of revolution. The reciprocal screws form a 4-system. All zero-pitch reciprocal screws either pass through the center of the universal joint or lie on a plane defined by the axes of the universal joint. Furthermore, there exists an infinite-pitch reciprocal screw that passes through the center of the universal joint and is perpendicular to both joint axes.

5.5.2 Reciprocal Screws of Some Kinematic Chains

Reciprocal screws associated with a kinematic chain can be found by an intersection of the systems of reciprocal screws associated with the joints of the kinematic chain.

Universal–Spherical Dyad. The joint screws associated with a universal–spherical dyad form a 5-system. Hence the reciprocal screw is a 1-system. Because of the presence of a spherical joint and a universal joint, the reciprocal screw is a zero-pitch screw passing through the centers of the two joints.

Revolute–Spherical Dyad. The joint screws associated with a revolute–spherical dyad form a 4-system. The reciprocal screws form a 2-system. Because of the presence of a spherical joint, all reciprocal screws are zero-pitch screws passing through the center of the spherical joint. Due to the presence of a revolute joint, the reciprocal screws must also lie on a plane containing the axis of the revolute joint. Hence all the reciprocal screws are zero-pitch screws forming a planar pencil, as shown in Fig. 5.10.

Prismatic–Spherical Dyad. The joint screws associated with a prismatic–spherical dyad form a 4-system. The reciprocal screws form a 2-system. Because of the presence of a spherical joint, all reciprocal screws are zero-pitch screws passing through the center of the sphere. Furthermore, due to the presence of a prismatic joint, the reciprocal screws must also lie on a plane that

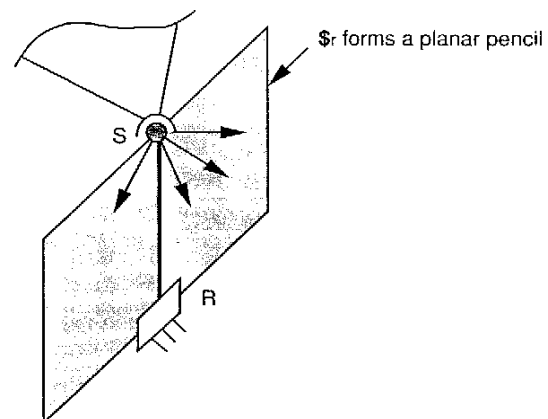


FIGURE 5.10. Revolute–spherical dyad and its reciprocal screw system.

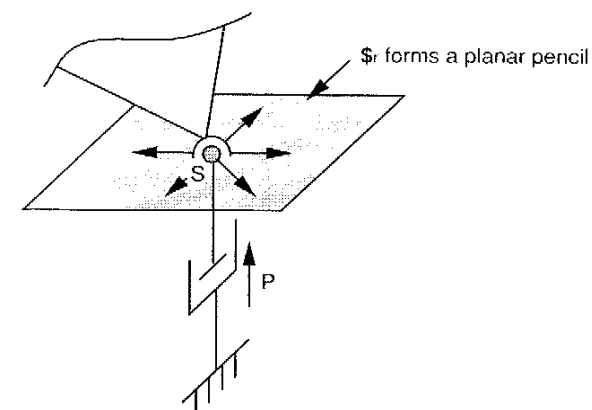


FIGURE 5.11. Prismatic-spherical dyad and its reciprocal screw system.

is perpendicular to the axis of the prismatic joint. Hence all the reciprocal screws are zero-pitch screws forming a planar pencil, as shown in Fig. 5.11.

Surface Contact Pair. Figure 5.12 shows a rigid body B that contacts another body A at point O , where the two contacting surfaces are free to roll

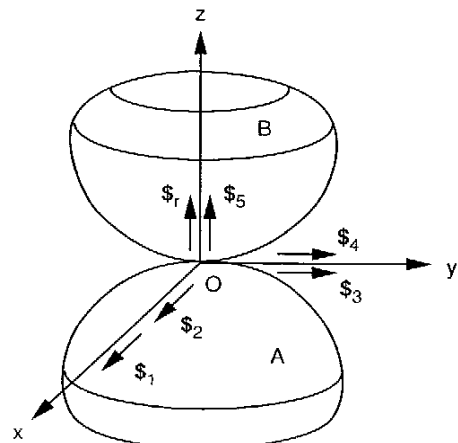


FIGURE 5.12. Two rigid bodies contacting at a point.

and slide with respect to one another. We wish to study the screws associated with this contact pair and its reciprocal screw.

The rigid body B possesses 5 degrees of freedom. Its instantaneous motion can be described by a linear combination of the following five unit screws:

$$\begin{aligned}\hat{\$}_1 &= [1, 0, 0, 0, 0, 0]^T, \\ \hat{\$}_2 &= [0, 0, 0, 1, 0, 0]^T, \\ \hat{\$}_3 &= [0, 1, 0, 0, 0, 0]^T, \\ \hat{\$}_4 &= [0, 0, 0, 0, 1, 0]^T, \\ \hat{\$}_5 &= [0, 0, 1, 0, 0, 0]^T.\end{aligned}\quad (5.43)$$

Since the screws associated with the contact pair form a 5-system, there exists a unique reciprocal screw. Because $\hat{\$}_1$, $\hat{\$}_3$, and $\hat{\$}_5$ are three intersecting zero-pitch screws, the reciprocal screw is a zero-pitch screw passing through the point of contact. Furthermore, due to the presence of two infinite-pitch screws, $\hat{\$}_2$ and $\hat{\$}_4$, the reciprocal screw must be perpendicular to both x and y axes. Hence we conclude that the reciprocal screw is given by

$$\hat{\$}_r = [0, 0, 0, 0, 0, 1]^T. \quad (5.44)$$

5.6 SCREW-BASED JACOBIAN

A parallel manipulator typically consists several limbs, say m . Each limb is made up of several links connected by various joints. Usually, one or more joints in each limb are driven by actuators, while the remaining joints are passive. Figure 5.13 shows the joint screws associated with a typical limb, where the first subscript denotes the joint number and the second subscript represents the limb number. Since we can always replace a cylindrical joint by a revolute joint plus a coaxial prismatic joint, and a spherical joint by three noncoplanar intersecting revolute joints, we may consider each limb as an open-loop chain connecting a moving platform to a fixed base by ℓ 1-dof joints. In this way, the instantaneous twist, $\$_p$, of the moving platform can be expressed as a linear combination of ℓ instantaneous twists (Mohamed and Duffy, 1985):

$$\$_p = \sum_{j=1}^{\ell} \dot{q}_{j,i} \hat{\$}_{j,i} \quad \text{for } i = 1, 2, \dots, m, \quad (5.45)$$

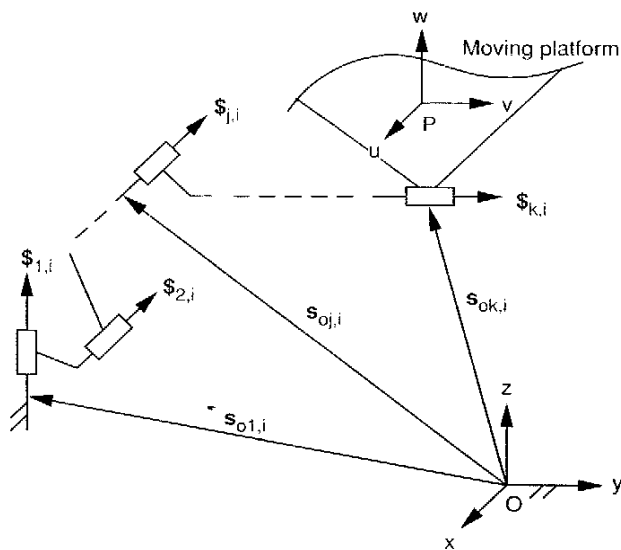


FIGURE 5.13. The i th limb of a parallel manipulator.

where $\dot{q}_{j,i}$ denotes the intensity and $\hat{\$}_j,i$ represents a unit screw associated with the j th joint of the i th limb. Recall that the end-effector twist is defined as

$$\$_p = \begin{bmatrix} \omega_n \\ \mathbf{v}_o \end{bmatrix}. \quad (5.46)$$

Equation (5.45) contains many unactuated joint screws which can be eliminated by applying the theory of reciprocal screws. Assuming that the actuated joints in each limb appear in the first g terms, we first identify g unit screws, $\hat{\$}_{rj,i}$ for $j = 1, 2, \dots, g$, each of which is reciprocal to all the unactuated joint screws in the i th limb. Then we perform the orthogonal product of both sides of Eq. (5.45) with each reciprocal screw. This produces g equations, which can be written in matrix form as

$$J_{x,i}\$_p = J_{q,i}\dot{\mathbf{q}}_i. \quad (5.47)$$

where

$$J_{x,i} = \begin{bmatrix} \hat{\$}_{r1,i}^T \\ \hat{\$}_{r2,i}^T \\ \vdots \\ \hat{\$}_{rg,i}^T \end{bmatrix},$$

$$J_{q,i} = \begin{bmatrix} \hat{\$}_{r1,i}^T \$_{1,i} & \hat{\$}_{r1,i}^T \$_{2,i} & \cdots & \hat{\$}_{r1,i}^T \$_{g,i} \\ \hat{\$}_{r2,i}^T \$_{1,i} & \hat{\$}_{r2,i}^T \$_{2,i} & \cdots & \hat{\$}_{r2,i}^T \$_{g,i} \\ \vdots & \vdots & \ddots & \vdots \\ \hat{\$}_{rg,i}^T \$_{1,i} & \hat{\$}_{rg,i}^T \$_{2,i} & \cdots & \hat{\$}_{rg,i}^T \$_{g,i} \end{bmatrix},$$

$$\dot{\mathbf{q}}_i = [\dot{q}_{1,i}, \dots, \dot{q}_{g,i}]^T.$$

Equation (5.47) written m times, once for each limb, yields $n = m \times g$ linear equations, which can be assembled in the form

$$J_x\$_p = J_q\dot{\mathbf{q}}, \quad (5.48)$$

where

$$J_x = \begin{bmatrix} J_{x,1} \\ J_{x,2} \\ \vdots \\ J_{x,m} \end{bmatrix},$$

$$J_q = \begin{bmatrix} [J_{q,1}] & 0 & \cdots & 0 \\ 0 & [J_{q,2}] & \cdots & 0 \\ \vdots & \vdots & \ddots & \vdots \\ 0 & 0 & \cdots & [J_{q,m}] \end{bmatrix},$$

$$\dot{\mathbf{q}} = [\dot{q}_{1,1}, \dots, \dot{q}_{g,1}, \dot{q}_{1,2}, \dots, \dot{q}_{g,2}, \dots, \dot{q}_{g,m}]^T.$$

Note that each row of J_x represents the transpose of a reciprocal screw.

The twists associated with all the joints of a limb form an ℓ -system provided that they are linearly independent. Let d be the dimension of the motion space ($d = 6$ for spatial and $d = 3$ for planar and spherical motions). Obviously, if $\ell = d$, there exists no screw reciprocal to the ℓ -system of twists. If $\ell < d$, there are $(d - \ell)$ linearly independent screws which form a $(d - \ell)$ -system. Every screw in the $(d - \ell)$ -system is reciprocal to the ℓ -system of twists. For a limb with k unactuated joints, there exist $(d - k)$ linearly inde-

pendent screws that form a $(d-k)$ -system. Every screw in the $(d-k)$ -system is reciprocal to every unactuated joint screw of the limb. Clearly, the $(d-k)$ -system contains the $(d-\ell)$ -system. Any screw taken from the $(d-k)$ -system, provided that it does not belong to the $(d-\ell)$ -system, can be used as a reciprocal screw, $\hat{\$}_{rj,i}$, to formulate of the Jacobian matrices. Hence there are plenty of reciprocal screws from which to choose. Furthermore, if each reciprocal screw is chosen to be reciprocal to all the joint screws, except for just one of the actuated joint screws, $J_{q,i}$ reduces to

$$J_{q,i} = \begin{bmatrix} \hat{\$}_{r1,i}^T \hat{\$}_{1,i} & 0 & \cdots & 0 \\ 0 & \hat{\$}_{r2,i}^T \hat{\$}_{2,i} & \cdots & 0 \\ \vdots & \vdots & \cdots & \vdots \\ 0 & 0 & \cdots & \hat{\$}_{rg,i}^T \hat{\$}_{g,i} \end{bmatrix}. \quad (5.49)$$

Hence J_q becomes a diagonal matrix, and the nonzero elements are given by the orthogonal products of the actuated joint screws with their corresponding reciprocal screws.

5.6.1 Screw-based Jacobian of a Stewart–Gough Platform

In this example, the Jacobian matrix of the Stewart–Gough platform shown in Fig. 3.15 is derived by applying the concept of reciprocal screws. Figure 5.14 depicts the equivalent kinematic chain of an *UPS* limb, where the lower spherical joint is replaced by two intersecting unit screws, $\hat{\$}_1$ and $\hat{\$}_2$, and the upper spherical joint is replaced by three intersecting unit screws, $\hat{\$}_4$, $\hat{\$}_5$, and $\hat{\$}_6$, respectively. The prismatic joint is denoted by $\hat{\$}_3$. Thus the passive degree of freedom between the *S–S* pair is eliminated.

As described in Chapter 3, two Cartesian coordinate systems $A(x, y, z)$ and $B(u, v, w)$ are attached to the fixed base and moving platform, respectively. Furthermore, we define an instantaneous reference frame $C(x', y', z')$, with its origin located at point P and the x' , y' , and z' axes parallel to the x , y , and z axes of the fixed frame. Then we express all the joint screws with respect to this instantaneous reference frame.

There are six joint screws associated with each limb. The third joint is the only actuated joint; the remaining five are passive. The actuated joint screw is an infinite pitch screw. Let $s_{j,i}$ be a unit vector along the j th joint axis of the i th limb. Then the six unit joint screws of a limb can be written as

$$\hat{\$}_{1,i} = \begin{bmatrix} s_{1,i} \\ (\mathbf{b}_i - \mathbf{d}_i) \times s_{1,i} \end{bmatrix},$$

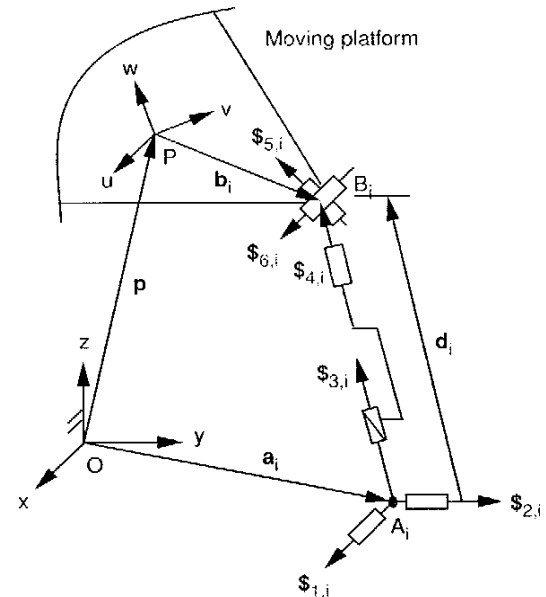


FIGURE 5.14. Equivalent kinematic structure of an *SPS* limb.

$$\begin{aligned} \hat{\$}_{2,i} &= \begin{bmatrix} s_{2,i} \\ (\mathbf{b}_i - \mathbf{d}_i) \times s_{2,i} \end{bmatrix}, \\ \hat{\$}_{3,i} &= \begin{bmatrix} \mathbf{0} \\ s_{3,i} \end{bmatrix}, \\ \hat{\$}_{4,i} &= \begin{bmatrix} s_{4,i} \\ \mathbf{b}_i \times s_{4,i} \end{bmatrix}, \\ \hat{\$}_{5,i} &= \begin{bmatrix} s_{5,i} \\ \mathbf{b}_i \times s_{5,i} \end{bmatrix}, \\ \hat{\$}_{6,i} &= \begin{bmatrix} s_{6,i} \\ \mathbf{b}_i \times s_{6,i} \end{bmatrix}, \end{aligned}$$

where $\mathbf{b}_i = \overline{PB_i}$, $\mathbf{d}_i = \overline{A_iB_i} = d_i s_{3,i}$, and $s_{3,i} = s_{4,i}$.

We now consider each limb as an open-loop chain and express the instantaneous twist of the moving platform in terms of the joint screws:

$$\dot{s}_p = \dot{\theta}_{1,i} \hat{s}_{1,i} + \dot{\theta}_{2,i} \hat{s}_{2,i} + \dot{d}_i \hat{s}_{3,i} + \dot{\theta}_{4,i} \hat{s}_{4,i} + \dot{\theta}_{5,i} \hat{s}_{5,i} + \dot{\theta}_{6,i} \hat{s}_{6,i}. \quad (5.50)$$

Since the axes of all the unactuated joints in each limb intersect the line passing through points A_i and B_i , a unique screw that is reciprocal to all the unactuated joint screws is readily identified as

$$\hat{s}_{r3,i} = \begin{bmatrix} s_{3,i} \\ \mathbf{b}_i \times s_{3,i} \end{bmatrix}. \quad (5.51)$$

Taking the orthogonal product of both sides of Eq. (5.50) with (5.51), we obtain

$$\hat{s}_{r3,i}^T \dot{s}_p = \dot{d}_i \quad \text{for } i = 1, 2, \dots, 6. \quad (5.52)$$

Writing Eq. (5.52) six times, once for each limb, we obtain

$$J_x \dot{\mathbf{x}} = J_q \dot{\mathbf{q}}, \quad (5.53)$$

where

$$J_x = \begin{bmatrix} (\mathbf{b}_1 \times s_{3,1})^T & s_{3,1}^T \\ (\mathbf{b}_2 \times s_{3,2})^T & s_{3,2}^T \\ \vdots & \vdots \\ (\mathbf{b}_6 \times s_{3,6})^T & s_{3,6}^T \end{bmatrix},$$

$$J_q = I(6 \times 6 \text{ identity matrix}),$$

$$\dot{\mathbf{x}} = [\omega_x, \omega_y, \omega_z, v_{px}, v_{py}, v_{pz}]^T,$$

$$\dot{\mathbf{q}} = [\dot{d}_1, \dot{d}_2, \dot{d}_3, \dot{d}_4, \dot{d}_5, \dot{d}_6]^T.$$

We note that $s_{3,i}$ represents the same unit vector, s_i , used in Eqs. (5.29)–(5.31). Hence when the first and the last three columns of J_x are interchanged, the screw-based Jacobian becomes the conventional Jacobian. We have arrived at the same result as that obtained earlier using the conventional velocity vector-loop method.

5.6.2 Screw-based Jacobian of a Platform Manipulator Driven by Three Planar Motors

Figure 5.15 shows a 6-dof parallel manipulator developed by Tsai and Tahmasebi (1993). This manipulator is made up of a moving platform, a fixed

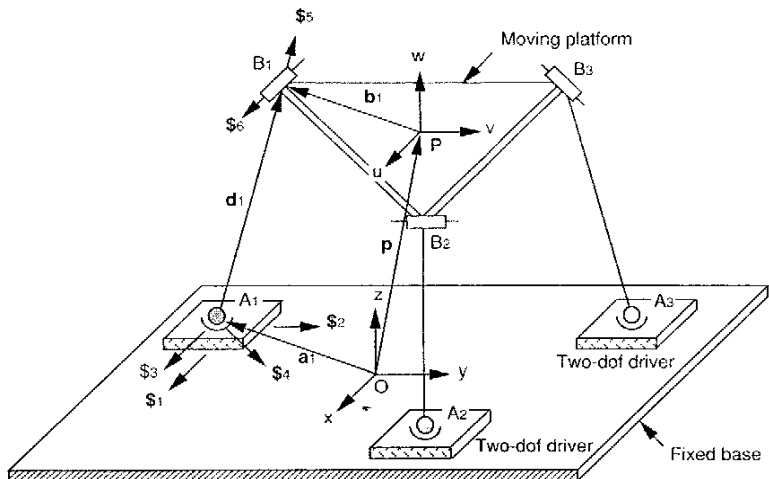


FIGURE 5.15. Platform manipulator driven by three planar motors.

base, and three inextensible limbs, $A_i B_i$ for $i = 1$ to 3. The upper end of each limb is connected to the moving platform by a revolute joint, while the lower end is connected to a planar 2-dof driver by a spherical joint. The revolute joint axes at B_1 , B_2 , and B_3 lie on a plane defined by B_1 , B_2 , and B_3 . The manipulator motion is obtained by moving the planar motors on the x - y plane of the fixed base. The direct kinematics of this manipulator can be found in Tahmasebi and Tsai (1994). In this section, we derive the Jacobian matrix of the manipulator by means of reciprocal screws.

As shown in Fig. 5.15, two Cartesian coordinate systems, $A(x, y, z)$ and $B(u, v, w)$, are attached to the fixed base and moving platform, respectively. The origin of the (u, v, w) frame is located at the centroid P of the moving platform with the u and v axes lying on the plane of $B_1 B_2 B_3$. The location of the moving platform relative to the fixed base is described by a rotation matrix ${}^A R_B$, and the position vector of the centroid \mathbf{p} .

Figure 5.15 also shows an equivalent limb in which the spherical joint is replaced by three noncoplanar intersecting revolute joints, $\hat{s}_{3,i}$, $\hat{s}_{4,i}$, and $\hat{s}_{5,i}$. The axis of $\hat{s}_{3,i}$ is aligned with the x -axis, the axis of $\hat{s}_{5,i}$ is aligned with the longitudinal axis of the limb, and the axis of $\hat{s}_{4,i}$ is perpendicular to both $\hat{s}_{3,i}$ and $\hat{s}_{5,i}$. The first joint screw, $\hat{s}_{1,i}$, points along the x -direction. The second joint screw, $\hat{s}_{2,i}$, points along the y -direction. The sixth joint screw, $\hat{s}_{6,i}$, lies on the $u-v$ plane. Overall, there are six joint screws associated with the

equivalent limb. The first two are actuated prismatic joints, while the remaining four are passive revolute joints.

To facilitate the analysis, we define an instantaneous reference frame, $C(x', y', z')$, with its origin located at point P and the x' , y' , and z' axes parallel to the x , y , and z axes of the fixed frame. Then we express all the unit joint screws with respect to this instantaneous reference frame as follows:

$$\begin{aligned}\hat{\$}_{1,i} &= \begin{bmatrix} \mathbf{0} \\ s_{1,i} \end{bmatrix}, \\ \hat{\$}_{2,i} &= \begin{bmatrix} \mathbf{0} \\ s_{2,i} \end{bmatrix}, \\ \hat{\$}_{3,i} &= \begin{bmatrix} \mathbf{s}_{3,i} \\ (\mathbf{b}_i - \mathbf{d}_i) \times \mathbf{s}_{3,i} \end{bmatrix}, \\ \hat{\$}_{4,i} &= \begin{bmatrix} \mathbf{s}_{4,i} \\ (\mathbf{b}_i - \mathbf{d}_i) \times \mathbf{s}_{4,i} \end{bmatrix}, \\ \hat{\$}_{5,i} &= \begin{bmatrix} \mathbf{s}_{5,i} \\ \mathbf{b}_i \times \mathbf{s}_{5,i} \end{bmatrix}, \\ \hat{\$}_{6,i} &= \begin{bmatrix} \mathbf{s}_{6,i} \\ \mathbf{b}_i \times \mathbf{s}_{6,i} \end{bmatrix},\end{aligned}$$

where $\mathbf{s}_{1,i} = \mathbf{s}_{3,i} = [1, 0, 0]^T$, $\mathbf{s}_{2,i} = [0, 1, 0]^T$, $\mathbf{a}_i = \overline{OA_i}$, $\mathbf{b}_i = \overline{PB_i}$, $\mathbf{d}_i = \overline{A_iB_i}$, $s_{5,i} = \mathbf{d}_i/d_i$, and $\mathbf{s}_{4,i} = \mathbf{s}_{5,i} \times \mathbf{s}_{3,i}$.

We now consider each limb as an open-loop chain and express the instantaneous twist, $\$_p$, of the moving platform in terms of the joint screws:

$$\$_p = v_{x,i}\hat{\$}_{1,i} + v_{y,i}\hat{\$}_{2,i} + \dot{\theta}_{3,i}\hat{\$}_{3,i} + \dots + \dot{\theta}_{6,i}\hat{\$}_{6,i} \quad i = 1, 2, 3, \quad (5.54)$$

where $v_{x,i}$ and $v_{y,i}$ denote the linear velocities of the planar motor along the x and y directions, and $\dot{\theta}_{3,i}, \dots, \dot{\theta}_{6,i}$ denote the passive joint rates.

Since there is a spherical joint at the lower end and a revolute joint at the upper end, all screws that are reciprocal to the unactuated joint screws form a planar pencil. Specifically, all the reciprocal screws are zero-pitch screws passing through A_i and lying on a plane H_i that contains the axis of $\hat{\$}_{6,i}$ and point A_i .

Theoretically, any two screws taken from the reciprocal screw system contained in H_i can be used to formulate the Jacobian matrix. Perhaps the most straightforward approach is to identify two reciprocal screws, each reciprocal to all the joint screws except for only one of the two infinite pitch screws, $\hat{\$}_{1,i}$ and $\hat{\$}_{2,i}$.

Let $\mathbf{n}_i = [n_{x,i}, n_{y,i}, n_{z,i}]^T$ be a unit vector defined by the cross product of $\mathbf{s}_{5,i}$ and $\mathbf{s}_{6,i}$; that is,

$$\mathbf{n}_i = \mathbf{s}_{5,i} \times \mathbf{s}_{6,i}. \quad (5.55)$$

Then a screw that is reciprocal to all screws except for $\hat{\$}_{1,i}$ is obtained by an intersection of the H_i -plane and a plane that passes point A_i and is parallel to the $x-z$ plane.

$$\hat{\$}_{r1,i} = \begin{bmatrix} \mathbf{s}_{r1,i} \\ (\mathbf{b}_i - \mathbf{d}_i) \times \mathbf{s}_{r1,i} \end{bmatrix}, \quad \text{where } \mathbf{s}_{r1,i} = \frac{[n_{z,i} \ 0 \ -n_{x,i}]^T}{\sqrt{1 - n_{y,i}^2}}. \quad (5.56)$$

Similarly, a screw that is reciprocal to all screws except for $\hat{\$}_{2,i}$ is obtained by an intersection of the H_i -plane and a plane that passes point A_i and is parallel to the $y-z$ plane.

$$\hat{\$}_{r2,i} = \begin{bmatrix} \mathbf{s}_{r2,i} \\ (\mathbf{b}_i - \mathbf{d}_i) \times \mathbf{s}_{r2,i} \end{bmatrix}, \quad \text{where } \mathbf{s}_{r2,i} = \frac{[0 \ n_{z,i} \ -n_{y,i}]^T}{\sqrt{1 - n_{x,i}^2}}. \quad (5.57)$$

Taking the orthogonal products of both sides of Eq. (5.54) with (5.56) and (5.57) in turn, the resulting equations can be arranged in matrix form:

$$\begin{bmatrix} ((\mathbf{b}_i - \mathbf{d}_i) \times \mathbf{s}_{r1,i})^T & \mathbf{s}_{r1,i}^T \\ ((\mathbf{b}_i - \mathbf{d}_i) \times \mathbf{s}_{r2,i})^T & \mathbf{s}_{r2,i}^T \end{bmatrix} \begin{bmatrix} \omega_p \\ \mathbf{v}_p \end{bmatrix} = \begin{bmatrix} \frac{n_{z,i}}{\sqrt{1 - n_{y,i}^2}} & 0 \\ 0 & \frac{n_{z,i}}{\sqrt{1 - n_{x,i}^2}} \end{bmatrix} \begin{bmatrix} v_{x,i} \\ v_{y,i} \end{bmatrix}. \quad (5.58)$$

Writing Eqs. (5.58) three times, once for each limb, we obtain

$$J_x \dot{\mathbf{x}} = J_q \dot{\mathbf{q}}, \quad (5.59)$$

where

$$J_x = \begin{bmatrix} ((\mathbf{b}_1 - \mathbf{d}_1) \times \mathbf{s}_{r1,1})^T & \mathbf{s}_{r1,1}^T \\ ((\mathbf{b}_1 - \mathbf{d}_1) \times \mathbf{s}_{r2,1})^T & \mathbf{s}_{r2,1}^T \\ ((\mathbf{b}_2 - \mathbf{d}_2) \times \mathbf{s}_{r1,2})^T & \mathbf{s}_{r1,2}^T \\ ((\mathbf{b}_2 - \mathbf{d}_2) \times \mathbf{s}_{r2,2})^T & \mathbf{s}_{r2,2}^T \\ ((\mathbf{b}_3 - \mathbf{d}_3) \times \mathbf{s}_{r1,3})^T & \mathbf{s}_{r1,3}^T \\ ((\mathbf{b}_3 - \mathbf{d}_3) \times \mathbf{s}_{r2,3})^T & \mathbf{s}_{r2,3}^T \end{bmatrix},$$

$$J_q = \begin{bmatrix} \frac{n_{z,1}}{\sqrt{1-n_{y,1}^2}} & 0 & 0 & 0 & 0 & 0 \\ 0 & \frac{n_{z,1}}{\sqrt{1-n_{x,1}^2}} & 0 & 0 & 0 & 0 \\ 0 & 0 & \frac{n_{z,2}}{\sqrt{1-n_{y,2}^2}} & 0 & 0 & 0 \\ 0 & 0 & 0 & \frac{n_{z,2}}{\sqrt{1-n_{x,2}^2}} & 0 & 0 \\ 0 & 0 & 0 & 0 & \frac{n_{z,3}}{\sqrt{1-n_{y,3}^2}} & 0 \\ 0 & 0 & 0 & 0 & 0 & \frac{n_{z,3}}{\sqrt{1-n_{x,3}^2}} \end{bmatrix},$$

$$\dot{x} = [\omega_x, \omega_y, \omega_z, v_{px}, v_{py}, v_{pz}]^T,$$

$$\dot{q} = [v_{x,1}, v_{y,1}, v_{x,2}, v_{y,2}, v_{x,3}, v_{y,3}]^T.$$

Although it is difficult to identify all the possible singular configurations of this manipulator, some of them can be found by inspection of the J_q and J_x matrices.

(a) Inverse Kinematic Singularities. We note that the nonzero elements of J_q are proportional to the z -components of the three unit vectors \mathbf{n}_i for $i = 1, 2$, and 3 . Hence an inverse kinematic singularity occurs when $n_{z,i} = 0$ for $i = 1$ or 2 or 3 . Physically, when one of the limbs points in the z -direction, the manipulator loses 2 degrees of freedom. Under such a condition, a differential motion of the planar motor about the x or y axis does not affect the velocity of the moving platform. If two or three limbs point in the z -direction simultaneously, 4 or 6 degrees of freedom will be lost.

(b) Direct Kinematic Singularities. A trivial direct kinematic singularity occurs when $n_{x,i} = n_{y,i} = 0$ for all the limbs. Under such a condition, the sixth column of J_x becomes zero identically, and the manipulator gains 1 degree of freedom. Physically, this corresponds to the configuration in which both the moving platform and the three limbs lie on the $x-y$ plane. Hence the moving platform can make an infinitesimal translation along the z -axis while all the actuators are locked.

A second direct kinematic singularity occurs when the following three conditions are satisfied simultaneously: (1) $\Delta B_1 B_2 B_3$ is an equilateral triangle; (2) the three limbs are of equal length; and (3) A_1, A_2 , and A_3 are placed directly under the centroid of the moving platform. When these conditions are

met, the third column of J_v goes to zero, the first and fifth columns become linearly dependent, and the second and fourth columns also become linearly dependent. Hence the manipulator gains 3 rotational degrees of freedom.

A third direct kinematic singularity occurs when $n_{z,i} = 0$ for $i = 1, 2$, and 3 . When the three limbs are all pointing along the z -direction, the fourth and fifth columns of J_x are both equal to zero. The moving platform can make an infinitesimal translation along any direction parallel to the $x-y$ plane. Hence the manipulator gains 2 degrees of freedom. In fact, this is a combined singularity, since under such a condition the manipulator is also under an inverse kinematic singularity.

5.7 SUMMARY

In this chapter, the Jacobian and singular conditions of parallel manipulators have been studied. Both the conventional and screw-based Jacobian matrices were discussed. The velocity vector-loop method was employed for the derivation of conventional Jacobians, while the concept of reciprocal screws was used for the derivation of screw-based Jacobians. It was shown that the Jacobian of a parallel manipulator can conveniently be split into two matrices: one associated with the direct kinematics and the other with the inverse kinematics. Depending on which matrix is singular, the singularities of a parallel manipulator can be classified into three types. At an inverse kinematic singular configuration, a manipulator loses 1 or more degrees of freedom, while at a direct kinematic singular configuration, a manipulator gains 1 or more degrees of freedom. A combined singularity results when the inverse and direct kinematic singularities occur simultaneously. Generally, a combined singularity depends not only on the manipulator configuration but also on the kinematic architecture. The classification and physical significance of each type of singularity were illustrated by several examples.

REFERENCES

- Baker, J. E., 1980, "On Relative Freedom Between Links in Kinematic Chains with Cross-Jointing," *Mech. Mach. Theory*, Vol. 15, pp. 397-413.
- Ball, R. S., 1900, *A Treatise on the Theory of Screws*, Cambridge University Press, Cambridge.
- Davies, T. H., 1981, "Kirchhoff's Circulation Law Applied to Multi-loop Kinematic Chains," *Mech. Mach. Theory*, Vol. 16, pp. 171-183.
- Davies, T. H. and Primrose, E. J. F., 1971, "An Algebra for the Screw Systems of a Pair of Bodies in a Kinematic Chain," *Proc. 3rd World Congress on the Theory of Machines and Mechanisms*, Paper D-14, pp. 199-212.

- Gosselin, C. and Angeles, J., 1990, "Singularity Analysis of Closed-Loop Kinematic Chains," *IEEE Trans. on Robot. Autom.*, Vol. 6, No. 3, pp. 281–290.
- Hunt, K. H., 1970, *Screw Systems in Spatial Kinematics*, Department of Mechanical Engineering, Monash University, Clayton, Victoria, Australia.
- Hunt, K. H., 1978, *Kinematic Geometry of Mechanisms*, Clarendon Press, Oxford.
- Merlet, J. P., 1989, "Singular Configurations of Parallel Manipulators and Grassmann Geometry," *Int. J. Robot. Res.*, Vol. 8, No. 5, pp. 45–56.
- Mohamed, M. G. and Duffy, J., 1985, "A Direct Determination of the Instantaneous Kinematics of Fully Parallel Robot Manipulators," *ASME J. Mech. Transm. Autom. Des.*, Vol. 107, No. 2, pp. 226–229.
- Mohamed, M. G., Sanger, J., and Duffy, J., 1983, "Instantaneous Kinematics of Fully Parallel Devices," *Proc. 6th IFTOMM Congress on Theory of Machines and Mechanisms*, New Delhi, India.
- Roth, B., 1984, "Screws, Motors, and Wrenches That Cannot Be Bought in a Hardware Store," *Proc. 1st International Symposium of Robotics Research*, pp. 679–693.
- St.-Onge, B. M. and Gosselin, C., 1996, "Singularity Analysis and Representation of Spatial Six-DOF Parallel Manipulators," *Recent Advances in Robot Kinematics*, edited by J. Lenarcic and V. Parenti-Castelli, Kluwer Academic Publishers, Dordrecht, The Netherlands, pp. 389–398.
- Sugimoto, K., 1987, "Kinematic and Dynamic Analysis of Parallel Manipulators by Means of Motor Algebra," *ASME J. Mech. Transm. Autom. Des.*, Vol. 109, No. 1, pp. 3–7.
- Tahmasebi, F. and Tsai, L. W., 1994, "Closed-Form Direct Kinematics Solution of a New Parallel Mini-manipulator," *ASME J. Mech. Des.*, Vol. 116, No. 4, pp. 1141–1147.
- Tsai, L. W. and Tahmasebi, F., 1993, "Synthesis and Analysis of a New Class of Six-DOF Parallel Mini-manipulators," *J. Robot. Sys.*, Vol. 10, No. 5, pp. 561–580.
- Waldron, K. J., 1966, "The Constraint Analysis of Mechanisms," *J. Mech.*, Vol. 2, pp. 101–114.
- Waldron, K. J., 1969, "The Mobility of Linkages," Ph.D. dissertation, Department of Mechanical Engineering, Stanford University, Stanford, CA.
- Waldron, K. J. and Hunt, K. H., 1988, "Series-Parallel Dualities in Actively Coordinated Mechanisms," *Proceedings of the 4th International Symposium on Robotic Research*, MIT Press, Cambridge, MA, pp. 175–181.
- Yuan, M. S. C., Freudenstein, F., and Woo, L. S., 1971, "Kinematic Analysis of Spatial Mechanisms by Means of Screw Coordinates, Part 1: Screw Coordinates," *ASME J. Eng. Ind.*, Vol. 93, Ser. B, No. 1, pp. 61–66.
- Zlatanov, D., Fenton, R. G., and Benhabib, B., 1994, "Singularity Analysis of Mechanisms and Robots Via a Motion-Space Model of the Instantaneous Kinematics," *Proceedings of the IEEE International Conference on Robotics and Automation*, Vol. 2, pp. 980–991.

EXERCISES

- Calculate the end-effector velocity v_q as a function of input joint angles and joint rates for the planar 5R manipulator shown in Fig. 1.7. Sketch the singular loci of the manipulator.
- Derive the Jacobian matrix of the planar 4R1P manipulator shown in Fig. 3.19. Identify the singular configurations.
- We wish to move the moving platform of the planar 3PRP manipulator shown in Fig. 3.3 along the x -axis with a linear velocity of v_q m/s and zero angular velocity. Calculate the linear velocities of the input actuators.
- Derive the conventional Jacobian matrix of the DELTA robot shown in Fig. 3.21 by using the velocity vector-loop approach. Under what conditions will the manipulator gain extra degree(s) of freedom?
- Derive the conventional Jacobian matrix of the 3×3 Stewart platform shown in Fig. 3.16 by the velocity vector-loop approach. Does this manipulator possess any inverse kinematics singularities?
- Find the reciprocal screws of a spherical-universal dyad assuming that the axes of the universal joints do not pass through the center of the sphere.
- Find the reciprocal screws of a spherical-cylindrical dyad assuming that the axis of the cylindrical joint does not pass through the center of the sphere.
- Formulate the Jacobian matrix of the 3×3 Stewart platform shown in Fig. 3.16 by the method of reciprocal screws.

CHAPTER 6

STATICS AND STIFFNESS ANALYSIS

6.1 INTRODUCTION

When a manipulator performs a given task, such as lifting up a workpiece from an NC machine as shown in Fig. 6.1, its end effector exerts force and moment to the external environment at the point(s) of contact. This force and moment are generated by actuators installed at various points of connection. For brevity, we often use the term *force* to imply both force and moment. For a serial manipulator, actuator forces are transmitted through an open-loop chain to the point of contact, while for a parallel manipulator, actuator forces are transmitted through several parallel paths to the end effector.

Static force analysis is of practical importance in determining the quality of force transmission through the various joints of a mechanism. It serves as a basis for sizing the links and bearings of a robot manipulator and for selecting appropriate actuators. The results can also be used for compliance control of a robot manipulator. The statics of spatial mechanisms can be treated by various methods, such as the vector method (Beyer, 1960; Chace, 1962), the dual vector and dual number quaternions (Yang, 1965), the screw calculus (Agrawal and Roth, 1992; Bagci, 1971; Denavit et al., 1965), and the principle of virtual work (Asada and Slotine, 1986; Gosselin, 1990; Paul, 1981; Tahmasebi and Tsai, 1995).

In this chapter we develop methods for representing static forces acting on a manipulator and for transforming them between coordinate systems. The transformation of force and moment between the actuator space and the end-effector space is the focal point of study. We show that the actuator input

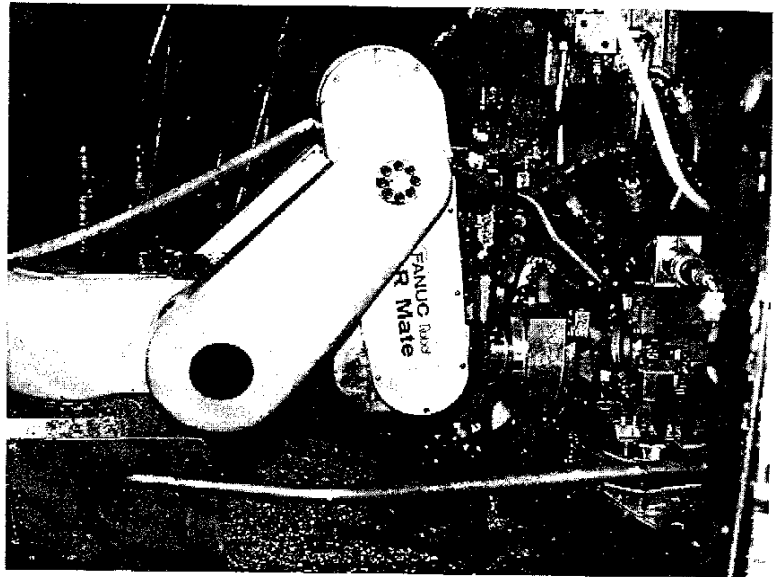


FIGURE 6.1. Fanuc LR Mate robot. (Courtesy of Fanuc Robotics North America, Inc., Rochester Hills, Michigan.)

forces are related to the end-effector output forces by the transpose of the manipulator Jacobian matrix. In addition, the free-body diagram method is introduced for the derivation of reaction forces generated at the various joints of a manipulator. A thorough understanding of the joint reaction forces is important for proper sizing of links and actuators at the design stage. Static force analysis is followed by stiffness analysis. It is shown that the end-effector output forces are related to its deflections by a matrix called the *stiffness matrix*. Both serial and parallel manipulators are studied.

6.2 STATICS OF SERIAL MANIPULATORS

In this section we study the statics of serial manipulators. First, we derive the basic equations governing the static balance of a link. Then these equations are applied for the static analysis of serial manipulators. The concept of equivalent joint torques and the transformation between the end-effector forces and equivalent joint torques are described.

6.2.1 Force and Moment Balance of a Link

In a serial manipulator, each link is connected to one or two other links by various joints. Figure 6.2 depicts the forces and moments acting on a typical link i that is connected to link $i - 1$ by joint i and to link $i + 1$ by joint $i + 1$. The forces acting on link $i + 1$ by link i in joint $(i + 1)$ can be reduced to a resultant force $\mathbf{f}_{i+1,i}$ and a resultant moment $\mathbf{n}_{i+1,i}$ about the origin O_i of the (x_i, y_i, z_i) link coordinate frame. Similarly, the forces acting on link i by link $i - 1$ in the i th joint can be reduced to a resultant force $\mathbf{f}_{i,i-1}$ and a moment $\mathbf{n}_{i,i-1}$ about the origin O_{i-1} of the $(x_{i-1}, y_{i-1}, z_{i-1})$ link coordinate frame. The following notations are defined:

$\mathbf{f}_{i+1,i}$: resulting force exerted on link $i + 1$ by link i at O_i , $\mathbf{f}_{i,i+1} = -\mathbf{f}_{i+1,i}$.

\mathbf{g} : acceleration of gravity.

m_i : mass of link i .

$\mathbf{n}_{i+1,i}$: resulting moment exerted on link $i + 1$ by link i , about point O_i ,

$$\mathbf{n}_{i,i+1} = -\mathbf{n}_{i+1,i}.$$

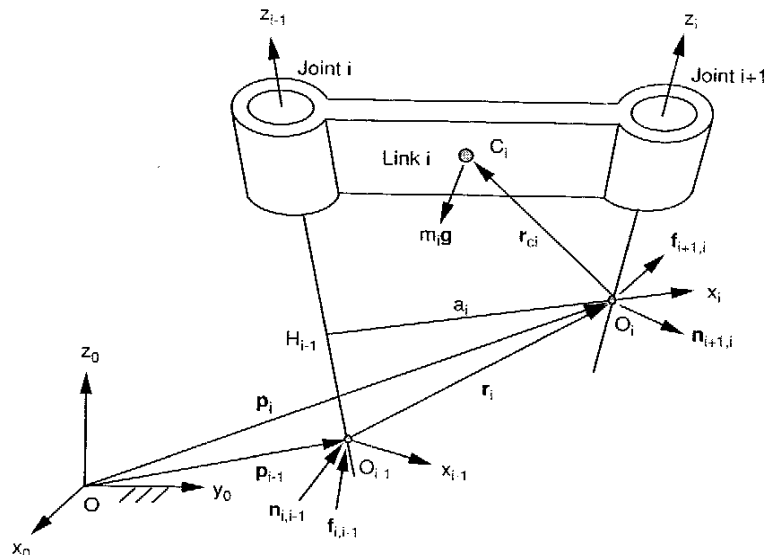


FIGURE 6.2. Forces and moments acting on link i .

\mathbf{r}_{ci} : position vector of the center of mass of link i relative to the i th link frame (i.e., $\mathbf{r}_{ci} = \overrightarrow{O_i C_i}$).

\mathbf{r}_i : position vector of O_i with respect to the $(i - 1)$ th link frame (i.e., $\mathbf{r}_i = \overrightarrow{O_{i-1} O_i}$).

First we consider the balance of forces. As shown in Fig. 6.2, there are three forces exerted on link i : $\mathbf{f}_{i,i-1}$, $-\mathbf{f}_{i+1,i}$, and $m_i \mathbf{g}$. Hence a force balance equation can be written as

$$\mathbf{f}_{i,i-1} - \mathbf{f}_{i+1,i} + m_i \mathbf{g} = \mathbf{0}. \quad (6.1)$$

Next, we consider the balance of moments about the origin O_i . As shown in Fig. 6.2, there are two moments acting on link i : $\mathbf{n}_{i,i-1}$ and $-\mathbf{n}_{i+1,i}$. In addition, the two forces $m_i \mathbf{g}$ and $\mathbf{f}_{i,i-1}$ produce moments about O_i . Summing these moments together, we obtain

$$\mathbf{n}_{i,i-1} - \mathbf{n}_{i+1,i} - \mathbf{r}_i \times \mathbf{f}_{i,i-1} + \mathbf{r}_{ci} \times m_i \mathbf{g} = \mathbf{0}. \quad (6.2)$$

We call $\mathbf{f}_{i+1,i}$ and $\mathbf{n}_{i+1,i}$ the reaction force and moment between link i and link $i + 1$. For $i = 0$, $\mathbf{f}_{i,0}$ and $\mathbf{n}_{i,0}$ represent the force and moment exerted on the first moving link by the base link. For $i = n$, $\mathbf{f}_{n+1,n}$ and $\mathbf{n}_{n+1,n}$ represent the force and moment exerted on the environment by the end effector. In this regard, the environment is treated as an additional link, numbered $n + 1$.

Equations (6.1) and (6.2) written once for every moving link, $i = 1, 2, \dots, n$, yield $2n$ vector equations in $2(n + 1)$ number of reaction forces and moments. Therefore, to yield a unique solution, two of the reaction forces and moments should be specified. When a manipulator performs a given task, such as insertion or grinding, the end effector exerts some force and/or moment to its environment. On the other hand, when a manipulator carries an object, the weight of the object becomes a load to the end effector. Hence by considering the end-effector output force and moment, $\mathbf{f}_{n+1,n}$ and $\mathbf{n}_{n+1,n}$, as known, Eqs. (6.1) and (6.2) can be solved for the remaining reaction forces and moments.

For convenience, we often combine the force and moment into a six-dimensional vector,

$$\mathbf{F}_{i,i-1} = \begin{bmatrix} \mathbf{f}_{i,i-1} \\ \mathbf{n}_{i,i-1} \end{bmatrix}. \quad (6.3)$$

We call the foregoing six-dimensional vector $\mathbf{F}_{i,i-1}$ a *wrench* about O_{i-1} .

6.2.2 Recursive Method

In this section we develop a recursive method for the static force analysis of serial manipulators. The recursive method solves joint reaction forces and moments one link at a time without the need of solving $2n$ vector equations simultaneously. To facilitate the analysis, we write Eqs. (6.1) and (6.2) in the following recursive form:

$$\mathbf{f}_{i,i-1} = \mathbf{f}_{i+1,i} - m_i \mathbf{g}, \quad (6.4)$$

$$\mathbf{n}_{i,i-1} = \mathbf{n}_{i+1,i} + \mathbf{r}_i \times \mathbf{f}_{i,i-1} - \mathbf{r}_{ci} \times m_i \mathbf{g}. \quad (6.5)$$

The vectors in Eqs. (6.4) and (6.5) are expressed in the fixed frame. However, the position vector \mathbf{r}_{ci} is often specified in the i th link frame. Similarly, the vector \mathbf{r}_i can conveniently be expressed, in terms of the D-H parameters, in the i th link frame as

$${}^i\mathbf{r}_i = \begin{bmatrix} a_i \\ d_i s\alpha_i \\ d_i c\alpha_i \end{bmatrix}. \quad (6.6)$$

Therefore, both ${}^i\mathbf{r}_{ci}$ and ${}^i\mathbf{r}_i$ should be transformed into the fixed frame before they are substituted into Eqs. (6.4) and (6.5). This can easily be done by the following transformations:

$$\mathbf{r}_{ci} = {}^0R_i {}^i\mathbf{r}_{ci}, \quad (6.7)$$

$$\mathbf{r}_i = {}^0R_i {}^i\mathbf{r}_i. \quad (6.8)$$

Applying Eqs. (6.4) and (6.5), the joint reaction forces can be computed recursively. The process starts at the end-effector link, one link at a time, and ends at the base link. For $i = n$, the end-effector output force and moment, $\mathbf{f}_{n+1,n}$ and $\mathbf{n}_{n+1,n}$, are considered as known. Hence Eqs. (6.4) and (6.5) give the reaction force and moment, $\mathbf{f}_{n,n-1}$ and $\mathbf{n}_{n,n-1}$, at the n th joint. The process is repeated for $i = n-1, n-2, \dots, 1$ until all the reaction forces are found.

Alternatively, we can compute the joint reaction forces in each individual link frame. Writing Eqs. (6.4) and (6.5) in the i th link frame, we obtain

$${}^i\mathbf{f}_{i,i-1} = {}^i\mathbf{f}_{i+1,i} - m_i {}^i\mathbf{g}, \quad (6.9)$$

$${}^i\mathbf{n}_{i,i-1} = {}^i\mathbf{n}_{i+1,i} + {}^i\mathbf{r}_i \times {}^i\mathbf{f}_{i,i-1} - {}^i\mathbf{r}_{ci} \times m_i {}^i\mathbf{g}. \quad (6.10)$$

Once the reaction forces are computed in the i th link frame, they are converted into the $(i-1)$ th link frame by the following transformations:

$${}^{i-1}\mathbf{f}_{i,i-1} = {}^{i-1}R_i {}^i\mathbf{f}_{i,i-1}, \quad (6.11)$$

$${}^{i-1}\mathbf{n}_{i,i-1} = {}^{i-1}R_i {}^i\mathbf{n}_{i,i-1}. \quad (6.12)$$

Note that the ${}^i\mathbf{g}$ term in Eqs. (6.9) and (6.10) denotes the acceleration of gravity expressed in the i th link frame. Since \mathbf{g} is usually specified in the fixed frame, it should be converted into the link frame before it is substituted into Eqs. (6.9) and (6.10). This can be accomplished by the following recursive formula. For $i = 0$, ${}^0\mathbf{g}$ is known. For $i = 1$ to n , we compute

$${}^i\mathbf{g} = {}^iR_{i-1} {}^{i-1}\mathbf{g} \quad (6.13)$$

in sequence. Furthermore, if the end-effector output force and moment are specified in the fixed frame, they should also be transformed into the end effector frame:

$${}^n\mathbf{f}_{n+1,n} = {}^nR_0 {}^0\mathbf{f}_{n+1,n}, \quad (6.14)$$

$${}^n\mathbf{n}_{n+1,n} = {}^nR_0 {}^0\mathbf{n}_{n+1,n}. \quad (6.15)$$

Equations (6.4) and (6.5) compute the joint reaction forces in the fixed frame, while Eqs. (6.9) and (6.10) calculate the same forces in the link frames. Both are equally useful for the static analysis of serial manipulators.

6.2.3 Equivalent Joint Torques

Once the reaction forces in the joints are known, the actuator forces and/or torques can be determined. For a serial manipulator, each joint is driven by an actuator that exerts either a force or a torque between two adjacent links. These actuator forces and/or torques can be found by projecting the reaction forces onto their corresponding joint axes.

For a prismatic joint, the actuator force is exerted along the i th joint axis. Assuming that frictional force at the joint is negligible, the actuator force, τ_i , is given by

$$\tau_i = \mathbf{z}_{i-1}^T \mathbf{f}_{i,i-1}, \quad (6.16)$$

where \mathbf{z}_{i-1} is a unit vector pointing along the positive i th joint axis. Equation (6.16) implies that the actuator only bears the component of $\mathbf{f}_{i,i-1}$ along the direction of the joint axis, while the other components of $\mathbf{f}_{i,i-1}$ are supported by the joint bearings.

Similarly, for a revolute joint, the actuator exerts a torque instead of force about the i th joint axis. This actuator torque, τ_i , is given by

$$\tau_i = \mathbf{z}_{i-1}^T \mathbf{n}_{i,i-1}. \quad (6.17)$$

Again, the actuator only carries the component of $\mathbf{n}_{i,i-1}$ along the direction of the joint axis, while other components of $\mathbf{n}_{i,i-1}$ are supported by the bearings. We call τ_i the equivalent joint torque.

Example 6.2.1 Statics of a Planar 3-DOF Manipulator Figure 6.3 shows the planar 3R manipulator studied in Chapters 2 and 4. A coordinate system with all the z -axes pointing out of the paper is defined for each link according to the D-H convention. Let the end-effector output force and moment be given by $\mathbf{f}_{4,3} = [f_x, f_y, 0]^T$ and $\mathbf{n}_{4,3} = [0, 0, n_z]^T$, respectively. Also let the acceleration of gravity, \mathbf{g} , be pointing along the negative y_0 -direction and the center of mass be located at the midpoint of each link. We wish to find the joint reaction forces and moments.

The D-H parameters and transformation matrices are given in Table 2.1 and Eqs. (2.6) through (2.8). The vectors ${}^i\mathbf{r}_i$ and ${}^i\mathbf{r}_{ci}$ are

$${}^i\mathbf{r}_i = \begin{bmatrix} a_i \\ 0 \\ 0 \end{bmatrix} \quad \text{and} \quad {}^i\mathbf{r}_{ci} = \begin{bmatrix} -a_i/2 \\ 0 \\ 0 \end{bmatrix}. \quad (6.18)$$

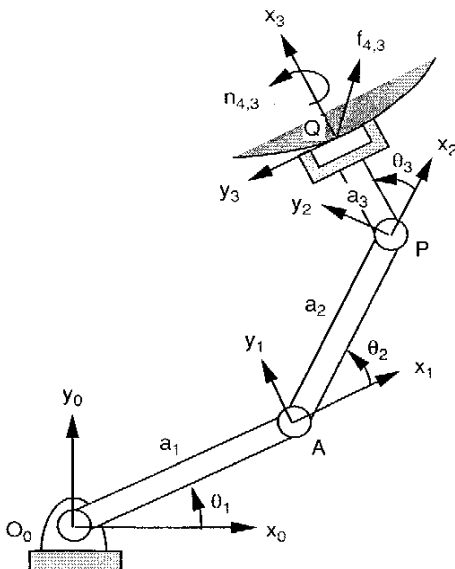


FIGURE 6.3. Planar 3R manipulator exerting a force $f_{4,3}$ and a moment $n_{4,3}$.

Substituting Eq. (6.18) for $i = 1$ to 3 into Eqs. (6.7) and (6.8) gives

$$\begin{aligned} \mathbf{r}_1 &= {}^0\mathbf{R}_1 {}^1\mathbf{r}_1 = a_1 \begin{bmatrix} c\theta_1 \\ s\theta_1 \\ 0 \end{bmatrix}, & \mathbf{r}_{c1} &= {}^0\mathbf{R}_1 {}^1\mathbf{r}_{c1} = -\frac{a_1}{2} \begin{bmatrix} c\theta_1 \\ s\theta_1 \\ 0 \end{bmatrix}, \\ \mathbf{r}_2 &= {}^0\mathbf{R}_2 {}^2\mathbf{r}_2 = a_2 \begin{bmatrix} c\theta_{12} \\ s\theta_{12} \\ 0 \end{bmatrix}, & \mathbf{r}_{c2} &= {}^0\mathbf{R}_2 {}^2\mathbf{r}_{c2} = -\frac{a_2}{2} \begin{bmatrix} c\theta_{12} \\ s\theta_{12} \\ 0 \end{bmatrix}, \\ \mathbf{r}_3 &= {}^0\mathbf{R}_3 {}^3\mathbf{r}_3 = a_3 \begin{bmatrix} c\theta_{123} \\ s\theta_{123} \\ 0 \end{bmatrix}, & \mathbf{r}_{c3} &= {}^0\mathbf{R}_3 {}^3\mathbf{r}_{c3} = -\frac{a_3}{2} \begin{bmatrix} c\theta_{123} \\ s\theta_{123} \\ 0 \end{bmatrix}. \end{aligned}$$

We now apply Eqs. (6.4) and (6.5) to compute the reaction forces exerted on link 3, then proceed to link 2 and 1 in sequence. For $i = 3$, substituting \mathbf{r}_{c3} , $\mathbf{f}_{4,3}$, and $\mathbf{n}_{4,3}$ into Eqs. (6.4) and (6.5) yields

$$\begin{aligned} \mathbf{f}_{3,2} &= \mathbf{f}_{4,3} - m_3\mathbf{g} = \begin{bmatrix} f_x \\ f_y + m_3g_c \\ 0 \end{bmatrix}, \\ \mathbf{n}_{3,2} &= \mathbf{n}_{4,3} + \mathbf{r}_3 \times \mathbf{f}_{3,2} - \mathbf{r}_{c3} \times m_3\mathbf{g} = \begin{bmatrix} 0 \\ 0 \\ n_{3,2z} \end{bmatrix}, \end{aligned}$$

where

$$n_{3,2z} = n_z + f_y a_3 c\theta_{123} - f_x a_3 s\theta_{123} + 0.5m_3 g_c a_3 c\theta_{123}.$$

For $i = 2$, we substitute $\mathbf{f}_{3,2}$ and $\mathbf{n}_{3,2}$ obtained in the preceding step along with \mathbf{r}_2 and \mathbf{r}_{c2} into Eqs. (6.4) and (6.5). As a result, we obtain

$$\begin{aligned} \mathbf{f}_{2,1} &= \mathbf{f}_{3,2} - m_2\mathbf{g} = \begin{bmatrix} f_x \\ f_y + (m_2 + m_3)g_c \\ 0 \end{bmatrix}, \\ \mathbf{n}_{2,1} &= \mathbf{n}_{3,2} + \mathbf{r}_2 \times \mathbf{f}_{2,1} - \mathbf{r}_{c2} \times m_2\mathbf{g} = \begin{bmatrix} 0 \\ 0 \\ n_{2,1z} \end{bmatrix}, \end{aligned}$$

where

$$\begin{aligned} n_{2,1z} &= n_z + f_y (a_2 c\theta_{12} + a_3 c\theta_{123}) - f_x (a_2 s\theta_{12} + a_3 s\theta_{123}) \\ &\quad + 0.5m_2 g_c a_2 c\theta_{12} + m_3 g_c (a_2 c\theta_{12} + 0.5a_3 c\theta_{123}). \end{aligned}$$

For $i = 1$, we substitute $\mathbf{f}_{2,1}$ and $\mathbf{n}_{2,1}$ obtained in the preceding step along with \mathbf{r}_1 and \mathbf{r}_{c1} into Eqs. (6.4) and (6.5). This produces

$$\mathbf{f}_{1,0} = \mathbf{f}_{2,1} - m_1 \mathbf{g} = \begin{bmatrix} f_x \\ f_y + (m_1 + m_2 + m_3) g_c \\ 0 \end{bmatrix},$$

$$\mathbf{n}_{1,0} = \mathbf{n}_{2,1} + \mathbf{r}_1 \times \mathbf{f}_{1,0} - \mathbf{r}_{c1} \times m_1 \mathbf{g} = \begin{bmatrix} 0 \\ 0 \\ n_{1,0z} \end{bmatrix},$$

where

$$\begin{aligned} n_{1,0z} = & n_z + f_y(a_1 c\theta_1 + a_2 c\theta_{12} + a_3 c\theta_{123}) - f_x(a_1 s\theta_1 + a_2 s\theta_{12} + a_3 s\theta_{123}) \\ & + 0.5m_1 g_c a_1 c\theta_1 + m_2 g_c(a_1 c\theta_1 + 0.5a_2 c\theta_{12}) \\ & + m_3 g_c(a_1 c\theta_1 + a_2 c\theta_{12} + 0.5a_3 c\theta_{123}). \end{aligned}$$

Finally, we apply Eq. (6.17) to compute the joint torques as follows:

$$\tau_1 = \mathbf{z}_0^T \mathbf{n}_{1,0} = n_{1,0z},$$

$$\tau_2 = \mathbf{z}_1^T \mathbf{n}_{2,1} = n_{2,1z},$$

$$\tau_3 = \mathbf{z}_2^T \mathbf{n}_{3,2} = n_{3,2z}.$$

We note that in the absence of gravity, the torques and end-effector output forces are related by the following equation:

$$\begin{bmatrix} \tau_1 \\ \tau_2 \\ \tau_3 \end{bmatrix} = J^T \begin{bmatrix} f_x \\ f_y \\ n_z \end{bmatrix}, \quad (6.19)$$

where

$$J = \begin{bmatrix} -(a_1 s\theta_1 + a_2 s\theta_{12} + a_3 s\theta_{123}) & -(a_2 s\theta_{12} + a_3 s\theta_{123}) & -a_3 s\theta_{123} \\ (a_1 c\theta_1 + a_2 c\theta_{12} + a_3 c\theta_{123}) & (a_2 c\theta_{12} + a_3 c\theta_{123}) & a_3 c\theta_{123} \\ 1 & 1 & 1 \end{bmatrix}.$$

Hence, in the absence of gravity, the transformation between the end-effector output forces and the joint torques is governed by the transpose of the conventional Jacobian matrix.

Example 6.2.2 Statics of the Stanford Manipulator As a second example, we consider the Stanford arm shown in Fig. 4.8. Let the end-effector output

force and moment be denoted as $\mathbf{f}_{7,6} = [f_x, f_y, f_z]^T$ and $\mathbf{n}_{7,6} = [n_x, n_y, n_z]^T$, respectively. Also let the acceleration of gravity be pointing in the negative z_0 -direction (i.e., $\mathbf{g} = [0, 0, -g_c]^T$). To simplify the analysis, we assume that the masses of links 1, 2, 4, 5, and 6 are negligible, and the center of mass of link 3 is located at the midpoint of the link. We wish to find the joint reaction forces.

The D-H parameters and the transformation matrices are given in Chapter 4. The unit vectors, \mathbf{z}_{i-1} for $i = 0$ to 5 are given in Eqs. (4.69) through (4.73). Some relevant ${}^i \mathbf{r}_i$ and ${}^i \mathbf{r}_{ci}$ vectors are as follows:

$$\begin{aligned} {}^2 \mathbf{r}_2 &= \begin{bmatrix} 0 \\ d_2 \\ 0 \end{bmatrix}, & {}^3 \mathbf{r}_3 &= \begin{bmatrix} 0 \\ 0 \\ d_3 \end{bmatrix}, & {}^3 \mathbf{r}_{c3} &= \begin{bmatrix} 0 \\ 0 \\ -d_3/2 \end{bmatrix}, \\ {}^1 \mathbf{r}_1 &= {}^4 \mathbf{r}_4 = {}^5 \mathbf{r}_5 = {}^6 \mathbf{r}_6 = \begin{bmatrix} 0 \\ 0 \\ 0 \end{bmatrix}. \end{aligned}$$

Transforming the vectors above into the fixed frame by Eqs. (6.7) and (6.8), we obtain

$$\begin{aligned} \mathbf{r}_2 &= {}^0 R_2 {}^2 \mathbf{r}_2 = d_2 \begin{bmatrix} -s\theta_1 \\ c\theta_1 \\ 0 \end{bmatrix}, \\ \mathbf{r}_3 &= {}^0 R_3 {}^3 \mathbf{r}_3 = d_3 \begin{bmatrix} c\theta_1 s\theta_2 \\ s\theta_1 s\theta_2 \\ c\theta_2 \end{bmatrix}, \\ \mathbf{r}_{c3} &= {}^0 R_3 {}^3 \mathbf{r}_{c3} = -\frac{d_3}{2} \begin{bmatrix} c\theta_1 s\theta_2 \\ s\theta_1 s\theta_2 \\ c\theta_2 \end{bmatrix}, \\ \mathbf{r}_4 &= \mathbf{r}_5 = \mathbf{r}_6 = \begin{bmatrix} 0 \\ 0 \\ 0 \end{bmatrix}. \end{aligned}$$

We now apply Eqs. (6.4) and (6.5) to compute the reaction forces one link at a time beginning from link 6. Due to negligible masses of links 4, 5, and 6, and the concurrence of the fourth, fifth, and sixth joint axes, the reaction forces at the last three joints are equal to one another; that is,

$$\mathbf{f}_{6,5} = \mathbf{f}_{5,4} = \mathbf{f}_{4,3} = \mathbf{f}_{7,6} = \begin{bmatrix} f_x \\ f_y \\ f_z \end{bmatrix},$$

$$\mathbf{n}_{6,5} = \mathbf{n}_{5,4} = \mathbf{n}_{4,3} = \mathbf{n}_{7,6} = \begin{bmatrix} n_x \\ n_y \\ n_z \end{bmatrix}.$$

For $i = 3$, substituting \mathbf{r}_3 , \mathbf{r}_{c3} , $\mathbf{f}_{4,3}$, and $\mathbf{n}_{4,3}$ into Eqs. (6.4) and (6.5) yields

$$\mathbf{f}_{3,2} = \mathbf{f}_{4,3} - m_3 \mathbf{g} = \begin{bmatrix} f_x \\ f_y \\ f_z + m_3 g_c \end{bmatrix},$$

$$\begin{aligned} \mathbf{n}_{3,2} &= \mathbf{n}_{4,3} + \mathbf{r}_3 \times \mathbf{f}_{3,2} - \mathbf{r}_{c3} \times m_3 \mathbf{g} \\ &= \begin{bmatrix} n_x + f_z d_3 s\theta_1 s\theta_2 - f_y d_3 c\theta_2 + 0.5 m_3 g_c d_3 s\theta_1 s\theta_2 \\ n_y - f_z d_3 c\theta_1 s\theta_2 + f_x d_3 c\theta_2 - 0.5 m_3 g_c d_3 c\theta_1 s\theta_2 \\ n_z + f_y d_3 c\theta_1 s\theta_2 - f_x d_3 s\theta_1 s\theta_2 \end{bmatrix}. \end{aligned}$$

For $i = 2$, we substitute $\mathbf{f}_{3,2}$ and $\mathbf{n}_{3,2}$ obtained in the preceding step along with \mathbf{r}_2 and \mathbf{r}_{c2} into Eqs. (6.4) and (6.5). As a result, we obtain

$$\mathbf{f}_{2,1} = \mathbf{f}_{3,2} - m_2 \mathbf{g} = \begin{bmatrix} f_x \\ f_y \\ f_z + m_3 g_c \end{bmatrix},$$

$$\begin{aligned} \mathbf{n}_{2,1} &= \mathbf{n}_{3,2} + \mathbf{r}_2 \times \mathbf{f}_{2,1} - \mathbf{r}_{c2} \times m_2 \mathbf{g} \\ &= \begin{bmatrix} n_x + f_z (d_3 s\theta_1 s\theta_2 + d_2 c\theta_1) - f_y d_3 c\theta_2 + m_3 g_c (0.5 d_3 s\theta_1 s\theta_2 + d_2 c\theta_1) \\ n_y - f_z (d_3 c\theta_1 s\theta_2 - d_2 s\theta_1) + f_x d_3 c\theta_2 - m_3 g_c (0.5 d_3 c\theta_1 s\theta_2 - d_2 s\theta_1) \\ n_z + f_y (d_3 c\theta_1 s\theta_2 - d_2 s\theta_1) - f_x (d_3 s\theta_1 s\theta_2 + d_2 c\theta_1) \end{bmatrix}. \end{aligned}$$

For $i = 1$, we substitute $\mathbf{f}_{2,1}$ and $\mathbf{n}_{2,1}$ obtained in the preceding step along with \mathbf{r}_1 and \mathbf{r}_{c1} into Eqs. (6.4) and (6.5). This produces

$$\mathbf{f}_{1,0} = \mathbf{f}_{2,1} - m_1 \mathbf{g} = \begin{bmatrix} f_x \\ f_y \\ f_z + m_3 g_c \end{bmatrix},$$

$$\begin{aligned} \mathbf{n}_{1,0} &= \mathbf{n}_{2,1} + \mathbf{r}_1 \times \mathbf{f}_{1,0} - \mathbf{r}_{c1} \times m_1 \mathbf{g} \\ &= \begin{bmatrix} n_x + f_z (d_3 s\theta_1 s\theta_2 + d_2 c\theta_1) - f_y d_3 c\theta_2 + m_3 g_c (0.5 d_3 s\theta_1 s\theta_2 + d_2 c\theta_1) \\ n_y - f_z (d_3 c\theta_1 s\theta_2 - d_2 s\theta_1) + f_x d_3 c\theta_2 - m_3 g_c (0.5 d_3 c\theta_1 s\theta_2 - d_2 s\theta_1) \\ n_z + f_y (d_3 c\theta_1 s\theta_2 - d_2 s\theta_1) - f_x (d_3 s\theta_1 s\theta_2 + d_2 c\theta_1) \end{bmatrix}. \end{aligned}$$

Finally, the joint torques are obtained by substituting the reaction forces above into Eqs. (6.16) and (6.17):

$$\begin{aligned} \tau_1 &= \mathbf{z}_0^T \mathbf{n}_{1,0} = n_z + f_y (d_3 c\theta_1 s\theta_2 - d_2 s\theta_1) - f_x (d_3 s\theta_1 s\theta_2 + d_2 c\theta_1), \\ \tau_2 &= \mathbf{z}_1^T \mathbf{n}_{2,1} \\ &= -s\theta_1 [n_x + f_z (d_3 s\theta_1 s\theta_2 + d_2 c\theta_1) - f_y d_3 c\theta_2 \\ &\quad + c\theta_1 [n_y - f_z (d_3 c\theta_1 s\theta_2 - d_2 s\theta_1) + f_x d_3 c\theta_2 \\ &\quad - m_3 g_c (0.5 d_3 c\theta_1 s\theta_2 - d_2 s\theta_1)]], \\ \tau_3 &= \mathbf{z}_2^T \mathbf{f}_{3,2} = f_x c\theta_1 s\theta_2 + f_y s\theta_1 s\theta_2 + (f_z + m_3 g_c) c\theta_2, \\ \tau_4 &= \mathbf{z}_3^T \mathbf{n}_{4,3} = n_x c\theta_1 s\theta_2 + n_y s\theta_1 s\theta_2 + n_z c\theta_2, \\ \tau_5 &= \mathbf{z}_4^T \mathbf{n}_{5,4} = n_x j_{45} + n_y j_{55} + n_z j_{65}, \\ \tau_6 &= \mathbf{z}_5^T \mathbf{n}_{6,5} = n_x j_{46} + n_y j_{56} + n_z j_{66}, \end{aligned}$$

where j_{45} , j_{55} , and j_{65} are the x , y , and z components of the unit vector \mathbf{z}_4 , and j_{46} , j_{56} , and j_{66} are the x , y , and z components of \mathbf{z}_5 .

In the absence of gravity, the input joint torques and the output forces are related by the following transformation:

$$\begin{bmatrix} \tau_1 \\ \tau_2 \\ \tau_3 \\ \tau_4 \\ \tau_5 \\ \tau_6 \end{bmatrix} = J^T \begin{bmatrix} f_x \\ f_y \\ f_z \\ n_x \\ n_y \\ n_z \end{bmatrix}, \quad (6.20)$$

where

$$J = \begin{bmatrix} -d_3 s\theta_1 s\theta_2 - d_2 c\theta_1 & d_3 c\theta_1 c\theta_2 & c\theta_1 s\theta_2 & 0 & 0 & 0 \\ d_3 c\theta_1 s\theta_2 - d_2 s\theta_1 & d_3 s\theta_1 c\theta_2 & s\theta_1 s\theta_2 & 0 & 0 & 0 \\ 0 & -d_3 s\theta_2 & c\theta_2 & 0 & 0 & 0 \\ 0 & -s\theta_1 & 0 & c\theta_1 s\theta_2 & j_{45} & j_{46} \\ 0 & c\theta_1 & 0 & s\theta_1 s\theta_2 & j_{55} & j_{56} \\ 1 & 0 & 0 & c\theta_2 & j_{65} & j_{66} \end{bmatrix}$$

is the conventional Jacobian matrix derived in Chapter 4.

From the two examples above, we observe that by neglecting the gravitational effect, the end-effector output forces are related to the input joint

torques by the transpose of the conventional Jacobian matrix. In the following section we show that this relation holds for all serial manipulators.

6.2.4 Application of the Principle of Virtual Work

In this section we apply the principle of virtual work to derive a transformation between the joint torques and end-effector forces (Asada and Slotine, 1986; Paul, 1981; Witney, 1972). A virtual displacement of a system refers to an infinitesimal change in the configuration of the system as a result of any arbitrary infinitesimal changes of the coordinates that are compatible with the forces and constraints imposed on the system at a given instant in time. The term *virtual displacement* is used to distinguish it from an *actual displacement*, for which the forces and constraints may be changing at the instant. We use the Greek letter delta, $\delta\mathbf{x}$, to denote a virtual displacement, as opposed to $d\mathbf{x}$ for an actual displacement.

For a serial manipulator, the virtual displacements at the joints can be written as $\delta\mathbf{q} = [\delta q_1, \delta q_2, \dots, \delta q_n]^T$, and the virtual displacement of the end effector can be expressed as $\delta\mathbf{x} = [\delta x, \delta y, \dots, \delta \psi]^T$. Let the end-effector output force and moment be denoted by

$$\mathbf{F} = \begin{bmatrix} \mathbf{f} \\ \mathbf{n} \end{bmatrix}. \quad (6.21)$$

Also let the vector of joint torques be denoted by

$$\boldsymbol{\tau} = \begin{bmatrix} \tau_1 \\ \tau_2 \\ \vdots \\ \tau_n \end{bmatrix}. \quad (6.22)$$

Assuming that frictional forces at the joints are negligible, the virtual work produced by the forces of constraint at the joints is zero. Hence, by neglecting the gravitational effect, the virtual work, δW , done by all the active forces is given by

$$\delta W = \boldsymbol{\tau}^T \delta\mathbf{q} - \mathbf{F}^T \delta\mathbf{x}. \quad (6.23)$$

The principle of virtual work states that a system is under equilibrium if and only if the virtual work vanishes for any infinitesimal virtual displacement. This is true if the virtual displacements are compatible with the constraints imposed on the system. In Eq. (6.23), however, the virtual displacements $\delta\mathbf{q}$ and $\delta\mathbf{x}$ are not independent. In fact, they are related by the

conventional Jacobian matrix as follows:

$$\delta\mathbf{x} = J \delta\mathbf{q}. \quad (6.24)$$

Substituting Eq. (6.24) into (6.23) yields

$$(\boldsymbol{\tau}^T - \mathbf{F}^T J) \delta\mathbf{q} = 0. \quad (6.25)$$

Since Eq. (6.25) holds for any arbitrary virtual displacement, $\delta\mathbf{q}$, we conclude that

$$\boldsymbol{\tau}^T - \mathbf{F}^T J = 0. \quad (6.26)$$

Taking the transpose of Eq. (6.26) yields

$$\boldsymbol{\tau} = J^T \mathbf{F}. \quad (6.27)$$

Equation (6.27) maps an m -dimensional end-effector output force into an n -dimensional joint torques. Since the Jacobian matrix is configuration dependent, the mapping is also configuration dependent.

6.2.5 Force Ellipsoid

Similar to the transformation of velocities, the transformation of forces for manipulators with only one type of joints and for one type of tasks can be characterized by a comparison of the end-effector force produced by a unit joint torque. Substituting Eq. (6.27) into $\boldsymbol{\tau}^T \boldsymbol{\tau} = 1$ yields

$$\mathbf{F}^T J J^T \mathbf{F} = 1. \quad (6.28)$$

At a given manipulator configuration, Eq. (6.28) represents an m -dimensional ellipsoid. Because the product $J J^T$ is symmetric positive semidefinite, its eigenvectors are orthogonal. The principal axes of the ellipsoid coincide with the eigenvectors of $J J^T$, and their lengths are equal to the reciprocals of the square roots of the eigenvalues.

Since the Jacobian matrix is configuration dependent, the force ellipsoid is also configuration dependent. As the end effector moves from one location to another, the shape and orientation of the force ellipsoid will also change accordingly. The closer the transmission ellipsoid to a sphere, the better the transmission characteristics are. The transformation is said to be *isotropic* when the principal axes are of equal lengths. At an isotropic point, an n -dimensional unit sphere in the joint torque space maps onto an m -dimensional sphere in the end-effector force space. On the other hand, at a singular point, an n -dimensional unit sphere in the joint torque space maps onto an m -

dimensional cylinder in the end-effector force space. Thus the mechanical advantage of the manipulator becomes infinitely large in some direction.

Example 6.2.3 Ellipsoid of a Planar 2 DOF Manipulator In this example we examine the transformation characteristics of the planar 2-dof manipulator shown in Fig. 6.4 to illustrate the principle. For this 2-dof manipulator, the end-effector output force and input joint torques can be written as $\mathbf{f} = [f_x, f_y]^T$ and $\tau = [\tau_1, \tau_2]^T$, respectively.

Substituting the Jacobian matrix, Eq. (4.66), into (6.27), we obtain

$$\begin{bmatrix} \tau_1 \\ \tau_2 \end{bmatrix} = \begin{bmatrix} -a_1 s\theta_1 - a_2 s\theta_{12} & a_1 c\theta_1 + a_2 c\theta_{12} \\ -a_2 s\theta_{12} & a_2 c\theta_{12} \end{bmatrix} \begin{bmatrix} f_x \\ f_y \end{bmatrix}. \quad (6.29)$$

Let the link lengths be $a_1 = \sqrt{2}$ m and $a_2 = 1$ m. At the posture where $\theta_1 = 0$ and $\theta_2 = \pi/2$, the Jacobian matrix reduces to

$$J = \begin{bmatrix} -1 & -1 \\ \sqrt{2} & 0 \end{bmatrix}.$$

Hence

$$JJ^T = \begin{bmatrix} 2 & -\sqrt{2} \\ -\sqrt{2} & 2 \end{bmatrix}.$$

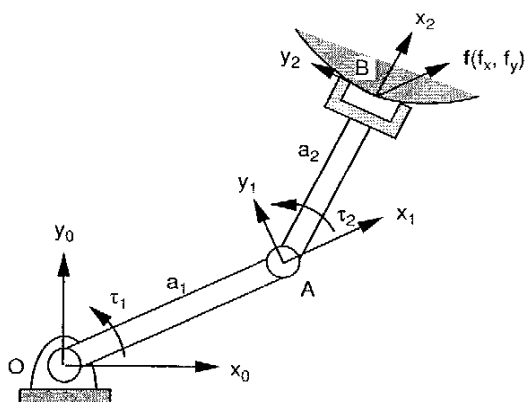


FIGURE 6.4. Planar 2R manipulator exerting a force $\mathbf{f}(f_x, f_y)$.

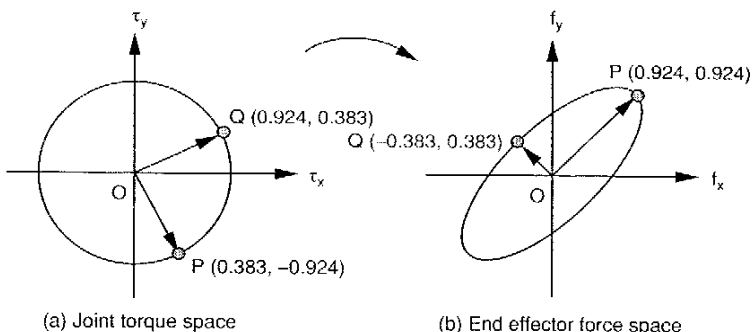


FIGURE 6.5. Force ellipsoid.

The eigenvalues of JJ^T are $\lambda_1 = 2 - \sqrt{2} = 0.5858$ and $\lambda_2 = 2 + \sqrt{2} = 3.4142$. The corresponding eigenvectors, normalized to unit length, are $(0.707, 0.707)$ and $(-0.707, 0.707)$, respectively. These two eigenvectors are at 45° angles with the f_x and f_y axes, respectively, and they are lined up with the principal axes of the ellipse.

Substituting JJ^T into (6.28), we obtain

$$2f_x^2 - 2\sqrt{2}f_x f_y + 2f_y^2 = 0.5858 \left(\frac{f_x}{\sqrt{2}} + \frac{f_y}{\sqrt{2}} \right)^2 + 3.4142 \left(\frac{f_x}{\sqrt{2}} - \frac{f_y}{\sqrt{2}} \right)^2 = 1.$$

Figure 6.5 shows the ellipse and its principal axes. The end-effector forces produced by a unit joint torque are $(f_x, f_y) = (0.924, 0.924)$ N along the major axis and $(f_x, f_y) = (-0.383, 0.383)$ N along the minor axis. The corresponding joint torques are $(\tau_1, \tau_2) = (0.383, -0.924)$ N·m along the major axis and $(\tau_1, \tau_2) = (0.924, 0.383)$ N·m along the minor axis. We note that the mechanical advantage along the major axis is larger than that along the minor axis.

6.3 TRANSFORMATION OF FORCES AND MOMENTS

In Chapter 4, we have shown that the coordinates of a twist can be transformed from one coordinate frame to another by a 6×6 transformation matrix ${}^i\tilde{T}_j$. Analogously, the coordinates of a wrench can be transformed from one

coordinate frame to another by the same matrix. Let \mathbf{f} denote the force acting along, and \mathbf{c} denote the couple about, the axis of a wrench. Then the wrench can be written as a six-dimensional column vector:

$$\mathbf{F} = \begin{bmatrix} \mathbf{s}_o \times \mathbf{f} + \mathbf{c} \end{bmatrix} = \begin{bmatrix} f_x \\ f_y \\ f_z \\ n_x \\ n_y \\ n_z \end{bmatrix}, \quad (6.30)$$

where \mathbf{s}_o denotes the position vector of any point on the wrench axis relative to a reference frame. The vector $\mathbf{s}_o \times \mathbf{f}$ denotes the moment contributed by the force \mathbf{f} about the origin of the reference frame chosen. We observe that the coordinates of a wrench depend on the choice of the reference frame, due to the fact that the effect of a force on the resulting moment, $\mathbf{n} = [n_x, n_y, n_z]^T$, depends on the point of application.

Figure 6.6 shows a wrench \mathbf{F} with reference to two reference frames: (x_i, y_i, z_i) and (x_j, y_j, z_j) . The position of the (x_j, y_j, z_j) frame relative to the (x_i, y_i, z_i) frame is denoted by a position vector ${}^i\mathbf{p} = [p_x, p_y, p_z]^T$, and the orientation of the (x_j, y_j, z_j) frame relative to the (x_i, y_i, z_i) frame is described by a rotation matrix iR_j . The wrench \mathbf{F} relative to the (x_i, y_i, z_i) frame is denoted by ${}^i\mathbf{F}$, and the same wrench relative to the (x_j, y_j, z_j) frame

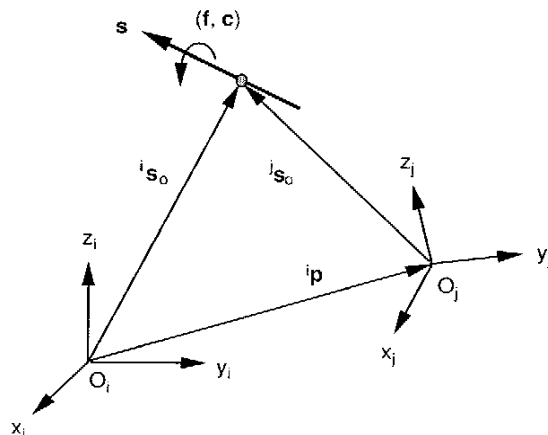


FIGURE 6.6. Transformation of force and moment between two coordinate systems.

is denoted by ${}^j\mathbf{F}$. Since the wrench has the properties of a screw, it follows that

$${}^i\mathbf{F} = {}^i\tilde{T}_j {}^j\mathbf{F}, \quad (6.31)$$

where ${}^i\tilde{T}_j$ is the 6×6 matrix derived in Chapter 4. Specifically,

$${}^i\tilde{T}_j = \begin{bmatrix} {}^iR_j & \mathbf{0} \\ \cdots & \cdots \\ {}^iW_j \ {}^iR_j & {}^iR_j \end{bmatrix}, \quad (6.32)$$

where

$${}^iW_j = \begin{bmatrix} 0 & -p_z & p_y \\ p_z & 0 & -p_x \\ -p_y & p_x & 0 \end{bmatrix}$$

is a 3×3 skew-symmetric matrix representing the vector of $\overrightarrow{O_i O_j}$ expressed in the (x_i, y_i, z_i) frame. Hence, given a wrench about one reference frame, we can transform it into another reference frame, and vice versa.

Example 6.3.1 Transformation between Tool Tip and Wrist Center Figure 6.7 shows a robot hand inserting a peg in a hole. We wish to monitor the force and moment acting on the peg. To accomplish this, a force sensor is mounted at the wrist center. Thus the force and moment are referred to two different locations: one with respect to the (x, y, z) frame at the peg and the other with respect to the (u, v, w) frame at the wrist center. The force and moment with respect to the (u, v, w) coordinate frame are known from the measurement made at the wrist center. The problem is to find the force and moment acting on the peg.

Assuming that these two coordinate frames are parallel at the instant and the wrist center Q relative to the peg coordinate frame is given by the vector $\mathbf{p} = [p_x, p_y, p_z]^T$, we have

$${}^{xyz}R_{uvw} = \begin{bmatrix} 1 & 0 & 0 \\ 0 & 1 & 0 \\ 0 & 0 & 1 \end{bmatrix},$$

$${}^{xyz}W_{uvw} = \begin{bmatrix} 0 & -p_z & p_y \\ p_z & 0 & -p_x \\ -p_y & p_x & 0 \end{bmatrix}.$$

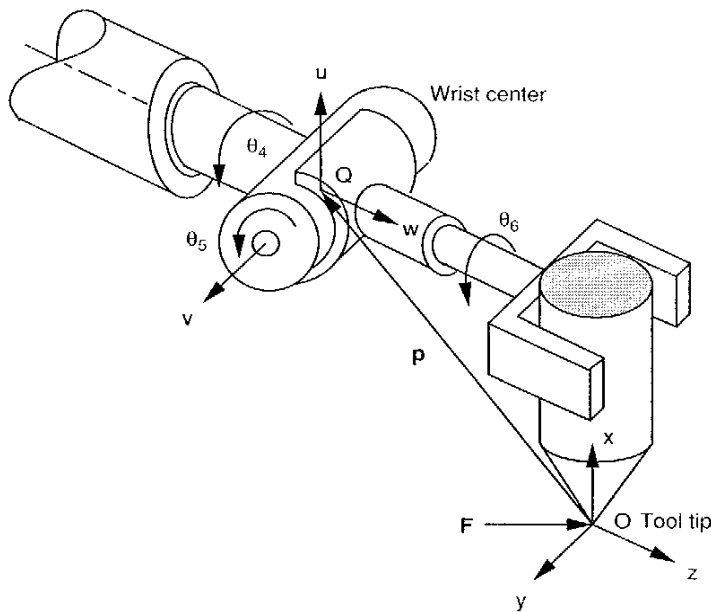


FIGURE 6.7. Transformation of force and moment from the tool tip to the wrist center.

Hence the transformation matrix ${}^{xyz}\tilde{T}_{uvw}$ is given by

$${}^{xyz}\tilde{T}_{uvw} = \begin{bmatrix} 1 & 0 & 0 & 0 & 0 & 0 \\ 0 & 1 & 0 & 0 & 0 & 0 \\ 0 & 0 & 1 & 0 & 0 & 0 \\ 0 & -p_z & p_y & 1 & 0 & 0 \\ p_z & 0 & -p_x & 0 & 1 & 0 \\ -p_y & p_x & 0 & 0 & 0 & 1 \end{bmatrix}. \quad (6.33)$$

Substituting Eq. (6.33) into Eq. (6.31), we obtain

$$\begin{bmatrix} f_x \\ f_y \\ f_z \\ n_x \\ n_y \\ n_z \end{bmatrix} = \begin{bmatrix} 1 & 0 & 0 & 0 & 0 & 0 \\ 0 & 1 & 0 & 0 & 0 & 0 \\ 0 & 0 & 1 & 0 & 0 & 0 \\ 0 & -p_z & p_y & 1 & 0 & 0 \\ p_z & 0 & -p_x & 0 & 1 & 0 \\ -p_y & p_x & 0 & 0 & 0 & 1 \end{bmatrix} \begin{bmatrix} f_u \\ f_v \\ f_w \\ n_u \\ n_v \\ n_w \end{bmatrix}. \quad (6.34)$$

Equation (6.34) provides a transformation of the force and moment measured at the wrist center to the output force and moment at the inserting point.

6.4 STIFFNESS ANALYSIS OF SERIAL MANIPULATORS

When a manipulator performs a given task, the end effector exerts some force and/or moment on its environment. This contact force and/or moment will cause the end effector to be deflected away from its desired location. Intuitively, the amount of deflection is a function of the applied force and stiffness of the manipulator. Thus the stiffness of a manipulator has a direct impact on the position accuracy. Furthermore, some advanced control strategies make use of the stiffness characteristics for feedback control of a robot manipulator (Bryfogle et al., 1993; Lebret et al., 1993).

The overall stiffness of a manipulator depends on several factors, including the size of and material used for the links, the mechanical transmission mechanisms, the actuators, and the controller. As the links become longer and more slender, link compliance becomes the major source of deflection. This is particularly true for space robots, for which light weight and compactness are the major concern (Nguyen and Ravindran, 1977). A few studies on the dynamics and control of flexible manipulators can be found in Cannon and Schmitz (1984), Chang and Hamilton (1991), and Hollars and Cannon (1985). On the other hand, most industrial robots are constructed with fairly rigid links, and the major sources of compliance come from the mechanical transmission mechanisms and control systems (Sunada and Dubowsky, 1983; Sweet and Good, 1984).

In what follows, we assume that the major links are perfectly rigid and consider the mechanical transmission mechanisms and the servo systems as the main sources of compliance.

6.4.1 Compliance Matrix

For a serial manipulator, each joint is typically driven by an actuator through a multiple-stage speed reducer along with several drive shafts. The speed reducer and the drive shafts may deflect when torque or force is transmitted. Further, the drive torque or force generated by a servo system usually depends on the position and velocity error signals and its feedback gains. The stiffness of the speed reducer, the drive shafts, and the servo system may be combined into an equivalent stiffness.

Let n be the dimension of the joint space, m be the dimension of the end-effector space, τ_i be the torque or force transmitted through the i th joint, and Δq_i be the corresponding deflection at the joint. Then for small deflections

we can relate τ_i and Δq_i by the linear approximation

$$\tau_i = k_i \Delta q_i, \quad (6.35)$$

where k_i is called the *stiffness constant*. For convenience, we write Eq. (6.35) for $i = 1, 2, \dots, n$ in matrix form:

$$\boldsymbol{\tau} = \chi \Delta \mathbf{q}, \quad (6.36)$$

where $\boldsymbol{\tau} = [\tau_1, \tau_2, \dots, \tau_n]^T$, $\Delta \mathbf{q} = [\Delta q_1, \Delta q_2, \dots, \Delta q_n]^T$, and $\chi = \text{diag}[k_1, k_2, \dots, k_n]$ is an $n \times n$ diagonal matrix.

For a serial manipulator, the joint displacement $\Delta \mathbf{q}$ is related to the end effector displacement $\Delta \mathbf{x}$ by the conventional $m \times n$ Jacobian matrix,

$$\Delta \mathbf{x} = J \Delta \mathbf{q}, \quad (6.37)$$

and the end-effector output force \mathbf{F} is related to the joint torque $\boldsymbol{\tau}$ by the transpose of the conventional Jacobian matrix,

$$\boldsymbol{\tau} = J^T \mathbf{F}. \quad (6.38)$$

Eliminating $\boldsymbol{\tau}$ and $\Delta \mathbf{q}$ from Eqs. (6.36), (6.37), and (6.38), we obtain

$$\Delta \mathbf{x} = C \mathbf{F}, \quad (6.39)$$

where

$$C = J \chi^{-1} J^T \quad (6.40)$$

is an $m \times m$ matrix called the *compliance matrix*.

From Eq. (6.40) we note that the compliance matrix is symmetric. It depends not only on the stiffness of each drive line but also on the Jacobian matrix. Since the Jacobian matrix is configuration dependent, the compliance matrix is also configuration dependent.

6.4.2 Stiffness Matrix

If $m = n$ and the Jacobian matrix is nonsingular, the compliance matrix is invertible. Multiplying both sides of Eq. (6.39) by C^{-1} , we obtain

$$\mathbf{F} = K \Delta \mathbf{x}, \quad (6.41)$$

where

$$K = C^{-1} = J^{-T} \chi J^{-1} \quad (6.42)$$

is called the *stiffness matrix*.

Obviously, the stiffness matrix is also configuration dependent. For manipulators with only one type of joint and for one type of task, we may characterize the stiffness of a manipulator by comparing the force required to generate one unit-length deflection at the end effector. Substituting Eq. (6.39) into $(\Delta \mathbf{x})^T (\Delta \mathbf{x}) = 1$, we obtain

$$\mathbf{F}^T C^T C \mathbf{F} = 1. \quad (6.43)$$

At a given manipulator configuration, Eq. (6.43) represents an m -dimensional force ellipsoid. Because $C^T C$ is symmetric positive semidefinite, its eigenvectors are orthogonal. The principal axes of the ellipsoid coincide with the eigenvectors of $C^T C$, and their lengths are equal to the reciprocals of the square roots of the eigenvalues. Hence the maximum and minimum forces required to produce a unit deflection are given by $1/\sqrt{\lambda_{\min}}$ and $1/\sqrt{\lambda_{\max}}$, respectively, where λ_{\min} and λ_{\max} are the minimum and maximum eigenvalues of $C^T C$.

Example 6.4.1 Stiffness Analysis of a Planar 2-DOF Manipulator Consider the planar 2-dof manipulator shown in Fig. 6.4 as an example. The end-effector deflection and output force are $\Delta \mathbf{x} = [\Delta x, \Delta y]^T$ and $\mathbf{F} = [f_x, f_y]^T$, respectively. We wish to examine the stiffness properties of this manipulator. Substituting the Jacobian matrix, Eq. (4.66), into (6.40), we obtain

$$C = \begin{bmatrix} \frac{(a_1 s_1 + a_2 s_{12})^2}{k_1} + \frac{a_2^2 s_{12}^2}{k_2} \\ - \frac{(a_1 s_1 + a_2 s_{12})(a_1 c_1 + a_2 c_{12})}{k_1} - \frac{a_2^2 s_{12} c_{12}}{k_2} \\ \frac{(a_1 s_1 + a_2 s_{12})(a_1 c_1 + a_2 c_{12})}{k_1} - \frac{a_2^2 s_{12} c_{12}}{k_2} \\ \frac{(a_1 c_1 + a_2 c_{12})^2}{k_1} + \frac{a_2^2 c_{12}^2}{k_2} \end{bmatrix}, \quad (6.44)$$

where $s_i = \sin \theta_i$, $c_i = \cos \theta_i$, $s_{ij} = \sin(\theta_i + \theta_j)$, and $c_{ij} = \cos(\theta_i + \theta_j)$.

For the purpose of demonstration, let $a_1 = \sqrt{2}$ m, $a_2 = 1$ m, $k_1 = k_2 = 1$ N·m, $\theta_1 = 0$, and $\theta_2 = \pi/2$. Then the compliance matrix reduces to

$$C = \begin{bmatrix} 2 & -\sqrt{2} \\ -\sqrt{2} & 2 \end{bmatrix}.$$

Hence

$$C^T C = \begin{bmatrix} 6 & -4\sqrt{2} \\ -4\sqrt{2} & 6 \end{bmatrix}.$$

Equation (6.43) reduces to

$$6f_x^2 + 8\sqrt{2} f_x f_y + 6f_y^2 = 0.343 \left(\frac{f_x}{\sqrt{2}} + \frac{f_y}{\sqrt{2}} \right)^2 + 11.657 \left(\frac{f_x}{\sqrt{2}} - \frac{f_y}{\sqrt{2}} \right)^2 = 1.$$

The equation above represents an ellipse in the end-effector force space. The eigenvalues of $C^T C$ are $\lambda_1 = 0.343$ and $\lambda_2 = 11.657$. The corresponding eigenvectors, normalized to unit length, are $(0.707, 0.707)$ and $(-0.707, 0.707)$, respectively. These two eigenvectors are at 45° angles with the f_x and f_y axes, respectively, and they line up with the principal axes of the ellipse.

6.5 STATICS OF PARALLEL MANIPULATORS

In this section we study the statics of parallel manipulators, which is more complicated than that of its serial counterpart. Due to the existence of several closed loops, the recursive method of analysis is no longer applicable. In general, it is necessary to derive the force and moment balance equations for each link and solve the equations simultaneously. However, if only the actuator drive forces and/or torques are of interest, the principle of virtual work can be applied (Bryfogle et al., 1993; Gosselin, 1990; Tahmasebi and Tsai, 1995).

6.5.1 Free-Body Diagram Approach

We first investigate the free-body diagram approach. A parallel manipulator typically consists of several limbs, each made up of several binary links. The analysis can be simplified greatly by making use of the fact that some of these binary links will bear only tension or compression forces. For example, if no external force or moment is applied to the binary link of a planar mechanism, the link will only be subject to tension or compression force along a line passing through the two revolute joints. Similarly, if no external force or moment is applied to a spherical-spherical binary link chain in a spatial mechanism, the link will only be subject to tension or compression force along a line pass-

ing through the two spherical centers. This method can best be demonstrated by examples.

Example 6.5.1 Statics of a Planar 3RRR Manipulator In this example we study the statics of the planar 3-dof parallel manipulator shown in Fig. 5.2. There are three limbs, each consisting of two members. The first member, a_i , is the input link; the second member, b_i , serves as a coupling link. Assuming that the acceleration of gravity is perpendicular to the plane of motion, we wish to find the joint torques, τ_1 , τ_2 , and τ_3 , required at the input links to produce an output force $\mathbf{f} = [f_x, f_y, 0]^T$ and an output moment $\mathbf{n} = [0, 0, n_z]^T$ at point G .

The forces exerted at the coupler link pass through its two end pivots, which can be written as

$$\mathbf{f}_i = \frac{\mathbf{f}_i \mathbf{b}_i}{b_i} \quad \text{for } i = 1, 2, 3, \quad (6.45)$$

where the subscript i denotes the i th limb, \mathbf{f}_i denotes the magnitude of \mathbf{f}_i , \mathbf{b}_i for $i = 1$ to 3 denote the vectors \overline{DA} , \overline{EB} , and \overline{FC} , respectively, and b_i denotes the magnitude of \mathbf{b}_i .

Summing all the forces acting on the moving platform, we obtain

$$\sum_{i=1}^3 \frac{\mathbf{f}_i \mathbf{b}_i}{b_i} = [f_x, f_y, 0]^T. \quad (6.46)$$

Summing the moments contributed by all forces about G , we obtain

$$\sum_{i=1}^3 \frac{\mathbf{e}_i \times \mathbf{f}_i \mathbf{b}_i}{b_i} = [0, 0, n_z]^T. \quad (6.47)$$

Equations (6.46) and (6.47) contain three nontrivial scalar equations in three unknowns, f_i for $i = 1, 2$, and 3. These three linear equations can be written in matrix form as

$$\begin{bmatrix} \frac{b_{1x}}{b_1} & \frac{b_{2x}}{b_2} & \frac{b_{3x}}{b_3} \\ \frac{b_{1y}}{b_1} & \frac{b_{2y}}{b_2} & \frac{b_{3y}}{b_3} \\ \frac{e_{1x}b_{1y} - e_{1y}b_{1x}}{b_1} & \frac{e_{2x}b_{2y} - e_{2y}b_{2x}}{b_2} & \frac{e_{3x}b_{3y} - e_{3y}b_{3x}}{b_3} \end{bmatrix} \begin{bmatrix} f_1 \\ f_2 \\ f_3 \end{bmatrix} = \begin{bmatrix} f_x \\ f_y \\ n_z \end{bmatrix}. \quad (6.48)$$

The vectors \mathbf{e}_i and \mathbf{b}_i are known from the kinematic analysis. Hence the three unknown forces, f_i for $i = 1, 2$, and 3 , can be found from the inverse transformation of Eq. (6.48). Once f_i for $i = 1, 2$, and 3 are known, the actuator torques can be found from the moment balance equation of each input link about its fixed pivot; that is,

$$\tau_i = \frac{f_i(a_{ix}b_{iy} - a_{iy}b_{ix})}{b_i}. \quad (6.49)$$

Eliminating f_i between Eqs. (6.48) and (6.49), we obtain

$$\begin{bmatrix} f_x \\ f_y \\ n_z \end{bmatrix} = \begin{bmatrix} \frac{b_{1x}}{a_{1x}b_{1y} - a_{1y}b_{1x}} & \frac{b_{2x}}{a_{2x}b_{2y} - a_{2y}b_{2x}} & \frac{b_{3x}}{a_{3x}b_{3y} - a_{3y}b_{3x}} \\ \frac{b_{1y}}{a_{1x}b_{1y} - a_{1y}b_{1x}} & \frac{b_{2y}}{a_{2x}b_{2y} - a_{2y}b_{2x}} & \frac{b_{3y}}{a_{3x}b_{3y} - a_{3y}b_{3x}} \\ \frac{a_{1x}b_{1y} - a_{1y}b_{1x}}{a_{1x}b_{1y} - a_{1y}b_{1x}} & \frac{a_{2x}b_{2y} - a_{2y}b_{2x}}{a_{2x}b_{2y} - a_{2y}b_{2x}} & \frac{a_{3x}b_{3y} - a_{3y}b_{3x}}{a_{3x}b_{3y} - a_{3y}b_{3x}} \end{bmatrix} \begin{bmatrix} \tau_1 \\ \tau_2 \\ \tau_3 \end{bmatrix}. \quad (6.50)$$

Equation (6.50) provides a transformation between the end-effector output forces and the input joint torques. Given the input joint torques, the end-effector output forces can be found directly from Eq. (6.50). On the other hand, given the end-effector output forces, we can find the input joint torques by the inverse transformation of Eq. (6.50).

Example 6.5.2 Statics of the Stewart–Gough Platform Consider the Stewart–Gough platform shown in Fig. 3.15. Let the origin O of the fixed (x, y, z) frame be located at the centroid of the fixed base with the x and y axes lying on the plane of the attachment points, A_i , for $i = 1$ to 6 . Also let the origin P of the moving (u, v, w) frame be located at the centroid of the moving platform, with its u and v axes lying on the plane of the attachment points, B_i , for $i = 1$ to 6 . Furthermore, let the gravitational effects be negligible. We wish to find the actuator forces, f_1, f_2, \dots, f_6 , required to produce an output force \mathbf{f} and an output moment \mathbf{n} at the centroid of the moving platform.

The forces and moments of constraint associated each prismatic joint can be considered as internal to the limb. Because of the spherical–spherical limb construction, no moment can be transmitted to the limb. In addition, the reaction force at each spherical joint points along line A_iB_i defined by the two spherical centers. Hence the force acting on the moving platform by each limb can be written as

$$\mathbf{f}_i = f_i \mathbf{s}_i \quad \text{for } i = 1, 2, \dots, 6, \quad (6.51)$$

where the subscript i denotes the i th limb, f_i denotes the magnitude of \mathbf{f}_i , and \mathbf{s}_i denotes a unit vector pointing from the base spherical joint to the moving spherical joint of the i th limb, namely, $\mathbf{s}_i = \mathbf{d}_i/d_i$.

We now form the force and moment balance equations of the moving platform. Summing all the forces acting on the moving platform, we obtain

$$\sum_{i=1}^6 f_i \mathbf{s}_i = \mathbf{f}. \quad (6.52)$$

Summing the moments contributed by all forces about the centroid P of the moving platform, we obtain

$$\sum_{i=1}^6 f_i \mathbf{b}_i \times \mathbf{s}_i = \mathbf{n}, \quad (6.53)$$

where $\mathbf{b}_i = \overline{PB_i}$. Equations (6.52) and (6.53) represent six linear scalar equations in f_i which can be written in matrix form as

$$\begin{bmatrix} \mathbf{f} \\ \mathbf{n} \end{bmatrix} = \begin{bmatrix} \mathbf{s}_1 & \mathbf{s}_2 & \cdots & \mathbf{s}_6 \\ \mathbf{b}_1 \times \mathbf{s}_1 & \mathbf{b}_2 \times \mathbf{s}_2 & \cdots & \mathbf{b}_6 \times \mathbf{s}_6 \end{bmatrix} \begin{bmatrix} f_1 \\ f_2 \\ \vdots \\ f_6 \end{bmatrix}. \quad (6.54)$$

Equation (6.54) provides a transformation between the end-effector output forces and the linear actuator forces. The vectors \mathbf{b}_i and \mathbf{s}_i are known from the kinematic analysis. Hence given the actuator forces, the end-effector output forces can be computed directly from Eq. (6.54). On the other hand, if the end-effector output forces are given, we can find the corresponding actuator forces by the inverse transformation of Eq. (6.54).

6.5.2 Application of the Principle of Virtual Work

As mentioned in Chapter 5, there are two types of joints in a parallel manipulator: actuated joints and passive joints. Assuming that the joints are frictionless and the gravitational effects are negligible, the reaction forces at the passive joints contribute to no virtual work.

Let $\mathbf{F} = [\mathbf{f}, \mathbf{n}]^T$ represent the vector of end-effector output force and moment, $\boldsymbol{\tau} = [\tau_1, \tau_2, \dots, \tau_n]^T$ represent the vector of actuated joint torques or forces, $\delta\mathbf{q} = [\delta q_1, \delta q_2, \dots, \delta q_n]^T$ represent the vector of virtual displacements associated with the actuated joints, and $\delta\mathbf{x} = [\delta x, \delta y, \dots, \delta \psi]^T$ represent the vector of virtual displacements associated with the end effector. Then

the virtual work contributed by all the active forces can be written as

$$\boldsymbol{\tau}^T \delta \mathbf{q} - \mathbf{F}^T \delta \mathbf{x} = 0. \quad (6.55)$$

However, the virtual displacements, $\delta \mathbf{q}$ and $\delta \mathbf{x}$, are related by the Jacobian matrix

$$\delta \mathbf{q} = J \delta \mathbf{x}, \quad (6.56)$$

where $J = J_q^{-1} J_x$ is as defined in Chapter 5.

Substituting Eq. (6.56) into (6.55) yields

$$(\boldsymbol{\tau}^T J - \mathbf{F}^T) \delta \mathbf{x} = 0. \quad (6.57)$$

Since Eq. (6.57) holds for any virtual displacement, $\delta \mathbf{x}$, we conclude that

$$\boldsymbol{\tau}^T J - \mathbf{F}^T = 0. \quad (6.58)$$

Taking the transpose of Eq. (6.58) yields

$$\mathbf{F} = J^T \boldsymbol{\tau}. \quad (6.59)$$

Equation (6.59) gives the end-effector output forces in terms of the actuated joint torques, and vice versa, via the inverse transformation. Because the Jacobian matrix for a parallel manipulator is defined as the inverse of that for a serial manipulator, Eq. (6.59) takes a different form from that of Eq. (6.27). Clearly, the transformation depends on the posture of a robot.

Example 6.5.3 Planar 3RRR Parallel Manipulator In this example we perform the static analysis of the planar 3-dof parallel manipulator shown in Fig. 5.2 by the principle of virtual work. The Jacobian of this manipulator was derived in Chapter 5. The vector of input joint rates is $\dot{\mathbf{q}} = [\dot{\theta}_1, \dot{\theta}_2, \dot{\theta}_3]^T$, and the vector of end-effector velocities is $\dot{\mathbf{x}} = [v_{gx}, v_{gy}, \dot{\phi}]^T$. The Jacobian matrices, derived in Chapter 5, are

$$J_x = \begin{bmatrix} b_{1x} & b_{1y} & e_{1x}b_{1y} - e_{1y}b_{1x} \\ b_{2x} & b_{2y} & e_{2x}b_{2y} - e_{2y}b_{2x} \\ b_{3x} & b_{3y} & e_{3x}b_{3y} - e_{3y}b_{3x} \end{bmatrix}, \quad (6.60)$$

$$J_q = \begin{bmatrix} a_{1x}b_{1y} - a_{1y}b_{1x} & 0 & 0 \\ 0 & a_{2x}b_{2y} - a_{2y}b_{2x} & 0 \\ 0 & 0 & a_{3x}b_{3y} - a_{3y}b_{3x} \end{bmatrix}. \quad (6.61)$$

Assuming that $\mathbf{a}_i \times \mathbf{b}_i \neq 0$, the overall Jacobian matrix is given by

$$J = J_q^{-1} J_x = \begin{bmatrix} \frac{b_{1x}}{a_{1x}b_{1y} - a_{1y}b_{1x}} & \frac{b_{1y}}{a_{1x}b_{1y} - a_{1y}b_{1x}} & \frac{e_{1x}b_{1y} - e_{1y}b_{1x}}{a_{1x}b_{1y} - a_{1y}b_{1x}} \\ \frac{b_{2x}}{a_{2x}b_{2y} - a_{2y}b_{2x}} & \frac{b_{2y}}{a_{2x}b_{2y} - a_{2y}b_{2x}} & \frac{e_{2x}b_{2y} - e_{2y}b_{2x}}{a_{2x}b_{2y} - a_{2y}b_{2x}} \\ \frac{b_{3x}}{a_{3x}b_{3y} - a_{3y}b_{3x}} & \frac{b_{3y}}{a_{3x}b_{3y} - a_{3y}b_{3x}} & \frac{e_{3x}b_{3y} - e_{3y}b_{3x}}{a_{3x}b_{3y} - a_{3y}b_{3x}} \end{bmatrix}. \quad (6.62)$$

Substituting Eq. (6.62) into (6.59), we obtain

$$\begin{bmatrix} f_x \\ f_y \\ n_z \end{bmatrix} = \begin{bmatrix} \frac{b_{1x}}{a_{1x}b_{1y} - a_{1y}b_{1x}} & \frac{b_{2x}}{a_{2x}b_{2y} - a_{2y}b_{2x}} & \frac{b_{3x}}{a_{3x}b_{3y} - a_{3y}b_{3x}} \\ \frac{b_{1y}}{a_{1x}b_{1y} - a_{1y}b_{1x}} & \frac{b_{2y}}{a_{2x}b_{2y} - a_{2y}b_{2x}} & \frac{b_{3y}}{a_{3x}b_{3y} - a_{3y}b_{3x}} \\ \frac{e_{1x}b_{1y} - e_{1y}b_{1x}}{a_{1x}b_{1y} - a_{1y}b_{1x}} & \frac{e_{2x}b_{2y} - e_{2y}b_{2x}}{a_{2x}b_{2y} - a_{2y}b_{2x}} & \frac{e_{3x}b_{3y} - e_{3y}b_{3x}}{a_{3x}b_{3y} - a_{3y}b_{3x}} \end{bmatrix} \begin{bmatrix} \tau_1 \\ \tau_2 \\ \tau_3 \end{bmatrix}. \quad (6.63)$$

Hence we have arrived at the same result as that derived by the free-body diagram analysis.

Example 6.5.4 Stewart-Gough Platform Let us consider the Stewart-Gough platform shown in Fig. 3.15 as a second example. Using the conventional approach, the end-effector velocity state is defined as

$$\dot{\mathbf{x}} = \begin{bmatrix} \mathbf{v}_p \\ \boldsymbol{\omega}_B \end{bmatrix}, \quad (6.64)$$

and the input joint rates are described by a six-dimensional vector,

$$\dot{\mathbf{q}} = [\dot{d}_1, \dot{d}_2, \dots, \dot{d}_6]^T. \quad (6.65)$$

The Jacobian matrices, derived in Chapter 5, are

$$J_x = \begin{bmatrix} \mathbf{s}_1^T & (\mathbf{b}_1 \times \mathbf{s}_1)^T \\ \mathbf{s}_2^T & (\mathbf{b}_2 \times \mathbf{s}_2)^T \\ \vdots & \vdots \\ \mathbf{s}_6^T & (\mathbf{b}_6 \times \mathbf{s}_6)^T \end{bmatrix} \quad (6.66)$$

$$J_q = I \quad (6.67)$$

Hence the overall Jacobian matrix is given by

$$J = J_q^{-1} J_x = \begin{bmatrix} s_1^T & (\mathbf{b}_1 \times s_1)^T \\ s_2^T & (\mathbf{b}_2 \times s_2)^T \\ \vdots & \vdots \\ s_6^T & (\mathbf{b}_6 \times s_6)^T \end{bmatrix}. \quad (6.68)$$

Substituting Eq. (6.68) into (6.59), we obtain

$$\begin{bmatrix} \mathbf{f} \\ \mathbf{n} \end{bmatrix} = \begin{bmatrix} s_1 & s_2 & \cdots & s_6 \\ \mathbf{b}_1 \times s_1 & \mathbf{b}_2 \times s_2 & \cdots & \mathbf{b}_6 \times s_6 \end{bmatrix} \begin{bmatrix} f_1 \\ f_2 \\ \vdots \\ f_6 \end{bmatrix}. \quad (6.69)$$

Again, we have arrived at the same result as that derived by the free-body diagram analysis.

6.6 STIFFNESS ANALYSIS OF PARALLEL MANIPULATORS

The stiffness analysis of parallel manipulators has been the subject of recent study by several workers (Gosselin, 1990; Kerr, 1989; Lebret et al., 1993; Tahmasebi and Tsai, 1995). We shall assume that, similar to serial manipulators, the links are perfectly rigid and consider the mechanical transmission mechanisms and servo systems as the only sources of compliance.

Let $\tau = [\tau_1, \tau_2, \dots, \tau_n]^T$ be the vector of actuated joint torques or forces and $\Delta \mathbf{q} = [\Delta q_1, \Delta q_2, \dots, \Delta q_n]^T$ be the corresponding vector of joint deflections. Then we can relate $\Delta \mathbf{q}$ to τ by an $n \times n$ diagonal matrix, $\chi = \text{diag}[k_1, k_2, \dots, k_n]$, as follows:

$$\tau = \chi \Delta \mathbf{q}. \quad (6.70)$$

For a parallel manipulator, the joint displacement, $\Delta \mathbf{q}$, is related to the end-effector deflection, $\Delta \mathbf{x} = [\Delta x, \Delta y, \Delta z, \Delta \phi, \Delta \theta, \Delta \psi]^T$, by the Jacobian matrix, J :

$$\Delta \mathbf{q} = J \Delta \mathbf{x}, \quad (6.71)$$

where $J = J_q^{-1} J_x$ is the conventional Jacobian matrix defined in Chapter 5. Substituting Eq. (6.71) into (6.70) and the resulting equation into (6.59) yields

$$\mathbf{F} = K \Delta \mathbf{x}, \quad (6.72)$$

where

$$K = J^T \chi J \quad (6.73)$$

is called the *stiffness matrix* of a parallel manipulator.

Equation (6.72) implies that the end-effector output force is related to its deflection by the stiffness matrix K . The stiffness matrix is symmetric, positive semidefinite, and manipulator configuration dependent. Furthermore, if the limbs are of the same type and the spring constants associated with all the drive lines are of the same value (i.e., $k_1 = k_2 = \dots = k_6 = k$), the stiffness matrix reduces to the form

$$K = k J^T J. \quad (6.74)$$

6.6.1 Stiffness Analysis of a 3-3 Stewart-Gough Platform

Figure 6.8 shows a schematic diagram of the 3-3 Stewart-Gough platform studied by Kerr (1989). There are six extensible limbs connecting a moving platform to a fixed base by two sets of concentric spherical joints located at points A_i and B_i , respectively. We wish to analyze the stiffness of this manipulator.

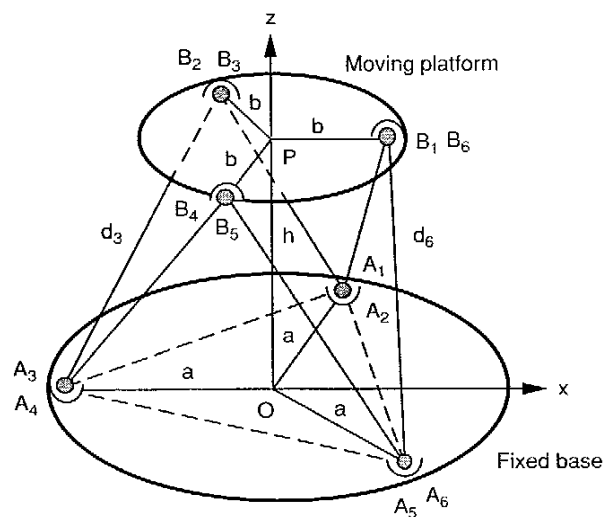


FIGURE 6.8. A 3-3 Stewart-Gough platform.

For the purpose of analysis, we attach an (x, y, z) coordinate frame to the fixed base with its origin O located at the centroid of the fixed base, its x and y axes lying on the plane of the attachment points, $A_i, i = 1, \dots, 6$, its x -axis pointing in the direction opposite to $\overline{OA_3}$, and its z -axis pointing out of the plane of the attachment points, as shown in Fig. 6.8. Furthermore, we assume that the two sets of concentric spherical joints form two equilateral triangles. Since the stiffness matrix depends on the position and orientation of the moving platform, in what follows we assume that the moving platform is located at a *central configuration*, where the moving platform is not rotated with respect to the fixed base and the centroid of the moving platform is at an elevation $\overline{OP} = h$ above the centroid of the fixed base, as shown in Figs. 6.8 and 6.9.

From the geometry of the platform shown in Figs. 6.8 and 6.9, we obtain the vectors \mathbf{a}_i , \mathbf{b}_i , and \mathbf{d}_i expressed in the fixed (x, y, z) frame as follows:

$$\mathbf{a}_1 = \mathbf{a}_2 = \left[\frac{a}{2}, \frac{\sqrt{3}a}{2}, 0 \right]^T,$$

$$\mathbf{a}_3 = \mathbf{a}_4 = [-a, 0, 0]^T,$$

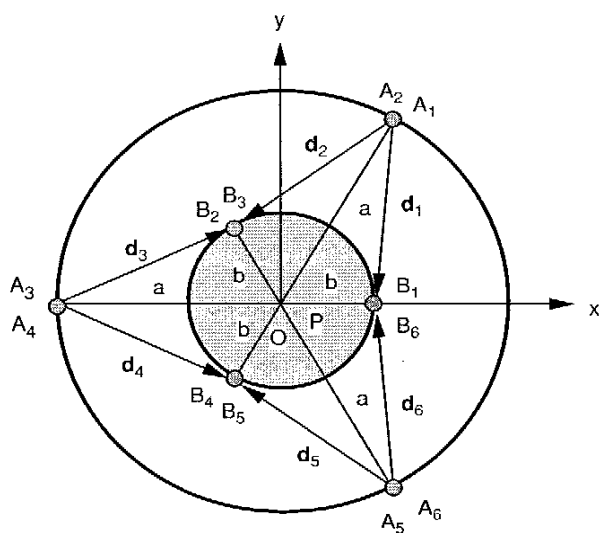


FIGURE 6.9. Top view of the 3-3 Stewart-Gough platform.

$$\mathbf{a}_5 = \mathbf{a}_6 = \left[\frac{a}{2}, -\frac{\sqrt{3}a}{2}, 0 \right]^T,$$

$$\mathbf{b}_1 = \mathbf{b}_6 = [b, 0, 0]^T,$$

$$\mathbf{b}_2 = \mathbf{b}_3 = \left[-\frac{b}{2}, \frac{\sqrt{3}b}{2}, 0 \right]^T,$$

$$\mathbf{b}_4 = \mathbf{b}_5 = \left[-\frac{b}{2}, -\frac{\sqrt{3}b}{2}, 0 \right]^T,$$

$$\mathbf{d}_1 = \left[\frac{2b-a}{2}, -\frac{\sqrt{3}a}{2}, h \right]^T,$$

$$\mathbf{d}_2 = \left[\frac{-b-a}{2}, \frac{\sqrt{3}(b-a)}{2}, h \right]^T,$$

$$\mathbf{d}_3 = \left[\frac{-b+2a}{2}, \frac{\sqrt{3}b}{2}, h \right]^T,$$

$$\mathbf{d}_4 = \left[\frac{-b+2a}{2}, -\frac{\sqrt{3}b}{2}, h \right]^T,$$

$$\mathbf{d}_5 = \left[\frac{-b-a}{2}, \frac{\sqrt{3}(-b+a)}{2}, h \right]^T,$$

$$\mathbf{d}_6 = \left[\frac{2b-a}{2}, \frac{\sqrt{3}a}{2}, h \right]^T.$$

At the central configuration, all the limbs are extended at equal lengths (i.e., $d_1 = d_2 = \dots = d_6 = d$). This leads to a simple relation between a, b, h , and d :

$$d^2 = a^2 + ab + b^2 + h^2. \quad (6.75)$$

Substituting the expressions above into Eq. (6.68), we obtain

$$J = \frac{1}{2d} \begin{bmatrix} 2b - a & -\sqrt{3}a & 2h & 0 & -2bh & -\sqrt{3}ab \\ -b - a & \sqrt{3}(b-a) & 2h & \sqrt{3}bh & bh & \sqrt{3}ab \\ -b + 2a & \sqrt{3}b & 2h & \sqrt{3}bh & bh & -\sqrt{3}ab \\ -b + 2a & -\sqrt{3}b & 2h & -\sqrt{3}bh & bh & \sqrt{3}ab \\ -b - a & \sqrt{3}(-b+a) & 2h & -\sqrt{3}bh & bh & -\sqrt{3}ab \\ 2b - a & \sqrt{3}a & 2h & 0 & -2bh & \sqrt{3}ab \end{bmatrix} \quad (6.76)$$

Substituting Eq. (6.76) and its transpose into (6.74), we obtain the stiffness matrix as

$$K = \frac{3k}{d^2} \times \begin{bmatrix} a^2 + b^2 - ab & 0 & 0 & 0 & bh(a/2 - b) & 0 \\ 0 & a^2 + b^2 - ab & 0 & -bh(a/2 - b) & 0 & 0 \\ 0 & 0 & 2h^2 & 0 & 0 & 0 \\ 0 & -bh(a/2 - b) & 0 & b^2h^2 & 0 & 0 \\ bh(a/2 - b) & 0 & 0 & 0 & b^2h^2 & 0 \\ 0 & 0 & 0 & 0 & 0 & 3a^2b^2/2 \end{bmatrix} \quad (6.77)$$

The upper left 3×3 submatrix represents the translational stiffness, the lower right 3×3 submatrix represents the torsional stiffness, and the other submatrices represent the cross-coupling effects between forces and moments, and between rotations and translations, respectively.

In practice, it is desirable to eliminate the cross-coupling terms. Fortunately, this can easily be achieved by choosing $a = 2b$ as a design condition. Substituting $a = 2b$ into (6.77) yields

$$K = \frac{3k}{d^2} \begin{bmatrix} 3b^2 & 0 & 0 & 0 & 0 & 0 \\ 0 & 3b^2 & 0 & 0 & 0 & 0 \\ 0 & 0 & 2h^2 & 0 & 0 & 0 \\ 0 & 0 & 0 & b^2h^2 & 0 & 0 \\ 0 & 0 & 0 & 0 & b^2h^2 & 0 \\ 0 & 0 & 0 & 0 & 0 & 6b^4 \end{bmatrix} \quad (6.78)$$

Observation of Eq. (6.78) reveals that three special designs are possible:

Case 1. $h^2 = 1.5b^2$ results in an isotropic translational stiffness, or

Case 2. $h^2 = 6b^2$ results in an isotropic torsional stiffness, or

Case 3. A compromise design between cases 1 and 2.

We note that without introducing additional design parameters, it is not possible to achieve both isotropic translational and isotropic torsional stiffness characteristics. Additional design parameters can be obtained by separating those concentric spherical joints located at either the moving platform or the fixed base.

6.7 SUMMARY

We have presented two methods of analysis, a free-body diagram method and the principle of virtual work, for the static analysis of serial and parallel manipulators. The free-body diagram method yields all the reaction forces acting on both the passive and actuated joints. While the principle of virtual work is more straightforward, it produces only the actuated joint forces. It was shown that in the absence of gravity, the actuated joint forces are related to the end-effector output forces by the transpose of the Jacobian matrix. The transformation characteristics were examined in detail by applying the theory of linear transformation. Furthermore, the stiffness characteristics of serial and parallel manipulators were examined. We have shown that the end-effector output forces are related to its deflections by a stiffness matrix. The stiffness matrix is a function of the stiffness constants of the drive lines and the Jacobian matrix of the manipulator. Since the Jacobian matrix is configuration dependent, the stiffness matrix is also configuration dependent. The statics and stiffness analyses of several manipulators were analyzed to illustrate the principles.

REFERENCES

- Agrawal, S. K. and Roth, B., 1992, "Statics of In-Parallel Manipulator Systems," *ASME J. Mech. Des.*, Vol. 114, pp. 564-568.
- Asada, H. and Slotine, J. J. E., 1986, *Robot Analysis and Control*, Wiley, New York.
- Bagci, C., 1971, "Static Force and Torque Analysis Using 3×3 Screw Matrix, and Transmission Criterion for Space Mechanisms," *ASME J. Eng. Ind.*, Vol. 93, Ser. B, No. 1, pp. 90-101.
- Beyer, R., 1960, "Statics and Dynamics in 3-D Mechanisms," *Trans. 6th Conference on Mechanisms*, Purdue University, West Lafayette, IN, pp. 94-112.
- Bryfogle, M. D., Nguyen, C. C., Antrazi, S. S., and Chiou, P. C., 1993, "Kinematics and Control of a Fully Parallel Force-Reflecting Hand Controller for Manipulator Teleoperation," *J. Robot. Syst.*, Vol. 10, No. 5, pp. 745-766.
- Cannon, R. H. and Schmitz, E., 1984, "Initial Experiments on the End-Point Control of a Flexible One-Link Robot," *Int. J. Robot. Res.*, Vol. 3, No. 3, pp. 62-75.

- Chace, M., 1962, "Mechanism Analysis by Vector Mathematics," *Trans. 7th Conference on Mechanisms*, Purdue University, West Lafayette, IN, pp. 100–113.
- Chang, L. and Hamilton, J. F., 1991, "Dynamics of Robot Manipulators with Flexible Links," *ASME J. Dyn. Syst. Meas. Control*, Vol. 113, pp. 54–59.
- Denavit, J. et al., 1965, "Velocity, Acceleration, and Static Force Analyses of Spatial Linkages," *ASME J. Appl. Mech.*, Ser. E, Vol. 32, pp. 903–910.
- Gosselin, C., 1990, "Stiffness Mapping of Parallel Manipulators," *IEEE Trans. Robot. Autom.*, Vol. 6, pp. 377–382.
- Hollars, M. G. and Cannon, R. H., 1985, "Initial Experiments on the End-Point Control of a Two-Link Manipulator with Flexible Tendons," *Proc. ASME Winter Annual Meeting*, Miami, FL.
- Kerr, D. R., 1989, "Analysis, Properties, and Design of a Stewart Platform Transducer," *ASME J. Mech. Transm. Autom. Des.*, Vol. 111, pp. 25–28.
- Lebret, G., Liu, K., and Lewis, F. L., 1993, "Dynamic Analysis and Control of a Stewart Platform Manipulator," *J. Robot. Syst.*, Vol. 10, No. 5, pp. 629–655.
- Nguyen, P. K. and Ravindran, R., 1977, "Kinematics and Control of the Space Shuttle Remote Manipulator System," *Proc. 7th Canadian Congress on Applied Mechanics*, Vancouver, British Columbia, Canada.
- Paul, R. P., 1981, *Robot Manipulators: Mathematics, Programming, and Control*, MIT Press, Cambridge, MA.
- Sunada, W. H. and Dubowsky, S., 1983, "On the Dynamic Analysis and Behavior of Industrial Robotic Manipulators with Elastic Members," *ASME J. Mech. Transm. Autom. Des.*, Vol. 105, pp. 42–51.
- Sweet, L. M. and Good, M. C., 1984, "Redefinition of the Robot Control Problem: Effects of Plant Dynamics, Drive System Constraints, and User Requirements," *Proc. IEEE Conference on Decision and Control*, Las Vegas, NV.
- Tahmasebi, F. and Tsai, L. W., 1995, "On the Stiffness of a Novel Six-Degree-of-Freedom Parallel Manipulator," *J. Robot. Syst.*, Vol. 12, No. 12, pp. 845–856.
- Witney, D. E., 1972, "The Mathematics of Coordinated Control of Prosthetic Arms and Manipulators," *ASME J. Dyn. Syst. Meas. Control*, Vol. 122, pp. 303–309.
- Yang, A. T., 1965, "Static Force and Torque Analysis of Spherical Four-Bar Mechanisms," *ASME J. Eng. Ind.*, Vol. 87, Ser. B, No. 2, pp. 221–227.

EXERCISES

- Figure 6.10 shows the planar five-bar 5R manipulator studied in Chapter 1. Calculate the actuator torques, τ_1 and τ_2 , required to produce an output force of $(0, f_y)$ N at point Q. Investigate the conditions that will result in infinite input torques.
- Figure 6.11 shows the pantograph mechanism studied in Chapter 1. Calculate the actuator forces, f_1 and f_2 , required to produce an output force of (f_x, f_y) N at point Q.

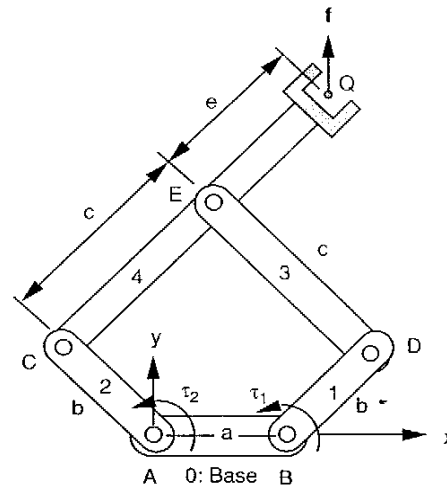


FIGURE 6.10. Statics of a five-bar manipulator.

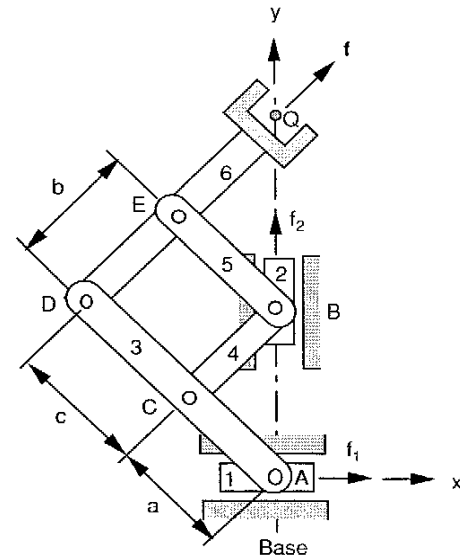


FIGURE 6.11. Statics of a pantograph.

- Using the free-body diagram method, determine the actuator torques and/or forces required to produce an end-effector output force of $(0, 0, f_z)$ N at point Q of the SCARA arm shown in Fig. 2.4. Express these torques as functions of joint angles.
- Using the free-body diagram method, find the actuator forces required to produce an output force of $(f_x, 0)$ N at the centroid of the planar 3RPR parallel manipulator shown in Fig. 6.12. Let the prismatic joints be the actuated joints.

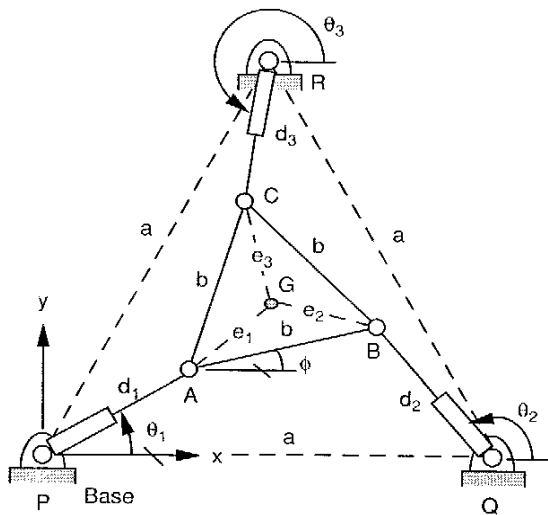


FIGURE 6.12. Schematic diagram of a planar 3RPR manipulator.

- For the DELTA robot shown in Fig. 3.21, let the moving platform be located directly on top of the fixed platform. Also let the sizes of the two platforms be the same. Calculate the joint torques required to produce an end effector output force of $(0, 0, f_z)$ N. Show that the actuator torques tend to infinity as the moving platform approaches the fully stretched location.
- Calculate the actuator torques required to generate an end-effector output force $\mathbf{f} = (f_x, f_y)$ N at point Q of the planar five-bar 4R1P manipulator shown in Fig. 3.19 by the principle of virtual work.

- Calculate the joint torques required to produce an end-effector output force $\mathbf{f} = (f_x, f_y, f_z)$ N at point Q of the SCARA arm shown in Fig. 2.4 by the principle of virtual work.
- Derive the stiffness matrix of the planar five-bar 5R manipulator shown in Fig. 6.10. Under what conditions will the manipulator lose its stiffness?
- Derive the stiffness matrix of the manipulator shown in Fig. 5.15, assuming that the moving platform is located at a central location. Under what conditions will the stiffness matrix become decoupled?

CHAPTER 7

WRIST MECHANISMS

7.1 INTRODUCTION

A robot manipulator needs at least 6 degrees of freedom to manipulate an object freely in space. Typically, the lengths of the first three moving links are much longer than those of the last three links. An end effector is attached to the last moving link for grasping or fine manipulation of an object. Thus the first three moving links are used primarily for manipulating the position, while the last three links are used for controlling the orientation of the end effector. For this reason, the subassembly associated with the first three moving links is called the *arm*, and the subassembly associated with the last three moving links is called the *wrist*. Furthermore, the last three joint axes are often designed to intersect at a common point called the *wrist center*. As discussed in Chapter 2, such a special arrangement leads to complete decoupling of the position from the orientation problem. The arm delivers the wrist center anywhere in its primary workspace, while the wrist controls the orientation of the end effector.

Figure 7.1 shows the kinematic structure of a 3-dof serial wrist mechanism with three intersecting joint axes, while Fig. 7.2 shows a wrist mechanism with a small offset distance between the first and second joint axes of the assembly. Theoretically, we can mount one motor with a proper gear reduction unit on each link to drive the joints. This kind of arrangement, however, requires the motors and their gear reduction units to be located close to the wrist subassembly, which will inevitably increase the inertia load to the motors of the arm subassembly. Therefore, it is highly desirable to incorporate some

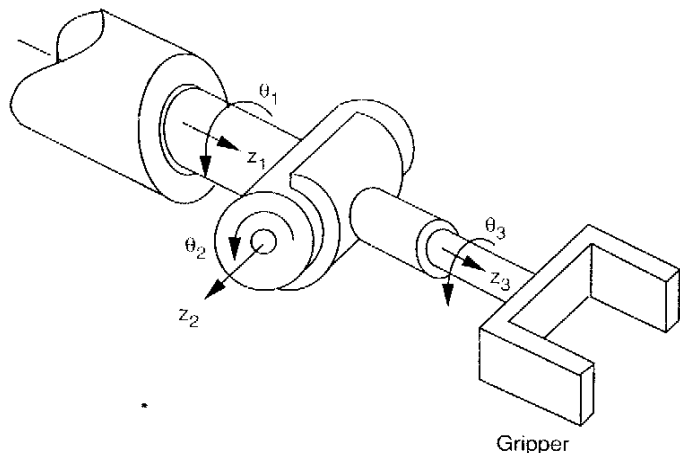


FIGURE 7.1. Spherical wrist mechanism.

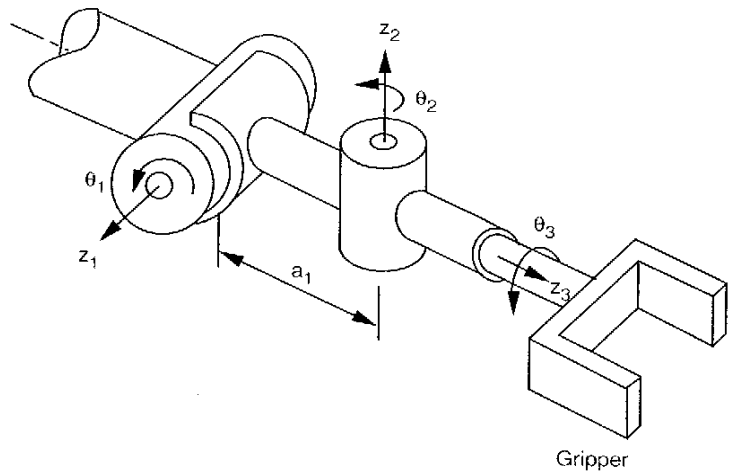


FIGURE 7.2. Nonspherical wrist mechanism.

kind of mechanical transmission mechanisms, which allow the actuators to be installed away from the wrist center.

In practice, a good wrist design should possess the following characteristics:

1. Three degrees of freedom
2. Spherical motion
3. Large workspace (i.e., large angular orientation range)
4. Remote drive capability
5. Compact size, light weight, and low inertia
6. High accuracy and repeatability
7. High mechanical stiffness
8. Low manufacturing cost
- 9.* Rugged and reliable design

The development of wrist mechanisms can be dated back to the early nineteenth century. It is related especially to the needs in handling nuclear materials, in space exploration, and for other hazardous tasks. To achieve the necessary characteristics, mechanical transmission mechanisms such as epicyclic gear trains, push-rod linkages, and tendon drives are often employed (Rivin, 1987; Rosheim, 1989). Rosheim's book provides a thorough survey of recent developments in wrist technology, with many published and patented mechanisms, design suggestions, and other relevant information for the design of wrist mechanisms. An atlas of simple bevel-gear wrist mechanisms can be found in Lin and Tsai (1989) and Lin (1990).

Epicyclic gear drives are commonly used for speed reduction and torque amplification in mechanical systems. Bevel-gear wrist mechanisms have been incorporated in most industrial robots because they are comparatively simple and compact in size, can be sealed in a metallic housing that keeps the gear trains free of contamination, and can be produced economically and reliably. Furthermore, using bevel gear trains for power transmission, actuators can be mounted remotely on the forearm, thereby reducing the weight and inertia of a robot manipulator.

In this chapter we focus on the kinematics and statics of epicyclic gear drives and, in particular, geared robotic wrist mechanisms. First we describe some of the commonly used bevel-gear wrist mechanisms, their structure characteristics, and classifications. Then we present a systematic methodology for the kinematic analysis using the concept of fundamental circuits and the equivalent open-loop chain. Finally, we introduce the concept of transmission lines for the static analysis of such mechanisms.

7.2 BEVEL-GEAR WRIST MECHANISMS

Epicyclic gear trains have been used to transmit motion for thousands of years. The earliest known example, perhaps, is the "South-Pointing Chariot," invented around 2600 B.C. by the ancient Chinese (Dudley, 1969). This device uses an ingenious differential gear train to constrain a figurehead mounted on top of the chariot always to point to the south. It is believed that the ancient Chinese used this device to keep them from getting lost in the Gobi desert. Other early examples of gear trains include water clocks, cord-winding and rope-laying machines, and steam engines (White, 1987, 1988). A survey of planetary gear trains, complete with angular velocity equations, can be found in Glover (1964, 1965). Dudley (1969) provides a review of the historical development of gear trains from 3000 B.C. to the 1960s.

The application of epicyclic gear trains to the development of robotic mechanisms did not occur until after the nineteenth century (Anonymous, 1982; Stackhouse, 1979; Trevelyan et al., 1986). A wrist requires at least 3 degrees of freedom to locate the end effector in an arbitrary orientation. This implies a minimum of three independent rotations about three noncoplanar intersecting joint axes. If such a motion is to be realized with gearing, this necessitates a 3-dof bevel gear train of gyroscopic complexity. Furthermore, the three input links of such a gear train should be coaxial to achieve remote drive capability.

Figure 7.3 shows the schematic diagram of a wrist mechanism developed by Cincinnati-Milacron (Stackhouse, 1979). The mechanism consists of seven links (including the forearm), six turning pairs, and three bevel gear

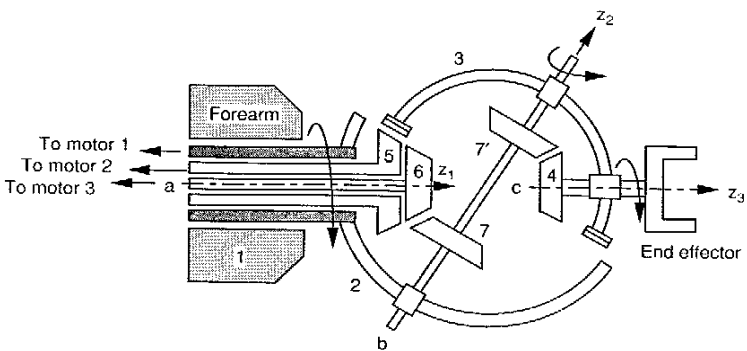


FIGURE 7.3. Cincinnati-Milacron T³ wrist mechanism.

pairs. There are three independent axes of rotation, z_1 , z_2 , and z_3 . The twist angle between the first and second joint axes is 60° , and between the second and third joint axes is -60° .

In the Cincinnati-Milacron wrist, link 2 serves as the carrier for the 5–3 and 6–7 bevel gear pairs, while link 3 serves as the carrier for the 7–4 bevel gear pair. Gears 7 and 7' are rigidly connected together by a single shaft that is housed in both carriers 2 and 3. Three coaxial members, numbered 2, 5, and 6, are supported by bearings housed in the forearm. Torques are transmitted from motors 1, 2, and 3 located in the proximal end of the forearm (not shown) to the three coaxial links. Rotation of link 5 is transmitted to link 3 via the 5–3 gear pair, while rotation of link 6 is transmitted to link 4 via the 6–7 and 7'–4 gear pairs. An end effector is attached to link 4, which is housed in the carrier 3. Furthermore, the three joint axes intersect at a common point. Therefore, the wrist mechanism is a 3-dof spherical mechanism.

The wrist roll motion is achieved by rotating link 2 with respect to link 1 about the z_1 -axis. The pitch motion is accomplished by rotating link 3 with respect to link 2 about the z_2 -axis. The end-effector roll motion is obtained by rotating link 4 with respect to link 3 about the z_3 -axis. An important feature of this wrist mechanism is that there is no mechanical interference between all the links. Therefore, continuously unobstructed rotations about the three joint axes can be achieved.

Figure 7.4 shows the schematic diagram of another wrist developed by the Bendix Corporation (Anonymous, 1982). The Bendix wrist consists of eight links (including the forearm), seven turning pairs, and four bevel gear pairs.

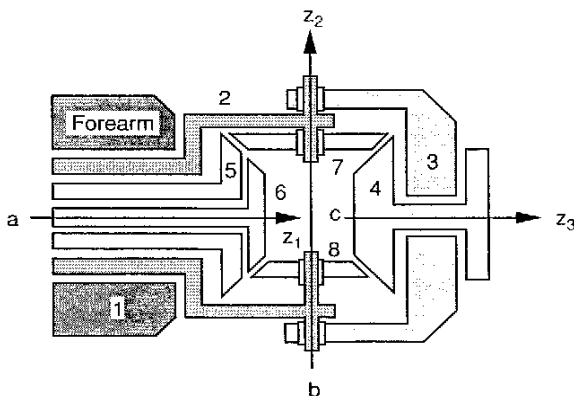


FIGURE 7.4. Bendix wrist mechanism.

There are three articulation points, axes z_1 , z_2 , and z_3 , respectively. The twist angles are 90° between the first and second joint axes, and -90° between the second and third joint axes.

In the Bendix wrist, link 2 serves as the carrier for the 5–7 and 6–8 bevel gear pairs, while link 3 serves as the carrier for the 7–4 and 8–4 bevel gear pairs. Three coaxial members, numbered 2, 5, and 6, are supported by bearings housed in the forearm. Torques are transmitted from motors located in the proximal end of the forearm (not shown) to the three coaxial links. Bevel gear pairs 5–7, 7–4, 6–8, and 8–4 transmit rotations of the coaxial input links to the end effector attached to link 4 and housed in carrier 3. Furthermore, the three joint axes intersect at a common point. Therefore, the Bendix wrist is also a 3-dof spherical mechanism. Unlike the Cincinnati-Milacron wrist, the Bendix wrist has a limited rotational range about the second joint axis.

7.3 STRUCTURE REPRESENTATION OF MECHANISMS

In this section we describe the functional schematic, graph, and canonical graph representations of the kinematic structure of a mechanism. The following assumptions are made for all representations:

1. For simplicity, all parallel redundant paths in a mechanism will be shown as a single path only. Parallel paths are generally used to increase load capacity and to achieve a better dynamic balance of a mechanism. For example, only one planet gear will be sketched for a basic planetary gear train with multiple planets. Similarly, when a link is supported by two bearings on one shaft, only one will be shown.
2. Two mechanical elements rigidly connected for the ease of manufacturing or assembling will be considered as one link. For example, two gears keyed together with a common shaft is considered as one link from the kinematic point of view.
3. All joints are assumed to be binary. A multiple joint will be replaced by a proper combination of several binary joints. For example, a ternary joint is replaced by two coaxial binary joints, a quaternary joint is replaced by three coaxial binary joints, and so on.

7.3.1 Functional Schematic Representation

The *functional schematic representation* of a mechanism refers to the conventional drawing of the mechanism. Shafts, gears, and other elements are identified as such. For the reason of clarity and simplicity, only those ele-

ments essential to the kinematic structure are shown. For examples, the diagrams in Figs. 7.3 and 7.4 are the functional schematic representations of the Cincinnati-Milacron T³ wrist and the Bendix wrist, respectively. In a more detailed functional schematic, link geometry and dimensions may also be shown. In this regard, two functional schematic representations of different physical embodiments may sometimes share the same kinematic structure topology.

7.3.2 Graph Representation

Since a kinematic chain is an assemblage of links and joints, this link and joint assemblage can be represented in a more abstract form known as the *graph representation*. In a graph representation, links are denoted by vertices and joints by edges. To distinguish the differences between pair connections, the edges can be colored or labeled. For epicyclic gear trains, gear pairs are denoted by heavy edges, turning pairs (revolute joints) are denoted by thin edges, and the thin edges are labeled according to their axis locations in space.

The graph of a mechanism is defined similarly, with the addition that the vertex denoting the fixed link is labeled accordingly, usually by two small concentric circles. For example, Fig. 7.5 shows the graph representation of Cincinnati-Milacron T³ wrist. The links and corresponding vertices are numbered from 1 to 7. As shown in Fig. 7.5, the three gear pairs, 5–3, 6–7 and 7–4, are sketched in heavy edges, the turning pairs, 1–2, 2–5, 2–7, 5–6, 7–3, and 3–4, are sketched in thin edges and are labeled *a*, *b*, and *c* according to their axis locations.

The advantages of using graph representation can be summarized as follows:

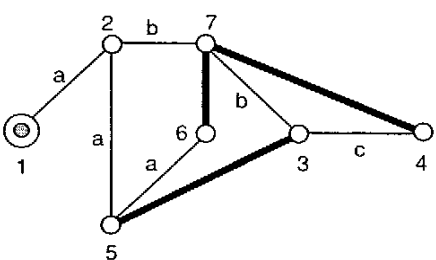


FIGURE 7.5. Graph representation of the Cincinnati-Milacron T³ wrist.

1. Many network properties of graphs are directly applicable.
2. The structure topology of a mechanism can be uniquely identified. Using graph representation, the similarities and differences between various mechanisms can be clearly identified.
3. A single atlas of graphs can be used to enumerate an enormous amount of mechanisms (Buchsbaum and Freudenstein, 1970; Chatterjee and Tsai, 1994; Freudenstein and Maki, 1979).
4. Graphs can be used to better organize kinematic and dynamic analysis of mechanisms (Freudenstein and Yang, 1972; Roberson and Schwerdtassek, 1988; Tsai et al., 1996).

7.3.3 Canonical Graph Representation

When there are three or more links in a mechanism sharing a common joint axis, the turning pairs among these coaxial links can be reconfigured without affecting the functionality of the mechanism. For example, links 2, 3, and 7 shown in Fig. 7.3 are connected by two coaxial revolute joints at axis *b*. These three coaxial links can be packaged in three different ways. Figure 7.6a shows the original construction, in which link 2 is connected to link 7 by a revolute joint while link 7 is connected to link 3 by another revolute joint. Figure 7.6b and c shows two alternative constructions. Also shown in Fig. 7.6a–c are the corresponding graph representations of the three alternative constructions.

The number of alternative joint connections increases with the number of coaxial links. Mechanisms constructed from these various joint connections are called *pseudoisomorphic mechanisms*, and the corresponding graphs, *pseudoisomorphic graphs*. This suggests a canonical representation of the graph. Among all the various pseudoisomorphic graphs, the one in which all the thin-edged paths beginning from the base link and ending at any other links have distinct edge labels is called a *canonical graph*. The Cincinnati-Milacron T³ wrist mechanism shown in Fig. 7.3 and its graph shown in Fig. 7.5 are not canonical, because the 2–7 and 7–3 edges in the 1–2–7–3–4 path are of the same label. Similarly, the 1–2, 2–5, and 5–6 edges in the 1–2–5–6 path are of the same label. After rearranging the revolute joints among the two sets of coaxial links (links 1, 2, 5, and 6) and (links 2, 3, and 7), the canonical functional schematic and graph representation of the mechanism are obtained, shown in Fig. 7.7. The canonical representation eliminates possible confusion among various pseudoisomorphic mechanisms. It leads to a systematic approach for the kinematic and dynamic analysis of geared robotic mechanisms (Tsai, 1988; Tsai et al., 1996).

In a canonical graph, the vertices can be divided into several levels. The ground-level vertex, called the *root*, denotes the base link. The first-level ver-

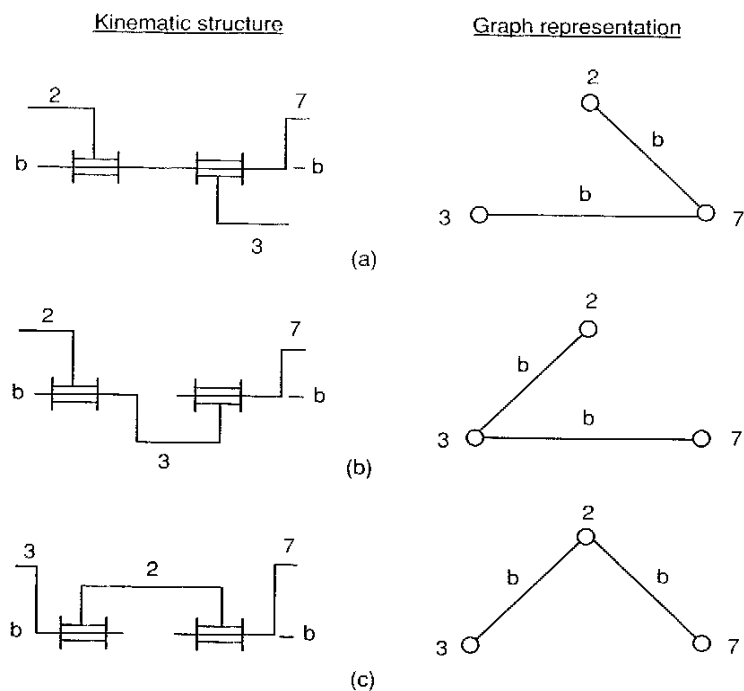


FIGURE 7.6. Three different ways of assembling three coaxial links.

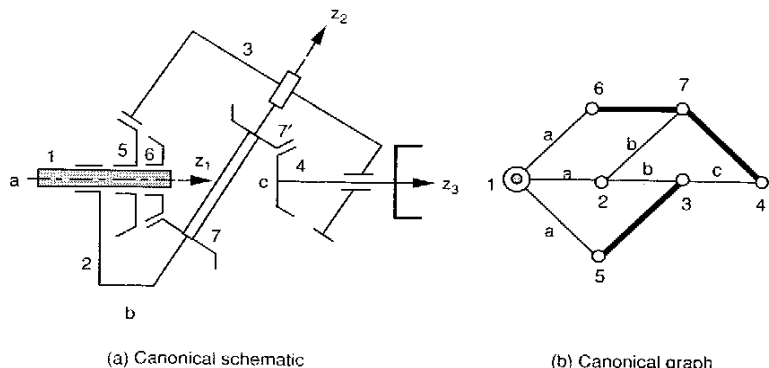


FIGURE 7.7. Canonical functional schematic and graph representation of the Cincinnati-Milacron T³ wrist.

tices denote those links that are connected directly to the base link by a turning pair. The first-level links can be potentially employed as the input links. The higher-level vertices denote revolving planet gears or carriers, including the end effector.

7.4 STRUCTURE CHARACTERISTICS OF EPICYCLIC GEAR TRAINS

In this section we describe the structure characteristics of epicyclic gear trains. To distinguish a geared linkage from an epicyclic gear train, we impose the following rules on the kinematic structure of all epicyclic gear trains:

1. An epicyclic gear train should obey the general degree-of-freedom equation. That is, no special link lengths are required to achieve a desired mobility.
2. There are no partially locked kinematic chains within a gear train.
3. Neglecting the mechanical limit, all links in an epicyclic gear train will have unlimited rotation capability. This implies that there should be no circuits formed exclusively by turning pairs.
4. Each gear in an epicyclic gear train has a turning pair on its axis to maintain a constant center distance between a gear pair.

Let n , j , j_t , j_g , f_i , and L denote the number of links, the total number of joints, the number of turning pairs, the number of gear pairs, the degrees of freedom associated with the i th joint, the degrees of freedom of the gear train, and the number of independent loops, respectively. The degree-of-freedom equation can be written

$$F = 3(n - j - 1) + \sum f_i. \quad (7.1)$$

Assuming that only gear pairs and turning pairs are used in an epicyclic gear train, it is obvious that

$$j = j_t + j_g. \quad (7.2)$$

Hence the total joint degrees of freedom is

$$\sum f_i = j_t + 2j_g. \quad (7.3)$$

Rules 3 and 4 imply that the subgraph formed by removing all the geared edges from the graph of an epicyclic gear train is a tree. It is well known from

graph theory that a tree of n vertices contains $n - 1$ edges:

$$j_t = n - 1. \quad (7.4)$$

Substituting Eq. (7.4) into (7.2) and (7.3) and the resulting equations into (7.1) yields

$$j_g = n - 1 - F. \quad (7.5)$$

Applying Euler's equation, we obtain

$$L = n - 1 - F = j_g. \quad (7.6)$$

From the discussions above, we summarize the structure characteristics of epicyclic gear trains as follows (Buchsbaum and Freudenstein, 1970):

1. The subgraph obtained by deleting all the geared edges from the graph of an epicyclic gear train is a tree.
2. The number of turning pairs is equal to the number of links diminished by one, $j_t = n - 1$.
3. The number of gear pairs is given by $j_g = n - 1 - F$.
4. Any geared edge added onto the tree forms one and only one circuit, called the *fundamental circuit*, or *f-circuit*. Each f-circuit contains one geared edge and several turning-pair edges.
5. The number of f-circuits is equal to the number of gear pairs, $L = j_g$.
6. Each turning-pair edge can be characterized by a label that identifies the location of its axis in space.
7. The differential degrees of freedom of any circuit must be no less than 1.
8. In each f-circuit, there is a vertex called the *transfer vertex* such that all thin edges on one side of the transfer vertex share the same label, and edges on the opposite side of the transfer vertex share a different label. The transfer vertex corresponds to the *carrier* of a gear pair.
9. Thin edges of the same label form a tree.

7.5 CLASSIFICATION OF WRIST MECHANISMS

Wrist mechanisms can be classified in several different ways. They can be classified by their degrees of freedom, type of motion (i.e., spherical versus nonspherical mechanisms), or other geometric considerations. In general, the joint axes of a wrist mechanism do not necessarily have to intersect at a common point, and the twist angles between adjacent joint axes are not

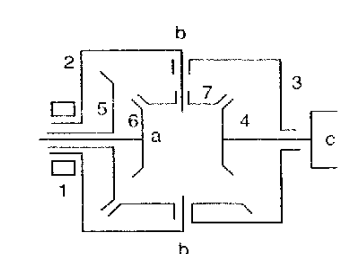
necessarily equal to $\pm 90^\circ$. A wrist is said to be a *spherical wrist* if its joint axes intersect at a common point. Otherwise, it is called a *nonspherical wrist*. A *simple* wrist is one in which the twist angles between adjacent joint axes are all equal to $\pm 90^\circ$. On the other hand, if any of the twist angles is not equal to $\pm 90^\circ$, it is called an *oblique wrist*. Following the definitions above, we observe that both the Cincinnati-Milacron T³ and Bendix wrists, shown in Figs. 7.3 and 7.4, respectively, are 3-dof spherical wrists. However, the Cincinnati-Milacron T³ wrist is an oblique wrist, whereas the Bendix wrist is a simple wrist.

Wrist mechanisms can also be classified according to their gearing arrangement. A wrist is called a *basic mechanism* if rotations of the input links are transmitted to the articulation points by gears mounted only on its axes of articulation, and it is called a *derived mechanism* if additional idler gears are incorporated between the axes of articulation points. Based on this definition and the concept of transmission lines, Chang and Tsai (1989) developed a systematic methodology for the enumeration and classification of robotic mechanisms.

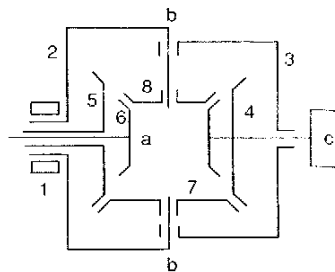
Figure 7.8 shows an atlas of basic 3-dof spherical wrist mechanisms with up to nine links. Figure 7.9 shows three wrist mechanisms derived from the seven-link wrist shown in Fig. 7.8a. In all cases, link 1 denotes the base link (forearm) and link 4 denotes the end effector. In Fig. 7.8a and b and Fig. 7.9a–c, links 2, 5, and 6 serve as the input links, while in Fig. 7.8c–e, links 5, 6, and 7 are the input links. We note that all the mechanisms shown in Figs. 7.8 and 7.9 are sketched in simple wrist configurations. These mechanisms can easily be reconfigured into oblique wrists. Many more derived wrist mechanisms can be found in Lin and Tsai (1989) and Lin (1990).

7.6 KINEMATICS OF EPICYCLIC GEAR DRIVES

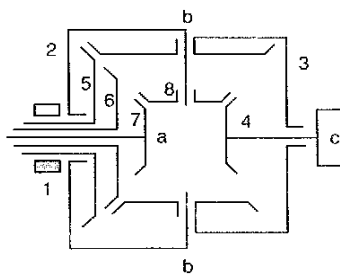
In the design of power transmission mechanisms such as speed reducers or automotive transmissions, it is often necessary to analyze the speed ratios between their input and output members and, sometimes, angular velocities of the intermediate members. The analysis is usually accomplished on a one-by-one basis using various methods, such as the tabular method (Merritt, 1947; Shigley and Uicker, 1980), the relative velocity method (Glover, 1964, 1965; Levai, 1968), the energy method (Wilkinson, 1960), the signal flow method (Ma and Gupta, 1989; Wojszarski and Lidwin, 1973), the bond graph method (Allen, 1979), and the velocity vector-loop approach (Smith, 1979; Willis, 1982). The amount of work involved in analyzing a compound epicyclic gear train is quite laborious and can often introduce human errors. Therefore, it is highly desirable to develop a systematic procedure for the



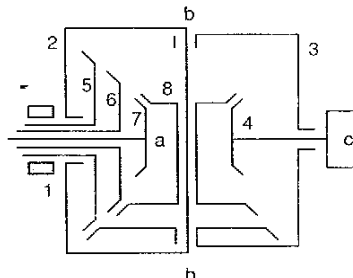
(a) Seven link wrist



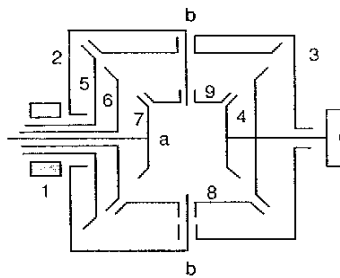
(b) Eight link wrist- 1



(c) Eight link wrist- 2

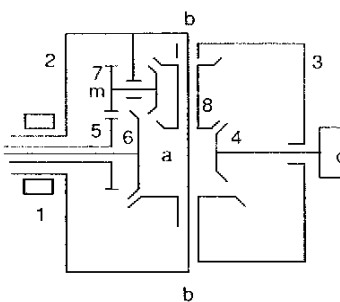


(d) Eight-link wrist- 3

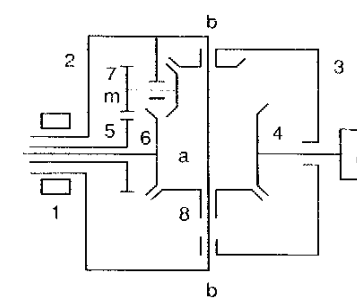


(e) Nine link wrist

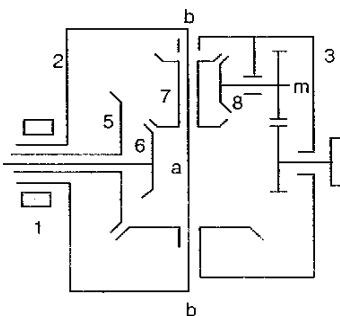
FIGURE 7.8. Five basic 3-dof wrist mechanisms.



(a) Eight link wrist-1



(b) Eight link wrist-2



(c) Eight link wrist - 3

FIGURE 7.9. Eight-link wrists derived form the seven-link wrist.

analysis (Hedman, 1989, 1993; Tsai, 1985). Perhaps the most promising approach is the systematic method introduced by Freudenstein and Yang (1972), which utilizes the theory of fundamental circuits. These workers showed that there exists a carrier for every gear pair in an epicyclic gear train and that a fundamental circuit equation can be written for each circuit. This results in a system of linear equations that can be solved for angular velocities of all the links. The method is very straightforward and can be implemented on a computer for automated analysis of epicyclic gear trains. The theory of fundamental circuits was further extended by other researchers (Belfiore and Pennestri, 1989; Pennestri and Freudenstein, 1993; Tsai, 1988).

In what follows, we introduce the theory of fundamental circuits and coaxiality condition. Then we analyze two industrial epicyclic gear drives to illustrate the theory.

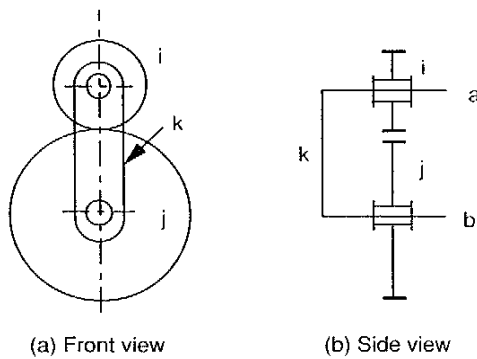


FIGURE 7.10. Gear pair.

7.6.1 Fundamental Circuit Equation

Figure 7.10 shows a meshing gear pair, i and j , in which k is the carrier. Links i , j , and k constitute a *fundamental circuit*. A *fundamental circuit equation* relating the angular displacements of the gears can be written as

$$\theta_{i,k} = \pm N_{ji}\theta_{j,k}, \quad (7.7)$$

where $\theta_{i,k}$ and $\theta_{j,k}$ denote the angular displacements of gears i and j relative to the carrier k , respectively. The gear ratio of a gear pair is defined as $N_{ji} = T_j/T_i$, where T_i and T_j denote the number of teeth on gears i and j , respectively. Following the definitions above, we have $\theta_{i,k} = -\theta_{k,i}$, and $N_{ij} = 1/N_{ji}$.

The sign in Eq. (7.7) is positive or negative depending on whether a positive rotation of gear i relative to the carrier k produces a positive or negative rotation of gear j . For planar gear trains it is convenient to assume that all the positive axes of rotation are pointing out of the paper. This results in a positive gear ratio for an internal gear mesh and a negative gear ratio for an external gear mesh. For spherical or spatial mechanisms, we assign a positive direction of rotation to each joint axis in accordance with the Denavit-Hartenberg convention. The sign of a gear ratio then follows the definition above.

Since Eq. (7.7) is written in terms of relative angular displacements, it is valid whether the gear train is planar or bevel gear type and whether the carrier is stationary or revolving. We can write one such equation for each f-circuit in an epicyclic gear mechanism, resulting in $n - F - 1$ fundamental circuit equations. Differentiating Eq. (7.7) with respect to time, we obtain an

equation relating the angular velocities of the links as follows:

$$\omega_{i,k} = \pm N_{ji}\omega_{j,k}. \quad (7.8)$$

7.6.2 Coaxiality Condition

Let i , j , and k be three coaxial links; the relative angular displacements among these coaxial links can be related by the following chain rule:

$$\theta_{i,j} = \theta_{i,k} - \theta_{j,k}. \quad (7.9)$$

Equation (7.9) is called the *coaxiality condition*. The fundamental circuit equation and the coaxiality condition together can be used to solve the kinematics of epicyclic gear trains. In what follows we analyze the speed ratios of two planar epicyclic gear trains to illustrate the theory.

Example 7.6.1 Minuteman Cover Drive Figure 7.11a shows the functional schematic of the Minuteman cover drive. In this mechanism, ring gear 1 is fixed to the ground, sun gear 2 is the input link, while the other ring gear, 5, serves as the output member. The compound planet gear meshes with sun gear 2 as well as the two ring gears, and is supported by the carrier, 3, with a revolute joint. Link 2 is connected to links 1, 3, and 5 by coaxial revolute joints. Together, it forms a five-link, 1-dof compound planetary gear train. We wish to find the overall speed reduction ratio of this mechanism.

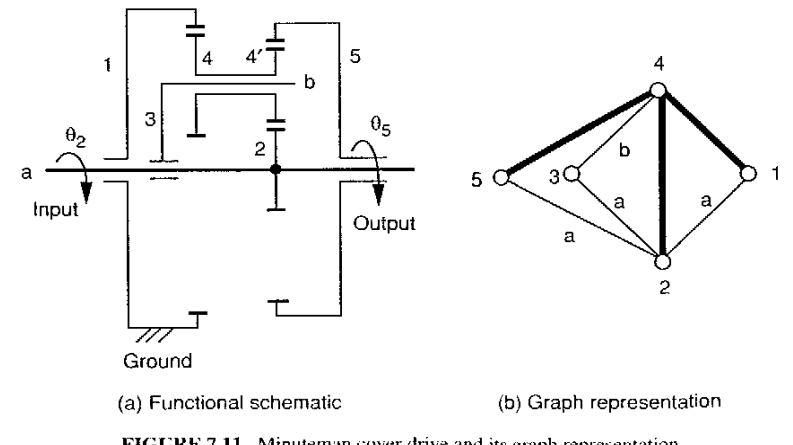


FIGURE 7.11. Minuteman cover drive and its graph representation.

Fundamental circuits. Since there are three gear pairs in the mechanism, the number of fundamental circuits is three. The graph representation of the mechanism is depicted in Fig. 7.11b. From the graph representation, the fundamental circuits can be easily identified. First, we remove all the heavy edges from the graph. This results in a tree (characteristic 1). Then we replace one heavy edge onto the tree at a time. According to the 4th characteristic, each time we replace a heavy edge onto the tree, we obtain a unique fundamental circuit. Finally, the transfer vertex or the carrier of each circuit is identified by applying the 8th characteristic. As a result, we obtain three fundamental circuits, (2,4,3), (1,4,3), and (4,5,3), where the first two numbers in the parentheses denote the gear pair, and the third number denotes the carrier. Hence the fundamental circuit equations can be written

$$f(2, 4, 3) : \theta_{2,3} = -N_{42}\theta_{4,3}, \quad (7.10)$$

$$f(1, 4, 3) : \theta_{1,3} = N_{41}\theta_{4,3}, \quad (7.11)$$

$$f(4, 5, 3) : \theta_{4,3} = N_{54}\theta_{5,3}. \quad (7.12)$$

Since link 1 is fixed, all angular displacements should be referred to link 1. That is, the input and output angular displacements can be written as $\theta_{2,1}$ and $\theta_{5,1}$, respectively. To derive an equation relating the output angular displacement to the input angular displacement, $\theta_{4,3}$ and $\theta_{1,3}$ should be eliminated, while $\theta_{2,3}$ and $\theta_{5,3}$ should be expressed in terms of $\theta_{2,1}$ and $\theta_{5,1}$ by applying the coaxiality conditions.

Coaxiality conditions. From Fig. 7.11 we observe that links 1, 2, 3, and 5 share a common joint axis. Two coaxiality conditions can be written as

$$\theta_{2,3} = \theta_{2,1} - \theta_{3,1}, \quad (7.13)$$

$$\theta_{5,3} = \theta_{5,1} - \theta_{3,1}. \quad (7.14)$$

Substituting (7.13) and (7.14) into (7.10) through (7.12) yields

$$\theta_{2,1} - \theta_{3,1} = -N_{42}\theta_{4,3}, \quad (7.15)$$

$$-\theta_{3,1} = N_{41}\theta_{4,3}, \quad (7.16)$$

$$\theta_{4,3} = N_{54}(\theta_{5,1} - \theta_{3,1}). \quad (7.17)$$

Equations (7.15), (7.16), and (7.17) represent a system of three linear equations in three unknowns: $\theta_{5,1}$, $\theta_{3,1}$, and $\theta_{4,3}$. Solving Eq. (7.16) for $\theta_{4,3}$ and substituting the resulting expression into Eqs. (7.15) and (7.17) yields

$$\theta_{2,1} - \theta_{3,1} - \frac{N_{42}}{N_{41}}\theta_{3,1} = 0, \quad (7.18)$$

$$\frac{1}{N_{41}}\theta_{3,1} + N_{54}(\theta_{5,1} - \theta_{3,1}) = 0. \quad (7.19)$$

Solving (7.18) for $\theta_{3,1}$ and substituting the resulting equation into (7.19) yields

$$\theta_{5,1} = \frac{N_{41}N_{54} - 1}{N_{54}(N_{41} + N_{42})}\theta_{2,1}. \quad (7.20)$$

Taking the derivative of Eq. (7.20) with respect to time and rearranging, we obtain the speed reduction ratio of the gear train as

$$\frac{\omega_{2,1}}{\omega_{5,1}} = \frac{N_{54}(N_{41} + N_{42})}{N_{41}N_{54} - 1}. \quad (7.21)$$

This compound planetary gear train can provide a very large speed reduction. For example, for $N_{41} = \frac{32}{74}$, $N_{42} = \frac{33}{9}$, and $N_{54} = \frac{75}{33}$, the speed reduction ratio is given by

$$\frac{\omega_{2,1}}{\omega_{5,1}} = \frac{\frac{75}{33}\left(\frac{32}{74} + \frac{33}{9}\right)}{\frac{32}{74} \cdot \frac{75}{33} - 1} = -541.7.$$

Example 7.6.2 Differential Speed Reducer Figure 7.12 shows the functional schematic of a planetary differential gear train. The mechanism uses its carrier, 2, as the input link, the larger sun gear, 3, as the output link, and the smaller sun gear, 1, as the fixed link. The compound planet gear, 4, meshes

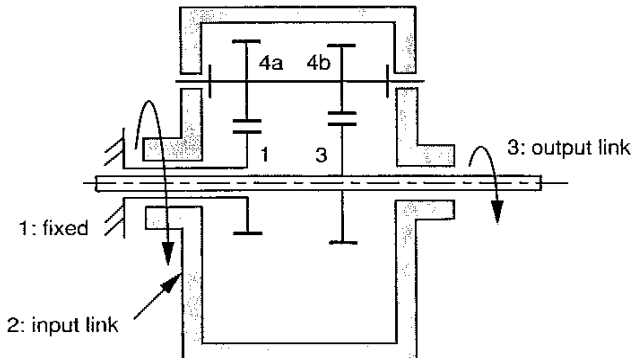


FIGURE 7.12. Differential speed reducer.

with both sun gears 1 and 3. We wish to find the speed ratio of the input link to the output link.

Since there are two gear pairs supported by a single carrier, two fundamental circuits are easily identified as (1,4,2) and (3,4,2). The fundamental circuit equations can be written

$$f(1, 4, 2) : \theta_{1,2} = -N_{41}\theta_{4,2}, \quad (7.22)$$

$$f(3, 4, 2) : \theta_{3,2} = -N_{43}\theta_{4,2}. \quad (7.23)$$

Since link 1 is fixed, all angular displacements should be referred to link 1. The input and output angular displacements can be written as $\theta_{2,1}$ and $\theta_{3,1}$, respectively. To derive an equation relating the output angular displacement to the input angular displacement, $\theta_{4,2}$ should be eliminated, while $\theta_{3,2}$ should be expressed in terms of $\theta_{2,1}$ and $\theta_{3,1}$ by applying the coaxiality condition. From Fig. 7.12 we observe that links 1, 2, and 3 share a common joint axis. A coaxiality condition can be written as

$$\theta_{3,2} = \theta_{3,1} - \theta_{2,1}. \quad (7.24)$$

Dividing Eq. (7.22) by (7.23) yields

$$-N_{43}\theta_{2,1} = N_{41}\theta_{3,2}. \quad (7.25)$$

Substituting Eq. (7.24) into (7.25) and simplifying yields

$$\frac{\theta_{2,1}}{\theta_{3,1}} = \frac{N_{41}}{N_{41} - N_{43}}. \quad (7.26)$$

Taking the derivative of Eq. (7.26) with respect to time and rearranging, we obtain the speed reduction ratio of the gear train as

$$\frac{\omega_{2,1}}{\omega_{3,1}} = \frac{N_{41}}{N_{41} - N_{43}}. \quad (7.27)$$

For example, let $N_{41} = \frac{33}{75}$ and $N_{43} = \frac{32}{76}$; then the speed reduction ratio is given by

$$\frac{\omega_{2,1}}{\omega_{3,1}} = \frac{\frac{33}{75}}{\frac{33}{75} - \frac{32}{76}} = 23.2.$$

7.7 KINEMATICS OF ROBOTIC WRIST MECHANISMS

In this section we study the kinematics of robotic wrist mechanisms of gyroscopic complexity. The analysis of bevel-gear wrist mechanisms is much more complex, due to the fact that the carriers and planet gears may possess simultaneous angular velocities about nonparallel axes. The conventional tabular or analytical method in textbooks, which concentrates on planar epicyclic gear trains, is no longer applicable. To overcome this difficulty, Yang and Freudenstein (1973) applied the dual relative velocity and dual matrix of transformation for the analysis of epicyclic bevel-gear trains and hypoid gears. Freudenstein et al. (1984) suggested using the conventional tabular method in conjunction with the Rodrigues equation. Recently, Tsai (1988) showed that the kinematic analysis of geared robotic mechanisms can be accomplished by applying the concept of *equivalent open-loop chain* and the theory of fundamental circuits. This method, which appears to be the simplest and most systematic approach, is the main focus of this section.

The method consists of two basic steps. The first step involves the identification of an equivalent open-loop chain and the derivation of the kinematic relationship between the orientation of the end effector and the joint angles of the equivalent open-loop chain. The second step involves the derivation of the kinematic relationship between the joint angles and the input actuator displacements. The first step results in a transformation between the end-effector space and the joint space of the equivalent open-loop chain, and the second step results in a transformation between the joint space and the input actuator space. The overall kinematic relation is obtained as a product of the two transformations.

In what follows, we use the Cincinnati-Milacron T³ wrist to illustrate the procedure.

7.7.1 Equivalent Open-Loop Chain

Recall that the graph of a geared robotic mechanism can always be transformed into a canonical form, and the removal of all the geared edges from the graph results in a tree. The tree represents an open-loop kinematic chain made up of links connected together by revolute pairs. In particular, we call the thin-edged path that starts from the base link and ends at the end-effector link the *equivalent open-loop chain*. For example, the canonical graph of the Cincinnati-Milacron T³ wrist shown in Fig. 7.7b contains vertex 1 as the base link and 4 as the end-effector. The thin-edged path that starts from the base link and ends at the end-effector link consists of vertices 1–2–3–4. Hence the equivalent open-loop chain is made up of links 1, 2, 3, and 4 connected in series by revolute joints as shown in Fig. 7.13.

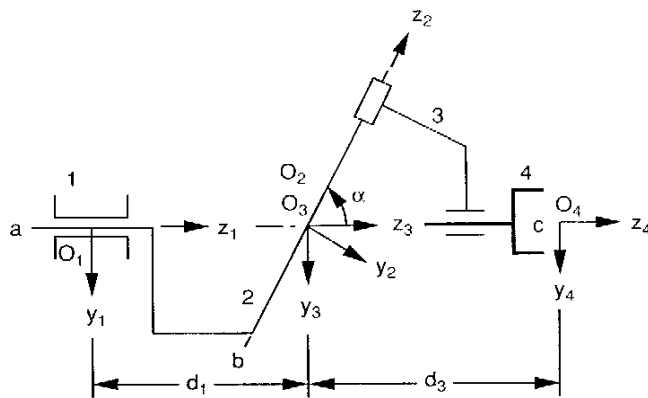


FIGURE 7.13. Equivalent open-loop chain of the Cincinnati-Milacron T^3 wrist.

To facilitate the analysis of such a mechanism, we first assign a positive direction of rotation to each joint axis and define a coordinate system for each link in accordance with the Denavit–Hartenberg convention. Thus the (x_1, y_1, z_1) coordinate frame is attached to link 1, the (x_2, y_2, z_2) coordinate frame is attached to link 2, the (x_3, y_3, z_3) coordinate frame is attached to link 3, and the (x_4, y_4, z_4) coordinate frame is attached to link 4. The origin O_1 and the x_1 -axis have been chosen arbitrarily since at this time we do not know how the wrist is attached to the forearm. The equivalent open-loop chain shown in Fig. 7.13 has been sketched in a configuration in which all the x_i , $i = 1$ to 4, axes are parallel to each other and are pointing out of the paper. We define this particular configuration as the *reference position* and refer the angular displacement of a link (or gear) in the mechanism as the rotation of the link from this reference position, positive or negative in accordance with the right-hand screw rule. The Denavit–Hartenberg parameters for this equivalent open-loop chain are given in Table 7.1.

The transformation between the end-effector space and the joint space of the equivalent open-loop chain can be derived by applying the Denavit–

TABLE 7.1. Link Parameters of the Cincinnati-Milacron T^3 Wrist

Joint i	α_i	a_i	d_i	$\theta_{j,i}$
1	α	0	d_1	$\theta_{2,1}$ (variable)
2	$-\alpha$	0	0	$\theta_{3,2}$ (variable)
3	0	0	d_3	$\theta_{4,3}$ (variable)

Hartenberg method or the method of successive screw displacements. Both methods have been discussed in detail in Chapter 2.

7.7.2 Transformation between Joint Space and Actuator Space

The second step is achieved by applying the theory of fundamental circuits and the coaxiality conditions. With the aid of graph representation, the fundamental circuits are identified and the fundamental circuit equation, Eq. (7.7), is written once for each fundamental circuit. Next, the coaxiality condition, Eq. (7.9), is written as many times as appropriate for the purpose of eliminating some of the unwanted angular displacements. This leads to a simple relationship between the actuator displacements and the joint angles of the equivalent open-loop chain.

For example, the Cincinnati–Milacron T^3 wrist shown in Fig. 7.7 is a 3-dof mechanism with three bevel gear pairs. Applying the structure characteristic no. 4, three fundamental circuits are identified as 7–2–3–4–7, 6–1–2–7–6, and 5–1–2–3–5. Applying the structure characteristic no. 8, we obtain vertices 3, 2, and 2 as the corresponding transfer vertices. Hence the fundamental circuit equations are given by

$$f(7, 4, 3) : \theta_{7,3} = -N_{47}\theta_{4,3}, \quad (7.28)$$

$$f(6, 7, 2) : \theta_{6,2} = -N_{76}\theta_{7,2}, \quad (7.29)$$

$$f(5, 3, 2) : \theta_{5,2} = N_{35}\theta_{3,2}. \quad (7.30)$$

Since link 1 is considered as the fixed link, all angular displacements should be referred to link 1. The input angular displacements are $\theta_{2,1}$, $\theta_{3,1}$, and $\theta_{6,1}$, while the joint angles of the equivalent open-loop chain are $\theta_{2,1}$, $\theta_{3,2}$, and $\theta_{4,3}$. All the other angular displacements should be eliminated by applying the coaxial conditions. From Fig. 7.7 we observe that links 2, 3, and 7 share a common joint axis, z_2 , and links 1, 2, 5, and 6 share another common joint axis, z_1 . Hence three coaxiality conditions can be written as

$$\theta_{7,3} = \theta_{7,2} - \theta_{3,2}, \quad (7.31)$$

$$\theta_{6,2} = \theta_{6,1} - \theta_{2,1}, \quad (7.32)$$

$$\theta_{5,2} = \theta_{5,1} - \theta_{2,1}. \quad (7.33)$$

Solving Eqs. (7.28) through (7.33) for $\theta_{5,1}$ and $\theta_{6,1}$ in terms of $\theta_{2,1}$, $\theta_{3,2}$, and $\theta_{4,3}$ yields

$$\theta_{5,1} = \theta_{2,1} + N_{35}\theta_{3,2}, \quad (7.34)$$

$$\theta_{6,1} = \theta_{2,1} - N_{76}\theta_{3,2} + N_{76}N_{47}\theta_{4,3}. \quad (7.35)$$

Since link 2 is an input link, we have

$$\theta_{2,1} = \dot{\theta}_{2,1}. \quad (7.36)$$

We can write Eqs. (7.34), (7.35), and (7.36) in matrix form as

$$\begin{bmatrix} \theta_{2,1} \\ \theta_{5,1} \\ \theta_{6,1} \end{bmatrix} = \begin{bmatrix} 1 & 0 & 0 \\ 1 & N_{35} & 0 \\ 1 & -N_{76} & N_{76}N_{47} \end{bmatrix} \begin{bmatrix} \dot{\theta}_{2,1} \\ \dot{\theta}_{3,2} \\ \dot{\theta}_{4,3} \end{bmatrix}, \quad (7.37)$$

or simply

$$\phi = A\theta, \quad (7.38)$$

where $\phi = [\theta_{2,1}, \theta_{5,1}, \theta_{6,1}]^T$ denotes the vector of input angular displacements, $\theta = [\theta_{2,1}, \theta_{3,2}, \theta_{4,3}]^T$ denotes the vector of joint angles, and

$$A = \begin{bmatrix} 1 & 0 & 0 \\ 1 & N_{35} & 0 \\ 1 & -N_{76} & N_{76}N_{47} \end{bmatrix}. \quad (7.39)$$

For the direct kinematics, the input angular displacements are given and the joint angles are found from inverse transformation of Eq. (7.38). Once the joint angles are known, the end-effector orientation is found by the direct Denavit–Hartenberg transformation. For the inverse kinematics, the end-effector orientation is given. We first find the joint angles from the inverse Denavit–Hartenberg transformation. Then we find the input angular displacements from Eq. (7.38).

7.7.3 Angular Velocity Relations

The angular velocity of the end effector with respect to the base link, $\omega_{4,1}$, can be expressed as a summation of the instantaneous twists about the three equivalent joint axes:

$$\omega_{4,3} = \dot{\theta}_{2,1}\mathbf{z}_1 + \dot{\theta}_{3,2}\mathbf{z}_2 + \dot{\theta}_{4,3}\mathbf{z}_3, \quad (7.40)$$

where \mathbf{z}_i denotes a unit vector pointing along the positive z_i -axis. Taking the time derivative of Eq. (7.37) yields

$$\begin{bmatrix} \dot{\theta}_{2,1} \\ \dot{\theta}_{5,1} \\ \dot{\theta}_{6,1} \end{bmatrix} = \begin{bmatrix} 1 & 0 & 0 \\ 1 & N_{35} & 0 \\ 1 & -N_{76} & N_{76}N_{47} \end{bmatrix} \begin{bmatrix} \dot{\theta}_{2,1} \\ \dot{\theta}_{3,2} \\ \dot{\theta}_{4,3} \end{bmatrix}. \quad (7.41)$$

Hence the joint rates can be expressed in terms of the actuator rotation rates by taking the inverse transformation of Eq. (7.41); that is,

$$\begin{bmatrix} \dot{\theta}_{2,1} \\ \dot{\theta}_{3,2} \\ \dot{\theta}_{4,3} \end{bmatrix} = \begin{bmatrix} 1 & 0 & 0 \\ -N_{53} & N_{53} & 0 \\ -N_{74}(N_{67} + N_{53}) & N_{74}N_{53} & N_{74}N_{67} \end{bmatrix} \begin{bmatrix} \dot{\theta}_{2,1} \\ \dot{\theta}_{5,1} \\ \dot{\theta}_{6,1} \end{bmatrix}. \quad (7.42)$$

For the direct velocity problem, the actuator rotation rates are given. We compute the joint rates from Eq. (7.42) and the angular velocity of the end effector from Eq. (7.40). For the inverse velocity problem, the angular velocity of the end effector is given. We solve the joint rates from the vector equation (7.40) and then the actuator rotation rates from Eq. (7.41).

7.8 STATIC FORCE ANALYSIS

In this section we apply the principle of virtual work to derive a transformation between the equivalent joint torques and the actuator torques.

7.8.1 Principle of Virtual Work

For a 3-dof wrist, the virtual displacements of the input actuators can be written as $\delta\phi = [\delta\phi_1, \delta\phi_2, \delta\phi_3]^T$, and the virtual displacements at the joints of the equivalent open-loop chain can be written as $\delta\theta = [\delta\theta_{2,1}, \delta\theta_{3,2}, \delta\theta_{4,3}]^T$. Let the actuator input torques be denoted by $\xi = [\xi_1, \xi_2, \xi_3]^T$ and the output joint torques be denoted by $\tau = [\tau_1, \tau_2, \tau_3]^T$, respectively. Neglecting the frictional forces and the gravitational effect, the virtual work, δW , produced by these active forces is given by

$$\delta W = \xi^T \delta\phi - \tau^T \delta\theta. \quad (7.43)$$

From Eq. (7.38) we obtain a relation between the virtual displacements $\delta\phi$ and $\delta\theta$ as

$$\delta\phi = A\delta\theta. \quad (7.44)$$

Substituting Eq. (7.44) into (7.43) yields

$$\delta W = (\xi^T A - \tau^T) \delta\theta. \quad (7.45)$$

The system is under equilibrium if and only if the virtual work vanishes for any independent infinitesimal virtual displacement. Hence

$$\xi^T A - \tau^T = 0. \quad (7.46)$$

Taking the transpose of Eq. (7.46) yields

$$\tau = B\xi, \quad (7.47)$$

where $B = A^T$ is called the *structure matrix*. For example, the structure matrix for the Cincinnati-Milacron T³ wrist is given by

$$B = A^T = \begin{bmatrix} 1 & 1 & 1 \\ 0 & N_{35} & -N_{76} \\ 0 & 0 & N_{76}N_{47} \end{bmatrix}.$$

We note that the structure matrix is a function of the structure topology and the gear ratios and is independent of end-effector orientation.

For a 3-dof spherical wrist, it can be shown that the vector of equivalent joint torques is related to the end-effector output torque, $\mathbf{n} = [n_x, n_y, n_z]^T$, by

$$\tau = J^T \mathbf{n}, \quad (7.48)$$

where J is a 3×3 Jacobian matrix relating the end-effector angular velocity to the joint rates of the equivalent open-loop chain. Combining Eqs. (7.47) and (7.48), we obtain an overall transformation as

$$\xi = B^{-1} J^T \mathbf{n}. \quad (7.49)$$

Using Eq. (7.49), we can compute the input actuator torques for any desired end-effector output torque. On the other hand, given the input actuator torques, we can compute the resulting end-effector torque by performing the inverse transformation of Eq. (7.49).

7.8.2 Transmission Lines

In this section we introduce the concept of *transmission line*. Taking the derivative of Eq. (7.47) yields

$$d\tau = B d\xi. \quad (7.50)$$

Hence the (i, j) element of the structure matrix B can be interpreted as the partial rate of change of the joint torque with respect to the input actuator torque; that is,

$$b_{ij} = \frac{\partial \tau_i}{\partial \xi_j}, \quad (7.51)$$

where b_{ij} denotes the (i, j) element of B .

The element $b_{ij} \neq 0$ implies that the input torque ξ_j is amplified by b_{ij} times when it is transmitted to the i th joint. Hence $b_{ij} = 0$ implies that the input torque ξ_j does not have any influence on the resultant torque at joint i . The i th row of the structure matrix B describes how the resultant torque about joint i is affected by all the input actuators. On the other hand, the j th column of the structure matrix B describes how the torque of the j th input actuator is transmitted to various joints of a mechanism. Since input torques are transmitted to the joints by gear trains, nonzero elements in a column of the structure matrix must be consecutive. The gear train that results in a series of nonzero elements in the j th column of B is therefore called a *transmission line* for the input actuator j . In a transmission line, the first gear is attached to the rotor of an actuator, and the last gear is attached to one of the links in the equivalent open-loop chain.

Following the discussion above, it can be concluded that the element b_{ij} is equal to the *train value* defined from the input-gear j to the gear pivoted about the i th joint axis of the equivalent open-loop chain. For example, the Cincinnati-Milacron T³ wrist shown in Fig. 7.7 has three transmission lines: (1) link 2 by itself, (2) gears 5 and 3, and (3) gears 6, 7, 7', and 4. The element b_{23} is equal to the train value $-N_{76}$ defined from the input gear 6 to gear 7 pivoted on the second joint axis, where the negative sign comes from the fact that when the input gear 6 makes a positive rotation about the z_1 -axis, gear 7 will make a negative rotation about the z_2 -axis. Similarly, the element b_{33} is equal to the train value $N_{76}N_{47}$ defined from the input gear 6 to gear 4 pivoted about the third joint axis. Hence the elements of B can be determined by inspection. Note that if the stator of a motor is mounted on the i th link and the rotor is connected to the $(i+1)$ th link without any gear reduction, we have a direct drive. The element of B for a direct drive is equal to 1.

7.8.3 Kinematics of the Bendix Wrist

In this section the kinematics of the Bendix wrist shown in Fig. 7.4 is analyzed. The canonical graph representation of the mechanism is shown in Fig. 7.14, where vertex 1 represents the base link and 4 represents the end effector. The thin-edged path, which starts from the base link and ends at the end-effector link, consists of vertices 1, 2, 3, and 4. Hence the equivalent open-loop chain is made up of links 1, 2, 3, and 4 connected in series by revolute joints as shown in Fig. 7.15. The transformation between the end-effector space and the joint space is similar to that for the Cincinnati-Milacron T³ wrist. The only difference is in the twist angles between the joint axes. In the Bendix design the twist angles are $\alpha_1 = 90^\circ$, $\alpha_2 = -90^\circ$, and $\alpha_3 = 0^\circ$.

There are four gear pairs and therefore four fundamental circuits. Applying the structure characteristic no. 4, we identify four fundamental circuits as 5-

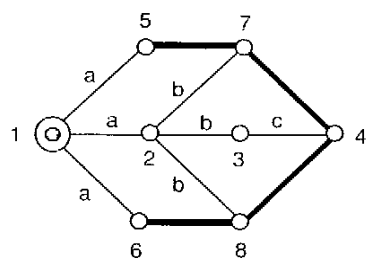


FIGURE 7.14. Canonical graph representation of the Bendix wrist.

1–2–7–5, 7–2–3–4–7, 8–2–3–4–8, and 6–1–2–8–6. Applying the structure characteristic no. 8, we obtain vertices 2, 3, 3, and 2 as the corresponding transfer vertices. Hence the fundamental circuit equations are given by

$$f(7, 5, 2) : \theta_{7,2} = N_{57}\theta_{5,2}, \quad (7.52)$$

$$f(4, 7, 3) : \theta_{4,3} = -N_{74}\theta_{7,3}, \quad (7.53)$$

$$f(4, 8, 3) : \theta_{4,3} = N_{84}\theta_{8,3}, \quad (7.54)$$

$$f(8, 6, 2) : \theta_{8,2} = -N_{68}\theta_{6,2}. \quad (7.55)$$

Since link 1 is considered the fixed link, all angular displacements should be referred to link 1. The input angular displacements are $\theta_{2,1}$, $\theta_{5,1}$, and $\theta_{6,1}$,

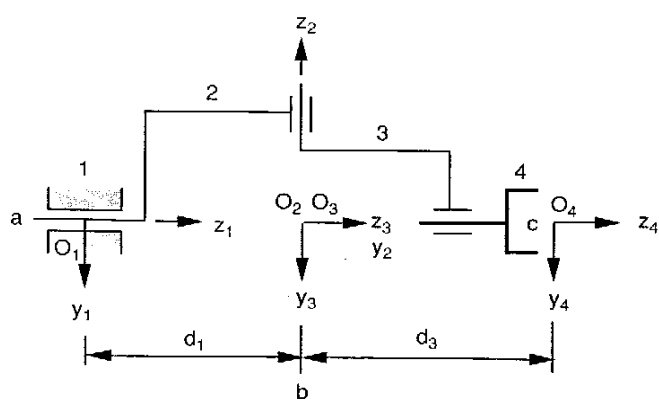


FIGURE 7.15. Equivalent open-loop chain of the Bendix wrist.

while the joint angles of the equivalent open-loop chain are $\theta_{2,1}$, $\theta_{3,2}$, and $\theta_{4,3}$. All the other angular displacements should be eliminated by applying the coaxiality conditions.

From Fig. 7.4 we observe that links 2, 3, 7, and 8 share one common joint axis, z_2 , and links 1, 2, 5, and 6 share another common joint axis, z_1 . Hence four coaxiality conditions can be written as

$$\theta_{7,3} = \theta_{7,2} - \theta_{3,2}, \quad (7.56)$$

$$\theta_{8,3} = \theta_{8,2} - \theta_{3,2}, \quad (7.57)$$

$$\theta_{5,2} = \theta_{5,1} - \theta_{2,1}, \quad (7.58)$$

$$\theta_{6,2} = \theta_{6,1} - \theta_{2,1}. \quad (7.59)$$

Solving Eqs. (7.52) through (7.59) for $\theta_{5,1}$ and $\theta_{6,1}$ in terms of $\theta_{2,1}$, $\theta_{3,2}$, and $\theta_{4,3}$, we obtain

$$\theta_{5,1} = \theta_{2,1} + N_{75}\theta_{3,2} - N_{75}N_{47}\theta_{4,3}, \quad (7.60)$$

$$\theta_{6,1} = \theta_{2,1} - N_{86}\theta_{3,2} - N_{86}N_{48}\theta_{4,3}. \quad (7.61)$$

Since link 2 is an input link, we have

$$\theta_{2,1} = \theta_{2,1}. \quad (7.62)$$

Writing Eqs. (7.60), (7.61), and (7.62) in matrix form, we obtain

$$\begin{bmatrix} \theta_{2,1} \\ \theta_{5,1} \\ \theta_{6,1} \end{bmatrix} = \begin{bmatrix} 1 & 0 & 0 \\ 1 & N_{75} & -N_{75}N_{47} \\ 1 & -N_{86} & -N_{86}N_{48} \end{bmatrix} \begin{bmatrix} \theta_{2,1} \\ \theta_{3,2} \\ \theta_{4,3} \end{bmatrix}. \quad (7.63)$$

Hence the structure matrix B is given by

$$B = A^T = \begin{bmatrix} 1 & 1 & 1 \\ 0 & N_{75} & -N_{86} \\ 0 & -N_{75}N_{47} & -N_{86}N_{48} \end{bmatrix}. \quad (7.64)$$

In view of the right angle between the z_1 and z_2 axes, and between the z_2 and z_3 axes, we have $N_{75} = N_{86} = 1/N_{47} = 1/N_{48}$. Hence the structure matrix reduces further to

$$B = A^T = \begin{bmatrix} 1 & 1 & 1 \\ 0 & N_{75} & -N_{75} \\ 0 & -1 & -1 \end{bmatrix}. \quad (7.65)$$

Once the structure matrix is known, the velocity and statics analyses can be performed by following the procedure outlined earlier for the Cincinnati Milacron wrist.

7.9 SUMMARY

The graph representation of the kinematic structures of epicyclic gear trains, including bevel-gear wrist mechanisms, has been described. Applying the network properties of graphs, the structure characteristics of epicyclic gear trains were derived and bevel-gear wrist mechanisms classified according to their structure characteristics. The theory of fundamental circuit and the coaxiality condition were introduced for the kinematic analysis of epicyclic gear trains. It was shown that the kinematics of bevel-gear wrist mechanisms can be analyzed in two basic steps. The first step involves the identification of an equivalent open-loop chain and the derivation of the kinematic relationship between the orientation of the end effector and the joint angles of the equivalent open-loop chain. The second step deals with the kinematic relationship between the joint angles and the input actuator displacements. The concepts of transmission lines and structure matrix were also introduced. It was shown that using the concept of transmission lines, the structure matrix of a wrist mechanism can be derived by an inspection of the kinematic structure of a mechanism. Several industrial gear reducers and wrist mechanisms were analyzed to illustrate the methodology.

REFERENCES

- Allen, R. R., 1979, "Multi-port Models of the Kinematic and Dynamic Analysis of Gear Power Transmission," *ASME J. Mech. Des.*, Vol. 101, pp. 258-392.
- Anonymous, 1982, "Bevel Gears Make Robot's Wrist More Flexible," *Mach. Des.*, Vol. 54, No. 18, p. 55.
- Belfiore, N. P. and Pennestri, E., 1989, "Kinematic and Static Force Analysis of Epicyclic Gear Trains," Paper AMR-6B-1, *Proc. First National Applied Mechanics and Robotics Conference*, Cincinnati, OH, Vol. 1.
- Buchsbaum, F. and Freudenstein, F., 1970, "Synthesis of Kinematic Structure of Geared Kinematic Chains and Other Mechanisms," *J. Mech.*, Vol. 5, pp. 357-392.
- Chang, S. L. and Tsai, L. W., 1989, "Topological Synthesis of Articulated Gear Mechanisms," *IEEE J. Robot. Autom.*, Vol. 6, No. 1, pp. 97-103.
- Chatterjee, G. and Tsai, L. W., 1994, "Enumeration of Epicyclic-Type Automatic Transmission Gear Trains," *SAE 1994 Trans.*, Vol. 103, Sec. 6, pp. 1415-1426.
- Dudley, D. W., 1969, *The Evolution of the Gear Art*, American Gear Manufacturers Association, Alexandria, VA, printed by Dual Printing, Inc., Buffalo, NY.
- Freudenstein, F. and Maki, E. R., 1979, "Creation of Mechanisms According to Kinematic Structure and Function," *J. Environ. Plann. B*, Vol. 6, pp. 375-391.
- Freudenstein, F. and Yang, A. T., 1972, "Kinematics and Statics of a Coupled Epicyclic Spur-Gear Train," *J. Mech. Mach. Theory*, Vol. 7, pp. 263-275.
- Freudenstein, F., Longman, R. W., and Chen, C. K., 1984, "Kinematic Analysis of Robotic Bevel-Gear Train," *ASME J. Mech. Transm. Autom. Des.*, Vol. 106, No. 3, pp. 371-375.
- Glover, J. H., 1964, "Planetary Gear Systems," *Product Eng.*, January, pp. 59-68.
- Glover, J. H., 1965, "Planetary Gear Systems," *Product Eng.*, September, pp. 72-79.
- Hedman, A., 1989, "Computer Aided Analysis of General Mechanical Transmission Systems," *Proc. 2nd International Conference on New Developments in Powertrain and Chassis Engineering*, Strasbourg, France, pp. 193-197.
- Hedman, A., 1993, "Transmission Analysis—Automatic Derivation of Relationships," *ASME J. Mech. Des.*, Vol. 115, No. 4, pp. 1031-1037.
- Levai, Z., 1968, "Structure Analysis of Planetary Gear Trains," *J. Mech.*, Vol. 3, pp. 131-148.
- Lin, C. C., 1990, "Kinematic Synthesis of Bevel-Gear-Type Robotic Wrist Mechanisms," Ph.D. dissertation, Department of Mechanical Engineering, University of Maryland, College Park, MD.
- Lin, C. C. and Tsai, L. W., 1989, "The Development of an Atlas of Bevel-Gear-Type Spherical Wrist Mechanisms," Paper 89-AMR-2A-3, *Proc. First National Conference on Applied Mechanisms and Robotics*, Cincinnati, OH.
- Ma, R. and Gupta, K. C., 1989, "On the Motion of Oblique Bevel Gear and Robot Wrists," *J. Robot. Sys.*, Vol. 5, pp. 509-520.
- Merritt, H. E., 1947, *Gear Trains*, Pitman, London.
- Paul, R. P. and Stevenson, C. N., 1983, "Kinematics of Robot Wrists," *Int. J. Robot. Res.*, Vol. 2, No. 1, pp. 31-38.
- Pennestri, E. and Freudenstein, F., 1993, "A Systematic Approach to Power-Flow and Static Force Analysis in Epicyclic Spur-Gear Trains," *ASME J. Mech. Des.*, Vol. 115, No. 3, pp. 639-644.
- Rivin, E. I., 1987, *Mechanical Design of Robots*, McGraw-Hill, New York.
- Roberson, R. E. and Schwertassek, R., 1988, *Dynamics of Multibody Systems*, Springer-Verlag, Berlin.
- Rosheim, M. E., 1989, *Robot Wrist Actuators*, Wiley, New York.
- Shigley, J. E. and Uicker, J. J., Jr., 1980, *Theory of Machines and Mechanisms*, McGraw-Hill, New York.
- Smith, D., 1979, "Analysis of Epicyclic Gear Trains via the Vector Loop Approach," Paper 10, *Proc. 6th Applied Mechanisms Conference*.
- Stackhouse, T., 1979, "A New Concept in Wrist Flexibility," *Proc. 9th International Symposium on Industrial Robots*, Washington, DC, pp. 589-599.
- Trevelyan, J. P., Kovesi, P. D., Ong, M., and Elford, D., 1986, "ET: A Wrist Mechanism without Singular Positions," *Int. J. Robot. Res.*, Vol. 4, No. 4, pp. 71-85.

- Tsai, L. W., 1985, "An Algorithm for the Kinematic Analysis of Epicyclic Gear Trains," *Proc. 9th Applied Mechanisms Conference*, Vol. II, Session VII.B-I, Kansas City, Missouri.
- Tsai, L. W., 1988, "The Kinematics of Spatial Robotic Bevel-Gear Trains," *IEEE J. Robot. Autom.*, Vol. 4, No. 2, pp. 150–156.
- Tsai, L. W., Chen, D. Z., and Lin, T. W., 1998, "Dynamic Analysis of Geared Robotic Mechanisms Using Graph Theory," *ASME J. Mech. Des.*, Vol. 120, No. 2, pp. 240–244.
- White, G., 1987, "Epicyclic Gears in Early Cord Winding and Rope Laying Machines," *J. Mech. Mach. Theory*, Vol. 22, No. 6, pp. 529–547.
- White, G., 1988, "Epicyclic Gears Applied to Early Steam Engines," *J. Mech. Mach. Theory*, Vol. 23, No. 1, pp. 25–37.
- Wilkinson, W. H., 1960, "Four Ways to Calculate Planetary Gear Trains," *Mach. Des.*, January, pp. 155–159.
- Willis, R. J., 1982, "On the Kinematics of the Closed Epicyclic Differential Gears," *ASME J. Mech. Des.*, Vol. 104, pp. 712–723.
- Wojnarowski, J. and Lidwin, A., 1973, "The Application of Signal Flow Graphs—The Kinematic Analysis of Planetary Gear Trains," *J. Mech. Mach. Theory*, Vol. 10, pp. 17–31.
- Yang, A. T. and Freudenstein, F., 1973, "Mechanics of Epicyclic Bevel-Gear Trains," *ASME J. Eng. Ind.*, Vol. 95, Ser. B, No. 2, pp. 497–502.

EXERCISES

- Sketch the graph and canonical graph of the mechanism shown in Fig. 7.16. Calculate the degrees of freedom of this mechanism.
- Sketch the graph and canonical graph of the wrist mechanism shown in Fig. 7.17. How many degrees of freedom does this mechanism have? What links can be used as the input links, and why?
- Discuss the advantages and disadvantages associated with simple and oblique wrist mechanisms from the kinematic structural point of view.
- Find the speed reduction ratio ω_1/ω_2 for the compound planetary gear train shown in Fig. 7.18, where link 1 is the input link and link 2 is the output link. Find a set of gears that will provide a reduction ratio of approximately 2 : 1.
- Find the speed reduction ratio ω_3/ω_4 for the planetary gear train shown in Fig. 7.19, where link 3 is the input link and link 4 is the output link. Find a set of gears that will provide a reduction ratio of approximately 3 : 1.

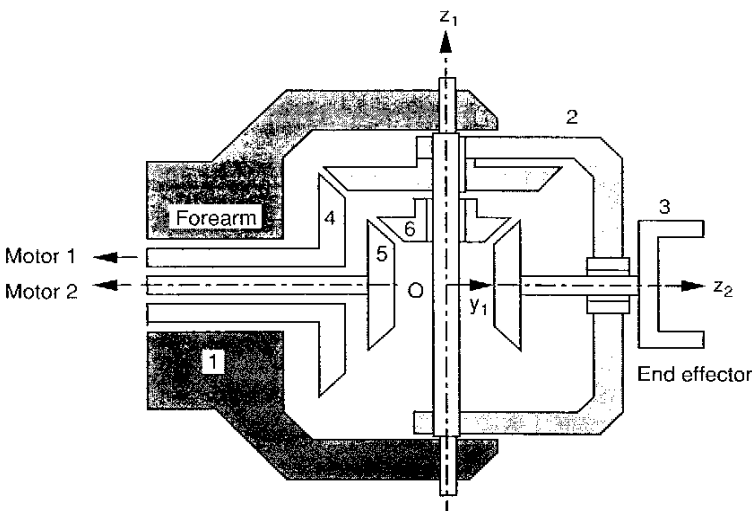


FIGURE 7.16. Spherical wrist mechanism—1.

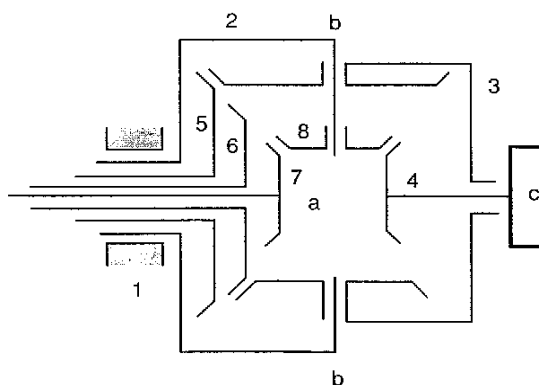


FIGURE 7.17. Spherical wrist mechanism—2.

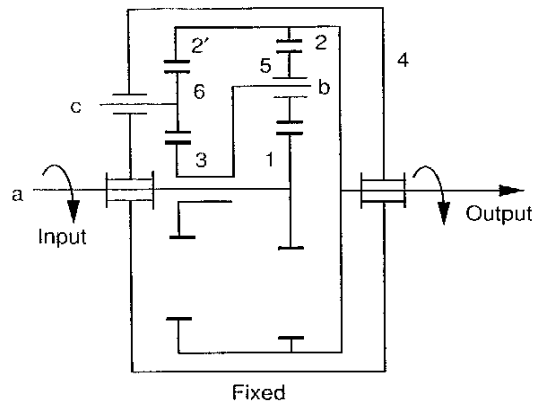


FIGURE 7.18. Compound planetary gear train—1.

6. Derive the structure matrix for the 3-dof spherical wrist mechanism shown in Fig. 7.20, where links 6, 9, and 10 are the input links and link 4 is the end effector.
7. Derive the structure matrix for the 3-dof spherical wrist mechanism shown in Fig. 7.21, where links 6, 9, and 10 are the input links and link 4 is the end effector.

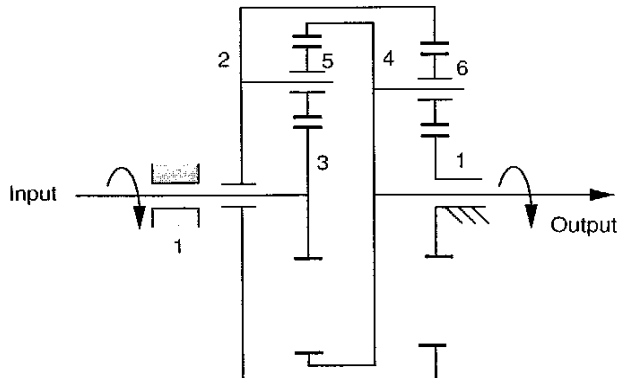


FIGURE 7.19. Compound planetary gear train—2.

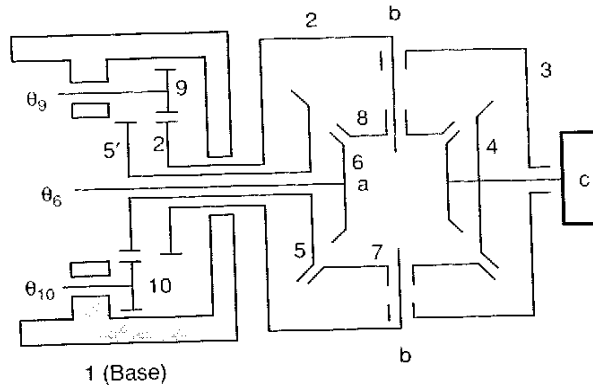


FIGURE 7.20. Spherical wrist mechanism—3.

8. For the spherical wrist mechanism shown in Fig. 7.17, let links 5, 6, and 7 be the input links and 4 be the end-effector link. Find the input rotation rates in terms of a given angular velocity and general posture of the end effector.
9. For the spherical wrist mechanism shown in Fig. 7.16, links 4 and 5 are the input links and 3 is the end-effector link. Assuming that the end effector is oriented at a general posture, calculate the input torques, τ_4 and τ_5 ,

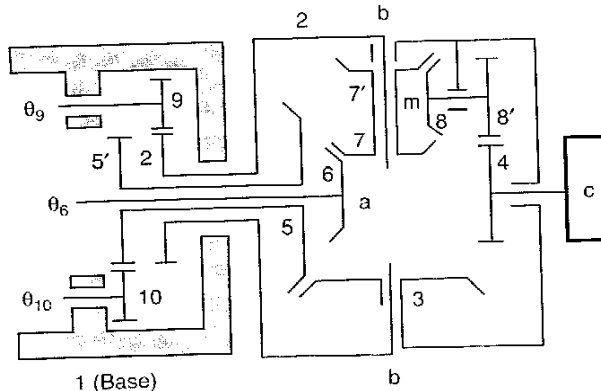


FIGURE 7.21. Spherical wrist mechanism—4.

required to produce an end-effector output moment of (n_x, n_y, n_z) about the center of the wrist.

10. For the 3-dof spherical wrist mechanism shown in Fig. 7.22, links 7, 9, and 10 are the input links and link 4 is the end effector. Applying the principle of virtual work, calculate the input torques, τ_7 , τ_9 and τ_{10} , required to generate an end-effector output moment of (n_x, n_y, n_z) about the center of the wrist. For the particular posture shown in Fig. 7.22, is it possible to generate an output moment in the x_1 -direction?

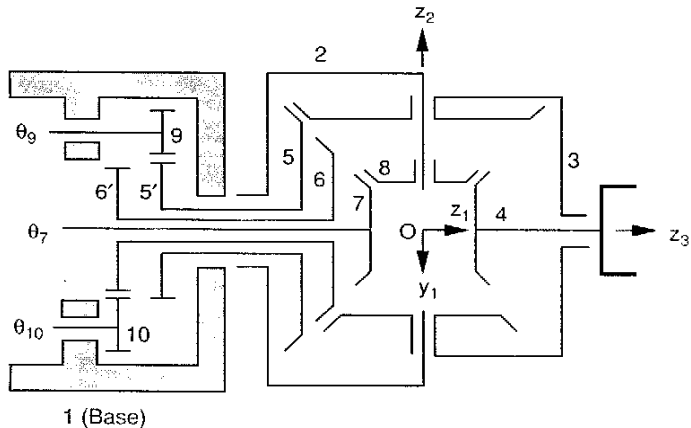


FIGURE 7.22. Spherical wrist mechanism - 5.

CHAPTER 8

TENDON-DRIVEN MANIPULATORS

8.1 INTRODUCTION

The kinematic structure of a robot manipulator often takes the form of an open-loop chain. An open-loop manipulator is mechanically simple and easy to construct. Theoretically, one actuator can be mounted on each link to drive the next link via a speed reduction unit. Using this approach, however, actuators and speed reducers installed on the distal end become the load for actuators installed on the proximal end of a manipulator, resulting in a bulky and heavy system. To reduce the size and inertia of a robot manipulator, it is often necessary to introduce some mechanical transmission system that permits actuators to be located remotely away from the joints.

Various mechanical transmission systems, including gear trains, tendon-and-pulley trains, tie-rod linkages, and so on, may be incorporated. The type of transmission system selected depends on the application and other design considerations. Generally, the power-to-weight ratio must be optimized, backlash and vibration minimized, and friction reduced. The application of gear trains as mechanical transmission mechanisms for robot wrists was discussed in Chapter 7. In this chapter we concentrate on the kinematics of tendon drives. The term *tendon* is widely used to imply belts, cables, or similar constructions. The main advantages of using tendon drives are: (1) All actuators can be installed on the fixed base, resulting in a compact and lightweight design; and (2) a well-designed tendon transmission system has little backlash. These merits have made tendons better suited than other mechanical transmission systems in applications such as dexterous hands, where the re-

quirements of small volume, light weight, and high speed are the most important factors. The main disadvantages of introducing a tendon transmission system are the extra cost of additional mechanical components and the possibility of creating some drawbacks, such as friction and vibration in the system.

In this chapter we address the fundamental mechanics of tendon-driven manipulators. Basic issues, including the structural characteristics, kinematics, and statics of tendon-driven manipulators, are studied.

8.2 CLASSIFICATION OF TENDON-DRIVEN MANIPULATORS

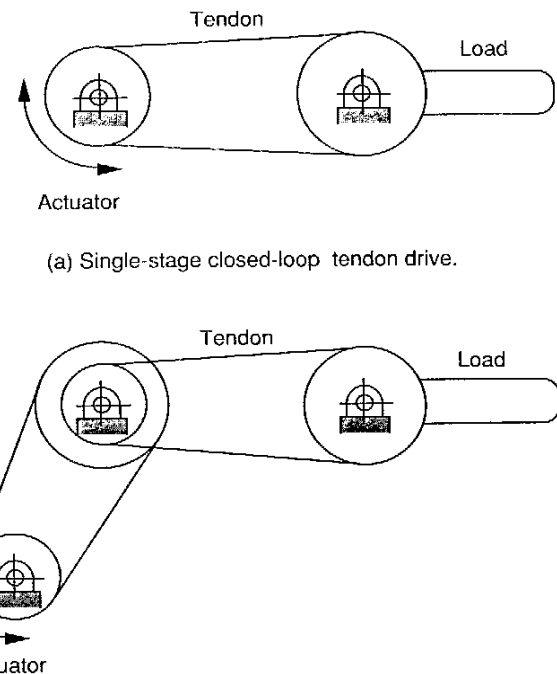
Tendon drives can generally be classified into two categories: (1) *closed-loop tendon drives* and (2) *open-ended tendon drives*. In what follows, we describe each of them in turn.

8.2.1 Closed-Loop Tendon Drives

Perhaps the most commonly known tendon-driven manipulating system is the *closed-loop tendon drive*, used in a variety of industrial machinery. Recently, these drives have also been incorporated in robot manipulators (Ali et al., 1993; Cannon and Schmitz, 1984; Hollars and Cannon, 1985; Melchiorri and Vassura, 1992; Okada, 1977; Sugano and Kato, 1987). This type of transmission system uses one motor to drive a closed-loop belt in both directions. Figure 8.1a shows a 1-dof mechanism driven by a rotary actuator through a closed-loop tendon. Power transmission in a closed-loop tendon transmission system usually relies on friction generated between pulleys and belts. To increase the efficiency, toothed belts known as the *timing belt* or *chain-and-sprocket devices* can be used. Closed-loop tendons can also be connected in series to form a multistage transmission system, as shown in Fig. 8.1b. In a closed-loop drive, a portion of each tendon will be under high tension while the other portion is under little tension. Although torque can be transmitted in both directions, pretension is often necessary to prevent tendons from slackening. Pretension, however, can introduce significant amount of friction and apparent backlash due to the elastic effect of tendons. Because a closed-loop belt can be driven in both directions, the number of actuators needed is equal to the number of degrees of freedom of a manipulator.

8.2.2 Open-Ended Tendon Drives

Another form of tendon transmission is called an *open-ended tendon drive*. Let n be the degrees of freedom and m the number of control tendons in an open-ended tendon drive. We call such a manipulator an $n \times m$ manipulator.



(a) Single-stage closed-loop tendon drive.

(b) Double-stage closed-loop tendon drive.

FIGURE 8.1. Closed-loop tendon drives.

For example, Fig. 8.2 shows a 2×3 tendon-driven manipulator. In an open-ended tendon transmission system, one end of each tendon is attached to a moving link while the other end is pulled by an actuator. Force is transmitted by pulling of the tendons. A unique feature associated with open-ended tendon drives is that tendons can exert tension but not compression. That is, actuator forces must be applied in a unidirectional sense. Morecki et al. (1980) showed that m should be greater than n to achieve independent control of all the degrees of freedom of a manipulator. Using this criterion, we can classify open-ended tendon-driven manipulators as follows.

(a) $m < n$. If the number of tendons is less than the number of degrees of freedom, the motion of a manipulator cannot be controlled at will. We call this type of manipulator an *insufficiently actuated manipulator*. An insufficiently

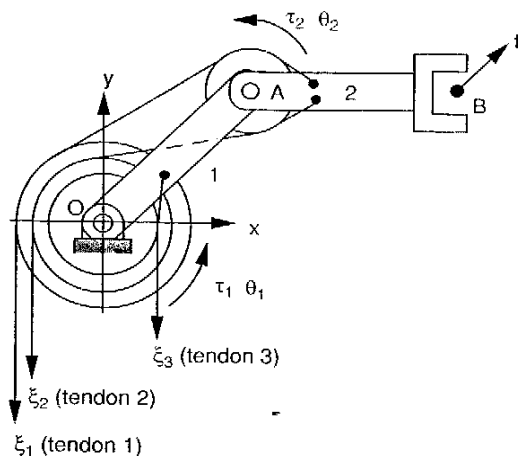


FIGURE 8.2. A 2-dof manipulator driven by three tendons.

actuated manipulator usually relies on mechanical constraints or structural characteristics to control its posture. Hirose and Umetani (1978, 1979) developed a soft gripper. The gripper consists of three multi-dof fingers. Each is controlled by only one grip tendon and one release tendon. The diameter of the grip pulley becomes smaller from its base joint toward the tip joint, while the diameter of the release pulley is uniform along its entire length. Although the joints cannot be controlled independently, the fingers can conform to an object of random shape with a uniform grasping force. Rovetta (1981) constructed a mechanical hand with two fingers and a palm. Each finger has four joints and is pulled by a single tendon against a spring-loaded palm. Insufficiently actuated manipulators have also been configured into *differential mechanisms* (Hirose, 1986).

(b) $m = n$. When the number of tendons is equal to the number of degrees of freedom, the manipulator is still an insufficiently actuated mechanism. This type of manipulator can often be found in hoisting cranes and elevators for raising, shifting, and lowering heavy objects. For such applications, tendons are usually designed to pull against the gravitational force. A robotic crane system utilizing the Stewart platform architecture was recently developed by Albus et al. (1992). In their design, six cables are used as parallel links to manipulate the location of a suspended moving platform, as shown in Fig. 8.3. Although the number of actuators is less than $n + 1$, complete control of

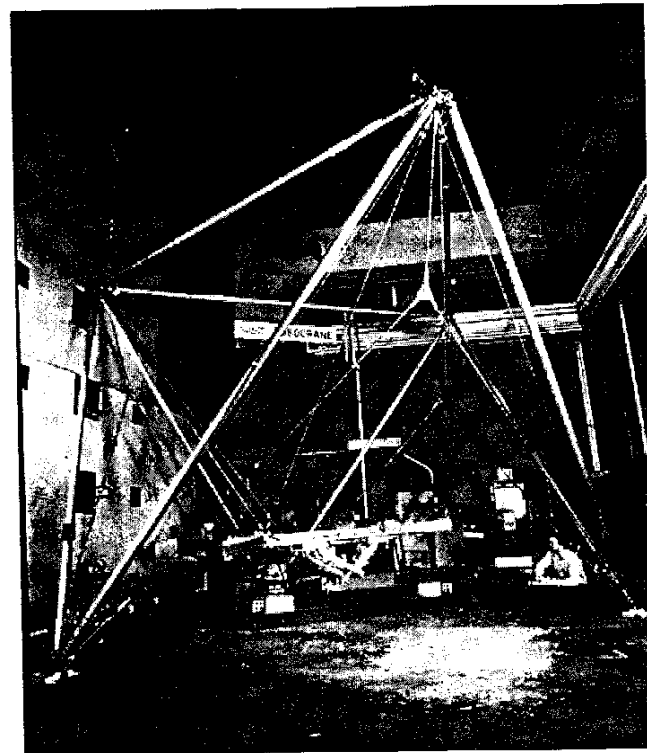


FIGURE 8.3. NIST RoboCrane. (Courtesy of NIST, Gaithersburg, Maryland.)

the end-effector location is possible. In fact, the gravitational force has been employed as the $(n + 1)$ th control force.

Another way of controlling an n -dof manipulator with n tendons is to let the actuators work against spring-loaded tendons or joints. For example, Rovetta (1977) built a mechanical gripper in which return springs were installed in the joints to serve as a bias torque. This approach, however, prohibits the system from fine manipulation and force control since the spring may exhibit some nonlinearity and cause asymmetric responses.

(c) $m > n$. If the number of tendons exceeds the number of degrees of freedom, the manipulator can be controlled at will. This is by far the most popular arrangement because it allows users complete control of the degrees

of freedom. We call this type of manipulator a *sufficiently actuated manipulator*. For example, Morecki et al. (1980) discussed some of the problems encountered in the design of their anthropomorphic two-handed manipulator and Salisbury designed a three-fingered hand known as the *Stanford/JPL hand* (Salisbury, 1982; Rouff and Salisbury, 1990). In the Stanford/JPL hand, each finger has three articulation points and is controlled by four tendons. The kinematics and statics of the transmission system were studied in detail by Salisbury and Craig (1982) and Salisbury and Roth (1983). As shown in Fig. 8.4, Jacobsen et al. (1984, 1986, 1989) developed a four-fingered hand



FIGURE 8.4. Utah/MIT dexterous hand. (Courtesy of SARCOS, Salt Lake City, Utah.)

called the *Utah/MIT hand*. Each finger of the Utah/MIT hand has four articulation points and is controlled by eight tendons. Many other tendon-driven manipulators are discussed in Pham and Heginbotham (1986).

8.3 PLANAR SCHEMATIC REPRESENTATION

In this section we present a planar schematic representation of the kinematic structure of tendon-driven manipulators. To reduce the scope of study, we consider only those mechanisms that obey the following assumptions:

1. The manipulator is an articulated type (i.e., after removal of tendons and pulleys, the mechanism becomes an open-loop chain).
2. Each tendon is routed from the base link to one of the moving links over pulleys mounted on the joint axes of an open-loop chain in a consecutive manner.
3. All tendons are under tension, and the amount of stretch in each tendon is negligible.
4. No slippage occurs between pulleys and tendons.

Figure 8.5 shows a functional schematic diagram of the Stanford/JPL finger (Mason and Salisbury, 1985). For the purpose of illustration, the fixed base is denoted by link 0, the moving links and joints are numbered sequentially from 1 to 3, and a positive direction of rotation is assigned to each joint axis, as shown in the figure. In the Stanford/JPL finger, the first joint axis, z_1 , is fixed to the base link; the second joint axis, z_2 , is perpendicular to the first; and the third joint axis, z_3 , is parallel to the second. Pulley 2 is attached to link 2, and pulley 3 is attached to link 3. Pulleys 4, 5, 6, and 7 are free to rotate about the first joint axis, pulleys 2 and 8 are free to rotate about the second joint axis, and pulley 3 is free to rotate about the third joint axis. The first tendon, s_1 , connects pulley 4 to 8 and then 3; the second tendon, s_2 , connects pulley 5 to 8 and then 3; the third tendon, s_3 , connects pulley 6 to 2; and the fourth tendon, s_4 , connects pulley 7 to 2. Overall, the mechanism consists of nine links and four control tendons.

The tendon routings in such a functional schematic diagram can sometimes be confusing due to the nature of spatial construction. For convenience, a planar schematic representation is defined to illustrate the routing of tendons (Tsai and Lee, 1989). To construct a planar schematic, we start from the second joint axis and twist every joint axis about the common normal defined by the joint axis itself and its preceding joint axis until all the axes are pointing in the same direction. In this way, the routing of tendons can be shown clearly without losing the tendon routing topology. Figure 8.6a shows a pla-

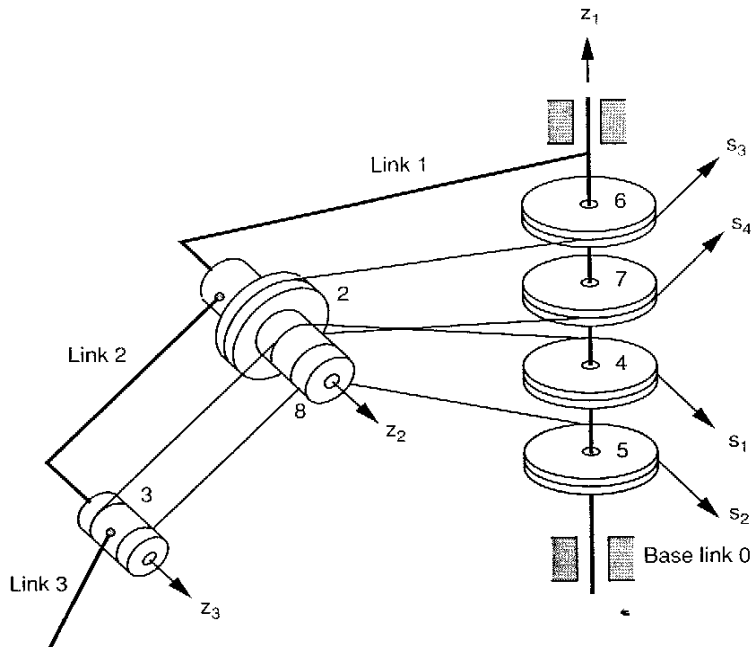


FIGURE 8.5. Functional schematic diagram of the Stanford/JPL finger.

nar schematic diagram of the Stanford/JPL finger. In a planar representation, all the positive joint axes point out of the paper. The routing of each tendon can also be sketched individually, as shown in Fig. 8.6b–e.

A more abstract planar representation of the tendon routing is shown in Fig. 8.7. In this abbreviated planar representation, a line passing by one side of a pulley implies that the tendon is routed over that pulley several times, beginning and ending at that side of the pulley. Similar to a gear train, we call each tendon routing arrangement a *transmission line*.

8.4 KINEMATICS OF TENDON-DRIVEN MANIPULATORS

The kinematics of tendon-driven manipulators is similar to that of geared robotic mechanisms. The analysis can be accomplished in two fundamental steps. The first step is the derivation of a kinematic relationship between

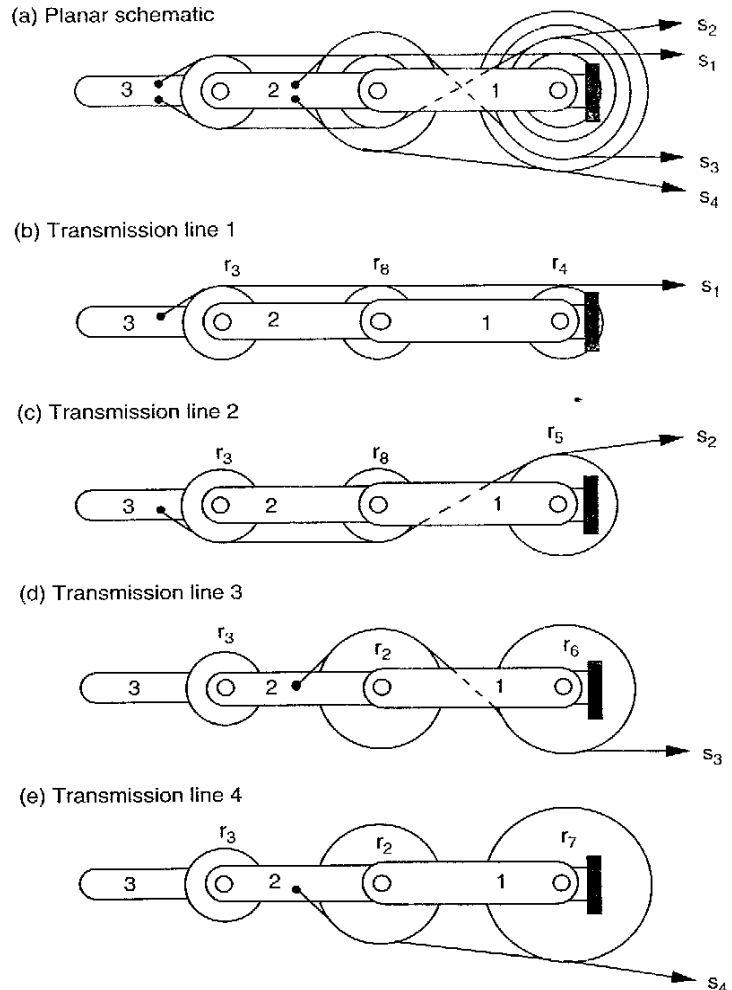


FIGURE 8.6. Planar schematic diagram of the Stanford/JPL finger.

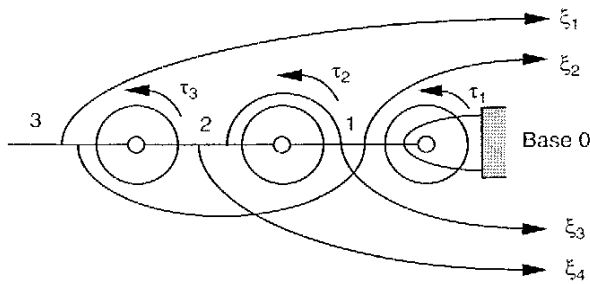


FIGURE 8.7. Abbreviated planar representation of the Stanford/JPL finger.

the location of the end effector and the joint angles of the open-loop chain. This step can be accomplished by the Denavit–Hartenberg method outlined in Chapter 2. The second step is the derivation of a kinematic relationship between the joint angles and the tendon displacements, and this is the main focus of this section.

Mathematically, the joint angles and tendon displacements are related by a linear transformation. In this section we apply the theory of fundamental circuits and the coaxiality conditions for the derivation of the transformation matrix. We will show that the transformation matrix can be obtained by an inspection of the tendon routing topology using the concept of transmission lines. In general, the transformation matrix is a function of the pulley size, the tendon routing topology, and the manipulator posture. However, for those open-loop manipulators in which tendons are routed from one joint to another along the open-loop chain in a consecutive manner, we show that the matrix is independent of the manipulator posture.

8.4.1 Fundamental Circuit Equations

Let i and j denote a pulley pair for which link k serves as the common carrier, as shown in Fig. 8.8. Then links i , j , and k constitute a simple tendon-and-pulley train. For the purpose of analysis, a positive direction of rotation is assigned to each joint axis of the pulley pair. A *fundamental circuit equation* relating the angular displacements of the two pulleys can be written as

$$r_i \theta_{i,k} = \pm r_j \theta_{j,k}, \quad (8.1)$$

where $\theta_{i,k}$ and $\theta_{j,k}$ denote the rotations of pulleys i and j with respect to the carrier k and r_i and r_j denote the radii of the two pulleys.

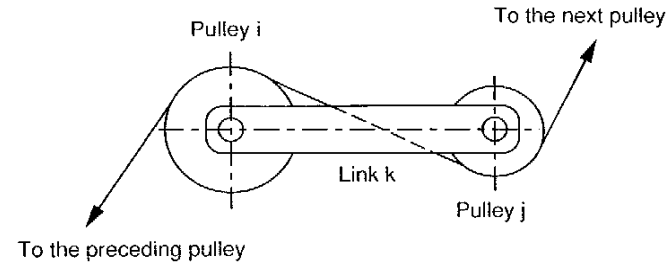


FIGURE 8.8. Planar schematic of a simple tendon-and-pulley train.

A tendon routing is called a *parallel type* if a rotation of one pulley about its prescribed positive joint axis produces a positive rotation of the other pulley. Otherwise, it is called a *crossed type*. For example, the routing shown in Fig. 8.8 is a crossed type. The sign in Eq. (8.1) is positive for parallel routing and negative for crossed routing. Equation (8.1) is valid whether or not the carrier is stationary.

8.4.2 Coaxiality Conditions

Let i , j , and k denote three links that share a common joint axis; then similar to an epicyclic gear train, the angular displacements of the three links are related by the following chain rule:

$$\theta_{i,j} = \theta_{i,k} - \theta_{j,k}. \quad (8.2)$$

Equation (8.2) is useful for relating the relative rotations among three coaxial links.

8.4.3 Transmission Lines

Figure 8.9 shows a typical transmission line in which the links are labeled sequentially from 0 to n and the pulleys are labeled from j to $j + n - 1$. Let $\theta_{j,i}$ denote the angular displacement of link j with respect to link i . We can write the fundamental circuit equation once for each pulley pair as follows:

$$r_{j+i-1} \theta_{j+i-1,i} = \pm r_{j+i} \theta_{j+i,i} \quad \text{for } i = 1, 2, \dots, n-1. \quad (8.3)$$

where the \pm sign is positive for a parallel routing and negative for a crossed routing.

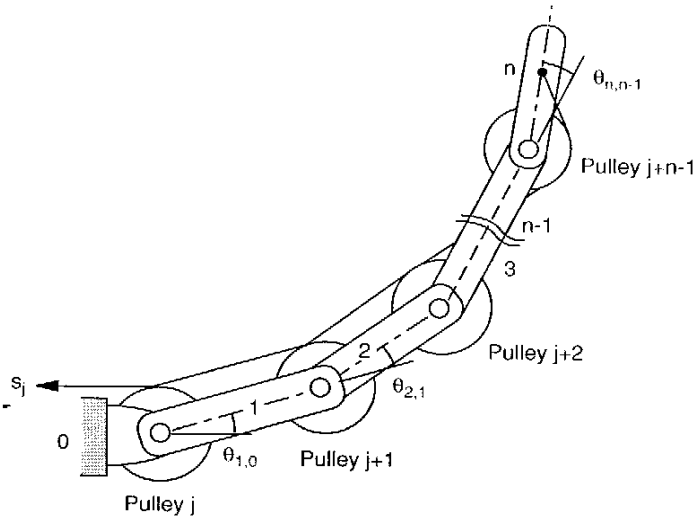


FIGURE 8.9. Typical transmission line.

Since links $i - 1$, i , and pulley $j + i - 1$ are coaxial, a coaxiality condition can be written as

$$\theta_{j+i-1,i} = \theta_{j+i-1,i-1} - \theta_{i,i-1} \quad \text{for } i = 1, 2, \dots, n. \quad (8.4)$$

Since pulley $j + n - 1$ is attached to link n , $\theta_{j+n-1,n} = 0$. Eliminating $\theta_{j+i-1,i}$ for $i = 2, 3, \dots, n$ from Eqs. (8.3) and (8.4) yields

$$\theta_{j,0} = \theta_{1,0} \pm (r_{j+1}/r_j)\theta_{2,1} \pm \dots \pm (r_{j+n-1}/r_j)\theta_{n,n-1}. \quad (8.5)$$

The \pm sign for each term of $\theta_{k,k-1}$ in Eq. (8.5) is determined by the number of crossed routings preceding the k th joint axis. The sign is positive if the number of crossed routings is even; otherwise, it is negative. Hence the equation can readily be obtained by an inspection of the tendon routing topology.

Let the displacement of tendon j from a fully stretched out reference position be denoted by s_j . It is obvious that the displacement of tendon j is related to the angular displacement of the base pulley by

$$s_j = \pm r_j \theta_{j,0}, \quad (8.6)$$

where the \pm sign is positive if a pull of the tendon results in a positive rotation of the base pulley, otherwise, it is negative.

Eliminating $\theta_{j,0}$ between Eqs. (8.6) and (8.5) and writing the resulting equation once for each tendon yields m linear equations relating the tendon displacements to the joint angles of the open-loop chain. These equations can be assembled in matrix form:

$$\mathbf{s} = \mathbf{A}\boldsymbol{\theta}, \quad (8.7)$$

where $\mathbf{s} = [s_1, s_2, \dots, s_m]^T$ denotes an m -dimensional vector of tendon displacements, $\boldsymbol{\theta} = [\theta_{1,0}, \theta_{2,1}, \dots, \theta_{n,n-1}]^T$ denotes an n -dimensional vector of the joint angles, and \mathbf{A} is an $m \times n$ transformation matrix. The elements of \mathbf{A} are functions of the pulley sizes and the tendon routing topology and are independent of the posture of a manipulator. Since $m \geq n + 1$, \mathbf{A} is not a square matrix.

Equation (8.7) constitutes a set of m linear equations. Given the joint angles of the open-loop chain, we can compute the tendon displacements directly from Eq. (8.7). On the other hand, since $m > n$, the tendon displacements cannot be specified arbitrarily. Specifically, only n of the m tendon displacements are needed to determine the joint angles. The displacements of the remaining $m - n$ tendons follow the constraints imposed by Eq. (8.7). This contributes to a major difference between a tendon-driven manipulator and a geared robotic mechanism.

Example 8.4.1 Kinematics of the Stanford/JPL Finger Let us apply the concept of transmission lines to the kinematic analysis of the Stanford/JPL finger shown in Fig. 8.5. The open-loop chain consists of links 0, 1, 2, and 3. The routing of four tendons is depicted clearly in Fig. 8.6.

Writing Eq. (8.5) once for each transmission line shown in Fig. 8.6 yields

$$\begin{aligned} \theta_{4,0} &= \theta_{1,0} + (r_8/r_4)\theta_{2,1} + (r_3/r_4)\theta_{3,2}, \\ \theta_{5,0} &= \theta_{1,0} - (r_8/r_5)\theta_{2,1} - (r_3/r_5)\theta_{3,2}, \\ \theta_{6,0} &= \theta_{1,0} - (r_2/r_6)\theta_{2,1}, \\ \theta_{7,0} &= \theta_{1,0} + (r_2/r_7)\theta_{2,1}. \end{aligned} \quad (8.8)$$

Note that we have made use of the following facts in the derivation of Eq. (8.8). The parallel-and-parallel routing of tendon 1 leads to positive second and third terms on the right-hand side of the first equation; the crossed-and-parallel routing of tendon 2 results in negative second and third terms on the right-hand side of the second equation; the crossed routing of tendon 3 leads to a negative second term on the right-hand side of the third equation;

and the parallel routing of tendon 4 results in a positive second term on the right-hand side of the fourth equation.

The tendon displacements are related to the base pulley rotations by the following equations:

$$\begin{aligned}s_1 &= -r_4\theta_{4,0}, \\ s_2 &= -r_5\theta_{5,0}, \\ s_3 &= r_6\theta_{6,0}, \\ s_4 &= r_7\theta_{7,0}.\end{aligned}\quad (8.9)$$

Eliminating $\theta_{4,0}$, $\theta_{5,0}$, $\theta_{6,0}$, and $\theta_{7,0}$ between Eqs. (8.8) and (8.9), we obtain

$$\mathbf{s} = \mathbf{A}\boldsymbol{\theta}, \quad (8.10)$$

where $\mathbf{s} = [s_1, s_2, s_3, s_4]^T$, $\boldsymbol{\theta} = [\theta_{1,0}, \theta_{2,1}, \theta_{3,2}]^T$, and

$$\mathbf{A} = \begin{bmatrix} -r_4 & -r_8 & -r_3 \\ -r_5 & r_8 & r_3 \\ r_6 & -r_2 & 0 \\ r_7 & r_2 & 0 \end{bmatrix}. \quad (8.11)$$

We observe that the elements of \mathbf{A} are functions of tendon routing and pulley sizes. The tendon displacements are highly coupled. The third joint angle, $\theta_{3,2}$, affects the displacements of tendons 1 and 2 only, while the first and second joint angles, $\theta_{1,0}$ and $\theta_{2,1}$, affect the displacements of all four tendons.

Example 8.4.2 Kinematics of the Utah/MIT Finger As a second example we consider a 4-dof manipulator controlled by eight tendons, resembling the Utah/MIT finger. In the Utah/MIT finger, the first joint axis is fixed to the base; the second joint axis is perpendicular to the first with a small offset distance; while the third and fourth joint axes are both parallel to the second joint axis. A planar schematic diagram of the mechanism is shown in Fig. 8.10. As shown in the figure, pulleys 1, 2, 3, and 4 are attached to links 1, 2, 3, and 4, respectively. Pulleys 1, 5, 6, and 7 are pivoted about the first joint axis; pulleys 2, 8, and 9 are pivoted about the second joint axis; pulleys 3 and 10 are pivoted about the third joint axis; and pulley 4 is pivoted about the fourth joint axis. The first and second tendons, s_1 and s_2 , wrap around the opposite sides of pulleys 5, 8, 10, and 4; the third and fourth tendons, s_3 and s_4 , wrap around the opposite sides of pulleys 6, 9, and 3; the fifth and sixth tendons, s_5 and s_6 , wrap around the opposite sides of pulleys 7 and 2; and the seventh and eighth tendons, s_7 and s_8 , wrap around the opposite sides of pulley 1.

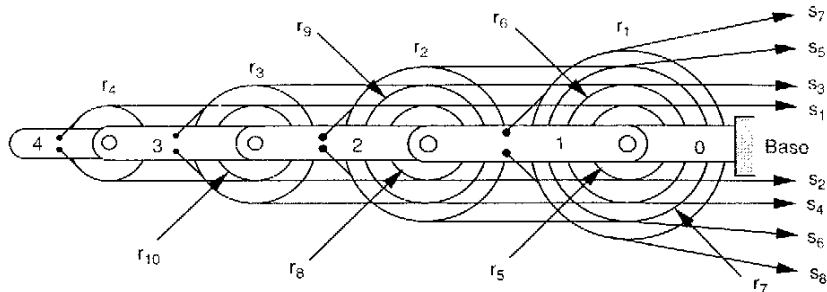


FIGURE 8.10. A 4-dof manipulator driven by eight tendons.

We wish to find the transformation between the joint angles and the tendon displacements.

Writing Eq. (8.5) once for each of the eight tendons yields

$$\begin{aligned}\theta_{5,0} &= \theta_{1,0} + (r_8/r_5)\theta_{2,1} + (r_{10}/r_5)\theta_{3,2} + (r_4/r_5)\theta_{4,3}, \\ \theta_{5,0} &= \theta_{1,0} + (r_8/r_5)\theta_{2,1} + (r_{10}/r_5)\theta_{3,2} + (r_4/r_5)\theta_{4,3}, \\ \theta_{6,0} &= \theta_{1,0} + (r_9/r_6)\theta_{2,1} + (r_3/r_6)\theta_{3,2}, \\ \theta_{6,0} &= \theta_{1,0} + (r_9/r_6)\theta_{2,1} + (r_3/r_6)\theta_{3,2}, \\ \theta_{7,0} &= \theta_{1,0} + (r_2/r_7)\theta_{2,1}, \\ \theta_{7,0} &= \theta_{1,0} + (r_2/r_7)\theta_{2,1}, \\ \theta_{1,0} &= \theta_{1,0}, \\ \theta_{1,0} &= \theta_{1,0}.\end{aligned}\quad (8.12)$$

Note that the first and second equations in Eq. (8.12) are identical, due to the fact that tendons 1 and 2 are wrapped around opposite sides of the same pulleys. Similar conditions occur for the remaining tendons. The tendon displacements are related to the angular displacements of the base pulley by

$$\begin{aligned}s_1 &= -r_5\theta_{5,0}, \\ s_2 &= r_5\theta_{5,0}, \\ s_3 &= -r_6\theta_{6,0}, \\ s_4 &= r_6\theta_{6,0}, \\ s_5 &= -r_7\theta_{7,0},\end{aligned}$$

$$\begin{aligned}s_6 &= r_7\theta_{7,0}, \\ s_7 &= -r_1\theta_{1,0}, \\ s_8 &= r_1\theta_{1,0}.\end{aligned}\quad (8.13)$$

Substituting Eq. (8.12) into (8.13), we obtain

$$\mathbf{s} = A\boldsymbol{\theta}, \quad (8.14)$$

where $\mathbf{s} = [s_1, s_2, \dots, s_8]^T$, $\boldsymbol{\theta} = [\theta_{1,0}, \theta_{2,1}, \theta_{3,2}, \theta_{4,3}]^T$, and

$$A = \begin{bmatrix} -r_5 & -r_8 & -r_{10} & -r_4 \\ r_5 & r_8 & r_{10} & r_4 \\ -r_6 & -r_9 & -r_3 & 0 \\ r_6 & r_9 & r_3 & 0 \\ -r_7 & -r_2 & 0 & 0 \\ r_7 & r_2 & 0 & 0 \\ -r_1 & 0 & 0 & 0 \\ r_1 & 0 & 0 & 0 \end{bmatrix}. \quad (8.15)$$

Equation (8.14) provides a transformation between the joint angles and the tendon displacements. Given the joint angles, we can compute the corresponding tendon displacements from Eq. (8.14).

8.5 STATIC FORCE ANALYSIS

In this section we apply the principle of virtual work to derive a transformation between the equivalent joint torques and the tendon forces. Let the vector of tendon forces be denoted by $\xi = [\xi_1, \xi_2, \dots, \xi_m]^T$ and the vector of output joint torques be denoted by $\tau = [\tau_1, \tau_2, \dots, \tau_n]^T$. Also let the virtual joint displacements be denoted by $\delta\boldsymbol{\theta} = [\delta\theta_{1,0}, \delta\theta_{2,1}, \dots, \delta\theta_{n,n-1}]^T$ and the virtual tendon displacements be denoted by $\delta\mathbf{s} = [\delta s_1, \delta s_2, \dots, \delta s_m]^T$. Then the virtual work, δW , done by the active forces is given by

$$\delta W = -\tau^T \delta\boldsymbol{\theta} + \xi^T \delta\mathbf{s}. \quad (8.16)$$

However, the virtual displacements $\delta\boldsymbol{\theta}$ and $\delta\mathbf{s}$ in Eq. (8.16) are related by

$$\delta\mathbf{s} = A\delta\boldsymbol{\theta}. \quad (8.17)$$

Substituting Eq. (8.17) into (8.16) yields

$$\delta W = (-\tau^T + \xi^T A) \delta\boldsymbol{\theta}. \quad (8.18)$$

Since the system is under equilibrium, the virtual work vanishes for any arbitrary virtual displacement $\delta\boldsymbol{\theta}$. Hence we conclude that

$$-\tau^T + \xi^T A = \mathbf{0}. \quad (8.19)$$

Taking the transpose of Eq. (8.19), we obtain

$$\tau = B\xi. \quad (8.20)$$

where $B = A^T$ is called the *structure matrix*. We note that each column of B represents a transmission line.

Equation (8.20) provides a transformation from the tendon forces to the joint torques. However, as described in Chapter 6, the joint torques are related to the end-effector output forces by the transpose of the Jacobian matrix:

$$\tau = J^T \mathbf{F}. \quad (8.21)$$

Eliminating τ from Eqs. (8.20) and (8.21), we obtain the overall transformation

$$B\xi = J^T \mathbf{F}. \quad (8.22)$$

Assuming that J is a nonsingular square matrix, Eq. (8.22) can be inverted as follows:

$$\mathbf{F} = J^{-T} B\xi. \quad (8.23)$$

Therefore, given the tendon forces, we can compute the end-effector output forces directly from Eq. (8.23). Since $m > n$, given the end-effector output force, there exist an infinitude of tendon forces. But only those positive tendon forces are permissible. This makes control of tendon-drive manipulators more complicated than that of conventional manipulators. A systematic method for the resolution of tendon forces is discussed in a later section.

Furthermore, assuming that pulleys mounted on the same joint axis are of the same size, the structure matrix can be decomposed into a product of two matrices,

$$B = R^* B^*, \quad (8.24)$$

where R^* is an $n \times n$ diagonal matrix whose nonzero elements are the radii of the pulleys installed on the consecutive joint axes of the open-loop chain and B^* is an $n \times m$ matrix whose (i, j) element takes the value $+1$, -1 , or 0 depending on whether a positive pull of tendon j produces a positive, negative, or no effect on the i th joint torque. Thus B^* contains the tendon routing topology, while R^* represents the pulley sizes.

Example 8.5.1 Structural Matrix of the Stanford/JPL Finger The structure matrix of the Stanford/JPL finger shown in Fig. 8.5 is obtained by taking the transpose of Eq. (8.11):

$$B = A^T = \begin{bmatrix} -r_4 & -r_5 & r_6 & r_7 \\ -r_8 & r_8 & -r_2 & r_2 \\ -r_3 & r_3 & 0 & 0 \end{bmatrix}. \quad (8.25)$$

Furthermore, if $r_2 = r_8$ and $r_4 = r_5 = r_6 = r_7$, the structure matrix can be written as $B = R^* B^*$, where

$$B^* = \begin{bmatrix} -1 & -1 & 1 & 1 \\ -1 & 1 & -1 & 1 \\ -1 & 1 & 0 & 0 \end{bmatrix}, \quad (8.26)$$

$$R^* = \begin{bmatrix} r_4 & 0 & 0 \\ 0 & r_2 & 0 \\ 0 & 0 & r_3 \end{bmatrix}. \quad (8.27)$$

The first column of B^* implies that a pull of tendon 1 will produce negative torques about the first, second, and third joint axes. The second column of B^* implies that a pull of tendon 2 will result in negative, positive, and positive torques about the first, second, and third joint axes, respectively. The effects of tendons 3 and 4 on the joint torques of the manipulator can be explained similarly.

Example 8.5.2 Structural Matrix of the Utah/MIT Finger The structure matrix of the 4-dof manipulator shown in Fig. 8.10 is obtained by taking the transpose of Eq. (8.15):

$$B = \begin{bmatrix} -r_5 & r_5 & -r_6 & r_6 & -r_7 & r_7 & -r_1 & r_1 \\ -r_8 & r_8 & -r_9 & r_9 & -r_2 & r_2 & 0 & 0 \\ -r_{10} & r_{10} & -r_3 & r_3 & 0 & 0 & 0 & 0 \\ -r_4 & r_4 & 0 & 0 & 0 & 0 & 0 & 0 \end{bmatrix}. \quad (8.28)$$

Furthermore, if $r_1 = r_5 = r_6 = r_7$, $r_2 = r_8 = r_9$, and $r_3 = r_{10}$, the structure matrix can be written as $B = R^* B^*$, where

$$B^* = \begin{bmatrix} -1 & 1 & -1 & 1 & -1 & 1 & -1 & 1 \\ -1 & 1 & -1 & 1 & -1 & 1 & 0 & 0 \\ -1 & 1 & -1 & 1 & 0 & 0 & 0 & 0 \\ -1 & 1 & 0 & 0 & 0 & 0 & 0 & 0 \end{bmatrix}, \quad (8.29)$$

$$R^* = \begin{bmatrix} r_1 & 0 & 0 & 0 \\ 0 & r_2 & 0 & 0 \\ 0 & 0 & r_3 & 0 \\ 0 & 0 & 0 & r_4 \end{bmatrix}. \quad (8.30)$$

The matrix B^* contains eight columns formed by four pairs of tendons: (1,2), (3,4), (5,6), and (7,8). For each pair of tendons, the corresponding column vectors are negatives of each other, indicating that the tendons are routed symmetrically around opposite sides of the pulleys.

8.6 FEASIBLE STRUCTURE MATRICES

In this section we discuss the fundamental structure characteristics of tendon-driven manipulators. We show that an n -dof open-loop manipulator requires at least $n + 1$ tendons, and these tendons must be routed in certain patterns such that independent control of the joints can be achieved. Finally, we introduce the notion of isomorphic structure matrices and present some feasible structure matrices.

8.6.1 Structure Characteristics

The structure matrix defines the force transmission characteristics between the tendon force space and the joint torque space. Given a set of tendon forces, the resulting joint torques of the open-loop chain can be computed directly from Eq. (8.20). Conversely, given a set of desired joint torques, Eq. (8.20) constitutes n linear equations in m unknowns. To maintain positive tendon forces, m must be greater than n such that the solutions of tendon forces can be written as a particular solution plus an $(m - n)$ -dimensional homogeneous solution. More specifically, for $m > n$, we can express the inverse transformation of Eq. (8.20) as

$$\xi = B^+ \tau + H\lambda, \quad (8.31)$$

where $B^+ = B^T [BB^T]^{-1}$ is the pseudoinverse of B , H is an $m \times (m - n)$ matrix with its column vectors spanning the null space of B , and λ is an arbitrary $(m - n)$ -dimensional vector.

The first term on the right-hand side of Eq. (8.31) is called the *particular solution*, and the second term, the *homogeneous solution*. The particular solutions form an n -dimensional subspace in the m -dimensional tendon-force space. The homogeneous solution gives the ratios of tendon forces that result in no net joint torques. Hence if the column space of H contains at least one

m -dimensional vector with all positive elements, by choosing a proper value of λ , positive tendon forces can always be maintained.

Based on the discussion above, we conclude that the structure matrix B must satisfy the following conditions (Lee and Tsai, 1991; Ou and Tsai, 1993):

1. The number of tendons must exceed the number of degrees of freedom by at least 1 (i.e., $m \geq n + 1$).
2. The rank of B must be equal to the degrees of freedom of the system. Furthermore, if $m = n + 1$, the determinant of a submatrix formed by deleting any column from B should not be equal to zero.
3. There exists at least one vector with all positive elements in the null space of B .
4. Since we assume that tendons are routed from joint to joint in a consecutive manner, nonzero elements in each column of B must be consecutive.
5. Exchanging any two columns of a structure matrix, which is equivalent to a renumbering of two tendons, does not have any effect on the mechanics of a manipulator. It follows that the structure matrix can always be arranged in a form such that all the zero elements appear on the lower right corner of the matrix.
6. Changing the sign of every element in a row does not have any effect on the mechanics of a manipulator. This is equivalent to a change in the definition of the positive direction of rotation of a joint axis.

8.6.2 Isomorphic Structure Matrices

We have shown in Eq. (8.5) that the elements of a structure matrix are determined by the routing of tendons and the definitions of positive directions of rotation of the joint axes. Therefore, if the positive direction of rotation of a joint axis is defined in the opposite sense, the sign for each element in the corresponding row of the structure matrix will be reversed. Since the definition of positive direction of rotation and the numbering of tendons have no effect on the functionality of a mechanism, two structure matrices are said to be structurally *isomorphic* if they satisfy one of the following conditions:

1. They are identical.
2. They become identical after changing the sign of every element in one or more rows of a matrix (structure characteristic 6).

3. They become identical after exchanging two or more columns of a matrix (structure characteristic 5).
4. They become identical after the combined operation of conditions 2 and 3.

Example 8.6.1 Two Isomorphic Tendon Routings Figure 8.11a and b show a 2-dof manipulator with two apparently different routings of tendons. We wish to show that these two routings are structurally isomorphic. Let the positive direction of rotation be pointing out of the paper. Then the structure matrices for the two routings of tendons are given by

$$(1) \quad B_1^* = \begin{bmatrix} -1 & -1 & 1 \\ -1 & 1 & 0 \end{bmatrix},$$

$$(2) \quad B_2^* = \begin{bmatrix} 1 & 1 & -1 \\ -1 & 1 & 0 \end{bmatrix},$$

respectively. It can be seen that after switching the sign of each element in the first row of B_2^* , the structure matrix B_2^* becomes identical to B_1^* . Physically, if we reverse the definition of positive direction of rotation of the first (proximal) joint axis of the mechanism shown in Fig. 8.11b, it becomes identical to that of Fig. 8.11a. Therefore, these two routings are structurally isomorphic.

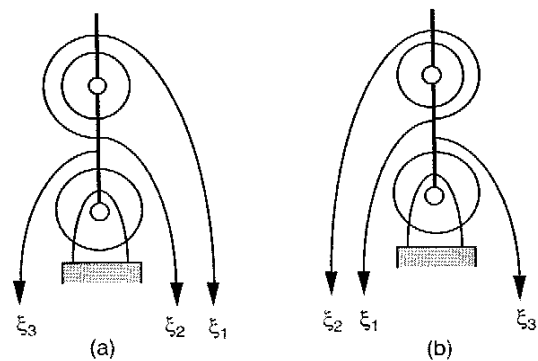


FIGURE 8.11. Two structurally isomorphic, 2-dof tendon-driven manipulators.

8.6.3 Feasible Pseudotriangular Structure Matrices

In the preceding section we have shown that an n -dof manipulator requires at least $n + 1$ tendons and that the routing of these tendons must satisfy the structure characteristics 1 through 6. We call a structure matrix that satisfies characteristics 1 through 6 a *feasible structure matrix*; otherwise, the manipulator is not controllable.

Assuming that all pulleys are of the same size, an atlas of nonisomorphic pseudotriangular structure matrices representing tendon-driven manipulators with up to 6 degrees of freedom was developed by Lee and Tsai (1991). Figure 8.12 shows the planar schematics of nonisomorphic tendon-driven manipulators with up to 3 degrees of freedom. Figures 8.13 and 8.14 list all feasible nonisomorphic routings of tendon-driven manipulators with 4 degrees of freedom. We note that the Stanford/JPL finger and Utah/MIT finger do not belong to this class of manipulators. Note that the number of feasible tendon routings increases tremendously if pulleys are permitted to take different sizes (Ou and Tsai, 1993).

8.7 REDUNDANT FORCES RESOLUTION

In this section we develop a systematic method for the resolution of redundant tendon forces. Since the joint space and the tendon space do not have the same dimension, the mapping from the joint torques to the tendon forces is not unique. Theoretically, the pseudoinverse technique can be used. However, the computation of the pseudoinverse can be very time consuming. In addition, the vector λ in Eq. (8.31) must be chosen properly such that all tendons are under tension at all times. To achieve this, the largest ratio of all the negative tendon forces in the particular solution to their corresponding components in the homogeneous solution must be identified. This process will inevitably increase the computation time and reduce the possibility for real-time control of a tendon-driven manipulator system. To overcome this difficulty, Salisbury (1982) supplemented Eq. (8.20) with an additional equation derived from one of the bearing forces for the resolution of redundant forces. Jacobsen et al. (1984, 1989) developed a *rectifier* concept for control of the Utah/MIT hand.

The rectifier concept uses circuitlike operators to convert joint torque signals into tendon force signals without using the pseudoinverse transformation. It provides a closed-form-like solution for the tendon forces. In this section we describe the rectifier concept for the resolution of redundant forces (Lee, 1991; Lee and Tsai, 1993). First, we study the characteristics of a 1-dof system to illustrate the basic principle of a rectifier. Then we extend it to multi-dof systems.

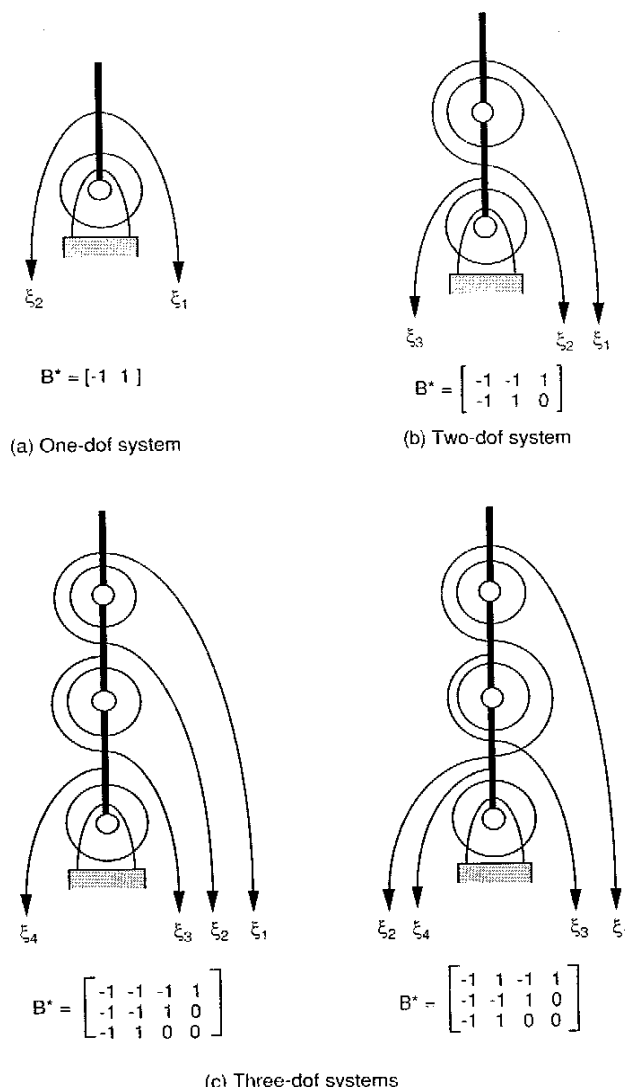
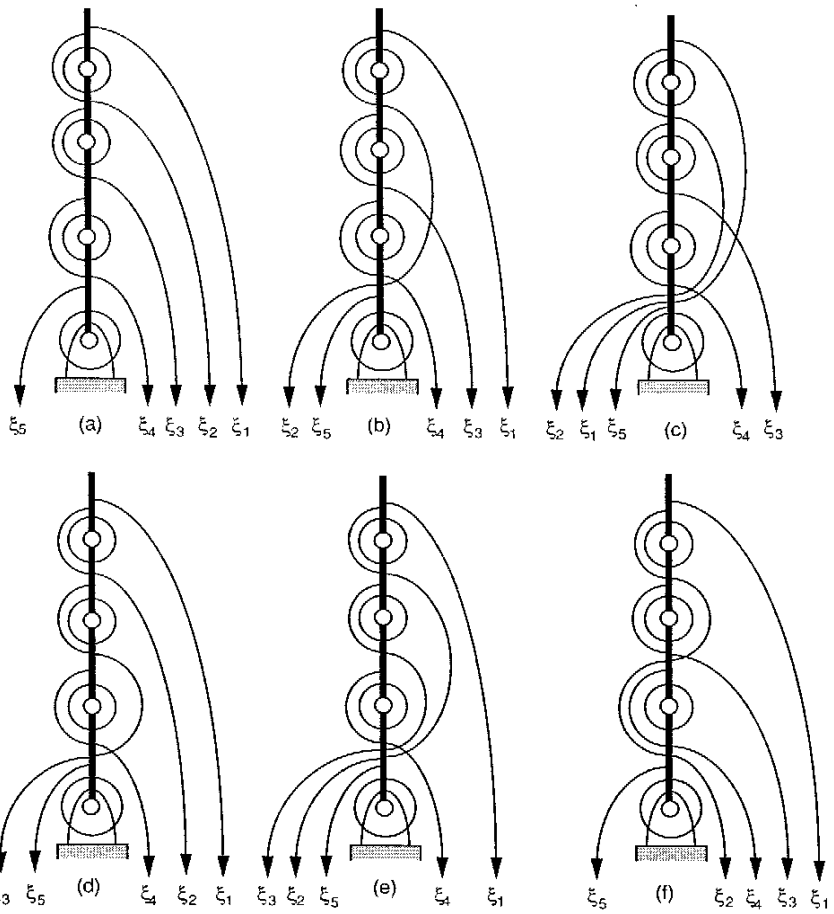
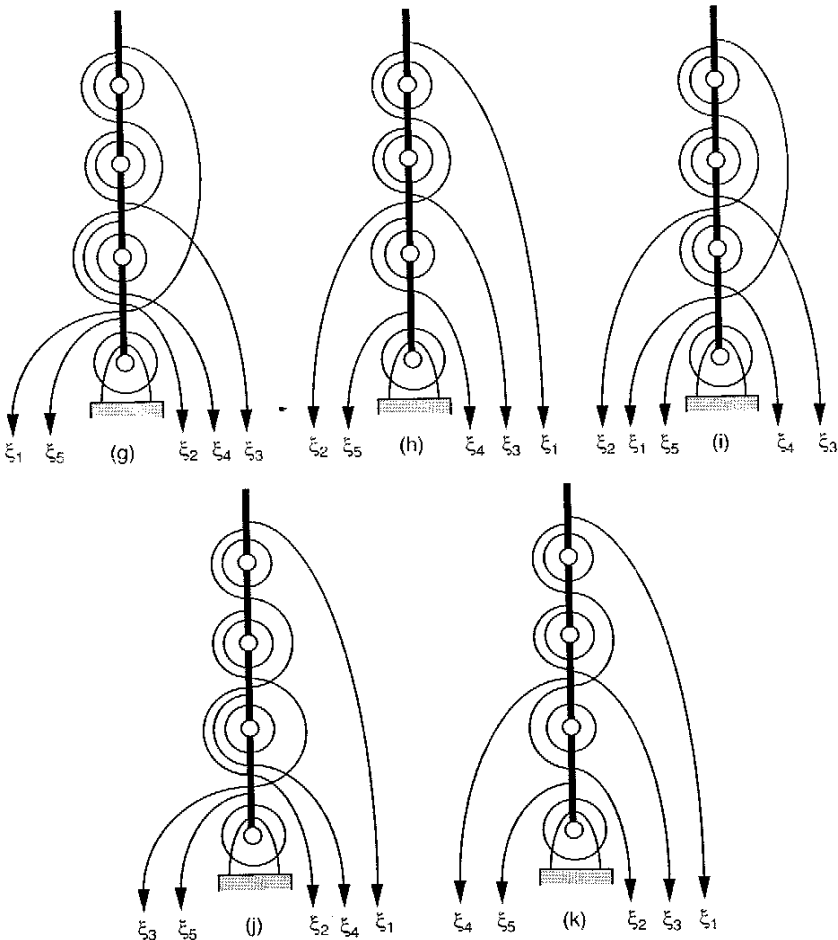


FIGURE 8.12. Feasible $n \times (n + 1)$ manipulators with up to 3 degrees of freedom.

FIGURE 8.13. Feasible 4 \times 5 tendon routings—part I.

8.7.1 Basic Principle

We first study a 1-dof system with two control tendons, shown in Fig. 8.15. Let the positive direction of rotation be pointing out of the paper and let τ be the resulting joint torque about the fixed pivot, O . Assuming that the pulley has a radius of r , a moment balance equation about the fixed pivot can be

FIGURE 8.14. Feasible 4 \times 5 tendon routings—part II.

written

$$\xi_1 - \xi_2 = \tau/r. \quad (8.32)$$

Equation (8.32) contains two tendon forces, ξ_1 and ξ_2 , both of which must be positive at all times. If τ is positive (counterclockwise), the minimum ten-

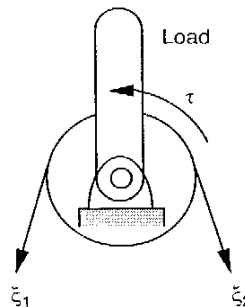


FIGURE 8.15. A 1-dof system controlled by two tendons.

don forces would be $\xi_1 = \tau/r$ and $\xi_2 = 0$. On the other hand, if τ is negative (clockwise), the minimum forces would be $\xi_1 = 0$ and $\xi_2 = -\tau/r$. This simple relation can be written in a mathematical form as

$$\text{for } \tau \geq 0, \begin{cases} \xi_1 = \tau/r + \delta, \\ \xi_2 = \delta, \end{cases} \quad (8.33)$$

$$\text{for } \tau < 0, \begin{cases} \xi_1 = \delta, \\ \xi_2 = -\tau/r + \delta, \end{cases} \quad (8.34)$$

where δ is a positive bias force that has no net effect on the resultant joint torque.

For convenience, we define two operators O^+ and O^- :

$$O^+(x) = \begin{cases} x, & x \geq 0, \\ 0, & x < 0, \end{cases} \quad (8.35)$$

$$O^-(x) = \begin{cases} 0, & x \geq 0, \\ -x, & x < 0, \end{cases} \quad (8.36)$$

where x is a dummy variable.

The characteristics of $O^+(x)$ and $O^-(x)$ can be described graphically as shown in Fig. 8.16. Mathematically, $O^+(x)$ and $O^-(x)$ can also be written as

$$O^+(x) = \frac{x + |x|}{2}, \quad (8.37)$$

$$O^-(x) = \frac{-x + |x|}{2}. \quad (8.38)$$

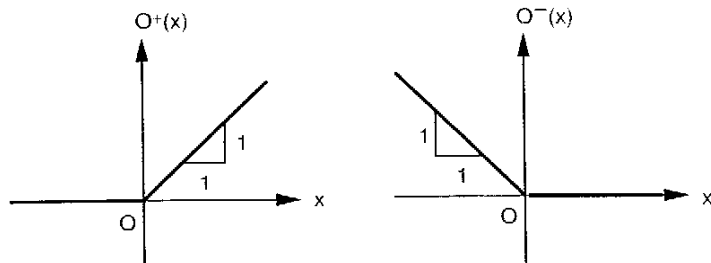


FIGURE 8.16. Characteristics of $O^+(x)$ and $O^-(x)$ operators.

Following the definitions above, it can be shown that

$$O^+(x) + O^-(x) = |x|, \quad (8.39)$$

$$O^+(x) - O^-(x) = x. \quad (8.40)$$

Expressing Eqs. (8.33) and (8.34) in terms of O^+ and O^- operators, we obtain

$$\begin{aligned} \xi_1 &= O^+(\tau/r) + \delta, \\ \xi_2 &= O^-(\tau/r) + \delta. \end{aligned} \quad (8.41)$$

We note that the O^+ operator goes with the tendon force that produces a positive joint torque, and the O^- operator goes with the one that results in a negative joint torque in Eq. (8.32). The physical meaning of Eq. (8.41) can readily be seen from Fig. 8.15. If the required joint torque is positive, ξ_1 must give a minimum pull of τ/r while ξ_2 remains zero. On the other hand, if the required joint torque is negative, ξ_2 must give a minimum pull of $|\tau/r|$ while ξ_1 remains zero. Adding a bias force δ to both ξ_1 and ξ_2 has no effect on the resulting joint torque. Furthermore, the ratio of the two bias forces, 1:1 for this simple system, is proportional to the homogeneous solution of Eq. (8.32). The addition of a bias force prevents the tendons from slackening.

The rectifier concept can be implemented in a conventional or other advanced controller. Figure 8.17 illustrates a PD controller using the rectifier concept for the control of the 1-dof manipulator shown in Fig. 8.15.

8.7.2 Application to Multi-DOF Systems

We now demonstrate how the tendon forces in an n -dof system can be determined systematically using the $O^+(x)$ and $O^-(x)$ operators. In general,

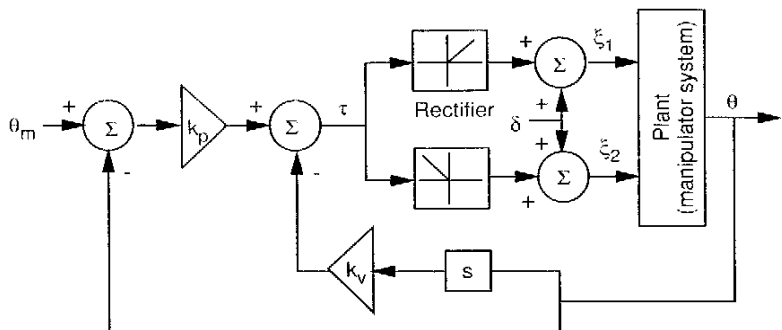


FIGURE 8.17. PD controller using the rectifier concept.

we first reduce the system of equations given by Eq. (8.20) to one equation in two unknown forces. Next, we solve these two unknown forces by applying the $O^+(x)$ and $O^-(x)$ operators. Then we substitute the results back into the original system of equations to obtain a reduced system of equations and repeat the process until all the variables are solved. The following examples serve to illustrate the methodology. For simplicity, we assume that pulleys mounted on the same joint axis are of the same size.

Example 8.7.1 A 3-DOF Manipulator with a Pseudotriangular Structure Matrix We first consider a spatial 3-dof manipulator controlled by four tendons, as shown in Fig. 8.18. The structure matrix B , obtained by an inspection of the tendon routing, is

$$B = R^* B^* = \begin{bmatrix} r_1 & 0 & 0 \\ 0 & r_2 & 0 \\ 0 & 0 & r_3 \end{bmatrix} \begin{bmatrix} -1 & -1 & -1 & 1 \\ -1 & -1 & 1 & 0 \\ -1 & 1 & 0 & 0 \end{bmatrix}. \quad (8.42)$$

Because of the routing topology, the structure matrix takes the pseudotriangular form. The null space of B^* is given by $H = [1, 1, 2, 4]^T$. Substituting the structure matrix above into Eq. (8.20) and multiplying both sides of the resulting equation by the inverse of R^* yields

$$-\xi_1 - \xi_2 - \xi_3 + \xi_4 = \tau_1/r_1, \quad (8.43)$$

$$-\xi_1 - \xi_2 + \xi_3 = \tau_2/r_2, \quad (8.44)$$

$$-\xi_1 + \xi_2 = \tau_3/r_3. \quad (8.45)$$

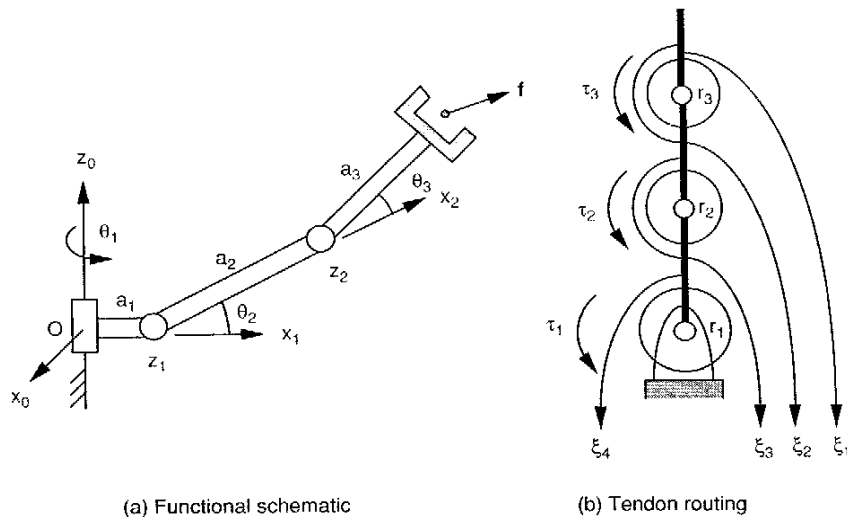


FIGURE 8.18. A 3-dof manipulator controlled by four tendons.

Since Eq. (8.45) contains only two unknown forces, ξ_1 and ξ_2 , and they must be positive at all times, we can express ξ_1 and ξ_2 in terms of the O^+ and O^- operators by applying Eq. (8.41):

$$\begin{aligned} \xi_1 &= O^-(\tau_3/r_3) + \delta_1, \\ \xi_2 &= O^+(\tau_3/r_3) + \delta_2, \end{aligned} \quad (8.46)$$

where δ_1 is a positive bias force that results in no net joint torque about the third joint axis.

To determine ξ_3 , we substitute Eq. (8.46) into (8.44) and then apply the relation $O^-(x) + O^+(x) = |x|$. This yields

$$-2\delta_1 + \xi_3 = \tau_2/r_2 + |\tau_3/r_3|. \quad (8.47)$$

We may consider Eq. (8.47) as one equation in two unknowns, δ_1 and ξ_3 . Applying the O^+ and O^- operators, we obtain

$$\begin{aligned} \delta_1 &= \frac{O^-(\tau_2/r_2 + |\tau_3/r_3|)}{2} + \frac{\delta_2}{2}, \\ \xi_3 &= O^+(\tau_2/r_2 + |\tau_3/r_3|) + \delta_2. \end{aligned} \quad (8.48)$$

where δ_2 is a positive bias force that results in no net joint torques about the second and third joint axes.

Combining Eqs. (8.46) and (8.48) yields

$$\begin{aligned}\xi_1 &= O^-(\tau_3/r_3) + \frac{O^-(\tau_2/r_2 + |\tau_3/r_3|)}{2} + \frac{\delta_2}{2}, \\ \xi_2 &= O^+(\tau_3/r_3) + \frac{O^-(\tau_2/r_2 + |\tau_3/r_3|)}{2} + \frac{\delta_2}{2}, \\ \xi_3 &= O^+(\tau_2/r_2 + |\tau_3/r_3|) + \delta_2.\end{aligned}\quad (8.49)$$

Substituting Eqs. (8.49) into Eq. (8.43) yields

$$-2\delta_2 + \xi_4 = \tau_1/r_1 + |\tau_2/r_2 + |\tau_3/r_3|| + |\tau_3/r_3|. \quad (8.50)$$

Equation (8.50) contains two unknowns, δ_2 and ξ_4 . Applying the O^+ and O^- operators again, we obtain

$$\begin{aligned}\delta_2 &= \frac{O^-(\tau_1/r_1 + |\tau_2/r_2 + |\tau_3/r_3|| + |\tau_3/r_3|) + \delta_3}{2} + \frac{\delta_3}{2}, \\ \xi_4 &= O^+(\tau_1/r_1 + |\tau_2/r_2 + |\tau_3/r_3|| + |\tau_3/r_3|) + \delta_3,\end{aligned}\quad (8.51)$$

where δ_3 is a positive bias force that results in no net joint torques about the first, second, and third joint axes.

Finally, combining Eqs. (8.49) and (8.51), we obtain

$$\begin{aligned}\xi_1 &= O^-(\tau_3/r_3) + \frac{O^-(\tau_2/r_2 + |\tau_3/r_3|)}{2} \\ &\quad + \frac{O^-(\tau_1/r_1 + |\tau_2/r_2 + |\tau_3/r_3|| + |\tau_3/r_3|)}{4} + \frac{\delta_3}{4}, \\ \xi_2 &= O^+(\tau_3/r_3) + \frac{O^-(\tau_2/r_2 + |\tau_3/r_3|)}{2} \\ &\quad + \frac{O^-(\tau_1/r_1 + |\tau_2/r_2 + |\tau_3/r_3|| + |\tau_3/r_3|)}{4} + \frac{\delta_3}{4}, \\ \xi_3 &= O^+(\tau_2/r_2 + |\tau_3/r_3|) + \frac{O^-(\tau_1/r_1 + |\tau_2/r_2 + |\tau_3/r_3|| + |\tau_3/r_3|)}{2} + \frac{\delta_3}{2}, \\ \xi_4 &= O^+(\tau_1/r_1 + |\tau_2/r_2 + |\tau_3/r_3|| + |\tau_3/r_3|) + \delta_3.\end{aligned}\quad (8.52)$$

Equation (8.52) provides an effective method for transforming joint torques to tendon forces. The computation is more straightforward than that of the pseudoinverse technique. The result guarantees that each tendon force is at

least equal to one-fourth of the bias force, δ_3 . Although the bias force can be chosen arbitrarily, its contribution to tendon forces is proportional to the vector of the homogeneous solution (i.e., 1 : 1 : 2 : 4).

Example 8.7.2 Stanford/JPL Finger In this example, we consider the Stanford/JPL finger, shown in Fig. 8.5. The abbreviated planar representation is shown in Fig. 8.7. Assuming that the pulleys mounted on the same joint axis are of the same size (i.e., $r_1 = r_4 = r_5 = r_6 = r_7$ and $r_2 = r_8$), the structure matrix can be written as a product of R^* and B^* , where R^* and B^* are given by Eqs. (8.27) and (8.26), respectively. The null space of B^* is given by $H = [1, 1, 1, 1]^T$.

Substituting $B = R^*B^*$ into Eq. (8.20) yields

$$\xi_1 + \xi_2 + \xi_3 + \xi_4 = \tau_1/r_1, \quad (8.53)$$

$$-\xi_1 + \xi_2 - \xi_3 + \xi_4 = \tau_2/r_2, \quad (8.54)$$

$$-\xi_1 + \xi_2 = \tau_3/r_3. \quad (8.55)$$

Since Eq. (8.55) contains only two unknowns, ξ_1 and ξ_2 can be written in terms of O^+ and O^- operators as

$$\begin{aligned}\xi_1 &= O^-(\tau_3/r_3) + \delta_1, \\ \xi_2 &= O^+(\tau_3/r_3) + \delta_1,\end{aligned}\quad (8.56)$$

where δ_1 is a positive bias force that produces no net joint torque about the third joint axis.

Substituting Eq. (8.55) into (8.54) yields

$$-\xi_3 + \xi_4 = \tau_2/r_2 - \tau_3/r_3. \quad (8.57)$$

Again, Eq. (8.57) contains only two unknowns, ξ_3 and ξ_4 . Hence they can be written in terms of O^+ and O^- operators as

$$\begin{aligned}\xi_3 &= O^-(\tau_2/r_2 - \tau_3/r_3) + \delta_2, \\ \xi_4 &= O^+(\tau_2/r_2 - \tau_3/r_3) + \delta_2,\end{aligned}\quad (8.58)$$

where δ_2 is a positive bias force that produces no net joint torque about the second joint axis.

Substituting Eqs. (8.56) and (8.58) into (8.53) and making use of Eq. (8.39) yields

$$-2\delta_1 + 2\delta_2 = \tau_1/r_1 + |\tau_3/r_3| - |\tau_2/r_2 - \tau_3/r_3|. \quad (8.59)$$

Hence δ_1 and δ_2 can be written in terms of the O^+ and O^- operators as

$$\begin{aligned}\delta_1 &= \frac{O^-(\tau_1/r_1 + |\tau_3/r_3| - |\tau_2/r_2 - \tau_3/r_3|)}{2} + \delta_3, \\ \delta_2 &= \frac{O^+(\tau_1/r_1 + |\tau_3/r_3| - |\tau_2/r_2 - \tau_3/r_3|)}{2} + \delta_3,\end{aligned}\quad (8.60)$$

where δ_3 is a positive bias force that produces no net joint torques about the first, second, and third joint axes. Substituting Eq. (8.60) into (8.56) and (8.58) yields

$$\xi_1 = O^-(\tau_3/r_3) + \frac{O^-(\tau_1/r_1 + |\tau_3/r_3| - |\tau_2/r_2 - \tau_3/r_3|)}{2} + \delta_3, \quad (8.61)$$

$$\xi_2 = O^+(\tau_3/r_3) + \frac{O^+(\tau_1/r_1 + |\tau_3/r_3| - |\tau_2/r_2 - \tau_3/r_3|)}{2} + \delta_3,$$

$$\xi_3 = O^-(\tau_2/r_2 - \tau_3/r_3) + \frac{O^+(\tau_1/r_1 + |\tau_3/r_3| - |\tau_2/r_2 - \tau_3/r_3|)}{2} + \delta_3,$$

$$\xi_4 = O^+(\tau_2/r_2 - \tau_3/r_3) + \frac{O^+(\tau_1/r_1 + |\tau_3/r_3| - |\tau_2/r_2 - \tau_3/r_3|)}{2} + \delta_3.$$

Although the bias force δ_3 can be chosen arbitrarily, its contribution on tendon forces is proportional to the vector of homogeneous solution. Figure 8.19 shows the design of a redundant force resolver in accordance with Eq. (8.61). This design can be implemented for computed torque control of the Stanford/JPL finger.

Example 8.7.3 Utah/MIT Finger Let us consider the Utah/MIT finger shown in Fig. 8.10. Assuming that the pulleys mounted at the same joint axis are of the same size (i.e., $r_1 = r_5 = r_6 = r_7$, $r_2 = r_8 = r_9$, and $r_3 = r_{10}$), the structure matrix can be written as a product of R^* and B^* , where R^* and B^* are given by Eqs. (8.30) and (8.29), respectively.

Since $n = 4$ and $m = 8$, the null space of B^* is an 8×4 matrix given by

$$H = \begin{bmatrix} 1 & 0 & 0 & 0 \\ 1 & 0 & 0 & 0 \\ 0 & 1 & 0 & 0 \\ 0 & 1 & 0 & 0 \\ 0 & 0 & 1 & 0 \\ 0 & 0 & 1 & 0 \\ 0 & 0 & 0 & 1 \\ 0 & 0 & 0 & 1 \end{bmatrix}. \quad (8.62)$$

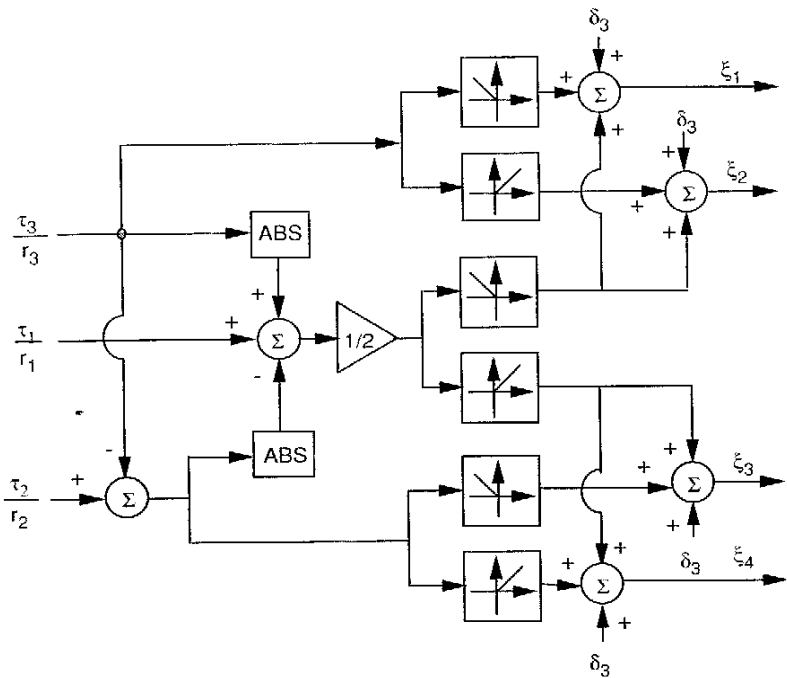


FIGURE 8.19. Force resolver schematic diagram for the Stanford/JPL finger.

Substituting $B = R^*B^*$ into Eq. (8.20) yields

$$-\xi_1 + \xi_2 - \xi_3 + \xi_4 - \xi_5 + \xi_6 - \xi_7 + \xi_8 = \tau_1/r_1, \quad (8.63)$$

$$-\xi_1 + \xi_2 - \xi_3 + \xi_4 - \xi_5 + \xi_6 = \tau_2/r_2, \quad (8.64)$$

$$-\xi_1 + \xi_2 - \xi_3 + \xi_4 = \tau_3/r_3, \quad (8.65)$$

$$-\xi_1 + \xi_2 = \tau_4/r_4. \quad (8.66)$$

Subtracting Eq. (8.64) from (8.63), (8.65) from (8.64), and (8.66) from (8.65), we obtain a simplified system of equations:

$$-\xi_7 + \xi_8 = \tau_1/r_1 - \tau_2/r_2,$$

$$-\xi_5 + \xi_6 = \tau_2/r_2 - \tau_3/r_3,$$

$$\begin{aligned} -\xi_3 + \xi_4 &= \tau_3/r_3 - \tau_4/r_4, \\ -\xi_1 + \xi_2 &= \tau_4/r_4. \end{aligned} \quad (8.67)$$

Since each equation in Eq. (8.67) contains only two unknowns, the four pairs of tendon forces can be written in terms of O^+ and O^- operators as follows:

$$\begin{aligned} \xi_1 &= O^+(\tau_4/r_4) + \delta_1, \\ \xi_2 &= O^+(\tau_4/r_4) + \delta_1, \\ \xi_3 &= O^-(\tau_3/r_3 - \tau_4/r_4) + \delta_2, \\ \xi_4 &= O^+(\tau_3/r_3 - \tau_4/r_4) + \delta_2, \\ \xi_5 &= O^-(\tau_2/r_2 - \tau_3/r_3) + \delta_3, \\ \xi_6 &= O^+(\tau_2/r_2 - \tau_3/r_3) + \delta_3, \\ \xi_7 &= O^-(\tau_1/r_1 - \tau_2/r_2) + \delta_4, \\ \xi_8 &= O^+(\tau_1/r_1 - \tau_2/r_2) + \delta_4, \end{aligned} \quad (8.68)$$

where $\delta_1, \delta_2, \delta_3$, and δ_4 are four positive bias forces. These four bias forces correspond to the four column vectors of H .

Figure 8.20 shows the design of a redundant force resolver in accordance with Eq. (8.68). In comparison with the two preceding examples, we observe that there are four bias forces for the Utah/MIT finger but only one for each of the Stanford/JPL finger and the 3×4 manipulator with a pseudotriangular structure matrix. Both the Stanford/JPL finger and the 3×4 manipulator utilize the minimum number of tendons ($m = n + 1$), whereas the Utah/MIT finger employs the maximum number of tendons ($m = 2n$). Although the Utah/MIT finger requires more tendons, it has the advantage of independently regulating the bias force for each pair of tendons. In addition, the computation of tendon forces for the Utah/MIT finger is greatly simplified.

8.8 SUMMARY

This chapter has covered the kinematics and static force analysis of tendon-driven manipulators. Tendon-driven manipulators were classified into closed-loop tendon drives and open-ended tendon drives. A planar schematic representation of tendon routing topology was defined. The fundamental circuit equations, coaxiality conditions, and the concept of transmission lines were introduced. It was also shown that tendon displacements are related to the joint angles by a structure matrix and that using the concept of transmission lines, the structure matrix can be derived by an inspection of the tendon

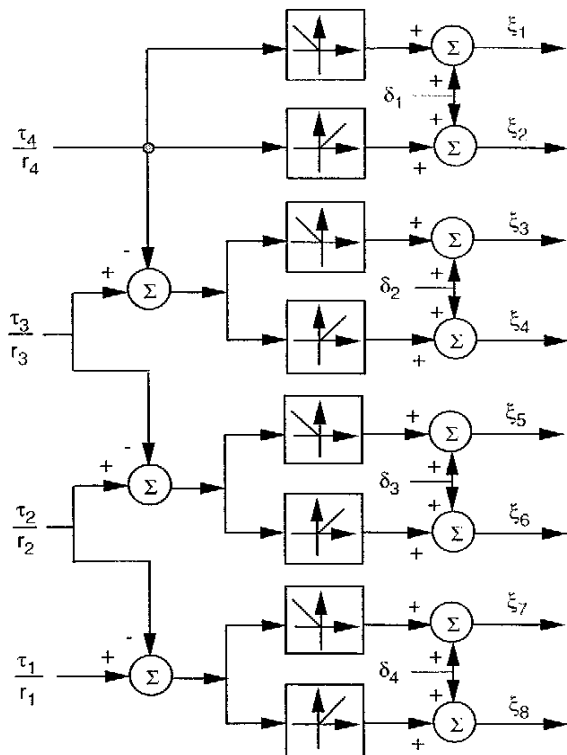


FIGURE 8.20. Force resolver schematic diagram for the Utah/MIT finger.

routing topology. From the static force analysis, structure characteristics associated with tendon-driven manipulators were identified. An atlas of tendon-driven manipulators with $n \times (n + 1)$ pseudotriangular structural matrices was developed. Finally, an efficient method for the resolution of redundant tendon forces was presented. To demonstrate the methodology, the Stanford/JPL finger and Utah/MIT finger were analyzed.

REFERENCES

- Albus, J., Bostelman, R., and Dagalakis, N., 1992, "The NIST Spider, a Robot Crane," *J. Res. NIST*, Vol. 97, No. 3, pp. 373–385.

- Ali, M., Kyriakopoulos, K. J., and Stephanou, H. E., 1993, "The Kinematics of the Anthrobots-2 Dextrous Hand," *Proc. IEEE International Conference on Robotics and Automation*, pp. 705-710.
- Cannon, R. H. and Schmitz, E., 1984, "Initial Experimentation on the End-Point Control of a Flexible One-Link Robot," *Int. J. Robot. Res.*, Vol. 3, No. 3, pp. 62-75.
- Hirose, S., 1986, "Connected Differential Mechanism and Its Applications," in *Robot Grippers*, edited by D. T. Pham and W. B. Heginbotham, Springer-Verlag, New York, pp. 141-153.
- Hirose, S. and Umetani, Y., 1978, "The Development of a Soft Gripper for the Versatile Robot Hand," *Mech. Mach. Theory*, Vol. 13, pp. 351-359.
- Hirose, S. and Umetani, Y., 1979, "The Kinematics and Control of a Soft Gripper for the Handling of Living or Fragile Objects," *Proc. 5th World Congress on the Theory of Machines and Mechanisms*, pp. 1175-1178.
- Hollars, M. and Cannon, R. H., 1985, "Initial Experiments on the End-Point Control of a Two-Link Manipulator with Flexible Tendons," *Proc. ASME Winter Annual Meeting*, Miami, FL.
- Jacobsen, S. C., Wood, J. E., Knutti, D.F., and Biggers, K.B., 1984, "The Utah/MIT Dextrous Hand: Work in Progress," *Int. J. Robot. Res.*, Vol. 3, No. 4, pp. 21-50.
- Jacobsen, S. C., Iversen, E. K., Knutti, D. F., Johnson, R. T., and Biggers, K. B., 1986, "The Design of the Utah/MIT Dextrous Hand," *Proc. IEEE International Conference on Robotics and Automation*, pp. 1520-1532.
- Jacobsen, S. C., Ko, H., Iversen, E. K., and Davis, C. C., 1989, "Antagonistic Control of a Tendon Driven Manipulator," *Proc. IEEE International Conference on Robotics and Automation*, pp. 1334-1339.
- Lee, J. J., 1991, "Tendon-Driven Manipulators: Analysis, Synthesis, and Control," Ph.D. dissertation, Department of Mechanical Engineering, University of Maryland, College Park, MD.
- Lee, J. J. and Tsai, L. W., 1991, "On the Structural Synthesis of Tendon-Driven Manipulators Having a Pseudo-triangular Matrix," *Int. J. Robot. Res.*, Vol. 10, No. 3, pp. 255-262.
- Lee, J. J. and Tsai, L. W., 1993, "Torque Resolver Design for Tendon-Driven Manipulators," *ASME J. Mech. Des.*, Vol. 115, pp. 877-883.
- Mason, M. T. and Salisbury, J. K., 1985, *Robot Hands and the Mechanics of Manipulation*, MIT Press, Cambridge, MA.
- Melchiorri, C. and Vassura, G., 1992, "Mechanical and Control Features of the University of Bologna Hand Version 2," *Proc. IEEE/RSJ International Conference on Intelligent Robots and Systems*, Raleigh, NC, pp. 187-193.
- Morecki, A., Busko, Z., Gasztold, H., and Jaworek, K., 1980, "Synthesis and Control of the Anthropomorphic Two-Handed Manipulator," *Proc. 10th International Symposium on Industrial Robots*, Milan, Italy, pp. 461-474.
- Okada, T., 1977, "On a Versatile Finger System," *Proc. 7th International Symposium on Industrial Robots*, Tokyo, pp. 345-352.

- Ou, Y. J. and Tsai, L. W., 1993, "Kinematic Synthesis of Tendon-Driven Manipulators with Isotropic Transmission Characteristics," *ASME J. Mech. Des.*, Vol. 115, pp. 884-891.
- Pham, D. T. and Heginbotham, W. B., 1986, *Robot Grippers*, Springer-Verlag, New York.
- Rouff, C. F. and Salisbury, J. K., 1990, "Multi-fingered Robotic Hand," U.S. Patent 4,921,293.
- Rovetta, A., 1977, "On Specific Problems of Design of Multipurpose of Mechanical Hands in Industrial Robots," *Proc. 7th International Symposium on Industrial Robots*, Tokyo, pp. 337-341.
- Rovetta, A., 1981, "On Functionality of a New Mechanical Hand," *ASME J. Mech. Des.*, Vol. 103, pp. 277-280.
- Salisbury, J. K., 1982, "Kinematic and Force Analysis of Articulated Mechanical Hands," Ph.D. dissertation, Mechanical Engineering Department, Stanford University, Stanford, CA.
- Salisbury, J. K. and Craig, J. J., 1982, "Articulated Hands: Force Control and Kinematic Issues," *Int. J. Robot. Res.*, Vol. 1, No. 1, pp. 4-17.
- Salisbury, J. K. and Roth, B., 1983, "Kinematic and Force Analysis of Articulated Mechanical Hands," *ASME J. Mech. Transm. Autom. Des.*, Vol. 105, No. 1, pp. 35-41.
- Sugano, S. and Kato, I., 1987, "WABOT-2: Autonomous Robot with Dextrous Finger Arm," *Proc. IEEE International Conference on Robotics and Automation*, pp. 90-97.
- Tsai, L. W. and Lee, J. J., 1989, "Kinematic Analysis of Tendon Driven Robotic Mechanisms Using Graph Theory," *ASME J. Mech. Transm. Autom. Des.*, Vol. 111, pp. 59-65.

EXERCISES

1. What is the structure matrix of the 2-dof manipulator shown in Fig. 8.2?
2. Assuming that the mass of the moving platform is 100 kg and the gravitational force points down vertically, derive the structure matrix for the 6-dof NIST RoboCrane shown in Fig. 8.21. Can the end effector resist an external force in excess of 100 kg acting in the direction opposite to gravity?
3. Derive the structure matrices for the 4-dof manipulators shown in Fig. 8.13a and b.
4. Derive the structure matrices for the 4-dof manipulators shown in Fig. 8.14h and k.
5. Are the two tendon routings shown in Fig. 8.22a and b isomorphic?

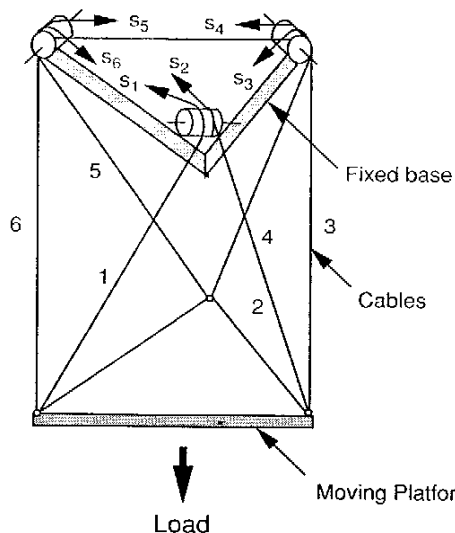


FIGURE 8.21. Functional schematic diagram of the NIST RoboCrane.

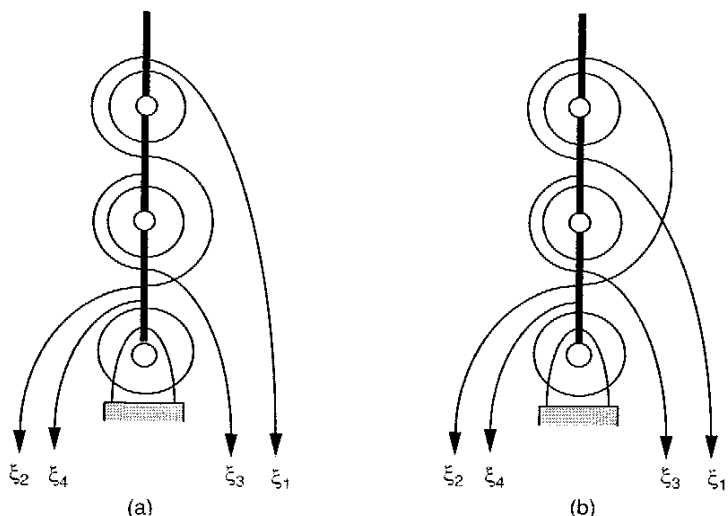


FIGURE 8.22. Two 3-dof tendon-driven manipulators with four tendons-- 1.

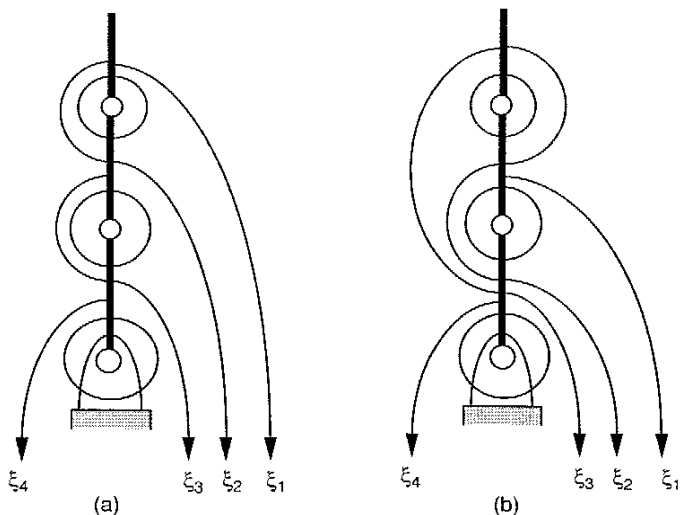


FIGURE 8.23. Two 3-dof tendon-driven manipulators with four tendons-- 2.

6. Prove that the two tendon routings shown in Fig. 8.23a and b are isomorphic.
7. For the 2-dof manipulator shown in Fig. 8.2, let $OA = 1$ m, $AB = 0.707$ m, $\theta_1 = 0$, and $\theta_2 = 3\pi/4$. Also let the radii of all pulleys be equal to 0.1 m. Calculate the tendon forces, (ξ_1, ξ_2, ξ_3) , required to generate an end-effector output force of $|f| = 100$ N. Plot the force as a function of the orientation angle of f .
8. For the 3-dof manipulator shown in Fig. 8.18, let the radii of all pulleys be equal to 1 unit. Calculate the tendon forces, $(\xi_1, \xi_2, \xi_3, \xi_4)$, required to produce an output force of $f = (100, 0, 0)$ N at the end effector assuming that $\theta_1 = \theta_2 = 0^\circ$ and $\theta_3 = 45^\circ$.
9. Using the rectifier concept, design a tendon force resolver for the 2-dof manipulator shown in Fig. 8.2.
10. Using the rectifier concept, design a tendon force resolver for the 3-dof manipulator shown in Fig. 8.22a. Compare the result with that for the 3×4 manipulator shown in Fig. 8.18. Can you distinguish which is the better design?

CHAPTER 9

DYNAMICS OF SERIAL MANIPULATORS

9.1 INTRODUCTION

In this chapter we extend our study from kinematics and statics to the dynamics of serial manipulators. For some applications, such as arc welding (Fig. 9.1), it is necessary to move the end effector of a manipulator from point to point rapidly. The dynamics of the manipulator plays an important role in achieving such high-speed performance. The purpose of this chapter is to develop a set of equations that describe the dynamical behavior of a manipulator. The development of a dynamical model is important in several ways. First, a dynamical model can be used for computer simulation of a robotic system. By examining the behavior of the model under various operating conditions, it is possible to predict how a robotic system will behave when it is built. Various manufacturing automation tasks can be examined without the need of a real system. Second, it can be used for the development of suitable control strategies. A sophisticated controller requires the use of a realistic dynamical model to achieve optimal performance under high-speed operations. Some control schemes rely directly on a dynamic model to compute actuator torques required to follow a desired trajectory. Third, the dynamics analysis of a manipulator reveals all the joint reaction forces (and moments) needed for the design and sizing of links, bearings, and actuators.

There are two types of dynamical problems: direct dynamics and inverse dynamics. The *direct dynamics problem* is to find the response of a robot arm corresponding to some applied torques and/or forces. That is, given a vector of joint torques or forces, we wish to compute the resulting motion of the

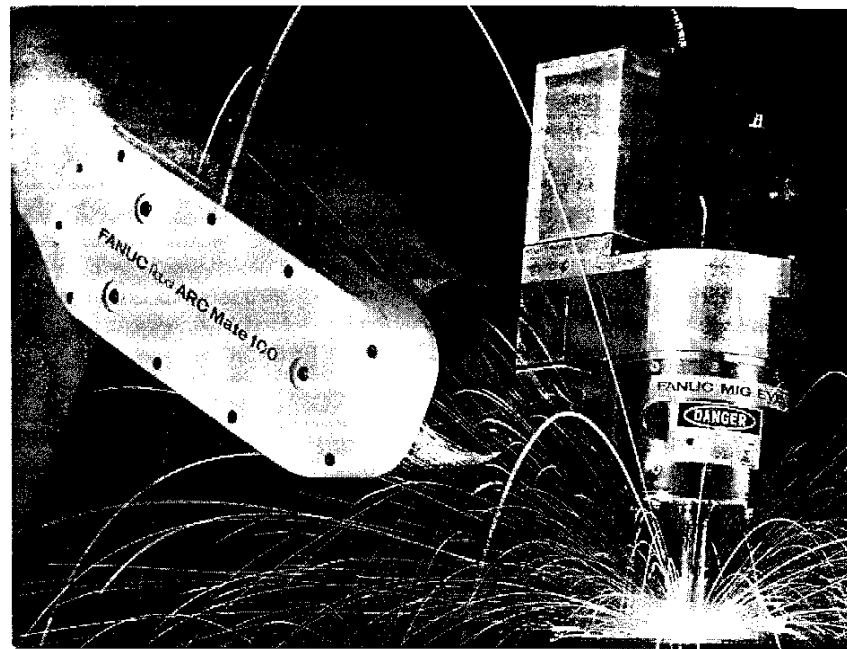


FIGURE 9.1. Arc welding robot. (Courtesy of Fanuc Robotics North America, Inc., Rochester Hills, Michigan.)

manipulator as a function of time. The *inverse dynamics problem* is to find the actuator torques and/or forces required to generate a desired trajectory of the manipulator. The problem can be formulated in the joint space, $\mathbf{q}(t)$, or the end effector space, $\mathbf{x}(t)$. The two formulations are related by the Jacobian matrix and its time derivative. In general, the efficiency of computation for direct dynamics is not as critical since it is used primarily for computer simulations of a manipulator. On the other hand, an efficient inverse dynamical model becomes extremely important for real-time feedforward control of a manipulator.

The dynamical equations of motion can be formulated by several methods. One approach is application of the Newton and Euler laws. Writing Newton's and Euler's equations once for each body of a mechanical system results in a system of equations that contains both the applied forces and the forces of constraint. The latter can be eliminated by considering the geometric and kinematic equations describing the nature of constraints. Another approach

is application of the principle of *d'Alembert* or *Hamilton*. Alternatively, one can apply *Lagrange's equations of motion* (Goldstein, 1980; Paul, 1981) or *Kane's method* (Kane and Levinson, 1980, 1985). The advantage of employing the Lagrangian approach is that it eliminates the forces of constraint at the outset. However, these forces of constraint must be restored at a later time if they are to be used for the purpose of design. On the other hand, the Newton–Euler approach produces a larger system of equations, and these equations can be solved simultaneously for all the forces, including the forces of constraint.

Recently, there has been an increasing interest in the development of general-purpose computer programs for dynamical analysis of mechanical systems. For example, the following programs were developed using the Lagrangian formulation.

- *ADAMS*: developed by Chace et al. at the University of Michigan and marketed by Mechanical Dynamics, Inc. (1981).
- *DADS*: developed by Haug et al. (Haug, 1989) at the University of Iowa and marketed by Computer Aided Design Software, Inc. (1995).
- *DYMAC*: developed by Paul et al. (Paul, 1979) at the University of Pennsylvania.
- *IMP*: developed by Uicker et al. (Uicker, 1965; Sheth and Uicker, 1972) at the University of Wisconsin.

Other computer programs, such as *NBOD2* developed at NASA Goddard Space Flight Center (Frisch, 1974) and *SD-EXACT* developed by Rosenthal and Sherman (1983), are based on Eulerian approach and Kane's method. General-purpose computer programs are great for computer simulations. However, they are not necessarily suitable for real-time control of a robot manipulator. Thus, more efficient methodologies specifically tailored for robotic systems have been proposed. These include the recursive Lagrangian equations (Hollerbach, 1980), the recursive Newton–Euler equations (Armstrong, 1979; Luh et al., 1980; Orin et al., 1979), and the generalized d'Alembert equations (Fu et al., 1987; Lee et al., 1983).

Dynamics is a huge subject by itself. Obviously, we will not be able to cover the subject in great detail. In what follows, we review some fundamental laws associated with the dynamics of a rigid body and present the recursive Newton–Euler and Lagrangian methods of analysis. In addition, the effects of rotor inertias are discussed. Several examples are used to demonstrate the principles.

9.2 MASS PROPERTIES

In this section, the center of mass, inertia matrix, parallel axis theorem, and principal moments of inertia of a rigid body are defined.

9.2.1 Center of Mass

Mass is a quantity of matter that forms a body of a certain shape and size. Referring to Fig. 9.2, $A(x, y, z)$ is a Cartesian reference frame, \mathbf{u} and \mathbf{w} are two unit vectors, dV represents a differential volume of the material body B , ρ is the material density, and \mathbf{p} is the position vector of the differential mass ρdV with respect to the reference frame A . The *center of mass* of such a material body is defined as the point C , whose position vector \mathbf{p}_c satisfies the following condition:

$$\mathbf{p}_c = \frac{1}{m} \int_V \mathbf{p} \rho dV, \quad (9.1)$$

where $m = \int_V \rho dV$ is the total mass of the material body B .

9.2.2 Inertia Matrix

The *second moment*, \mathbf{I}_u^O , of a rigid body B relative to a line L_u that passes through a reference point O and is parallel to a unit vector \mathbf{u} is defined as

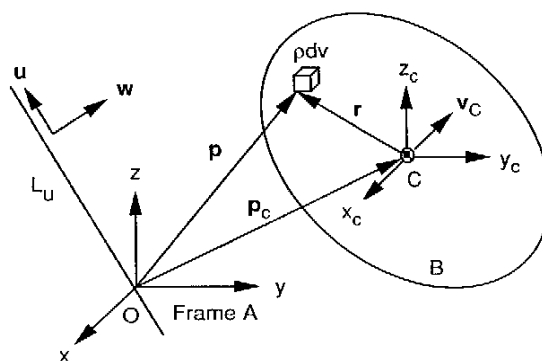


FIGURE 9.2. Moments of mass about a reference point.

(Roberson and Schwertassek, 1988)

$$\mathbf{I}_u^O = \int_V [\mathbf{p} \times (\mathbf{u} \times \mathbf{p})] \rho dV, \quad (9.2)$$

where the trailing superscript O denotes the reference point and the trailing subscript u denotes the direction of the reference line. Expanding the triple product in Eq. (9.2) yields

$$\mathbf{I}_u^O = \int_V [\mathbf{p}^2 \mathbf{u} - (\mathbf{p}^T \mathbf{u}) \mathbf{p}] \rho dV. \quad (9.3)$$

The scalar product of \mathbf{I}_u^O with a unit vector \mathbf{w} is called the *product of inertia* of B relative to O for \mathbf{u} and \mathbf{w} ,

$$I_{uw} = \mathbf{I}_u^O \cdot \mathbf{w} = \int_V [(\mathbf{u}^T \mathbf{w}) \mathbf{p}^2 - (\mathbf{p}^T \mathbf{u})(\mathbf{p}^T \mathbf{w})] \rho dV. \quad (9.4)$$

It follows from the definition above that $I_{uw} = I_{wu}$. In particular, when \mathbf{u} and \mathbf{w} represent the same vector, the corresponding product of inertia, I_{uu} , is called the *moment of inertia* of B about L_u :

$$I_{uu} = \int_V [\mathbf{p}^2 - (\mathbf{p}^T \mathbf{u})^2] \rho dV = mr_a^2, \quad (9.5)$$

where $r_a = \mathbf{p}^2 - (\mathbf{p}^T \mathbf{u})^2 = (\mathbf{u} \times \mathbf{p})^2$ is a nonnegative real quantity called the *radius of gyration* of B with respect to L_u .

Equation (9.3) can be written in matrix form as

$$\mathbf{I}_u^O = \mathbf{I}_B^O \mathbf{u}, \quad (9.6)$$

where

$$\mathbf{I}_B^O \equiv \begin{bmatrix} I_{xx} & I_{xy} & I_{xz} \\ I_{yx} & I_{yy} & I_{yz} \\ I_{zx} & I_{zy} & I_{zz} \end{bmatrix} \quad (9.7)$$

is called the *inertia matrix* or *inertia tensor* of B about O , and

$$I_{xx} = \int_V (y^2 + z^2) \rho dV,$$

$$I_{yy} = \int_V (z^2 + x^2) \rho dV,$$

$$I_{zz} = \int_V (x^2 + y^2) \rho dV,$$

$$\begin{aligned} I_{xy} &= I_{yx} = - \int_V xy \rho dV, \\ I_{yz} &= I_{zy} = - \int_V yz \rho dV, \\ I_{xz} &= I_{zx} = - \int_V xz \rho dV, \end{aligned} \quad (9.8)$$

where x , y , and z are the coordinates of a differential volume of mass ρdV with respect to a reference frame A whose origin is located at O . Note that each element of \mathbf{I}_B^O represents either a moment of inertia or a product of inertia of B about the coordinate axes of the reference frame A .

The inertia matrix is symmetric. Its elements depend on the choice of a reference point and a reference frame. For brevity, we often omit the trailing superscript whenever the reference point is clearly understood or is the center of mass of a rigid body. For a rigid body of simple geometry, the inertia matrix can be computed by using the volumetric integration given by Eq. (9.8). For objects of irregular shape, the inertia matrix is often determined experimentally.

9.2.3 Parallel Axis Theorem

Let $C(x_c, y_c, z_c)$ be a Cartesian coordinate frame attached to the center of mass C of a rigid body B with its coordinate axes parallel to those of A , as shown in Fig. 9.2. Then it can be shown that

$$\begin{aligned} I_{xx}^O &= I_{xx}^C + m(y_c^2 + z_c^2), \\ I_{yy}^O &= I_{yy}^C + m(z_c^2 + x_c^2), \\ I_{zz}^O &= I_{zz}^C + m(x_c^2 + y_c^2), \\ I_{xy}^O &= I_{xy}^C + mx_c y_c, \\ I_{yz}^O &= I_{yz}^C + my_c z_c, \\ I_{zx}^O &= I_{zx}^C + mz_c x_c, \end{aligned} \quad (9.9)$$

where x_c , y_c , and z_c are the coordinates of the center of mass in frame A . Equation (9.9) is called the *parallel axes theorem*.

9.2.4 Principal Moments of Inertia

We have shown that the inertia matrix depends on the choice of a reference point and the orientation of a reference frame. It turns out that for a certain

orientation of a reference frame, the products of inertia will vanish. These special coordinate axes are called the *principal axes*, and the corresponding moments of inertia are called the *principal moments of inertia*.

Let I_B^O be the inertia matrix of a rigid body B about a point O expressed in a reference frame A . Also, let L_u be a principal axis that passes through the origin O and points in the direction of \mathbf{u} . By definition, \mathbf{u} is parallel to the vector of the second moment of B about L_u . That is,

$$I_B^O \mathbf{u} = \lambda \mathbf{u}. \quad (9.10)$$

Equation (9.10) contains three linear homogeneous equations in three unknowns: u_x , u_y , and u_z . The condition for existence of nontrivial solutions is

$$\begin{vmatrix} I_{xx} - \lambda & I_{xy} & I_{xz} \\ I_{yx} & I_{yy} - \lambda & I_{yz} \\ I_{zx} & I_{zy} & I_{zz} - \lambda \end{vmatrix} = 0. \quad (9.11)$$

Hence the eigenvalues and eigenvectors of the inertia matrix I_B^O correspond to the principal moments of inertia and the directions of principal axes, respectively. In general, corresponding to each reference point there exists at least one set of three mutually perpendicular principal axes of inertia (Kane and Levinson, 1985).

Example 9.2.1 Inertia Matrix of a Rectangular Bar Consider a rectangular bar of cross section $a \times b$ and length c as shown in Fig. 9.3. Assuming that the material of the bar is homogeneous, the mass m of the bar is equal to ρabc . It can be shown that the axes of the center-of-mass coordinate system shown in Fig. 9.3 are already aligned with the principal axes of the bar. Hence the products of inertia are all zero, and the resulting inertia matrix is

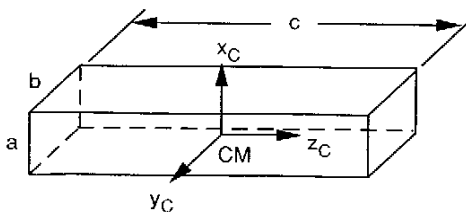


FIGURE 9.3. Rectangular bar.

$$I_B^C = \frac{m}{12} \begin{bmatrix} b^2 + c^2 & 0 & 0 \\ 0 & c^2 + a^2 & 0 \\ 0 & 0 & a^2 + b^2 \end{bmatrix}. \quad (9.12)$$

For a slender rod, a and b are much smaller than c . The inertia matrix can be approximated by

$$I_B^C = \frac{mc^2}{12} \begin{bmatrix} 1 & 0 & 0 \\ 0 & 1 & 0 \\ 0 & 0 & 0 \end{bmatrix}. \quad (9.13)$$

9.3 MOMENTUM

In this section the linear and angular momentum of a rigid body are defined.

9.3.1 Linear Momentum

The *linear momentum* of a mass element ρdV about a point O , expressed in a reference frame A , as shown in Fig. 9.2, is defined as

$$d\mathbf{l}^O = \frac{d\mathbf{p}}{dt} \rho dV. \quad (9.14)$$

Hence the total linear momentum of the material body B about O is given by

$$\mathbf{l}^O = \int_V \frac{d\mathbf{p}}{dt} \rho dV. \quad (9.15)$$

With reference to the center of mass, the position vector \mathbf{p} of the mass element ρdV can be written as

$$\mathbf{p} = \mathbf{p}_c + \mathbf{r}, \quad (9.16)$$

where $\mathbf{r} = {}^A R_C {}^C \mathbf{r}$ denotes the position of the mass element with respect to the center of mass C and expressed in the reference frame A . Here the rotation matrix ${}^A R_C$ is used to transform the vector ${}^C \mathbf{r}$ from frame C to A .

Substituting Eq. (9.16) into (9.15), we obtain

$$\mathbf{l}^O = \int_V \frac{d\mathbf{p}_c}{dt} \rho dV + \int_V \frac{d\mathbf{r}}{dt} \rho dV. \quad (9.17)$$

For a rigid body of constant mass, it can be shown that the integral and the time derivative in the second term on the right-hand side of Eq. (9.17) can be interchanged. Hence following the definition of a center of mass, the second

term vanishes and Eq. (9.17) reduces to

$$\mathbf{I}^O = \frac{d\mathbf{p}_c}{dt} \int_V \rho dV = m\mathbf{v}_c, \quad (9.18)$$

where $\mathbf{v}_c \equiv d\mathbf{p}_c/dt$ denotes the linear velocity of the center of mass with respect to the reference frame A . Equation (9.18) implies that the total linear momentum of a rigid body is equal to the linear momentum of a point mass with mass m located at the center of mass.

9.3.2 Angular Momentum

Referring to Fig. 9.2, the *angular momentum* $d\mathbf{h}^O$ of a mass element ρdV about a reference point O and expressed in a reference frame A is defined as the moment of its linear momentum about O :

$$d\mathbf{h}^O = \left(\mathbf{p} \times \frac{d\mathbf{p}}{dt} \right) \rho dV. \quad (9.19)$$

Therefore, the total angular momentum of B about O is

$$\mathbf{h}^O = \int_V \left(\mathbf{p} \times \frac{d\mathbf{p}}{dt} \right) \rho dV. \quad (9.20)$$

Substituting Eq. (9.16) into (9.20), we obtain

$$\begin{aligned} \mathbf{h}^O &= \left(\mathbf{p}_c \times \frac{d\mathbf{p}_c}{dt} \right) \int_V \rho dV + \int_V \left(\mathbf{r} \times \frac{d\mathbf{r}}{dt} \right) \rho dV \\ &\quad + \mathbf{p}_c \times \left(\frac{d}{dt} \int_V \mathbf{r} \rho dV \right) + \int_V \mathbf{r} \rho dV \times \left(\frac{d\mathbf{p}_c}{dt} \right). \end{aligned} \quad (9.21)$$

The last two terms in the expression above vanish since both contain the factor

$$\int_V \mathbf{r} \rho dV = 0.$$

Hence the total angular momentum about O is given by

$$\mathbf{h}^O = m(\mathbf{p}_c \times \mathbf{v}_c) + \mathbf{h}^C, \quad (9.22)$$

where

$$\mathbf{h}^C = \int_V \left(\mathbf{r} \times \frac{d\mathbf{r}}{dt} \right) \rho dV = \int_V \mathbf{r} \times (\boldsymbol{\omega}_B \times \mathbf{r}) \rho dV \quad (9.23)$$

denotes the angular momentum of motion about the center of mass, $\boldsymbol{\omega}_B$ is the angular velocity of B , and \mathbf{v}_c denotes the linear velocity of the center of mass with respect to the reference frame A .

Equation (9.22) states that the total angular momentum of B about the origin O is equal to the angular momentum of a point mass with mass m concentrated at the center of mass, plus the angular momentum of rotation about the center of mass. Since Eq. (9.23) takes the same form as Eq. (9.2), it follows from Eq. (9.6) that \mathbf{h}^C can be written as

$$\mathbf{h}^C = I_B^C \boldsymbol{\omega}_B, \quad (9.24)$$

where I_B^C denotes the inertia matrix of B about the center of mass C and expressed in the reference frame A . In this book, unless otherwise specified, the center of mass is taken as the reference point and the trailing superscript is omitted.

9.4 TRANSFORMATION OF INERTIA MATRIX

The angular momentum given in Eq. (9.24) can be expressed in any reference frame. Expressing Eq. (9.24) in the fixed reference frame A and dropping the trailing superscript C , we obtain

$${}^A\mathbf{h} = {}^A\mathbf{I}_B {}^A\boldsymbol{\omega}_B, \quad (9.25)$$

where a leading superscript denotes the frame in which a vector or an inertia matrix is expressed. Expressing Eq. (9.24) in a body-fixed, center-of-mass, coordinate frame C , we have

$${}^C\mathbf{h} = {}^C\mathbf{I}_B {}^C\boldsymbol{\omega}_B, \quad (9.26)$$

where ${}^C\boldsymbol{\omega}_B$ denotes the angular velocity of body B relative to the fixed frame A and expressed in the body frame C . That is, ${}^C\boldsymbol{\omega}_B = {}^A\mathbf{R}_C^T {}^A\boldsymbol{\omega}_B$, where ${}^A\mathbf{R}_C$ is a rotation matrix describing the orientation of C relative to A .

Since \mathbf{h} is a vector, its transformation follows that of a vector. Specifically,

$${}^A\mathbf{h} = {}^A\mathbf{R}_C {}^C\mathbf{h}. \quad (9.27)$$

Substituting Eqs. (9.25) and (9.26) into (9.27), we obtain

$${}^A\mathbf{I}_B {}^A\boldsymbol{\omega}_B = {}^A\mathbf{R}_C {}^C\mathbf{I}_B {}^C\boldsymbol{\omega}_B. \quad (9.28)$$

Substituting ${}^C\omega_B = {}^A R_C^T {}^A\omega_B$ into Eq. (9.28) results in

$${}^A I_B = {}^A R_C {}^C I_B {}^A R_C^T. \quad (9.29)$$

Equation (9.29) transforms an inertia matrix expressed in one reference frame into another. Both inertia matrices are taken about the center of mass C . The elements of ${}^C I_B$ are constant since they are expressed in the body-fixed coordinate frame C . However, the elements of ${}^A I_B$ are not because they are expressed in the fixed frame A and the orientation of B relative to A may be time dependent. The dependence of ${}^A I_B$ arises from the rotation matrix ${}^A R_C$.

9.5 KINETIC ENERGY

Referring to Fig. 9.2, the *kinetic energy* dK of a mass element ρdV with respect to a reference frame A is defined as

$$dK = \frac{1}{2} \mathbf{v}^T \mathbf{v} \rho dV, \quad (9.30)$$

where \mathbf{v} denotes the velocity of a mass element ρdV . Therefore, the total kinetic energy of B is given by

$$K = \frac{1}{2} \int_V \mathbf{v}^T \mathbf{v} \rho dV. \quad (9.31)$$

We can express \mathbf{v} in terms of the linear velocity of the center of mass and the angular velocity of the moving body as

$$\mathbf{v} = \mathbf{v}_c + \boldsymbol{\omega}_B \times \mathbf{r}. \quad (9.32)$$

Substituting Eq. (9.32) into (9.31), we obtain

$$\begin{aligned} K &= \frac{1}{2} \mathbf{v}_c^T \mathbf{v}_c \int_V \rho dV + (\mathbf{v}_c \times \boldsymbol{\omega}_B)^T \int_V \mathbf{r} \rho dV \\ &\quad + \frac{1}{2} \boldsymbol{\omega}_B^T \left(\int_V \mathbf{r} \times (\boldsymbol{\omega}_B \times \mathbf{r}) \rho dV \right). \end{aligned} \quad (9.33)$$

The second term in Eq. (9.33) vanishes because it follows the definition of the center of mass. The integrand in the third term represents the angular momentum of B about the center of mass. Hence Eq. (9.33) reduces to

$$K = \frac{1}{2} \mathbf{v}_c^T m \mathbf{v}_c + \frac{1}{2} \boldsymbol{\omega}_B^T I_B \boldsymbol{\omega}_B. \quad (9.34)$$

In words, the kinetic energy of a rigid body B is equal to the kinetic energy of a point mass of mass m located at the center of mass, plus the kinetic energy of rotation about the center of mass.

9.6 NEWTON-EULER LAWS

In this section the Newton–Euler laws of motion are reviewed. Based on these laws, a recursive method of analysis is developed in the next section.

9.6.1 General Reference Point

We assume that there exists an *inertia frame* with respect to which the Newton–Euler laws can be applied. As shown in Fig. 9.4, let $A(x, y, z)$ be an inertia frame, \mathbf{l}^O the linear momentum of a rigid body B about the origin O and expressed in A , and \mathbf{h}^O the corresponding angular momentum. Also let \mathbf{f}^O and \mathbf{n}^O be the resultants of forces and moments exerted on the rigid body B about the origin O . Then the Newton–Euler laws can be stated as

$$\mathbf{f}^O = \frac{d\mathbf{l}^O}{dt}, \quad (9.35)$$

$$\mathbf{n}^O = \frac{d\mathbf{h}^O}{dt}. \quad (9.36)$$

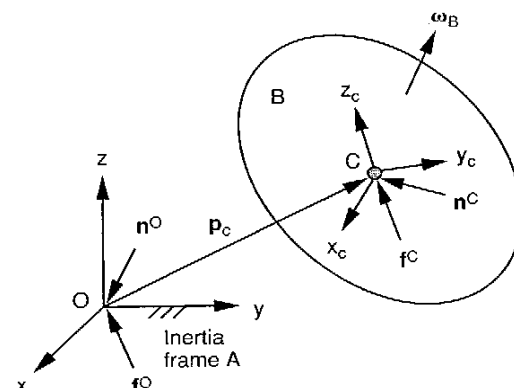


FIGURE 9.4. Resultant force and moment acting on a rigid body.

Equations (9.35) into (9.36) are two fundamental dynamical equations of motion. The main difference between dynamical and kinematical equations is that dynamical equations apply only in an inertia frame, whereas kinematical equations are valid in any frame of reference. For engineering applications, any frame that is fixed to the ground can be considered as an inertia frame. In this book we use the terms *inertia frame*, *base frame*, and *fixed frame* interchangeably. Any vector that is described in a fixed frame is called *absolute* as opposed to *relative*.

9.6.2 Center of Mass as the Reference Point

When an arbitrary point is taken as the reference point, it may be inconvenient to apply the basic laws of motion. In what follows, we show that when the center of mass is used as the reference point, the motion of a rigid body can naturally be split into two parts: a linear motion of its center of mass plus a rotational motion of the rigid body about the center of mass.

Referring to Fig. 9.4, let C be the center of mass of a rigid body B . First, we apply Newton's law. Substituting Eq. (9.18) into (9.35) gives

$$\mathbf{f}^O = \frac{d(m\mathbf{v}_c)}{dt}. \quad (9.37)$$

For a body of constant mass, Eq. (9.37) reduces to

$$\mathbf{f}^O = m \frac{d\mathbf{v}_c}{dt}. \quad (9.38)$$

Equation (9.38) is called *Newton's equation of motion* for the center of mass.

Next, we consider the rotational motion of the rigid body B . Differentiating Eq. (9.22) with respect to time yields

$$\frac{d\mathbf{h}^O}{dt} = \frac{d\mathbf{h}^C}{dt} + m \left(\mathbf{p}_c \times \frac{d\mathbf{v}_c}{dt} \right). \quad (9.39)$$

Let \mathbf{f}^C and \mathbf{n}^C be the resultants of forces and moments exerted at the center of mass C as shown in Fig. 9.4. Then it can be shown that

$$\mathbf{f}^O = \mathbf{f}^C, \quad (9.40)$$

$$\mathbf{n}^O = \mathbf{n}^C + \mathbf{p}_c \times \mathbf{f}^C. \quad (9.41)$$

Substituting Eqs. (9.39) and (9.41) into (9.36), we obtain

$$\mathbf{n}^C + \mathbf{p}_c \times \mathbf{f}^C = \frac{d\mathbf{h}^C}{dt} + m \left(\mathbf{p}_c \times \frac{d\mathbf{v}_c}{dt} \right). \quad (9.42)$$

Because of Eqs. (9.38) and (9.40), Eq. (9.42) reduces further to

$$\mathbf{n}^C = \frac{d\mathbf{h}^C}{dt}. \quad (9.43)$$

In words, the rate of change of angular momentum of B about its center of mass C is equal to the resulting moment exerted at the same point.

The derivative of \mathbf{h}^C can be developed most conveniently in the body-fixed, center-of-mass, coordinate frame C because the inertia components of B are constant in C . Substituting Eq. (9.26) into (9.43), dropping the trailing superscript C , and expressing the resulting equation in frame C yields

$${}^C\mathbf{n} = \frac{d({}^CI_B {}^C\omega_B)}{dt}. \quad (9.44)$$

Note that the differentiation of \mathbf{h}^C in Eq. (9.44) is taken with respect to the inertia frame A . Applying Eq. (4.19) to (9.44) yields

$${}^C\mathbf{n} = {}^CI_B {}^C\dot{\omega}_B + {}^C\omega_B \times ({}^CI_B {}^C\omega_B). \quad (9.45)$$

Equation (9.45) is called *Euler's equation of motion* for the center-of-mass coordinate frame.

Euler's equation of motion can also be written in the fixed frame A . Multiplying both sides of Eq. (9.45) by AR_C and making use of the relationships ${}^C\dot{\omega}_B = {}^AR_C {}^A\dot{\omega}_B$ and ${}^C\omega_B = {}^AR_C {}^A\omega_B$, we obtain

$${}^A\mathbf{n} = ({}^AR_C {}^CI_B {}^AR_C) {}^A\dot{\omega}_B + {}^A\omega_B \times [({}^AR_C {}^CI_B {}^AR_C) {}^A\omega_B], \quad (9.46)$$

or simply

$${}^A\mathbf{n} = {}^AI_B {}^A\dot{\omega}_B + {}^A\omega_B \times ({}^AI_B {}^A\omega_B). \quad (9.47)$$

Equation (9.47) is called *Euler's equation of motion* for a nonbody fixed frame, a coordinate frame that is located instantaneously at the center of mass with its coordinate axes parallel to those of the inertia frame A . Although Eqs. (9.45) and (9.47) have similar form, they are fundamentally different. The inertia elements in Eq. (9.45) are constant, whereas those in Eq. (9.47) are time dependent. Hence we often use Eq. (9.45) instead of (9.47) to avoid any possible confusion.

For the direct dynamics problem, the resulting forces are given and the motion of a rigid body is obtained by integrating the differential equations (9.38) and (9.45). For the inverse dynamics problem, the motion of a rigid body is prescribed as a function of time, and the forces required to produce that motion are obtained by substituting the position, velocity, and acceleration of the rigid body directly into Eqs. (9.38) and (9.45) or (9.47).

Special Case When the axes of the center-of-mass coordinate frame coincide with the principal axes of B , Eq. (9.45) reduces further to

$$\begin{aligned} n_x &= I_{xx}\dot{\phi}_x - \omega_y\omega_z(I_{yy} - I_{zz}), \\ n_y &= I_{yy}\dot{\phi}_y - \omega_z\omega_x(I_{zz} - I_{xx}), \\ n_z &= I_{zz}\dot{\phi}_z - \omega_x\omega_y(I_{xx} - I_{yy}), \end{aligned} \quad (9.48)$$

where I_{xx} , I_{yy} , and I_{zz} are the principal moments of inertia about the center-of-mass coordinate frame.

9.7 RECURSIVE NEWTON-EULER FORMULATION

In this section we present a recursive Newton-Euler formulation for the dynamical analysis of serial manipulators. The Newton-Euler formulation incorporates all the forces acting on the individual links of a robot arm. Hence the resulting dynamical equations include all the forces of constraint between two adjacent links. These forces of constraint are useful for sizing the links and bearings during the design stage. The method consists of a *forward computation* of the velocities and accelerations of each link, followed by a *backward computation* of the forces and moments in each joints.

The forces and moments acting on a typical link i of a serial manipulator are shown in Fig. 9.5. For the purpose of analysis, the following notations are employed:

- $\mathbf{f}_{i,i-1}$: resulting force exerted on link i by link $i - 1$ at point O_{i-1} .
- \mathbf{f}_i^* : inertia force exerted at the center of mass of link i .
- \mathbf{I}_i : inertia matrix of link i about its center of mass and expressed in the i th link frame.
- $\mathbf{n}_{i,i-1}$: resulting moment exerted on link i by link $i - 1$ at point O_{i-1} .
- \mathbf{n}_i^* : inertia moment exerted at the center of mass of link i .
- \mathbf{p}_i : position vector of the origin of the i th link frame with respect to the base link frame, $\mathbf{p}_i = \overline{O_0 O_i}$.
- \mathbf{p}_{ci} : position vector of the center of mass of the i th link with respect to the base link frame, $\mathbf{p}_{ci} = \overline{O_0 C_i}$.
- \mathbf{r}_i : position vector of the origin of the i th link frame with respect to the $(i - 1)$ th link frame, $\mathbf{r}_i = \overline{O_{i-1} O_i}$.
- \mathbf{r}_{ci} : position vector of the center of mass of link i with respect to the i th link frame, $\mathbf{r}_{ci} = \overline{O_i C_i}$.
- \mathbf{v}_i : absolute linear velocity of the origin O_i .

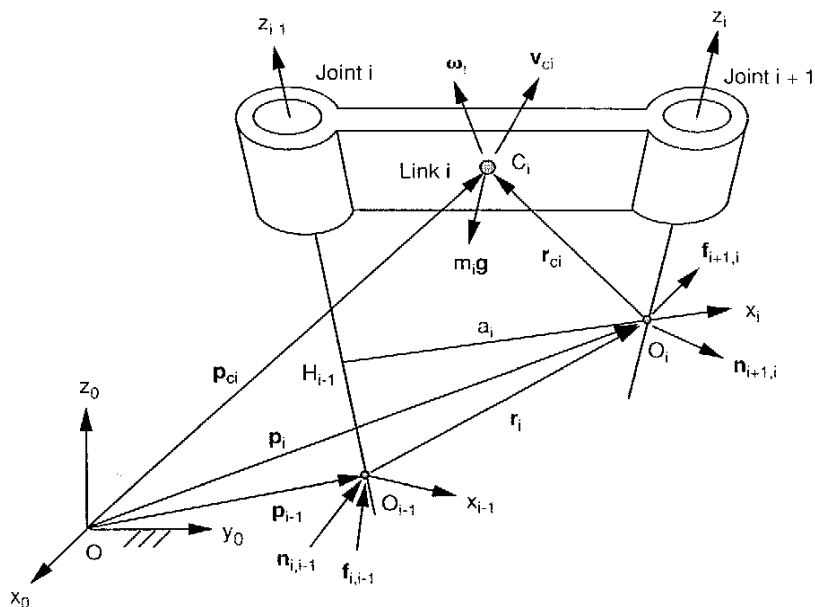


FIGURE 9.5. Forces and moments exerted on link i .

- \mathbf{v}_{ci} : absolute linear velocity of the center of mass of link i .
- $\dot{\mathbf{v}}_i$: absolute linear acceleration of the origin O_i .
- $\ddot{\mathbf{v}}_{ci}$: absolute linear acceleration of the center of mass of link i .
- \mathbf{z}_i : unit vector pointing along the z_i -axis.
- $\boldsymbol{\omega}_i$: absolute angular velocity of link i .
- $\boldsymbol{\dot{\omega}}_i$: absolute angular acceleration of link i .

9.7.1 Forward Computation

We first compute the angular velocity, angular acceleration, linear velocity, and linear acceleration of each link in terms of its preceding link. These velocities can be computed in a recursive manner, starting at the first moving link and ending at the end-effector link. The initial conditions for the base link are $\mathbf{v}_0 = \dot{\mathbf{v}}_0 = \boldsymbol{\omega}_0 = \dot{\boldsymbol{\omega}}_0 = 0$.

(a) Angular Velocity Propagation. Due to the serial construction of a manipulator, the angular velocity of link i relative to link $i - 1$ is equal to

$\mathbf{z}_{i-1}\dot{\theta}_i$ for a revolute joint and 0 for a prismatic joint, where \mathbf{z}_{i-1} denotes a unit vector pointing along the i th joint axis. Hence the angular velocity of link i can be written as

$$\boldsymbol{\omega}_i = \begin{cases} \boldsymbol{\omega}_{i-1} + \mathbf{z}_{i-1}\dot{\theta}_i & \text{for a revolute joint,} \\ \boldsymbol{\omega}_{i-1} & \text{for a prismatic joint.} \end{cases} \quad (9.49)$$

Expressing Eq. (9.49) in the i th link frame, we obtain

$$\boldsymbol{\omega}_i = \begin{cases} {}^iR_{i-1}({}^{i-1}\boldsymbol{\omega}_{i-1} + {}^{i-1}\mathbf{z}_{i-1}\dot{\theta}_i) & \text{for a revolute joint,} \\ {}^iR_{i-1}{}^{i-1}\boldsymbol{\omega}_{i-1} & \text{for a prismatic joint,} \end{cases} \quad (9.50)$$

where

$${}^iR_{i-1} = \begin{bmatrix} c\theta_i & s\theta_i & 0 \\ -c\alpha_i s\theta_i & c\alpha_i c\theta_i & s\alpha_i \\ s\alpha_i s\theta_i & -s\alpha_i c\theta_i & c\alpha_i \end{bmatrix}, \quad (9.51)$$

and ${}^{i-1}\mathbf{z}_{i-1} = [0, 0, 1]^T$ is a unit vector pointing along the i th joint axis and expressed in the $(i-1)$ th link coordinate system.

(b) Angular Acceleration Propagation. The angular acceleration of link i is obtained by differentiating Eq. (9.49) with respect to time:

$$\ddot{\boldsymbol{\omega}}_i = \begin{cases} \ddot{\boldsymbol{\omega}}_{i-1} + \mathbf{z}_{i-1}\ddot{\theta}_i + \boldsymbol{\omega}_{i-1} \times \mathbf{z}_{i-1}\dot{\theta}_i & \text{for a revolute joint,} \\ \ddot{\boldsymbol{\omega}}_{i-1} & \text{for a prismatic joint.} \end{cases} \quad (9.52)$$

Expressing Eq. (9.52) in the i th link frame, we obtain

$$\ddot{\boldsymbol{\omega}}_i = \begin{cases} {}^iR_{i-1}({}^{i-1}\ddot{\boldsymbol{\omega}}_{i-1} + {}^{i-1}\mathbf{z}_{i-1}\ddot{\theta}_i \\ \quad + {}^{i-1}\boldsymbol{\omega}_{i-1} \times {}^{i-1}\mathbf{z}_{i-1}\dot{\theta}_i) & \text{for a revolute joint,} \\ {}^iR_{i-1}{}^{i-1}\ddot{\boldsymbol{\omega}}_{i-1} & \text{for a prismatic joint.} \end{cases} \quad (9.53)$$

Equation (9.53) provides a recursive formula for computing the angular acceleration of link i in terms of link $i-1$.

(c) Linear Velocity Propagation. Referring to Fig. 9.5, we observe that (1) if the i th joint is a revolute joint, link i does not translate along the i th joint axis, and (2) if the i th joint is a prismatic joint, there is a translational velocity of \dot{d}_i along the i th joint axis. Hence the velocity of O_i can be written in terms of O_{i-1} as follows:

$$\mathbf{v}_i = \begin{cases} \mathbf{v}_{i-1} + \boldsymbol{\omega}_i \times \mathbf{r}_i & \text{for a revolute joint,} \\ \mathbf{v}_{i-1} + \boldsymbol{\omega}_i \times \mathbf{r}_i + \mathbf{z}_{i-1}\dot{d}_i & \text{for a prismatic joint.} \end{cases} \quad (9.54)$$

We may express Eq. (9.54) in the i th link frame as

$$\begin{cases} {}^i\mathbf{v}_i = {}^iR_{i-1}{}^{i-1}\mathbf{v}_{i-1} + {}^i\boldsymbol{\omega}_i \times {}^i\mathbf{r}_i & \text{for a revolute joint,} \\ {}^i\mathbf{v}_i = {}^iR_{i-1}({}^{i-1}\mathbf{v}_{i-1} + {}^{i-1}\mathbf{z}_{i-1}\dot{d}_i) + {}^i\boldsymbol{\omega}_i \times {}^i\mathbf{r}_i & \text{for a prismatic joint,} \end{cases} \quad (9.55)$$

where

$${}^i\mathbf{r}_i = \begin{bmatrix} a_i \\ d_i s\alpha_i \\ d_i c\alpha_i \end{bmatrix}. \quad (9.56)$$

The vector ${}^i\mathbf{r}_i$ is a constant vector for a revolute joint and a variable for a prismatic joint. Equation (9.55) is a recursive formula for computing the linear velocity of the origin of link i in terms of link $i-1$.

(d) Linear Acceleration Propagation. Linear acceleration of the origin O_i of frame i can be obtained by differentiating Eq. (9.54) with respect to time:

$$\begin{cases} \dot{\mathbf{v}}_i = \dot{\mathbf{v}}_{i-1} + \dot{\boldsymbol{\omega}}_i \times \mathbf{r}_i + \boldsymbol{\omega}_i \times (\boldsymbol{\omega}_i \times \mathbf{r}_i) & \text{for a revolute joint,} \\ \dot{\mathbf{v}}_i = \dot{\mathbf{v}}_{i-1} + \mathbf{z}_{i-1}\ddot{d}_i + \dot{\boldsymbol{\omega}}_i \times \mathbf{r}_i \\ \quad + \boldsymbol{\omega}_i \times (\boldsymbol{\omega}_i \times \mathbf{r}_i) + 2\boldsymbol{\omega}_i \times (\mathbf{z}_{i-1}\dot{d}_i) & \text{for a prismatic joint.} \end{cases} \quad (9.57)$$

Expressing Eq. (9.57) in the i th link frame, we obtain

$$\begin{cases} {}^i\dot{\mathbf{v}}_i = {}^iR_{i-1}{}^{i-1}\dot{\mathbf{v}}_{i-1} + {}^i\dot{\boldsymbol{\omega}}_i \times {}^i\mathbf{r}_i \\ \quad + {}^i\boldsymbol{\omega}_i \times ({}^i\boldsymbol{\omega}_i \times {}^i\mathbf{r}_i) & \text{for a revolute joint,} \\ {}^i\dot{\mathbf{v}}_i = {}^iR_{i-1}({}^{i-1}\dot{\mathbf{v}}_{i-1} + {}^{i-1}\mathbf{z}_{i-1}\ddot{d}_i) + {}^i\dot{\boldsymbol{\omega}}_i \times {}^i\mathbf{r}_i \\ \quad + {}^i\boldsymbol{\omega}_i \times ({}^i\boldsymbol{\omega}_i \times {}^i\mathbf{r}_i) \\ \quad + 2{}^i\boldsymbol{\omega}_i \times ({}^iR_{i-1}{}^{i-1}\mathbf{z}_{i-1}\dot{d}_i) & \text{for a prismatic joint.} \end{cases} \quad (9.58)$$

Equation (9.58) is a recursive formula for computing the linear acceleration of link i in terms of link $i-1$.

(e) Linear Acceleration of the Center of Mass. The linear acceleration of the center of mass is computed by:

$$\dot{\mathbf{v}}_{ci} = \dot{\mathbf{v}}_i + \dot{\boldsymbol{\omega}}_i \times {}^i\mathbf{r}_{ci} + \boldsymbol{\omega}_i \times ({}^i\boldsymbol{\omega}_i \times {}^i\mathbf{r}_{ci}). \quad (9.59)$$

(f) Acceleration of Gravity. Finally, we transform the acceleration of gravity from the $(i-1)$ link frame to the i th link frame as follows:

$${}^i\mathbf{g} = {}^iR_{i-1}{}^{i-1}\mathbf{g}. \quad (9.60)$$

9.7.2 Backward Computation

Once the velocities and accelerations of the links are found, the joint forces can be computed one link at a time starting from the end-effector link and ending at the base link. We first apply Eqs. (9.38) and (9.45) to compute the inertia force and inertia moment exerted at the center of mass of link i :

$${}^i\mathbf{f}_i^* \equiv -m_i {}^i\dot{\mathbf{v}}_{ci}, \quad (9.61)$$

$${}^i\mathbf{n}_i^* \equiv -{}^iI_i {}^i\dot{\boldsymbol{\omega}}_i - {}^i\boldsymbol{\omega}_i \times ({}^iI_i {}^i\boldsymbol{\omega}_i). \quad (9.62)$$

Next, we write the force and moment balance equations about the center of mass of link i . Referring to Fig. 9.5, we have

$${}^i\mathbf{f}_i^* + {}^i\mathbf{f}_{i,i-1} - {}^i\mathbf{f}_{i+1,i} + m_i {}^i\mathbf{g} = 0, \quad (9.63)$$

$${}^i\mathbf{n}_i^* + {}^i\mathbf{n}_{i,i-1} - {}^i\mathbf{n}_{i+1,i} - ({}^i\mathbf{r}_i + {}^i\mathbf{r}_{ci}) \times {}^i\mathbf{f}_{i,i-1} + {}^i\mathbf{r}_{ci} \times {}^i\mathbf{f}_{i+1,i} = 0. \quad (9.64)$$

Writing the Eqs. (9.63) and (9.64) in recursive forms, we obtain

$${}^i\mathbf{f}_{i,i-1} = {}^i\mathbf{f}_{i+1,i} - m_i {}^i\mathbf{g} - {}^i\mathbf{f}_i^*, \quad (9.65)$$

$${}^i\mathbf{n}_{i,i-1} = {}^i\mathbf{n}_{i+1,i} + ({}^i\mathbf{r}_i + {}^i\mathbf{r}_{ci}) \times {}^i\mathbf{f}_{i,i-1} - {}^i\mathbf{r}_{ci} \times {}^i\mathbf{f}_{i+1,i} - {}^i\mathbf{n}_i^*. \quad (9.66)$$

Once the reaction force and moment are computed in the i th link frame, they are converted into the $(i-1)$ th link frame by the following transformations:

$${}^{i-1}\mathbf{f}_{i,i-1} = {}^{i-1}R_i {}^i\mathbf{f}_{i,i-1}, \quad (9.67)$$

$${}^{i-1}\mathbf{n}_{i,i-1} = {}^{i-1}R_i {}^i\mathbf{n}_{i,i-1}. \quad (9.68)$$

Equations (9.65) through (9.68) can be used to solve for ${}^i\mathbf{f}_{i,i-1}$ and ${}^i\mathbf{n}_{i,i-1}$ recursively, starting from the end-effector link. For the end-effector link, ${}^n\mathbf{f}_{n+1,n}$ and ${}^n\mathbf{n}_{n+1,n}$ represent the end-effector output force and moment and are considered as known.

9.7.3 Joint Torque Equations

Actuator torques or forces, τ_i , are obtained by projecting the forces of constraint onto their corresponding joint axes; that is,

$$\tau_i = \begin{cases} {}^{i-1}\mathbf{n}_{i,i-1}^T {}^{i-1}\mathbf{z}_{i-1} & \text{for a revolute joint,} \\ {}^{i-1}\mathbf{f}_{i,i-1}^T {}^{i-1}\mathbf{z}_{i-1} & \text{for a prismatic joint.} \end{cases} \quad (9.69)$$

If there are viscous forces in the joints, the actuator torques or forces are computed as follows:

$$\tau_i = \begin{cases} {}^{i-1}\mathbf{n}_{i,i-1}^T {}^{i-1}\mathbf{z}_{i-1} + b_i \dot{\theta}_i & \text{for a revolute joint,} \\ {}^{i-1}\mathbf{f}_{i,i-1}^T {}^{i-1}\mathbf{z}_{i-1} + b_i \dot{d}_i & \text{for a prismatic joint.} \end{cases} \quad (9.70)$$

where b_i is the damping coefficient for joint i .

Given the desired joint velocities and joint accelerations, we compute the velocities and accelerations of the links followed by the forces of constraint, recursively. The instantaneous velocities and accelerations of link i are computed from those of link $i-1$ by Eqs. (9.50), (9.53), (9.58), and (9.59). The process starts with the first moving link and ends at the end-effector link. Once the velocities and accelerations of the links are found, the reaction forces between two adjacent links are solved by a backward procedure. Namely, the forces of constraint at joint i are calculated from those of joint $i+1$ by Eqs. (9.65) and (9.66), and the process begins with the end-effector link and ends at the first moving link.

Example 9.7.1 Newton-Euler Dynamics of a Planar 2-DOF Manipulator Let us consider the planar 2-dof manipulator shown in Fig. 6.4 as an example. The D-H transformation matrices are

$${}^0A_1 = \begin{bmatrix} c\theta_1 & -s\theta_1 & 0 & a_1 c\theta_1 \\ s\theta_1 & c\theta_1 & 0 & a_1 s\theta_1 \\ 0 & 0 & 1 & 0 \\ 0 & 0 & 0 & 1 \end{bmatrix}, \quad {}^1A_2 = \begin{bmatrix} c\theta_2 & -s\theta_2 & 0 & a_2 c\theta_2 \\ s\theta_2 & c\theta_2 & 0 & a_2 s\theta_2 \\ 0 & 0 & 1 & 0 \\ 0 & 0 & 0 & 1 \end{bmatrix}. \quad (9.71)$$

Assuming that the links are homogeneous, the vectors ${}^i\mathbf{r}_i$ and ${}^i\mathbf{r}_{ci}$ are given by

$${}^i\mathbf{r}_i = \begin{bmatrix} a_i \\ 0 \\ 0 \end{bmatrix} \quad \text{and} \quad {}^i\mathbf{r}_{ci} = \begin{bmatrix} -a_i/2 \\ 0 \\ 0 \end{bmatrix} \quad \text{for } i = 1, 2. \quad (9.72)$$

Let the two links be square beams of relatively small cross-sectional area. Then the inertia matrix of link i about its center of mass coordinate frame is

given by

$$I_i = \frac{m_i a_i^2}{12} \begin{bmatrix} 0 & 0 & 0 \\ 0 & 1 & 0 \\ 0 & 0 & 1 \end{bmatrix} \quad \text{for } i = 1, 2.$$

Assuming that the acceleration of gravity points in the $-y_0$ -direction, ${}^0\mathbf{g} = [0, -g_c, 0]^T$. We now apply the Newton-Euler method to calculate the link velocities and accelerations, and then forces and moments, recursively.

(a) *Forward computation* ($i = 1, 2$). First, we compute the velocities and accelerations of link 1. Substituting ${}^0\omega_0 = {}^0\mathbf{v}_0 = {}^0\dot{\omega}_0 = {}^0\ddot{\mathbf{v}}_0 = \mathbf{0}$ into Eqs. (9.50), (9.53), (9.58), and (9.59), we obtain

$${}^1\omega_1 = \begin{bmatrix} 0 \\ 0 \\ \dot{\theta}_1 \end{bmatrix},$$

$${}^1\dot{\omega}_1 = \begin{bmatrix} 0 \\ 0 \\ \ddot{\theta}_1 \end{bmatrix},$$

$${}^1\dot{\mathbf{v}}_1 = a_1 \begin{bmatrix} -\dot{\theta}_1^2 \\ \ddot{\theta}_1 \\ 0 \end{bmatrix},$$

$${}^1\ddot{\mathbf{v}}_{c1} = \frac{a_1}{2} \begin{bmatrix} -\dot{\theta}_1^2 \\ \ddot{\theta}_1 \\ 0 \end{bmatrix}.$$

The acceleration of gravity expressed in the first link frame is

$${}^1\mathbf{g} = {}^1R_0 {}^0\mathbf{g} = [-g_c s\theta_1 \quad -g_c c\theta_1 \quad 0]^T.$$

Next, we compute the velocities and accelerations of link 2. Substituting the velocities and accelerations of link 1 into Eqs. (9.50), (9.53), (9.58), and (9.59), we obtain

$${}^2\omega_2 = \begin{bmatrix} 0 \\ 0 \\ \dot{\theta}_1 + \dot{\theta}_2 \end{bmatrix},$$

$${}^2\dot{\omega}_2 = \begin{bmatrix} 0 \\ 0 \\ \ddot{\theta}_1 + \ddot{\theta}_2 \end{bmatrix},$$

$${}^2\dot{\mathbf{v}}_2 = \begin{bmatrix} a_1(\ddot{\theta}_1 s\theta_2 - \dot{\theta}_1^2 c\theta_2) - a_2(\dot{\theta}_1 + \dot{\theta}_2)^2 \\ a_1(\ddot{\theta}_1 c\theta_2 + \dot{\theta}_1^2 s\theta_2) + a_2(\dot{\theta}_1 + \dot{\theta}_2) \\ 0 \end{bmatrix},$$

$${}^2\ddot{\mathbf{v}}_2 = \begin{bmatrix} a_1(\ddot{\theta}_1 s\theta_2 - \dot{\theta}_1^2 c\theta_2) - \frac{1}{2}a_2(\dot{\theta}_1 + \dot{\theta}_2)^2 \\ a_1(\ddot{\theta}_1 c\theta_2 + \dot{\theta}_1^2 s\theta_2) + \frac{1}{2}a_2(\dot{\theta}_1 + \dot{\theta}_2) \\ 0 \end{bmatrix}.$$

The acceleration of gravity expressed in the second link frame is

$${}^2\mathbf{g} = {}^2R_1 {}^1\mathbf{g} = [-g_c s\theta_{12} \quad -g_c c\theta_{12} \quad 0]^T.$$

(b) *Backward computation* ($i = 2, 1$). For the backward computation, we first compute the forces exerted on link 2 and then link 1. Assuming that there are no externally applied forces, ${}^2\mathbf{f}_{3,2} = {}^2\mathbf{n}_{3,2} = \mathbf{0}$. Substituting ${}^2\mathbf{f}_{3,2} = \mathbf{0}$ along with the velocities and accelerations of link 2 obtained from the forward computation into Eqs. (9.61), (9.62), (9.65), and (9.66) for $i = 2$, we obtain

$${}^2\mathbf{f}_2^* = -m_2 \begin{bmatrix} a_1(\ddot{\theta}_1 s\theta_2 - \dot{\theta}_1^2 c\theta_2) - \frac{1}{2}a_2(\dot{\theta}_1 + \dot{\theta}_2)^2 \\ a_1(\ddot{\theta}_1 c\theta_2 + \dot{\theta}_1^2 s\theta_2) + \frac{1}{2}a_2(\dot{\theta}_1 + \dot{\theta}_2) \\ 0 \end{bmatrix},$$

$${}^2\mathbf{n}_2^* = -\frac{m_2 a_2^2}{12} \begin{bmatrix} 0 \\ 0 \\ \dot{\theta}_1 + \dot{\theta}_2 \end{bmatrix},$$

$${}^2\mathbf{f}_{2,1} = m_2 \begin{bmatrix} a_1(\ddot{\theta}_1 s\theta_2 - \dot{\theta}_1^2 c\theta_2) - \frac{1}{2}a_2(\dot{\theta}_1 + \dot{\theta}_2)^2 + g_c s\theta_{12} \\ a_1(\ddot{\theta}_1 c\theta_2 + \dot{\theta}_1^2 s\theta_2) + \frac{1}{2}a_2(\dot{\theta}_1 + \dot{\theta}_2) + g_c c\theta_{12} \\ 0 \end{bmatrix},$$

$${}^2\mathbf{n}_{2,1} = \begin{bmatrix} 0 \\ 0 \\ \frac{1}{3}m_2 a_2^2(\dot{\theta}_1 + \dot{\theta}_2) + \frac{1}{2}m_2 a_1 a_2(\dot{\theta}_1 c\theta_2 + \dot{\theta}_1^2 s\theta_2) + \frac{1}{2}m_2 g_c a_2 c\theta_{12} \end{bmatrix}.$$

Substituting the foregoing forces and moments obtained for link 2 along with the velocities and accelerations of link 1 into Eqs. (9.61), (9.62), (9.65), and (9.66) for $i = 1$, and making use of Eqs. (9.67) and (9.68), we obtain

$${}^1\mathbf{f}_1^* = -\frac{m a_1}{2} \begin{bmatrix} -\dot{\theta}_1^2 \\ \ddot{\theta}_1 \\ 0 \end{bmatrix},$$

$$\begin{aligned} {}^1\mathbf{n}_1^* &= -\frac{m_1 a_1^2}{12} \begin{bmatrix} 0 \\ 0 \\ \ddot{\theta}_1 \end{bmatrix}, \\ {}^1\mathbf{f}_{1,0} &= \begin{bmatrix} m_2[-a_1\dot{\theta}_1^2 - \frac{1}{2}a_2(\dot{\theta}_1 + \dot{\theta}_2)^2c\theta_2 - \frac{1}{2}a_2(\dot{\theta}_1 + \dot{\theta}_2)s\theta_2 + g_c s\theta_1] \\ +m_1(-\frac{1}{2}a_1\dot{\theta}_1^2 + g_c s\theta_1) \\ m_2[a_1\ddot{\theta}_1 - \frac{1}{2}a_2(\dot{\theta}_1 + \dot{\theta}_2)^2s\theta_2 + \frac{1}{2}a_2(\dot{\theta}_1 + \dot{\theta}_2)c\theta_2 + g_c c\theta_1] \\ +m_1(\frac{1}{2}a_1\dot{\theta}_1 + g_c c\theta_1) \\ 0 \\ 0 \end{bmatrix}, \\ {}^1\mathbf{n}_{1,0} &= \begin{bmatrix} 0 \\ 0 \\ (\frac{1}{3}m_1a_1^2 + \frac{1}{3}m_2a_2^2 + m_2a_1^2 + m_2a_1a_2c\theta_2)\ddot{\theta}_1 \\ +(\frac{1}{3}m_2a_2^2 + \frac{1}{2}m_2a_1a_2c\theta_2)\ddot{\theta}_2 - m_2a_1a_2s\theta_2(\dot{\theta}_1\dot{\theta}_2 + \frac{1}{2}\dot{\theta}_2^2) \\ +\frac{1}{2}m_1g_c a_1c\theta_1 + m_2g_c a_1c\theta_1 + \frac{1}{2}m_2g_c a_2c\theta_{12} \end{bmatrix}. \end{aligned}$$

(c) *Joint torques computation.* Finally, we apply Eq. (9.69) to compute the required joint torques. This results in two dynamical equations:

$$\begin{aligned} \tau_1 &= [(\frac{1}{3}m_1 + m_2)a_1^2 + m_2a_1a_2c\theta_2 + \frac{1}{3}m_2a_2^2]\ddot{\theta}_1 \\ &+ (\frac{1}{2}m_2a_1a_2c\theta_2 + \frac{1}{3}m_2a_2^2)\ddot{\theta}_2 - m_2a_1a_2s\theta_2(\dot{\theta}_1\dot{\theta}_2 + \frac{1}{2}\dot{\theta}_2^2) \\ &+ g_c[(\frac{1}{2}m_1 + m_2)a_1c\theta_1 + \frac{1}{2}m_2a_2c\theta_{12}], \quad (9.73) \end{aligned}$$

$$\begin{aligned} \tau_2 &= (\frac{1}{2}m_2a_1a_2c\theta_2 + \frac{1}{3}m_2a_2^2)\ddot{\theta}_1 + \frac{1}{3}m_2a_2^2\ddot{\theta}_2 + \frac{1}{2}m_2a_1a_2s\theta_2\dot{\theta}_1^2 \\ &+ \frac{1}{2}m_2g_c a_2c\theta_{12}. \quad (9.74) \end{aligned}$$

As expected, the dynamical equation for the second joint is simpler than that for first joint. The various dynamical effects, including the Coriolis and centrifugal velocity coupling, and gravitational effects are demonstrated clearly in this example. It can be seen from Eqs. (9.73) and (9.74) that the dynamical model is fairly complex even for such a simple 2-dof manipulator. Using the Newton-Euler recursive method, all the joint reaction forces are also found.

9.8 LAGRANGIAN FORMULATION

The Newton-Euler equations of motion contain all the forces of constraint between adjacent links as variables. Therefore, additional operations are needed to eliminate these forces of constraint in order to obtain closed-form equations. The Lagrangian method, on the other hand, formulates the equations of motion by using a set of *generalized coordinates*. It eliminates all or some of the forces of constraint at the outset. The following notations are used throughout this section:

G: vector of gravitational forces.

I_i: inertia matrix of link *i* about its center of mass and expressed in the base link frame.

J_i: link *i* Jacobian matrix.

J_{vi}: Jacobian submatrix associated with the linear velocity of the center of mass of link *i*.

J_{ωi}: Jacobian submatrix associated with the angular velocity vector of link *i*.

K: kinetic energy of a mechanical system.

L: Lagrange function, $L = K - U$.

M: manipulator inertia matrix.

M_{ij}: (*i*, *j*) element of **M**.

n: number of generalized coordinates.

p_{ci}*: position vector of the center of mass of the *i*th link with respect to the *k*th link frame and expressed in the fixed base frame.

Q_i: generalized active force corresponding to the *i*th generalized coordinate.

Q: vector of generalized forces, $\mathbf{Q} = [Q_1, Q_2, \dots, Q_n]^T$.

q_i: *i*th generalized coordinate.

q: vector of generalized coordinates, $\mathbf{q} = [q_1, q_2, \dots, q_n]^T$.

U: potential energy of a mechanical system.

V: velocity coupling vector.

δW: virtual work.

The *Lagrangian function* is defined as the difference between the kinetic and potential energy of a mechanical system:

$$L = K - U. \quad (9.75)$$

Note that the kinetic energy depends on both location and velocity of the links of a manipulator system, whereas the potential energy depends only on the location of the links. Lagrange's equations of motion are formulated in terms of the Lagrangian function as (Goldstein, 1980)

$$\frac{d}{dt} \left(\frac{\partial L}{\partial \dot{q}_i} \right) - \frac{\partial L}{\partial q_i} = Q_i, \quad i = 1, 2, \dots, n. \quad (9.76)$$

In what follows, we first define the generalized coordinates. Then we formulate expressions for the kinetic energy, potential energy, and generalized force of a robot manipulator.

9.8.1 Generalized Coordinates

Various constraints exist in a mechanical system. A kinematic constraint imposes some conditions on the relative motion between a pair of bodies. Perhaps the most frequently encountered *constraints* are those provided by the *joints* that physically connect several links to form a mechanical system.

Constraints can be classified into holonomic and nonholonomic constraints. A kinematic constraint is said to be *holonomic* if the conditions of constraint can be expressed as algebraic equations of their coordinates, and possibly the time, of the form

$$f(\mathbf{x}_1, \mathbf{x}_2, \dots, t) = 0, \quad (9.77)$$

where \mathbf{x}_i denotes the coordinates of a particle or a rigid body. A constraint that cannot be expressed in the foregoing form is said to be *nonholonomic*. The equations of constraint can be derived from the geometry of a joint. For example, the constraints imposed by a spherical joint can be stated as the position vector of the center of the sphere of one body always being equal to that of the enclosing socket of the other. Hence the constraints imposed by a spherical joint are holonomic. Similarly, the constraints provided by revolute, prismatic, and cylindrical joints are also holonomic.

The *configuration* of a mechanical system is known completely if the position and orientation of all the bodies in the system with respect to a reference frame are known. Since a rigid body has 6 degrees of freedom, a mechanical system with m moving bodies requires $6m$ coordinates to specify its configuration completely in a three-dimensional space. In a mechanical system such as a robot arm, however, these bodies are often subject to mechanical constraints imposed by the joints. As a result, these $6m$ coordinates are no longer independent. Fortunately, most of the constraints encountered in a robotic system are holonomic. If there exist c holonomic constraints, we

may use these constraints to eliminate c of the $6m$ coordinates. Hence we are left with $n = 6m - c$ independent coordinates and the system is said to have n degrees of freedom. The elimination of dependent coordinates can also be accomplished by the introduction of n new independent variables, say q_1, q_2, \dots, q_n , such that the $6m$ old coordinates can be expressed in terms of the n new independent variables. We call these n new independent variables a set of *independent generalized coordinates*. Thus the number of independent generalized coordinates is equal to the number of degrees of freedom of a multibody mechanical system. We observe that given a mechanical system, the generalized coordinates can be defined in several different ways.

Lagrangian equations of motion formulated in terms of a set of independent generalized coordinates and generalized forces are called *Lagrangian equations of the second type*. Using the second type of formulation, all the forces of constraint in the joints do not appear in the equations, and the number of equations is exactly equal to the number of degrees of freedom. In formulating the equations of motion, however, it is sometimes more convenient to employ more coordinates than the number of degrees of freedom. Under such a situation, the coordinates are no longer independent and the resulting equations of motion must be solved along with an appropriate set of constraint equations using, for example, the method of Lagrangian multipliers. We call such a set of nonindependent coordinates *redundant Lagrangian coordinates*. Equations of motion formulated in terms of a set of redundant Lagrangian coordinates are called *Lagrangian equations of the first type*. The first type of formulation will contain some unknown forces of constraint as the Lagrange multipliers.

Lagrange's equations of the first type are applicable to mechanical systems with either holonomic or nonholonomic constraints. The equations of constraint and their first and second derivatives must be adjoined to the equations of motion to produce a number of equations that is equal to the number of unknowns. In this regard, Lagrange's equations of the first type are more suitable for modeling the dynamics of parallel manipulators, where there are numerous kinematical constraints due to the presence of several closed loops.

Although Lagrange's equations of the second type are only applicable to mechanical systems with holonomic constraints, they are particularly suitable for modeling the dynamics of serial manipulators. For a serial manipulator, it turns out that the number of joints is equal to the number of degrees of freedom. Therefore, the joint variables, $\mathbf{q} = [q_1, q_2, \dots, q_n]^T$, constitute a set of independent generalized coordinates. Each component of \mathbf{q} represents either the joint angle of a revolute joint or the translational distance of a prismatic joint. Consequently, a generalized coordinate q_i does not necessarily have the dimension of length, and the corresponding generalized force, Q_i , does not

necessarily have the dimension of force. However, the product $Q_i^T q_i$ always has the dimension of work.

9.8.2 Kinetic Energy

Let us examine the kinetic energy of a typical link as shown in Fig. 9.5. Applying Eq. (9.34), the kinetic energy of link i can be written as

$$K_i = \frac{1}{2} \mathbf{v}_{ci}^T m_i \mathbf{v}_{ci} + \frac{1}{2} \boldsymbol{\omega}_i^T I_i \boldsymbol{\omega}_i. \quad (9.78)$$

The velocity vectors and the inertia matrix in Eq. (9.78) can be expressed in any reference frame. Let I_i be the inertia matrix of link i about its center of mass and expressed in the base frame, and ${}^i I_i$ be the inertia matrix of link i about its center of mass and expressed in the link frame i . Then following Eq. (9.29), we have

$$I_i = {}^0 R_i {}^i I_i ({}^0 R_i)^T. \quad (9.79)$$

We note that ${}^i I_i$ is time invariant. However, I_i depends on the robot arm posture, because it is expressed in the base frame and the orientation of link i with respect to the base is a function of joint variables.

The velocity of the center of mass and the angular velocity of link i can be found by using the recursive method developed in the preceding section. Alternatively, they can also be found by applying the theory of instantaneous screw motion. Either way, we can express them in matrix form as

$$\dot{\mathbf{x}}_{ci} = J_i \dot{\mathbf{q}}, \quad (9.80)$$

where

$$\dot{\mathbf{x}}_{ci} = \begin{bmatrix} \mathbf{v}_{ci} \\ \boldsymbol{\omega}_i \end{bmatrix} \quad \text{and} \quad J_i = \begin{bmatrix} J_{vi} \\ J_{\omega i} \end{bmatrix}.$$

Here J_i is a $6 \times n$ matrix that maps the instantaneous joint rates into the instantaneous velocity of the center of mass and the angular velocity of link i , and J_{vi} and $J_{\omega i}$ are two $3 \times n$ submatrices of J_i . We call J_i the *link Jacobian matrix* and J_{vi} and $J_{\omega i}$ the *link Jacobian submatrices*.

Let J_{vi}^j and $J_{\omega i}^j$ be the j th column vectors of J_{vi} and $J_{\omega i}$, respectively. Then applying the theory of instantaneous screw motion for $j \leq i$, we obtain

$$J_{vi}^j = \begin{cases} \mathbf{z}_{j-1} \times {}^{j-1} \mathbf{p}_{ci}^* & \text{for a revolute joint,} \\ \mathbf{z}_{j-1} & \text{for a prismatic joint,} \end{cases} \quad (9.81)$$

$$J_{\omega i}^j = \begin{cases} \mathbf{z}_{j-1} & \text{for a revolute joint,} \\ \mathbf{0} & \text{for a prismatic joint.} \end{cases} \quad (9.82)$$

where ${}^{j-1} \mathbf{p}_{ci}^*$ is a position vector defined from the origin of the $j-1$ link frame to the center of mass of link i and expressed in the base frame. We note that J_{vi}^j and $J_{\omega i}^j$ denote the partial rate of change of the velocity of the center of mass and the angular velocity of link i with respect to the j th joint motion. Since the motion of link i depends only on joints 1 through i , the two column vectors above are set to zero for $j > i$. Furthermore, since both \mathbf{z}_{j-1} and ${}^{j-1} \mathbf{p}_{ci}^*$ depend on \mathbf{q} , the submatrices J_{vi} and $J_{\omega i}$ are configuration dependent. Using the notations above, J_{vi} and $J_{\omega i}$ can be written as

$$J_{vi} = [J_{vi}^1, J_{vi}^2, \dots, J_{vi}^i, \mathbf{0}, \mathbf{0}, \dots, \mathbf{0}], \quad (9.83)$$

$$J_{\omega i} = [J_{\omega i}^1, J_{\omega i}^2, \dots, J_{\omega i}^i, \mathbf{0}, \mathbf{0}, \dots, \mathbf{0}]. \quad (9.84)$$

Substituting Eq. (9.80) into (9.78) and then summing over all links, we obtain an expression for the kinetic energy of the system as

$$\begin{aligned} K &= \frac{1}{2} \sum_{i=1}^n (\mathbf{v}_{ci}^T m_i \mathbf{v}_{ci} + \boldsymbol{\omega}_i^T I_i \boldsymbol{\omega}_i) \\ &= \frac{1}{2} \sum_{i=1}^n [(J_{vi} \dot{\mathbf{q}})^T m_i (J_{vi} \dot{\mathbf{q}}) + (J_{\omega i} \dot{\mathbf{q}})^T I_i (J_{\omega i} \dot{\mathbf{q}})] \\ &= \frac{1}{2} \dot{\mathbf{q}}^T \left[\sum_{i=1}^n (J_{vi}^T m_i J_{vi} + J_{\omega i}^T I_i J_{\omega i}) \right] \dot{\mathbf{q}}. \end{aligned} \quad (9.85)$$

For convenience, we define an $n \times n$ manipulator inertia matrix as

$$M = \sum_{i=1}^n (J_{vi}^T m_i J_{vi} + J_{\omega i}^T I_i J_{\omega i}). \quad (9.86)$$

In this way, the total kinetic energy of a robot arm can be expressed in terms of the manipulator inertia matrix and the vector of joint rates:

$$K = \frac{1}{2} \dot{\mathbf{q}}^T M \dot{\mathbf{q}}. \quad (9.87)$$

We note that the manipulator inertia matrix M defined in Eq. (9.86) involves the link Jacobian submatrices J_{vi} and $J_{\omega i}$. Therefore, the manipulator inertia matrix is configuration dependent. Similar to the inertia matrix of a rigid body, the manipulator inertia matrix is a symmetric, positive-definite matrix. The quadratic form of the equation indicates that the kinetic energy is always positive unless the system is at rest.

9.8.3 Potential Energy

The potential energy stored in link i of a robot arm is defined as the amount of work required to raise the center of mass of link i from a horizontal reference plane to its present position under the influence of gravity. With reference to the inertia frame, the work required to displace link i to position \mathbf{p}_{ci} is given by $-m_i \mathbf{g}^T \mathbf{p}_{ci}$. Hence the total potential energy stored in a robot arm is

$$U = - \sum_{i=1}^n m_i \mathbf{g}^T \mathbf{p}_{ci}. \quad (9.88)$$

9.8.4 Generalized Forces

In this section we investigate various contributions to the vector of generalized forces. Except for gravitational and inertia forces, the generalized forces account for all the other forces acting on a robot arm that are consistent with the mechanical constraints. The vector of generalized forces, $\mathbf{Q} = [Q_1, Q_2, \dots, Q_n]^T$, is defined by the principle of virtual work as

$$\delta W = \mathbf{Q}^T \delta \mathbf{q}. \quad (9.89)$$

We first consider the case in which actuators exert forces or torques at the joints and external force and moment are applied at the end effector. Let $\boldsymbol{\tau} = [\tau_1, \dots, \tau_n]^T$ be an n -dimensional vector of joint torques generated by the actuators and $\mathbf{F}_e = [\mathbf{f}_e^T, \mathbf{n}_e^T]^T$ be a six-dimensional vector of resultant force and moment exerted at the end effector. Then the virtual work produced by these forces and moments is

$$\delta W = \boldsymbol{\tau}^T \delta \mathbf{q} + \mathbf{F}_e^T \delta \mathbf{x}, \quad (9.90)$$

where $\delta \mathbf{x}$ denotes a six-dimensional virtual displacement vector of the end effector. Substituting the relation $\delta \mathbf{x} = J \delta \mathbf{q}$ into Eq. (9.90) and then equating the resulting virtual work to that of Eq. (9.89) yields the vector of generalized forces as

$$\mathbf{Q} = \boldsymbol{\tau} + J^T \mathbf{F}_e. \quad (9.91)$$

The contribution of friction to the generalized force vector can also be formulated. Frictional force is a highly nonlinear phenomenon that is difficult to model accurately (Armstrong-Helouvry, 1991), yet it can have significant effects on system dynamics. In a grease- or oil-lubricated bearing, there are four regimes of lubrication: static friction, boundary lubrication, partial fluid lubrication, and full fluid lubrication. In the fourth regime, frictional force is proportional to the relative velocity between the contacting bodies. It can

be modeled by a simple expression: $-b_i \dot{q}_i$. Therefore the virtual work contributed by this type of frictional forces is given by

$$\delta W = -\mathbf{f}_r^T \delta \mathbf{q}, \quad (9.92)$$

where $\mathbf{f}_r = [b_1 \dot{q}_1, b_2 \dot{q}_2, \dots, b_n \dot{q}_n]^T$ denotes the frictional torques or forces in the joints and the minus sign indicates that the direction of frictional torque or force is always opposite to the joint velocity. Adding this contribution to the vector of generalized forces in Eq. (9.91), we obtain

$$\mathbf{Q} = \boldsymbol{\tau} + J^T \mathbf{F}_e - \mathbf{f}_r. \quad (9.93)$$

We notice that in the absence of friction and externally applied force, the vector of generalized forces and the vector of joint torques are equivalent (i.e., $\mathbf{Q} = \boldsymbol{\tau}$). In this case, the components of the generalized force vector are the actuator forces for prismatic joints and torques for revolute joints.

9.8.5 General Form of Dynamical Equations

Now we are in a position to formulate the dynamical equations of a serial manipulator. First, we substitute Eqs. (9.87) and (9.88) into (9.75) to obtain a compact expression for the Lagrangian function:

$$L = \frac{1}{2} \dot{\mathbf{q}}^T M \dot{\mathbf{q}} + \sum_{i=1}^n m_i \mathbf{g}^T \mathbf{p}_{ci}. \quad (9.94)$$

Next, we differentiate the Lagrangian function with respect to q_i , \dot{q}_i , and t to formulate the dynamical equations of motion. To facilitate the derivation, we expand the term for the kinetic energy into a sum of scalars. Let M_{ij} be the (i, j) element of the manipulator inertia matrix M ; then Eq. (9.94) can be written as

$$L = \frac{1}{2} \sum_{i=1}^n \sum_{j=1}^n M_{ij} \dot{q}_i \dot{q}_j + \sum_{i=1}^n m_i \mathbf{g}^T \mathbf{p}_{ci}. \quad (9.95)$$

Since the potential energy does not depend on \dot{q}_i , taking the partial derivative of Eq. (9.95) with respect to \dot{q}_i , we obtain

$$\frac{\partial L}{\partial \dot{q}_i} = \sum_{j=1}^n M_{ij} \dot{q}_j. \quad (9.96)$$

Taking the total derivative of Eq. (9.96) with respect to time yields

$$\frac{d}{dt} \left(\frac{\partial L}{\partial \dot{q}_i} \right) = \sum_{j=1}^n M_{ij} \ddot{q}_j + \sum_{j=1}^n \left(\frac{dM_{ij}}{dt} \right) \dot{q}_j = \sum_{j=1}^n M_{ij} \ddot{q}_j + \sum_{j=1}^n \sum_{k=1}^n \frac{\partial M_{ij}}{\partial q_k} \dot{q}_k \dot{q}_j. \quad (9.97)$$

Taking the partial derivative of Eq. (9.95) with respect to q_i yields

$$\frac{\partial L}{\partial q_i} = \frac{1}{2} \frac{\partial}{\partial q_i} \left(\sum_{j=1}^n \sum_{k=1}^n M_{jk} \dot{q}_j \dot{q}_k \right) + \sum_{j=1}^n m_j \mathbf{g}^T \left(\frac{\partial \mathbf{p}_{ej}}{\partial q_i} \right). \quad (9.98)$$

Note that the partial derivative of \mathbf{p}_{ej} with respect to q_i is equal to the i th column vector of the link Jacobian submatrix J_{vj} . Hence Eq. (9.98) can be written as

$$\frac{\partial L}{\partial q_i} = \frac{1}{2} \sum_{j=1}^n \sum_{k=1}^n \frac{\partial M_{jk}}{\partial q_i} \dot{q}_j \dot{q}_k + \sum_{j=1}^n m_j \mathbf{g}^T J_{vj}^i. \quad (9.99)$$

Finally, we substitute Eqs. (9.97) and (9.99) into (9.76) to obtain the dynamical equations of motion:

$$\sum_{j=1}^n M_{ij} \ddot{q}_j + V_i + G_i = Q_i \quad \text{for } i = 1, 2, \dots, n. \quad (9.100)$$

where

$$V_i = \sum_{j=1}^n \sum_{k=1}^n \left(\frac{\partial M_{ij}}{\partial q_k} - \frac{1}{2} \frac{\partial M_{jk}}{\partial q_i} \right) \dot{q}_j \dot{q}_k, \quad (9.101)$$

$$G_i = - \sum_{j=1}^n m_j \mathbf{g}^T J_{vj}^i. \quad (9.102)$$

The first term in Eq. (9.100) accounts for the inertia forces, the second term represents the *Coriolis* and *centrifugal* forces, and the third term gives the gravitational effects. The n scalar equations given by Eq. (9.100) can be written in matrix form as

$$M \ddot{\mathbf{q}} + \mathbf{V} + \mathbf{G} = \mathbf{Q}, \quad (9.103)$$

where $\mathbf{V} = [V_1, \dots, V_n]^T$, $\mathbf{G} = [G_1, \dots, G_n]^T$, and $\mathbf{Q} = [Q_1, \dots, Q_n]^T$.

Equation (9.103) is called the *general form of dynamical equations*. The vector \mathbf{V} is called the *velocity coupling vector*. The vector \mathbf{G} is called the vector of gravitational forces. There are two distinct types of velocity cou-

pling between joints. The velocity-squared terms correspond to the centrifugal forces, and the velocity product terms correspond to the Coriolis forces. The manipulator inertia matrix M is symmetric and positive definite and therefore is always invertible. The off-diagonal terms of M represent the acceleration coupling effect between joints.

Example 9.8.1 Lagrangian Dynamics of a Planar 2-DOF Manipulator In this example we formulate Lagrange's equations of motion for the planar 2-dof manipulator shown in Fig. 6.4. We note that the link coordinate axes are aligned with the principal axes of each link. The two D-H transformation matrices are given by Eq. (9.71). The center of mass of link i , expressed in link frame i , is given by Eq. (9.72). Let θ_1 and θ_2 be a set of two independent generalized coordinates. We compute the link inertia matrices, link Jacobian matrices, gravitational effects, and Lagrange's equations of motion as follows.

(a) *Link inertia matrices.* Assuming that the moving links are homogeneous with a relatively small cross section, the inertia matrix of link i about its center of mass and expressed in the i th link frame is

$$I_i = \frac{1}{12} m_i a_i^2 \begin{bmatrix} 0 & 0 & 0 \\ 0 & 1 & 0 \\ 0 & 0 & 1 \end{bmatrix} \quad \text{for } i = 1, 2. \quad (9.104)$$

The inertia matrices of links 1 and 2 about their respective centers of mass and expressed in the base frame are obtained by substituting Eq. (9.104) for $i = 1$ and 2 into (9.79). As a result, we obtain

$$I_1 = \frac{1}{12} m_1 a_1^2 \begin{bmatrix} s^2 \theta_1 & -s\theta_1 c\theta_1 & 0 \\ -s\theta_1 c\theta_1 & c^2 \theta_1 & 0 \\ 0 & 0 & 1 \end{bmatrix}, \quad (9.105)$$

$$I_2 = \frac{1}{12} m_2 a_2^2 \begin{bmatrix} s^2 \theta_{12} & -s\theta_{12} c\theta_{12} & 0 \\ -s\theta_{12} c\theta_{12} & c^2 \theta_{12} & 0 \\ 0 & 0 & 1 \end{bmatrix}. \quad (9.106)$$

(b) *Link Jacobian matrices.* The position vectors of the centers of mass of links 1 and 2 with respect to the various link frames and expressed in the base frame are given by

$${}^0 \mathbf{p}_{e1}^* = \begin{bmatrix} \frac{1}{2} a_1 c\theta_1 \\ \frac{1}{2} a_1 s\theta_1 \\ 0 \end{bmatrix}, \quad (9.107)$$

$${}^1\mathbf{p}_{e2}^* = \begin{bmatrix} \frac{1}{2}a_2c\theta_{12} \\ \frac{1}{2}a_2s\theta_{12} \\ 0 \end{bmatrix}, \quad (9.108)$$

$${}^0\mathbf{p}_{e2}^* = \begin{bmatrix} a_1c\theta_1 + \frac{1}{2}a_2c\theta_{12} \\ a_1s\theta_1 + \frac{1}{2}a_2s\theta_{12} \\ 0 \end{bmatrix}. \quad (9.109)$$

The link Jacobian submatrices, J_{vi} and $J_{\omega i}$, are obtained by substituting Eqs. (9.107) through (9.109) into (9.83) and (9.84):

$$J_{v1} = \begin{bmatrix} -\frac{1}{2}a_1s\theta_1 & 0 \\ \frac{1}{2}a_1c\theta_1 & 0 \\ 0 & 0 \end{bmatrix}, \quad (9.110)$$

$$J_{\omega 1} = \begin{bmatrix} 0 & 0 \\ 0 & 0 \\ 1 & 0 \end{bmatrix}, \quad (9.111)$$

$$J_{v2} = \begin{bmatrix} -a_1s\theta_1 - \frac{1}{2}a_2s\theta_{12} & -\frac{1}{2}a_2s\theta_{12} \\ a_1c\theta_1 + \frac{1}{2}a_2c\theta_{12} & \frac{1}{2}a_2c\theta_{12} \\ 0 & 0 \end{bmatrix}, \quad (9.112)$$

$$J_{\omega 2} = \begin{bmatrix} 0 & 0 \\ 0 & 0 \\ 1 & 1 \end{bmatrix}. \quad (9.113)$$

(c) *Manipulator inertia matrix.* The manipulator inertia matrix is obtained by substituting Eqs. (9.105), (9.106), and (9.110) through (9.113) into (9.86):

$$\begin{aligned} M &= J_{v1}^T m_1 J_{v1} + J_{\omega 1}^T I_1 J_{\omega 1} + J_{v2}^T m_2 J_{v2} + J_{\omega 2}^T I_2 J_{\omega 2} \\ &= \begin{bmatrix} \frac{1}{3}m_1a_1^2 + m_2(a_1^2 + a_1a_2c\theta_2 + \frac{1}{3}a_2^2) & m_2(\frac{1}{2}a_1a_2c\theta_2 + \frac{1}{3}a_2^2) \\ m_2(\frac{1}{2}a_1a_2c\theta_2 + \frac{1}{3}a_2^2) & \frac{1}{3}m_2a_2^2 \end{bmatrix}. \end{aligned} \quad (9.114)$$

(d) *Velocity coupling vector.* Taking the partial derivatives of the manipulator inertia matrix, Eq. (9.114), with respect to θ in accordance with Eq. (9.101) yields

$$\begin{aligned} V_1 &= \sum_{j=1}^2 \sum_{k=1}^2 \left(\frac{\partial M_{1j}}{\partial \theta_k} - \frac{1}{2} \frac{\partial M_{jk}}{\partial \theta_1} \right) \dot{\theta}_j \dot{\theta}_k \\ &= -m_2 a_1 a_2 s \theta_2 \left(\dot{\theta}_1 \dot{\theta}_2 + \frac{1}{2} \dot{\theta}_2^2 \right), \end{aligned} \quad (9.115)$$

$$V_2 = \sum_{j=1}^2 \sum_{k=1}^2 \left(\frac{\partial M_{2j}}{\partial \theta_k} - \frac{1}{2} \frac{\partial M_{jk}}{\partial \theta_2} \right) \dot{\theta}_j \dot{\theta}_k = \frac{1}{2} m_2 a_1 a_2 s \theta_2 \dot{\theta}_1^2. \quad (9.116)$$

(e) *Gravitational vector.* The gravitational terms are obtained by substituting Eqs. (9.110) and (9.112) into (9.102),

$$G_1 = \frac{1}{2}m_1 g_c a_1 c \theta_1 + m_2 g_c a_1 c \theta_1 + \frac{1}{2}m_2 g_c a_2 c \theta_{12}, \quad (9.117)$$

$$G_2 = \frac{1}{2}m_2 g_c a_2 c \theta_{12}. \quad (9.118)$$

(f) *Lagrange's equations of motion.* Assuming that there are no external forces exerted at the end effector and the joint friction is negligible, the vector of joint torques and the vector of generalized forces are equivalent. Lagrange's equations of motion are obtained by substituting Eqs. (9.114) through (9.118) into (9.100). This results in the following two dynamical equations of motion:

$$\begin{aligned} \tau_1 &= [(\frac{1}{3}m_1 + m_2) a_1^2 + m_2 a_1 a_2 c \theta_2 + \frac{1}{3}m_2 a_2^2] \ddot{\theta}_1 \\ &\quad + (\frac{1}{2}m_2 a_1 a_2 c \theta_2 + \frac{1}{3}m_2 a_2^2) \ddot{\theta}_2 - m_2 a_1 a_2 s \theta_2 (\dot{\theta}_1 \dot{\theta}_2 + \frac{1}{2} \dot{\theta}_2^2) \\ &\quad + g_c [(\frac{1}{2}m_1 + m_2) a_1 c \theta_1 + \frac{1}{2}m_2 a_2 c \theta_{12}], \end{aligned} \quad (9.119)$$

$$\begin{aligned} \tau_2 &= (\frac{1}{2}m_2 a_1 a_2 c \theta_2 + \frac{1}{3}m_2 a_2^2) \ddot{\theta}_1 + \frac{1}{3}m_2 a_2^2 \ddot{\theta}_2 + \frac{1}{2}m_2 a_1 a_2 s \theta_2 \dot{\theta}_1^2 \\ &\quad + \frac{1}{2}m_2 g_c a_2 c \theta_{12}. \end{aligned} \quad (9.120)$$

Hence we have arrived at the same equations obtained by using the recursive Newton–Euler formulation. Using the Lagrangian formulation, forces of constraint do not appear in the equations of motion.

Example 9.8.2 Langrangian Dynamics of a SCARA Arm Let us study the dynamics of a SCARA arm as a second example. The SCARA arm is constructed with four parallel joint axes. The first two and the fourth are revolute joints, and the third is a prismatic joint. To simplify the problem, we consider the motion of the first three moving links and combine the mass of the fourth link and the load, if any, with the third link. In this way, we will be dealing with a pure position problem. Figure 9.6 shows a schematic diagram of the

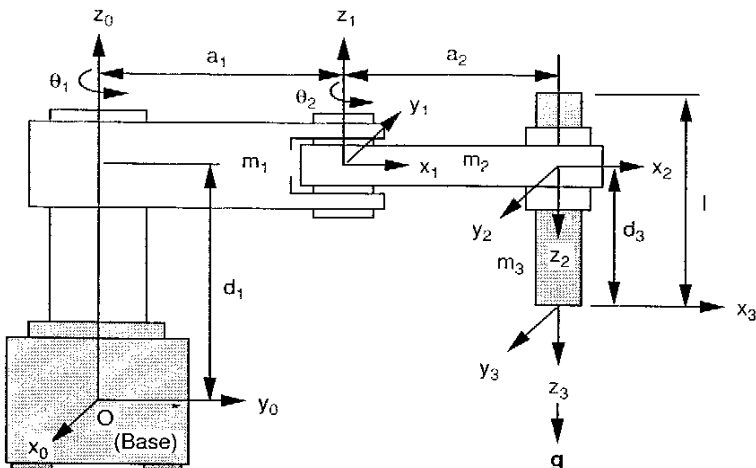


FIGURE 9.6. Schematic diagram of a SCARA arm.

first three moving links in which the coordinate axes of each link frame are aligned with the principal axes of the link. The Denavit–Hartenberg parameters are listed in Table 2.2, and the D–H transformation matrices are given by Eqs. (2.9) to (2.11).

Assuming that all links are homogeneous with relatively small cross section, the position vectors of the centers of mass are given by

$${}^1\mathbf{p}_{c1} = [-a_1/2, 0, 0]^T,$$

$${}^2\mathbf{p}_{c2} = [-a_2/2, 0, 0]^T,$$

$${}^3\mathbf{p}_{c3} = [0, 0, -\ell/2]^T,$$

where ℓ is the third link length. Let θ_1 , θ_2 , and d_3 be a set of independent generalized coordinates. We compute the link inertia matrices, link Jacobian matrices, and the gravitational effects for the links, and substitute them into Eq. (9.100) to obtain Lagrange's equations of motion as follows.

(a) *Link inertia matrices.* The link inertia matrices about their centers of mass and expressed in their respective link frames are

$${}^1I_l = \frac{1}{12}m_1a_1^2 \begin{bmatrix} 0 & 0 & 0 \\ 0 & 1 & 0 \\ 0 & 0 & 1 \end{bmatrix}, \quad (9.121)$$

$${}^2I_l = \frac{1}{12}m_2a_2^2 \begin{bmatrix} 0 & 0 & 0 \\ 0 & 1 & 0 \\ 0 & 0 & 1 \end{bmatrix}, \quad (9.122)$$

$${}^3I_l = \frac{1}{12}m_3\ell^2 \begin{bmatrix} 1 & 0 & 0 \\ 0 & 1 & 0 \\ 0 & 0 & 0 \end{bmatrix}. \quad (9.123)$$

The link inertia matrices about their centers of mass and expressed in the base frame are obtained by substituting Eqs. (9.121) through (9.123) along with their rotation matrices into (9.79):

$$I_l = \frac{1}{12}m_la_l^2 \begin{bmatrix} s^2\theta_l & -s\theta_lc\theta_l & 0 \\ -s\theta_lc\theta_l & c^2\theta_l & 0 \\ 0 & 0 & 1 \end{bmatrix}, \quad (9.124)$$

$$I_2 = \frac{1}{12}m_2a_2^2 \begin{bmatrix} s^2\theta_{12} & -s\theta_{12}c\theta_{12} & 0 \\ -s\theta_{12}c\theta_{12} & c^2\theta_{12} & 0 \\ 0 & 0 & 1 \end{bmatrix}, \quad (9.125)$$

$$I_3 = \frac{1}{12}m_3\ell^2 \begin{bmatrix} 1 & 0 & 0 \\ 0 & 1 & 0 \\ 0 & 0 & 0 \end{bmatrix}. \quad (9.126)$$

(b) *Link Jacobian matrices.* The position vectors of the centers of mass of links 1, 2, and 3 with respect to the various link frames and expressed in the base frame are

$${}^0\mathbf{p}_{c1}^* = \begin{bmatrix} \frac{1}{2}a_1c\theta_1 \\ \frac{1}{2}a_1s\theta_1 \\ d_1 \end{bmatrix}, \quad (9.127)$$

$${}^1\mathbf{p}_{c2}^* = \begin{bmatrix} \frac{1}{2}a_2c\theta_{12} \\ \frac{1}{2}a_2s\theta_{12} \\ 0 \end{bmatrix}, \quad (9.128)$$

$${}^0\mathbf{p}_{c2}^* = \begin{bmatrix} a_1c\theta_1 + \frac{1}{2}a_2c\theta_{12} \\ a_1s\theta_1 + \frac{1}{2}a_2s\theta_{12} \\ d_1 \end{bmatrix}, \quad (9.129)$$

$${}^2\mathbf{p}_{c3}^* = \begin{bmatrix} 0 \\ 0 \\ d_3 - \frac{1}{2}\ell \end{bmatrix}, \quad (9.130)$$

$${}^1\mathbf{p}_{c3}^* = \begin{bmatrix} a_2 c \theta_{12} \\ a_2 s \theta_{12} \\ -d_3 + \frac{1}{2}\ell \end{bmatrix}, \quad (9.131)$$

$${}^0\mathbf{p}_{c3}^* = \begin{bmatrix} a_1 c \theta_1 + a_2 c \theta_{12} \\ a_1 s \theta_1 + a_2 s \theta_{12} \\ d_1 - d_3 + \frac{1}{2}\ell \end{bmatrix}. \quad (9.132)$$

The link Jacobian submatrices, J_{vi} and $J_{\omega i}$, are obtained by substituting the equations above into Eqs. (9.83) and (9.84):

$$J_{v1} = \begin{bmatrix} -\frac{1}{2}a_1 s \theta_1 & 0 & 0 \\ \frac{1}{2}a_1 c \theta_1 & 0 & 0 \\ 0 & 0 & 0 \end{bmatrix}, \quad (9.133)$$

$$J_{\omega 1} = \begin{bmatrix} 0 & 0 & 0 \\ 0 & 0 & 0 \\ 1 & 0 & 0 \end{bmatrix}, \quad (9.134)$$

$$J_{v2} = \begin{bmatrix} -a_1 s \theta_1 - \frac{1}{2}a_2 s \theta_{12} & -\frac{1}{2}a_2 s \theta_{12} & 0 \\ a_1 c \theta_1 + \frac{1}{2}a_2 c \theta_{12} & \frac{1}{2}a_2 c \theta_{12} & 0 \\ 0 & 0 & 0 \end{bmatrix}, \quad (9.135)$$

$$J_{\omega 2} = \begin{bmatrix} 0 & 0 & 0 \\ 0 & 0 & 0 \\ 1 & 1 & 0 \end{bmatrix}, \quad (9.136)$$

$$J_{v3} = \begin{bmatrix} -a_1 s \theta_1 - a_2 s \theta_{12} & -a_2 s \theta_{12} & 0 \\ a_1 c \theta_1 + a_2 c \theta_{12} & a_2 c \theta_{12} & 0 \\ 0 & 0 & -1 \end{bmatrix}, \quad (9.137)$$

$$J_{\omega 3} = \begin{bmatrix} 0 & 0 & 0 \\ 0 & 0 & 0 \\ 1 & 1 & 0 \end{bmatrix}. \quad (9.138)$$

(c) *Manipulator inertia matrix.* The manipulator inertia matrix is obtained by substituting Eqs. (9.124) through (9.126) and (9.133) through (9.138) into (9.86):

$$\begin{aligned} M &= J_{v1}^T m_1 J_{v1} + J_{\omega 1}^T I_1 J_{\omega 1} + J_{v2}^T m_2 J_{v2} + J_{\omega 2}^T I_2 J_{\omega 2} + J_{v3}^T m_3 J_{v3} + J_{\omega 3}^T I_3 J_{\omega 3} \\ &= m_1 \begin{bmatrix} \frac{1}{3}a_1^2 & 0 & 0 \\ 0 & 0 & 0 \\ 0 & 0 & 0 \end{bmatrix} \\ &\quad + m_2 \begin{bmatrix} a_1^2 + a_1 a_2 c \theta_2 + \frac{1}{3}a_2^2 & -\frac{1}{2}a_1 a_2 c \theta_2 + \frac{1}{3}a_2^2 & 0 \\ \frac{1}{2}a_1 a_2 c \theta_2 + \frac{1}{3}a_2^2 & \frac{1}{3}a_2^2 & 0 \\ 0 & 0 & 0 \end{bmatrix} \\ &\quad + m_3 \begin{bmatrix} a_1^2 + 2a_1 a_2 c \theta_2 + a_2^2 & a_1 a_2 c \theta_2 + a_2^2 & 0 \\ a_1 a_2 c \theta_2 + a_2^2 & a_2^2 & 0 \\ 0 & 0 & 1 \end{bmatrix}. \end{aligned} \quad (9.139)$$

(d) *Velocity coupling vector.* Taking the partial derivatives of the manipulator inertia matrix with respect to q_i in accordance with Eq. (9.101) yields

$$\begin{aligned} V_1 &= \sum_{j=1}^3 \sum_{k=1}^3 \left(\frac{\partial M_{1j}}{\partial q_k} - \frac{1}{2} \frac{\partial M_{jk}}{\partial q_1} \right) \dot{q}_j \dot{q}_k \\ &= -(m_2 + 2m_3)a_1 a_2 s \theta_2 \left(\dot{\theta}_1 \dot{\theta}_2 + \frac{1}{2} \dot{\theta}_2^2 \right), \end{aligned} \quad (9.140)$$

$$\begin{aligned} V_2 &= \sum_{j=1}^3 \sum_{k=1}^3 \left(\frac{\partial M_{2j}}{\partial q_k} - \frac{1}{2} \frac{\partial M_{jk}}{\partial q_2} \right) \dot{q}_j \dot{q}_k \\ &= \left(\frac{1}{2}m_2 + m_3 \right) a_1 a_2 s \theta_2 \dot{\theta}_1^2, \end{aligned} \quad (9.141)$$

$$V_3 = \sum_{j=1}^3 \sum_{k=1}^3 \left(\frac{\partial M_{3j}}{\partial q_k} - \frac{1}{2} \frac{\partial M_{jk}}{\partial q_3} \right) \dot{q}_j \dot{q}_k = 0. \quad (9.142)$$

(e) *Gravitational vector.* Assuming that the acceleration of gravity points in the negative z_0 -direction (i.e., $\mathbf{g} = [0, 0, -g_e]^T$), the gravitational terms are obtained by substituting Eqs. (9.133), (9.135), and (9.137) into (9.102):

$$G_1 = - \sum_{j=1}^3 m_j \mathbf{g}^T J_{vj}^1 = 0, \quad (9.143)$$

$$G_2 = - \sum_{j=1}^3 m_j \mathbf{g}^T J_{vj}^2 = 0, \quad (9.144)$$

$$G_3 = - \sum_{j=1}^3 m_j \mathbf{g}^T J_{vj}^3 - m_3 g_c. \quad (9.145)$$

(f) *Lagrange's equations of motion.* Assuming that there are no external forces and moments exerted at the end effector and that the joint friction is negligible, the vector of joint torques and the vector of generalized forces are equivalent. Substituting Eqs. (9.139) through (9.145) into (9.100) yields

$$\begin{aligned} \tau_1 &= [(\frac{1}{3}m_1 + m_2 + m_3) a_1^2 + (m_2 + 2m_3)a_1 a_2 c\theta_2 + (\frac{1}{3}m_2 + m_3) a_2^2] \ddot{\theta}_1 \\ &\quad + [(\frac{1}{2}m_2 + m_3) a_1 a_2 c\theta_2 + (\frac{1}{3}m_2 + m_3) a_2^2] \ddot{\theta}_2 \\ &\quad - (m_2 + 2m_3) a_1 a_2 s\theta_2 (\dot{\theta}_1 \dot{\theta}_2 + \frac{1}{2} \dot{\theta}_2^2), \end{aligned} \quad (9.146)$$

$$\begin{aligned} \tau_2 &= [(\frac{1}{2}m_2 + m_3) a_1 a_2 c\theta_2 + (\frac{1}{3}m_2 + m_3) a_2^2] \ddot{\theta}_1 + (\frac{1}{3}m_2 + m_3) a_2^2 \ddot{\theta}_2 \\ &\quad + (\frac{1}{2}m_2 + m_3) a_1 a_2 s\theta_2 \dot{\theta}_1^2, \end{aligned} \quad (9.147)$$

$$\tau_3 = m_3 \ddot{d}_3 - m_3 g_c. \quad (9.148)$$

Equations (9.146) through (9.148) are the dynamical equations of motion for the 3-dof SCARA arm. The model is slightly more complex than the planar 2-dof manipulator. This is because the construction of first two joint axes of the SCARA arm is essentially the same as that of the planar 2-dof manipulator. In a SCARA manipulator, the first two joint axes control the horizontal position of the end effector, while the third prismatic joint controls the vertical position. The gravitational effects do not appear in the first two equations, because the acceleration of gravity is parallel to the first two joint axes. We observe that the motion of the third joint is completely independent of the first two, and the third link merely acts as a load to the motion of the first two joints.

9.9 INERTIA EFFECTS OF THE ROTORS

In previous sections we have assumed that each joint in a serial manipulator is driven directly by a motor and that the inertia effects of gears and rotors are negligible. Strictly speaking, the resulting equations are valid only for direct-drive manipulators. In a non-direct-drive manipulator, typically each joint is driven by a motor through a gear reduction unit. Although the inertias of gears and rotors are relatively small, their effects on the dynamics of a manipulator can be significant. This is because their inertia effects, when reflected in the joint space, are functions of the squares or products of the gear ratios (Tsai and Chang, 1994). Therefore, a more accurate dynamical model should take

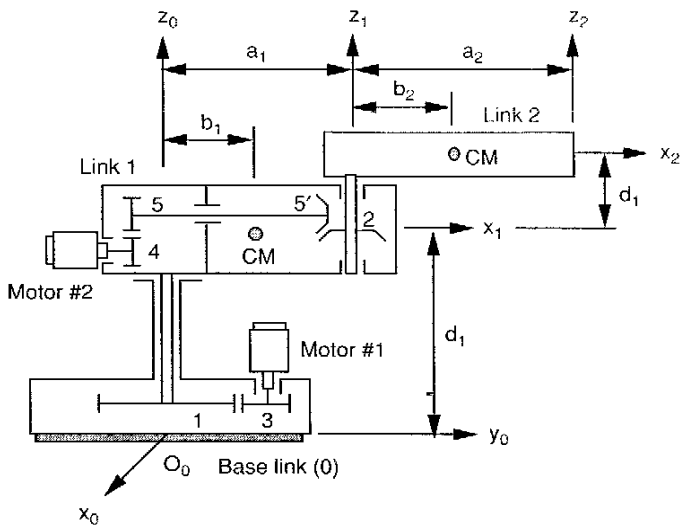


FIGURE 9.7. Schematic diagram of a geared 2-dof robot.

this into consideration. In this section we use a planar 2-dof manipulator as an example to illustrate the principle.

Figure 9.7 shows a geared planar 2-dof manipulator, where link 1 rotates with respect to the fixed base about the z_0 -axis, and link 2 rotates with respect to link 1 about the z_1 -axis. For brevity, only a few gears are shown. In practice, there may be multiple stages of gear reduction in each transmission line. As shown in the figure, motor 1 drives the first moving link through a gear pair attached to the shafts of motor 1 and link 1, and motor 2 drives link 2 through a spur gear pair attached to motor 2 and an intermediate shaft 5 followed by a bevel gear pair attached to the other end of the intermediate shaft 5 and link 2. Motor 1 is mounted on the fixed base, while motor 2 is mounted on the rear end of link 1. Assuming that the acceleration of gravity points in the negative z_0 -direction, we wish to develop a dynamical model for the manipulator.

9.9.1 Kinematic Analysis

In Chapter 7, we have shown that the kinematic analysis of geared robotic mechanisms can be achieved in two basic steps. The first step involves the identification of an *equivalent open-loop chain* and the derivation of a kine-

matic relationship between the location of the end effector and the joint angles of the equivalent open-loop chain. The second step involves the derivation of a kinematic relationship between the joint angles and the input actuator displacements. The kinematic relation between the end-effector location and the joint angles has been described in Chapter 2. In this section we apply the theory of fundamental circuits to derive the kinematic relation between the joint angles and the input actuator displacements. As shown in Fig. 9.7, the equivalent open-loop chain consists of three *primary links*: base link 0, link 1, and link 2. All the other links are called *secondary links*. Link 0 carries gear 3; link 1 carries gears 4 and 5; link 2 does not carry any secondary link.

We now apply the theory of fundamental circuits to derive the kinematic relationship between the joint angles and the input actuator displacements. There are three gear pairs. Link 0 serves as the carrier for the 3–1 gear pair; link 1 serves as the carrier for the 4–5 and 5'–2 gear pairs. Let N_{ij} be the gear ratio between gears i and j . The fundamental circuit equations can be written as

$$f(3, 1, 0) : \theta_{3,0} = -N_{13}\theta_{1,0}, \quad (9.149)$$

$$f(4, 5, 1) : \theta_{4,1} = -N_{54}\theta_{5,1}, \quad (9.150)$$

$$f(5', 2, 1) : \theta_{5,1} = -N_{25}\theta_{2,1}, \quad (9.151)$$

where $\theta_{i,j}$ denotes the relative rotation of link i with respect to link j .

Since $\theta_{1,0}$ and $\theta_{2,1}$ are the joint angles of the equivalent open-loop chain, we should express all the other angular displacements in terms of these two joint angles. Substituting Eq. (9.151) into (9.150) gives

$$\theta_{4,1} = N_{54}N_{25}\theta_{2,1}. \quad (9.152)$$

Combining Eqs. (9.149), (9.151), and (9.152), we obtain

$$\begin{bmatrix} \theta_{3,0} \\ \theta_{4,1} \\ \theta_{5,1} \end{bmatrix} = \begin{bmatrix} -N_{13} & 0 \\ 0 & N_{54}N_{25} \\ 0 & -N_{25} \end{bmatrix} \begin{bmatrix} \theta_1 \\ \theta_2 \end{bmatrix}. \quad (9.153)$$

For brevity, we have used θ_i to replace $\theta_{i,i-1}$ for $i = 1$ and 2 in Eq. (9.153). Hence, given the joint angles, one can compute the corresponding rotations of the rotors and the intermediate shaft.

9.9.2 Kinetic Energy of a Revolving Rotor

Before we formulate the dynamical equations of motion, we study the kinetic energy of a rotor j that is carried by a primary link i , as shown in Fig. 9.8. We

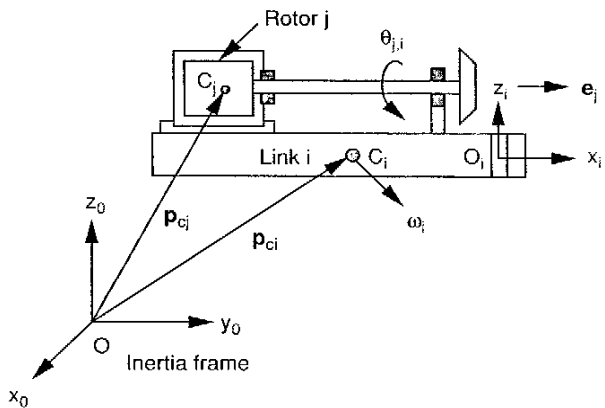


FIGURE 9.8. Typical rotor j that is carried by link i .

assume that the mass of the rotor is symmetrically distributed about its axis of rotation. This is a reasonable assumption, since rotors, gears, and shafts are all symmetric about their axes of rotation.

Let \mathbf{v}_{cj} be the absolute velocity of the center of mass of the rotor, ω_j the absolute angular velocity of the rotor, and I_j the inertia matrix of the rotor about its center of mass and expressed in the inertia frame. Then the kinetic energy of link j can be written as

$$K_j = \frac{1}{2} [\mathbf{v}_{cj}^T m_j \mathbf{v}_{cj} + \omega_j^T I_j \omega_j]. \quad (9.154)$$

The absolute angular velocity of link j can be expressed in terms of the absolute angular velocity of the carrier, ω_i , and the angular velocity of the rotor relative to the carrier; that is,

$$\omega_j = \omega_i + \dot{\theta}_{j,i} \mathbf{e}_j, \quad (9.155)$$

where \mathbf{e}_j denotes the direction of the rotor axis and $\dot{\theta}_{j,i}$ denotes the relative rotation of link j with respect to link i .

Substituting Eq. (9.155) into (9.154) and making use of the symmetric property of the inertia matrix, we obtain

$$K_j = \frac{1}{2} [\mathbf{v}_{cj}^T m_j \mathbf{v}_{cj} + \omega_i^T I_j \omega_i + 2\omega_i^T I_j \mathbf{e}_j \dot{\theta}_{j,i} + \mathbf{e}_j^T I_j \mathbf{e}_j \dot{\theta}_{j,i}^2]. \quad (9.156)$$

Here $\mathbf{e}_j^T I_j \mathbf{e}_j = I_{j,z}$ is called the *axial moment of inertia* of the rotor j . We observe that only the last two terms on the right-hand side of Eq. (9.156)

depend exclusively on the relative rotation of the rotor. For an axisymmetric rotor, the center of mass always lies on its axis of rotation and therefore can be considered as a point fixed on the carrier. Further, due to symmetry, the rotor inertia matrix, I_j , is invariant in the link frame i . Hence the contributions of the first two terms can conveniently be combined with link i to form an equivalent link. In this way, the inertia effects of a rotor due to its relative rotation with respect to the carrier can be written as

$$\hat{K}_j = \frac{1}{2} I_{j,z} \dot{\theta}_{j,i}^2 + I_{j,z} (\omega_i^T \mathbf{e}_j) \dot{\theta}_{j,i}. \quad (9.157)$$

In general, $\dot{\theta}_{j,i}$ is a linear function of the joint rates of the equivalent open-loop chain. For a manipulator with each joint individually driven by an actuator, $\dot{\theta}_{j,i}$ is related to the joint rate, $\dot{q}_{i+1,i}$, by a simple gear ratio, N . Substituting $\dot{\theta}_{j,i} = N\dot{q}_{i+1,i}$ into Eq. (9.157) gives

$$\hat{K}_j = \frac{1}{2} N^2 I_{j,z} \dot{q}_{i+1,i}^2 + N I_{j,z} (\omega_i^T \mathbf{e}_j) \dot{q}_{i+1,i}. \quad (9.158)$$

It is worth noting that the common wisdom of simply adding $N^2 I_{j,z}$ to the inertia of a robotic system is valid only if the carrier is stationary or its angular velocity is perpendicular to the rotor axis of rotation, $\omega_i^T \mathbf{e}_j = 0$.

9.9.3 Dynamic Analysis

In this section we perform the dynamic analysis of the example manipulator. First, we apply the recursive method to compute the angular velocity, the velocity of the center of mass, and the potential energy of each link. Then we substitute these quantities directly into Lagrange's equations of motion. We provide just sufficient information leading to the solution without detailed derivations.

The first equivalent link consists of link 1, rotor 4, intermediate shaft 5, and the gears attached to them. The second equivalent link consists of link 2 and the bevel gear attached to it. Let m_i be the mass of the equivalent link i . To simplify the analysis, we assume that the inertia matrix of an equivalent link i about its combined center of mass and expressed in the link i frame takes the following form:

$${}^i I_i = \begin{bmatrix} I_{i,x} & 0 & 0 \\ 0 & I_{i,y} & 0 \\ 0 & 0 & I_{i,z} \end{bmatrix}.$$

(a) Kinetic and Potential Energies of Link 1. The initial conditions of the base link are ${}^0 \omega_0 = {}^0 \mathbf{v}_0 = \mathbf{0}$. The angular velocity and the velocity of the center of mass of link 1 expressed in link 1 frame are

$${}^1 \omega_1 = \begin{bmatrix} 0 \\ 0 \\ \dot{\theta}_1 \end{bmatrix},$$

$${}^1 \mathbf{v}_{c1} = \begin{bmatrix} 0 \\ b_1 \dot{\theta}_1 \\ 0 \end{bmatrix},$$

where b_1 locates the combined center of mass of link 1 along the x_1 -axis as shown in Fig. 9.7. Note that the acceleration information is not needed for the Lagrangian formulation. Therefore, the kinetic energy of link 1 is given by

$$K_1 = \frac{1}{2} {}^1 \mathbf{v}_{c1}^T m_1 {}^1 \mathbf{v}_{c1} + \frac{1}{2} {}^1 \omega_1^T {}^1 I_1 {}^1 \omega_1 = \frac{1}{2} (m_1 b_1^2 + I_{1,z}) \dot{\theta}_1^2, \quad (9.159)$$

and the potential energy of link 1 is given by

$$U_1 = m_1 g_c d_1. \quad (9.160)$$

(b) Kinetic and Potential Energies of Link 2. The angular velocity and the linear velocity of the combined center of mass of link 2 are computed and expressed in frame 2 as

$${}^2 \omega_2 = \begin{bmatrix} 0 \\ 0 \\ \dot{\theta}_1 + \dot{\theta}_2 \end{bmatrix},$$

$${}^2 \mathbf{v}_{c2} = \begin{bmatrix} a_1 s \theta_2 \dot{\theta}_1 \\ a_1 c \theta_2 \dot{\theta}_1 + b_2 (\dot{\theta}_1 + \dot{\theta}_2) \\ 0 \end{bmatrix},$$

where b_2 locates the combined center of mass of link 2 along the x_2 -axis as shown in Fig. 9.7. Therefore, the kinetic energy of link 2 is given by

$$K_2 = \frac{1}{2} {}^2 \mathbf{v}_{c2}^T m_2 {}^2 \mathbf{v}_{c2} + \frac{1}{2} {}^2 \omega_2^T {}^2 I_2 {}^2 \omega_2$$

$$= \frac{1}{2} m_2 [a_1^2 \dot{\theta}_1^2 + b_2^2 (\dot{\theta}_1 + \dot{\theta}_2)^2 + 2a_1 b_2 c \theta_2 \dot{\theta}_1 (\dot{\theta}_1 + \dot{\theta}_2)] + \frac{1}{2} I_{2,z} (\dot{\theta}_1 + \dot{\theta}_2)^2, \quad (9.161)$$

and the potential energy of link 2 is given by

$$U_2 = m_2 g_c (d_1 + d_2). \quad (9.162)$$

(c) Kinetic Energies of the Rotors and Gears. We note that $\omega_i^T \mathbf{e}_j = 0$ for both $i = 0$ and 1. Substituting Eq. (9.153) into (9.157), we obtain the

additional kinetic energies contributed by the rotors and gears:

$$K_r = \frac{1}{2} [N_{13}^2 I_{3,z} \dot{\theta}_1^2 + (N_{54}^2 I_{4,z} + I_{5,z}) N_{25}^2 \dot{\theta}_2^2]. \quad (9.163)$$

(d) Lagrangian Function and Its Derivatives. Substituting Eqs. (9.159) through (9.163) into (9.75), we obtain the Lagrangian function

$$L = \frac{1}{2} [(\kappa_1 + 2m_2 a_1 b_2 c \theta_2) \dot{\theta}_1^2 + \kappa_2 \dot{\theta}_2^2 + 2(\kappa_4 + m_2 a_1 b_2 c \theta_2) \dot{\theta}_1 \dot{\theta}_2] - m_1 g_c d_1 - m_2 g_c (d_1 + d_2), \quad (9.164)$$

where

$$\begin{aligned}\kappa_1 &= \kappa_3 + \kappa_4 + N_{13}^2 I_{3,z} + m_2 a_1^2, \\ \kappa_2 &= \kappa_4 + N_{54}^2 N_{25}^2 I_{4,z} + N_{25}^2 I_{5,z}, \\ \kappa_3 &= I_{1,z} + m_1 b_1^2, \\ \kappa_4 &= I_{2,z} + m_2 b_2^2.\end{aligned}$$

We note that κ_3 represents the mass moment of inertia of link 1 about the z_0 -axis, and κ_4 represents the mass moment of inertia of link 2 about the z_1 -axis. The effects of rotor and gear inertias are clearly shown as functions of the squares of their respective gear ratios.

Taking the partial derivatives of L with respect to θ_1 , θ_2 , $\dot{\theta}_1$ and $\dot{\theta}_2$ yields

$$\frac{\partial L}{\partial \theta_1} = 0, \quad (9.165)$$

$$\frac{\partial L}{\partial \theta_2} = -m_2 a_1 b_2 s \theta_2 \dot{\theta}_1 (\dot{\theta}_1 + \dot{\theta}_2), \quad (9.166)$$

$$\frac{\partial L}{\partial \dot{\theta}_1} = (\kappa_1 + 2m_2 a_1 b_2 c \theta_2) \dot{\theta}_1 + (\kappa_4 + m_2 a_1 b_2 c \theta_2) \dot{\theta}_2, \quad (9.167)$$

$$\frac{\partial L}{\partial \dot{\theta}_2} = \kappa_2 \dot{\theta}_2 + (\kappa_4 + m_2 a_1 b_2 c \theta_2) \dot{\theta}_1. \quad (9.168)$$

Taking the total derivatives of Eqs. (9.167) and (9.168) with respect to time yields

$$\begin{aligned}\frac{d}{dt} \left(\frac{\partial L}{\partial \dot{\theta}_1} \right) &= (\kappa_1 + 2m_2 a_1 b_2 c \theta_2) \ddot{\theta}_1 + (\kappa_4 + m_2 a_1 b_2 c \theta_2) \ddot{\theta}_2 \\ &\quad - m_2 a_1 b_2 s \theta_2 \dot{\theta}_2 (2\dot{\theta}_1 + \dot{\theta}_2),\end{aligned} \quad (9.169)$$

$$\frac{d}{dt} \left(\frac{\partial L}{\partial \dot{\theta}_2} \right) = (\kappa_4 + m_2 a_1 b_2 c \theta_2) \ddot{\theta}_1 + \kappa_2 \ddot{\theta}_2 - m_2 a_1 b_2 s \theta_2 \dot{\theta}_1 \dot{\theta}_2. \quad (9.170)$$

(e) Lagrange's Equations of Motion. Substituting Eqs. (9.165), (9.166), (9.169), and (9.170) into (9.76) produces Lagrange's equations of motion as

$$M(\theta) \ddot{\theta} + \mathbf{V}(\theta, \dot{\theta}) + \mathbf{G}(\theta) = \boldsymbol{\tau}, \quad (9.171)$$

where

$$\theta = \begin{bmatrix} \theta_1 \\ \theta_2 \end{bmatrix},$$

$$M(\theta) = \begin{bmatrix} \kappa_1 + 2m_2 a_1 b_2 c \theta_2 & \kappa_4 + m_2 a_1 b_2 c \theta_2 \\ \kappa_4 + m_2 a_1 b_2 c \theta_2 & \kappa_2 \end{bmatrix},$$

$$\mathbf{V}(\theta, \dot{\theta}) = \begin{bmatrix} -m_2 a_1 b_2 s \theta_2 \dot{\theta}_2 (2\dot{\theta}_1 + \dot{\theta}_2) \\ m_2 a_1 b_2 s \theta_2 \dot{\theta}_1^2 \end{bmatrix},$$

$$\mathbf{G}(\theta) = \begin{bmatrix} 0 \\ 0 \end{bmatrix}.$$

Equation (9.171) is the dynamical model for the two-link manipulator. Although the rotor inertias may be small, their effects can be significant since they are multiplied by the squares or products of the gear ratios. A gear reduction on the order of 50 to 100 is commonly used in an industrial robot. For example, for a gear ratio of 60, the inertia of a rotor will be multiplied by 3600.

9.10 END-EFFECTOR SPACE DYNAMICAL EQUATIONS

In previous sections we have derived the dynamical equations of motion in terms of the joint angles, \mathbf{q} , or in the *joint space*. We assume that a desired trajectory of the end effector can be expressed in terms of the joint angles, velocities, and accelerations. Based on the joint space formulation, various control schemes have been developed. However, in practice, we often wish to program the end-effector trajectories in the Cartesian space, \mathbf{x} , and for the joint-based control schemes to work these Cartesian space trajectories should be converted into joint space trajectories. Theoretically, the conversion can be accomplished by applying

$$\begin{aligned}\mathbf{q}_d &= \text{inverse kinematics of } \mathbf{x}_d, \\ \dot{\mathbf{q}}_d &= J^{-1} \dot{\mathbf{x}}_d, \\ \ddot{\mathbf{q}}_d &= J^{-1} \ddot{\mathbf{x}}_d + J^{-1} \ddot{\mathbf{x}}_d,\end{aligned} \quad (9.172)$$

where J is the Jacobian matrix and the subscript d is used to indicate a desired quantity.

In reality, it is quite difficult to compute the equations above efficiently for real-time control purpose. Therefore, usually only the desired joint angles, $\dot{\mathbf{q}}_d$, are computed from the inverse kinematics, and the joint velocities and accelerations are computed numerically by the first and second differences. However, for certain control techniques (Khatib, 1983), it may be desirable to express the dynamical equations in the *end-effector space*. This can be accomplished by the following procedure.

The end-effector velocity is related to the joint velocity by

$$\dot{\mathbf{x}} = J\dot{\mathbf{q}}. \quad (9.173)$$

Assuming that J is a nonsingular square matrix, we substitute the inverse transformation of Eq. (9.173) into (9.87) to obtain an expression for the kinetic energy in terms of the end-effector velocity:

$$K = \frac{1}{2}\dot{\mathbf{x}}^T \tilde{M} \dot{\mathbf{x}}, \quad (9.174)$$

where

$$\tilde{M} = (J^{-1})^T M J^{-1}, \quad (9.175)$$

is the manipulator inertia matrix expressed in the end-effector space. We refer to \tilde{M} as the *end-effector space inertia matrix* or *Cartesian inertia matrix*.

Taking the derivative of Eq. (9.173) with respect to time yields

$$\ddot{\mathbf{x}} = J\ddot{\mathbf{q}} + \dot{J}\dot{\mathbf{q}}. \quad (9.176)$$

Multiplying both sides of Eq. (9.176) by J^{-1} and rearranging yields

$$\ddot{\mathbf{q}} = J^{-1}(\ddot{\mathbf{x}} - \dot{J}\dot{\mathbf{q}}). \quad (9.177)$$

Multiplying Eq. (9.103) by J^{-T} and then substituting Eqs. (9.175) and (9.177) into the resulting equation, we obtain

$$\tilde{M}\ddot{\mathbf{x}} + \tilde{\mathbf{V}} + \tilde{\mathbf{G}} = \tilde{\mathbf{Q}}, \quad (9.178)$$

where

$$\tilde{\mathbf{V}} = J^{-T}(\mathbf{V} - MJ^{-1}\dot{J}\dot{\mathbf{q}}),$$

$$\tilde{\mathbf{G}} = J^{-T}\mathbf{G},$$

$$\tilde{\mathbf{Q}} = J^{-T}\mathbf{Q}.$$

Hence once the dynamical equations are derived in the joint space, they can be converted into the end-effector space. Although the equations of motion

above are expressed in the end-effector space, some of the terms, such as $\tilde{\mathbf{V}}$, $\tilde{\mathbf{G}}$, and $\tilde{\mathbf{Q}}$, are still written as functions of the joint variables, $\dot{\mathbf{q}}$. Due to the nonlinearity of the inverse kinematics, it is practically impossible to express everything in terms of the end-effector variables, \mathbf{x} . We note that as the robot arm approaches a singular configuration, the Jacobian matrix is not invertible and certain quantities in the end-effector space become very large.

9.11 SUMMARY

In this chapter we first reviewed the inertia properties, the momentum, and the kinetic energy of a rigid body. It was shown that the angular momentum and the kinetic energy of a rigid body can be divided into two parts: one associated with the motion of the center of mass and the other with the motion of the rigid body about its center of mass. Next, we reviewed the Newton–Euler laws. Both the Newton and Euler equations of motion were derived. Then we presented two methods for the dynamical analysis of serial manipulators. The recursive Newton–Euler formulation consists of a forward computation followed by a backward computation. In the forward computation, link velocities and accelerations are calculated, one link at a time, from link 1 to link n , using the kinematical equations derived in Chapter 4. In the backward computation, joint reaction forces are calculated one link at a time from link n back to link 1 using the Newton–Euler equations of motion. Although the recursive method is more tedious, it renders all the joint reaction forces that may be useful for sizing the links and bearings during the design phase. Lagrange’s method formulates the problem with all the forces of constraint eliminated at the outset. The link Jacobian submatrices, the manipulator inertia matrix, and the derivation of the generalized forces have been described and a general matrix form of the dynamical equations of motion was presented. The effects of rotor inertia were also discussed. It has been shown that rotor inertias, which have been ignored in most textbooks, may have significant effects on the dynamics of a manipulator. Finally, the transformation of dynamical equations into the end-effector space was described briefly.

REFERENCES

- Armstrong, W. M., 1979, “Recursive Solution to the Equations of Motion of an N-link Manipulator,” *Proc. 5th World Congress on the Theory of Machines and Mechanisms*, Vol. 2, pp. 1343–1346.
- Armstrong-Helouvry, B., 1991, *Control of Machines with Friction*, Kluwer Academic Publishers, Boston.

- Computer Aided Design Software, Inc., CADSI, 1995, *DADS User's Manual, Rev. 8*, Oakdale, IA.
- Frisch, H. P., 1974, "A Vector-Dyadic Development of the Equations of Motion for N -Coupled Rigid Bodies and Point Masses" (NBOD2), NASA TN D-7767, NASA, Washington, DC.
- Fu, K. S., Gonzalez, R. C., and Lee, C. S. G., 1987, *Robotics: Control, Sensing, Vision, and Intelligence*, McGraw-Hill, New York.
- Goldstein, H., 1980, *Classical Mechanics*, 2nd ed., Addison-Wesley, Reading, MA.
- Haug, E. J., 1989, *Computer Aided Kinematics and Dynamics of Mechanical Systems*, Allyn and Bacon, Needham Heights, MA.
- Hollerbach, J. M., 1980, "A Recursive Lagrangian Formulation of Manipulator Dynamics and a Comparative Study of Dynamics Formulation Complexity," *IEEE Trans. Syst. Man Cybern.*, Vol. SMC-10, No. 11, pp. 730-736.
- Kane, T. R. and Levinson, D. A., 1980, "Formulation of Equations of Motion for Complex Spacecraft," *J. Guidance Control*, Vol. 3, pp. 99-112.
- Kane, T. R. and Levinson, D. A., 1985, *Dynamics: Theory and Application*, McGraw-Hill, New York.
- Khatib, O., 1983, "Commande dynamique dans l'espace opérationnel des robots manipulateurs en présence d'obstacles," Docteur Ingénieur Thèse, École Nationale Supérieure de l'Aéronautique et de L'Espace, Toulouse, France.
- Lee, C. S. G., Lee, B. H., and Nigam, R., 1983, "Development of the Generalized d'Alembert Equations of Motion for Mechanical Manipulators," *Proc. 22nd Conference on Decision and Control*, San Antonio, TX, pp. 1205-1210.
- Luh, J. Y. S., Walker, M. W., and Paul, R. P., 1980, "On-Line Computational Scheme for Mechanical Manipulators," *ASME J. Dyn. Syst. Meas. Control*, Vol. 120, pp. 69-76.
- Mechanical Dynamics, Inc., MDI, 1981, *User's Guide to ADAMS*, Ann Arbor, MI.
- Orin, D. E., McGhee, R. B., Vukobratovic, M., and Hartoch, G., 1979, "Kinematic and Kinetic Analysis of Open-Chain Linkages Utilizing Newton-Euler Methods," *Math. Biosci.*, Vol. 43, pp. 107-130.
- Paul, B., 1979, *Kinematics and Dynamics of Planar Machinery*, Prentice Hall, Upper Saddle River, NJ.
- Paul, R. P., 1981, *Robot Manipulators: Mathematics, Programming and Control*, MIT Press, Cambridge, MA.
- Roberson, R. E. and Schwertassek, R., 1988, *Dynamics of Multibody Systems*, Springer-Verlag, New York.
- Rosenthal, D. E. and Sherman, M. A., 1983, "Symbolic Multibody Equations via Kane's Method," (SD-EXACT) AIAA Paper 83-803, *Proc. AAS/AIAA Astrodynamics Special Conference*, pp. 1-20.
- Sheth, P. N. and Uicker, J. J., 1972, "IMP (Integrated Mechanisms Program): A Computer-Aided Design Analysis System for Mechanisms and Linkages," *ASME J. Eng. Ind.*, Vol. 94, pp. 454-464.

- Tsai, L. W. and Chang, S. L., 1994, "Backlash Control via Redundant Drives: An Experimental Verification," *ASME J. Mech. Des.*, Vol. 116, No. 3, pp. 963-967.
- Uicker, J. J., 1965, "On the Dynamic Analysis of Spatial Linkages Using 4×4 Matrices," Ph.D. dissertation, Northwestern University, Evanston, IL.

EXERCISES

- Derive the parallel axis theorem given by Eq. (9.9).
- The inertia matrix of a rectangular bar about a center-of-mass coordinate frame, (x_c, y_c, z_c) , is given by Eq. (9.12). What is the inertia matrix about O expressed in the (x, y, z) coordinate frame, as shown in Fig. 9.9?

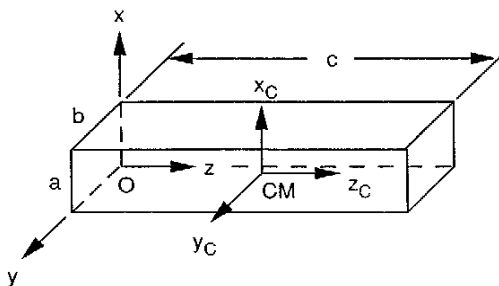


FIGURE 9.9. Inertia matrix of a rectangular bar.

- The inertia matrix of a rectangular bar about a center-of-mass coordinate frame, (x_c, y_c, z_c) , is given by Eq. (9.12). What is the inertia matrix about the center of mass and expressed in an (x, y, z) coordinate frame that is rotated with respect to the (x_c, y_c, z_c) frame by an angle ϕ about the z_c -axis, as shown in Fig. 9.10?

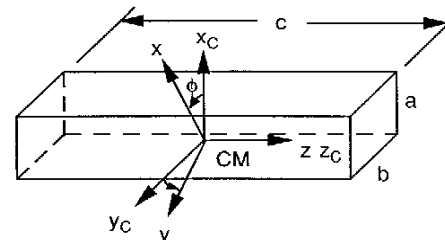


FIGURE 9.10. Inertia matrix of a rectangular bar.

4. Figure 9.11 shows a 2-dof 2R pointer, in which the first joint axis points up vertically along the positive z_0 -axis and the second joint axis intersects the first perpendicularly. Assuming that the second moving link is a slender homogeneous rod of mass m , what is the inertia matrix of this link about O expressed in the (x_0, y_0, z_0) coordinate frame?

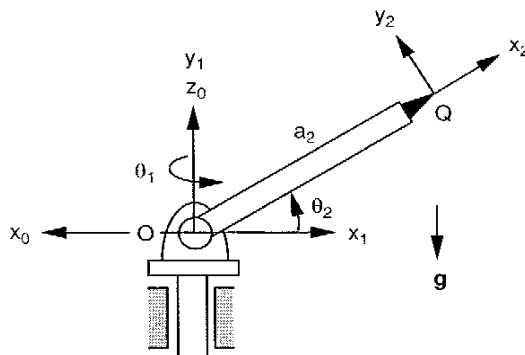


FIGURE 9.11. A 2-dof pointer.

5. Consider the 2-dof 2R pointer shown in Fig. 9.11. Assuming that the inertia of the first moving link is negligible and that the second moving link is a slender homogeneous rod of mass m , calculate the angular momentum of the system about the origin O expressed in the (x_0, y_0, z_0) coordinate frame.
6. Show that when the axes of a center-of-mass coordinate system coincide with the principal axes of a rigid body, Euler's equations of motion reduce to Eq. (9.48).
7. For the 2-dof 2R pointer shown in Fig. 9.11, assume that the inertia of the first moving link is negligible and that the second moving link is a slender homogeneous rod of mass m . Develop the dynamical equations of motion by the recursive Newton–Euler method. Identify the contributions due to Coriolis, centrifugal, and gravitational effects.
8. For the planar 3-dof manipulator shown in Fig. 2.3, assume that the acceleration of gravity points in the negative z_0 -direction and that the three moving links are slender homogeneous rods of masses m_1 , m_2 , and m_3 , respectively. Derive the dynamical equations of motion by the recursive Newton–Euler method. Express the resulting equations in matrix form.

9. Figure 9.12 shows a spatial 3-dof, 3R manipulator in which the second joint axis intersects the first perpendicularly and the third joint axis is parallel to the second. Assuming that the link inertias are negligible and that there is a point mass m attached to the end effector at point Q , derive the dynamical equations of motion by the recursive Newton–Euler method.

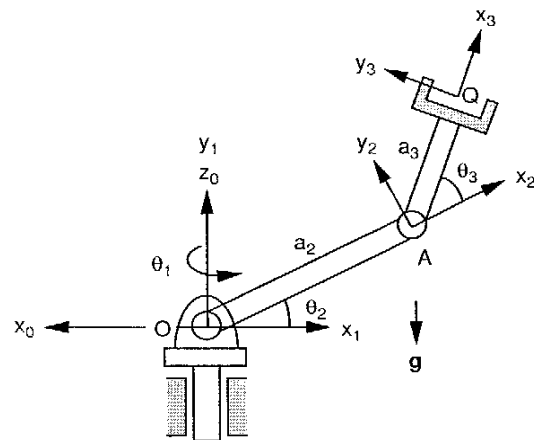


FIGURE 9.12. Spatial 3-dof, 3R manipulator.

10. Consider the 2-dof pointer shown in Fig. 9.11. Assuming that the inertia of the first moving link is negligible and that the second moving link is a slender homogeneous rod of mass m , derive the dynamical equations of motion by the Lagrangian method using θ_1 and θ_2 as the generalized coordinates.
11. Describe two possible sets of generalized coordinates for the spatial 3R manipulator shown in Fig. 9.12.
12. Derive the dynamical equations of motion for the spatial 3-dof manipulator shown in Fig. 9.12 by the Lagrangian method, assuming that the link inertias are negligible and that there is a point mass m attached to the end effector at point Q .

CHAPTER 10

DYNAMICS OF PARALLEL MANIPULATORS

10.1 INTRODUCTION

In this chapter we investigate the dynamics of parallel manipulators such as the VARIAX machining center developed by Giddings & Lewis, shown in Fig. 10.1. While the kinematics of parallel manipulators have been studied extensively during the last two decades, fewer papers can be found on the dynamics of parallel manipulators. The dynamical analysis of parallel manipulators is complicated by the existence of multiple closed-loop chains. Several approaches have been proposed, including the Newton–Euler formulation (Do and Yang, 1988; Guglielmetti and Longchamp, 1994; Tsai and Kohli, 1990), the Lagrangian formulation (Lebret et al., 1993; Miller and Clavel, 1992; Pang and Shahingpoor, 1994), and the principle of virtual work (Codourey and Burdet, 1997; Miller, 1995; Tsai, 1998; Wang and Gosselin, 1997; Zhang and Song, 1993). Other approaches have also been suggested (Baiges and Duffy, 1996; Freeman and Tesar, 1988; Luh and Zheng, 1985; Murray and Lovell, 1989; Sugimoto, 1987).

The traditional Newton–Euler formulation requires the equations of motion to be written once for each body of a manipulator, which inevitably leads to a large number of equations and results in poor computational efficiency. The Lagrangian formulation eliminates all of the unwanted reaction forces and moments at the outset. It is more efficient than the Newton–Euler formulation. However, because of the numerous constraints imposed by closed loops of a parallel manipulator, deriving explicit equations of motion in terms

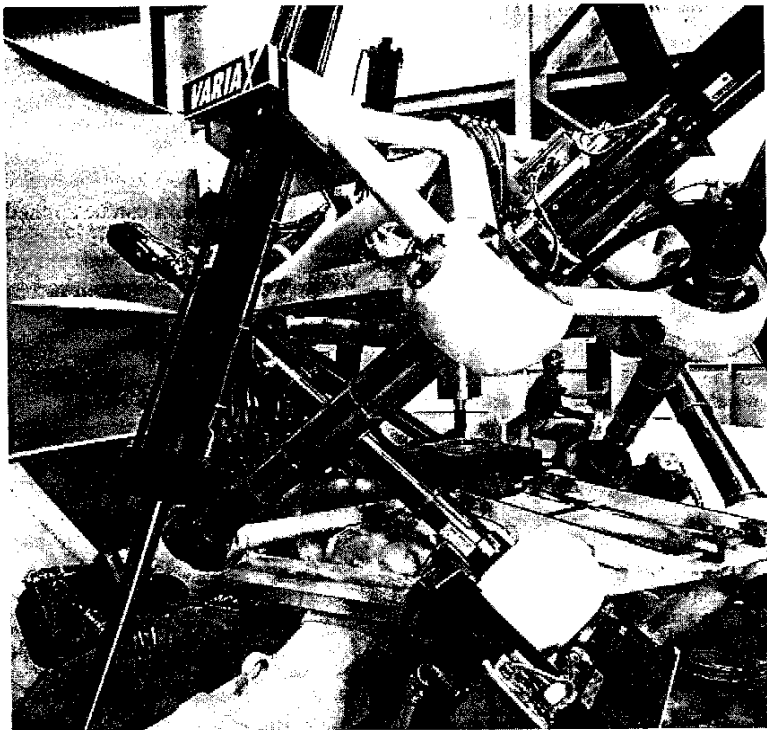


FIGURE 10.1. VARIAX® machining center. (Courtesy of Giddings & Lewis Machine Tools, Fond du Lac, Wisconsin.)

of a set of independent generalized coordinates becomes a prohibitive task. To simplify the problem, additional coordinates along with a set of Lagrangian multipliers are often introduced. In some cases, limbs are approximated by point masses by arguing that such approximation does not introduce significant modeling errors (Lebret et al., 1993; Pfreundschuh et al., 1994; Stamper, 1997; Stamper and Tsai, 1998). In this regard, the principle of virtual work appears to be the most efficient method of analysis. A comparison study of the inverse dynamics of manipulators with closed-loop geometry can be found in the work of Lin and Song (1990).

In this chapter we first describe the Newton–Euler method of analysis for parallel manipulators. Then we present a more efficient technique using the

principle of virtual work. Finally, we show that the dynamical model of some simple parallel manipulators can be developed by the Lagrangian formulation.

10.2 NEWTON-EULER FORMULATION

In this section we illustrate how Newton and Euler's equations can be applied for the dynamical analysis of a Stewart-Gough platform.

10.2.1 Kinematics of a Stewart-Gough Platform

Figure 10.2 shows the schematic diagram of a Stewart-Gough platform, studied in Chapters 3 and 5. For the purpose of analysis, we attach a coordinate

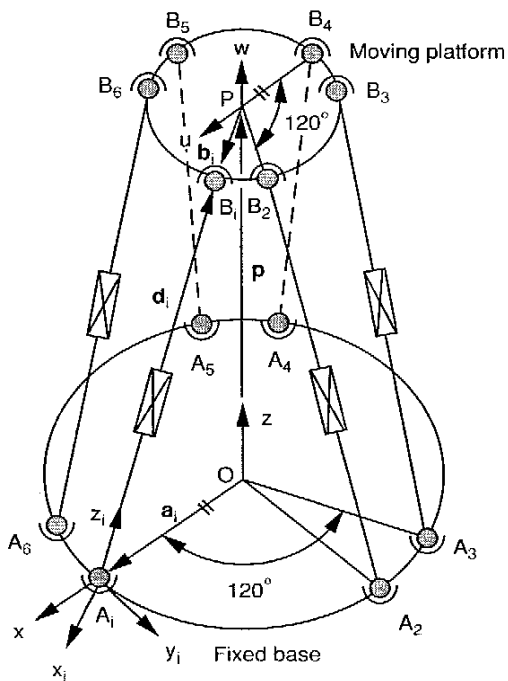


FIGURE 10.2. Schematic diagram of a Stewart-Gough platform.

frame $A(x, y, z)$ to the fixed base and another coordinate frame $B(u, v, w)$ to the moving platform. The $x-y$ plane contains the ball joints A_i , for $i = 1$ to 6, and the $u-v$ plane contains the ball joints B_i , for $i = 1$ to 6. The origin of the moving frame B is located at the centroid, P , of the moving platform, whereas the origin of the fixed frame A is located at the centroid, O , of the fixed base. Each of the six limbs is denoted by a vector d_i . Furthermore, we attach a coordinate frame $C(x_i, y_i, z_i)$ to each limb with the origin located at A_i . The z_i -axis points from A_i to B_i . The y_i -axis is parallel to the cross product of two unit vectors along the z_i and z axes, and the x_i -axis is defined by the right-hand rule.

For the inverse dynamics problem, the time history of a desired trajectory is given and the problem is to determine the actuator forces and/or torques required to produce that motion. The time history of the moving platform can be described by a position vector of the centroid, \mathbf{p} , and three Euler angles, ϕ , θ , and ψ . The velocity and acceleration of the centroid P are obtained by taking the derivatives of \mathbf{p} with respect to time; that is, $\mathbf{v}_p = \dot{\mathbf{p}}$ and $\ddot{\mathbf{v}}_p = \ddot{\mathbf{p}}$.

Let the three Euler angles be defined as a rotation of ϕ about the z -axis, followed by a second rotation of θ about the rotated v -axis, and a third rotation of ψ about the rotated w -axis. Then the rotation matrix of the moving platform relative to the fixed base is given by

$${}^A R_B = \begin{bmatrix} c\phi c\theta c\psi - s\phi s\psi & -c\phi c\theta s\psi - s\phi c\psi & c\phi s\theta \\ s\phi c\theta c\psi + c\phi s\psi & -s\phi c\theta s\psi + c\phi c\psi & s\phi s\theta \\ -s\theta c\psi & s\theta s\psi & c\theta \end{bmatrix}. \quad (10.1)$$

The angular velocity of the moving platform, $\boldsymbol{\omega}_p$, written in terms of the Euler angles and the body-fixed \mathbf{w} , \mathbf{v}' , and \mathbf{w}'' unit vectors, is

$$\boldsymbol{\omega}_p = \dot{\phi}\mathbf{w} + \dot{\theta}\mathbf{v}' + \dot{\psi}\mathbf{w}''. \quad (10.2)$$

In Eq. (10.2), \mathbf{w} , \mathbf{v}' , and \mathbf{w}'' are not orthogonal. Expressing \mathbf{w} , \mathbf{v}' , and \mathbf{w}'' in the fixed reference frame A , we obtain

$$\boldsymbol{\omega}_p = \begin{bmatrix} \dot{\psi}c\phi s\theta - \dot{\theta}s\phi \\ \dot{\psi}s\phi s\theta + \dot{\theta}c\phi \\ \dot{\psi}c\theta + \dot{\phi} \end{bmatrix}. \quad (10.3)$$

The angular acceleration of the moving platform is obtained by taking the derivative of Eq. (10.3) with respect to time:

$$\dot{\boldsymbol{\omega}}_p = \begin{bmatrix} \ddot{\psi}c\phi s\theta - \dot{\psi}\dot{\phi}s\phi s\theta + \dot{\psi}\dot{\theta}c\phi c\theta - \ddot{\theta}s\phi - \dot{\theta}\dot{\phi}c\phi \\ \ddot{\psi}s\phi s\theta + \dot{\psi}\dot{\phi}c\phi s\theta + \dot{\psi}\dot{\theta}s\phi c\theta + \ddot{\theta}c\phi - \dot{\theta}\dot{\phi}s\phi \\ \ddot{\psi}c\theta - \dot{\psi}\dot{\theta}s\theta + \ddot{\phi} \end{bmatrix}. \quad (10.4)$$

Both ω_p and $\dot{\omega}_p$ in Eqs. (10.3) and (10.4) are expressed in the fixed frame A . These two vectors can be transformed into the moving frame B by premultiplying ${}^A R_B^\top$.

(a) Position Analysis. First, we derive the location of each limb in terms of the location of the moving platform. Referring to Fig. 10.2, a vector-loop equation can be written as

$$\mathbf{a}_i + d_i \mathbf{s}_i = \mathbf{p} + \mathbf{b}_i, \quad (10.5)$$

where $\mathbf{a}_i = [a_{ix}, a_{iy}, 0]^\top$ denotes the position vector of A_i with respect to the fixed frame, ${}^B \mathbf{b}_i = [b_{ix}, b_{iy}, 0]^\top$ denotes the position vector of B_i with respect to the moving frame, $\mathbf{b}_i = [b_{ix}, b_{iy}, b_{iz}]^\top$ represents the vector ${}^B \mathbf{b}_i$ expressed in the fixed frame (i.e., $\mathbf{b}_i = {}^A R_B {}^B \mathbf{b}_i$), \mathbf{s}_i is a unit vector pointing from A_i to B_i , and d_i is the length of limb i . Solving Eq. (10.5) for \mathbf{s}_i , we obtain

$$\mathbf{s}_i = \frac{\mathbf{p} + \mathbf{b}_i - \mathbf{a}_i}{d_i}, \quad (10.6)$$

where

$$d_i = |\mathbf{p} + \mathbf{b}_i - \mathbf{a}_i|. \quad (10.7)$$

Assuming that each limb is connected to the fixed base by a universal joint such that it cannot rotate about the longitudinal axis, the orientation of limb i with respect to the fixed base can be described by two Euler angles, namely a rotation of ϕ_i about the z_i -axis resulting in a (x'_i, y'_i, z'_i) system, followed by another rotation of θ_i about the rotated y'_i -axis as shown in Fig. 10.3. Hence the rotation matrix of the i th limb can be written as

$${}^A R_i = \begin{bmatrix} c\phi_i c\theta_i & -s\phi_i & c\phi_i s\theta_i \\ s\phi_i c\theta_i & c\phi_i & s\phi_i s\theta_i \\ -s\theta_i & 0 & c\theta_i \end{bmatrix}. \quad (10.8)$$

The unit vector \mathbf{s}_i expressed in the i th limb frame is given by

$${}^i \mathbf{s}_i = \begin{bmatrix} 0 \\ 0 \\ 1 \end{bmatrix}. \quad (10.9)$$

Upon substitution of ${}^i \mathbf{s}_i$ into $\mathbf{s}_i = {}^A R_i {}^i \mathbf{s}_i$, we obtain

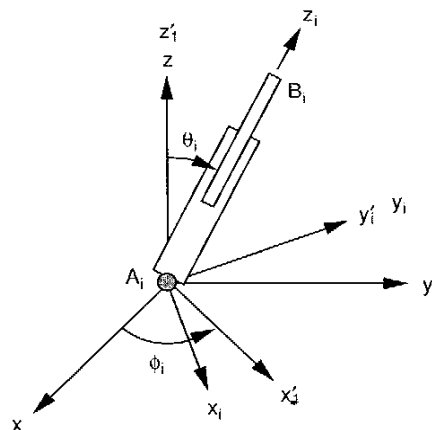


FIGURE 10.3. Euler angles of a limb.

$$\mathbf{s}_i = \begin{bmatrix} c\phi_i s\theta_i \\ s\phi_i s\theta_i \\ c\theta_i \end{bmatrix}. \quad (10.10)$$

Solving Eq. (10.10) for θ_i and ϕ_i yields

$$\begin{aligned} c\theta_i &= s_{iz}, \\ s\theta_i &= \sqrt{s_{ix}^2 + s_{iy}^2} \quad (0 \leq \theta \leq \pi), \\ s\phi_i &= s_{iy}/s\theta_i, \\ c\phi_i &= s_{ix}/s\theta_i, \end{aligned} \quad (10.11)$$

where s_{ix} , s_{iy} , and s_{iz} are the x , y , and z components of \mathbf{s}_i . Equations (10.6) and (10.11) together determine the direction and Euler angles of the i th limb in terms of the moving platform location.

As shown in Fig. 10.4, each limb consists of a cylinder (link 1) and a piston (link 2). Let e_1 be the distance between A_i and the center of mass of the i th cylinder, and let e_2 be the distance between B_i and the center of mass of the i th piston. Then the position vectors of the centers of mass of the i th cylinder and piston, \mathbf{r}_{1i} and \mathbf{r}_{2i} , can be written as

$$\mathbf{r}_{1i} = \mathbf{a}_i + e_1 \mathbf{s}_i \quad (10.12)$$

$$\mathbf{r}_{2i} = \mathbf{a}_i + (d_i - e_2) \mathbf{s}_i. \quad (10.13)$$

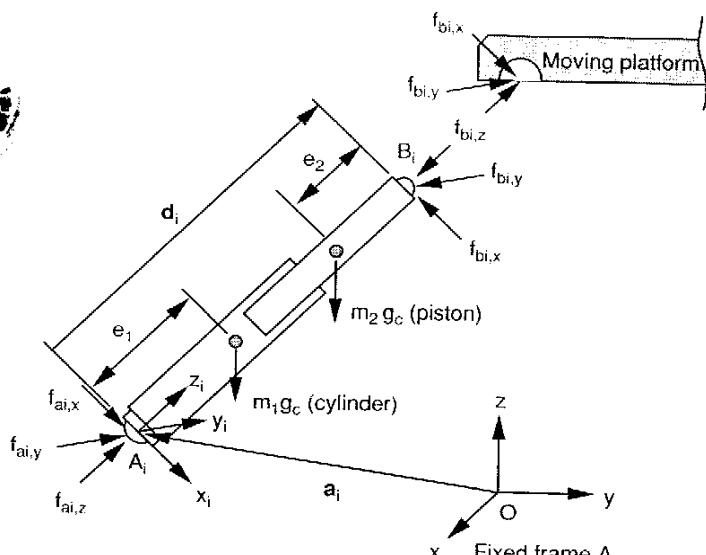


FIGURE 10.4. Free-body diagram of a typical limb.

(b) Velocity Analysis. Next, we compute the linear and angular velocities of each limb in terms of the velocity and angular velocity of the moving platform. The velocity of a ball point B_i , denoted as \mathbf{v}_{bi} , is found by taking the time derivative of the right-hand side of Eq. (10.5):

$$\mathbf{v}_{bi} = \mathbf{v}_p + \boldsymbol{\omega}_p \times \mathbf{b}_i. \quad (10.14)$$

Transforming \mathbf{v}_{bi} to the i th limb frame yields

$${}^i\mathbf{v}_{bi} = {}^iR_A \mathbf{v}_{bi}, \quad (10.15)$$

where ${}^i\mathbf{v}_{bi} = [{}^i\mathbf{v}_{bix}, {}^i\mathbf{v}_{biy}, {}^i\mathbf{v}_{biz}]^T$ denotes the velocity of B_i expressed in the i th limb frame, and ${}^iR_A = {}^A\mathbf{R}_i^T$.

The velocity of B_i can also be written in terms of the angular velocity of the i th limb by taking the derivative of the left-hand side of Eq. (10.5) with respect to time:

$${}^i\mathbf{v}_{bi} = d_i {}^i\boldsymbol{\omega}_i \times {}^i\mathbf{s}_i + \dot{d}_i {}^i\mathbf{s}_i. \quad (10.16)$$

Dot-multiplying both sides of Eq. (10.16) by ${}^i\mathbf{s}_i$ yields

$$\dot{d}_i = {}^i\mathbf{v}_{bix}. \quad (10.17)$$

Since each limb does not spin about its longitudinal axis, ${}^i\boldsymbol{\omega}_i \cdot {}^i\mathbf{s}_i = 0$. Cross-multiplying both sides of Eq. (10.16) by \mathbf{s}_i , we obtain the angular velocity of limb i :

$${}^i\boldsymbol{\omega}_i = \frac{1}{d_i} ({}^i\mathbf{s}_i \times {}^i\mathbf{v}_{bi}) = \frac{1}{d_i} \begin{bmatrix} -{}^i\mathbf{v}_{biy} \\ {}^i\mathbf{v}_{bix} \\ 0 \end{bmatrix}. \quad (10.18)$$

Once the angular velocity of the i th limb is found, the velocities of the centers of mass of the i th cylinder and piston, ${}^i\mathbf{v}_{1i}$ and ${}^i\mathbf{v}_{2i}$, are found by differentiating Eqs. (10.12) and (10.13) with respect to time:

$${}^i\mathbf{v}_{1i} = e_1 {}^i\boldsymbol{\omega}_i \times {}^i\mathbf{s}_i = \frac{e_1}{d_i} \begin{bmatrix} {}^i\mathbf{v}_{bix} \\ {}^i\mathbf{v}_{biy} \\ 0 \end{bmatrix} \quad (10.19)$$

$${}^i\mathbf{v}_{2i} = (d_i - e_2) {}^i\boldsymbol{\omega}_i \times {}^i\mathbf{s}_i + \dot{d}_i {}^i\mathbf{s}_i = \frac{1}{d_i} \begin{bmatrix} (d_i - e_2) {}^i\mathbf{v}_{bix} \\ (d_i - e_2) {}^i\mathbf{v}_{biy} \\ d_i {}^i\mathbf{v}_{biz} \end{bmatrix}. \quad (10.20)$$

(c) Acceleration Analysis. The acceleration of the ball point B_i , expressed in the fixed frame, is found by taking the time derivative of Eq. (10.14):

$$\ddot{\mathbf{v}}_{bi} = \ddot{\mathbf{v}}_p + \dot{\boldsymbol{\omega}}_p \times \mathbf{b}_i + \boldsymbol{\omega}_p \times (\dot{\boldsymbol{\omega}}_p \times \mathbf{b}_i). \quad (10.21)$$

Expressing $\ddot{\mathbf{v}}_{bi}$ in the i th limb frame gives

$${}^i\ddot{\mathbf{v}}_{bi} = {}^iR_A \ddot{\mathbf{v}}_{bi}. \quad (10.22)$$

The acceleration of B_i can also be expressed in terms of the angular acceleration of the i th limb by taking the derivative of Eq. (10.16) with respect to time:

$${}^i\ddot{\mathbf{v}}_{bi} = \ddot{d}_i {}^i\mathbf{s}_i + d_i {}^i\dot{\boldsymbol{\omega}}_i \times {}^i\mathbf{s}_i + d_i {}^i\boldsymbol{\omega}_i \times ({}^i\boldsymbol{\omega}_i \times {}^i\mathbf{s}_i) + 2\dot{d}_i {}^i\boldsymbol{\omega}_i \times {}^i\mathbf{s}_i. \quad (10.23)$$

Since each limb does not spin about its own axis, ${}^i\dot{\boldsymbol{\omega}}_{iz} = 0$. Dot-multiplying both sides of Eq. (10.23) by ${}^i\mathbf{s}_i$, we obtain

$$\ddot{d}_i = {}^i\dot{\mathbf{v}}_{bix} + d_i {}^i\boldsymbol{\omega}_i^2 = {}^i\dot{\mathbf{v}}_{bix} + \frac{{}^i\mathbf{v}_{bix}^2 + {}^i\mathbf{v}_{biy}^2}{d_i}. \quad (10.24)$$

Cross-multiplying both sides of Eq. (10.23) by ${}^i\mathbf{s}_i$, we obtain the angular acceleration of limb i :

$${}^i\ddot{\boldsymbol{\omega}}_i = \frac{1}{d_i} {}^i\mathbf{s}_i \times {}^i\dot{\mathbf{v}}_{bi} - \frac{2\dot{d}_i}{d_i} {}^i\boldsymbol{\omega}_i = \frac{1}{d_i} \begin{bmatrix} -{}^i\dot{v}_{biy} + \frac{2{}^i v_{bix} {}^i v_{biy}}{d_i} \\ {}^i\dot{v}_{bix} - \frac{2{}^i v_{bix} {}^i v_{biy}}{d_i} \\ 0 \end{bmatrix}. \quad (10.25)$$

Once the angular acceleration of the i th limb is found, the accelerations of the centers of mass of the i th cylinder and piston are obtained by differentiating Eqs. (10.19) and (10.20) with respect to time:

$$\begin{aligned} {}^i\ddot{\mathbf{v}}_{1i} &= e_1 {}^i\dot{\boldsymbol{\omega}}_i \times {}^i\mathbf{s}_i + e_1 {}^i\boldsymbol{\omega}_i \times ({}^i\dot{\boldsymbol{\omega}}_i \times {}^i\mathbf{s}_i) \\ &= \frac{e_1}{d_i} \begin{bmatrix} {}^i\dot{v}_{bix} - \frac{2{}^i v_{bix} {}^i v_{biy}}{d_i} \\ {}^i\dot{v}_{biy} - \frac{2{}^i v_{bix} {}^i v_{biy}}{d_i} \\ -\frac{{}^i v_{bix}^2 + {}^i v_{biy}^2}{d_i} \end{bmatrix}, \end{aligned} \quad (10.26)$$

$$\begin{aligned} {}^i\ddot{\mathbf{v}}_{2i} &= \ddot{d}_i {}^i\mathbf{s}_i + (d_i - e_2) {}^i\dot{\boldsymbol{\omega}}_i \times {}^i\mathbf{s}_i + (d_i - e_2) {}^i\boldsymbol{\omega}_i \times ({}^i\dot{\boldsymbol{\omega}}_i \times {}^i\mathbf{s}_i) \\ &\quad + 2\dot{d}_i {}^i\boldsymbol{\omega}_i \times {}^i\mathbf{s}_i \\ &= \frac{1}{d_i} \begin{bmatrix} (d_i - e_2) {}^i\dot{v}_{bix} + \frac{2e_2 {}^i v_{bix} {}^i v_{biy}}{d_i} \\ (d_i - e_2) {}^i\dot{v}_{biy} + \frac{2e_2 {}^i v_{bix} {}^i v_{biy}}{d_i} \\ d_i {}^i\dot{v}_{bix} + \frac{e_2 ({}^i v_{bix}^2 + {}^i v_{biy}^2)}{d_i} \end{bmatrix}. \end{aligned} \quad (10.27)$$

10.2.2 Dynamics of the Limbs

We are now in a position to perform dynamical analysis of the manipulator. To simplify the analysis, we decompose the manipulator into a moving platform and six open-loop chains (limbs). The free-body diagram of a typical limb is shown in Fig. 10.4. We combine the cylinder and piston of each limb into a subsystem and formulate the dynamical equations directly for the subsystem. In this way, reaction forces and moments between the cylinder and piston will not enter into the equations of motion. Euler's equation of motion, written

about point A_i , is

$${}^i\mathbf{n}_i^A = \frac{d}{dt} ({}^i\mathbf{h}_i^A), \quad (10.28)$$

where ${}^i\mathbf{n}_i^A$ denotes the resultant moment exerted on the i th limb about point A_i and ${}^i\mathbf{h}_i^A$ denotes combined angular momentum of the i th cylinder and piston about the same point. Both vectors are expressed in the i th limb frame.

The combined angular momentum of the i th cylinder and piston about point A_i is given by

$${}^i\mathbf{h}_i^A = m_1 e_1 ({}^i\mathbf{s}_i \times {}^i\mathbf{v}_{1i}) + m_2 (d_i - e_2) ({}^i\mathbf{s}_i \times {}^i\mathbf{v}_{2i}) + {}^i\mathbf{h}_{1i}^C + {}^i\mathbf{h}_{2i}^C, \quad (10.29)$$

where

$$\begin{aligned} {}^i\mathbf{h}_{1i}^C &= {}^iI_{1i} {}^i\boldsymbol{\omega}_i, \\ {}^i\mathbf{h}_{2i}^C &= {}^iI_{2i} {}^i\boldsymbol{\omega}_i \end{aligned}$$

are the angular momentums of the cylinder and piston about their respective centers of mass, and where ${}^iI_{1i}$ and ${}^iI_{2i}$ are the inertia matrices of the cylinder and piston about their respective centers of mass and expressed in the i th limb frame. Differentiating Eq. (10.29) with respect to time, we obtain

$$\begin{aligned} \frac{d}{dt} ({}^i\mathbf{h}_i^A) &= m_1 e_1 ({}^i\mathbf{s}_i \times {}^i\dot{\mathbf{v}}_{1i}) + m_2 (d_i - e_2) ({}^i\mathbf{s}_i \times {}^i\dot{\mathbf{v}}_{2i}) + {}^iI_{1i} {}^i\dot{\boldsymbol{\omega}}_i \\ &\quad + {}^i\boldsymbol{\omega}_i \times ({}^iI_{1i} {}^i\boldsymbol{\omega}_i) + {}^iI_{2i} {}^i\dot{\boldsymbol{\omega}}_i + {}^i\boldsymbol{\omega}_i \times ({}^iI_{2i} {}^i\boldsymbol{\omega}_i). \end{aligned} \quad (10.30)$$

The external moment exerted on limb i about A_i is due to the gravitational force exerted at the centers of mass of the two links and the reaction forces exerted at the ball joint B_i . Since the acceleration of gravity \mathbf{g} is defined in the fixed frame, it should be transformed into the limb frame. Referring to Fig. 10.4, let ${}^i\mathbf{f}_{bi} = [{}^i\mathbf{f}_{bix}, {}^i\mathbf{f}_{biy}, {}^i\mathbf{f}_{biz}]^T$ be the force acting on the moving platform by the i th limb and ${}^A\mathbf{g} = [0, 0, -g_c]^T$ be the acceleration of gravity. Then the resulting moment acting on the i th limb about point A_i is given by

$$\begin{aligned} {}^i\mathbf{n}_i^A &= d_i {}^i\mathbf{s}_i \times (-{}^i\mathbf{f}_{bi}) + [m_1 e_1 + m_2 (d_i - e_2)] ({}^i\mathbf{s}_i \times {}^iR_A {}^A\mathbf{g}) \\ &= \begin{bmatrix} d_i {}^i\mathbf{f}_{bix} \\ -d_i {}^i\mathbf{f}_{bix} + m_1 e_1 g_c s\theta_i + m_2 (d_i - e_2) g_c s\theta_i \\ 0 \end{bmatrix}. \end{aligned} \quad (10.31)$$

The dynamical equations of motion for the i th limb are obtained by substituting Eqs. (10.30) and (10.31) into (10.28). These equations of motion can

be further simplified by assuming that the limbs are made up of slender cylindrical rods. Substituting Eqs. (10.30) and (10.31) into (10.28) and making use of the fact that the products of inertia are all equal to zero, I_{iz} is negligibly small, and $\dot{\omega}_{iz} = 0$, we obtain

$$\begin{aligned} {}^i f_{bi_x} &= \frac{1}{d_i} [m_1 e_1 g_c s\theta_i + m_2 (d_i - e_2) g_c s\theta_i - m_1 e_1 {}^i \dot{v}_{1iy}] \\ &\quad - m_2 (d_i - e_2) {}^i \dot{v}_{2ix} - I_{1iy} {}^i \dot{\omega}_{iy} - I_{2iy} {}^i \dot{\omega}_{iy}, \end{aligned} \quad (10.32)$$

$$\begin{aligned} {}^i f_{bi_y} &= \frac{1}{d_i} [-m_1 e_1 {}^i \dot{v}_{1iy} - m_2 (d_i - e_2) {}^i \dot{v}_{2iy}] \\ &\quad + I_{1ix} {}^i \dot{\omega}_{ix} + I_{2ix} {}^i \dot{\omega}_{ix}], \end{aligned} \quad (10.33)$$

where I_{jix} and I_{jiy} denote the x and y components of the principal moments of inertia of the cylinder ($j = 1$) or piston ($j = 2$) about their respective centers of mass and expressed in the i th limb frame. Equations (10.32) and (10.33) determine ${}^i f_{bi_x}$ and ${}^i f_{bi_y}$ for each limb in terms of its inertia forces and moments.

10.2.3 Dynamics of the Moving Platform

In this section we formulate the dynamical equations of motion of the moving platform. These equations of motion are expressed either in the fixed frame A or in the moving frame B . Since the reaction forces, ${}^i \mathbf{f}_{bi}$, obtained in the preceding section are expressed in the i th limb frame, they should be transformed into either the fixed frame A or the moving frame B before they are substituted into the equations of motion.

First, we apply Newton's equation of motion to the moving platform and express the resulting equation in the fixed frame:

$$\sum_{i=1}^6 {}^A \mathbf{f}_{bi} + m_p {}^A \mathbf{g} = m_p {}^A \dot{\mathbf{v}}_p, \quad (10.34)$$

where

$${}^A \mathbf{f}_{bi} = {}^A R_i {}^i \mathbf{f}_{bi} \quad (10.35)$$

denotes the reaction force exerted on the moving platform by the i th limb at a ball joint B_i and expressed in the fixed frame A . Substituting Eq. (10.8) into (10.35) and then the resulting equation into (10.34), we obtain

$$\sum_{i=1}^6 ({}^i f_{bi_x} c\phi_i c\theta_i - {}^i f_{bi_y} s\phi_i + {}^i f_{bi_z} c\phi_i s\theta_i) = m_p \dot{v}_{px}, \quad (10.36)$$

$$\sum_{i=1}^6 ({}^i f_{bi_x} s\phi_i c\theta_i + {}^i f_{bi_y} c\phi_i + {}^i f_{bi_z} s\phi_i s\theta_i) = m_p \dot{v}_{py}, \quad (10.37)$$

$$\sum_{i=1}^6 (-{}^i f_{bi_x} s\theta_i + {}^i f_{bi_z} c\theta_i) = m_p \dot{v}_{pz} + m_p g_c. \quad (10.38)$$

The resulting moment, ${}^B \mathbf{n}_p$, taken about the center of mass of the moving platform and expressed in the moving frame B is

$${}^B \mathbf{n}_p = \sum_{i=1}^6 {}^B \mathbf{b}_i \times {}^B \mathbf{f}_{bi}, \quad (10.39)$$

where

$${}^B \mathbf{f}_{bi} = {}^B R_A {}^A \mathbf{f}_{bi} = {}^B R_i {}^i \mathbf{f}_{bi} \quad (10.40)$$

denotes the reaction force exerted on the moving platform by the i th limb at the ball joint B_i and expressed in the moving frame B .

Assuming that u , v , and w are the principal axes of the moving platform, substituting Eq. (10.39) into Euler's equations of motion, Eq. (9.48), and making use of the fact that the products of inertia are all equal to zero and that $I_{pu} = I_{pv}$, we obtain

$$\sum_{i=1}^6 b_{iv} (a_{31} {}^i f_{bi_x} + a_{32} {}^i f_{bi_y} + a_{33} {}^i f_{bi_z}) = I_{pu} \dot{\omega}_{pu} - \omega_{pv} \omega_{pw} (I_{pv} - I_{pw}), \quad (10.41)$$

$$\sum_{i=1}^6 -b_{iu} (a_{31} {}^i f_{bi_x} + a_{32} {}^i f_{bi_y} + a_{33} {}^i f_{bi_z}) = I_{pv} \dot{\omega}_{pv} - \omega_{pu} \omega_{pw} (I_{pw} - I_{pu}), \quad (10.42)$$

$$\begin{aligned} \sum_{i=1}^6 [b_{iu} (a_{21} {}^i f_{bi_x} + a_{22} {}^i f_{bi_y} + a_{23} {}^i f_{bi_z}) \\ - b_{iv} (a_{11} {}^i f_{bi_x} + a_{12} {}^i f_{bi_y} + a_{13} {}^i f_{bi_z})] = I_{pw} \dot{\omega}_{pw}, \end{aligned} \quad (10.43)$$

where a_{ij} are the (i, j) elements of ${}^B R_i$, ${}^B \boldsymbol{\omega}_p = [\omega_{pu}, \omega_{pv}, \omega_{pw}]^T$ is the angular velocity of the moving platform expressed in the moving frame B , and I_{pu} , I_{pv} , and I_{pw} are the u , v , and w components of the principal moments of inertia of the moving platform about its center of mass and expressed in the moving frame B .

Hence once ${}^i f_{bi,x}$ and ${}^i f_{bi,y}$ are determined from Eqs. (10.32) and (10.33), Eqs. (10.36) through (10.38) and (10.41) through (10.43) constitute a set of six linear equations in six unknowns, ${}^i f_{bi,z}$ for $i = 1, 2, \dots, 6$. These six equations can easily be solved by, for example, the Gauss elimination method.

10.2.4 Actuator and Ground Reaction Forces

Once the reaction forces at the moving ball joints are found, the actuating force τ_i is obtained by summing all the forces acting on the i th piston along the z_i -axis.

$$\tau_i = {}^i f_{bi,z} + m_2 g_c c\theta_i + m_2 {}^i \ddot{v}_{2i}. \quad (10.44)$$

Note that the moment in Eq. (10.31) is taken about the fixed ball point A_i such that the reaction forces \mathbf{f}_{ai} at the fixed ball joints do not enter into the equations of motion. These reaction forces, if interested, can be found by formulating Newton's equation, one limb at a time, as follows:

$${}^i \mathbf{f}_{ai} + {}^i \mathbf{f}_{bi} + (m_1 + m_2) {}^i R_A {}^A \mathbf{g} = m_1 {}^i \dot{\mathbf{v}}_{1i} + m_2 {}^i \dot{\mathbf{v}}_{2i}. \quad (10.45)$$

10.2.5 Newton–Euler's Procedure

The procedure for solving the inverse dynamics of a Stewart–Gough platform can be summarized in five basic steps:

1. Perform the inverse kinematic analysis of the mechanism. We first compute the position, velocity, and acceleration of the moving ball points in terms of a prescribed motion of the moving platform. Then we derive the position, velocity, and acceleration of the center of mass and the angular velocity and angular acceleration of each limb. Specifically, for $i = 1$ to 6, we compute:
 - $\mathbf{b}_i = {}^A R_B {}^B \mathbf{b}_i$.
 - d_i and \mathbf{s}_i from Eqs. (10.7) and (10.6).
 - $c\phi_i, s\phi_i, c\theta_i, s\theta_i$, and ${}^A R_i$ from Eqs. (10.11) and (10.8).
 - \mathbf{v}_{bi} and ${}^i \mathbf{v}_{bi}$ from Eqs. (10.14) and (10.15).
 - ${}^i \omega_i$ from Eq. (10.18).
 - $\dot{\mathbf{v}}_{bi}$ and ${}^i \dot{\mathbf{v}}_{bi}$ from Eqs. (10.21) and (10.22).
 - ${}^i \dot{\omega}_i$ from Eq. (10.25).
 - ${}^i \ddot{\mathbf{v}}_{ii}$ and ${}^i \ddot{\mathbf{v}}_{2i}$ from Eqs. (10.26) and (10.27).
2. Decompose the manipulator into a moving platform and several open-loop chains by cutting open at the moving ball joints. Assign appropri-

ate action and reaction forces at the points of connection between the moving platform and the six limbs.

3. Consider each limb as a subsystem and formulate Euler's equations of motion about the fixed ball joint for each limb. In this way, some of the reaction forces at the moving ball points can be determined independent of the equations of motion of the moving platform. Specifically, we solve Eqs. (10.32) and (10.33) for ${}^i f_{fix}$ and ${}^i f_{hiy}$.
4. Solve the remaining reaction forces by formulating Newton's and Euler's equations of motion of the moving platform. That is, solve Eqs. (10.36) through (10.38) and Eqs. (10.41) through (10.43) for ${}^i f_{bi,z}$ for $i = 1, 2, \dots, 6$.
5. Find the actuator force τ_i by Eq. (10.44).

10.3 PRINCIPLE OF VIRTUAL WORK

In this section we illustrate how to apply the *principle of virtual work* or *d'Alembert's principle* for the dynamic analysis of parallel manipulators. The following conventions are employed:

- \mathbf{f}_i : resulting force (excluding the actuator force) exerted at the center of mass of link i .
- \mathbf{f}_i^* : inertia force exerted at the center of mass of link i , $\mathbf{f}_i^* = -m_i \dot{\mathbf{v}}_i$.
- $\hat{\mathbf{f}}_i$: $\mathbf{f}_i + \mathbf{f}_i^*$.
- \mathbf{f}_p : resulting force exerted at the center of mass of the moving platform.
- \mathbf{f}_p^* : inertia force exerted at the center of mass of the moving platform, $\mathbf{f}_p^* = -m_p \dot{\mathbf{v}}_p$.
- $\hat{\mathbf{f}}_p$: $\mathbf{f}_p + \mathbf{f}_p^*$.
- \mathbf{n}_i : resulting moment (excluding the actuator torque) exerted at the center of mass of link i .
- \mathbf{n}_i^* : inertia moment exerted at the center of mass of link i , $\mathbf{n}_i^* = -i I_i {}^i \dot{\omega}_i - {}^i \omega_i \times (i I_i {}^i \omega_i)$.
- $\hat{\mathbf{n}}_i$: $\mathbf{n}_i + \mathbf{n}_i^*$.
- \mathbf{n}_p : resulting moment exerted at the center of mass of the moving platform.
- \mathbf{n}_p^* : inertia moment exerted at the center of mass of the moving platform, $\mathbf{n}_p^* = -I_p \dot{\omega}_p - \omega_p \times (I_p \omega_p)$.
- $\hat{\mathbf{n}}_p$: $\mathbf{n}_p + \mathbf{n}_p^*$.
- \mathbf{q} : vector of actuated limb lengths, $\mathbf{q} = [d_1, d_2, \dots, d_n]^T$.

\mathbf{x}_i : six-dimensional vector describing the position and orientation of link i .

$\dot{\mathbf{x}}_{ji}$: six-dimensional vector describing the linear and angular velocities of the cylinder ($j = 1$) or piston ($j = 2$) of the i th limb, $\dot{\mathbf{x}}_{ji} = [v_{jix}, v_{jiy}, \dots, \omega_{iz}]^T$.

\mathbf{x}_p : six-dimensional vector describing the position and orientation of the moving platform.

$\dot{\mathbf{x}}_p$: six-dimensional vector describing the linear and angular velocities of the moving platform, $\dot{\mathbf{x}}_p = [v_{px}, v_{py}, \dots, \omega_{pz}]^T$.

$\boldsymbol{\tau}$: vector of actuated joint torques and/or forces.

$\delta(\cdot)$: virtual displacement of (\cdot) .

For convenience, we introduce a six-dimensional wrench, $\hat{\mathbf{F}}_i$, as the sum of applied and inertia wrenches about the center of mass of link i :

$$\hat{\mathbf{F}}_i = \begin{bmatrix} \hat{\mathbf{f}}_i \\ \hat{\mathbf{n}}_i \end{bmatrix}. \quad (10.46)$$

Similarly, we introduce a six-dimensional wrench, $\hat{\mathbf{F}}_p$, as the sum of applied and inertia wrenches about the center of mass of the moving platform:

$$\hat{\mathbf{F}}_p = \begin{bmatrix} \hat{\mathbf{f}}_p \\ \hat{\mathbf{n}}_p \end{bmatrix}. \quad (10.47)$$

Then the principle of virtual work for a parallel manipulator can be stated as

$$\delta\mathbf{q}^T \boldsymbol{\tau} + \delta\mathbf{x}_p^T \hat{\mathbf{F}}_p + \sum_i \delta\mathbf{x}_i^T \hat{\mathbf{F}}_i = 0, \quad (10.48)$$

where the summation goes over all links of the limbs. Note that in Eq. (10.48) we have isolated the actuator torques and/or forces from other applied forces for convenience of derivation.

The virtual displacements in Eq. (10.48), however, must be compatible with the kinematic constraints imposed by the joints. Therefore, it is necessary to relate these virtual displacements to a set of independent generalized virtual displacements. For parallel manipulators, the coordinates of the moving platform, $\mathbf{x}_p = [x_p, y_p, \dots, \psi]^T$, can conveniently be chosen as the generalized coordinates. This is because the virtual displacement of actuated joints, $\delta\mathbf{q}$, is related to the virtual displacement of the moving platform, $\delta\mathbf{x}_p$, by the manipulator Jacobian matrix J_p :

$$\delta\mathbf{q} = J_p \delta\mathbf{x}_p. \quad (10.49)$$

Furthermore, the virtual displacement of the i th link of a limb, $\delta\mathbf{x}_i$, can be related to the virtual displacement of the moving platform, $\delta\mathbf{x}_p$, by a link Jacobian matrix J_i :

$$\delta\mathbf{x}_i = J_i \delta\mathbf{x}_p. \quad (10.50)$$

Substituting Eqs. (10.49) and (10.50) into (10.48), we obtain

$$\delta\mathbf{x}_p^T (J_p^T \boldsymbol{\tau} + \hat{\mathbf{F}}_p + \sum_i J_i^T \hat{\mathbf{F}}_i) = 0. \quad (10.51)$$

Since Eq. (10.51) is valid for any virtual displacement $\delta\mathbf{x}_p$, it follows that

$$J_p^T \boldsymbol{\tau} + \hat{\mathbf{F}}_p + \sum_i J_i^T \hat{\mathbf{F}}_i = 0. \quad (10.52)$$

Equation (10.52) describes the dynamics of a parallel manipulator that is similar to Kane's formulation (Kane and Levinson, 1985). Note that the wrenches in Eq. (10.52) are taken about the center of mass of each link. Hence if an external wrench is applied at a point other than the center of mass, it should be transformed into the center-of-mass coordinate frame before it is substituted into the equations of motion.

In general, if the number of actuators is equal to the number of degrees of freedom of a manipulator, J_p is a square matrix. Hence $\boldsymbol{\tau}$ can be uniquely determined:

$$\boldsymbol{\tau} = -J_p^{-T} (\hat{\mathbf{F}}_p + \sum_i J_i^T \hat{\mathbf{F}}_i), \quad \text{provided that } J_p \text{ is nonsingular.} \quad (10.53)$$

On the other hand, if the number of actuators is greater than the number of degrees of freedom, $\boldsymbol{\tau}$ has an infinitude of solutions from which a minimum norm solution can be obtained by applying the pseudoinverse technique.

In what follows, we use the Stewart–Gough platform shown in Fig. 10.2 as an example to illustrate the methodology. Since the inverse kinematic analysis of the manipulator was carried out in the preceding section, we proceed directly to the formulation of link Jacobian matrices, link inertia wrenches, and the equations of motion.

10.3.1 Link Jacobian Matrices

A critical step in formulating d'Alembert's equations of motion is the derivation of the manipulator Jacobian matrix and link Jacobian matrices. To identify the manipulator Jacobian matrix, J_p , we write Eq. (10.14) in matrix form:

$$\mathbf{v}_{bi} = J_{bi} \dot{\mathbf{x}}_p, \quad (10.54)$$

where

$$J_{bi} = \begin{bmatrix} 1 & 0 & 0 & 0 & b_{iz} & -b_{iy} \\ 0 & 1 & 0 & -b_{iz} & 0 & b_{ix} \\ 0 & 0 & 1 & b_{iy} & -b_{ix} & 0 \end{bmatrix}. \quad (10.55)$$

Substituting Eq. (10.54) into (10.15), we obtain

$${}^i\mathbf{v}_{bi} = {}^iJ_{bi} \dot{\mathbf{x}}_p = \begin{bmatrix} {}^iJ_{bi,x} \\ {}^iJ_{bi,y} \\ {}^iJ_{bi,z} \end{bmatrix} \dot{\mathbf{x}}_p, \quad (10.56)$$

where ${}^iJ_{bi} = {}^iR_A J_{bi}$ is a 3×6 matrix whose row vectors are given by

$$\begin{aligned} {}^iJ_{bi,x} &= [c\phi_i c\theta_i, s\phi_i c\theta_i, -s\theta_i, -b_{iz} s\phi_i c\theta_i - b_{iy} s\theta_i, b_{iz} c\phi_i c\theta_i + b_{ix} s\theta_i, \\ &\quad -b_{iy} c\phi_i c\theta_i + b_{ix} s\phi_i c\theta_i], \\ {}^iJ_{bi,y} &= [-s\phi_i, c\phi_i, 0, -b_{iz} c\phi_i, -b_{iz} s\phi_i, b_{iy} s\phi_i + b_{ix} c\phi_i], \\ {}^iJ_{bi,z} &= [c\phi_i s\theta_i, s\phi_i s\theta_i, c\theta_i, -b_{iz} s\phi_i s\theta_i + b_{iy} c\theta_i, b_{iz} c\phi_i s\theta_i - b_{ix} c\theta_i, \\ &\quad -b_{iy} c\phi_i s\theta_i + b_{ix} s\phi_i s\theta_i]. \end{aligned} \quad (10.57)$$

Making use of the row matrices above, Eq. (10.17) can be written as

$$\dot{d}_i = {}^iJ_{bi,z} \dot{\mathbf{x}}_p. \quad (10.58)$$

Writing Eq. (10.58) six times, once for each limb, yields six scalar equations which can be assembled in the matrix form

$$\dot{\mathbf{q}} = J_p \dot{\mathbf{x}}_p, \quad (10.59)$$

where

$$J_p = \begin{bmatrix} {}^1J_{b1z} \\ {}^2J_{b2z} \\ \vdots \\ {}^6J_{b6z} \end{bmatrix} \quad (10.60)$$

is known as the *manipulator Jacobian matrix*.

Similarly, Eqs. (10.18), (10.19), and (10.20) can be written as

$${}^i\omega_i = \frac{1}{d_i} \begin{bmatrix} -{}^iJ_{bi,y} \\ {}^iJ_{bi,x} \\ \mathbf{0}_{1 \times 6} \end{bmatrix} \dot{\mathbf{x}}_p, \quad (10.61)$$

$${}^i\mathbf{v}_{li} = \frac{e_1}{d_i} \begin{bmatrix} {}^iJ_{bi,x} \\ {}^iJ_{bi,y} \\ \mathbf{0}_{1 \times 6} \end{bmatrix} \dot{\mathbf{x}}_p, \quad (10.62)$$

$${}^i\mathbf{v}_{2i} = \frac{1}{d_i} \begin{bmatrix} (d_i - e_2) {}^iJ_{bi,x} \\ (d_i - e_2) {}^iJ_{bi,y} \\ d_i {}^iJ_{bi,z} \end{bmatrix} \dot{\mathbf{x}}_p. \quad (10.63)$$

Combining Eqs. (10.61), (10.62), and (10.63), we obtain

$${}^i\dot{\mathbf{x}}_{1i} = {}^iJ_{1i} \dot{\mathbf{x}}_p, \quad (10.64)$$

$${}^i\dot{\mathbf{x}}_{2i} = {}^iJ_{2i} \dot{\mathbf{x}}_p, \quad (10.65)$$

where

$${}^iJ_{1i} = \frac{1}{d_i} \begin{bmatrix} e_1 {}^iJ_{bi,x} \\ e_1 {}^iJ_{bi,y} \\ \mathbf{0}_{1 \times 6} \\ -{}^iJ_{bi,y} \\ {}^iJ_{bi,x} \\ \mathbf{0}_{1 \times 6} \end{bmatrix}, \quad (10.66)$$

$${}^iJ_{2i} = \frac{1}{d_i} \begin{bmatrix} (d_i - e_2) {}^iJ_{bi,x} \\ (d_i - e_2) {}^iJ_{bi,y} \\ d_i {}^iJ_{bi,z} \\ -{}^iJ_{bi,y} \\ {}^iJ_{bi,x} \\ \mathbf{0}_{1 \times 6} \end{bmatrix} \quad (10.67)$$

are called the *link Jacobian matrices* of the i th cylinder and piston, respectively.

10.3.2 Inertia and Applied Wrenches

Assume that gravitational force is the only force acting on the manipulator. Then the vector sum of applied and inertia wrenches exerted at the center of mass of the moving platform is given by

$$\hat{\mathbf{F}}_p = \begin{bmatrix} \hat{\mathbf{f}}_p \\ \hat{\mathbf{n}}_p \end{bmatrix} = \begin{bmatrix} m_p \mathbf{g} - m_p \dot{\mathbf{v}}_p \\ -{}^A I_p \dot{\boldsymbol{\omega}}_p - \boldsymbol{\omega}_p \times ({}^A I_p \boldsymbol{\omega}_p) \end{bmatrix}, \quad (10.68)$$

where ${}^A I_p = {}^A R_B {}^B I_p {}^B R_A$ denotes the inertia matrix of the moving platform taken about its center of mass and expressed in the fixed frame A .

Similarly, the vector sum of external and inertia wrenches exerted at the centers of mass of the cylinder and piston and expressed in the i th limb frame are given by

$${}^i\hat{\mathbf{F}}_{li} = \begin{bmatrix} {}^i\hat{\mathbf{f}}_{li} \\ {}^i\hat{\mathbf{n}}_{li} \end{bmatrix} = \begin{bmatrix} m_{li} {}^iR_A \mathbf{g} + m_{li} {}^i\dot{\mathbf{v}}_{li} \\ -{}^iI_{li} {}^i\dot{\boldsymbol{\omega}}_i - {}^i\boldsymbol{\omega}_i \times ({}^iI_{li} {}^i\boldsymbol{\omega}_i) \end{bmatrix}, \quad (10.69)$$

$${}^i\hat{\mathbf{F}}_{2i} = \begin{bmatrix} {}^i\hat{\mathbf{f}}_{2i} \\ {}^i\hat{\mathbf{n}}_{2i} \end{bmatrix} = \begin{bmatrix} m_{2i} {}^iR_A \mathbf{g} - m_{2i} {}^i\dot{\mathbf{v}}_{2i} \\ -{}^iI_{2i} {}^i\dot{\boldsymbol{\omega}}_i - {}^i\boldsymbol{\omega}_i \times ({}^iI_{2i} {}^i\boldsymbol{\omega}_i) \end{bmatrix}. \quad (10.70)$$

Note that due to symmetry, the inertia matrices of the moving platform and the six limbs are all diagonal.

10.3.3 Equations of Motion

We now apply the principle of virtual work for derivation of the equations of motion. Equation (10.52) can be written specifically for the Stewart–Gough platform as follows:

$$J_p^T \boldsymbol{\tau} + \hat{\mathbf{F}}_p + \sum_{i=1}^6 ({}^iJ_{li}^T {}^i\hat{\mathbf{F}}_{li} + {}^iJ_{2i}^T {}^i\hat{\mathbf{F}}_{2i}) = 0. \quad (10.71)$$

Note that in Eq. (10.71), $\hat{\mathbf{F}}_p$ is expressed in the fixed frame A , while ${}^i\hat{\mathbf{F}}_{li}$ and ${}^i\hat{\mathbf{F}}_{2i}$ are expressed in the limb frame i and then transformed into the fixed frame by the transpose of the link Jacobian matrices. Similarly, the vector of actuator forces, $\boldsymbol{\tau}$, is specified in the actuator joint space and then transformed into the fixed frame by the transpose of the manipulator Jacobian matrix.

Substituting Eqs. (10.66) and (10.67) into (10.71) and simplifying yields

$$J_p^T (\boldsymbol{\tau} + \hat{\mathbf{F}}_z) + \hat{\mathbf{F}}_p + J_x^T \hat{\mathbf{F}}_x + J_y^T \hat{\mathbf{F}}_y = 0, \quad (10.72)$$

where

$$J_x = \begin{bmatrix} 1J_{b1x} \\ 2J_{b2x} \\ \vdots \\ 6J_{b6x} \end{bmatrix}, \quad (10.73)$$

$$J_y = \begin{bmatrix} 1J_{b1y} \\ 2J_{b2y} \\ \vdots \\ 6J_{b6y} \end{bmatrix}, \quad (10.74)$$

$$\hat{\mathbf{F}}_x = \begin{bmatrix} e_1 \hat{f}_{11x} + (d_1 - e_2) \hat{f}_{21x} + \hat{n}_{11y} + \hat{n}_{21y} \\ d_1 \\ e_1 \hat{f}_{12x} + (d_2 - e_2) \hat{f}_{22x} + \hat{n}_{12y} + \hat{n}_{22y} \\ d_2 \\ \vdots \\ e_1 \hat{f}_{16x} + (d_6 - e_2) \hat{f}_{26x} + \hat{n}_{16y} + \hat{n}_{26y} \\ d_6 \end{bmatrix}, \quad (10.75)$$

$$\hat{\mathbf{F}}_y = \begin{bmatrix} e_1 \hat{f}_{11y} + (d_1 - e_2) \hat{f}_{21y} - \hat{n}_{11x} - \hat{n}_{21x} \\ d_1 \\ e_1 \hat{f}_{12y} + (d_2 - e_2) \hat{f}_{22y} - \hat{n}_{12x} - \hat{n}_{22x} \\ d_2 \\ \vdots \\ e_1 \hat{f}_{16y} + (d_6 - e_2) \hat{f}_{26y} - \hat{n}_{16x} - \hat{n}_{26x} \\ d_6 \end{bmatrix}, \quad (10.76)$$

$$\hat{\mathbf{F}}_z = \begin{bmatrix} \hat{f}_{21z} \\ \hat{f}_{22z} \\ \vdots \\ \hat{f}_{26z} \end{bmatrix}, \quad (10.77)$$

where \hat{f}_{jix} , \hat{f}_{jiy} , and \hat{f}_{jiz} are the x -, y -, and z -components of ${}^i\hat{\mathbf{f}}_{ji}$, and \hat{n}_{jix} , \hat{n}_{jiy} , and \hat{n}_{jiz} are the x -, y -, and z -components of ${}^i\hat{\mathbf{n}}_{ji}$. From Eq. (10.72), the actuator forces required to produce a desired motion characteristics can be computed by using, for example, the Gauss elimination method. Note that the actuator forces depend on the inverse of the transpose of the manipulator Jacobian matrix, J_p^{-T} . Therefore, the computation of actuator forces may become numerically unstable when the manipulator approaches a singular configuration.

We observe that using the principle of virtual work, the constraint forces and moments are eliminated from the equations of motion. This method is, therefore, more efficient than the Newton–Euler formulation and the Lagrangian formulation. It is potentially useful for real-time control of a parallel manipulator.

10.3.4 d'Alembert's Procedure

In this section we summarize the procedure for solving the inverse dynamics of a Stewart–Gough platform by using the principle of virtual work. It is assumed that the time history of the moving platform is specified in terms of the

position of the centroid, \mathbf{p} , and three Euler's angles, ϕ , θ , and ψ . The velocity and acceleration of the centroid are calculated by taking the derivatives of \mathbf{p} with respect to time. The rotation matrix of the moving platform, ${}^A R_B$, is calculated from Eq. (10.1). The angular velocity and angular acceleration of the moving platform are calculated from Eqs. (10.3) and (10.4). At any instant in time, the actuator forces are computed by the following five steps:

1. Determine the position, velocity, and acceleration of all links by performing the inverse kinematic analysis. Specifically, for $i = 1$ to 6, we compute:
 - (a) $\mathbf{b}_i = {}^A R_B {}^B \mathbf{b}_i$ and ${}^A I_p = {}^A R_B {}^B I_p {}^B R_A$.
 - (b) d_i and s_i from Eqs. (10.7) and (10.6).
 - (c) $c\phi_i$, $s\phi_i$, $c\theta_i$, $s\theta_i$, and ${}^A R_i$ from Eqs. (10.11) and (10.8).
 - (d) ${}^B v_{bi}$ and ${}^I v_{bi}$ from Eqs. (10.14) and (10.15).
 - (e) ${}^I \omega_i$ from Eq. (10.18).
 - (f) ${}^B \dot{v}_{bi}$ and ${}^I \dot{v}_{bi}$ from Eqs. (10.21) and (10.22).
 - (g) ${}^I \ddot{\omega}_i$ from Eq. (10.25).
 - (h) ${}^I \dot{v}_{1i}$ and ${}^I \dot{v}_{2i}$ from Eqs. (10.26) and (10.27).
2. Determine the platform and link Jacobian matrices.
 - (a) For $i = 1$ to 6, calculate J_{bi} and then ${}^I J_{bi}$ from Eqs. (10.55) and (10.57).
 - (b) Calculate J_p by Eq. (10.60).
3. Determine the resultants of the applied and inertia wrenches.
 - (a) Calculate $\hat{\mathbf{F}}_p$ by Eq. (10.68).
 - (b) For $i = 1$ to 6, calculate ${}^I \hat{\mathbf{F}}_{1i}$ and ${}^I \hat{\mathbf{F}}_{2i}$ from Eqs. (10.69) and (10.70), respectively.
4. Formulate the dynamical equations of motion. Calculate J_x , J_y , $\hat{\mathbf{F}}_x$, $\hat{\mathbf{F}}_y$, and $\hat{\mathbf{F}}_z$ from Eqs. (10.73) through (10.77), and then substitute the resulting expressions into Eq. (10.72).
5. Solve the resulting dynamical equations of motion, Eq. (10.72), by the Gaussian elimination method.

10.3.5 Numerical Examples

Based on the algorithm above, a computer program was developed to solve the inverse dynamics of the Stewart-Gough platform shown in Fig. 10.2, using MATLAB software. Figure 10.5 shows the locations of the ball joints and the initial location of the moving platform. The manipulator system parameters are $m_p = 32$ kg, $m_{1,i} = 2$ kg, $m_{2,i} = 2$ kg, $b_i = 0.5$ m, $a_i = 1$ m, $e_1 =$

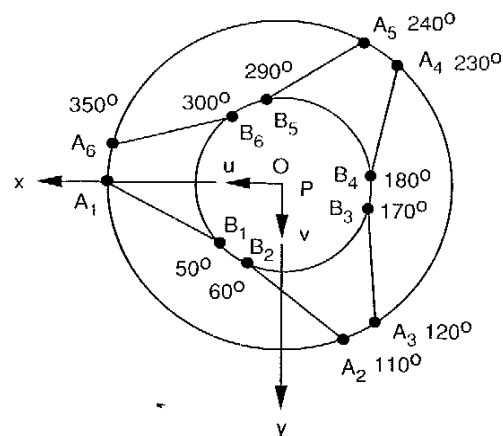


FIGURE 10.5. Top view of the Stewart-Gough platform.

$$0.2 \text{ m}, e_2 = 0.75 \text{ m}, {}^B I_p = \text{diag}[2, 2, 4] \text{ kg}\cdot\text{m}^2, {}^I I_{1i} = \text{diag}[1, 1, 0.001] \text{ kg}\cdot\text{m}^2, {}^I I_{2i} = \text{diag}[0.4, 0.4, 0.0001] \text{ kg}\cdot\text{m}^2, \text{ and } \mathbf{g} = [0, 0, -9.8]^T \text{ m/s}^2.$$

The following examples are solved to illustrate the algorithm. In all examples it is assumed that the platform starts at rest and accelerates with a constant acceleration for a period of 0.4 second. Furthermore, at the initial location, the moving platform is assumed to be located 1 m above the fixed base, namely, at $t = 0$, $\mathbf{p} = [0, 0, 1]^T \text{ m}$, and $\phi = \theta = \psi = 0$.

For the first example, the moving platform moves along the x -direction with a constant acceleration of $\ddot{p}_x = 5 \text{ m/s}^2$ while all the other parameters are held constant, $\ddot{p}_y = \ddot{p}_z = \ddot{\phi} = \ddot{\theta} = \ddot{\psi} = 0$. The actuating forces versus time calculated by the program are plotted in Fig. 10.6.

For the second example, the moving platform moves along the z -direction with a constant acceleration of $\ddot{p}_z = 5 \text{ m/s}^2$ while all the other parameters are held constant, $\ddot{p}_x = \ddot{p}_y = \ddot{\phi} = \ddot{\theta} = \ddot{\psi} = 0$. As can be seen from Fig. 10.7, to accelerate the platform along the z -axis, all actuating forces are equal to one another. As the moving platform moves away from the fixed base, the limbs become more vertically oriented, therefore reducing the actuating forces.

For the third example, the moving platform rotates about the y -axis with a constant angular acceleration of $\ddot{\theta} = 2 \text{ rad/s}^2$ while all the other parameters are held constant, $\ddot{p}_x = \ddot{p}_y = \ddot{p}_z = \ddot{\phi} = \ddot{\psi} = 0$. The actuating forces versus time are plotted in Fig. 10.8.

For the fourth example, the moving platform rotates about the z -axis with a constant angular acceleration of $\ddot{\phi} = 2 \text{ rad/s}^2$ while all the other parameters

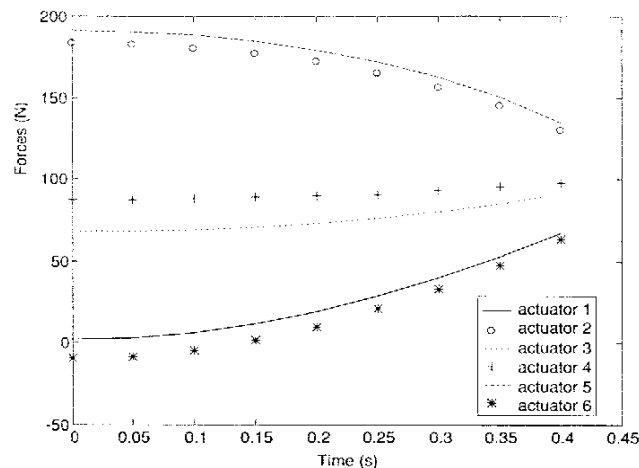


FIGURE 10.6. Actuating forces versus time, $\ddot{p}_x = 5 \text{ m/s}^2$.

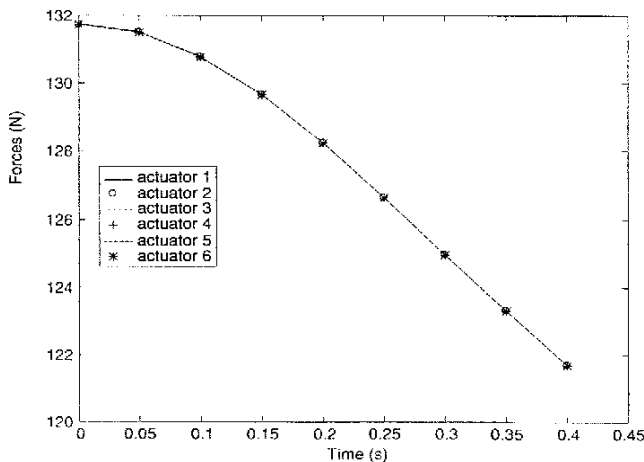


FIGURE 10.7. Actuating forces versus time, $\ddot{p}_z = 5 \text{ m/s}^2$.

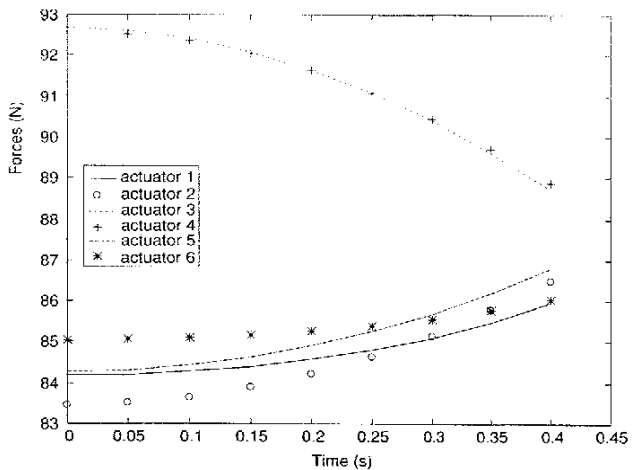


FIGURE 10.8. Actuating forces versus time, $\ddot{\theta} = 2 \text{ rad/s}^2$.

are held constant, $\ddot{p}_x = \ddot{p}_y = \ddot{p}_z = \ddot{\theta} = \ddot{\psi} = 0$. As can be seen from Fig. 10.9, due to the symmetrical arrangement of the limbs, the forces exerted by actuators 1, 3, and 5 are equal to one another, and the forces exerted by actuators 2, 4, and 6 are also equal to one another.

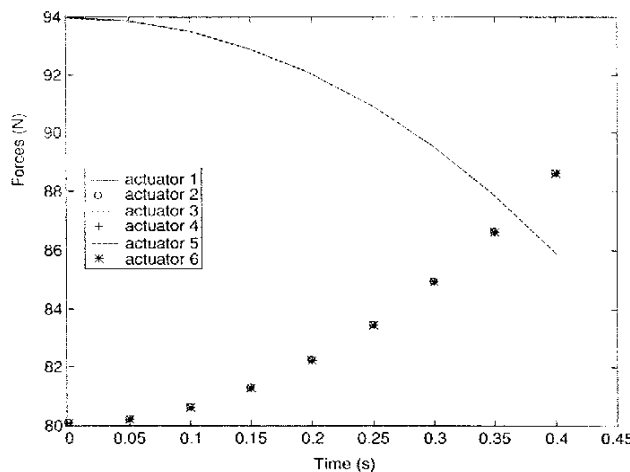
10.4 LAGRANGIAN FORMULATION

In this section we show that the inverse dynamics of relatively simple parallel manipulators can be solved by applying the Lagrangian equations of the first type. The Lagrangian equations of the first type are written in terms of a set of redundant coordinates. Therefore, the formulation requires a set of constraint equations derived from the kinematics of a mechanism. These constraint equations and their derivatives must be adjoined to the equations of motion to produce a number of equations that is equal to the number of unknowns.

The Lagrangian equations of the first type can be written as

$$\frac{d}{dt} \left(\frac{\partial L}{\partial \dot{q}_j} \right) - \frac{\partial L}{\partial q_j} = Q_j + \sum_{i=1}^k \lambda_i \frac{\partial \Gamma_i}{\partial q_j} \quad \text{for } j = 1 \text{ to } n, \quad (10.78)$$

FIGURE 10.7. Actuating forces versus time, $\ddot{p}_z = 5 \text{ m/s}^2$.

FIGURE 10.9. Actuating forces versus time, $\ddot{\phi} = 2 \text{ rad/s}^2$.

where Γ_i denotes the i th constraint function, k is the number of constraint functions, and λ_i is the Lagrangian multiplier. The number of coordinates, n , exceeds the number of degrees of freedom by k . Solving the equations of motion is made easier by arranging the Lagrangian equations into two sets. One contains the Lagrange multipliers as the only unknowns, and the other contains the generalized forces contributed by the actuators as the additional unknowns. Let the first k equations be associated with the redundant coordinates and the remaining $n - k$ equations be associated with the actuated joint variables. Then the first set of equations can be written in the form

$$\sum_{i=1}^k \lambda_i \frac{\partial \Gamma_i}{\partial q_j} = \frac{d}{dt} \left(\frac{\partial L}{\partial \dot{q}_j} \right) - \frac{\partial L}{\partial q_j} - \hat{Q}_j, \quad (10.79)$$

where \hat{Q}_j , if any, represents the generalized force contributed by an externally applied force. For the inverse dynamics, \hat{Q}_j is given. Hence the right-hand side of Eq. (10.79) is known. Writing Eq. (10.79) once for each redundant coordinate yields a set of k linear equations that can be solved for the k Lagrangian multipliers.

Once the Lagrange multipliers are found, the actuator torques and/or forces can be determined directly from the remaining equations. Specifically, the

second set of equations can be written as

$$Q_j = \frac{d}{dt} \left(\frac{\partial L}{\partial \dot{q}_j} \right) - \frac{\partial L}{\partial q_j} - \sum_{i=1}^k \lambda_i \frac{\partial \Gamma_i}{\partial q_j} \quad \text{for } j = k+1 \text{ to } n, \quad (10.80)$$

where Q_j is the actuator force or torque.

In what follows, we analyze the dynamics of a 3-dof parallel manipulator as an example to illustrate the principle.

10.4.1 Lagrangian Dynamics of the University of Maryland Manipulator

In this section we analyze the dynamics of the University of Maryland manipulator as an example to illustrate the methodology. For convenience, the schematic diagram is repeated in Fig. 10.10. The coordinate frames, link lengths, and the joint angles of the manipulator are shown in more detail in Fig. 3.11. In this manipulator, θ_{11} , θ_{12} , and θ_{13} are the actuated joints.

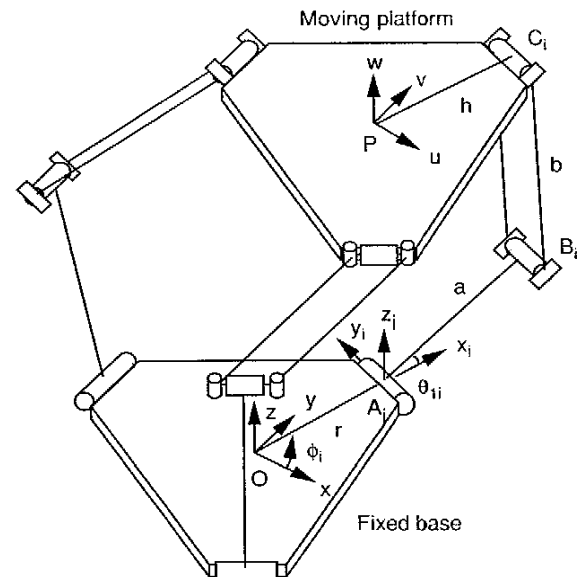


FIGURE 10.10. University of Maryland's manipulator.

Theoretically, the dynamic analysis can be accomplished by using just three generalized coordinates since this is a 3-dof manipulator. However, this would lead to a cumbersome expression for the Lagrange function, due to the complex kinematics of the manipulator. Instead, Lagrange's equations of the first type will be employed by introducing three redundant coordinates, p_x , p_y , and p_z . Thus we have p_x , p_y , p_z , θ_{11} , θ_{12} , and θ_{13} as the generalized coordinates. Equation (10.78) represents a system of six equations in six variables. The six variables are λ_i for $i = 1$ to 3, and the three actuator torques, Q_j for $j = 4$, 5, and 6. Note that the generalized forces, Q_i for $i = 1$ to 3, represent the x , y , and z components of an external force exerted at the centroid P of the moving platform.

This formulation requires three constraint equations, Γ_i for $i = 1$ to 3. The constraint equations are obtained from the fact that the distance between joints B and C is always equal to the length of the connecting rod of the upper arm, b ; that is,

$$\begin{aligned}\Gamma_i &= \overline{B_i C_i}^2 - b^2 \\ &= (p_x + hc\phi_i - rc\phi_i - ac\phi_i c\theta_{1i})^2 + (p_y + hs\phi_i - rs\phi_i - as\phi_i c\theta_{1i})^2 \\ &\quad + (p_z - as\theta_{1i})^2 - b^2 \\ &= 0\end{aligned}\quad (10.81)$$

for $i = 1, 2$, and 3.

To simplify the analysis, we assume that the mass of each connecting rod, m_b , in the upper arm assembly is divided evenly and concentrated at the two endpoints B_i and C_i . Then we derive the Lagrangian function L as follows. The total kinetic energy of the manipulator is

$$K = K_p + \sum_{i=1}^3 (K_{ai} + K_{bi}), \quad (10.82)$$

where K_p is the kinetic energy of the moving platform, K_{ai} the kinetic energy of the input link and the rotor on limb i , and K_{bi} the kinetic energy of the two connecting rods of limb i . Specifically,

$$\begin{aligned}K_p &= \frac{1}{2}m_p(\dot{p}_x^2 + \dot{p}_y^2 + \dot{p}_z^2), \\ K_{ai} &= \frac{1}{2}(I_m + \frac{1}{3}m_a a^2)\dot{\theta}_{1i}^2, \\ K_{bi} &= \frac{1}{2}m_b(\dot{p}_x^2 + \dot{p}_y^2 + \dot{p}_z^2) + \frac{1}{2}m_b a^2 \dot{\theta}_{1i}^2,\end{aligned}$$

where m_p is the mass of the moving platform, m_a the mass of the input link, m_b the mass of one of the two connecting rods, and I_m the axial moment of

inertia of the rotor mounted on the i th limb. Assuming that the acceleration of gravity points in the $-z$ -direction, the total potential energy of the manipulator relative to the fixed x - y plane is

$$U = U_p + \sum_{i=1}^3 (U_{ai} + U_{bi}), \quad (10.83)$$

where U_p is the potential energy of the moving platform, U_{ai} the potential energy of the input link on limb i , and U_{bi} the potential energy of the two connecting rods of the i th limb. Specifically,

$$\begin{aligned}U_p &= m_p g_c p_z, \\ U_{ai} &= \frac{1}{2}m_a g_c as\theta_{1i}, \\ U_{bi} &= m_b g_c(p_z + as\theta_{1i}).\end{aligned}$$

Therefore, the Lagrangian function is

$$\begin{aligned}L &= \frac{1}{2}(m_p + 3m_b)(\dot{p}_x^2 + \dot{p}_y^2 + \dot{p}_z^2) \\ &\quad + \frac{1}{2}(I_m + \frac{1}{3}m_a a^2 + m_b a^2)(\dot{\theta}_{11}^2 + \dot{\theta}_{12}^2 + \dot{\theta}_{13}^2) - (m_p + 3m_b)g_c p_z \\ &\quad - (\frac{1}{2}m_a + m_b)g_c a(s\theta_{11} + s\theta_{12} + s\theta_{13}).\end{aligned}\quad (10.84)$$

Taking the derivatives of the Lagrangian function with respect to the six generalized coordinates, we obtain

$$\begin{aligned}\frac{d}{dt} \left(\frac{\partial L}{\partial \dot{p}_x} \right) &= (m_p + 3m_b)\ddot{p}_x, & \frac{\partial L}{\partial p_x} &= 0, \\ \frac{d}{dt} \left(\frac{\partial L}{\partial \dot{p}_y} \right) &= (m_p + 3m_b)\ddot{p}_y, & \frac{\partial L}{\partial p_y} &= 0, \\ \frac{d}{dt} \left(\frac{\partial L}{\partial \dot{p}_z} \right) &= (m_p + 3m_b)\ddot{p}_z, & \frac{\partial L}{\partial p_z} &= -(m_p + 3m_b)g_c,\end{aligned}$$

$$\begin{aligned}\frac{d}{dt} \left(\frac{\partial L}{\partial \dot{\theta}_{11}} \right) &= (I_m + \frac{1}{3}m_a a^2 + m_b a^2)\ddot{\theta}_{11}, & \frac{\partial L}{\partial \theta_{11}} &= -(\frac{1}{2}m_a + m_b)g_c a c\theta_{11}, \\ \frac{d}{dt} \left(\frac{\partial L}{\partial \dot{\theta}_{12}} \right) &= (I_m + \frac{1}{3}m_a a^2 + m_b a^2)\ddot{\theta}_{12}, & \frac{\partial L}{\partial \theta_{12}} &= -(\frac{1}{2}m_a + m_b)g_c a c\theta_{12}, \\ \frac{d}{dt} \left(\frac{\partial L}{\partial \dot{\theta}_{13}} \right) &= (I_m + \frac{1}{3}m_a a^2 + m_b a^2)\ddot{\theta}_{13}, & \frac{\partial L}{\partial \theta_{13}} &= -(\frac{1}{2}m_a + m_b)g_c a c\theta_{13}.\end{aligned}$$

Taking the partial derivatives of the constraint function Γ_i with respect to the six generalized coordinates yields

$$\frac{\partial \Gamma_i}{\partial p_x} = 2(p_x + hc\phi_i - rc\phi_i - ac\phi_i c\theta_{1i}) \quad \text{for } i = 1, 2, 3,$$

$$\frac{\partial \Gamma_i}{\partial p_y} = 2(p_y + hs\phi_i - rs\phi_i - as\phi_i c\theta_{1i}) \quad \text{for } i = 1, 2, 3,$$

$$\frac{\partial \Gamma_i}{\partial p_z} = 2(p_z - as\theta_{1i}) \quad \text{for } i = 1, 2, 3,$$

$$\frac{\partial \Gamma_1}{\partial \theta_{11}} = 2a[(p_x c\phi_1 + p_y s\phi_1 + h - r)s\theta_{11} - p_z c\theta_{11}],$$

$$\frac{\partial \Gamma_i}{\partial \theta_{11}} = 0 \quad \text{for } i = 2, 3,$$

$$\frac{\partial \Gamma_i}{\partial \theta_{12}} = 0 \quad \text{for } i = 1, 3,$$

$$\frac{\partial \Gamma_2}{\partial \theta_{12}} = 2a[(p_x c\phi_2 + p_y s\phi_2 + h - r)s\theta_{12} - p_z c\theta_{12}],$$

$$\frac{\partial \Gamma_i}{\partial \theta_{13}} = 0 \quad \text{for } i = 1, 2,$$

$$\frac{\partial \Gamma_3}{\partial \theta_{13}} = 2a[(p_x c\phi_3 + p_y s\phi_3 + h - r)s\theta_{13} - p_z c\theta_{13}].$$

Substituting the derivatives above into Eqs. (10.79) and (10.80), we obtain a system of dynamical equations. For $j = 1, 2$, and 3:

$$2 \sum_{i=1}^3 \lambda_i (p_x + hc\phi_i - rc\phi_i - ac\phi_i c\theta_{1i}) = (m_p + 3m_b) \ddot{p}_x - f_{px}, \quad (10.85)$$

$$2 \sum_{i=1}^3 \lambda_i (p_y + hs\phi_i - rs\phi_i - as\phi_i c\theta_{1i}) = (m_p + 3m_b) \ddot{p}_y - f_{py}, \quad (10.86)$$

$$2 \sum_{i=1}^3 \lambda_i (p_z - as\theta_{1i}) = (m_p + 3m_b) \ddot{p}_z + (m_p + 3m_b) g_c - f_{pz}, \quad (10.87)$$

where f_{px} , f_{py} , and f_{pz} are the x -, y -, and z -components of an external force exerted on the moving platform. For $j = 4, 5$, and 6:

$$\begin{aligned} \tau_1 &= (I_m + \frac{1}{3}m_a a^2 + m_b a^2) \ddot{\theta}_{11} + (\frac{1}{2}m_a + m_b) g_c a c \theta_{11} \\ &\quad - 2a\lambda_1 [(p_x c\phi_1 + p_y s\phi_1 + h - r)s\theta_{11} - p_z c\theta_{11}], \end{aligned} \quad (10.88)$$

$$\begin{aligned} \tau_2 &= (I_m + \frac{1}{3}m_a a^2 + m_b a^2) \ddot{\theta}_{12} + (\frac{1}{2}m_a + m_b) g_c a c \theta_{12} \\ &\quad - 2a\lambda_2 [(p_x c\phi_2 + p_y s\phi_2 + h - r)s\theta_{12} - p_z c\theta_{12}], \end{aligned} \quad (10.89)$$

$$\begin{aligned} \tau_3 &= (I_m + \frac{1}{3}m_a a^2 + m_b a^2) \ddot{\theta}_{13} + (\frac{1}{2}m_a + m_b) g_c a c \theta_{13} \\ &\quad - 2a\lambda_3 [(p_x c\phi_3 + p_y s\phi_3 + h - r)s\theta_{13} - p_z c\theta_{13}]. \end{aligned} \quad (10.90)$$

Equations (10.85) through (10.87) form a set of three linear equations in three unknowns from which the three Lagrange multipliers can be determined. Once the Lagrange multipliers are found, the actuator torques are determined from the second set of equations, Eqs. (10.88) through (10.90). These two sets of equations can be used for real-time control of the manipulator (Stampfer, 1997).

10.5 SUMMARY

The inverse dynamics of parallel manipulators has been studied in this chapter. First, a numerical solution technique based on the Newton-Euler equations was presented. It was shown that by considering each limb as a subsystem, the reaction forces and moments at the joint connecting the upper and lower members of a limb can be eliminated from the equations of motion. It was also shown that by writing the equations of motion of each limb about the fixed ball joint and by expressing the resulting equations in the link frame, reaction forces at the fixed ball joint are eliminated at the outset while some of the reaction forces at the moving ball joint can be solved independently of the equations of motion of the moving platform. Hence the computational efficiency is greatly improved.

Second, a more efficient method based on the principle of virtual work has been developed. A critical step in applying this method is the development of link Jacobian matrices that relate the velocity states of the limbs to the velocity state of the moving platform. A Stewart-Gough platform with six extensible limbs was used as an example to illustrate the methodology. It was shown that using the principle of virtual work, dynamical equations of motion for such a complex manipulator can be reduced to solving a system

of six equations in six unknowns. To demonstrate the algorithm, a computer algorithm was developed and several numerical examples were solved. It is believed that this method is more efficient than the Newton–Euler method. It can potentially be employed for real-time control of a Stewart–Gough platform.

Although it is nearly impossible to derive explicit dynamical equations for a general 6-dof parallel manipulator, it has been shown that explicit equations of motion for some relatively simple manipulators can be derived by applying Lagrangian equations of the first type. The dynamics of the University of Maryland manipulator were analyzed to illustrate the method.

REFERENCES

- Baiges, I. J. and Duffy, J., 1996, "Dynamic Modeling of Parallel Manipulators," Paper 96-DETC/MECH-1136. *Proc. 1996 ASME Design Engineering Technical Conferences*.
- Codourey, A. and Burdet, E., 1997, "A Body-Oriented Method for Finding a Linear Form of the Dynamic Equation of Fully Parallel Robots," *Proc. 1997 IEEE International Conference on Robotics and Automation*, Albuquerque, NM, pp. 1612–1618.
- Do, W. Q. D. and Yang, D. C. H., 1988, "Inverse Dynamic Analysis and Simulation of a Platform Type of Robot," *J. Robot. Syst.*, Vol. 5, No. 3, pp. 209–227.
- Freeman, R. A. and Tesar, D., 1988, "Dynamic Modeling of Serial and Parallel Mechanisms/Robotic Systems: Part I, Methodology; Part II, Applications," *Proc. ASME Mechanisms Conference: Trends and Developments in Mechanisms, Machines, and Robotics*, Vol. 3, pp. 7–27.
- Guglielmetti, P. and Longchamp, R., 1994, "A Closed Form Inverse Dynamics Model of the Delta Parallel Robot," *Proc. 1994 International Federation of Automatic Control Conference on Robot Control*, pp. 39–44.
- Kane, T. R. and Levinson, D. A., 1985, *Dynamics: Theory and Application*, McGraw-Hill, New York.
- Lebret, G., Liu, K., and Lewis, F. L., 1993, "Dynamic Analysis and Control of a Stewart Platform Manipulator," *J. Robot. Syst.*, Vol. 10, No. 5, pp. 629–655.
- Lin, Y. J. and Song, S. M., 1990, "A Comparative Study of Inverse Dynamics of Manipulators with Closed-Chain Geometry," *J. Robot. Syst.*, Vol. 7, pp. 507–534.
- Luh, J. Y. S. and Zheng, Y. F., 1985, "Computation of Input Generalized Forces for Robots with Closed Kinematic Chain Mechanisms," *IEEE J. Robot. Autom.*, Vol. 1, pp. 95–103.
- Miller, K., 1995, "Experimental Verification of Modeling of Delta Robot Dynamics by Application of Hamilton's Principle," *Proc. 1995 IEEE International Conference on Robotics and Automation*, pp. 532–537.
- Miller, K. and Clavel, R., 1992, "The Lagrange-Based Model of Delta-4 Robot Dynamics," *Robotersysteme*, Vol. 8, pp. 49–54.
- Murray, J. J. and Lovell, G. H., 1989, "Dynamic Modeling of Closed-Chain Robotic Manipulators and Implications for Trajectory Control," *IEEE Trans. Robot. Autom.*, Vol. 5, pp. 522–528.
- Pang, H. and Shahinpoor, M., 1994, "Inverse Dynamics of a Parallel Manipulator," *J. Robot. Syst.*, Vol. 11, No. 8, pp. 693–702.
- Pfreundschuh, G. H., Suger, T. G., and Kumar, V., 1994, "Design and Control of a Three-Degree-of-Freedom, In-Parallel, Actuated Manipulator," *J. Robot. Syst.*, Vol. 11, No. 2, pp. 103–115.
- Stamper, R., 1997, "A Three-Degree-of-Freedom Parallel Manipulator with Only Translational Degrees of Freedom," Ph.D. dissertation, Department of Mechanical Engineering, University of Maryland, College Park, MD.
- Stamper, R. and Tsai, L. W., 1998, "Dynamic Modeling of a Parallel Manipulator with Three Translational Degrees of Freedom," DETC98/MECH-5956, *Proc. ASME Design Engineering Technical Conferences*, Atlanta, GA.
- Sugimoto, K., 1987, "Kinematic and Dynamic Analysis of Parallel Manipulators by Means of Motor Algebra," *ASME J. Mech. Transm. Autom. Des.*, Vol. 109, No. 1, pp. 3–5.
- Tsai, L. W., 1998, "Solving the Inverse Dynamics of Parallel Manipulators by the Principle of Virtual Work," DETC98/MECH-5865, *Proc. ASME Design Engineering Technical Conferences*, Atlanta, GA.
- Tsai, K. Y. and Kohli, D., 1990, "Modified Newton–Euler Computational Scheme for Dynamic Analysis and Simulation of Parallel Manipulators with Applications to Configuration Based on R-L Actuators," *Proc. 1990 ASME Design Engineering Technical Conferences*, Vol. 24, pp. 111–117.
- Wang, J. and Gosselin, C. M., 1997, "Dynamic Analysis of Spatial Four-Degree-of-Freedom Parallel Manipulators," DETC97/DAC-3759, *Proc. 1997 ASME Design Engineering Technical Conferences*, Sacramento, CA.
- Zhang, C. D. and Song, S. M., 1993, "An Efficient Method for Inverse Dynamics of Manipulators Based on the Virtual Work Principle," *J. Robot. Syst.*, Vol. 10, No. 5, pp. 605–627.

EXERCISES

- Derive the dynamic equations of motion for the planar five-bar manipulator shown in Fig. 1.7 by the Newton–Euler formulation. To simplify the analysis, let the inertias of links 1, 2, and 3 be negligible, link 4 be a slender homogeneous rod of mass m , and the acceleration of gravity be pointing in the negative y -direction.
- For the planar 3RPR manipulator shown in Fig. 6.12, let the inertias of the limbs be negligible, the moving platform be a triangular plate of uniform

density of mass m , and the acceleration of gravity be pointing out of the plane of motion. Develop the dynamical equations of motion by the Newton–Euler formulation.

3. Derive the dynamical equations of motion for the planar five-bar manipulator shown in Fig. 3.19 by the principle of virtual work. To simplify the analysis, let the inertias of links 1, 2, and 3 be negligible, link 4 be a slender homogeneous rod of mass m , and the acceleration of gravity be pointing in the $-y$ -direction.
4. Derive the dynamical equations of motion for the University of Maryland manipulator shown in Fig. 3.10 using the principle of virtual work. Assume that the inertias of the limbs are negligible, the moving platform is triangular plate of uniform density of mass m , and the acceleration of gravity points in the $-z$ -direction.
5. For the planar five-bar manipulator shown in Fig. 3.19, let a point mass m be attached to the end effector at point Q , the inertias of all links be negligible, and the acceleration of gravity be pointing in the $-y$ -direction. Derive the dynamical equations of motion by the Lagrangian formulation.

APPENDIX A

CONTINUATION METHOD

The inverse kinematics problem of a serial manipulator can often be reduced to a single polynomial in one variable if the manipulator has three consecutive joint axes intersecting at a common point or parallel to one another. However, for a manipulator of general kinematic structure, closed-form solutions become a nearly impossible task. In this case, it may be necessary to solve the problem numerically. In this appendix we introduce a numerical method known as the *continuation* or *homotopy method*. Readers are referred to Garcia and Li (1980), Garcia and Zangwill (1979, 1981), Morgan (1983, 1986), Li (1983), and Li et al. (1987a, b, 1988) for more detailed description of the method.

Freudenstein and Roth (1963) introduced a numerical method called the *bootstrap method* or the *parameter perturbation method* for solving a very difficult problem associated with the coupler-point synthesis of geared five-bar linkages. This work attracted much attention from mathematicians and scientists and was subsequently refined and perfected into the modern continuation method (Saaty, 1981). Perhaps the two most important concepts in a successful implementation of the method are (1) the use of complex number to represent real parameters and variables, and (2) the introduction of m -homogeneous variables (Wampler et al., 1990). The homogeneous formulation may lead to a smaller number of solution paths and reduce the computing time needed in following some diverging paths.

In what follows, we first introduce the concept of polynomial homogenization and then the concept of homotopy. Tsai and Morgan's solution is used to demonstrate the methodology. Finally, a *cheater's homotopy* is introduced.

A.1 BEZOUT NUMBER

The Bezout number accounts for the number of solutions to a system of polynomial equations. First, we consider a single polynomial equation in one complex variable:

$$f(x) = \sum_{j=0}^n a_j x^{n-j} = 0, \quad (\text{A.1})$$

where a_j are constant coefficients and x is a complex variable. A fundamental theorem of algebra states that by counting multiplicity of a solution, an n -degree polynomial equation has n solutions. That is, the *Bezout number* of a single polynomial is equal to the degree of the equation.

Next, we consider a system of n polynomial equations in n variables. The degree of a multivariable polynomial term is defined as the sum of its exponents, the degree of a polynomial equation is defined as the highest degree of all the terms in the equation, and the *total degree* of a polynomial system is defined as the product of the degrees of all the equations. For the system of polynomials

$$\begin{aligned} f_1(x_1, x_2, \dots, x_n) &= 0, \\ f_2(x_1, x_2, \dots, x_n) &= 0, \\ &\vdots \\ f_n(x_1, x_2, \dots, x_n) &= 0, \end{aligned} \quad (\text{A.2})$$

if the degree of equation $f_i(\mathbf{x})$ is d_i , the total degree of the system is $d = \prod_{i=1}^n d_i$.

The *Bezout theorem* states that a polynomial system of total degree d has at most d isolated solutions in the complex Euclidean space. If all solutions of a polynomial system are nonsingular, the number of solutions is exactly equal to the total degree of the system. Including solutions at infinity, the *Bezout number* of a polynomial system is equal to the total degree of the system.

A.2 TRADITIONAL HOMOGENEOUS FORMULATION

Solutions at infinity can properly be accounted for by introducing homogeneous coordinates. Let (x_1, x_2, \dots, x_n) be n variables of a polynomial system. The homogeneous coordinates $(y_1, y_2, \dots, y_{n+1})$ are obtained by extending the number of variables from n to $n+1$ using the relations $x_i = y_i/y_{n+1}$, for $i = 1, 2, \dots, n$, where y_{n+1} is a scaling factor. Substituting $x_i = y_i/y_{n+1}$

into the original system of equations and then multiplying each equation by $y_{n+1}^{d_i}$ to clear the denominators, we obtain a new system of equations that are homogeneous in y_i . In this way, solutions at infinity become finite nonzero solutions with $y_{n+1} = 0$, and a solution to the original system of equations is obtained by dividing the homogeneous solution by y_{n+1} . This is known as the traditional *1-homogeneous formulation*.

For example, the system of equations, Eqs. (2.106) through (2.110), derived for the inverse kinematics of a general 6R manipulator can be written as

$$\left\{ \begin{array}{l} f_i(\mathbf{x}) = a_{i,1}x_1x_3 + a_{i,2}x_1x_4 + a_{i,3}x_2x_3 + a_{i,4}x_2x_4 \\ \quad + a_{i,5}x_5x_7 + a_{i,6}x_5x_8 + a_{i,7}x_6x_7 + a_{i,8}x_6x_8 \\ \quad + a_{i,9}x_1 + a_{i,10}x_2 + a_{i,11}x_3 + a_{i,12}x_4 \\ \quad + a_{i,13}x_5 + a_{i,14}x_6 + a_{i,15}x_7 + a_{i,16}x_8 \\ \quad + a_{i,17} = 0 \quad (i = 1, \dots, 4), \\ f_5(\mathbf{x}) = x_1^2 + x_2^2 - 1 = 0, \\ f_6(\mathbf{x}) = x_3^2 + x_4^2 - 1 = 0, \\ f_7(\mathbf{x}) = x_5^2 + x_6^2 - 1 = 0, \\ f_8(\mathbf{x}) = x_7^2 + x_8^2 - 1 = 0, \end{array} \right. \quad (\text{A.3})$$

where $a_{i,j}$'s are the coefficients and x_i 's are the variables of the eight polynomials. The coefficients represent the constant link parameters, and the variables are the sines and cosines of four joint angles. For this system of equations, the degree of $f_i(\mathbf{x}) = 0$ is 2 for $i = 1$ to 8. Hence the total degree of the system is $\prod_{i=1}^8 d_i = 2^8 = 256$.

The traditional 1-homogeneous system is obtained by substituting $x_i = y_i/y_9$, for $i = 1, 2, \dots, 8$ into Eq. (A.3) and then multiplying each equation by y_9^2 to clear the denominators. This results in a system of eight homogeneous equations in nine unknowns:

$$\left\{ \begin{array}{l} \tilde{f}_i(\mathbf{y}) = a_{i,1}y_1y_3 + a_{i,2}y_1y_4 + a_{i,3}y_2y_3 + a_{i,4}y_2y_4 \\ \quad + a_{i,5}y_5y_7 + a_{i,6}y_5y_8 + a_{i,7}y_6y_7 + a_{i,8}y_6y_8 \\ \quad + a_{i,9}y_1y_9 + a_{i,10}y_2y_9 + a_{i,11}y_3y_9 + a_{i,12}y_4y_9 \\ \quad + a_{i,13}y_5y_9 + a_{i,14}y_6y_9 + a_{i,15}y_7y_9 + a_{i,16}y_8y_9 \\ \quad + a_{i,17}y_9^2 = 0 \quad (i = 1, \dots, 4), \\ \tilde{f}_5(\mathbf{y}) = y_1^2 + y_2^2 - y_9^2 = 0, \\ \tilde{f}_6(\mathbf{y}) = y_3^2 + y_4^2 - y_9^2 = 0, \\ \tilde{f}_7(\mathbf{y}) = y_5^2 + y_6^2 - y_9^2 = 0, \\ \tilde{f}_8(\mathbf{y}) = y_7^2 + y_8^2 - y_9^2 = 0. \end{array} \right. \quad (\text{A.4})$$

For a traditional 1-homogeneous system, if (y_1, \dots, y_{n+1}) is a solution, $(\rho y_1, \dots, \rho y_{n+1})$ is also a solution, where ρ is any nonzero constant. Hence each solution of the original system corresponds to a line passing the origin in the homogeneous coordinates called the *projective space*. Using homogeneous coordinates, the Bezout number of a system of polynomial equations is equal to the total degree of the system. Hence the Bezout number for the system of equations in Eq. (A.4) is 256.

A.3 M-HOMOGENIZATION

In this section we introduce the concept of *m-homogenization*. It has been shown that the use of multihomogeneous variables can sometimes reduce the number of extraneous solutions. The main tasks involved in multihomogenization are the association of variables in groups and the transformation of each group into a separate homogeneous set of variables. A polynomial system is said to be under *m-homogeneous formulation* if its variables are arranged into m homogeneous groups. For example, we may arrange the variables in the system of equations given by Eq. (A.3) into two groups: (x_1, x_2, x_5, x_6) and (x_3, x_4, x_7, x_8) . Then we substitute $x_i = y_i/y_9$ for $i = 1, 2, 5$, and 6, and $x_i = y_i/y_{10}$ for $i = 3, 4, 7$, and 8 into the equations and clear the denominators to obtain a 2-homogeneous system:

$$\begin{cases} \tilde{f}_i(\mathbf{y}) = a_{i,1}y_1y_3 + a_{i,2}y_1y_4 + a_{i,3}y_2y_3 + a_{i,4}y_2y_4 \\ \quad + a_{i,5}y_5y_7 + a_{i,6}y_5y_8 + a_{i,7}y_6y_7 + a_{i,8}y_6y_8 \\ \quad + a_{i,9}y_1y_{10} + a_{i,10}y_2y_{10} + a_{i,11}y_3y_9 + a_{i,12}y_4y_9 \\ \quad + a_{i,13}y_5y_{10} + a_{i,14}y_6y_{10} + a_{i,15}y_7y_9 + a_{i,16}y_8y_9 \\ \quad + a_{i,17}y_9y_{10} = 0 \quad (i = 1, \dots, 4), \\ \tilde{f}_5(\mathbf{y}) = y_1^2 + y_2^2 - y_9^2 = 0, \\ \tilde{f}_6(\mathbf{y}) = y_3^2 + y_4^2 - y_{10}^2 = 0, \\ \tilde{f}_7(\mathbf{y}) = y_5^2 + y_6^2 - y_9^2 = 0, \\ \tilde{f}_8(\mathbf{y}) = y_7^2 + y_8^2 - y_{10}^2 = 0. \end{cases} \quad (\text{A.5})$$

Let β_j for $j = 1$ to m denote m groups of variables. To compute the Bezout number, we first form a sum over j of the product $d_{ij}\beta_j$ for each m -homogeneous equation, where d_{ij} is the degree of equation i with respect to the variables of the j th group. This results in n linear equations in β_j with d_{ij} as their coefficients. Next we form the product of these linear equations to

TABLE A.1. Degrees of the 2-Homogeneous System

Equation <i>i</i>	Group 1 (<i>j</i> = 1)	Group 2 (<i>j</i> = 2)
1	1	1
2	1	1
3	1	1
4	1	1
5	2	0
6	0	2
7	2	0
8	0	2

obtain a nonlinear polynomial in β_j :

$$\prod_{i=1}^n \left(\sum_{j=1}^m d_{ij} \beta_j \right) = (d_{11}\beta_1 + \dots + d_{1m}\beta_m)(d_{21}\beta_1 + \dots + d_{2m}\beta_m) \dots (d_{n1}\beta_1 + \dots + d_{nm}\beta_m). \quad (\text{A.6})$$

The *multihomogeneous Bezout number* is defined as the coefficient of the term $\prod_{j=1}^m \beta_j^{k_j}$ in Eq. (A.6), where k_j is the number of variables in group j .

For the 2-homogeneous system given in Eq. (A.5), the variables are arranged in two groups: (x_1, x_2, x_5, x_6) and (x_3, x_4, x_7, x_8) . The degrees of the eight equations in the variables of each group are listed in Table A.1. To find the Bezout number, we form the product

$$\prod_{i=1}^8 \left(\sum_{j=1}^2 d_{ij} \beta_j \right) = (\beta_1 + \beta_2)^4 (2\beta_1)^2 (2\beta_2)^2,$$

where d_{ij} is taken from the (i, j) element of Table A.1. Since both groups contain four variables and the coefficient of the term $\beta_1^4\beta_2^4$ in the polynomial above is 96, the 2-homogeneous Bezout number is 96. Hence the 2-homogeneous formulation of the system results in at most 96 solutions.

A.4 SOLUTIONS AT INFINITY

As mentioned earlier, using the homogeneous coordinates, solutions at infinity can be accounted for by setting the last coordinate in each group of variables to zero. For example, solutions at infinity for the 2-homogeneous

system given in Eq. (A.5) consist of three categories: (1) $y_9 = y_{10} = 0$, (2) $y_9 = 0, y_{10} = 1$, and (3) $y_9 = 1, y_{10} = 0$. For case (1), $y_9 = y_{10} = 0$, the last four equations of (A.5) reduce to

$$\begin{aligned}\tilde{f}_5(\mathbf{y}) &= y_1^2 + y_2^2 = 0, \\ \tilde{f}_6(\mathbf{y}) &= y_3^2 + y_4^2 = 0, \\ \tilde{f}_7(\mathbf{y}) &= y_5^2 + y_6^2 = 0, \\ \tilde{f}_8(\mathbf{y}) &= y_7^2 + y_8^2 = 0.\end{aligned}\quad (\text{A.7})$$

Hence $y_2 = \pm iy_1, y_4 = \pm iy_3, y_6 = \pm iy_5$, and $y_8 = \pm iy_7$. There are 16 combinations. For a typical combination, say $y_2 = iy_1, y_4 = iy_3, y_6 = iy_5, y_8 = iy_7$, the first four equations of (A.5) reduce to

$$\begin{aligned}\tilde{f}_1(\mathbf{y}) &= [(a_{i,1} - a_{i,4}) + i(a_{i,2} + a_{i,3})]y_1y_3 \\ &\quad + [(a_{i,5} - a_{i,8}) + i(a_{i,6} + a_{i,7})]y_5y_7 \\ &= 0,\end{aligned}\quad (\text{A.8})$$

for $i = 1, 2, 3$, and 4.

We may consider Eq. (A.8) as a system of four linear equations in two variables, y_1y_3 and y_5y_7 . Then it becomes obvious that the only feasible solutions are $y_1y_3 = 0$ and $y_5y_7 = 0$ for generic parameters. However, y_1 and y_5 cannot be zero simultaneously, otherwise $(y_1, y_2, y_3, y_4, y_5, y_6, y_7, y_8) = (0, 0, 0, 0, 0, 0, 0, 0)$, which is not in the projective space. Similarly, y_3 and y_7 cannot be zero simultaneously. Hence for this combination there are two solutions: $(y_1, y_2, y_3, y_4, y_5, y_6, y_7, y_8) = (1, i, 0, 0, 0, 0, 1, i)$ and $(0, 0, 1, i, 1, i, 0, 0)$. Since there are 16 combinations for case (1), a total of 32 isolated solutions exist at infinity.

Similarly, it can be shown that there are 16 solutions at infinity for each of cases (2) and (3). Overall, there are 64 solutions at infinity. Hence the system of equations has at most 32 solutions. Although these 32 solutions do satisfy Eq. (A.3), it can be shown that 16 of them do not satisfy the original loop-closure equations. Those solutions that do not satisfy the original loop-closure equations are called *extraneous solutions*, while the others are *significant*.

A.5 CONTINUATION METHOD

In this section we describe briefly a numerical solution method called the *continuation method*. Suppose that we would like to solve a system of n poly-

nomial equations in n variables:

$$F(\mathbf{x}) : \begin{cases} f_1(x_1, x_2, \dots, x_n) = 0, \\ f_2(x_1, x_2, \dots, x_n) = 0, \\ \vdots \\ f_n(x_1, x_2, \dots, x_n) = 0. \end{cases} \quad (\text{A.9})$$

We call $F(\mathbf{x}) = (f_1, f_2, \dots, f_n)$ the *target system*. The idea of the continuation method is to embed the target system in a family of polynomial systems parameterized by a real parameter t , called the *continuation parameter*. All solutions to one system in the family, called the *initial system* $G(\mathbf{x}) = 0$, can be solved in closed form. Furthermore, the solutions of the initial system should be connected to all isolated solutions of the target system via smooth paths called the *homotopy paths*. More specifically, we construct a *homotopy function* $H(\mathbf{x}, t) = 0$ with a new parameter t such that $H(\mathbf{x}, 1) = F(\mathbf{x})$, $H(\mathbf{x}, 0) = G(\mathbf{x})$, and the following properties are satisfied:

1. *Triviality.* The solutions of $G(\mathbf{x}) = 0$ can be solved in closed form.
2. *Smoothness.* The solution set of $H(\mathbf{x}, t) = 0$ for $0 \leq t < 1$ consists of a finite number of smooth paths, each parameterized by t .
3. *Accessibility.* Every isolated solution of $F(\mathbf{x}) = 0$ is reached by a solution of $G(\mathbf{x}) = 0$.

Properties 1 to 3 ensure that the solution paths can be followed from the solutions of $G(\mathbf{x}) = 0$ at $t = 0$ to all solutions of $F(\mathbf{x}) = 0$ at $t = 1$ using a conventional numerical technique involving differential equation solvers. We note that even though properties 1 to 3 imply that each solution of $F(\mathbf{x}) = 0$ will lie at the end of a solution path, some of the paths may diverge to infinity as the continuation parameter t approaches 1. This usually occurs when $G(\mathbf{x}) = 0$ possesses more solutions than $F(\mathbf{x}) = 0$. Under such a condition, some of the solutions of $G(\mathbf{x}) = 0$ are extraneous and typically diverge to infinity.

We see that the continuation method requires an initial system $G(\mathbf{x}) = 0$, a homotopy function $H(\mathbf{x}, t) = 0$, and a numerical technique for tracking the homotopy function from $t = 0$ to $t = 1$. In what follows, we briefly describe each of these in turn.

A.5.1 Homotopy Function

The homotopy function provides a way of tracking the solutions of an initial system to the solutions of a target system. The solution paths must be smooth

and nonsingular. A commonly used generic homotopy function is

$$H(\mathbf{x}, t) = \gamma(1-t)G(\mathbf{x}) + tF(\mathbf{x}), \quad (\text{A.10})$$

where γ is a random complex constant. We note that at $t = 0$ the solutions of $H(\mathbf{x}, 0) = 0$ are those of $G(\mathbf{x}) = 0$ and at $t = 1$ its solutions are those of $F(\mathbf{x}) = 0$.

In constructing a homotopy function, the triviality property can easily be satisfied. However, the smoothness and accessibility properties can only be satisfied with a careful choice of $G(\mathbf{x})$ and γ . The parameter γ is needed to ensure the accessibility of a homotopy function. This can be demonstrated by an example in which the initial system is the negative of the original system; that is, $G(\mathbf{x}) = -F(\mathbf{x})$. For $\gamma = 1$, the homotopy function $H(\mathbf{x}, t) = (1-t)G(\mathbf{x}) + tF(\mathbf{x})$ would vanish at $t = 0.5$, while for other choices of γ , it would not. Therefore, it is necessary to choose γ at random to avoid this problem.

A.5.2 Initial System

All the solutions of an initial system must be known, each solution must be nonsingular, and the system must maintain the same *polynomial structure* as the target system. Otherwise, several things can go wrong: (1) $H(\mathbf{x}, t) = 0$ might have no solution for some increment of t , or it might have several nearby solutions which are hard to distinguish or find; (2) $G(\mathbf{x}) = 0$ might not have enough solutions to match the solutions of $F(\mathbf{x}) = 0$, or $F(\mathbf{x}) = 0$ might have some solutions with no continuation paths converging on them; and (3) as t approaches 1, the solutions of $H(\mathbf{x}, t) = 0$ might diverge to infinity.

Perhaps the simplest initial system for a 1-homogeneous polynomial system is (Li, 1983)

$$G(\mathbf{x}) : \begin{cases} g_1(\mathbf{x}) = a_1x_1^{d_1} - b_1 = 0, \\ g_2(\mathbf{x}) = a_2x_2^{d_2} - b_2 = 0, \\ \vdots \\ g_n(\mathbf{x}) = a_nx_n^{d_n} - b_n = 0, \end{cases} \quad (\text{A.11})$$

where a_i and b_i are random complex coefficients. Because of the simple structure of $G(\mathbf{x})$ in Eq. (A.11), the triviality property is clearly satisfied. It can be shown that the smoothness and accessibility properties are satisfied for almost all choices of a_i and b_i . That is, $G(\mathbf{x}) = 0$ consists of $d = \prod_{i=1}^n d_i$ smooth

paths, which either converge to the solutions of $F(\mathbf{x}) = 0$ or diverge to infinity as t approaches 1, and each isolated solution of $F(\mathbf{x}) = 0$ has a path converging to it. Hence the only bad behavior is that as t is incremented, the solution to $H(\mathbf{x}, t) = 0$ might diverge to infinity. Nevertheless, all isolated solutions of $F(\mathbf{x}) = 0$ can be found. The random choice of a_j and b_j is a key factor for the success of this method.

Another possible generic initial system is

$$G(\mathbf{x}) : \begin{cases} g_1(\mathbf{x}) = \prod_{j=1}^{d_1} (x_1 - b_{1j}) = 0, \\ g_2(\mathbf{x}) = \prod_{j=1}^{d_2} (x_2 - b_{2j}) = 0, \\ \vdots \\ g_n(\mathbf{x}) = \prod_{j=1}^{d_n} (x_n - b_{nj}) = 0, \end{cases} \quad (\text{A.12})$$

where b_{ij} are random complex coefficients. Again it can be shown that Eq. (A.12) satisfies the triviality, smoothness, and accessibility properties for almost all choices b_{ij} .

The foregoing initial systems are generic in nature and can be applied to any polynomial system. It is also possible to construct an initial system for a specific problem of interest. A straightforward approach is to randomly perturb the coefficients of a target system without damaging the basic structure of the polynomials. For an m -homogeneous system, an initial system with identical polynomial structure as the target system can often be generated by a product of factors:

$$g_i(\mathbf{x}) = \prod_{j=1}^{m_i} h_{ij}(x_{1j}, x_{2j}, \dots, x_{kj}) = 0, \quad (\text{A.13})$$

where h_{ij} is a polynomial of degree d_{ij} with respect to group j , d_{ij} is the degree of equation i with respect to the variables of group j , and k_j denotes the number of variables in group j . The factors h_{ij} should be chosen with sufficiently random coefficients to satisfy the triviality, smoothness, and accessibility properties.

For example, an initial system for the 2-homogeneous system given in Eq. (A.5) can be formulated as

$$G(\mathbf{y}) : \begin{cases} g_1(\mathbf{y}) = (y_1 - b_{11}y_9)(y_3 - b_{12}y_{10}) = 0, \\ g_2(\mathbf{y}) = (y_2 - b_{21}y_9)(y_4 - b_{22}y_{10}) = 0, \\ g_3(\mathbf{y}) = (y_5 - b_{31}y_9)(y_7 - b_{32}y_{10}) = 0, \\ g_4(\mathbf{y}) = (y_6 - b_{41}y_9)(y_8 - b_{42}y_{10}) = 0, \\ g_5(\mathbf{y}) = y_1^2 + y_2^2 - b_{51}y_9^2 = 0, \\ g_6(\mathbf{y}) = y_3^2 + y_4^2 - b_{61}y_{10}^2 = 0, \\ g_7(\mathbf{y}) = y_5^2 + y_6^2 - b_{71}y_9^2 = 0, \\ g_8(\mathbf{y}) = y_7^2 + y_8^2 - b_{81}y_{10}^2 = 0, \end{cases} \quad (\text{A.14})$$

where the b_{ij} are random complex constants.

A.5.3 Path Tracking

To implement the continuation method, we start at a solution of $G(\mathbf{x}) = 0$, increment t by a small number δt and solve for the function $H(\mathbf{x}, \delta t) = 0$. Increment t again and solve for $H(\mathbf{x}, 2\delta t) = 0$, and so on, until t reaches $t = 1$. Each time we increment t by δt , we use the solution of $H(\mathbf{x}, t) = 0$ obtained at the preceding step as the initial guess and solve for the function $H(\mathbf{x}, t + \delta t) = 0$. We repeat this process for each solution of $G(\mathbf{x}) = 0$ to find all solutions of $F(\mathbf{x}) = 0$.

The method can be implemented on a computer. The implementation involves the formulation of a set of differential equations whose solutions are the continuation paths. Typically, these differential equations are solved by using a numerical integration technique. The integration is followed by Newton's iteration to refine the final solution estimates at the end of each solution path (Morgan, 1983, 1986).

A.5.4 Tsai and Morgan's Solution

As an example, let us consider the inverse kinematics of the general 6R manipulator studied in Chapter 2. Expanding Eqs. (2.106) through (2.110), we obtain a system of eight polynomials as shown in Eq. (A.15), where $x_1 = c\theta_1$, $x_2 = s\theta_1$, $x_3 = c\theta_2$, $x_4 = s\theta_2$, $x_5 = c\theta_4$, $x_6 = s\theta_4$, $x_7 = c\theta_5$, and $x_8 = s\theta_5$ are the variables of the eight polynomials; a_i , d_i , and α_i are the constant D-H link parameters; θ_i , $i = 1, 2, 4$, and 5 are the joint angles; $\mathbf{p} = [p_x, p_y, p_z]^T$ is a position vector of the origin of the fifth link frame; and $\mathbf{e} = [e_x, e_y, e_z]^T$ is a unit vector along the z_5 -axis, as shown in Fig. 2.11. The position vector \mathbf{p} and the unit vector \mathbf{e} are computed by Eqs. (2.100) and (2.101) using the given end-effector position and orientation.

$$\begin{aligned} f_1(\mathbf{x}) &= -c\alpha_1s\alpha_2p_yx_1x_3 + s\alpha_2p_xx_1x_4 + c\alpha_1s\alpha_2p_xx_2x_3 + s\alpha_2p_yx_2x_4 \\ &\quad - s\alpha_3c\alpha_4a_5x_5x_8 - s\alpha_3a_5x_6x_7 - s\alpha_1c\alpha_2p_yx_1 + s\alpha_1c\alpha_2p_xx_2 \\ &\quad - s\alpha_1s\alpha_2(p_z - d_1)x_3 - s\alpha_2a_1x_4 + s\alpha_3s\alpha_4d_5x_5 - s\alpha_3a_4x_6 \\ &\quad - c\alpha_3s\alpha_4a_5x_8 + (c\alpha_1c\alpha_2p_z - c\alpha_1c\alpha_2d_1 - c\alpha_2d_2 - d_3 \\ &\quad - c\alpha_3d_4 - c\alpha_3c\alpha_4d_5) = 0, \\ f_2(\mathbf{x}) &= c\alpha_1s\alpha_2e_yx_1x_3 + s\alpha_2e_xx_1x_4 + c\alpha_1s\alpha_2e_xx_2x_3 + s\alpha_2e_yx_2x_4 \\ &\quad + s\alpha_3c\alpha_4s\alpha_5x_5x_7 - s\alpha_3s\alpha_5x_6x_8 - s\alpha_1c\alpha_2e_yx_1 + s\alpha_1c\alpha_2e_xx_2 \\ &\quad - s\alpha_1s\alpha_2e_zx_3 + s\alpha_3s\alpha_4c\alpha_5x_5 + c\alpha_3s\alpha_4s\alpha_5x_7 \\ &\quad + (c\alpha_1c\alpha_2e_z - c\alpha_3c\alpha_4c\alpha_5) = 0, \\ f_3(\mathbf{x}) &= a_2e_xx_1x_3 + c\alpha_1a_2e_yx_1x_4 + a_2e_yx_2x_3 - c\alpha_1a_2e_xx_2x_4 \\ &\quad - s\alpha_3c\alpha_4s\alpha_5d_3x_5x_7 + s\alpha_5a_3x_5x_8 + c\alpha_4s\alpha_5a_3x_6x_7 \\ &\quad + s\alpha_3s\alpha_5d_3x_6x_8 + (a_1e_x - s\alpha_1d_2e_z)x_1 + (a_1e_y + s\alpha_1d_2e_z)x_2 \\ &\quad + s\alpha_1a_2e_zx_4 - s\alpha_3s\alpha_4c\alpha_5d_3x_5 + s\alpha_4c\alpha_5a_3x_6 \\ &\quad - s\alpha_4s\alpha_5(d_4 + c\alpha_3d_3)x_7 + s\alpha_5a_4x_8 + (d_1e_z + c\alpha_1d_2e_z \\ &\quad + c\alpha_3c\alpha_4c\alpha_5d_3 + c\alpha_4c\alpha_5d_4 + c\alpha_5d_5 - p_xe_x - p_ye_y \\ &\quad - p_ze_z) = 0, \\ f_4(\mathbf{x}) &= a_2p_xx_1x_3 + c\alpha_1a_2p_yx_1x_4 + a_2p_yx_2x_3 - c\alpha_1a_2p_xx_2x_4 \\ &\quad + a_3a_5x_5x_7 + s\alpha_3c\alpha_4a_5d_3x_5x_8 + s\alpha_3a_5d_3x_6x_7 - c\alpha_4a_3a_5x_6x_8 \\ &\quad + (a_1p_x - s\alpha_1d_2p_y)x_1 + (a_1p_y + s\alpha_1d_2p_x)x_2 - a_1a_2x_4 \\ &\quad - s\alpha_1a_2(d_1 - p_2)x_4 + (a_3a_4 - s\alpha_3s\alpha_4d_3d_5)x_5 \\ &\quad + (s\alpha_4a_3d_5 + s\alpha_3a_4d_3)x_6 + a_4a_5x_7 + (s\alpha_4a_5d_4 \\ &\quad + c\alpha_3s\alpha_4a_5d_3)x_8 + 0.5(-a_1^2 - d_1^2 - a_2^2 - d_2^2 + a_3^2 + d_3^2 \\ &\quad + a_4^2 + d_4^2 + a_5^2 + d_5^2 - p_x^2 - p_y^2 - p_z^2) = 0, \\ f_5(\mathbf{x}) &= x_1^2 + x_2^2 - 1 = 0, \\ f_6(\mathbf{x}) &= x_3^2 + x_4^2 - 1 = 0, \\ f_7(\mathbf{x}) &= x_5^2 + x_6^2 - 1 = 0, \\ f_8(\mathbf{x}) &= x_7^2 + x_8^2 - 1 = 0, \end{aligned} \quad (\text{A.15})$$

Tsai and Morgan (1985) used Eq. (A.10) with $\gamma = 1$ as the homotopy function to solve for the system of equations above. The D-H parameters of a 6R manipulator are given in Table A.2, and the given end-effector position and orientation are listed in Table A.3. Using Eq. (A.11) as the initial system, there are 256 generic starting points. A continuation path is generated for each

TABLE A.2. D-H Parameters of a 6R Manipulator

i	a_i (unit)	d_i (unit)	α_i (deg)
1	0.5000	0.1875	80
2	1.0000	0.375	15
3	0.1250	0.250	120
4	0.6250	0.875	75
5	0.3125	0.500	100
6	0.2500	0.125	60

TABLE A.3. Given End-Effector Position and Orientation

Given Vector	x-Component	y-Component	z-Component
q	0.22441776	0.71549788	0.79551628
u	-0.71511545	0.65150320	0.25328538
v	-0.69899036	-0.66895464	-0.25280857
w	0.00473084	0.35783135	0.93377425

starting point. Some of these paths converge to solutions of Eq. (A.15), and the remaining diverge to infinity as the continuation parameter t approaches $t = 1$. Each isolated solution to the system has a path converging to it. All solutions are isolated unless the system has an infinite number of solutions, that is, when the manipulator is in a singular configuration. In the latter case, some solutions will be isolated and others will form algebraic hypersurfaces, most commonly curves. Hence the continuation method will find all solutions unless there are an infinite number of solutions. For the general 6R manipulator, the continuation method always has 32 converging paths, of which 16 are significant. For the example above, the continuation method found 12 significant real solutions listed in Table A.4.

Following Eq. (A.13), an alternative initial system can be constructed:

$$G(\mathbf{x}) : \begin{cases} g_1(\mathbf{x}) = -x_6x_7 + x_2 = 0, \\ g_2(\mathbf{x}) = -x_6x_8 + x_2 = 0, \\ g_3(\mathbf{x}) = x_1x_3 + x_5x_8 + x_1 + x_2 - x_7 - 5 = 0, \\ g_4(\mathbf{x}) = x_1x_3 + x_5x_7 + x_1 + x_2 - x_3 + x_8 - 5 = 0, \\ g_5(\mathbf{x}) = x_1^2 + x_2^2 - 1 = 0, \\ g_6(\mathbf{x}) = x_3^2 + x_4^2 - 1 = 0, \\ g_7(\mathbf{x}) = x_5^2 + x_6^2 - 1 = 0, \\ g_8(\mathbf{x}) = x_7^2 + x_8^2 - 2 = 0. \end{cases} \quad (\text{A.16})$$

It can be shown that the system above has exactly 32 isolated solutions, which can easily be obtained by straightforward elimination. Using a generic homotopy function, every isolated solution of the system of equations (A.15) can be reached by a solution of Eq. (A.16). Since there are exactly 32 paths to follow, this results in a great saving of computation time. The algorithm was implemented by Li and Wang (1990) and executed without any failure for various sets of parameters.

TABLE A.4. Real Solutions Found

No.	θ_1 (deg.)	θ_2 (deg.)	θ_4 (deg.)	θ_5 (deg.)
1	167.68	83.55	65.84	-88.67
2	-143.00	100.07	18.46	-59.49
3	115.86	-168.65	157.17	-111.41
4	107.56	2.00	166.77	-173.54
5	-106.07	-140.86	-161.28	35.54
6	-65.37	142.24	-70.90	51.63
7	120.52	31.27	114.15	-143.62
8	7.75	103.87	-21.37	-79.90
9	-16.69	97.90	-80.98	25.72
10	47.26	163.44	28.32	-41.13
11	20.93	58.74	-27.07	-125.66
12	38.93	-56.45	12.28	72.23

A.6 CHEATER'S HOMOTOPY

The *cheater's homotopy* was introduced for solving a system of polynomial equations which needs to be solved repetitively with varying coefficients (Li et al., 1988). Let

$$F(\mathbf{x}, \mathbf{a}) : \begin{cases} f_1(x_1, \dots, x_n; a_1, \dots, a_k) = 0, \\ f_2(x_1, \dots, x_n; a_1, \dots, a_k) = 0, \\ \vdots \\ f_n(x_1, \dots, x_n; a_1, \dots, a_k) = 0 \end{cases} \quad (\text{A.17})$$

be the target system, where $\mathbf{x} = (x_1, \dots, x_n)$ are the variables and $\mathbf{a} = (a_1, \dots, a_k)$ are the coefficients. Also let

$$G(\mathbf{x}) : \begin{cases} g_1(x_1, \dots, x_n) = f_1(x_1, \dots, x_n; a_1^0, \dots, a_k^0) + b_1^0 = 0, \\ g_2(x_1, \dots, x_n) = f_2(x_1, \dots, x_n; a_1^0, \dots, a_k^0) + b_2^0 = 0, \\ \vdots \\ g_n(x_1, \dots, x_n) = f_n(x_1, \dots, x_n; a_1^0, \dots, a_k^0) + b_n^0 = 0 \end{cases} \quad (\text{A.18})$$

be a system of polynomial equations obtained by substituting the coefficients \mathbf{a} of the original system with the random complex numbers $\mathbf{a}^0 = (a_1^0, a_2^0, \dots, a_k^0)$ and by adding the constants $\mathbf{b}^0 = (b_1^0, b_2^0, \dots, b_n^0)$. It can be shown that the smoothness and accessibility properties hold for the homotopy function

$$H(\mathbf{x}, t) = F(\mathbf{x}, (1-t)\mathbf{a}^0 + t\mathbf{a}) + (1-t)\mathbf{b}^0 = 0. \quad (\text{A.19})$$

Note that at $t = 0$, $H(\mathbf{x}, 0) = G(\mathbf{x}) = 0$, and at $t = 1$, $H(\mathbf{x}, 1) = F(\mathbf{x}, \mathbf{a}) = 0$.

The cheater's homotopy is accomplished in two steps.

1. Solve the system of equations in Eq. (A.18) using conventional homotopy. The number of nonsingular solutions found, d_0 , is bounded by the total degree of the original system (i.e., $d_0 \leq d$).
2. For each new choice of coefficients $\mathbf{a} = (a_1, a_2, \dots, a_k)$, follow the d_0 paths defined by $H(\mathbf{x}, t) = 0$ in Eq. (A.19) to find all solutions of $F(\mathbf{x}, \mathbf{a}) = 0$.

Using this method, we follow all $d = d_1 d_2 \cdots d_n$ paths of the system of equations with random complex coefficients \mathbf{a}^0 and \mathbf{b}^0 only once to find d_0 nonsingular solutions. These d_0 solutions are then used to initialize the paths for subsequent runs. This results in a fewer number of paths to follow and therefore drastically increases the efficiency of the method.

It is important for \mathbf{a}^0 and \mathbf{b}^0 to be complex numbers, although the original system $F(\mathbf{x}, \mathbf{a}) = 0$ may have real coefficients. For real \mathbf{a}^0 and \mathbf{b}^0 , the homotopy function may fail to satisfy the smoothness and accessibility properties. Freudenstein and Roth (1963) did not use complex numbers to represent real parameters in their original *bootstrap method*. As a result, they encountered some difficulties in finding the solutions. The cheater's homotopy is called the *parameter homotopy* by Wampler et al. (1990).

REFERENCES

- Freudenstein, F. and Roth, B., 1963, "Numerical Solution of Systems of Non-linear Equations," *J. Assoc. Comput. Mach.*, Vol. 10, pp. 550–556.
- Garcia, C. B. and Li, T. Y., 1980, "On the Number of Solutions to Polynomial Systems of Equations," *SIAM J. Numer. Anal.*, Vol. 17, pp. 540–546.
- Garcia, C. B. and Zangwill, W. I., 1979, "Finding All Solutions to Polynomial Systems and Other Systems of Equations," *Math Program*, Vol. 16, pp. 159–176.
- Garcia, C. B. and Zangwill, W. I., 1981, *Pathways to Solutions, Fixed Points, and Equilibria*, Prentice Hall, Upper Saddle River, NJ.
- Li, T. Y., 1983, "On Chow, Mallet-Paret and Yorke Homotopy for Solving Systems of Polynomials," *Bull. Inst. Math. Acad. Sinica*, Vol. 11, pp. 433–437.
- Li, T. Y., Sauer, T., and York, J. A., 1987a, "Numerical Solution of a Class of Deficient Polynomial Systems," *SIAM J. Numer. Anal.*, Vol. 24, pp. 435–451.
- Li, T. Y., Sauer, T., and York, J. A., 1987b, "The Random Product Homotopy and Deficient Polynomial Systems," *Numer. Math.*, Vol. 51, pp. 481–500.
- Li, T. Y., Sauer, T., and York, J. A., 1988, "The Cheater's Homotopy: An Efficient Procedure for Solving Systems of Polynomial Equations," *SIAM J. Numer. Anal.*, Vol. 18, No. 2, pp. 173–177.
- Li, T. Y. and Wang, X., 1990, "A Homotopy for Solving the Kinematics of the Most General Six- and Five-Degree-of-Freedom Manipulators," *Proc. ASME Conference on Mechanism Synthesis and Analysis*, DE-Vol. 25, pp. 249–252.
- Morgan, A. P., 1983, "A Method for Computing All Solutions to Systems of Polynomial Equations," *ACM Trans. Math. Software*, Vol. 9, No. 1, pp. 1–17.
- Morgan, A. P., 1986, "A Homotopy for Solving Polynomial Systems," *Appl. Math. Comput.*, Vol. 18, pp. 87–92.
- Saaty, T. L., 1981, *Modern Nonlinear Equations*, McGraw-Hill, New York (1967) and Dover, New York (1981).
- Tsai, L. W. and Morgan, A., 1985, "Solving the Kinematics of the Most General Six- and Five-Degree-of-Freedom Manipulators by Continuation Methods," *ASME J. Mech. Transm. Autom. Des.*, Vol. 107, pp. 189–200.
- Wampler, C., Morgan, A., and Sommese, A., 1990, "Numerical Continuation Methods for Solving Polynomial Systems Arising in Kinematics," *ASME J. Mech. Des.*, Vol. 112, pp. 59–68.

APPENDIX B

SYLVESTER DIALYTIC ELIMINATION METHOD

In this appendix we introduce an elimination method for reduction of a system of polynomial equations. The elimination method was introduced by Cayley (1848). The method requires the derivation of an equation known as the *eliminant* or *resultant*. Various methods of formulating the eliminant can be found in Salmon (1964). Perhaps the most widely used method in the field of kinematics is the *Sylvester dialytic elimination method* (Roth, 1993). Theoretically, the method will reduce any system of multivariable polynomial equations to a single polynomial in one unknown. Practically, the method can be applied only to a relatively small set of polynomial equations. This is because the resulting polynomial equation can explode exponentially with the number and degree of equations and can possibly introduce a large number of extraneous solutions.

B.1 ELIMINATION PROCEDURE

The Sylvester dialytic elimination procedure consists of the following six basic steps:

1. Rewrite all equations with one variable suppressed.
2. Define the power products of the remaining variables as new “linear unknowns.” Here *power products* refers to the terms in a polynomial equation. For example, the power products of the polynomial $x^2z + 6xy + 3yz + 4z + 1 = 0$ are x^2z , xy , yz , z , and 1.

3. From the original equations, generate as many new linearly independent equations as the number of the linear unknowns.
4. Set the determinant of the coefficient matrix to zero to obtain a polynomial in the suppressed variable.
5. Find the roots of the characteristic polynomial of the matrix. This results in all possible solutions of the suppressed variable.
6. Substitute the suppressed variable, one at a time, into the original system of equations and repeat the process for the remaining variables.

Perhaps the most crucial step of the elimination procedure is step 3. The new linear equations are usually generated by multiplying the original equations by the powers of one or more of the variables (Salmon, 1964). This can best be illustrated by an example.

B.2 EXAMPLE

We wish to solve the following two polynomial equations in two unknowns, x_1 and x_2 :

$$e_{11}x_1^2 + e_{12}x_2^2 + e_{13}x_1x_2 + e_{14}x_1 + e_{15}x_2 + e_{16} = 0, \quad (\text{B.1})$$

$$e_{21}x_1^2 + e_{22}x_2^2 + e_{23}x_1x_2 + e_{24}x_1 + e_{25}x_2 + e_{26} = 0, \quad (\text{B.2})$$

where e_{ij} 's are constant coefficients.

Step 1. We rewrite Eqs. (B.1) and (B.2) with the variable x_2 suppressed:

$$Ax_1^2 + Bx_1 + C = 0, \quad (\text{B.3})$$

$$A'x_1^2 + B'x_1 + C' = 0, \quad (\text{B.4})$$

where $A = e_{11}$, $B = e_{13}x_2 + e_{14}$, $C = e_{12}x_2^2 + e_{15}x_2 + e_{16}$, $A' = e_{21}$, $B' = e_{23}x_2 + e_{24}$, and $C' = e_{22}x_2^2 + e_{25}x_2 + e_{26}$.

Step 2. We consider the power products x_1^2 , x_1 , and 1 as new linear variables. Then Eqs. (B.3) and (B.4) become two linear equations in these new variables.

Step 3. We generate additional equations by multiplying Eqs. (B.3) and (B.4) by the powers of the variable x_1 . Multiplying Eqs. (B.3) and (B.4) by x_1 , we obtain

$$Ax_1^3 + Bx_1^2 + Cx_1 = 0, \quad (\text{B.5})$$

$$A'x_1^3 + B'x_1^2 + C'x_1 = 0. \quad (\text{B.6})$$

Step 4. We consider Eqs. (B.3), (B.4), (B.5), and (B.6) as four linear equations in four unknowns: x_1^3 , x_1^2 , x_1 , and 1. Setting the determinant of the coefficient matrix of the four linearly independent equations to zero yields an eliminant:

$$\begin{vmatrix} A & B & C & 0 \\ 0 & A & B & C \\ A' & B' & C' & 0 \\ 0 & A' & B' & C' \end{vmatrix} = 0. \quad (\text{B.7})$$

Expanding Eq. (B.7), we obtain

$$(AC' - CA')^2 + (AB' - BA')(CB' - BC') = 0. \quad (\text{B.8})$$

Step 5. Equation (B.8) is a fourth-degree polynomial in x_2 . Hence, counting multiplicities and solutions at infinity, there are exactly four solutions.

Step 6. We substitute each solution of x_2 into Eqs. (B.1) and (B.2) and solve the resulting equations for x_1 . There should be only one solution of x_1 corresponding to each solution of x_2 , since Eqs. (B.1) and (B.2) must be satisfied simultaneously.

REFERENCES

- Cayley, A., 1848, "On the Theory of Elimination," *Cambridge Dublin Math. J.*, Vol. 3.
- Roth, B., 1993, "Computations in Kinematics," in *Computational Kinematics*, edited by J. Angeles, G. Hommel, and P. Kovacs, Kluwer Academic Publishers, Dordrecht, The Netherlands, pp. 3–14.
- Salmon, G., 1964, *Lessons Introductory to the Modern Higher Algebra*, 5th ed., Chelsea Publishing Co., New York.

APPENDIX C

RAGHAVAN AND ROTH'S SOLUTION

The Sylvester dialytic elimination method described in Appendix B is effective for a small system of polynomial equations of relatively low degree. For more complicated polynomial systems, the method can make a problem unmanageably large. Therefore, it is desirable to develop alternative methods of generating new linearly independent equations that introduce no new power products, or at worst a small number of new power products. In this appendix we describe a technique employed by Raghavan and Roth (1990a,b) for solving the inverse kinematics of the general 6R manipulator.

C.1 LOOP-CLOSURE EQUATION

Let us consider the general 6R manipulator shown in Fig. 2.11. For convenience, we decompose 1A_2 as a product of two matrices:

$${}^1A_2 = {}^1G_2 {}^1H_2, \quad (\text{C.1})$$

where

$${}^1G_2 = \begin{bmatrix} c\theta_2 & -s\theta_2 & 0 & 0 \\ s\theta_2 & c\theta_2 & 0 & 0 \\ 0 & 0 & 1 & 0 \\ 0 & 0 & 0 & 1 \end{bmatrix} \quad \text{and} \quad {}^1H_2 = \begin{bmatrix} 1 & 0 & 0 & a_2 \\ 0 & c\alpha_2 & -s\alpha_2 & 0 \\ 0 & s\alpha_2 & c\alpha_2 & d_2 \\ 0 & 0 & 0 & 1 \end{bmatrix}.$$

Note that 1G_2 contains only the joint variable and 1H_2 contains only the link parameters.

Substituting Eq. (C.1) into (2.99), we obtain

$${}^0A_1^{-1}G_2^{-1}H_2^{-2}A_3^{-3}A_4^{-4}A_5^{-5}A_6 = {}^0A_6. \quad (\text{C.2})$$

Premultiplying both sides of Eq. (C.2) by $({}^0A_1^{-1}G_2)^{-1}$ and postmultiplying both sides by ${}^5A_6^{-1}$, we obtain

$${}^1H_2^{-2}A_3^{-3}A_4^{-4}A_5 = {}^1G_2^{-1}{}^0A_1^{-1}{}^0A_6^{-5}A_6^{-1}. \quad (\text{C.3})$$

Note that by moving θ_1 , θ_2 , and θ_6 to the right-hand side of the equation, we have effectively lowered the degrees of the equations. When the matrix multiplication is carried out, Eq. (C.3) takes the form

$$\begin{aligned} & \left[\begin{array}{cccc} f_{11}(\theta_3, \theta_4, \theta_5) & f_{12}(\theta_3, \theta_4, \theta_5) & f_{13}(\theta_3, \theta_4, \theta_5) & f_{14}(\theta_3, \theta_4, \theta_5) \\ f_{21}(\theta_3, \theta_4, \theta_5) & f_{22}(\theta_3, \theta_4, \theta_5) & f_{23}(\theta_3, \theta_4, \theta_5) & f_{24}(\theta_3, \theta_4, \theta_5) \\ f_{31}(\theta_4, \theta_5) & f_{32}(\theta_4, \theta_5) & f_{33}(\theta_4, \theta_5) & f_{34}(\theta_4, \theta_5) \\ 0 & 0 & 0 & 1 \end{array} \right] \\ &= \left[\begin{array}{cccc} f'_{11}(\theta_1, \theta_2, \theta_6) & f'_{12}(\theta_1, \theta_2, \theta_6) & f'_{13}(\theta_1, \theta_2, \theta_6) & f'_{14}(\theta_1, \theta_2, \theta_6) \\ f'_{21}(\theta_1, \theta_2, \theta_6) & f'_{22}(\theta_1, \theta_2, \theta_6) & f'_{23}(\theta_1, \theta_2, \theta_6) & f'_{24}(\theta_1, \theta_2, \theta_6) \\ f'_{31}(\theta_1, \theta_2, \theta_6) & f'_{32}(\theta_1, \theta_2, \theta_6) & f'_{33}(\theta_1, \theta_2, \theta_6) & f'_{14}(\theta_1, \theta_2, \theta_6) \\ 0 & 0 & 0 & 1 \end{array} \right]. \quad (\text{C.4}) \end{aligned}$$

Equation (C.4) only reveals the variables appearing in the elements of Eq. (C.3). An examination of Eq. (C.4) reveals that the six scalar equations obtained from the third and fourth columns are free of the variable θ_6 . These six equations can be written in vector form, denoted as \mathbf{a} and \mathbf{b} , as follows:

$$\mathbf{a}: \begin{bmatrix} c\theta_3 & s\theta_3 & 0 \\ -c\alpha_2 s\theta_3 & c\alpha_2 c\theta_3 & s\alpha_2 \\ s\alpha_2 s\theta_3 & -s\alpha_2 c\theta_3 & c\alpha_2 \end{bmatrix} \begin{bmatrix} \mu_x \\ \mu_y \\ \mu_z \end{bmatrix} + \begin{bmatrix} a_2 \\ 0 \\ d_2 \end{bmatrix} = \begin{bmatrix} c\theta_2 & s\theta_2 & 0 \\ s\theta_2 & -c\theta_2 & 0 \\ 0 & 0 & 1 \end{bmatrix} \begin{bmatrix} h_x \\ h_y \\ h_z \end{bmatrix}, \quad (\text{C.5})$$

$$\mathbf{b}: \begin{bmatrix} c\theta_3 & s\theta_3 & 0 \\ -c\alpha_2 s\theta_3 & c\alpha_2 c\theta_3 & s\alpha_2 \\ s\alpha_2 s\theta_3 & -s\alpha_2 c\theta_3 & c\alpha_2 \end{bmatrix} \begin{bmatrix} v_x \\ v_y \\ v_z \end{bmatrix} = \begin{bmatrix} c\theta_2 & s\theta_2 & 0 \\ s\theta_2 & -c\theta_2 & 0 \\ 0 & 0 & 1 \end{bmatrix} \begin{bmatrix} n_x \\ n_y \\ n_z \end{bmatrix}, \quad (\text{C.6})$$

where

$$\mu_x = g_x c\theta_4 + g_y s\theta_4 + a_3,$$

$$\mu_y = -(g_x s\theta_4 - g_y c\theta_4) c\alpha_3 + g_z s\alpha_3,$$

$$\mu_z = (g_x s\theta_4 - g_y c\theta_4) s\alpha_3 + g_z c\alpha_3 + d_3,$$

$$v_x = m_x c\theta_4 + m_y s\theta_4,$$

$$v_y = -(m_x s\theta_4 - m_y c\theta_4) c\alpha_3 + m_z s\alpha_3,$$

$$v_z = (m_x s\theta_4 - m_y c\theta_4) s\alpha_3 + m_z c\alpha_3,$$

and where g_x , g_y , g_z , h_x , h_y , h_z , m_x , m_y , m_z , n_x , n_y , and n_z are defined in Chapter 2 under Eqs. (2.106) and (2.107). We note that μ_x , μ_y , μ_z , v_x , v_y , and v_z are linear functions of the terms $s\theta_4 s\theta_5$, $s\theta_4 c\theta_5$, $c\theta_4 s\theta_5$, $c\theta_4 c\theta_5$, $s\theta_4$, $c\theta_4$, $s\theta_5$, $c\theta_5$, and 1, whereas h_x , h_y , h_z , n_x , n_y , and n_z are linear functions of the terms $s\theta_1$, $c\theta_1$, and 1.

The two vectors \mathbf{a} and \mathbf{b} in Eqs. (C.5) and (C.6) represent six scalar equations in five unknowns: θ_1 , θ_2 , \dots , θ_5 . To eliminate several variables at a time, we treat some of the power products as new variables with the other power products suppressed. Toward this end, we write Eqs. (C.5) and (C.6) in the matrix form

$$A \begin{bmatrix} s\theta_4 s\theta_5 \\ s\theta_4 c\theta_5 \\ c\theta_4 s\theta_5 \\ c\theta_4 c\theta_5 \\ s\theta_4 \\ c\theta_4 \\ s\theta_5 \\ c\theta_5 \\ 1 \end{bmatrix} = B \begin{bmatrix} s\theta_1 s\theta_2 \\ s\theta_1 c\theta_2 \\ c\theta_1 s\theta_2 \\ c\theta_1 c\theta_2 \\ s\theta_1 \\ c\theta_1 \\ s\theta_2 \\ c\theta_2 \end{bmatrix}, \quad (\text{C.7})$$

where A is a 6×9 matrix whose elements are linear combinations of $s\theta_3$, $c\theta_3$, and 1, and B is a 6×8 matrix whose elements are all constants.

It can be shown that the products $\mathbf{a}^T \mathbf{a}$, $\mathbf{a}^T \mathbf{b}$, $\mathbf{a} \times \mathbf{b}$, and $(\mathbf{a}^T \mathbf{a}) \mathbf{b} - 2(\mathbf{a}^T \mathbf{b}) \mathbf{a}$ result in eight additional polynomials which take the same form as Eq. (C.7) (Raghavan and Roth, 1990a). Combining these eight equations with Eq. (C.7), we obtain 14 linearly independent equations, which can be written

$$A' \begin{bmatrix} s\theta_4 s\theta_5 \\ s\theta_4 c\theta_5 \\ c\theta_4 s\theta_5 \\ c\theta_4 c\theta_5 \\ s\theta_4 \\ c\theta_4 \\ s\theta_5 \\ c\theta_5 \\ 1 \end{bmatrix} = B' \begin{bmatrix} s\theta_1 s\theta_2 \\ s\theta_1 c\theta_2 \\ c\theta_1 s\theta_2 \\ c\theta_1 c\theta_2 \\ s\theta_1 \\ c\theta_1 \\ s\theta_2 \\ c\theta_2 \end{bmatrix}, \quad (\text{C.8})$$

where A' is a 14×9 matrix whose elements are linear combinations of $s\theta_3$, $c\theta_3$, and 1, and B' is a 14×8 matrix whose elements are constants.

C.2 ELIMINATION OF θ_1 AND θ_2

In this section we show how θ_1 and θ_2 can be eliminated simultaneously from Eq. (C.8). Toward this goal, we treat $s\theta_1s\theta_2$, $s\theta_1c\theta_2$, $c\theta_1s\theta_2$, $c\theta_1c\theta_2$, $s\theta_1$, $c\theta_1$, $s\theta_2$, and $c\theta_2$ in Eq. (C.8) as eight independent variables, and the left-hand-side terms as constants. Then Eq. (C.8) represents 14 linearly independent equations in eight unknowns. We can solve these eight variables from any eight of the 14 equations and substitute them back into the remaining six equations. This results in six independent equations, free of θ_1 and θ_2 , which can be arranged in matrix form:

$$E \begin{bmatrix} s\theta_4s\theta_5 \\ s\theta_4c\theta_5 \\ c\theta_4s\theta_5 \\ c\theta_4c\theta_5 \\ s\theta_4 \\ c\theta_4 \\ s\theta_3 \\ c\theta_5 \\ 1 \end{bmatrix} = [0], \quad (C.9)$$

where E is a 6×9 matrix whose elements are linear combinations of $s\theta_3$, $c\theta_3$, and 1.

C.3 ELIMINATION OF θ_4 AND θ_5

In this section we eliminate θ_4 and θ_5 simultaneously. We note that the six equations in Eq. (C.9) are already written with the variable θ_3 suppressed. We make use of the following trigonometric identities to convert the equations into polynomials,

$$c\theta_i = \frac{1 - t_i^2}{1 + t_i^2}, \quad (C.10)$$

$$s\theta_i = \frac{2t_i}{1 + t_i^2}, \quad (C.11)$$

where $t_i = \tan(\theta_i/2)$.

Substituting Eqs. (C.10) and (C.11) for $i = 4$ and 5 into Eq. (C.9) and then multiplying each equation by $(1 + t_4^2)(1 + t_5^2)$ to clear the denominators, we obtain

$$E' \begin{bmatrix} t_4^2t_5^2 \\ t_4^2t_5 \\ t_4^2 \\ t_4t_5^2 \\ t_4t_5 \\ t_4 \\ t_5^2 \\ t_5 \\ 1 \end{bmatrix} = [0], \quad (C.12)$$

where E' is a 6×9 matrix whose elements are linear combinations of $s\theta_3$, $c\theta_3$, and 1. Substituting Eqs. (C.10) and (C.11) for $i = 3$ into Eq. (C.12) and multiplying the first four resulting equations by $(1 + t_3^2)$, we obtain

$$E'' \begin{bmatrix} t_4^2t_5^2 \\ t_4^2t_5 \\ t_4^2 \\ t_4t_5^2 \\ t_4t_5 \\ t_4 \\ t_5^2 \\ t_5 \\ 1 \end{bmatrix} = [0], \quad (C.13)$$

where E'' is a 6×9 matrix. Note that the elements in the first four rows of E'' are quadratic in t_3 , whereas the elements in the last two rows are rational functions of t_3 , the numerators being quadratic polynomials in t_3 and the denominators being $(1 + t_3^2)$. Multiplying Eq. (C.13) by t_4 yields the following six additional linearly independent equations:

$$E'' \begin{bmatrix} t_4^3t_5^2 \\ t_4^3t_5 \\ t_4^3 \\ t_4^2t_5^2 \\ t_4^2t_5 \\ t_4^2 \\ t_4t_5^2 \\ t_4t_5 \\ t_4 \end{bmatrix} = [0]. \quad (C.14)$$

Finally, we combine Eqs. (C.13) and (C.14) in matrix form:

$$\begin{bmatrix} E'' & 0 \\ 0 & E'' \end{bmatrix} \begin{bmatrix} t_4^3 t_5^2 \\ t_4^3 t_5 \\ t_4^3 \\ t_4^2 t_5^2 \\ t_4^2 t_5 \\ t_4^2 t_5 \\ t_4 t_5 \\ t_4 \\ t_5 \\ t_5 \\ 1 \end{bmatrix} = [0]. \quad (\text{C.15})$$

We may consider $t_4^3 t_5^2$, $t_4^3 t_5$, t_4^3 , $t_4^2 t_5^2$, $t_4^2 t_5$, $t_4 t_5$, t_4 , t_5^2 , t_5 , and 1 as 12 unknowns. Then Eq. (C.15) constitutes a set of 12 linearly independent equations. The compatibility condition for nontrivial solution to exist is that the coefficient matrix must be singular. Setting the determinant of the coefficient matrix to zero yields a 16th-degree polynomial in t_3 . See Raghavan and Roth (1990a) for a more detailed derivation of the equation. Once θ_3 is solved, the other variables can be solved by back substitution. We conclude that the inverse kinematics of the general 6R robot has at most 16 real solutions.

REFERENCES

- Raghavan, M. and Roth, B., 1990a, "Kinematic Analysis of the 6R Manipulator of General Geometry," *Proc. 5th International Symposium on Robotics Research*, edited by H. Miura and S. Arimoto, MIT Press, Cambridge, MA.
 Raghavan, M. and Roth, B., 1990b, "A General Solution for the Inverse Kinematics of All Series Chains," *Proc. 8th CISM-IFToMM Symposium on Robots and Manipulators (ROMANSY-90)*, Cracow, Poland.

APPENDIX D

LIST OF SYMBOLS

In this appendix we summarize some commonly used symbols. In general, vectors are represented by boldface lowercase characters and matrices are represented by uppercase characters. A trailing superscript denotes the inverse or transpose of a matrix. A trailing subscript may represent the component of a vector, the link number, or the position number of a rigid body. A leading superscript denotes a frame in which a vector or a screw is expressed. The leading superscript is often omitted when the fixed frame serves as the reference frame. In each case, a symbol is defined in the text where it first appears.

A : fixed frame.

A : transpose of a structure matrix, $A = B^T$.

A : $m \times n$ matrix.

A' : $m \times n$ matrix.

A, B, C : coefficients of a polynomial equation.

A', B', C' : coefficients of a polynomial equation.

A_i : 4×4 matrix of transformation associated with the i th screw displacement.

A_i : i th ball point on the fixed base of a parallel manipulator.

$i^{-1}A_i$: 4×4 matrix of transformation between the i th and $(i-1)$ th link frames.

- ${}^0\Lambda_n$: 4×4 matrix describing the position and orientation of an end effector (link n) with respect to a fixed frame (link 0).
- a : link length.
- a_i : offset distance between two adjacent joint axes (D-H parameter).
- a_i : coefficient of a polynomial system.
- a_i^0 : complex coefficient of an initial polynomial system.
- a_{ij} : (i, j) element of a transformation matrix.
- \mathbf{a} : vector of constants, $\mathbf{a} = [a_1, a_2, \dots, a_k]^T$.
- \mathbf{a}^0 : vector of constants, $\mathbf{a}^0 = [a_1^0, a_2^0, \dots, a_k^0]^T$.
- \mathbf{a}_i : position vector of a ball point A_i .
- B : moving link frame.
- B : structure matrix that transforms a set of actuator torques to joint torques.
- B : $m \times n$ matrix.
- B_i : i th ball point on the moving platform of a parallel manipulator.
- B' : $m \times n$ matrix.
- B^* : structure matrix whose elements assume the value +1, -1, or 0.
- B^+ : pseudoinverse of B , $B^+ = B^T [BB^T]^{-1}$.
- b : link length.
- b_i : damping coefficient.
- b_i : random complex constant.
- b_i^0 : complex constant of an initial polynomial system.
- b_{ij} : complex constant.
- \mathbf{b}^0 : vector of constants, $\mathbf{b}^0 = [b_1^0, b_2^0, \dots, b_n^0]^T$.
- \mathbf{b}_i : position vector of a ball point B_i relative to a moving frame B , expressed in a fixed frame A .
- ${}^B\mathbf{b}_i$: position vector of a point B_i relative to and expressed in a moving frame B .
- C : cylindrical joint.
- C : compliance matrix.
- C_k : connectivity number associated with limb k .
- C_p : cam pair.
- c : link length.

- c_i : degrees of constraint on relative motion imposed by joint i .
- $c\theta_i$: shorthand notation for $\cos \theta_i$.
- \mathbf{c} : couple.
- d : total degree of a polynomial system.
- d_i : translational distance along the i th joint axis (D-H parameter).
- d_i : i th limb length.
- d_i : degree of equation i .
- d_{ij} : degree of equation i with respect to the variables of group j .
- $d(\cdot)$: derivative of (\cdot) .
- \mathbf{d}_i : vector of a limb i , $\mathbf{d}_i = \overline{A_i B_i}$.
- $\det(\cdot)$: determinant of (\cdot) .
- E : planar pair.
- E, E', E'' : $m \times n$ matrices.
- e : link length.
- e_i : link length i .
- e_{ij} : coefficient of a polynomial equation.
- \mathbf{e} : unit vector.
- \mathbf{e}_i : unit vector directed along the i th joint axis.
- F : degrees of freedom of a mechanism or mechanical manipulator.
- $F(\mathbf{x})$: system of polynomial equations that are functions of \mathbf{x} .
- \mathbf{F} : end-effector output wrench.
- \mathbf{F}_e : external wrench exerted at the center of mass on an end effector.
- $\mathbf{F}_{i,i-1}$: wrench exerted on link i by link $i - 1$.
- $\hat{\mathbf{F}}_i$: sum of applied and inertia wrenches exerted at the center of mass of link i .
- $\hat{\mathbf{F}}_{ji}$: sum of applied and inertia wrenches exerted at the center of mass of link j , which is a part of limb i .
- $\hat{\mathbf{F}}_p$: sum of applied and inertia wrenches exerted at the center of mass of a moving platform.
- f_i : degrees of freedom associated with joint i .
- f_i : i th polynomial equation of $F(\mathbf{x})$.

- f:** end-effector output force.
- f:** system of constraint equations.
- f^C:** resultant force exerted at the center of mass *C* of a rigid body.
- f^O:** resultant force exerted at point *O* of a rigid body.
- f_{ai}:** force exerted at point *A_i* of limb *i*.
- f_{bi}:** force exerted at point *B_i* of a moving platform by limb *i*.
- f^B_{bi}:** f_{bi} expressed in a moving frame *B*.
- fⁱ_{bi}:** f_{bi} expressed in the *i*th limb frame.
- f_i:** resultant force exerted at the center of mass of link *i*.
- f_i^{*}:** inertia force exerted at the center of mass of link *i*, $f_i^* = -m_i \dot{v}_i$.
- f̂_i:** sum of applied and inertia forces exerted at the center of mass of link *i*, $\hat{f}_i = f_i + f_i^*$.
- f̂_i:** f_i expressed in the *i*th link frame.
- f̂_i^{*}:** f_i^{*} expressed in the *i*th link frame.
- f_{i,j}:** force exerted on link *i* by link *j*.
- f^k_{i,j}:** f_{i,j} expressed in the *k*th link frame.
- f_{ji}^{*}:** inertia force exerted at the center of mass of link *j*, which is a part of limb *i*.
- f̂_{ji}:** f_{ji}^{*} expressed in the *i*th limb frame.
- f_p:** resultant force exerted at the center of mass of a moving platform.
- f_p^{*}:** inertia force exerted at the center of mass of a moving platform, $f_p^* = -m_p \dot{v}_p$.
- f̂_p:** sum of applied and inertia forces exerted at the center of mass of a moving platform, $\hat{f}_p = f_p + f_p^*$.
- f_r:** vector of friction torques and/or forces.
- G:** gear pair.
- G(x):** initial system of polynomial equations used by a continuation method.
- G_i:** *i*th component of **G**.
- i⁻¹G_i:** 4 × 4 transformation matrix that contains only link parameters.
- G:** vector of gravitational effects,

$$\mathbf{G} = [G_1, G_2, \dots, G_n]^T$$

- Ĝ:** **G** expressed in the end-effector space.
- g:** link length.
- g_c:** gravitational constant.
- g_i(x):** *i*th polynomial equation of **G(x)**.
- g:** acceleration of gravity.
- ĝ_i:** **g** expressed in the *i*th link frame.
- H:** helical joint.
- H:** $m \times (m - n)$ matrix whose column vectors span the null space of a structure matrix **B**.
- H(x, t):** homotopy function.
- i⁻¹H_i:** 4 × 4 transformation matrix that contains only one joint variable.
- h:** link length.
- h_{ij}(x):** polynomial of degree d_{ij} with respect to the variables of group *j*.
- h^A_i:** angular momentum of limb *i* taken about point *A_i*.
- ĥ_i^A:** h^A_i expressed in the *i*th limb frame.
- h^C:** angular momentum of a rigid body taken about the center of mass *C*.
- ĥ_{ji}^C:** angular momentum of link *j* of the *i*th limb taken about the center of mass of link *j*.
- h^O:** angular momentum of a rigid body taken about point *O*.
- I:** identity matrix.
- I^C_B:** shorthand notation for ${}^A I_B^C$.
- I^O_B:** shorthand notation for ${}^A I_B^O$.
- AI^C_B:** inertia matrix of a rigid body *B* taken about the center of mass and expressed in a fixed frame *A*.
- AI^O_B:** inertia matrix of a rigid body *B* taken about a point *O* and expressed in a fixed frame *A*.
- I_i:** inertia matrix of link *i* taken about the center of mass and expressed in a fixed frame *A*.
- Î_i:** inertia matrix of link *i* taken about the center of mass and expressed in the *i*th link frame.
- Î_{ji}:** inertia matrix of link *j* taken about the center of mass link *j* and expressed in the *i*th limb frame.
- I_{j,x}, I_{j,y}, I_{j,z}:** principal moment of inertia of link *j* about the coordinate axes of a fixed frame.

- $I_{j,u}, I_{j,v}, I_{j,w}$: principal moment of inertia of link j about the coordinate axes of a moving frame.
- I_{xx}, I_{yy}, I_{zz} : principal moment of inertia of a rigid body about the coordinate axes of a fixed frame.
- I_{xy}, I_{yz}, I_{zx} : product of inertia of a rigid body about the coordinate axes of a fixed frame.
- I_{uu}, I_{vv}, I_{ww} : principal moment of inertia of a rigid body about the coordinate axes of a moving frame.
- I_{uv}, I_{vw}, I_{wu} : product of inertia of a rigid body about the coordinate axes of a moving frame.
- I_{uv}^O : product of inertia of a rigid body relative to a reference point O for \mathbf{u} and \mathbf{v} .
- I_u^O : second moment of inertia of a rigid body relative to a line that passes through a point O and is parallel to a unit vector \mathbf{u} .
- \mathbf{i} : unit vector pointing along the x -axis in a Cartesian coordinate system.
- J : Jacobian matrix.
- J_{bi} : 3×6 matrix transforming the velocity of the center of mass of a moving platform to a ball point B_i .
- $J_{bi,x}$: first row of J_{bi} .
- $J_{bi,y}$: second row of J_{bi} .
- $J_{bi,z}$: third row of J_{bi} .
- J_i : i th link Jacobian matrix.
- J_{ji} : j th link Jacobian matrix of the i th limb.
- J_p : Jacobian matrix of a moving platform.
- J_q : Jacobian matrix associated with the rates of change of the input joint variables.
- J_{vi} : link Jacobian submatrix associated with the linear velocity of the center of mass of link i .
- J_{vi}^j : j th column of J_{vi} .
- J_{mi} : link Jacobian submatrix associated with the angular velocity vector of link i .
- J_{wi}^j : j th column of J_{wi} .
- J_x : Jacobian matrix associated with the rates of change of the end effector coordinates.
- j : number of joints in a mechanism.
- j_g : number of gear pairs.

- j_i : number of joints with i degrees of freedom.
- j_t : number of turning pairs.
- \mathbf{j} : unit vector pointing along the y -axis in a Cartesian coordinate system.
- K : kinetic energy of a system of rigid bodies.
- K : stiffness matrix.
- K_j : kinetic energy of link j .
- K_r : kinetic energy of rotor r .
- k_i : constant coefficient.
- k_i : stiffness constant associated with joint i .
- k_p : position feedback gain.
- k_v : velocity feedback gain.
- \mathbf{k} : unit vector pointing along the z -axis in a Cartesian coordinate system.
- L : Lagrangian function.
- L : number of independent loops in a mechanism.
- L, M, N, P, Q, R : Plücker coordinates of a line.
- \mathbf{l}^O : linear momentum of a rigid body about a reference point O .
- M : manipulator inertia matrix.
- \tilde{M} : M expressed in the end-effector space.
- M_{ij} : (i, j) element of M .
- m : mass of a rigid body.
- m : number of tendons.
- m_i : mass of link i .
- \mathbf{m}_i : unit vector.
- N_{ij} : gear ratio between a gear pair i and j , $N_{ij} = T_j/T_i$.
- n : number of links in a mechanism (including the fixed link).
- n : number of degrees of freedom of a manipulator.
- n : last link of a manipulator.
- n : number of generalized coordinates.
- n : end effector output moment.
- \mathbf{n}^C : resulting moment exerted at the center of mass C of a rigid body.
- \mathbf{n}^O : resulting moment taken about point O of a rigid body.

- \mathbf{n}_i : unit vector.
- \mathbf{n}_i : resulting moment exerted at the center of mass of link i .
- $\hat{\mathbf{n}}_i$: sum of applied and inertia moments exerted at the center of mass of link i , $\hat{\mathbf{n}}_i = \mathbf{n}_i + \mathbf{n}_i^*$.
- \mathbf{n}_A^i : resulting moment taken about point A of link i .
- \mathbf{n}_i^* : inertia moment exerted at the center of mass of link i ,
- $$\mathbf{n}_i^* = -I_i \dot{\omega}_i - \boldsymbol{\omega}_i \times (I_i \boldsymbol{\omega}_i).$$
- ${}^i \mathbf{n}_i$: \mathbf{n}_i expressed in the i th link frame.
- ${}^i \mathbf{n}_i^*$: \mathbf{n}_i^* expressed in the i th link frame.
- $\mathbf{n}_{i,j}$: moment exerted on link i by link j .
- ${}^k \mathbf{n}_{i,j}$: $\mathbf{n}_{i,j}$ expressed in the k th link frame.
- \mathbf{n}_{ji}^* : inertia moment exerted at the center of mass of link j which is a part of limb i .
- ${}^i \mathbf{n}_{ji}^*$: \mathbf{n}_{ji}^* expressed in the i th limb frame.
- \mathbf{n}_p : resulting moment exerted at the center of mass of a moving platform.
- ${}^B \mathbf{n}_p$: \mathbf{n}_p expressed in a moving frame B .
- \mathbf{n}_p^* : inertia moment exerted at the center of mass of a moving platform, $\mathbf{n}_p^* = -I_p \dot{\boldsymbol{\omega}}_p - \boldsymbol{\omega}_p \times (I_p \boldsymbol{\omega}_p)$.
- $\hat{\mathbf{n}}_p$: sum of applied and inertia moments exerted at the center of mass of a moving platform, $\hat{\mathbf{n}}_p = \mathbf{n}_p + \mathbf{n}_p^*$.
- O : origin of a fixed frame, $O = O_0$.
- $O^+(x)$: “+” operator that takes the value of x when $x \geq 0$, and 0 otherwise.
- $O^-(x)$: “−” operator that takes the value of $-x$ when $x < 0$, and 0 otherwise.
- O_i : origin of the i th link frame.
- P : point of a rigid body.
- P : point located at a wrist center of a serial manipulator.
- P : point located at the center of mass of a moving platform.
- p_x, p_y, p_z : x , y , and z coordinates of \mathbf{p} .
- p_u, p_v, p_w : u , v , and w coordinates of \mathbf{p} .
- \mathbf{p} : abbreviated form of ${}^A \mathbf{p}$.
- ${}^A \mathbf{p}$: position vector of a point P with respect to a fixed frame A .

- ${}^A \mathbf{p}$: position vector of the wrist center with respect to a fixed frame A .
- ${}^A \mathbf{p}$: position vector of the center of mass of a moving platform with respect to a fixed frame A .
- ${}^B \mathbf{p}$: position vector of a point P with respect to a moving frame B .
- ${}^j \mathbf{p}$: position vector of a point P relative to the j th link frame.
- \mathbf{p}_c : position vector of the center of mass of a rigid body.
- \mathbf{p}_{ci} : position vector of the center of mass of link i with respect to a fixed frame.
- ${}^j \mathbf{p}_{ci}$: position vector of the center of mass of link i with respect to the j th link frame.
- ${}^j \mathbf{p}_{ci}^*$: position vector of the center of mass of link i with respect to the j th link frame, expressed in a fixed frame.
- \mathbf{p}_i : position vector of the origin O_i of the i th link frame with respect to a fixed frame.
- ${}^j \mathbf{p}_i$: $\overline{O_j O_i}$ expressed in the j th link frame.
- ${}^j \mathbf{p}_i^*$: $\overline{O_j O_i}$ expressed in a fixed frame.
- ${}^j \mathbf{p}_n$: $\overline{O_j O_n}$ expressed in the j th link frame.
- ${}^j \mathbf{p}_n^*$: $\overline{O_j O_n}$ expressed in a fixed frame.
- Q : origin of an end-effector coordinate frame.
- Q_i : generalized active force associated with the i th generalized coordinate.
- \mathbf{Q} : vector of generalized forces,
- $$\mathbf{Q} = [Q_1, Q_2, \dots, Q_n]^T.$$
- $\tilde{\mathbf{Q}}$: \mathbf{Q} expressed in the end-effector space.
- q_i : i th joint variable or generalized coordinate.
- \mathbf{q} : vector of joint angles or generalized coordinates,
- $$\mathbf{q} = [q_1, q_2, \dots, q_n]^T.$$
- ${}^A \mathbf{q}$: abbreviated form of ${}^A \mathbf{q}$.
- ${}^A \mathbf{q}$: position vector of the origin of a moving frame with respect to a fixed frame A .
- ${}^A \mathbf{q}$: position vector of the end-effector coordinate frame with respect to a fixed frame A .
- R : revolute joint.

- R^* : $n \times n$ diagonal matrix whose nonzero elements represent the radii of the pulleys installed on the joint axes of a tendon-driven manipulator.
- ${}^A R_B$: 3×3 rotation matrix that describes the orientation of frame B with respect to frame A .
- ${}^B R_A$: inverse transformation of ${}^A R_B$, ${}^B R_A = {}^A R_B^{-1}$.
- r : link length.
- r_d : radius of gyration.
- r_i : radius of pulley i .
- \mathbf{r} : position vector of a point relative to a center-of-mass coordinate frame.
- \mathbf{r}_{ci} : position vector of the center of mass of link i relative to the i th link frame, expressed in a fixed frame.
- ${}^i \mathbf{r}_{ci}$: \mathbf{r}_{ci} expressed in the i th link frame.
- \mathbf{r}_i : $\overline{O_{i-1} O_i}$ expressed in a fixed frame.
- ${}^i \mathbf{r}_i$: \mathbf{r}_i expressed in link frame i , ${}^i \mathbf{r}_i = [a_i, d_i s\alpha, d_i c\alpha]^T$.
- S : spherical joint.
- S_i : i th coordinate of a screw $\$$.
- S_{ri} : i th coordinate of a reciprocal screw $\$_r$.
- s_i : linear displacement of tendon i .
- \mathbf{s} : vector of tendon displacements, $\mathbf{s} = [s_1, s_2, \dots, s_m]^T$.
- \mathbf{s}_i : unit vector pointing along the axis of a screw $\$_i$.
- ${}^i \mathbf{s}_i$: \mathbf{s}_i expressed in the i th limb frame.
- \mathbf{s}_o : position vector of a screw axis defined from the origin of a fixed frame to any point on the screw axis.
- s_{oi} : position vector of a screw axis defined from the origin of a fixed frame to any point on the i th screw axis.
- ${}^j s_{oi}$: position vector of a screw axis defined from the origin of a reference frame j to any point on the screw axis i .
- \mathbf{s}_r : unit vector pointing along the axis of a reciprocal screw $\$_r$.
- s_{ro} : position vector of a screw axis defined from the origin of a fixed frame to any point on the reciprocal screw $\$_r$.
- $s\theta_i$: shorthand notation for $\sin \theta_i$.
- T_i : number of teeth on gear i .

- ${}^A T_B$: 4×4 matrix describing the transformation of frame B to frame A .
- ${}^i \tilde{T}_j$: 6×6 matrix describing the transformation of a screw or wrench from coordinate frame j to i .
- t : time.
- t : continuation parameter.
- t : translational distance along the axis of a screw.
- t_i : translational distance along the i th screw axis.
- t_i : shorthand notation for $\tan(\theta_i/2)$.
- U : potential energy of a mechanical system.
- U_i : potential energy of link i .
- u_x, u_y, u_z : x , y , and z components of \mathbf{u} .
- \mathbf{u} : unit vector pointing along the u -axis of a moving frame.
- V_i : i th component of \mathbf{V} .
- \mathbf{V} : vector of velocity coupling terms, $\mathbf{V} = [V_1, V_2, \dots, V_n]^T$.
- $\tilde{\mathbf{V}}$: \mathbf{V} expressed in the end-effector space.
- v_x, v_y, v_z : x , y , and z components of \mathbf{v} .
- \mathbf{v} : unit vector pointing along the v -axis of a moving frame.
- \mathbf{v} : abbreviated form of ${}^A \mathbf{v}$.
- ${}^A \mathbf{v}$: vector \mathbf{v} expressed in a fixed frame A .
- \mathbf{v}_{bi} : velocity of a ball point B_i expressed in a fixed frame.
- ${}^i \mathbf{v}_{bi}$: \mathbf{v}_{bi} expressed in the i th limb frame.
- \mathbf{v}_{ci} : velocity of the center of mass of link i relative to a fixed frame.
- ${}^j \mathbf{v}_{ci}$: \mathbf{v}_{ci} expressed in the j th link frame.
- $\dot{\mathbf{v}}_{ci}$: linear acceleration of the center of mass of link i relative to a fixed frame.
- ${}^j \dot{\mathbf{v}}_{ci}$: $\dot{\mathbf{v}}_{ci}$ expressed in the j th link frame.
- \mathbf{v}_i : velocity of the origin O_i of the i th link frame relative to a fixed frame.
- $\ddot{\mathbf{v}}_i$: linear acceleration of the origin O_i of the i th link frame relative to a fixed frame.
- ${}^i \mathbf{v}_i$: \mathbf{v}_i expressed in the i th link frame.
- \mathbf{v}_{ji} : velocity of the center of mass of link j , which is a part of limb i .

- \mathbf{v}_n : velocity of the origin of an end-effector coordinate frame.
- \mathbf{v}_o : velocity of a point in the end effector which instantaneously coincides with the origin of a fixed frame.
- \mathbf{v}_P : velocity of a point P relative to a fixed frame.
- \mathbf{v}_p : velocity of the center of mass of a moving platform relative to a fixed frame.
- $\ddot{\mathbf{v}}_p$: acceleration of a point P relative to a fixed frame.
- $\ddot{\mathbf{v}}_p$: acceleration of the center of mass of a moving platform relative to a fixed frame.
- \mathbf{v}_q : velocity of a point Q relative to a fixed frame.
- iW_j : 3×3 skew-symmetric matrix whose nonzero elements represent the vector $\overline{O_i O_j}$ expressed in the i th link frame.
- w_x, w_y, w_z : x, y , and z components of \mathbf{w} .
- \mathbf{w} : unit vector pointing along the w -axis of a moving frame.
- x_c, y_c, z_c : x, y , and z axes of a coordinate frame attached to the center of mass of link i .
- x_i : i th variable of a polynomial system.
- x_i, y_i, z_i : x, y , and z axes of the i th link frame.
- \mathbf{x} : n -dimensional vector describing the position and orientation of an end effector.
- $\dot{\mathbf{x}}$: n -dimensional vector describing the linear and angular velocities of an end effector,
 $\dot{\mathbf{x}}_i = [v_x, v_y, \dots, v_z]^T$ for conventional Jacobian and
 $\dot{\mathbf{x}}_i = [\omega_x, \omega_y, \dots, \omega_z]^T$ for screw-based Jacobian.
- \mathbf{x}_i : n -dimensional vector describing the position and orientation of link i .
- $\dot{\mathbf{x}}_i$: n -dimensional vector describing the linear and angular velocities of link i .
- $\dot{\mathbf{x}}_{ji}$: n -dimensional vector describing the linear and angular velocities of the j th link, which is a part of limb i .
- $\dot{\mathbf{x}}_p$: n -dimensional vector describing the linear and angular velocities of a moving platform.
- y_i : i th variable of a polynomial system.

- ${}^{i-1}Z_{i-1}$: 3×3 skew-symmetric matrix whose nonzero elements represent a unit angular velocity of link i relative to link $i - 1$, expressed in the $(i - 1)$ th link frame.
- \mathbf{z}_i : unit vector pointing along the z_i axis, expressed in a fixed frame.
- ${}^i\mathbf{z}_i$: \mathbf{z}_i expressed in the i th link frame, ${}^i\mathbf{z}_i = [0, 0, 1]^T$.
- α : angle.
- α_i : twist angle between two adjacent joint axes of link i (D-H parameter).
- β : angle.
- β_i : variable.
- Γ_i : i th constraint function.
- γ : random complex constant.
- $\boldsymbol{\gamma}$: 1×3 perspective transformation matrix.
- $\Delta\mathbf{q}$: vector of infinitesimal joint displacements.
- $\Delta\mathbf{x}$: vector of infinitesimal end-effector displacement.
- δ : bias force.
- δ_i : i th bias force.
- $\delta\mathbf{x}_i$: virtual displacement of link i .
- $\delta\mathbf{x}_p$: virtual displacement of a moving platform.
- δW : virtual work.
- η : virtual coefficient.
- θ : angle.
- θ : Euler angle.
- θ_i : i th joint angle (D-H parameter).
- θ_{ij} : shorthand notation for $\theta_i + \theta_j$.
- θ_{ijk} : shorthand notation for $\theta_i + \theta_j + \theta_k$.
- $\theta_{i,j}$: angular displacement of link i relative to link j .
- θ_{ji} : angular displacement associated with the j th joint of limb i .
- $\boldsymbol{\theta}$: vector of joint angles.
- κ_i : i th constant coefficient of an equation.
- λ : degrees of freedom of the space in which a mechanism is intended to function.
- λ : eigenvalue.
- λ : constant.

λ :	pitch of a screw.
λ_i :	i th Lagrange multiplier.
λ :	vector of some constants.
μ :	constant.
μ_i :	i th constant.
v :	constant.
v_i :	i th constant.
ξ_i :	i th tendon force.
ξ_i :	i th actuator torque or force.
ξ :	vector of tendon forces.
ξ :	vector of actuator torques and/or forces.
ρ :	scaling factor.
ρ :	material density.
τ_i :	i th joint torque or force.
τ :	vector of joint torques and/or forces.
ϕ :	angle.
ϕ :	Euler angle.
ϕ_i :	angle i .
ϕ :	vector of actuator rotation angles.
χ :	$n \times n$ diagonal matrix whose elements represent the stiffness constants of actuated joints.
ψ :	angle.
ψ :	Euler angle.
ψ_i :	angle i .
Ω :	3×3 skew symmetric matrix whose nonzero elements represent the angular velocity of a rigid body, $\Omega = {}^A\dot{R}_B {}^A R_B^T$.
$\omega_x, \omega_y, \omega_z$:	x, y , and z components of ω_i .
ω :	angular velocity of a rigid body.
${}^A\omega_B$:	angular velocity of a moving frame B relative to a fixed frame A .
ω_i :	angular velocity of link i .
$\dot{\omega}_i$:	angular acceleration of link i .
${}^j\omega_i$:	ω_i expressed in the j th link frame.
${}^j\dot{\omega}_i$:	$\dot{\omega}_i$ expressed in the j th link frame.
ω_p :	angular velocity of a moving platform.
$\dot{\omega}_p$:	angular acceleration of a moving platform.

$\$$:	screw.
$\hat{\$}$:	unit screw.
${}^j\$$:	screw expressed in the j th link frame.
$\$_i$:	screw displacement associated with the i th joint axis.
$\hat{\$}_{j,i}$:	unit screw associated with the j th joint of the i th limb.
$\$_p$:	screw displacement associated with a moving platform.
$\$,$:	reciprocal screw.
$\hat{\$,}$:	unit reciprocal screw.
$[]$:	product convention.
\sum :	summation convention.
\int :	integration convention.
${}^k(\cdot)$:	(\cdot) expressed in the k th link frame.
$(\cdot)^T$:	transpose of (\cdot).
$(\cdot)^{-1}$:	inverse of (\cdot).
$(\cdot)'$:	derivative of (\cdot) with respect to time.
$ (\cdot) $:	absolute value of (\cdot).
$ (\cdot) $:	determinant of (\cdot).



INDEX

- Accessibility, 463–465
Actuator force(s), 260, 265
Actuator space, 260, 317, 319
Actuator torque(s), 321–322
ADAMS, 374
Adept gripper, 19
Adept-one robot, 20–22, 24
Amplitude, 182
Angular momentum, 380–381
Angular velocity, 171–174
Arm, 25–26, 298
 $\text{Atan2}(x, y)$, 39, 41, 72, 75–76, 83–85,
 102–103, 107–109
Automation
 flexible, 1
 hard, 1
Base, 9, 54, 116
Base frame, 384
Bendix wrist, 302
 canonical graph representation,
 323–324
 equivalent open-loop chain, 323–324
 kinematics 323–326
Bezout number, 147, 149, 155–156, 158,
 458
 multihomogeneous, 461
Bezout theorem, 458, 460
Bootstrap method, 457
Canonical graph, 305–306, 324
Carrier, 302–303, 308, 312
Center of mass, 375
Central configuration, 290
Centrifugal forces, 402–403
Characteristic equation, 34
Characteristic value, 34
Chasles' theorem, 42, 91
Cheater's homotopy, 469–470
Cincinnati-Milacron wrist, 301, 317–319
 canonical graph representation, 306
 equivalent open-loop chain, 318
 graph representation, 304
Classification of robots, 19–29
 by degrees of freedom, 19
 by drive technology, 21
 by kinematic structure, 20
 by motion characteristics, 27
 by workspace geometry, 25
Closed-form solution(s), 55, 70
Closed-loop chain, 8
Coaxiality condition(s), 313–314, 316,
 343–344
Compatibility condition, 173

Compliance matrix, 279–281
 Composite homogeneous transformation, 45
 Condition number, 211–212
 Configuration, 10, 47, 396
 folded back, 72, 82, 216
 fully stretched, 72, 82, 216
 Connectivity, 118–119, 121–123
 Constraints, 396
 holonomic, 396
 nonholonomic, 396
 Constraint equation(s), 447, 450
 Constraint function(s), 448
 Continuation method, 56, 117, 156, 457, 462–463
 Continuation parameter, 463
 Coordinate systems
 base, 60
 end effector, 58
 hand, 58, 60
 link, 56–60
 Coriolis forces, 402–403
 d'Alembert's principle, 374, 437
 DADS, 374
 Degree of a polynomial system, 458–460, 470
 Degrees of freedom, 6, 9–15, 118, 298, 307, 334–337, 396–397, 448
 passive, 12–13, 122, 152
 DELTA robot, 134, 166, 167
 Denavit and Hartenberg's convention, 57
 Denavit–Hartenberg method, 69, 123–124
 Dextrous hand, 18
 Differential kinematics, 171, 177
 Differential speed reducer, 315
 Differential transformation matrix
 link, 178
 overall, 179
 Direct dynamics, 47, 372
 Direct kinematics, 46, 54, 66, 98, 117
 Direct position problem, 54
 Direct velocity problem, 169
 Direction cosine representation, 31
 DOF, 6
 Dual matrix method, 55
 DYMAC, 374
 Dynamic analysis, 47

Dynamic synthesis, 48
 Dynamical equations
 end effector space, 417
 general form, 401
 Dynamics, 47, 372, 424
 Eigenvalue(s), 34, 212–213, 273, 275, 281–282, 378
 Eigenvectors, 35, 212–213, 273, 275, 281–282, 378
 Elbow manipulator
 position analysis, 98–103
 screw-based Jacobian, 198–202
 singular configurations, 218–219
 Eliminant, 150–151, 473
 Elimination method, 56, 473, 477
 Ellipsoid, 212–213, 215, 273–275, 281
 End effector, 17–18, 54, 65–66
 End-effector force space, 274–275, 282
 End-effector space, 169, 185, 213, 215–216, 260, 279, 317–318
 Equivalent joint torque(s), 261, 265–266, 321–322, 348
 Equivalent open-loop chain, 300, 317–319, 323–326, 411–412, 414
 Euler angle(s), 31, 37–41, 65, 131, 133, 427–429
 roll-pitch-yaw angles, 38
 w–u–w Euler angles, 39
 w–v–w Euler angles, 41
 Euler's equation, 16
 Euler's equation of motion, 385, 432
 Euler's theorem, 34
 Extraneous solutions, 56, 155, 460, 462, 473
 F-circuit, *see* Fundamental circuit(s)
 Fanuc arc welding robot, 373
 Fanuc LR Mate robot, 261
 Fanuc S-900W robot, 4, 20–21, 77, 109, 115
 position analysis, 77–85
 Fanuc spray painting robot, 170
 Five-bar linkage, 11–12
 Forward kinematics, 46, 142
 Four-bar linkage, 11
 Frame
 Fixed frame, 29
 Moving frame, 29

Free-body diagram, 261, 282, 288, 293
 Functional schematic representation, 303–304
 Fundamental circuit(s), 300, 308, 311–312, 314, 316, 319, 323
 Fundamental circuit equation(s), 312, 314, 316, 319, 324, 342, 343
 General 6R manipulator, 85–86, 459, 466
 Generalized coordinates, 395–397, 438, 450–452
 independent, 397, 403, 406, 425
 redundant, 397, 447–448, 450
 Generalized forces, 395, 400–401, 405, 410, 448, 450
 Generalized inner product, 243
 Geometric method, 55–56, 123
 Grübler criterion, 11–12, 14
 Graph representation, 304
 Gripper, 18
 universal, 18
 Hamilton, 374
 Home position, 98
 Homogeneous coordinates, 42–44
 Homogeneous formulation, 457
 m-homogeneous formulation, 460
 1-homogeneous formulation, 459
 2-homogeneous formulation, 461
 traditional, 458
 Homogeneous solution, 351
 Homogeneous transformation
 matrix(es), 43
 D–H transformation matrices, 60–62
 Homogeneous variables, 457
 Homotopy function, 463–464, 467, 470
 Homotopy method, 85, 457
 Homotopy paths, 463
 Humanoids, 2–3
 Hybrid kinematic chain, 8
 IMP, 374
 Inertia effects of rotors, 410
 Inertia frame, 383–385, 400
 Inertia matrix(es), 375–378, 381–382, 386, 395, 414
 Cartesian, 418
 end-effector space, 418
 Kane's method, 374
 Kinematic analysis, 46

Kinematic chain(s), 9
 Kinematic pair(s), 7. *See also* Joint(s)
 cam pair, 8
 gear pair, 8
 higher pairs, 7–8
 lower pairs, 7–8
 plane pair, 7
 screw pair, 7
 sliding pair, 7
 surface contact, 246
 Kinematic synthesis, 46
 Kinematics, 46
 Kinetic energy, 382–383, 395–396,
 398–399, 401, 412, 413, 418, 450
 Kutzbach criterion, 11

Lagrangian equations, 374
 of the first type, 397, 447
 of the second type, 397
 Lagrangian formulation, 374, 395, 424,
 426, 443, 447
 Lagrangian function, 395, 401, 450–451
 Lagrangian method(s), 374, 395
 Lagrangian multiplier, 425, 448
 Legs, 116
 Limb(s), 116
 Line coordinates, 184
 Linear momentum, 379–380
 Linear velocity, 174
 Link Jacobian submatrix(es), 395,
 398–399, 402
 Link parameters, 56, 58–60
 Links, 6
 Location, 29
 description of, 41
 Loop mobility criterion, 6, 15–16
 Loop-closure equation(s), 16, 65–66,
 69–70, 85, 97, 124, 228, 231, 235

Machine(s), 8–9
 Manipulator(s), 1. *See also* Robot(s)
 direct drive, 23
 hybrid, 21
 master-slave, 2
 mechanical, 2, 17
 open-loop, 20, 54
 parallel, 20–21
 planar, 27
 serial, 20

spatial, 28
 spherical, 28
 Matrix method, 55
 Mechanics, 45
 Mechanism(s), 6, 8–9
 overconstrained, 14
 planar, 27
 spatial, 28
 spherical, 29
 Members, 6
 Method of successive screw
 Minuteman cover drive, 313
 Moment(s) of inertia, 375–377
 axial, 413
 principal, 375, 377–378, 386
 Motion
 planar, 27
 spatial, 28
 spherical, 28
 NBOD2, 374
 Newton–Euler laws, 383
 Newton's equation of motion, 384
 Newton–Euler equations, 374, 395
 Newton–Euler formulation, 386, 424,
 426
 NIST RoboCrane, 337, 370
 Norm, 212
 Number synthesis, 46
 O^+ operator, 358–366
 O^- operator, 358–366
 Open-loop chain, 8, 15
 Orientation, 25, 29, 31, 35, 37, 44
 Orthogonal conditions, 33, 66, 144, 151,
 153–156
 Orthogonal product, 243, 248, 252
 Orthogonal transformation, 34
 Orthogonality conditions, *see* orthogonal
 condition
 Pair element, 7
 Pantograph mechanism, 12–13, 16, 164,
 294
 Parallel axes theorem, 375, 377
 Parallel manipulators, 20–21, 116
 asymmetrical, 118
 classification of, 118–123

dynamics, 424
 Jacobian analysis, 223
 planar, 119
 position analysis, 116
 spatial, 121
 spherical, 28, 119
 statics, 282
 stiffness analysis, 288
 symmetrical, 118
 Parameter homotopy, 470
 Parameter perturbation method, 457
 Particular solution, 351, 354
 Path tracking, 466
 Pathfinder, 6
 Perspective transformation, 43–44
 Pitch(es), 39, 176, 182–183, 207, 241,
 243–247
 Plücker coordinates, 184
 Planar 2-dof manipulator
 conventional Jacobian, 187–188
 force ellipsoid, 275
 locus of isotropic points, 214
 Lagrangian dynamics, 403–405
 Newton–Euler dynamics, 391–394
 stiffness analysis, 281–282
 velocity ellipsoid, 215
 Planar 3-dof manipulator
 conventional Jacobian, 188–189
 D–H transformation matrices, 62–63
 position analysis, 70–74
 singular configurations, 216–217
 statics, 266–268
 Planar 3-dof, 3-PRP manipulator, 120,
 165
 Planar 3-RRR manipulator, 50, 120
 conventional Jacobian, 227–231
 position analysis, 124–129
 statics, 283–284, 286–287
 Planar linkages, 27
 Planar schematic representation, 339
 Platform manipulators, 116, 136
 Position vector, 29–30
 Posture, 47, 55
 Potential energy, 395–396, 400–401,
 414–415
 Power product(s), 473–474, 477, 479
 Primary links, 412
 Principal axes, 212, 273, 281–282, 378,
 386, 435
 Principle of virtual work, 272, 285, 321,
 348, 437–438, 442–443
 Prismatic-spherical dyad, 245
 Product of inertia, 376–377
 Projective space, 460, 462
 Pseudoisomorphic graphs, 305
 Pseudoisomorphic mechanisms, 305
 Pseudotriangular structure matrix(es),
 354, 360, 366
 Quaternion algebra method, 55
 Radius of gyration, 376
 Raghavan and Roth's solution, 477–482
 Reciprocal screw(s), 241–250, 253–254
 of some kinematic chains, 245
 of some kinematic pairs, 244
 Rectifier, 354, 359–360
 Recursive method, 264
 Redundant forces resolution, 354
 Reference coordinate system, 29
 Reference frame, 30, 42, 44
 instantaneous, 193–195, 199, 203,
 205
 Reference position, 96–100, 104, 318
 Resultant, 473
 Resultant screw, 91, 95
 Revolute-spherical dyad, 245
 Robot(s), 2. *See also* Manipulator(s)
 articulated, 26
 Cartesian, 25, 26
 Cincinnati Milacron T³, 4
 cylindrical, 25, 27
 deficient, 19
 gantry, 25
 general-purpose, 19
 historical development, 2–6
 master-slave, 5
 PUMA, 4
 redundant, 19
 SCARA, 26. *See also* SCARA arm
 serial, 20
 spherical, 25
 Unimate, 3
 Robotic systems, 17
 Robotics, 45
 Rodrigues's formula, 36, 93
 Roll, 39
 Root, 305

Rotation matrix(es), 33, 36–42
basic, 38

Scaling factor, 43–44, 458

SCARA arm, 26, 64, 112, 406

D-H transformation matrices, 63–65
Lagrangian dynamics, 405, 410

Scorbot robot, 56–57, 67, 114

D-H transformation matrices, 64–65
loop-closure equation, 66–69
position analysis, 74–76

Scorbot-ER III robot, 24

Screw algebra method, 55

Screw axis, 34–35, 92, 94–95, 182–183, 241

Screw axis representation, 31, 35–37

Screw coordinates, 182–184

Screw cylindroid, 183

Screw displacement(s), 91, 182

Screw parameters, 92, 94

Screw systems, 182–183

- n*-system, 183
- one-system, 183
- two-system, 183

Screw(s)

- reciprocal, 241–247
- transpose of, 243

SD-EXACT, 374

Second moment, 375

Secondary links, 412

Self motion, 218

Serial manipulators, 20

- dynamics, 372
- Jacobian analysis, 169
- position analysis, 54
- statics, 260
- stiffness analysis, 279

Significant solutions, 88, 462

Singular condition(s), 170, 216, 225–226

Singular configuration(s), 84, 108, 127, 215, 223, 225–226

Singularity(ies), 215

- boundary, 216
- combined, 226, 230, 234, 238
- direct kinematic, 226, 229, 232, 236, 240, 256
- interior, 216
- inverse kinematic, 225, 228, 232, 236, 240, 256

Skew-symmetric matrix, 172–173, 176, 179–180, 207, 277

Slider-and-crank mechanism, 9

Smoothness, 463–465

Solutions at infinity, 461–462

Spatial 3-PPSR, 168

- screw-based Jacobian, 252–257

Spatial 3-RPS manipulator, 51

- position analysis, 142–151

Spatial 3-UPU manipulator, 52, 165–166

Spatial orientation mechanism, 129

- conventional Jacobian, 231–234
- position analysis, 129–134

Spherical 3-RRR manipulator, 28

Stanford manipulator, 113

- conventional Jacobian, 189–192
- position analysis, 103–109
- screw-based Jacobian, 195–198
- singular configurations, 217–218
- statics, 268–271

Stanford/JPL finger, 339–342

- abbreviated planar representation, 342
- force resolver schematic diagram, 365
- kinematics, 345–346
- planar schematic diagram, 341
- redundant forces resolution, 363–365
- schematic diagram, 340
- structural matrix, 350

Stanford/JPL hand, 18, 338

Statics, 47, 260

Stewart–Gough platform, 13, 14, 426

- conventional Jacobian, 239–240
- dynamics, 432–436
- equations of motion, 442–443
- kinematics, 426–432
- link Jacobian matrices, 439–441
- position analysis, 151–158
- screw-based Jacobian, 250–252
- statics, 284–285, 287–288
- 3–3 Stewart–Gough platform

 - position analysis, 158–161
 - stiffness analysis, 289–293

Stiffness analysis

- parallel manipulators, 288
- serial manipulators, 279

Stiffness constant, 280

Stiffness matrix, 261, 280–281, 289, 292

Structure characteristics, 300, 307, 351, 354

epicyclic gear trains, 308

tendon-driven manipulators, 352

Structure matrix, 322–323, 349–350

Successive screw displacements, 56, 91, 95–96, 98

Sylvester, 150, 158, 473

Target position, 96–98, 100, 105

Target system, 463–465, 469

Tendon driven manipulators

- classification of, 334–339
- closed-loop tendon drives, 334
- feasible structure matrices, 351
- kinematics, 340
- open-ended tendon drives, 334
- planar schematic representation, 339
- redundant forces resolution, 354
- static force analysis, 348
- structure characteristics, 352

Tendon force space, 351

Tendon routing, 339, 340, 342–345

- crossed type, 343–344
- parallel type, 343

Train value, 323

Transfer vertex, 308

Transformation

- of forces, 273
- of force(s) and moment(s), 260, 275
- of screw coordinates, 205

Transmission line(s), 309, 322–323, 340, 342–345, 349

Trigonometric identities, 82, 88, 127, 134, 149, 480

Triviality, 463–465

Tsai and Morgan's solution, 85, 466

Twist, 182–183

Type synthesis, 46

Universal-spherical dyad, 245

University of Maryland manipulator

- conventional Jacobian, 234–239
- Lagrangian dynamics, 449–453
- position analysis, 134–142

Utah/MIT finger

- force resolver schematic diagram, 367
- kinematics, 346–348

Yaw, 39

Zero position, 96

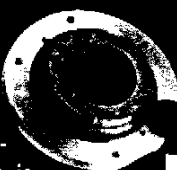
Complete, state-of-the-art coverage of robot analysis

This unique book provides the fundamental knowledge needed for understanding the mechanics of both serial and parallel manipulators. Presenting fresh and authoritative material on parallel manipulators that is not available in any other resource, it offers an in-depth treatment of position analysis, Jacobian analysis, statics and stiffness analysis, and dynamical analysis of both types of manipulators, including a discussion of industrial and research applications. It also features:

- The homotopy continuation method and dialytic elimination method for solving polynomial systems that apply to robot kinematics
- Numerous worked examples and problems to reinforce learning
- An extensive bibliography offering many resources for more advanced study

Drawing on Dr. Lung-Wen Tsai's vast experience in the field as well as recent research publications, *Robot Analysis* is a first-rate text for upper-level undergraduate and graduate students in mechanical engineering, electrical engineering, and computer studies, as well as an excellent desktop reference for robotics researchers working in industry or in government.

LUNG-WEN TSAI, PhD, is a professor in the Department of Mechanical Engineering and the Institute for Systems Research at the University of Maryland in College Park, Maryland. He received his PhD from Stanford University in 1973 and has had an extensive career in engineering, education, and industry. He is a fellow of the ASME. An internationally recognized expert in automotive engineering, mechanisms and machine theory, and robot manipulators, he is well published in leading robotics journals, including numerous articles in the *Journal of Robotics Systems* (Wiley), the ASME *Journal of Mechanical Design*, and *IEEE Transactions on Robotics and Automation*.



Cover Design: Paul DiNovo

WILEY-INTERSCIENCE

John Wiley & Sons, Inc.

Professional/Trade Division

605 Third Avenue, New York, N.Y. 10158-0012

ISBN 0-471-32593-7

90000

